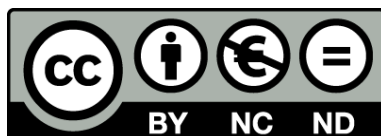# UNIVERSITAT DE BARCELONA

Understanding and predicting magnetic coupling in complex systems: from inorganic complexes to organic polyradicals

Daniel Reta Mañeru

Memória presentada per

Daniel Reta Mañeru

per a optar al grau de Doctor per la Universitat de Barcelona

Programa de doctorat en Química Teòrica i Computational

Understanding and predicting magnetic coupling in complex systems: from inorganic complexes to organic polyradicals

Dirigida per:

Dr. Francesc Illas i Riera   Dr. Ibério de Pinho Ribeiro Moreira

(Universitat de Barcelona)   (Universitat de Barcelona)

Tutor:

Dr. Ibério de Pinho Ribeiro Moreira

(Universitat de Barcelona)

UNIVERSITAT DE BARCELONA

Barcelona, 2016

UNIVERSITAT DE BARCELONA

FACULTAT DE QUÍMICA

DEPARTAMENT DE QUÍMICA FÍSICA

INSTITUT DE QUÍMICA TEÒRICA I COMPUTACIONAL

UNDERSTANDING AND PREDICTING MAGNETIC COUPLING IN COMPLEX SYSTEMS: FROM INORGANIC COMPLEXES TO ORGANIC POLYRADICALS

Daniel Reta Mañeru

2016

A Kinga

A mi familia

Agradecimientos

Quisiera expresar aquí mi más sincero agradecimiento a todas aquellas personas que, de un modo u otro, han contribuido a este trabajo y lo han hecho posible.

Particularmente, a mis directores de tesis, el Dr. Francesc Illas y el Dr. Ibério de P. R. Moreira. Sólo gracias a la generosa actitud de Francesc al ofrecerme un contrato, tuve los medios para poder embarcarme en la carrera académica. La más absoluta confianza que ambos depositaron en mí desde el inicio y su incesante disponibilidad para dedicarme su tiempo y responder mis dudas, facilitaron enormemente mi incorporación al campo de la química teórica y computacional, que era desconocido para mí. Además, ser testigo inmediato del carácter tan excepcional y al mismo tiempo dispar de Francesc e Ibério, me ha ofrecido una serie de vivencias científicas y personales que han influenciado muy positivamente mi manera de entender la ciencia y de ser. Estoy profundamente agradecido por haber podido compartir este tiempo con ellos y por la sincera amistad desarrollada.

Al Prof. Sambhu N. Datta, y al Prof Vincent Robert por la cálida y generosa acogida que me ofrecieron durante las estancias que realicé en sus respectivos grupos, en el *IIT Bombay*, y el *Laboratoire de Chimie Quantique* de Stasbourg. El interés del Prof. Datta en los radicales orgánicos fue lo que marcó gran parte de la línea de investigación de esta tesis. Estoy en deuda con él por la increíble oportunidad que me ofreció para asomarme a la cultura India, lo cual me ha enriquecido personalmente en todos los aspectos. No me puedo olvidar de mis compañeros pre-doctorales durante mi estancia en India: Arun K. Pal, Shekhar Hansda y Tumpa Sadhukhan, con quienes compartí momentos memorables en India. Debo un especial agradecimiento y reconocimiento a la dimensión científica y personal del Prof. Robert, quien me hizo sentir en casas cuando me acogió en su grupo. Su modo de enfocar los problemas me resultan excepcionales e inspiradores.

A todas aquellas personas con las que he ido coincidiendo en el camino, y que han ido contribuyendo a mi formación como científico. Quisiera dedicar especial atención a los Profesores Iker Zuriguel, Diego Maza y Ángel Garcimartín, de la Universidad de Navarra, ya que fueron ellos los primeros que alentaron y promovieron una actitud científica en mi formación. No puedo dejar de mencionar tampoco a la doctora Carolina Sañudo, quien me ofreció generosamente su laboratorio para realizar mi tesis de máster.

También él juzga que todo está bien. Este universo en adelante sin dueño no le parece estéril ni fútil. Cada uno de los granos de esa piedra, cada fragmento mineral de esa montaña llena de noche, forma por sí solo un mundo. La lucha por llegar a las cumbres basta para llenar un corazón de hombre. Hay que imaginarse a Sísifo feliz.

El mito de Sísifo

Albert Camus

GENERAL INDEX

Theoretical Background   CHAPTER 2

Theoretical Study of High-Spin Ground State Odd Alternant Hydrocarbons   CHAPTER 4

Magnetism in Organic and Organometallic Compounds

1.1. Introduction.

The challenge for understanding the origin of magnetism in matter and the associated phenomena have required a remarkable effort by some of the brightest scientific minds, which, in the process, has offered fundamentally new ways of describing matter and prompted deep technological transformations of societies. A detailed discussion on the scientific contributions that led to the formulation of quantum theory and consequently the explanation of the origin of magnetism is out of the scope of this brief introduction. Nevertheless, some historical remarks are required.

Till the beginning of XIX century, electric and magnetic phenomena were thought to be independent. This changed with the contributions by Ampère, Oersted, Faraday and Henry who carried out some of the most important scientific studies manifesting a correlation between magnetic and electric fields. Maxwell, in 1865, provided a mathematical formalism allowing for a classical explanation and unification of the electromagnetic waves. Despite that, the explanation to the origin of magnetism remained an open question.

Magnetism is a macroscopic expression of the basic constituents of matter. It is then reasonable to think that a proper theory of matter was prior to the description of the origin of magnetism. Thus, the explanation of the origin of magnetism is the story of the development of quantum theory. Maxwell was succeeded as the director of the Cavendish laboratory by J. J. Thomson who, in 1897, demonstrated the existence of a basic constituent of the atom, the electron, which is ultimately responsible for the appearance of magnetism. These early steps were followed by consecutive developments brought by Bohr in 1913 on the atomic structure, by Stern and Gerlach in 1922 concerning the magnetic moment of the atom and by Hund in 1925 studying atomic spectra. Taken together, they collected the necessary evidence and called for a new interpretation of reality and of how matter interacts with radiation. This ultimately took place between 1925 and 1926 with two formulations of quantum mechanics: the theory of matrix mechanics by Heisenberg, Born and Jordan and the theory of wave mechanics by Schrodinger. Finally, in 1928 Dirac unified both theories bringing together the concepts of electron spin developed by Uhlenbeck and Goudsmit in 1925, the Pauli exclusion principle proposed in 1925 and the Fermi-Dirac (1926) and Bose-Einstein (1924) statistics. At that point, a theory capable of rationalizing most of the

properties of matter and its interaction with radiation was introduced,[1,2] including magnetic phenomena.[3]

The first attempts to apply the new-born quantum theory to the field of magnetism were pursued by Heisenberg in 1928. He was devoted to rationalizing the observed ferromagnetism (and consequent appearance of unpaired electrons) in metals, where the assumption of localized spins is fulfilled due to the nature of *d* and *f* shells of the metallic ions. This model would also provide a theoretical explanation to the molecular field by Weiss (1907). Further joint theoretical and experimental research carried out by Bethe, Kramers (1929), Pauling (1931) and Peney, Schlapp, Van Vleck (1932) among others, established the fundamental role of the crystalline field on the electronic structure of the metallic ion centres, responsible for the magnetic response of the material. This was generalized by Jahn and Teller in 1937 by means of group theory, which linked the symmetry of the crystalline field with the electronic structure of the paramagnetic centres. Finally, the rationalization of the several exhibited magnetic behaviours in solids was completed with the contribution of Neél (1932-1936) on anti- and ferrimagnetism, and the introduction of superexchange by Anderson[4] in order to explain antiferromagnetism through a diamagnetic centre. These works settled the basis for studying the electronic structure together with the origin and temperature dependence of magnetic properties in a diversity of systems, which boosted the development of solid state physics. The interaction of the unpaired electrons determine the magnetic order within a range of temperature, being ferromagnetic or antiferromagnetic if the alignment of the spins is parallel or antiparallel, respectively. The collective behaviour arising from these interactions is what defines the magnetic properties of the material, where the dimensionality of the network composed by the spins plays a crucial role.[5,6]

Ultimately, the interaction between localized spin moments can be described by the phenomenological Hamiltonian introduced by Heisenberg[7]

$$\hat{H} = -\sum_{\langle i,j \rangle} J_{ij} \hat{\boldsymbol{S}}_i \cdot \hat{\boldsymbol{S}}_j \tag{1}$$

where J_{ij} is the exchange coupling constant between the $\hat{\boldsymbol{S}}_i$ and $\hat{\boldsymbol{S}}_j$ localized spin moments and the $\langle i,j \rangle$ symbol indicates that the sum refers to nearest neighbour interactions only. Here, a positive or negative value implies a ferromagnetic or

antiferromagnetic interaction, respectively. A simplification of the previous Hamiltonian was introduced by Ising,[8] considering only the z components of spin moments

$$\hat{H}^{Ising} = -\sum_{\langle i,j \rangle} J_{ij} \hat{S}_i^z \cdot \hat{S}_j^z \tag{2}$$

These models are essential for the interpretation of many different magnetic phenomena arising from the existence of localized spin moments. Hence, these two Hamiltonians are central to the work presented in this thesis, and they will be found all along the discussion.

The previous reasoning was devoted to the appearance of unpaired electrons and their subsequent magnetic order in systems where the spin moment is localized on a metallic centre. The assumptions of the models that rationalized these properties were initially thought for d and f orbitals. A detailed discussion on how to use some of the current computational methods to accurately extract the coupling constants in related compounds is presented in chapter 3. However, since the establishment of quantum theory, the study of magnetic properties has spread throughout many fields of research and has gathered a large collection of examples demonstrating that magnetism can also be originated in systems with no metallic centres. Particularly important are these compounds where the unpaired electrons are shared among heteroatoms presenting different electronegativities[9,10] or delocalized over a π–conjugated system.[11] Of relevant interest to the purpose of this thesis is the latter case, which is extensively treated in chapter 4.

1.2. General Considerations.

The forthcoming discussion presents the basic arguments behind the characterization of magnetic properties, as it is done for most of the compounds discussed in this thesis.

1.2.1. Magnetization and Magnetic Susceptibility.

Consider 1 mol of a molecular sample, subject to a homogeneous external magnetic field $\vec{H}$. The acquired molar magnetization can be expressed as

$$\vec{M}(\vec{H}) = -\frac{\partial E(\vec{H})}{\partial \vec{H}} \tag{3}$$

where E is the total energy under the presence of $\vec{H}$ and can be expressed as a sum of the possible states of the system with energies $E_n(\vec{H})$ (n=1, 2, …). Each of the sublevels contribute to the total magnetization with a microscopic magnetization

$$\vec{M}_n(\vec{H}) = -\frac{\partial E_n(\vec{H})}{\partial \vec{H}} \tag{4}$$

For a given temperature *T*, assuming thermal equilibrium, the macroscopic molar magnetization (eqn (3)) can be rewritten as a sum of the microscopic magnetizations weighted according to a Boltzman distribution

$$\vec{M}(\vec{H}, T) = \frac{N \sum_n \left(-\partial E_n(\vec{H})/\partial \vec{H}\right) e^{\left(-E_n(\vec{H})/kT\right)}}{\sum_n e^{\left(-E_n(\vec{H})/kT\right)}} \tag{5}$$

It is worth noting that in order to apply eqn (5), one must know the variation of the energy of each of the thermally populated states $E_n(\vec{H})$ (n=1, 2, ⋯) with the applied field. As a preliminary discussion, consider the two limiting cases where H/kT is either very small or very large. The case where H/kT is very small stands for the simplifications introduced by Van Vleck, as discussed later. The situation in which H/kT is very large is associated with the saturation magnetization, and allows knowing the total multiplicity (*S* value) of the sample. In order to exemplify this, consider an ideal paramagnet, which is a simplified case of *N* non-interacting paramagnetic centres. In such case, the magnetization can be expressed as

$$M = Ng\beta S B_s(y) \tag{6}$$

where $B_s(y)$ is a Brillouin functions,[12] *N* Avogadro's number, β the electronic Bohr magneton and *g* the g-factor. If H/kT is large, as stated, $B_s(y)$ tends to unity and *M* approaches the saturation value M_S, which expressed in *N*β units ($1N\beta = 5585 \; cm^3 Gmol^{-1}$) yields:

$$M_S = gS \tag{7}$$

Therefore, by recording the magnetization at large H/kT, one can access the S value of the sample.

Now, the quantity relating the acquired magnetization with the applied field is the magnetic susceptibility,

$$\chi = \frac{\partial \vec{M}(\vec{H})}{\partial \vec{H}} \tag{8}$$

The magnetic susceptibility χ is a second rank tensor whereas the magnetization $\vec{M}$ is an axial vector. Then, it is always possible to define the reference axis so χ is diagonal with the $\chi_u (u = x, y, z)$ principal values. If the magnetization of the sample does not depend on the angle associated to the applied external field, the sample is said to be magnetically isotropic, and χ becomes a scalar. Additionally, for weak enough magnetic fields, $\vec{M}$ and $\vec{H}$ are almost parallel, leading to an expression for χ

$$\chi = \frac{M}{H} \tag{9}$$

that is very useful for molecular magnetism, where the systems are generally isotropic, do not present hysteresis neither remanent magnetization. The fields generally applied in experiments are constant and of low intensity, so eqn (9) holds. In these conditions, χ depends only on the temperature and on the nature of the sample, which is closely related to the microscopic properties.

1.2.2. Diamagnetism and Paramagnetism.

It has been observed experimentally that samples react following two opposing behaviours under the presence of an external applied field. Thus, the expression of the magnetic susceptibility can be presented as a sum of two contributions, which are associated with different phenomena:

$$\chi = \chi^D + \chi^P \tag{10}$$

In this expression, χ^D and χ^P stand for the diamagnetic and paramagnetic susceptibilities, respectively. Their opposing nature manifests in the fact that the former is negative while the latter is positive. Both are present in paramagnets and metals, but the interplay among them determines how they react to an external applied field. Thus, if χ^D dominates, the sample is repelled due to the appearance of an induced magnetic

moment opposing the applied field; the sample is said to be diamagnetic. Contrarily, if χ^P dominates, the sample is attracted by the applied field and is considered as paramagnetic. The origin of both phenomena arises from the specific electronic structure of the sample, but corresponds to two different types of interactions.

Diamagnetism is an intrinsic property of matter, since it arises from the motion of the electrons interacting with the applied field. It is fundamentally related to the closed-shell electrons and therefore it is always present. In fact, it is associated to Lenz's law, which states that a circular electric flow induces a magnetic field that opposes the applied one. Some theoretical models[5] have helped understanding the origin and nature of the phenomenon, which is independent of the temperature and intensity of the applied field. However, to calculate its contribution by *ab initio* methods for medium and large size molecules is too complicated, and empirical formulas to estimate its effect have been proposed. Particularly, Pascal[13] proposed an expression

$$\chi^D = kM10^{-6}cm^3mol^{-1} \tag{11}$$

where M is the molecular weight of the compound and k an adjusting factor varying among 0.4 and 0.5, is generally considered as a reasonable approximation to estimate diamagnetic contribution for low molecular weight cases. For large molecular weights, the diamagnetic contribution needs to be estimated by means of complex experimental setups based on the contribution of different chemical groups. Once the overall χ^D contribution is estimated, the value of χ can be corrected to extract χ^P

The appearance of paramagnetic susceptibility, however, is due to the existence of unpaired electrons in matter, and if these exist, always overcome χ^D. From a microscopic point of view, it is more appealing because its study offers a manner to extract information about the nature of the electronic structure. From now on, magnetic susceptibly χ stands for paramagnetic susceptibility χ^P. Next section describes a theoretical model accounting for the behaviour of a system under the influence of an external magnetic field, for the description of the different contributions to magnetic susceptibility.

1.2.3. Van Vleck Formula.

As previously mentioned, knowledge of the expression of the magnetization allows to access the magnetic susceptibility, for given conditions of temperature and applied field. However, eqn (5) is too difficult to apply directly in its general form due to the $E_n(\vec{H})$. As a strategy, Van Vleck proposed a simplification based on two approximations:[14]

- The energies E_n are expanded as increasing powers of applied field $\vec{H}$ as

$$E_n(\vec{H}) = E_n^{(0)} + E_n^{(1)}\vec{H} + E_n^{(2)}\vec{H} + \cdots \tag{12}$$

where $E_n^{(0)}$ is the energy of level n in the absence of an applied field. The contributions $E_n^{(1)}$ and $E_n^{(2)}$ are the so called first- and second-order Zeeman coefficients. The contribution to the magnetization of each microscopic state is given by

$$\vec{M}_n = -E_n^{(1)} - 2E_n^{(2)}\vec{H} + \cdots \tag{13}$$

- The applied field $\vec{H}$ is assumed to be not too large and the temperature T not too small, so $\vec{H}/kT \ll 1$. Thus, the exponent in eqn (5) may be written as

$$e^{-E_n/kT} \approx e^{-E_n^{(0)}/kT}\left(1 - \frac{E_n^{(1)}\vec{H}}{kT}\right) \tag{14}$$

Considering these simplifications, and keeping in mind that in zero field the magnetization vanishes $\sum_n E_n^{(1)} e^{\left(-E_n^{(0)}/kT\right)} = 0$, the resulting expression for the magnetization is

$$\vec{M} = \frac{N\vec{H}\sum_n\left(E_n^{(1)2}/kT - 2E_n^{(2)}\right)e^{\left(-E_n^{(0)}/kT\right)}}{e^{\left(-E_n^{(0)}/kT\right)}} \tag{15}$$

which, after derivation with respect the external field $\vec{H}$ the Van Vleck formula for molar magnetic susceptibility is obtained

$$\chi = \frac{N\sum_n\left(E_n^{(1)2}/kT - 2E_n^{(2)}\right)e^{\left(-E_n^{(0)}/kT\right)}}{e^{\left(-E_n^{(0)}/kT\right)}} \tag{16}$$

To apply this formula, at variance with eqn (5), it is only required to know $E_n^{(0)}$, $E_n^{(1)}$ and $E_n^{(2)}$ values. Theory ensures that if one knows all eigenvalues $E_n^{(0)}$ and eigenfunctions $|n\rangle$ of the Hamiltonian in zero-field, it is then possible to calculate $E_n^{(1)}$ and $E_n^{(2)}$ through perturbation theory as

$$E_n^{(1)} = \langle n|\mathbf{H}_{ZE}|n\rangle \tag{17}$$

$$E_n^{(2)} = \sum_{m \neq n} \frac{\langle n|\mathbf{H}_{ZE}|n\rangle^2}{\left(E_n^{(0)} - E_m^{(0)}\right)} \tag{18}$$

where $\mathbf{H}_{ZE}$ is the Zeeman operator, accounting for the interaction between the magnetic field and the electronic angular momenta, and is expressed as

$$\mathbf{H}_{ZE} = \beta \sum_i (\mathbf{I}_i + g_e \mathbf{s}_i) H \tag{19}$$

where $\mathbf{I}_i$ and $\mathbf{s}_i$ are the orbital angular and spin momentum of electron i, repectively. β is the Bohr magneton and g_e is the gyromagnetic factor of the free electron. It is worth pointing out again that Van Vleck formula is only applicable for magnetic field ranges in which a linear dependence of $\vec{M}$ *vs* $\vec{H}$ is ensured.

1.2.4. Curie and Curie-Weiss Law.

Before the introduction of quantum mechanics, Curie proposed in 1914 a phenomenological expression relating the molar magnetic susceptibility to the temperature. It is characterized by a horizontal straight line for the χT *vs* T plots. Keeping in mind the previous discussion, this particular behaviour can be understood as an expression of certain characteristics in a given set of experimental conditions.

Consider the simplest example in molecular magnetism, which is an isolated magnetic centre with a $^{2S+1}\Gamma$ ground state displaying no first-order angular momentum and a large energetic separation from any excited state, so coupling with excited states can be neglected. Assume that the $^{2S+1}\Gamma$ energy is the origin. The application of an external field $\vec{H}$ splits the $2S + 1$ sublevels, according to Zeeman as

$$E_n = M_S g \beta H \tag{20}$$

M_S varies from $-S$ to $+S$. g is isotropic and takes the value of an independent electron $g_e = 2.0023$ due to the large energetic gap with any excited state. Thus, provided that H/kT is small, which is precisely the condition for Curie law to hold, one can use Van Vleck formula, obtaining the expression for Curie Law

$$\chi = \frac{Ng^2\beta^2 S(S+1)}{3k} \cdot \frac{1}{T} = \frac{C}{T} \tag{21}$$

Naturally, this is a limiting case but it is useful for explanatory purposes. The majority of situations found experimentally correspond to more complex cases, where the ground state is not so well isolated from the excited states, and a diversity of couplings occur either due to crystal field effects, zero-field splitting or interaction of magnetic centres. In these situations, the dependence of χT *vs* T plots is more complicated, but arises from different considerations on the exposed arguments.

So far, it has been assumed that the macroscopic magnetic response arises solely from isolated centres with unpaired electrons where no first-order orbital momentum occurs. A step further towards the description of magnetic properties concerns considering interaction among the different magnetic centres, which in the case of being strong enough, might result in a macroscopic magnetic ordering over a range of temperature. From a theoretical perspective, it is relatively easy to modify Curie law to account for weak intermolecular interactions, by introducing a perturbation to the Zeeman term. Thus, the resulting Hamiltonian takes the form

$$\mathbf{H} = g\beta S_z H - zJ\langle S_z\rangle \mathbf{S}_z \tag{22}$$

where the $\langle S_z\rangle$ is the mean value of the $\mathbf{S}_z$ component of the spin operator. J is the exchange coupling constant between two nearest neighbouring centres, and z the number of those nearest neighbours. In Chapter 3 the J value receives large attention, and here it will be enough to say that positive values are associated with a ferromagnetic interaction of the spins (parallel alignment is more stable) whereas negative values correspond to antiferromagnetic interactions (antiparallel alignment is more stable). The inclusion of this perturbation term allows rewriting the molar magnetic susceptibility, which under the same assumptions as in Curie expression, writes

$$\chi = \frac{Ng^2\beta^2 S(S+1)}{3kT - zJS(S+1)} = \frac{C}{T - \theta} \tag{23}$$

with $\theta = JS(S+1)/3k$ is the Weiss constant. A system obeying Curie-Weiss law gives a straight line with slope C^{-1} when plotting $\chi^{-1} = f(T)$. Note that such plot yields both the sign and value of θ. Weiss interpreted the behaviour of ferromagnets as arising from an averaged interaction of localized non-interacting spin centres, under the influence of a molecular field. This model applies for $T \gg T_C$, and describes relatively well ferromagnetic compounds. T_C is the temperature at which ferromagnetic materials lose their permanent magnetic properties, to be replaced by induced magnetism. On the other hand, the description of antiferrro and ferrimagnetism based on a local molecular field was provided by Néel.[15] As compared to the Curie temperature, Néel temperature T_N is the temperature above which an antiferromagnetic material behaves as a paramagnet, since the thermal energy provides enough energy to suppress the macroscopic magnetic ordering within the material. The applicability of this model is also restricted to $T \gg T_N$. These models fail to describe magnetic susceptibility in regions where $T < T_C$ or T_N since in these situations the magnetic centres cannot be considered independent anymore and an explicit interaction among the centres need to be considered. This is because the magnitude of the interaction and the crystal structure define the magnetic topology, which in turn defines the magnetic behaviour of the system. When these interactions were modelled by spin model Hamiltonians, such as Heisenberg or Ising the energy expressions included in eqn (16) started to successfully describe magnetic susceptibilities of simple single crystals such as $CuCl_2·H_2O$.[16]

Figure 1 c) presents two cases of systems following the Curie-Weiss law, presenting alternatively antiferromagnetic ($\theta < 0$) and ferromagnetic interaction ($\theta > 0$). As illustrative examples, some magnetic orderings arising from these types of interactions in one and two dimensions are presented in Figure 1 a) and b). In these representations, the circles represent spin bearing units, which can range from single ions to large molecular entities and the dashed lines are associated to the nature of the coupling among them, i.e. either through-space or through-bond. Note that such coupling is crucial for defining the sign and strength of the magnetic interaction and the impact that structural features might have in both the building blocks and the resulting extended system. From now till the end of the chapter, the focus will be on compounds where the spin bearing centre is purely organic-based, showing both through-space and through-bond interactions, as exemplified in the forthcoming section where several reported organic magnetic systems are discussed. Yet, whichever the through-space or

through-bond coupling, it is key to ensure that the unpaired electrons remain coupled, and in the best of the cases, ferromagnetically coupled in a wide range of temperature. In that sense, one of the aims of this thesis is to show that the most promising approach relies on the use of π–conjugated polyradicals interacting through-bond. The coupling unit facilitating the through-bond path is then critical, and appropriate conditions must be fulfilled. These particularities are the structural arguments along this thesis, and are extensively treated in Chapter 4.
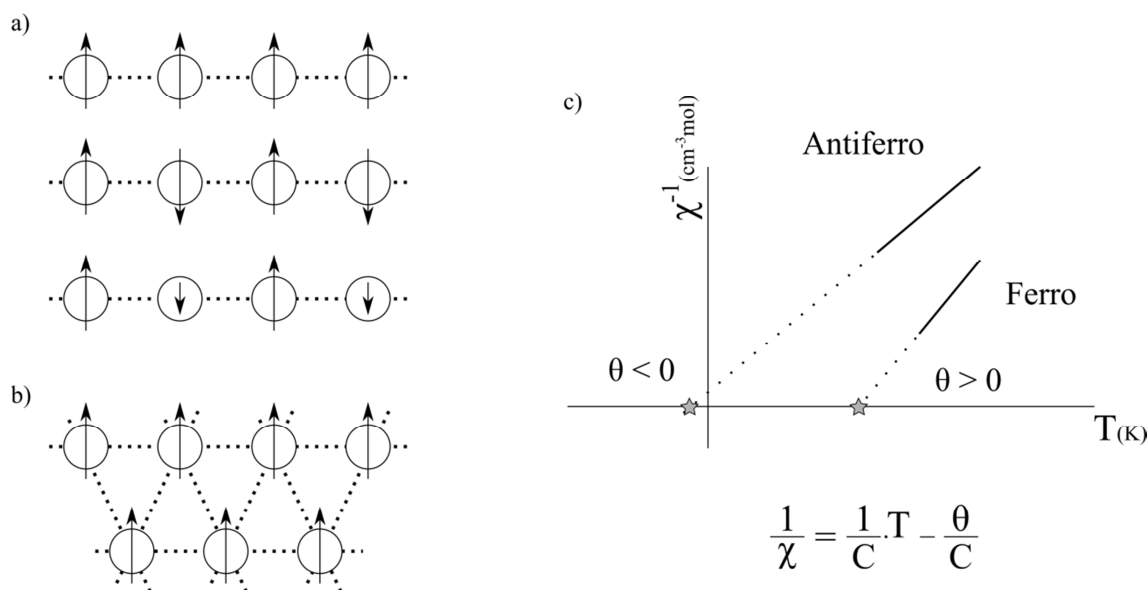
Figure 1. Schematic representation of different magnetic orders in a) collinear chains showing ferromagnetic, antiferromagnetic and ferrimagnetic order. b) Two-dimensional lattice showing ferromagnetic order. Dashed lines indicate that the interaction might transmit either through-space or through-bond. c) is a χ^{-1} *vs T* plot of two assemblies of molecules obeying Curie-Weiss law, with different type of interaction.

Now that the underlying common features for magnetic properties to appear in all molecules discussed throughout the thesis have been presented, next section provides a brief summary of how these magnetic properties manifest in organic compounds.

1.3. Molecular Magnetism.

Historically, magnetism has been devoted to inorganic compounds, mostly ionic solids with paramagnetic metallic centres (Fe, Co, Ni, Cu, Mn), responsible for their macroscopic magnetic properties. However, in the past decades, the field of magnetism has spread towards molecule-based approaches, getting to cover diverse areas such as

organometallic compounds or purely organic radical systems. The variety of systems is boosted by the possibilities offered by synthetic chemistry.[17,18]

The principal goal of this section is to present the main families of different organic radicals showing magnetic interaction (section 3.2), and on the basis of promoting robust ferromagnetism, the arguments for choosing one family over the others are discussed. This family is through-bond interacting odd alternant π–conjugated hydrocarbons, which are extensively treated in chapter 4 and appear as the best candidates for achieving the desired magnetic properties. However, for completeness, a brief discussion on metal-based compounds, including ionic solids and organometallic systems is also presented in this section. The comparison between the units bearing the unpaired electrons, i.e. organic molecules or metal-based complexes, allows introducing a crucial aspect that contributes to define how robust the magnetic interactions of the system are: the structural flexibility. It is reasonable to think that the magnetic interaction among spin-bearing centres depends on the relative arrangement of the units, which is essentially different for purely organic- and metal-based systems.

A feature that structures the forthcoming discussion is the nature of the bond between magnetic units, which in turn defines the through-space or through-bond character of the magnetic interaction. Thus, if the bond is ionic, the force acting between units is electrostatic (strong) and very isotropic, as is the case in ionic solids. Covalent bonds, which define the molecular skeleton, are strong and very directional. The bond between the metal and the ligand in coordination compounds is weaker than the covalent bond, but also directional. Finally, dispersion interactions are the weakest of all mentioned forces, and are crucial for keeping together the crystal structure. In coordination compounds covalent bonds define the ligands and coordination forces link the metal atoms to the ligands. Depending on the nature of the ligand, there might be large dispersion forces resulting in an ordered crystal of coordination units. In purely organic compounds, covalent and dispersive forces define the spatial arrangement of the molecular units.

1.3.1.   Metal-Based Compounds.
1.3.1.1. Ionic Solids.

The origin of magnetic properties in metal-based compounds is associated with the appearance of unpaired electrons over the metallic centres. A limiting case in terms of

structural flexibility is the family of ionic solids. Despite not being representative of molecule-based approaches, they serve as a good illustration of a system where magnetic properties occur in a fixed crystalline structure. Roughly speaking, the unpaired electrons responsible for the macroscopic magnetic properties appear from a variety of metallic ions tightly packed in a solid lattice, experiencing an orbital splitting induced by the ligand field. Structural freedom in these compounds is rather limited, as a consequence of the electrostatic potential that holds together the atoms through ionic bonds. This results in well-defined magnetic properties that do not vary over a wide range of temperature.

1.3.1.2. Coordination Compounds.

Coordination compounds represent a molecule-based approach, where an enormous amount of work has been reported in the last decades.[17–19] In these compounds, magnetic properties arise mostly from the molecular unit, although interaction among different molecular units is also important. The spin moments appear from d and/or f orbitals, where other kinds of perturbations, such as zero-field splitting or first-order angular momentum become important. In this situation, the magnetic interaction is rationalized in terms of superexchange.[4,20] Interestingly, the magnetic properties are no longer due to single atoms packed in a solid lattice where electrostatic forces spread equally in three directions of space, but rather from molecules that are forming a crystal. The forces that keep together the molecular entity (covalent bonds) are different in nature from the forces constituting the order in the solid (long-range interactions). The role of the bridging ligand is also paramount, presenting a large variability and introducing different distances and π–conjugations among the metallic centres. In general, the ligands are closed-shell molecules, although currently stable organic radicals, like carbenes, are also used.

The study of magnetic properties in coordination compounds has been mainly related to the study of Single Molecule Magnets (SMMs)[21,22] and Single Ion Magnets (SIMs).[23] The main idea is that magnetic properties arise from the individual molecular unit, rather than from collective phenomena. SMMs contain several metallic centres per molecular unit, while SIMs only presents one metallic centre per molecular unit. The most characteristic experimental signature of these compounds is a dependence of the imaginary (out-of-phase) contribution to the magnetic susceptibility on the angular

frequency with which the magnetic field oscillates in alternating current (ac) susceptibility measurements.[24] The main interest lies in the potential application for information storage, due to the existence of an energetic barrier to the re-orientation of the molecule's magnetisation. Thus, a particular orientation of the magnetisation can be associated to a state. The origin of the barrier resides in the magnetic anisotropy, which relates to the zero-field splitting (ZFS). ZFS may arise in molecules with $S > 1/2$ ground state and symmetry lower than the cubic. The Hamiltonian associated with ZFS can be expressed as

$$\hat{H} = D\left[\hat{S}_z^2 - S(S + 1)/3\right] + E\left(\hat{S}_x^2 - \hat{S}_y^2\right) \tag{24}$$

where $D = D_{zz} - \frac{1}{2}\left(D_{xx} + D_{yy}\right)$ and $E = \frac{1}{2}\left(D_{xx} - D_{yy}\right)$ are the axial and rhombic ZFS parameter, respectively, and $\hat{S}$ is the spin projection along a given axis. The effect of ZFS in the electronic levels of a molecule with a S ground state, when no external magnetic field is applied is depicted in Figure 2.
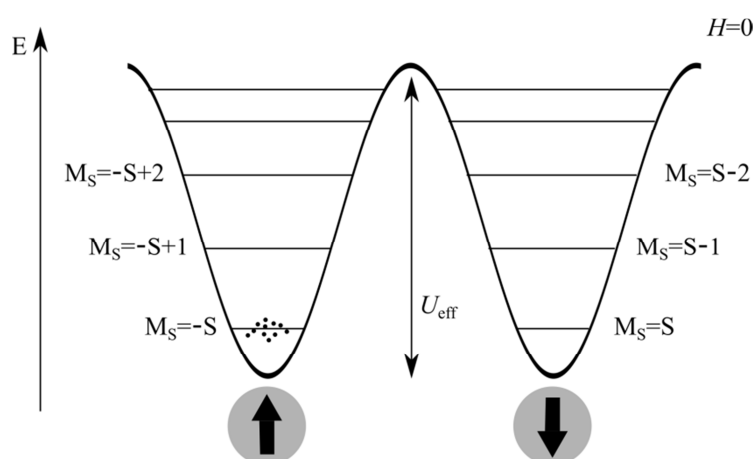
Figure 2. Representation of the double-well generated as a consequence of the zero-field splitting in a molecule with *S* multiplicity, in the absence of an applied external magnetic field.

The energetic barrier that the molecule would have to overcome to reverse its magnetisation can be expressed as[24]

$$U_{\text{eff}} = |D| \cdot S^2 \tag{25}$$

In view of eqn (25), synthetic routes have aimed at obtaining each time larger D and S values.[24–26] However, Neese and Pantazis[27] pointed out the relationship between the two D and S parameters, which prevents using polynuclear compounds as an effective strategy to increase U_{eff}. Instead, they propose using mononuclear species with a large

number of centres. Other theoretical investigations, as for instance the work by Maurice, de Graaf and Guihéry[28] have brought very important insights into the theoretical determination of anisotropic magnetic parameters that might help the experimentalist in the design of new SMMs. Finally, a recent review by Malrieu *et al.*[29] constitutes an excellent source for understanding the theoretical description of magnetic interactions in a vast collection of highly-correlated materials.

In order to close this section, it is worth mentioning that the success in describing magnetic properties in this sort of coordination compounds lies in the capacity for establishing magneto-structural relationships. The forthcoming section deals with compounds with an extra difficulty arising from a more delocalized character of the unpaired electrons over a π−conjugated system and an inherent structural flexibility that needs to be addressed for the correct description of magnetic properties.

1.3.2. Organic Radicals.

Magnetism in purely organic compounds represents a totally different approach. For these systems, all phenomena arise from *s* and *p* orbitals, and the absence of heavy atoms implies that significant spin-orbit coupling is not expected. Moreover, the spin density is delocalized to a larger extent, generally over a set of atoms participating in a π−conjugated system, as compared to the well-defined metallic centres in ionic solids or coordination compounds. The most commonly encountered systems of this kind can be divided, in a first approximation, depending on whether the interaction between the magnetic centres is through-space[9,10,30,31] (e.g. nitronyl nitroxides and charge transfer compounds) or through-bond[32–34] (e.g. π−conjugated molecules).

There is an important difference derived from these different mechanisms: in through-space interacting radicals, the radical centres are found in each of the molecular entities forming a crystal, which is held together by means of long-range interactions. The critical parameter affecting the magnetic properties is the distance between those units, which is largely dependent on the temperature. However, in through-bond interacting radicals, the magnetic interaction occurs within a covalently bonded molecular unit with a variable number of radical centres, which might be structurally flexible. This introduces some implicit difficulties that cannot be overlooked, as for instance low energetic cost molecular deformations, which affect the interaction path in a much more complex way than in molecular crystals. Ultimately, structural flexibility

might be responsible for the appearance of secondary structures, which is a degree of order that needs to be addressed for a proper description of the possible occurring magnetic interactions.

1.3.2.1. Remarks on the Stability of Organic Radical Centres.

Apart from purely fundamental interest, organic magnetism presents some attractive advantages, such as the capacity, by means of carbon chemistry, to tune the desired shapes and sizes of the final products, as an effective manner to modulate the macroscopic properties, together with the low cost of the raw materials. But, for any interaction to occur, the existence of unpaired electrons is required. In metal-based compounds, the unpaired electrons arise from the valence of a stable metallic centre in a given complex. However, in purely organic molecules, the situation is not as obvious. In fact the term *free radical* has a connotation of reactive intermediate species in chemical reactions. It is then appropriate to address few words on how to increase the stability of the unpaired electrons as a previous requirement for studying their magnetic interaction.

There are two main strategies to stabilize unpaired electrons in organic molecules. The first one relies on a steric protection of the radical centre, known as kinetic stabilization. Its representative example is the increase in stability when going from the Gomberg radical[35] to its perchlorinated derivative, the PTM.[36] The second strategy is based on the introduction of a π–conjugated system that enables an effective delocalization of the unpaired electron, promoting participation on several resonant forms, which results in a net energetic stabilization.[37–40] A representative example of this kind are molecules with a strong electronic acceptor or donor character enabling redox processes, which result in charged radicals, as for instance the tetracyanoethenide (TCNE)[41] and tetracyanoquinodimethane (TCNQ).[42] Here, the unpaired electron appears as a consequence of a charge-transfer process. However, the focus of this thesis is on neutral organic radicals presenting an even number of electrons. The reasons behind why these systems present unpaired electrons are given in chapter 4.

Overall, the stabilization of unpaired electrons in organic compounds is complicated because it involves a subtle interplay between stability and functionality. If the property of interest is magnetism, as it is the case in this thesis, the spins need to be exposed in a way that they can interact. However, too much of exposure also means possibilities of dimerization and consequent loss of any magnetic property. Similarly,

the incorporation of bulky substituents to prevent dimerization might turn into an effective isolation of the spins, suppressing any magnetic interaction.

1.3.2.2. Through-Space *vs* Through-Bond Interaction.

Once the stability of the unpaired electrons in ensured, the main goal is to promote a robust ferromagnetic ordering over a wide range of temperatures, aiming at ultimately achieving a device with controllable properties. As previously stated, magnetism in purely organic compounds occurs as a consequence of unpaired electrons interacting either through-space[30,31] or through-bond.[32–34]

In order for the through-bond compounds to show ferromagnetic interaction between the radical centres, one has to ensure that the orbitals associated with the unpaired electrons are orthogonal and share large regions of space. Topological arguments (as explained in chapter 4) are very useful to define the specific molecular architectures that promote such characteristics. Particularly, odd alternant polycyclic hydrocarbons with non-disjoint singly occupied molecular orbitals (SOMOs) are the most widely used structures. An example of this kind of molecules, relevant because of its ubiquity in this thesis, is the 1,3-phenylene unit, which is used as a strong ferromagnetic coupler between two unpaired electrons.[32,33,43] For through-space interacting organic radicals compounds to show ferromagnetic interaction, the mechanism is not so clear, and the most widely used model is the so-called McConnell mechanism, explained in the next section. By comparing through-space and through-bond scenarios and introducing the comparative advantages, as exemplified in a set of selected experimentally reported cases, it is intended to justify the choice of $\pi-$conjugated through-bond interacting systems as the most promising approach towards purely organic magnetic ordering. Additionally, this discussion allows putting in perspective the contribution to the literature found in chapter 4.

- The McConnell Mechanism.

Up to date, a grounded microscopic theoretical treatment able to correlate the intermolecular geometry of a pair of radicals with the resulting net magnetic response is still missing, presumably due to the complexity and diversity of molecular conformations in organic radicals. Despite that, this section presents the most widely used mechanism to explain the occurrence of magnetic interaction in through-space

interacting compounds. i.e. the McConnell mechanism,[44] given that through-bond interacting mechanisms are treated in chapter 4. The present discussion on McConnell mechanism is reduced only to the most important conclusions. For an extended discussion on the foundations of the mechanism and application to real case examples, as nitronyl nitroxides, see chapter 1 and 3 of Miller and Drillon's books[9,10] respectively, and the references they include. Particularly enlightening are the theoretical works by Novoa *et al.* (chapter 3 in[10] and chapter 2 in[11]) on the validity of this mechanism. Here, only the most important conclusions are provided.
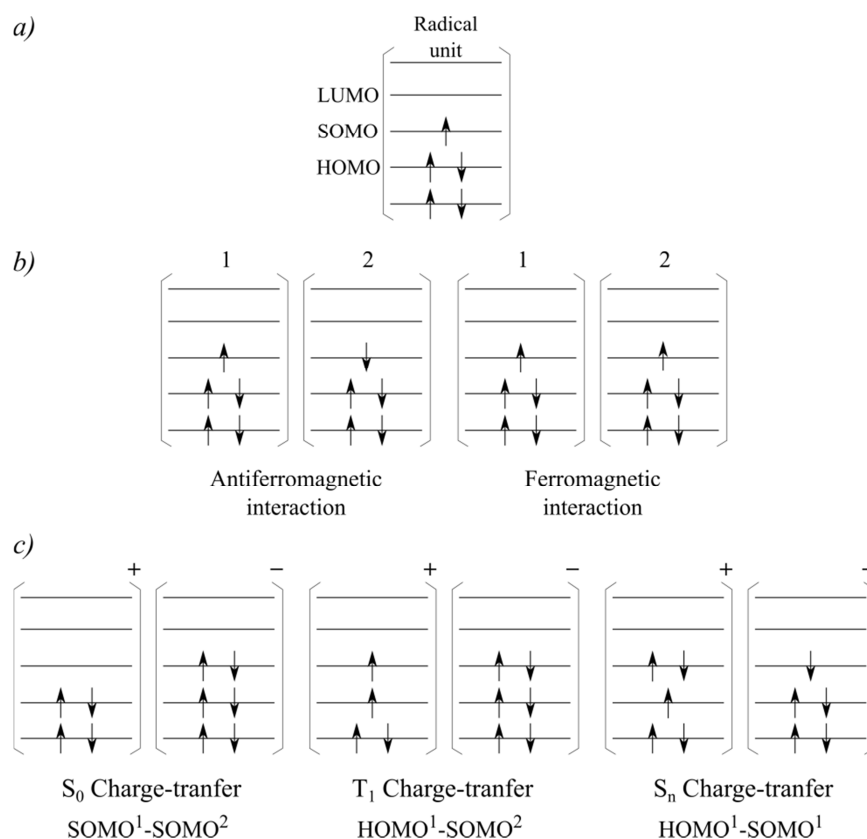
Figure 3. *a)* Depiction of a given radical unit with an unpaired electron in the singly occupied molecular orbital (SOMO). *b)* Possible magnetic states resulting from the interaction of two radical units. *c)* Some single excitations leading to different charge transfer states. HOMO and LUMO stand for highest occupied and lowest unoccupied molecular orbital, repectively.

Originally, McConnell made two proposals for explaining intermolecular magnetic interactions. The first one (mechanism I)[44] was prposed for hydrocarbon radicals units held together by $\pi-\pi$ interactions and relies on the sign of the atomic spin polarization between the atoms making the shortest contacts within the interacting molecules. If the packing of the crystals favours a π-orbital overlap between atoms with spin density of opposing sign via $\pi-$stacking, a ferromagnetic interaction is predicted. On the contrary,

if the overlap occurs among moieties with the same spin density sign, the interaction is said to be antiferromagnetic. The second mechanism (mechanism II)[45] implies charge-transfer between different molecular units displaying ground states of different spin multiplicities, which results in a stabilization of the triplet state.

Comparatively, mechanism II has deserved much less attention since Kollmar and Kahn[46] proved it wrong for bulk ferromagnet $Fe(III)(C_5Me_5)_2^+$ $(TCNE)^{-}$. They showed that higher-order charge-transfer mixing terms result in a stabilization of the singlet state, rather than the triplet, and that spin polarization effects need to be included.[47] As an illustration, the low-order mixings that can be expected in a charge-transfer compound are depicted in Figure 3. Note that the introduced charge-transfer states arise only from single-excitations from the highest occupied molecular orbital (HOMO) and SOMO orbitals only, but in organic systems with a large π conjugation this restriction does not necessarily hold and one could think of excitations involving other doubly occupied and virtual orbitals. The stabilization of ferromagnetic interaction implies that T_1 states must be close in energy from the ground state, which requires a strong overlap between the $HOMO^1$-$SOMO^2$. However, this also decreases the excitation energy to access various singlet excited states, which promote antiferromagnetism. A fine tune of the molecular orbital levels allows enhancing one state at the expense of the other, but ultimately magnetic interaction is subject to the crystal packing, which in turn depends on external factors such as temperature or pressure. Thus, it appears that a reliable control of the parameters affecting magnetism in these charge-transfer compounds is hard to achieve.

On the other hand, the experimental validation of mechanism I was provided by Izuoka et al.[48,49] in a series of [2.2]cyclophanes presenting two carbene (carbon atom with two unpaired electrons in two orthogonal orbitals) in *ortho-*, *meta-* and *para-* positions, as indicated in Scheme 1. According to McConnell mechanism I,[44] only in the meta compound the overlap occurs between spin densities of the same sign, promoting antiferromagnetism. Experimentally, the EPR signal associated with the *ortho* and *para* diphenylcarbenes is indeed associated to a quintet ground state (the four unpaired electrons interacting ferromagnetically), whereas such signal was not present in the
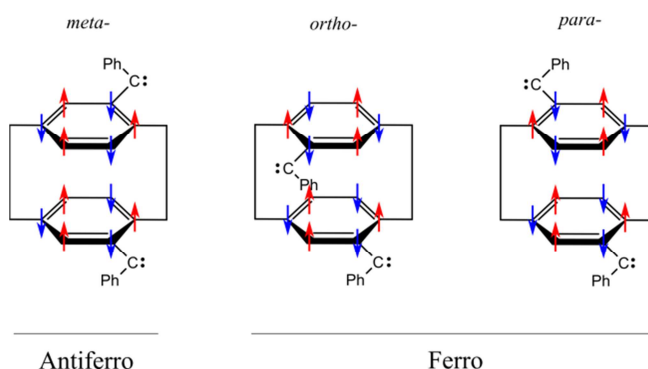
Scheme 1. Representation of the meta- ortho- and para-cyclophanes and the associated superposition of spin densities, resulting either in ferro- or antiferromagnetic interactions.

meta case. Despite this success, there are cases in which McConnell mechanism does not successfully account for the experimentally available data (for a detailed discussion see chapter 3 in[10]). The reason for that has been assigned to the specific molecular requirements that must be fulfilled for the assumptions of the model to hold. Specifically, this mechanism is valid if

$$\rho_i^A \rho_j^B \equiv P_{ij}^S - P_{ij}^T \qquad (26)$$

where ρ_i^A is the atomic spin population of atom i in frangent A and P_{ij}^S (P_{ij}^T) is the exchange density matrix of the singlet (triplet). This is true in cases of high symmetry, as the mentioned cyclophanes, but it is not for more general cases, like nitronyl nitroxides crystals.[50] Nevertheless, McConnell I mechanism remains to be the most widely used model to explain magnetic behaviour in through-space interacting radicals.

- Radicals with Unpaired Electron on:

This section introduces a selection of the most relevant examples reported so far in organic magnetism, arising from the interactions between stable radicals.[51] The underlying reasoning in the discussion aims at qualitatively compare the spatial arrangement of the radical centres that resuls from either a through-space or through-bond interaction, and how this can affect the magnetic coupling, mostly through structural parameters. On the basis of promoting robust ferromagnetism in purely organic compounds, this comparison allows choosing one set of molecules over the others.

Figure 4 presents some representative organic molecules in which magnetism has been studied. They are the basic units bearing the magnetic moments, which, when

extended and arranged in space, give rise to the magnetic properties. In Figure 4 the molecules are classified as follows: Each row corresponds to the different atoms bearing the unpaired electron, including carbon, nitrogen, oxygen and sulfur-containing heterocycles, classified in *a), b), c)* and *d)* respectively. Each column represents how the unpaired electrons interact. The leftmost column stands for through-space interacting compounds, resulting in a molecular crystal packing when extended in space. The crystal packing is crucial for the observed magnetic properties, since it determines the relative position of the molecular units and consequently the SOMO-SOMO overlap. The rightmost column stands for through-bond interacting species, which generally results in disordered oligomeric and conjugated polymeric structures when going to extended systems. Here, the magnetic properties arise from intramolecular interactions between the unpaired electrons along the covalent π-conjugated backbone of the molecule. As mentioned, to promote ferromagnetic interaction among the unpaired electrons, a widely used scheme consists of using 1,3-phenylene as coupling units, as evidenced by the abundance of reported cases.[32,33] Finally, the column in the middle corresponds to the so-called radical polymers, which are polymers bearing organic robust radicals as pendant groups per repeating unit. When polymerized, this strategy results in one dimensional-like (1D) structures, referred to the σ-skeleton. In a sense, this approach represents an intermediate between the two other cases, since the interaction between the radical centres is mostly through-space, dictated by how the pendant radicals are distributed with respect to each other, but also shares a characteristic of through-bond interacting compounds since the interaction happens within the same molecular unit. For radical polymers there is an important correlation between the adopted conformation and the associated magnetic properties.

Interestingly, the spatial distribution of the unpaired electrons depends on which of the three strategies is adopted, which in turn results in a total different response of magnetic properties to thermally induced vibrations or chemical and structural defects in the compound. In fact, the inherent structural flexibility of the constituent building blocks in purely organic magnetic compounds is the main feature affecting the resulting properties, which expresses differently in compounds where the interaction is through-space or through-bond. Figure 5 is an oversimplified illustration to exemplify such problematic for specific cases in through-space interacting compounds, radical polymers and through-bond interacting compounds, in *a), b)* and *c)* respectively.
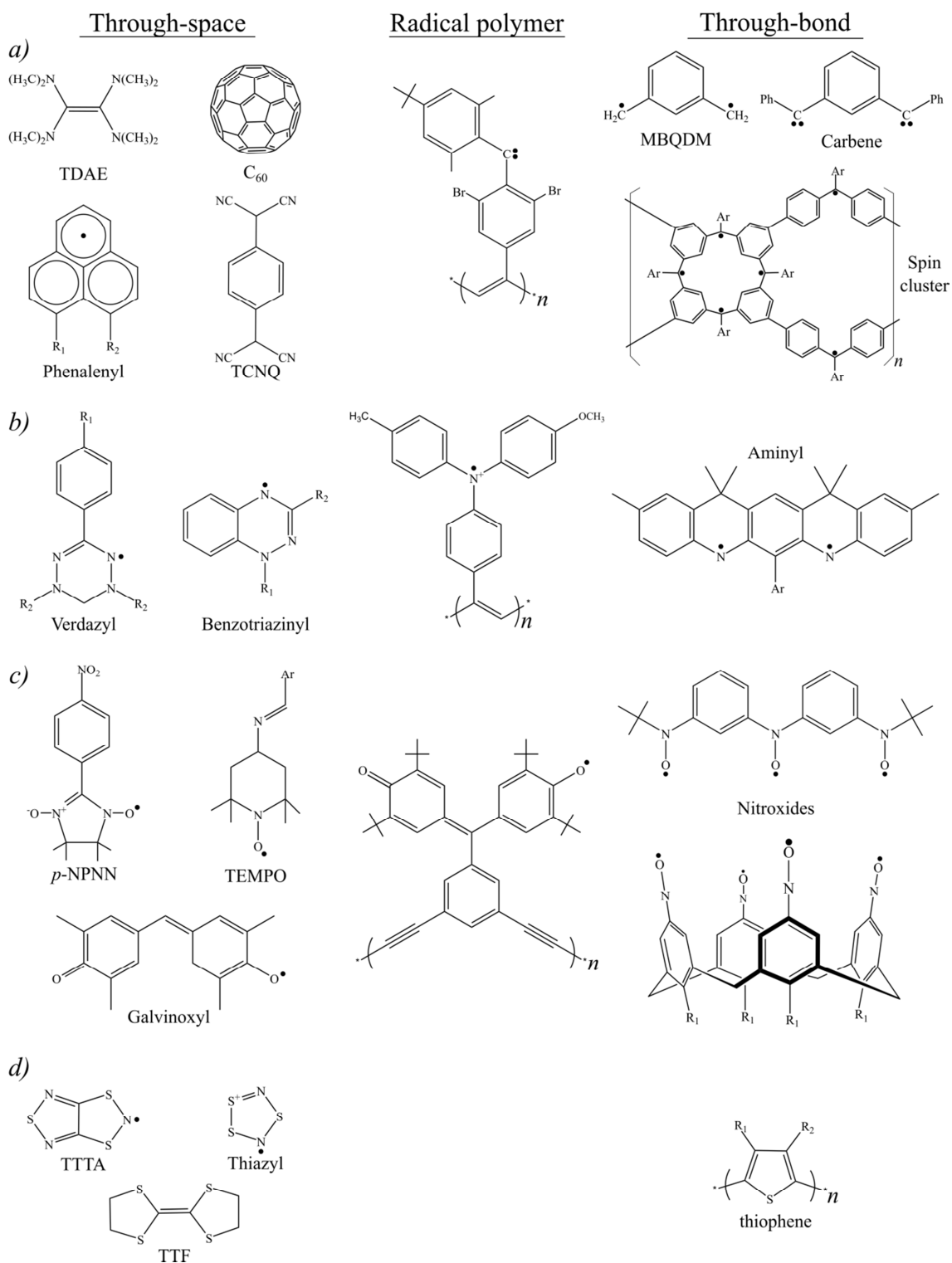
Figure 4. Molecular structure of some experimentally reported organic radical compounds. Each row corresponds to the different atom bearing the unpaired electron. *a), b)* and *c)* represent carbon, nitrogen, and oxygen respectively. *d)* present sulfur-based compounds. Each column represents the type of interaction between the unpaired electrons.
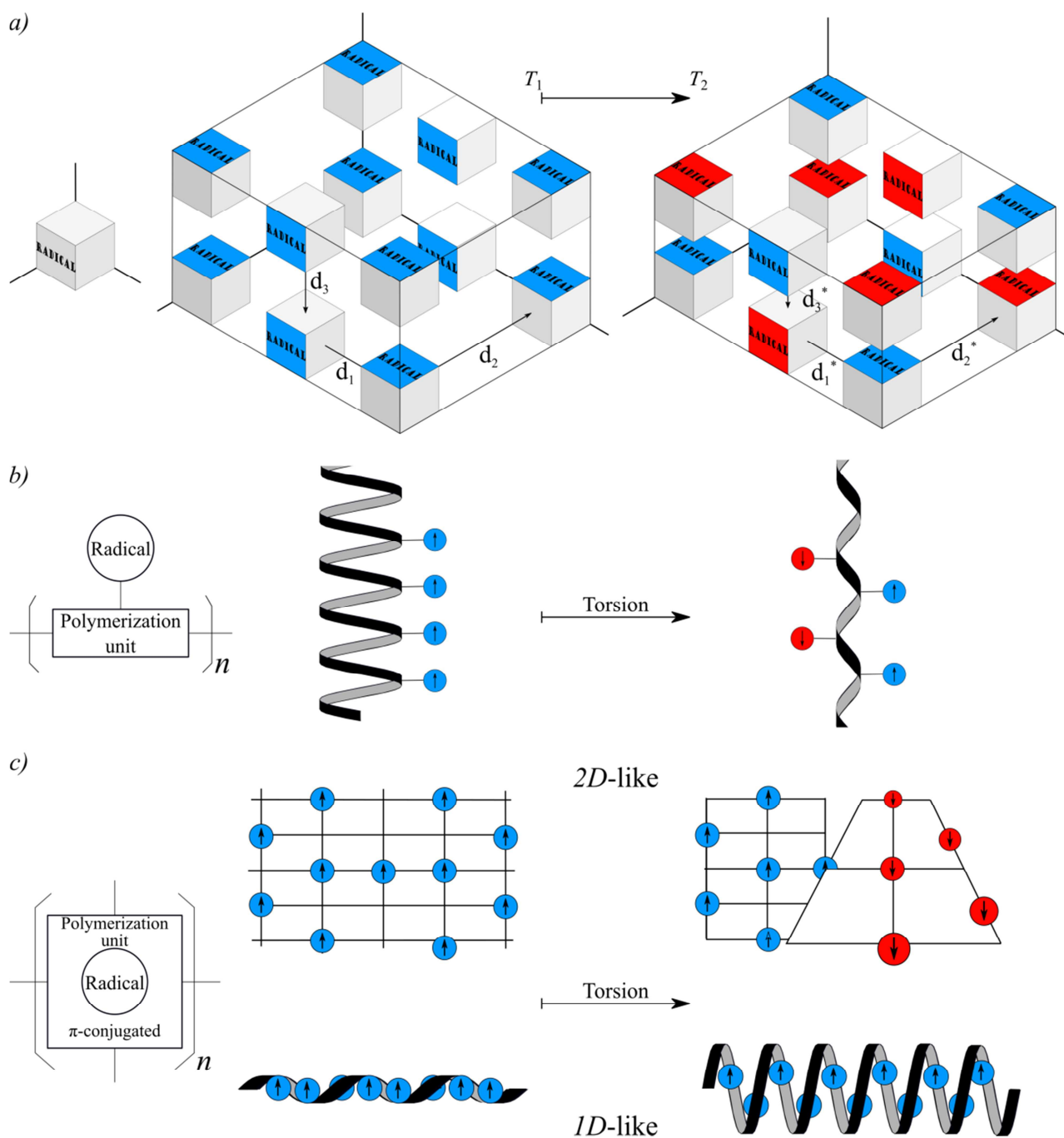
Figure 5. *(From left to right).* Schematic representation of the radical building block, possible resulting arrangements in space and impact of external perturbations on the magnetic interactions. *a)* discrete molecular radicals leading to a molecular crystal. It corresponds to the *Through-space column* in Figure 4 *b)* radical polymers leading to *1D*-like structures. This corresponds to the *Radical polymer* column in Figure 4*c)* π−conjugated polyradicals extended in either *2D*- or *1D*-fashion. This corresponds to the *Through-bond* column in Figure 4. Blue (red) circles indicate spin-up (spin-down) spins.

For instance, consider Figure 5 *a)*. It represents a given molecular crystal, in which each molecule bears an unpaired electron, as for instance nitronyl nitroxides does. In this sort of compounds, magnetic properties arise from the through-space interaction in the crystal and a change in the distance relating the magnetic units affects entirely the magnetic interaction. As a consequence, the obtained Curie or Néel temperature (T_C, T_N) are often very low. Figure 5 *b)* introduces the idea of radical polymers, and exemplifies the dependence of the magnetic interaction on the adopted conformation. This is an early indication about the importance that secondary structure might have in organic magnetism. Finally, Figure 5 *c)* exemplifies a strategy in which the radical centres belong to the covalent π-conjugated backbone of a polymeric unit, resulting in a through-bond mediated interaction of the unpaired electrons. The conjugated polymeric unit offers the possibility of achieving extended polyradicals systems in one and two dimensions.

The above qualitative discussion was introduced as guidance for the next sections, in which some of the reported organic examples showing magnetic properties are presented. The classification is based on the nature of the radical-bearing centre, and the order of the discussion follows the reasoning in Figure 4. Since the extent of the section might make it hard to follow, it may be useful to keep in mind the correspondence between the columns of Figure 4 and rows in Figure 5, in order to facilitate the line of thought. Therefore, when, for instance, discussing the crystal structure of *p*-NPNN (Figure 4, through-space column, *c)*) and how the magnetic interaction are affected by the distances between the molecular units, one can use the schematic representation in Figure 5 *a)* as example. In the same manner, when the discussion concerns radical polymers and how the adopted conformation determines the interaction between the magnetic centres, a pictorial representation is shown by Figure 5 *b)*.

Finally, the common goal for all discussed strategies (through-space, through-bond, and radical polymer) is the achievement of purely organic systems that are stable at ambient conditions, with many magnetic centres strongly coupled in order to present magnetic ordering at room temperature (i.e. polyradicals with large *S* values).

a)   Radicals with Unpaired Electrons on Carbon Atoms.

The molecular structures discussed in this section are depicted in Figure 4 *a)*. The amount of works concerning purely carbon-bearing radicals interacting through-space is

limited when compared to other organic radical-bearing atoms, as for instance nitrogen and oxygen. The reason behind it might be that for obtaining a molecular crystal it is necessary to have large dipole moments to promote interaction between the units, which is not present in purely hydrocarbon compounds. Related examples are found in buckminsterfullerene C_{60} and derivatives, as reported in the seminal work by Allemand et al.[52] Here, a mixture of TDAE-C_{60} promoting acceptor-donor dyad resulted in ferromagnetism at 16 K. However, successive experiments demonstrated that the magnetic properties were dependent on the sample preparation.[30] An extensive review on this topic can be found in chapter four of the book.[9] Another type of carbon-based molecular radicals is based on π−conjugated hydrocarbons. Phenalenyl (Figure 4), an odd-alternant hydrocarbon resulting from the triangular fusion of three benzene rings, is a representative example of stable radicals.[51] It constitutes one of the most basic elements of graphene and it is consider as a case study of the so called *synthetic organic spin chemistry*.[53] In the crystalline phase, phenalenyl-derivatives form π−dimer units. The study of magnetic properties of π−dimer resulting from neutral tri-*t*-butyl substituted phenalenyl radical (TBPLY),[54] indicated a very strong antiferromagnetic interaction between the two unpaired electrons located in each of the π−dimer units ($2J/K_B > 2000$ K). Theoretical studies indicated that the origin of such interaction is due to a large singly occupied molecular orbital (SOMO-SOMO) overlap.[55] Similarly, spiro-biphenalenyl (SBP) boron radicals represents a family of phenalenyl-derivatives showing interesting magnetic and optical properties.[56] Of particular interest are ethyl- and butyl-SBPs, since they show a spin transition connecting a low-temperature diamagnetic phase and a high-temperature paramagnetic phase. Theoretical studies on the ethyl-SBP have disentangled the factors dominating the spin transition,[57] recognizing the fine interplay between SOMO−SOMO overlap, which stabilizes the singlet states of the π-dimers, and the electrostatic interactions between radicals, which stabilizes the triplet states. In line with TBPLY, ethyl- and butyl-SBPs dimers show a strong antiferromagnetic interaction between the unpaired electrons in the high-temperature phase.[57,58] As previously mentioned, another crucial factor that allows an improvement of the material's properties concerns the stability of the radical centres. The synthesis of remarkable stable phenalenyl-derivatives radicals has been reported.[59] This behaviour has been assigned to an electronic stabilization promoted by the introduction of heteroatoms. Additionally, the crystal structures of the parent cations

were also reported. Despite that, no magnetic interaction among the stable centres is mentioned in this work.[59] Taken together, it seems reasonable to conclude that phenalenyl-derivatives offer great opportunities for achieving functional organic materials, but robust ferromagnetism is not among them.

Attempts for achieving radical polymers where the robust pendant radical is carbon-based have also been reported. Especially relevant is the work by Itoh et al,[60] where a persistent triplet carbene is used as spin source. However, despite successful generation of the carbene centres by photolysis of the diazo precursors, the synthesized polycarbenes presented low multiplicities, which was ascribed to an intramolecular antiferromagnetic interaction among the carbene centres.

Finally, through-bond interacting radical compounds with a carbon as the radical-bearing centre represent the most important conceptual approach for this thesis. In fact, chapter 4 is entirely devoted to this class of molecules and for that reason here only the most relevant works are highlighted. It is reasonable to think that if the magnetic interaction is through-bond, the nature of the coupling unit plays a crucial role in defining the magnetic interaction. As a matter of fact, it is well accepted that *meta*-phenylene units promote ferromagnetic interactions; π–conjugation helps in the delocalization of the unpaired electrons increasing their interaction, and *1,3-* connection through a six-membered ring does not allow closed-shell resonant forms to pair the unpaired electrons. For that reason, most of the though-bond interacting compounds discussed in this section present this topology. This field of research has experienced two major contributions. One was introduced by Rajca[61] using spin clusters, as an effective manner to avoid the suppression of magnetic interaction between the unpaired electrons. Such interruption often appears due to the experimental route required to generate the radical centres (the carbanion method, involving the oxidation of polyether precursors, Figure 6) and to the inherent structural flexibility of the compounds, which might result in a complete disruption of the π–conjugated system (Figure 5 *c)* upper part). Following this approach, first magnetic ordering in a purely organic polymer was reported.[61] The other contribution was based on C_{60}, but it is not free of controversy. The first work setting the precedent on the field[62] was retracted five years later, because the samples were found to have iron.[63] Yet, independent research groups reported similar results[64,65] before the retraction was announced. Additionally, ferromagnetic properties were also found in polymerized states of C_{60} with different structural defects

and light-element content (O, B, N).[66] It is thought that the observed ferromagnetism arise as a combination of through-space and through-bond interactions between the C_{60} units, although a model accounting for their magnetic properties is still missing.
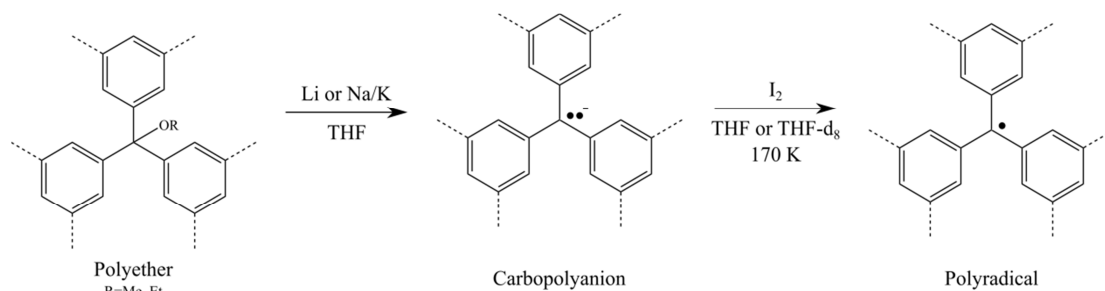
Figure 6. Carbanion method for the preparation of polyarylmethyl polyradicals.

b) Radicals with Unpaired Electrons on Nitrogen Atoms.

The molecular structures discussed in this section are in Figure 4 *b)*. As done for the carbon atom case, we first discuss examples in the leftmost column. Through-space interacting compounds displaying a nitrogen atom as radical-bearing centre have received large attention. Among them, verdazyl molecules and derivatives[67,68] constitute representative examples. They offer a large variability because there are several positions subject to chemical substitutions (R_1 and R_2 in Figure 4 *b)*). However, most of the reported examples show a very small and negative Weiss constant, indicating antiferromagnetic interaction. Other type of compounds belonging to this class is the benzotriazinyl family, which proved to be good candidates to promote ferromagnetic interactions even at room temperature.[69,70] The versatility introduced by the different substituents at several positions of the benzo rings has facilitated a large variability in the crystal packing and the subsequent magnetic properties associated. In fact, the benzotriazinyl derivative with R_1 = Phenyl and R_2 = CF_3 (see Figure 4 *b)*), shows a sharp spin transitions between low temperature diamagnetic and high temperature paramagnetic phases.[71] The origin of this phase transition has been computationally revealed,[72] which allowed the authors to propose, based on structural and electronic features, modifications on the molecule to increase and/or enable spin transitions in related compounds. These investigations point to benzotriazinyl as candidates for interesting switching materials, but in general, due to inherent dependence of magnetic interactions on the crystal packing, they are not good candidates to promote robust ferromagnetic properties in a material.

Within the radical polymer strategy, there are several reported examples based on different approaches. For instance, verdazyl has also been used as a robust pendant radical attached to a non-conjugated polymeric unit,[67] obtaining weak antiferromagnetic exchange couplings between the verdazyls. Alternatively, attempts using a sterically protected polyaminium salt (aminium is a cation formed protonation of an amine R_3NH^+) the pending from a polyacetylene as π–conjugated polymeric unit, as indicated in Figure 4, were pursued.[73] The choice of monosubstituted acetylene is important in order to promote stereoregular polyacetylene, aiming at obtaining optically active polymers, i.e. chiral and helical. This strategy proved successful for obtaining high-spin ground states at room temperature, as well as demonstrating the importance of secondary structure for defining the magnetic properties. Nevertheless, the maximum multiplicities obtained reached only 4 unpaired electrons, even if the spin concentration is almost one, interacting antiferromagnetically with a very small and negative Weiss constant.[73]

As far as the through-bond interacting species are concerned, the success is more evident. Verdazyl units have also been employed within this approach, linked to phenyl or thiophene rings mostly.[67] However, one cannot reach further than three verdazyl units linked together through a phenyl ring, and thus, it is a poor approach for extended polyradicals. Another strategy that allows a higher concentration of radical centres is based on ammonium radical cations, as reported in *meta-* and *para-* aniline cation radicals derivatives, which proved successful for coupling ferromagnetically three unpaired electrons.[74] However, there is strong evidence for discarding this route as an effective manner for achieving polyradicals systems.[75] An alternative approach relies on polyaniline (PANI) polymer, which is well-known for its conductive properties. Doping of the neutral polymer alters its electronic structure and affords the open-shell states. The protonated form of the polymer results in a metallic state with a temperature-independent magnetic susceptibility[76] and the introduction of tetracyanoquinodimethane (TCNQ, see Figure 4 *a)*) promotes charge-transfer states responsible for the appearance of the radical centres, which yield a room temperature magnetic order.[77] However, within this approach, it is very difficult to control structural parameters, and the disordered nature of the product prevents any magneto-structural relationship. There is recent evidence that neutral PANI (not doped) presents a helical-induced magnetization, although its value is extremely low.[78] This is an indication of the role that secondary

structure has in defining magnetic properties in these structurally flexible molecules. Following a different reasoning, Rajca *et al.*[79–82] have devoted a large amount of work to the synthesis, stabilization, isolation and characterization of the so-called family of aminyls, which stands for nitrogen-centred radicals. It is worth noting that in order to avoid disruption of magnetic interaction, the molecular design adopted imposes planarity of the π–conjugated system. Within this approach it has been possible to obtain a series of diradicals of increasing stability. Those include a molecule with a persistent triplet state showing a half-life of 30 minutes at −70ºC,[79] an aza-derivative of *m*-xylylene (MBQDM in Figure 4 *a)*) persistent in solution with a half-life of 10 minutes at room temperature and a triplet-singlet gap of 10 Kcal/mol,[80] and another room temperature persistent triplet radical that was isolated.[81] Additionally, and aiming at achieving high-spin ground state polyradicals, a room temperature persistent quintet ground state tetraradical was also synthesized and characterized.[82] Currently, large attention is being devoted to achieve aminyl polyradical polymers with very large magnetic moment.[43]

c) Radicals with Unpaired Electrons on Oxygen Atoms.

The molecular structures discussed in this section are in Figure 4 *c)*. Molecular crystals of oxygen-centred radicals are very abundant in the literature, and exemplify very well how, if the radical unit is stable but the crystal packing is not favourable to appropriate interactions, magnetic interactions might not occur, leading to paramagnetic systems with very low T_C. This generally manifests at different temperatures, as a consequence of a change in the crystal packing, as depicted in Figure 5 *a)*. One of the first examples demonstrating ferromagnetic interactions between organic molecules was based on galvinoxyl.[83] Magnetic susceptibility measurements resulted in a positive Weiss constant (11 K). Interestingly, the crystal structure undergoes a phase transition at 85 K to a low temperature phase. Thus, the recorded susceptibility at high temperature fits with a one dimensional ferromagnetic model showing a $J/k_B = 13$ K, while the one at low temperature is consistent with a singlet-triplet model showing strong antiferromagnetic interaction ($J/k_B = -230$ K). The transition is a first-order phase transition with a hysteresis of 5 K.[84] Another representative example of ferromagnetic interaction in an organic crystal is found in the nitronyl nitroxides family. Particularly, *p*-nitrophenyl nitronyl nitroxide (*p*-NPNN) became a milestone after the discovery of long-range ferromagnetic interaction in one of its crystal phases (β phase),

although the transition temperature was 0.65 K.[85] *p*-NPNN presents four polymorphic structures and, fortunately, the most thermodynamically stable is the *β* phase, which happens to be the one showing ferromagnetic ordering. A deeper account on the broad literature in these compounds can be found elsewhere.[9,10,30] Again, as discussed for the previous carbon- and nitrogen-centred through-space interacting radicals, this indicates the subtle interplay between crystal packing and magnetic properties and suggests that looking for robust magnetic properties within molecular crystals might not be the best strategy, due to the lack of control over the structural parameters influencing magnetic coupling.

Following the ongoing discussion, now the radical polymer strategy will be commented. It appears evident that oxygen-bearing radical molecules present a remarkable stability as derived from the large number of reported examples. Such stability is related to the degree of localization of the unpaired electron over the oxygen atom, which shows a large electronegativity. Thus, these compounds are good candidates as robust pendant radicals that can be attached to a variable number of polymeric units, which results in the several reported radical polymers. In fact, one can find various polymeric units, including thiophene,[86] 1,3-phenyleneethynylene[87–89] (see Figure 4) and polyacetylene[90] together with different pendant radicals, such as galvinoxyl,[86,88,89] TEMPO[87] and nitroxide.[90] For the purpose of this thesis, the most important consideration derived from these works is the crucial impact that secondary structure, generally in the form of a helical form, has in defining the interaction among the unpaired electrons and consequently the resulting magnetic properties.[87,88]

As it was similarly done with the previous radical-bearing centres discussed, a possible manner of reducing the impact of the adopted conformation on the magnetic properties is to include the radical centres in the backbone of the polymeric unit, as comparatively depicted in Figure 5 *b)* and *c)*. This results in through-bond interacting compounds. As far as the oxygen-bearing radical is concerned, several works deal with this strategy, mostly using a 1,3-phenylene as a coupling unit. One of the first examples consists of a dinitroxide.[91] The observed magnetic behaviour is interpreted in terms of a triplet ground state with best fit parameters of $\theta = -7.8$ K and $2J/k \gg 500$ K.[92] However, it is not a persistent triplet and it transforms into an isomeric aminoquinone imine N-oxide in a few hours in solution, which prevents its use as a building block. Aiming at improving the stability of related nitroxides, synthesis of a sterically

protected trinitroxide was successful in providing a quartet ground state with best fit parameters of $\theta = -19$ K and $2J/k \gg 240$ K,[92] but was discarded by the same authors as a strategy to keep extending the polyradical to polymeric system. Following a different approach, another manner of increasing stability is by means of conformational restriction, avoiding torsion of the π–conjugated system connecting the nitroxide units. This strategy afforded the first isolated nitroxide diradical with two diarylnitroxide moieties presenting a persistent triplet state ground state, even at room temperature.[93] Additionally, the annelated nitroxide diradical is stable at ambient conditions, in the solid state and in solution.[93] At variance with all previously discussed through-space interacting cases where the molecular unit bears only one unpaired electron, the stability of triplet dinitroxides permits obtaining crystal packings between units presenting high-spin ground states. Unfortunately, even if the local triplet remains within the molecule, the interaction among molecules is antiferromagnetic.[94] Finally, a strategy combining both through-space and through-bond interactions has also been investigated by Rajca et al. by means of stable calix[4]arene tetraradicals (see Figure 4).[95] The macrostructure of the calix[4]arene can be either alternate or conical, and there is a correlation between the exchange coupling constant and the adopted conformation. Particularly, through-bond interaction is ferro- and antiferromagnetic in the conical and alternate conformation, respectively; through-space interaction is always antiferromagnetic. However, the magnetic coupling constant between the unpaired electrons is very low, of the order of ± 1 K.

d) Radicals with Unpaired Electrons on Sulfur-containing Heterocycles.

The molecular structures discussed in this section can be found in Figure 4 *d)*. This last group of molecules does not necessarily present an unpaired electron localized on sulfur centres, but their common characteristic is the presence of sulfur-containing heterocycles. Additionally, most of the reported examples are cation radicals, as compared to the majority of neutral molecules discussed in the previous sections. One of the results that boosted this field of research was the discovery of a spontaneous magnetization in *p*-NC(C$_6$F$_4$)(CNSSN) dithiadiazolyl β crystal phase below 35 K,[96] which is well above the typical values reported for nitroxides counterparts. A review by Rawson[97] presents the latest achievements in different thiazyl radicals and provides an insightful discussion on structure-property relationships. Very recent studies have

showed that external pressure can modify the magnetic and transport properties of neutral bisdithiazolyl radicals.[98]

To the best of my knowledge, regarding the radical polymer strategy, there are no reported examples with pendant radicals constituted by sulfur-containing heterocycles.

Finally, through-bond interacting sulfur-based compounds showing paramagnetic/ferromagnetic interactions are almost entirely referred to thiophene derivatives. Tiophene can be found in a variety of sizes (oligomers) and with different substituents. However, in this brief discussion, only thiophene polymers, also known as polythiophenes, are of interest. When it is partially oxidized (p-doped), it is considered as a suitable species for optoelectronic materials due to its electrical conducting properties. Doping has also proved a good strategy for promoting magnetic properties, resulting even in ferromagnetism at room temperature.[99,100] As an example of other successful kind of doping, room temperature ferromagnetism arises from charge transfer states in a crystalline blend film of poly(3-hexylthiophene) (P3HT) mixed with phenyl-C_{61}-butyric acid methyl ester (PCBM).[101] However, magnetic properties are not limited to doped systems, either chemical or electrochemically, of this kind of conjugated polymers. As a matter of fact, remarkable interest has been devoted to study the impact of different structural parameters on the magnetic properties of undoped polythiophenes- particularly, the effect of the substituent (R_1 and R_2 in Figure 4 *d)*, including alkyl, alkoxy, thioalkyl), the substitution pattern (head-to-tail *vs* head-to-head–tail-to-tail) and the regioregularity of the polymer.[102] Interestingly, all investigated polymers showed a magnetic hysteresis loop resulting from spin densities, which were found to be determined by the nature of the substituent. Additionally, the interaction among the spin moments seemed to depend on the supramolecular structure of the conjugated polymers. In a more recent study by the same authors, this hypothesis was further investigated in a variety of different molar mass head-to-tail coupled poly(3-alkylthiophene)s (P3AT).[103] The purpose of varying the molar mass is to promote a differential π–stacking as an effective way to control supramolecular organization and study its effect on the magnetic properties. It is concluded that the magnitude of the saturation magnetization is mainly governed by the fraction of planar polymer chains, and the coercivity is influenced by the molecular structure, which relates to the π–interactions between different polymer chains. As it has been intentionally

highlighted during the previous discussion, this is another example of the critical role that supramolecular, or secondary structure has in defining the magnetic properties of extended conjugated systems.

In view of the previous discussion, and keeping in mind that the objective is to promote robust ferromagnetic interactions in organic radicals, we choose π–conjugated through-bond interacting radicals as building blocks. Particularly, through-space interacting radicals are not good candidates because the magnetic interaction depends critically on the crystal packing, which is subject to large variations depending on external factors such as temperature or pressure (see Figure 5 a)). On the other hand, the magnetic interaction in the radical polymers strategy is largely dependent on the secondary structure adopted by the polymer (see Figure 5 b)), which is difficult to control. Hence, similarly to the through-space case, radical polymers are not good candidates to promote robust ferromagnetic interactions. Finally, π–conjugated through-bond interacting radicals provide the radical centres within the backbone of the polymeric unit, offering the possibility for extending the system in different dimensionalities, introducing steric protection of the radical centres and reducing the impact of structural flexibility (see Figure 5 c)). Altogether, this constitutes efficient manners of designing high-spin ground state polyradical systems with robust ferromagnetic properties and chemical stability, as it will be explained in chapter 4.

1.4. Motivation and objectives of the thesis.

In view of all discussed evidences, one can conclude that up to date, a purely organic system showing strong ferromagnetic properties in a wide enough range of temperature does not exist. In general, through-space interacting compounds present too low T_C and magnetic coupling constants, whereas through-bond interacting systems, although showing larger coupling constant values, suffer from lack of stability due to the reactivity of the radical-bearing centres.

Particularly, we choose π–conjugated through-bond interacting neutral radicals as building blocks for achieving robust ferromagnetic properties in an organic material. The appearance of ferromagnetism in a neutral purely carbon-based compound with an even number of electrons does not only represent a fundamental challenge, but it also appears as a very promising approach for obtaining technologically relevant, low cost, materials. This relies on the possibilities offered by the organic synthetic route for

controlling shapes and sizes of the final products, as an effective manner to modulate the macroscopic shapes and properties.

Therefore, this thesis aims at reaching two particular goals:

• To propose and exploit an accurate manner for extracting magnetic coupling constants in a variety of compounds of increasing complexity, including coordination compounds and organic radicals. The proposal is based on an alternative formulation of the mapping approach following previous studies carried out in the group, and exploits the relation between pure spin states and energy expectation values using broken symmetry solutions. This is presented and applied in chapter 3 to extract the relevant magnetic coupling constants in complex magnetic topologies. This approach is validated by comparison to experiment and by means of effective Hamiltonian theory for model and real systems with three unpaired electrons in three centres.

• To provide new arguments for obtaining stable, high-spin ground state, $\pi-$conjugated polyradicals interacting through-bond with large ferromagnetic coupling constants, profiting from the inherent structural flexibility of these compounds, which in fact has been generally overlooked in previous theoretical studies. Therefore, several structural (i.e. derived from σ-bond covalent structure) and magnetic (i.e. arising from magnetic interactions) topologies offered by different combinations of the 1,3-phenylene coupling unit are investigated, including discrete molecular units and extended systems in one and two dimensions. The impact of a secondary structure, as a consequence of the structural flexibility, on the electronic structure and stability of the investigated compounds is expected to play a relevant role. These results are presented in chapter 4.

To conclude, this thesis aims to contribute to the accurate extraction of magnetic exchange interaction in complex systems, by means of the mapping approach, and to establish reliable criteria to define purely organic systems, showing high-spin ground state, chemical stability and robust ferromagnetic properties.

(1)   Heisenberg, W. *The Physical Principles of the Quantum Theory*; University of Chicago Press: Chicago, 1930.

(2)   Dirac, P. A. M. *The Principles of Quantum Mechanics*; Clarendon Press: Oxford, 1958.

(3)   Tomonaga, S. I. *The Story of Spin*; University of Chicago Press, 1997.

(4)   Anderson, P. W. Antiferromagnetism. Theory of Superexchange Interaction. *Phys. Rev.* **1950**, *79* (2), 350–356.

(5)   Ashcroft, N. W. Mermin, N. D. *Ashcroft & Mermin*; Saunders College Publishing: New York, 1976.

(6)   Caspers, W. J. *Spin Systems*; World Scientific Publishing: Singapur, 1989.

(7)   Heisenberg, W. Zur Theorie Des Ferromagnetismus. *Zeitschrift für Phys.* **1928**, *49* (9-10), 619–636.

(8)   Ising, E. Beitrag Zur Theorie Des Ferromagnetismus. *Zeitschrift für Phys.* **1925**, *31* (1), 253–258.

(9)   Miller, J. S.; Drillon, M. *Magnetism: Molecules to Materials II*; Miller, J. S., Drillon, M., Eds.; Wiley-VCH Verlag GmbH & Co. KGaA, 2002.

(10)   Miller, J. S.; Drillon, M. *Magnetism: Molecules to Materials IV*; Miller, J. S., Drillon, M., Eds.; Wiley-VCH Verlag GmbH & Co. KGaA, 2002.

(11)   Veciana, J. *Π-Electron Magnetism From Molecules to Magnetic Materials*; Veciana, J., Ed.; Springer-Verlag: Berlin, 2001.

(12)   Darby, M. I. Tables of the Brillouin Function and of the Related Function for the Spontaneous Magnetization. *Br. J. Appl. Phys.* **1967**, *18* (10), 1415–1417.

(13)   Bain, G. A.; Berry, J. F. Diamagnetic Corrections and Pascal's Constants. *J. Chem. Educ.* **2008**, *85* (4), 532.

(14)   Van Vleck, J. H. *The Theory of Electric and Magnetic Susceptibilities*; Oxford University Press: Oxford, 1932.

(15)   Néel, L. Magnetism and Local Molecular Field. *Science (80-.).* **1971**, *174* (4013), 985–992.

(16)   Poulis, N. J.; van den Handel, J.; Ubbink, J.; Poulis, J. A.; Gorter, C. J. On Antiferromagnetism in a Single Crystal. *Phys. Rev.* **1951**, *82* (4), 552–552.

(17)   Kahn, O. *Molecular Magnetism*; VCH: New York, 1993.

(18)   Carlin, R. L. *Magnetochemistry*; Springer-Verlag, 1986.

(19)   Gispert, J. R. *Coordination Chemistry*; Wiley-VCH Verlag GmbH & Co. KGaA: Weinheim, 2008.

(20)   Anderson, P. W. Theory of Magnetic Exchange Interactions:Exchange in Insulators and Semiconductors. *Solid State Phys.* **1963**, *14*, 99–214.

(21)   Sessoli, R.; Gatteschi, D.; Caneschi, A.; Novak, M. A. Magnetic Bistability in a Metal-Ion Cluster. *Nature* **1993**, *365* (6442), 141–143.

(22)   Christou, G.; Gatteschi, D.; Hendrickson, D. N.; Sessoli, R. Single-Molecule Magnets. *MRS Bull.* **2001**, *25* (11), 66–71.

(23)   Craig, G. A.; Murrie, M. 3d Single-Ion Magnets. *Chem. Soc. Rev.* **2015**, *44* (8), 2135–2147.

(24)   Gatteschi, D.; Sessoli, R.; Villain, J. *Molecular Nanomagnets*; Oxford University Press: Oxford, 2006.

(25)   Cirera, J.; Ruiz, E.; Alvarez, S.; Neese, F.; Kortus, J. How to Build Molecules with Large Magnetic Anisotropy. *Chemistry* **2009**, *15* (16), 4078–4087.

(26)   Rosado Piquer, L.; Sañudo, E. C. Heterometallic 3d-4f Single-Molecule Magnets. *Dalton Trans.* **2015**, *44* (19), 8771–8780.

(27)   Neese, F.; Pantazis, D. A. What Is Not Required to Make a Single Molecule Magnet. *Faraday Discuss.* **2011**, *148*, 229–238.

(28)   Maurice, R.; Graaf, C. de; Guihéry, N. Theoretical Determination of Spin Hamiltonians with Isotropic and Anisotropic Magnetic Interactions in Transition Metal and Lanthanide Complexes. *Phys. Chem. Chem. Phys.* **2013**, *15* (43), 18784–18804.

(29)   Malrieu, J. P.; Caballol, R.; Calzado, C. J.; De Graaf, C.; Guihéry, N. Magnetic Interactions in Molecules and Highly Correlated Materials: Physical Content, Analytical Derivation, and Rigorous Extraction of Magnetic Hamiltonians. *Chem. Rev.* **2014**, *114*, 429–492.

(30)   Blundell, S. J.; Pratt, F. L. Organic and Molecular Magnets. *J. Phys. Condens. Matter* **2004**, *16* (24), R771–R828.

(31)   Blundell, S. J. Molecular Magnets. *Contemp. Phys.* **2008**, *48* (5), 275–290.

(32)   Rajca, A. Organic Diradicals and Polyradicals: From Spin Coupling to Magnetism? *Chem. Rev.* **1994**, *94*, 871–893.

(33)   Rajca, A. The Physical Organic Chemistry of Very High-Spin Polyradicals. *Adv. Phys. Org. Chem.* **2005**, *40*, 153–199.

(34)   Shishlov, N. M. From the Gomberg Radical to Organic Magnets. *Russ. Chem. Rev.* **2007**, *75*, 863–884.

(35) Gomberg, M. An Instance of Trivalent Carbon: Triphenylmethyl. *J. Am. Chem. Soc.* **1900**, *22* (11), 757–771.

(36) Ballester, M.; Riera-Figueras, J.; Castaner, J.; Badfa, C.; Monso, J. M. Inert Carbon Free Radicals. I. Perchlorodiphenylmethyl and Perchlorotriphenylmethyl Radical Series. *J. Am. Chem. Soc.* **1971**, *93* (9), 2215–2225.

(37) Malrieu, J.-P.; Robert, V. Evaluation of the Aromatic Contribution to the Energy of Periodic Lattices. *J. Phys. Org. Chem.* **2006**, *19* (1), 10–17.

(38) Trinquier, G.; Malrieu, J.-P. Kekulé versus Lewis: When Aromaticity Prevents Electron Pairing and Imposes Polyradical Character. *Chemistry* **2015**, *21* (2), 814–828.

(39) Feixas, F.; Matito, E.; Poater, J.; Solà, M. Quantifying Aromaticity with Electron Delocalisation Measures. *Chem. Soc. Rev.* **2015**, *44* (18), 6434–6451.

(40) Zeng, Z.; Shi, X.; Chi, C.; López Navarrete, J. T.; Casado, J.; Wu, J. Pro-Aromatic and Anti-Aromatic Π-Conjugated Molecules: An Irresistible Wish to Be Diradicals. *Chem. Soc. Rev.* **2015**, *44*, 6578–6596.

(41) Zheludev, A.; Grand, A.; Ressouche, E.; Schweizer, J.; Morin, B. G.; Epstein, A. J.; Dixon, D. A.; Miller, J. S. Experimental Determination of the Spin Density in the Tetracyanoethenide Free Radical, [TCNE].bul. -, by Single-Crystal Polarized Neutron Diffraction. A View of a .pi.* Orbital. *J. Am. Chem. Soc.* **1994**, *116* (16), 7243–7249.

(42) Acker, D. S.; Harder, R. J.; Hertler, W. R.; Mahler, W.; Melby, L. R.; Benson, R. E.; Mochel, W. E. 7,7,8,8-Tetracyanoquinodimethane and Its Electrically Conducting Anion-Radical Derivatives. *J. Am. Chem. Soc.* **1960**, *82* (24), 6408–6409.

(43) Gallagher, N. M.; Olankitwanit, A.; Rajca, A. High-Spin Organic Molecules. *J. Org. Chem.* **2015**, *80* (1), 1291–1298.

(44) McConnell, H. M. Ferromagnetism in Solid Free Radicals. *J. Chem. Phys.* **1963**, *39*, 1910.

(45) McConnell, H. M. No Title. *Proc. Robert A. Welch Found. Conf. Chem Res.* **1967**, *11*, 144.

(46) Kollmar, C.; Kahn, O. Is the McConnell Mechanism a Suitable Strategy for the Design of Molecular Ferromagnets? **1991**, *113* (21), 7987–7994.

(47) Kollmar, C.; Kahn, O. Ferromagnetic Spin Alignment in Molecular Systems: An Orbital Approach. *Acc. Chem. Res.* **1993**, *26* (5), 259–265.

(48) Izuoka, A.; Murata, S.; Sugawara, T.; Iwamura, H. Ferro- and Antiferromagnetic Interaction between Two Diphenylcarbene Units Incorporated in the [2.2]paracyclophane Skeleton. *J. Am. Chem. Soc.* **1985**, *107* (6), 1786–1787.

(49)   Izuoka, A.; Murata, S.; Sugawara, T.; Iwamura, H. Molecular Design and Model
        Experiments of Ferromagnetic Intermolecular Interaction in the Assembly of
        High-Spin Organic Molecules. Generation and Characterization of the Spin
        States of Isomeric bis(phenylmethylenyl)[2.2]paracyclophanes. *J. Am. Chem.
        Soc.* **1987**, *109* (9), 2631–2639.

(50)   Deumal, M.; Cirujeda, J.; Veciana, J.; Novoa, J. J. Structure-Magnetism
        Relationships in α-Nitronyl Nitroxide Radicals: Pitfalls and Lessons to Be
        Learned. *Adv. Mater.* **1998**, *10* (17), 1461–1466.

(51)   Hicks, R. G. What's New in Stable Radical Chemistry? *Org. Biomol. Chem.*
        2007, *5* (9), 1321–1338.

(52)   Allemand, P. M.; Khemani, K. C.; Koch, A.; Wudl, F.; Holczer, K.; Donovan, S.;
        Grüner, G.; Thompson, J. D. Organic Molecular Soft Ferromagnetism in a
        Fullerene C60. *Science* **1991**, *253* (5017), 301–302.

(53)   Morita, Y.; Suzuki, S.; Sato, K.; Takui, T. Synthetic Organic Spin Chemistry for
        Structurally Well-Defined Open-Shell Graphene Fragments. *Nat. Chem.* **2011**, *3*
        (3), 197–204.

(54)   Goto, K.; Kubo, T.; Yamamoto, K.; Nakasuji, K.; Sato, K.; Shiomi, D.; Takui, T.;
        Kubota, M.; Kobayashi, T.; Yakusi, K.; et al. A Stable Neutral Hydrocarbon
        Radical: Synthesis, Crystal Structure, and Physical Properties of 2,5,8-Tri- Tert -
        Butyl-Phenalenyl. *J. Am. Chem. Soc.* **1999**, *121* (7), 1619–1620.

(55)   Takano, Y.; Taniguchi, T.; Isobe, H.; Kubo, T.; Morita, Y.; Yamamoto, K.;
        Nakasuji, K.; Takui, T.; Yamaguchi, K. Hybrid Density Functional Theory
        Studies on the Magnetic Interactions and the Weak Covalent Bonding for the
        Phenalenyl Radical Dimeric Pair. *J. Am. Chem. Soc.* **2002**, *124* (37), 11122–
        11130.

(56)   Pal, S. K.; Itkis, M. E.; Reed, R. W.; Oakley, R. T.; Cordes, A. W.; Tham, F. S.;
        Siegrist, T.; Haddon, R. C. Synthesis, Structure and Physical Properties of the
        First One-Dimensional Phenalenyl-Based Neutral Radical Molecular Conductor.
        J. Am. Chem. Soc. **2004**, *126* (5), 1478–1484.

(57)   Fumanal, M.; Mota, F.; Novoa, J. J.; Ribas-Arino, J. Unravelling the Key Driving
        Forces of the Spin Transition in Π-Dimers of Spiro-Biphenalenyl-Based
        Radicals. *J. Am. Chem. Soc.* **2015**, *137* (40), 12843–12855.

(58)   Huang, J.; Kertesz, M. Theoretical Analysis of Intermolecular Covalent π-π
        Bonding and Magnetic Properties of Phenalenyl and Spiro-Biphenalenyl Radical
        π-Dimers. *J. Phys. Chem. A* **2007**, *111* (28), 6304–6315.

(59)   Anamimoghadam, O.; Symes, M. D.; Long, D.-L.; Sproules, S.; Cronin, L.;
        Bucher, G. Electronically Stabilized Nonplanar Phenalenyl Radical and Its Planar
        Isomer. *J. Am. Chem. Soc.* **2015**, *137* (47), 14944–14951.

(60) Itoh, T.; Jinbo, Y.; Hirai, K.; Tomioka, H. Preparation of Poly(phenyl)acetylenes Having Diazo Groups and Magnetic Characterization of Poly(carbene). *J. Am. Chem. Soc.* **2005**, *127* (6), 1650–1651.

(61) Rajca, A.; Wongsriratanakul, J.; Rajca, S. Magnetic Ordering in an Organic Polymer. *Science* **2001**, *294*, 1503–1505.

(62) Makarova, T. L.; Sundqvist, B.; Höhne, R.; Esquinazi, P.; Kopelevich, Y.; Scharff, P.; Davydov, V. A.; Kashevarova, L. S.; Rakhmanina, A. V. Magnetic Carbon. *Nature* **2001**, *413* (6857), 716–718.

(63) Makarova, T. L.; Sundqvist, B.; Höhne, R.; Esquinazi, P.; Kopelevich, Y.; Scharff, P.; Davydov, V.; Kashevarova, L. S.; Rakhmanina, A. V. Retraction: Magnetic Carbon. *Nature* **2006**, *440* (7084), 707.

(64) Wood, R. A.; Lewis, M. H.; Lees, M. R.; Bennington, S. M.; Cain, M. G.; Kitamura, N. Ferromagnetic Fullerene. *J. Phys. Condens. Matter* **2002**, *14* (22), L385–L391.

(65) Narozhnyi, V. Ferromagnetic Carbon with Enhanced Curie Temperature. *Phys. B Condens. Matter* **2003**, *329-333*, 1217–1218.

(66) Makarova, T. L.; Han, K.-H.; Esquinazi, P.; da Silva, R. R.; Kopelevich, Y.; Zakharova, I. B.; Sundqvist, B. Magnetism in Photopolymerized Fullerenes. *Carbon N. Y.* **2003**, *41* (8), 1575–1584.

(67) Koivisto, B. D.; Hicks, R. G. The Magnetochemistry of Verdazyl Radical-Based Materials. *Coord. Chem. Rev.* **2005**, *249* (23), 2612–2630.

(68) Train, C.; Norel, L.; Baumgarten, M. Organic Radicals, a Promising Route towards Original Molecule-Based Magnetic Materials. *Coord. Chem. Rev.* **2009**, *253* (19-20), 2342–2351.

(69) Yan, B.; Cramen, J.; McDonald, R.; Frank, N. L. Ferromagnetic Spin-Delocalized Electron Donors for Multifunctional Materials: Π-Conjugated Benzotriazinyl Radicals. *Chem. Commun.* **2011**, *47* (11), 3201–3203.

(70) Constantinides, C. P.; Koutentis, P. A.; Rawson, J. M. Ferromagnetic Interactions in a 1D Alternating Linear Chain of Π-Stacked 1,3-Diphenyl-7-(thien-2-Yl)-1,4-Dihydro-1,2,4-Benzotriazin-4-Yl Radicals. *Chemistry* **2012**, *18* (23), 7109–7116.

(71) Constantinides, C. P.; Berezin, A. A.; Zissimou, G. A.; Manoli, M.; Leitus, G. M.; Bendikov, M.; Probert, M. R.; Rawson, J. M.; Koutentis, P. A. A Magnetostructural Investigation of an Abrupt Spin Transition for 1-Phenyl-3-Trifluoromethyl-1,4-dihydrobenzo[e][1,2,4]triazin-4-Yl. *J. Am. Chem. Soc.* **2014**, *136* (34), 11906–11909.

(72) Fumanal, M.; Vela, S.; Novoa, J. J.; Ribas-Arino, J. Towards the Tailored Design of Benzotriazinyl-Based Organic Radicals Displaying a Spin Transition. *Chem. Commun.* **2015**, *51* (87), 15776–15779.

(73)   Murata, H.; Miyajima, D.; Nishide, H. A High-Spin and Helical Organic
       Polymer: Poly{[4-(dianisylaminium)phenyl]acetylene}. *Macromolecules* **2006**,
       39 (19), 6331–6335.

(74)   Wienk, M. M.; Janssen, R. A. J. High-Spin Cation Radicals of Meta − Para
       Aniline Oligomers. *J. Am. Chem. Soc.* **1997**, *119* (19), 4492–4501.

(75)   Bushby, R. J.; Kilner, C. a.; Taylor, N.; Vale, M. E. Disjoint and Coextensive
       Amminium Radical Cations: A General Problem in Making Amminium Radical
       Cation Based High-Spin Polymers. *Tetrahedron* **2007**, *63* (46), 11458–11466.

(76)   Cao, Y.; Heeger, A. J. Magnetic Susceptibility of Polyaniline in Solution in Non-
       Polar Organic Solvents and in Polyblends in Poly(methyl Methacrylate). *Synth.
       Met.* **1992**, *52* (2), 193–200.

(77)   Zaidi, N. A.; Giblin, S. R.; Terry, I.; Monkman, A. P. Room Temperature
       Magnetic Order in an Organic Magnet Derived from Polyaniline. *Polymer
       (Guildf).* **2004**, *45* (16), 5683–5689.

(78)   Li, Y.; Ma, L.; Gan, M.; Tang, J.; Hu, H.; Ge, C.; Yu, L.; Huang, H.; Yang, F.
       Magnetic PANI Controlled by Morphology with Enhanced Microwave
       Absorbing Property. *Mater. Lett.* **2015**, *140*, 192–195.

(79)   Rajca, A.; Shiraishi, K.; Pink, M.; Rajca, S. Triplet (S=1) Ground State Aminyl
       Diradical. *J. Am. Chem. Soc.* **2007**, *129* (23), 7232–7233.

(80)   Rajca, A.; Olankitwanit, A.; Rajca, S. Triplet Ground State Derivative of Aza- M
       -Xylylene Diradical with Large Singlet-Triplet Energy Gap. *J. Am. Chem. Soc.*
       2011, *133*, 4750–4753.

(81)   Boratyński, P. J.; Pink, M.; Rajca, S.; Rajca, A. Isolation of the Triplet Ground
       State Aminyl Diradical. *Angew. Chemie - Int. Ed.* **2010**, *49*, 5459–5462.

(82)   Rajca, A.; Olankitwanit, A.; Wang, Y.; Boratyński, P. J.; Pink, M.; Rajca, S.
       High-Spin S = 2 Ground State Aminyl Tetraradicals. *J. Am. Chem. Soc.* **2013**,
       135, 18205–18215.

(83)   Mukai, K. Anomalous Magnetic Properties of Stable Crystalline Phenoxyl
       Radicals. *Bull. Chem. Soc. Jpn.* **1969**, *42* (1), 40–46.

(84)   Sugano, T. Magnetic Phase Transitions in Organic Radicals. *Polyhedron* **2001**,
       20 (11-14), 1285–1289.

(85)   Awaga, K.; Maruyama, Y. Ferromagnetic Intermolecular Interaction of the
       Organic Radical, 2-(4-Nitrophenyl)-4,4,5,5-Tetramethyl-4,5-Dihydro-1h-
       Imidazolyl-1-Oxy 3-Oxide. *Chem. Phys. Lett.* **1989**, *158* (6), 556–558.

(86)   Miyasaka, M.; Yamazaki, T.; Nishide, H. Poly(3-Phenylgalvinoxylthiophene). A
       New Conjugated Polyradical with High Spin Concentration. *Polym. J.* **2001**, *33*
       (11), 849–856.

(87)   Matsuda, K.; Stone, M. T.; Moore, J. S. Helical Pitch of M-Phenylene Ethynylene Foldamers by Double Spin Labeling. *J. Am. Chem. Soc.* **2002**, *124* (40), 11836–11837.

(88)   Kaneko, T.; Abe, H.; Teraguchi, M.; Aoki, T. Folding-Induced Through-Space Magnetic Interaction of Poly(1,3-Phenyleneethynylene)-Based Polyradicals. *Macromolecules* **2013**, *46* (7), 2583–2598.

(89)   Kaneko, T.; Iwamura, K.; Nishikawa, R.; Teraguchi, M.; Aoki, T. Synthesis of Sequential poly(1,3-Phenyleneethynylene)-Based Polyradicals and through-Space Antiferromagnetic Interaction of Their Solid State. *Polymer (Guildf).* **2014**, *55* (5), 1097–1102.

(90)   Nishide, H.; Kaneko, T.; Igarashi, M.; Tsuchida, E.; Yoshioka, N.; Lahti, P. M. Magnetic Characterization and Computational Modeling of Poly(phenylacetylenes) Bearing Stable Radical Groups. *Macromolecules* **1994**, *27* (11), 3082–3086.

(91)   Calder, A.; Forrester, A. R.; James, P. G.; Luckhurst, G. R. Nitroxide Radicals. V. N,N'-Di-Tert-Butyl-M-Phenylenebinitroxide, a Stable Triplet. *J. Am. Chem. Soc.* **1969**, *91* (14), 3724–3727.

(92)   Ishida, T.; Iwamura, H. Bis[3-Tert-Butyl-5-(N-Oxy-Tert-Butylamino)phenyl] Nitroxide in a Quartet Ground State: A Prototype for Persistent High-Spin Poly[(oxyimino)-1,3-Phenylenes]. *J. Am. Chem. Soc.* **1991**, *113* (11), 4238–4241.

(93)   Rajca, A.; Shiraishi, K.; Rajca, S. Stable Diarylnitroxide Diradical with Triplet Ground State. *Chem. Commun.* **2009**, No. 29, 4372–4374.

(94)   Rajca, A.; Takahashi, M.; Pink, M. Conformationally Constrained , Stable , Triplet Ground State (S = 1) Nitroxide Diradicals . Antiferromagnetic Chains of S = 1 Diradicals. *J. Am. Chem. Soc.* **2007**, *129* (13), 10159–10170.

(95)   Rajca, A.; Mukherjee, S.; Maren Pink; Rajca, S. Exchange Coupling Mediated Through-Bonds and Through-Space in Conformationally Constrained Polyradical Scaffolds: Calix[4]arene Nitroxide Tetraradicals and Diradical. *J. Am. Chem. Soc.* **2006**, *128* (41), 13497–13507.

(96)   Palacio, F.; Antorrena, G.; Castro, M.; Burriel, R.; Rawson, J.; Smith, J. N. B.; Bricklebank, N.; Novoa, J.; Ritter, C. High-Temperature Magnetic Ordering in a New Organic Magnet. *Phys. Rev. Lett.* **1997**, *79* (12), 2336–2339.

(97)   Rawson, J. M.; Alberola, A.; Whalley, A. Thiazyl Radicals: Old Materials for New Molecular Devices. *J. Mater. Chem.* **2006**, *16* (26), 2560.

(98)   Tian, D.; Winter, S. M.; Mailman, A.; Wong, J. W. L.; Yong, W.; Yamaguchi, H.; Jia, Y.; Tse, J. S.; Desgreniers, S.; Secco, R. A.; et al. The Metallic State in Neutral Radical Conductors: Dimensionality, Pressure and Multiple Orbital Effects. *J. Am. Chem. Soc.* **2015**, *137* (44), 14136–14148.

(99)   Nascimento, O. R.; de Oliveira, A. J. A.; Correa, A. A.; Bulhões, L. O. S.; Pereira, E. C.; Souza, V. M.; Walmsley, L. Magnetic Behavior of poly(3-Methylthiophene): Metamagnetism and Room-Temperature Weak Ferromagnetism. *Phys. Rev. B* **2003**, *67* (14), 144422.

(100)   Nascimento, O. R.; de Oliveira, A. J. A.; Pereira, E. C.; Correa, A. A.; Walmsley, L. The Ferromagnetic Behaviour of Conducting Polymers Revisited. *J. Phys. Condens. Matter* **2008**, *20* (3), 035214.

(101)   Yang, B.; Xiao, Z.; Yuan, Y.; Jayaraman, T. V.; Shield, J. E.; Skomski, R.; Huang, J. Room-Temperature Organic Ferromagnetism in the Crystalline poly(3-Hexylthiophene): Phenyl-C61-Butyric Acid Methyl Ester Blend Film. *Polymer (Guildf).* **2013**, *54* (2), 490–494.

(102)   Vandeleene, S.; Jivanescu, M.; Stesmans, A.; Cuppens, J.; Van Bael, M. J.; Yamada, H.; Sato, N.; Verbiest, T.; Koeckelberghs, G. Magnetic Properties of Substituted Poly(thiophene)s in Their Neutral State. *Macromolecules* **2010**, *43* (6), 2910–2915.

(103)   Vandeleene, S.; Jivanescu, M.; Stesmans, A.; Cuppens, J.; Van Bael, M. J.; Verbiest, T.; Koeckelberghs, G. Influence of the Supramolecular Organization on the Magnetic Properties of Poly(3-Alkylthiophene)s in Their Neutral State. *Macromolecules* **2011**, *44* (12), 4911–4919.

CHAPTER TWO

Theoretical Background

The aim of this chapter is to introduce the basic concepts that allow using quantum theory to calculate the electronic structure of a given ensemble of particles, i.e. a molecule, as an accurate manner to describe its properties. Among the vast amount of properties that can be calculated within the current methods, magnetic properties are central in this thesis, which orientates the discussion towards some specific formulations capable of accounting for it.

2.1. Wave Function-Based Methods.

2.1.1. The Electronic Problem.

For a given system of N electrons and M nuclei interacting described by position vectors $\mathbf{r}_i$ and $\mathbf{R}_A$ respectively, the stationary quantum states defining the system are obtained by solving the non-relativistic, time-independent Schrodinger equation:

$$\hat{H}\Psi = E\Psi \tag{1}$$

where $\hat{H}$ is the Hamiltonian operator associated to the system, E is the energy of a given stationary state and Ψ the wave function describing it. In atomic units,[1] the Hamiltonian is written as

$$H = -\sum_{i=1}^{N}\frac{1}{2}\nabla_i^2 - \sum_{A=1}^{M}\frac{1}{2M_A}\nabla_A^2 + \sum_{A=1}^{M}\sum_{B>A}^{M}\frac{Z_A Z_B}{R_{AB}} + \sum_{i=1}^{N}\sum_{j>i}^{N}\frac{1}{r_{ij}} - \sum_{i=1}^{N}\sum_{A=1}^{M}\frac{Z_A}{r_{iA}} \tag{2}$$

In this equation, M_A is the ratio of the mass of nucleus A to the mass of an electron, Z_A is the atomic number of nucleus A, ∇_A^2 and ∇_i^2 are the Laplacian operators involving differentiation with respect to the coordinates of the Ath nucleus and i^{th} electron respectively, $r_{iA} = |\bar{r}_i - \bar{r}_A|$ is the distance between the ith electron and the Ath nucleus and $r_{ij} = |\bar{r}_i - \bar{r}_j|$ is the distance between the ith and j^{th} electron and $R_{AB} = |\bar{R}_A - \bar{R}_B|$ is distance between the Ath and B^{th} nuclei. This equation can be expressed in a more compact way as

$$\hat{H} = \hat{T}_N + \hat{T}_e + V_N + V_e + V_{Ne} \tag{3}$$

The first and second terms are the nuclear and electronic kinetic energy operators, respectively. Third and fourth terms stand for the nucleus-nucleus and electron-electron

repulsion, respectively. The last term represents the coulomb attraction between electrons and nuclei.

2.1.1.1. The Born-Oppenheimer Approximation.

Equation (1) is a second-order differential equation in $3(N+M)$ variables that needs to be simplified in order to be solved. Such simplification can be achieved by means of Born-Oppenheimer approximation.[2] Given the different mass between electrons and nuclei, the description of the electronic motion can be assumed to accommodate almost instantaneously any change in the position of the nuclei. Thus, the description of their motion can be separated; the electrons experience the nuclei as fixed force centres and follow adiabatically any change in the nuclear positions. Conversely, the nuclei experience an average potential created by the electrons. This allows assuming that the kinetic energy of the nuclei $\hat{T}_N$ can be neglected and that the repulsion between the nuclei V_N is constant. Within this approximation, the total Hamiltonian of the system becomes

$$\hat{H} = \hat{T}_N + \hat{H}_{elec} + V_N \rightarrow \hat{H}_{elec} + V_N \tag{4}$$

where the electronic Hamiltonian operator is given by

$$\hat{H}_{elec} = \hat{T}_e + V_e + V_{Ne} \tag{5}$$

Since

$$\left[\hat{H}_{elec}, \mathbf{R}\right] = 0 \tag{6}$$

The eigenvalues of the electronic Hamiltonian may be determined for a particular value of the nuclear position vectors $\mathbf{R}$. Thus, the Schrödinger equation can be rewritten as

$$\left(\hat{H}_{elec} + V_N\right)|\Phi_m(\mathbf{r}; \mathbf{R})\rangle = E_m(\mathbf{r}; \mathbf{R})|\Phi_m(\mathbf{r}; \mathbf{R})\rangle \tag{7}$$

Here, $\mathbf{r}$ and $\mathbf{R}$ denote an implicit and parametric dependence on the electronic and nuclear coordinates respectively. The term arising from repulsions between the nuclei may be treated as an additive constant.

Because the electronic wave functions $|\Phi_m(\mathbf{r}; \mathbf{R})\rangle$ form a complete orthonormal set, they can be used to expand the total molecular wave function with the expansion coefficients being functions of the nuclear coordinates:

$$\Psi(\mathbf{r}_1, \mathbf{r}_2, \cdots, \mathbf{r}_N, \mathbf{R}) = \sum_m \chi_m(\mathbf{R})\Phi_m(\mathbf{r}_1, \mathbf{r}_2, \cdots, \mathbf{r}_N; \mathbf{R}) \tag{8}$$

This will be useful for the description of the nuclear motion. By introducing eqn (8) into eqn (1), the Schródinger equation can be rewritten as

$$\sum_m \{\chi_m E_m(\mathbf{R})\Phi_m + \hat{T}_N(\chi_m \Phi_m) - E(\chi_m \Phi_m)\} = 0 \tag{9}$$

Multiplying eqn (9) from the left by Φ_n^*, integrating over the coordinates of all electrons and expanding the expression,[3] it is obtained an expression of the nuclear kinetic operator $\hat{T}_N$ where the electronic and nuclear contributions have been separated

$$\sum_m \langle \Phi_n | \hat{T}_N | \chi_m \Phi_m \rangle = \hat{T}_N \chi_m + \sum_m C_{mn}(\mathbf{R}, \nabla)\chi_m(\mathbf{R}) \tag{10}$$

Note that the first term $\hat{T}_N \chi_m$ the electronic terms have been removed. The second term contains

$$C_{mn} = -\sum_A \frac{1}{M_A}\left(\langle \Phi_n | \nabla_A | \Phi_m \rangle \nabla_A + \frac{1}{2}\langle \Phi_n | \nabla_A^2 | \Phi_m \rangle\right) \tag{11}$$

which mixes the electronic wave functions through the first and second derivatives of nuclear positions, also called first and second non-adiabatic coupling elements. Finally, substituting eqn (10,11) in eqn (9),[3] it is obtained

$$\left(\hat{T}_N + E_{Nn}(\mathbf{R}) - E\right)\chi_n + \sum_{m \neq n} C_{mn}\chi_m = 0 \tag{12}$$

where

$$E_{Nn}(\mathbf{R}) = E_n(\mathbf{R}) - \sum_A \frac{1}{M_A}\frac{1}{2}\langle \Phi_n | \nabla_A^2 | \Phi_m \rangle \tag{13}$$

is an effective potential for the nuclei.

In the adiabatic approximation, the form of the total wave function is restricted to one electronic surface. This means that all non-adiabatic coupling elements are neglected, except those involving $n = m$. Except for spatially degenerate wave functions, the diagonal first order non-adiabatic coupling element is zero, leading to

$$C_{mn} = -\sum_A \frac{1}{2M_A} \left(\langle \Phi_m | \nabla_A^2 | \Phi_m \rangle \right) \tag{14}$$

also known as the diagonal correction.[4] If this is also set to zero, one gets

$$\left(\hat{T}_N + E_{Nn}(\mathbf{R}) \right) \chi_n(\mathbf{R}) = E_n \chi_n(\mathbf{R}) \tag{15}$$

which is the nuclear eigenvalue equation. A further approximation, the Born-Oppenheimer approximation,[2] it is assumed that the effective potential for the nuclei is equal to the electronic energy function, i.e. $E_{Nn}(\mathbf{R}) = E_n(\mathbf{R})$.

$$\left(\hat{T}_N + E_n(\mathbf{R}) \right) \chi_n(\mathbf{R}) = E_n \chi_n(\mathbf{R}) \tag{16}$$

In the Born-Oppenheimer picture, the nuclei move on a potential energy surface (PES) which is a solution to the electronic Schrödinger equation. Solving eqn(16) for the nuclear wave functions at each nuclear configuration leads to energy levels for the molecular vibrations and rotations. By doing so till a minimum in the surface is found, offers a way of optimizing the geometry of the problem investigated.

So far, in the electronic Hamiltonian, only the coordinates of the electrons have been considered. However, to fulfil the requirements of quantum mechanics, another intrinsic variable of the electrons must be considered: the spin, which happens to be the ultimate reason for the existence of magnetism. In order to do so, two spin functions α and β corresponding to spin up and down respectively, can be introduced. They represent a complete and orthonormal basis set. Then, the variables defining the ith electron are represented by $\mathbf{x}_i$ and include the Cartesian coordinates and spin.

Given that the non-relativistic electronic Hamiltonian does not explicitly refer to the spin property of the electrons, it has to be imposed *ad hoc*, which is achieved by constructing a wave function that not only satisfies the Schrödinger equation but also the antisymmetry principle, also known as Pauli principle. Such additional requirement makes the wave function antisymmetrical with respect to the interchange of the spin coordinates $\mathbf{x}$ of any two electrons. It is achieved by means of Slater determinants, which for a N-electron system writes as

$$\Psi(\mathbf{x}_1, \mathbf{x}_2, \cdots \mathbf{x}_N) = (N!)^{-1/2} \begin{vmatrix} \chi_i(\mathbf{x}_1) & \chi_j(\mathbf{x}_1) & \cdots & \chi_k(\mathbf{x}_1) \\ \chi_i(\mathbf{x}_2) & \chi_j(\mathbf{x}_2) & \cdots & \chi_k(\mathbf{x}_2) \\ \vdots & \vdots & \ddots & \vdots \\ \chi_i(\mathbf{x}_N) & \chi_j(\mathbf{x}_N) & \cdots & \chi_k(\mathbf{x}_N) \end{vmatrix} \tag{17}$$

This Slater determinant describes N electrons in N spin orbitals $(\chi_i, \chi_j, \cdots, \chi_k)$ without specifying which electron is in which orbital and where $(N!)^{-1/2}$ is a normalization factor. It fulfils the antisymmetry principle because exchanging the coordinates of two electrons imply the exchange of two rows, which changes the sign of the determinant. More details on the definition of the spin orbitals are given below.

2.1.1.2. Molecular orbitals.

An orbital is defined as a wave function for a single electron. The wave function describing i^{th} electron consists of a spatial and spin part. The former spatial orbital $\phi_i(\mathbf{r})$ is a function of the position vector $\mathbf{r}$ and its square, $|\phi_i(\mathbf{r})|^2 d\mathbf{r}$ describes the probability of finding the electron in the differential volume element $d\mathbf{r}$ around $\mathbf{r}$. The latter accounts for the spin part, which can be spin up or down. From each spatial orbital, two different possibilities for the spin part can be written

$$\chi(\mathbf{x}) = \begin{cases} \phi(\mathbf{r})\alpha(\omega) \\ or \\ \phi(\mathbf{r})\beta(\omega) \end{cases} \tag{18}$$

the resulting function is $\chi(\mathbf{x})$, the so called spin orbital, accounts for both spatial $\mathbf{r}$ and spin ω part. Ideally, the set of spatial orbital would form a complete basis set where to expand the wave function, but this requires an infinite set. Instead, one expands a finite set of K spatial orbitals $\{\phi_i | i = 1, 2, \cdots, K\}$ which imply $2K$ spin orbitals $\{\chi_i | i = 1, 2, \cdots, 2K\}$. The solutions are exact within the subspace spanned by the finite set of orbitals. In general, the convergence in energy is checked by improving the quality of the basis set, which is explained in forthcoming sections. Also, if the spatial part $\phi(\mathbf{r})$ for the spin up and down is assumed to be equal, it is a restricted formalism, whereas if one allows different spatial orbitals, it is an unrestricted formalism. This is further explained in next sections.

A molecule is an ensemble of atoms held together by covalent bonds. The theoretical description of a molecule with N electrons is therefore based on $2N$ atomic orbitals, which can be combined to define the molecular orbitals (MOs). Each of these orbitals are constructed following the linear combination of atomic orbitals (LCAO), which simply consists of

$$\psi_i = \sum_{\mu}^{2N} C_{\mu i} \phi_{\mu} \qquad (19)$$

Of particular interest are the alternant hydrocarbons, for which topological arguments provide useful insights on the properties of MOs and consequently on the electronic structure of the ground state. An alternant hydrocarbon is a compound consisting of carbon and hydrogen atoms only, presenting a conjugated system of π electrons where all carbon atoms can be divided into two sets (starred, not-starred) so that no atom of one set is directly linked to other atom of the same set. Generally, those compounds are assumed to be planar, which is not always true but provides a simplification for drawing some very important conclusions. For instance, it allows a strict separation of σ and π electrons because symmetric arguments do not allow their mixing. The first works dealing with these compounds were based on the simple Hückel model, which led to the Coulson and Rushbrooke pairing theorem[5] stating that for any alternant hydrocarbon: (1) the π-electron energy levels are symmetrically distributed about the zero energy level; (2) the LCAO-MO associated with the energy level ε_i is the same as that belonging to the energy level $-\varepsilon_i$ except for a difference of sign (only) in every other atomic orbital coefficient; (3) the total π-electron charge density at any carbon atom in the molecule equals unity. This theorem is important because it is at the basis of the topological arguments discussed in chapter 4, which allow rationalizing the appearance of unpaired electrons in neutral molecules with an even number of electrons.

There is a large amount of theoretical works dealing with alternant hydrocarbons, which cover very diverse areas such as graph theory and topology. A sound explanation on the mathematical concepts behind these arguments can be found in the book by Gutman and Polanksy.[6]

2.1.1.3. Spin-Adapted Configurations.

The computational investigation of magnetic properties requires working with energies of solutions that have been calculated taking into proper account the quantum mechanical nature of spin. Therefore, it is necessary to briefly define the spin.

For a single electron, its spin angular momentum is defined as

$$\vec{s} = s_x \vec{\imath} + s_y \vec{\jmath} + s_z \vec{k} \tag{20}$$

The squared magnitude of the vector $\vec{s}$ is a scalar operator

$$s^2 = \vec{s} \cdot \vec{s} = s_x^2 + s_y^2 + s_z^2 \tag{21}$$

where each of the components satisfy the commutation relations

$$[s_x, s_y] = is_z \qquad [s_y, s_z] = is_x \qquad [s_z, s_x] = is_y \tag{22}$$

It is generally more convenient to work with the ladder operators, expressed as

$$s_+ = s_x + is_y \qquad\qquad s_+ = s_x - is_y \tag{23}$$

which allows rewriting the squared spin operator as

$$s^2 = s_+ s_- - s_z + s_z^2 \qquad\qquad s^2 = s_- s_+ + s_z + s_z^2 \tag{24}$$

In a given many-electron system, the total spin angular momentum operator is the vector sum of the spin vectors of each electron

$$\vec{S} = \sum_{i=1}^{N} \vec{s}(i) \tag{25}$$

From here it follows that the total squared-magnitude, total spin components and ladder operators are, respectively:

$$S^2 = \vec{S} \cdot \vec{S} = \sum_{i=1}^{N} \sum_{j=1}^{N} \vec{s}(i) \cdot \vec{s}(j) \qquad S_I = \sum_{I=1}^{N} s_I(i) \quad I = x, y, z \qquad S_\pm = \sum_{i=1}^{N} s_\pm(i) \tag{26}$$

The action of these spin operators on specific functions is exemplified in section 2 of chapter 3.

Now, the spin of a system is defined by the complete set of states $|S, M_S\rangle$ which are simultaneously eigenfunctions of the squared total spin $\hat{S}^2$ and its z component $\hat{S}_z$ operators.

$$S^2|S, M_S\rangle = S(S + 1)|S, M_S\rangle \tag{27}$$

$$S_z|S, M_S\rangle = M_S|S, M_S\rangle \tag{28}$$

where S is a quantum number defining the total spin and multiplicity $(2S + 1)$ and M_S is another quantum number describing the z component of the total spin.

Within the time-independent non-relativistic formulation, the electronic Hamiltonian used (eqn (3)) does not contain any spin coordinates. This implies that the operators S^2 and S_z commute with the electronic Hamiltonian $[H, S^2] = 0 = [H, S_z]$, and consequently the exact electronic eigenfunctions are also eigenfunctions of the spin operators.

$$S^2|\Phi\rangle = S(S + 1)|\Phi\rangle \tag{29}$$

$$S_z|\Phi\rangle = M_S|\Phi\rangle \tag{30}$$

This correspondence and its extension to some spin Hamiltonians is at the core of the mapping approach discussed in next chapter. Any single determinant is an eigenfunction of S_z, but not necessarily of S^2. However, by combining certain determinants it is possible to construct a wave function that is eigenfunctions of S^2, resulting in a spin-adapted configuration

$$|\Phi\rangle = \sum_1^N c_N |\psi_i\psi_j \cdots \psi_k\rangle \tag{31}$$

An exhaustive review on how to obtain the c_N coefficients and construct the spin eigenfunctions can be found in the book by Pauncz.[7]

2.1.2.   Single Determinant Approach: Hartree-Fock Approximation.

For a *N*-electron system, the simplest antisymmetric wave function describing its ground state is a single Slater determinant

$$|\Psi_0\rangle = |\chi_i \chi_j \cdots \chi_N\rangle \tag{32}$$

Within the approximations discussed, the variational principle allows obtaining the optimum set of spin orbitals $\{\chi_i\}$ that minimize the electronic energy and is the best approximation to the ground state of the *N*-electron system

$$E_0 = \langle \Psi_0 | \hat{H}_{elec} | \Psi_0 \rangle = \sum_i \langle i|h|i\rangle + \frac{1}{2} \sum_{ij} \langle ij\|ij\rangle \tag{33}$$

An additional constrain to the spin orbitals is that they remain orthonormal $\langle \chi_i | \chi_j \rangle = \delta_{ij}$. The equation for the best spin orbitals is the Hartree-Fock integro-differential equation

$$
\begin{aligned}
h(1)\chi_i(1) &+ \sum_{i \neq j} \left[\int d\mathbf{x}_2 |\chi_j(2)|^2 r_{ij}^{-1} \right] \chi_i(1) - \sum_{i \neq j} \left[\int d\mathbf{x}_2 \chi_j^*(2)\chi_i(2)r_{ij}^{-1} \right] \chi_j(1) \\
&= \varepsilon_i \chi_i(1)
\end{aligned}
\tag{34}
$$

where

$$h(1) = -\frac{1}{2}\nabla_i^2 - \sum_A \frac{Z_A}{r_{iA}} \tag{35}$$

is a one-electron operator describing the kinetic energy and potential energy for attraction to the nuclei of a single electron. The two other terms in the left-hand side represent two electron operators, named the Coulomb J_j and Exchange K_j operators, respectively. The orbital energy of spin orbital χ_i is ε_i. The integrals associated with these operators are

$$h_{ii} = \langle \chi_i(1)|h|\chi_i(1)\rangle \tag{36}$$
$$J_{ij} = \langle \chi_i(1)\chi_j(2)|r_{ij}^{-1}|\chi_i(1)\chi_j(2)\rangle \tag{37}$$
$$K_{ij} = \langle \chi_i(1)\chi_j(2)|r_{ij}^{-1}|\chi_j(1)\chi_i(2)\rangle \tag{38}$$

The Coulomb integral (J_{ij}) represents the repulsion that electron *i* causes to the electron *j*, while the exchange integral (K_{ij}) does not have a classical physical meaning, since its origin is set in the antisymmetry principle. It accounts for the correlation of electrons

with the same spin. A deeper insight is given in chapter 4, when discussing different strategies to increase the value of the K_{ij} integral as a manner to stabilize open-shell states in purely organic compounds.

It is possible to define an operator including the three operators, which results in the Fock operator

$$f(1) = h(1) + \sum_j J_j(1) - K_j(1) \tag{39}$$

or alternatively $f(1) = h(1) + v^{HF}(1)$. $v^{HF}(1)$ stands for the average potential experienced by the electron-1 due to the presence of the other electrons. Thus, the Hartree-Fock equation can be rewritten as an eigenvalue problem

$$f(\mathbf{x}_1)\chi_i(\mathbf{x}_1) = \varepsilon_i\chi_i(\mathbf{x}_1) \tag{40}$$

Within the HF formalism, the whole problematic reduces to which set of orbitals are used to solve eqn (40); either restricted spatial orbitals, resulting in the Roothaan equation, or unrestricted spin orbitals leading to Pople-Nesbet equations.

2.1.2.1. Restricted Closed-Shell Hartree-Fock: Roothaan Equations.

For the description of closed-shell systems, where all spin orbitals are doubly occupied such as standard neutral molecules, a further simplification can be introduced, by assuming that the spatial part for α and β in each spin orbital is the same

$$\chi_i(\mathbf{x}) = \begin{cases} \psi_j(\mathbf{r})\alpha(\omega) \\ or \\ \psi_j(\mathbf{r})\beta(\omega) \end{cases} \tag{41}$$

This fact allows integration over the spin part, thus leaving only the spatial part of each monoelectronic function. Thus, the closed-shell restricted Hartree-Fock (RHF) ground state is $|\Psi_0\rangle = |\chi_1\chi_2\cdots\chi_N\rangle = |\psi_1\bar{\psi}_1\psi_2\bar{\psi}_2\cdots\psi_{N/2}\bar{\psi}_{N/2}\rangle$ and the expression for the associated energy is

$$E_0 = \langle\Psi_0|\hat{H}_{elec}|\Psi_0\rangle = 2\sum_i h_{ii} + \sum_i\sum_j(2J_{ij} - K_{ij}) \tag{42}$$

where J_{ij} and K_{ij} are the two-electron integrals associated with the Coulomb and Exchange operators.

The introduction of a basis, like the one in eqn (19), allowed Roothaan to redefine the RHF equations, leading to Roothaan equations.[8]

$$\mathbf{FC} = \mathbf{SC}\boldsymbol{\varepsilon} \tag{43}$$

where **F** is the Fock matrix, the elements of which write as $F_{\mu v} = \int d\mathbf{r}_1\, \phi_\mu^*(1) f(1) \phi_v(1)$, **S** is the overlap matrix with elements $S_{\mu v} = \int d\mathbf{r}_1\, \phi_\mu^*(1)\phi_v(1)$, **C** is the matrix of expansion coefficients $C_{\mu i}$ and $\boldsymbol{\varepsilon}$ is a diagonal matrix of the orbital energies ε_i. Through iteratively solving this equation with a given initial guess of atomic orbitals as starting point, by means of the Self Consistent Field (SC) approach, one gets the best set of spatial orbitals that approximate the ground state of the *N*-electron system and their corresponding energies.

2.1.2.2. Unrestricted Open-Shell Hartree-Fock: Pople-Nesbet Equations.

The electronic structure of a given molecule, or *N*-electron system, cannot always be described by means of doubly occupied orbitals. The existence of unpaired electrons ultimately explains the appearance of magnetic properties in matter, which is a fact. Therefore, it is necessary to count with methodologies capable of describing the electronic structure of compounds with a marked open-shell character. The two more common approaches are the restricted open-shell (ROHF) and the unrestricted open-shell (UHF) formalisms. Comparatively, in the former all electrons except the unpaired ones occupy closed-shell orbitals, whereas the latter does not impose this restriction to any electron. Additionally, at variance with ROHF, UHF wave functions are not eigenfunctions of the S^2 operator.

While for the Roothaan equations one works with a set of restricted spatial orbitals, for deriving Pople-Nesbet equations one uses a set of unrestricted spin orbitals

$$\chi_i(\mathbf{x}) = \begin{cases} \psi_j^\alpha(\mathbf{r})\alpha(\omega) \\ \quad or \\ \psi_j^\beta(\mathbf{r})\beta(\omega) \end{cases} \tag{44}$$

meaning that electrons with α spin are described by a set of spatial orbitals $\{\psi_j^\alpha | j = 1, 2, \cdots, K\}$ which is different from the set of spatial orbitals $\{\psi_j^\beta | j = 1, 2, \cdots, K\}$ used to describe β electrons. Introducing this set in eqn (40) and deriving the expressions for the Fock operator, the total energy can be expressed as a sum of all contributions

$$E_0 = \sum_i^{N^\alpha} h_{ii}^\alpha + \sum_i^{N^\beta} h_{ii}^\beta + \frac{1}{2}\sum_i^{N^\alpha}\sum_j^{N^\beta}\left(J_{ij}^{\alpha\alpha} - K_{ij}^{\alpha\alpha}\right) - \frac{1}{2}\sum_i^{N^\alpha}\sum_j^{N^\beta}\left(J_{ij}^{\beta\beta} - K_{ij}^{\beta\beta}\right)$$
$$+ \sum_i^{N^\alpha}\sum_j^{N^\beta} J_{ij}^{\alpha\beta} \tag{45}$$

As done for the restricted case, the introduction of a basis function to expand the molecular orbitals leads to the Pople-Nesbet equations, defined for each of the α and β orbitals

$$\mathbf{F}^\alpha \mathbf{C}^\alpha = \mathbf{S}\mathbf{C}^\alpha \boldsymbol{\varepsilon}^\alpha \tag{46}$$
$$\mathbf{F}^\beta \mathbf{C}^\beta = \mathbf{S}\mathbf{C}^\beta \boldsymbol{\varepsilon}^\beta \tag{47}$$

where the different terms hold the same meaning as in eqn (43). As mentioned, the wave functions obtained are not eigenfunctions of S^2 operator.

To summarize, HF method represents a good first approximation to the electronic electronic problem and provides a reasonably accurate description of the ground state of a *N*-electron system. However, it lacks a correct description of electron correlation, because the electron-electron interaction is replaced by an average interaction ($v^{HF}(1)$ eqn (39)). Electron correlation can be defined as the difference in energy between the HF and the exact energy in a given basis set within the Born-Oppenheimer approximation, and is of crucial importance in molecules with open-shell states and multi reference character, as is the case for the investigated molecules in this thesis. For magnetic properties, one usually uses calculated energies of electronic states with different multiplicities, for which the effect of correlation might be very different. Therefore it is necessary to count with methodologies capable of addressing electron correlation. Those normally start with a HF wave function and include electron correlation either via configuration interaction (CI), perturbation theory (PT) or Coupled Clusted (CC). The first two will be outlined in the forthcoming section.

2.1.2.3. Full Configuration Interaction (CI): Electron Correlation.

Consider a determinant as a result of promoting one electron occupying the χ_a spin orbital of the HF ground state to a virtual spin orbital χ_r. The obtained singly excited determinant has the form will be referred to as $|\Psi_a^r\rangle$. Similarly, a doubly excited determinant would be $|\Psi_{ab}^{rs}\rangle$. All $\binom{2K}{N}$ determinant can thus be classified as either HF

ground state or singly, doubly, $\cdots$, *N*-tuply excited determinants, which are used to expand the exact ground state wave function $|\Phi_0\rangle$ of the system

$$|\Phi_0\rangle = c_0|\Psi_0\rangle + \sum_{ra} c_a^r|\Psi_a^r\rangle + \sum_{\substack{a<b \\ r<s}} c_{ab}^{rs}|\Psi_{ab}^{rs}\rangle + \sum_{\substack{a<b<c \\ r<s<t}} c_{abc}^{rst}|\Psi_{abc}^{rst}\rangle + \cdots \tag{48}$$

This is the form of the full CI. The summation over $a < b$ means summing over all a and over all b greater than a. The exact solutions are the eigenvalues of the Hamiltonian matrix with elements $\langle\Psi_i|H|\Psi_i\rangle$ formed by the complete set $\{|\Psi_i\rangle\}$, where each $|\Psi_i\rangle$ is called a configuration interaction (CI). However, the introduction of a set of spin orbitals $\{\chi_i|i = 1,2,\cdots,2K\}$ implies that the $\binom{2K}{N}$ determinants formed from them do not constitute a complete *N*-electron basis. Still, by diagonalizing the finite Hamiltonian matrix spanned in the complete set of determinants would lead to the exact energy within this basis.

Correlation energy is then defined, as stated by Löwdin in 1959, as:

"The correlation energy for a certain state with respect to a specified Hamiltonian is the difference between the exact eigenvalue of the Hamiltonian and its expectation value in the HF approximation for the state under consideration."

• Truncated CI.

Despite the fact of being able of accessing the exact energy of the ground state by means of full CI, it is practically impossible to perform a full CI calculation on a system of interest, further than H_2 dimers. With a one-electron basis of moderate size, there are so many possible spin-adapted configurations that the full CI matrix becomes impossibly large.

A manner of reducing the complexity of the full CI matrix, is by truncating the CI expansion for the wave function in eqn (48). The most used truncations consist of neglecting all *N*-tuply excited determinants except those associated with single and double excitations. The resulting energy is no longer the exact one, but due to the variational principle, it constitutes an upper-bound for the energy. However, truncating the CI presents the size-consistency problem.

- •   Rayleigh-Schrödinger Perturbation Theory and Møller-Plesset Partitioning.

Another widely used way of including electronic correlation is by means of perturbation theory (PT), as originally developed by Rayleigh and Schrödinger. Before commenting on Møller-Plesset, approach, some conclusions and expressions of PT are highlighted An extensive review on the foundations and applications of perturbation theory can be found elsewhere.[9]

The main idea is to split the Hamiltonian in two terms: a zero[th] order unperturbed Hamiltonian $\hat{H}_0$, the energies and eigenvalues of which are known (for instance through HF equations), and a perturbation term $\hat{V}$ assumed to be small when compared to $\hat{H}_0$.

$$\hat{H} = \hat{H}_0 + \lambda\hat{V} \tag{49}$$

where $\lambda \in [0,1]$ is the perturbation parameter. If $\lambda = 0$ or $\lambda = 1$, the system is not perturbed of fully perturbed, respectively. Thus, the eigenvalue problem to solve is expressed as

$$\hat{H}|\Phi_i\rangle = (\hat{H}_0 + \lambda\hat{V})|\Phi_i\rangle = \varepsilon_i|\Phi_i\rangle \tag{50}$$

where $\hat{H}_0|\Psi_i^0\rangle = E_i^0|\Psi_i^0\rangle$, or written more compactly, $\hat{H}_0|i\rangle = E_i^0|i\rangle$. Then, expanding the eigenfunctions and eigenvalues of the perturbed system in a Taylor series in λ, gives

$$\varepsilon_i = E_i^0 + \lambda E_i^1 + \lambda^2 E_i^2 + \cdots \tag{51}$$
$$|\Phi_i\rangle = |i\rangle + \lambda|\Psi_i^1\rangle + \lambda^2|\Psi_i^2\rangle + \cdots \tag{52}$$

where E_i^n is the *n* th-order energy. Assuming the wave functions of $\hat{H}_0$ as normalized ($\langle i|i\rangle = 1$), the normalization for $|\Phi_i\rangle$ is the intermediate normalization $\langle i|\Phi_i\rangle = 1$. Substituting eqn (51 and 52) into eqn (50), one gets

$$\begin{aligned}(\hat{H}_0 + \lambda\hat{V})(|i\rangle + \lambda|\Psi_i^1\rangle + \lambda^2|\Psi_i^2\rangle + \cdots) \\ = (E_i^0 + \lambda E_i^1 + \lambda^2 E_i^2 + \cdots)|i\rangle + \lambda|\Psi_i^1\rangle + \lambda^2|\Psi_i^2\rangle \\ + \cdots\end{aligned} \tag{53}$$

And equating coefficients on λ^n, the following expressions are obtained

$$\hat{H}_0|i\rangle = E_i^0|i\rangle \qquad\qquad n = 0 \quad (54.1)$$
$$\hat{H}_0|\Psi_i^1\rangle + \hat{V}|i\rangle = E_i^0|\Psi_i^1\rangle + E_i^1|i\rangle \qquad\qquad n = 1 \quad (54.2)$$
$$\hat{H}_0|\Psi_i^2\rangle + \hat{V}|\Psi_i^1\rangle = E_i^0|\Psi_i^2\rangle + E_i^1|\Psi_i^1\rangle + E_i^2|i\rangle \qquad n = 1 \quad (54.3)$$
$$\cdots$$

Now, multiplying each of the equations by $\langle i|$ and using the intermediate normalization, the expressions for the n*th*-order energies are

$$E_i^0 = \langle i|\hat{H}_0|i\rangle \tag{55.1}$$

$$E_i^1 = \langle i|\hat{V}|i\rangle \tag{55.2}$$

$$E_i^2 = \langle i|\hat{V}|\Psi_i^1\rangle \tag{55.2}$$

$$\cdots$$

Then, solving eqns (54) for $|\Psi_i^n\rangle$ one can obtain the nth order energies from eqns (55).

Since $\hat{H}_0$ is hermitian and thus has a set of non-degenerate eigenfunctions that are orthogonal and form a complete space, each $|\Psi_i^n\rangle$ correction can be expressed as a linear combination of $\hat{H}_0$ eigenfunctions $|n\rangle$. For instance, for the first-order wave function can be expressed as

$$|\Psi_i^1\rangle = \sum_n c_n^1 |n\rangle \qquad \text{with } \langle n|\Psi_i^1\rangle = c_n^1 \tag{56}$$

and from eqn (54.2), rewritten in the form

$$\left(E_i^0 - \hat{H}_0\right)|\Psi_i^1\rangle = \left(\hat{V} - E_i^1\right)|i\rangle = \left(\hat{V} - \langle i|\hat{V}|i\rangle\right)|i\rangle \tag{57}$$

multiplied by $\langle n|$, and using the orthogonality of the zero[th] order wave functions, we obtain

$$(E_i^0 - E_n^0)\langle n|\Psi_i^1\rangle = \langle n|\hat{V}|i\rangle \tag{58}$$

Using the expansion in eqn (56) in the expression for the second order energy eqn (55.2), we have

$$E_i^2 = \langle i|\hat{V}|\Psi_i^1\rangle = {\sum_n}' \langle i|\hat{V}|n\rangle\langle n|\Psi_i^1\rangle \tag{59}$$

where the prime in the summation indicates that the term $n = i$ is excluded. Finally, using eqn (58), we obtain

$$E_i^2 = {\sum_n}' \frac{\langle i|\hat{V}|n\rangle\langle n|\hat{V}|i\rangle}{E_i^0 - E_n^0} = {\sum_n}' \frac{|\langle i|\hat{V}|n\rangle|^2}{E_i^0 - E_n^0} \tag{60}$$

which is the expression for the second order energy, expressed in terms of the zero[th] order energies and the perturbation elements between the eigenfunctions of the $\hat{H}_0$.

Møller-Plesset (MP), based on the Rayleigh-Schrödinger perturbation theory, published in 1934 an approach to introduce electron correlation in atomic and molecular systems[10] starting from the HF wavefunction as its zero[th] order wavefunction.

By analogy with the Rayleigh-Schrödinger PT, here the zero[th] order Hamiltonian is the sum of fock operators (see eqn (39)) and is expressed as

$$\widehat{H}_0 = \sum_i \hat{f}(i) = \sum_i \left(\hat{h}(i) + \sum_j \hat{J}_j(i) - \widehat{K}_j(i) \right) \tag{61}$$

while the perturbed Hamiltonian is defined as

$$\hat{V} = \sum_i \sum_{j>i} \frac{1}{r_{ij}} - \sum_i \sum_j \hat{J}_j(i) - \widehat{K}_j(i) \tag{62}$$

Now, from eqns (55.1 and 55.2) we can obtain the first order correction to the energy, which is precisely the closed-shell HF energy,

$$E_i^0 + E_i^1 = \langle i | \widehat{H}_0 | i \rangle + \langle i | \hat{V} | i \rangle = 2 \sum_i \varepsilon_i + \sum_i \sum_j (2J_{ij} - K_{ij}) = E_{RHF} \tag{63}$$

meaning that for obtaining any correction, it is necessary to go to second order terms. From eqn (55.2) and using Condon-Slater rules and Brillouin's theorem, which states that only double excitations bring non-zero contributions to the energy, the second order energy correction is expressed as

$$E_i^2 = \sum_{a<b} \sum_{r<s} \frac{\left| \langle i | \hat{V} | \Psi_{ab}^{rs} \rangle \right|^2}{\varepsilon_a + \varepsilon_b - \varepsilon_r - \varepsilon_s} \tag{64}$$

Where Ψ_{ab}^{rs} is the doubly-excited Slater determinant and ε are the orbital energies of the corresponding occupied ($\varepsilon_a, \varepsilon_b$) and unoccupied ($\varepsilon_r, \varepsilon_s$) canonical orbitals. The sum of the HF energy and the second order energy correction, yields the total MP2 energy

$$E_{MP2} = E_{HF} + \sum_{a<b} \sum_{r<s} \frac{\left| \langle i | \hat{V} | \Psi_{ab}^{rs} \rangle \right|^2}{\varepsilon_a + \varepsilon_b - \varepsilon_r - \varepsilon_s} \tag{65}$$

Higher order terms can be similarly obtained, but MP2 provides already a good description, provided that the ground state can be approached with a single determinant. At variance with variational methods like CI, perturbation theory does not present an

upper bound to energy, which implies that moving to a higher order correction does not guarantee a better description.

2.1.3. Multi Reference Approaches.

The previous section has dealt with single determinant approaches, meaning that the ground state is described with only one Slater determinant. However, open-shell systems normally are multi-configurational in nature, due to the low-lying states, and more than one Slater determinant is required for their description. Those are the multi reference approaches, among which multi-configurational self-consitent fielf (MSCSF) and multi-reference perturbation theory (MRPT) are widely used throughout this thesis.

2.1.3.1. Multi-Configuration Self- Consistent Field Method.

Consider a multideterminantal wave function that is expressed as a linear combination of configuration state functions (CSF), which are symmetry-adapted linear combinations of Slater determinant (see section 2.1.13).

$$|\Psi_{MCSCF}\rangle = \sum_I c_I |\Psi_I\rangle \tag{66}$$

The multi configurational self-consistent field (MCSCF) wave function represents a truncation of the CI expansion. The key point is that in this approach, both the coefficients of the determinants (c_I) and the coefficients of the orbitals used to expand the determinants are variationally optimized within the SCF procedure. For a closed-shell system, if only one determinant is included in the expansion of eqn (66), MCSCF and HF methods become identical.

A significant problem is the choice of configurations to be included in eqn (66). The most commonly used approach is defining a complete active space (CAS), which divides the initial set of orbitals into three subsets: inactive, active, and external orbital spaces. The first consists of a set of orbitals that remain doubly occupied in all CSF. The active orbital space allows all possible CSF combination among the number of electrons chosen and the orbitals of this subset. Finally, all external orbitals remain unoccupied in all CSF. Within the CAS, all excitations of any order are allowed, trying to capture the most relevant terms to describe the molecular properties of interest. For instance, in a benzene molecule, a reasonable CAS space would be six electrons in six

centres, since this defines the delocalization of the π–system. This would be denoted as CAS(6,6). Within the CAS subset, the accounted energy is normally referred to as static correlation energy, while the obtained from excitation of the CAS space with the rest of configurations is called dynamic correlation. If the coefficients of the orbitals are not optimized, the corresponding approach is denoted as CASCI, and within the CAS space it would correspond to a full CI. CASCI is a particular case of multi reference CI approach.

What makes MCSCF approaches so appealing is their capacity for optimizing the orbital coefficients. A self-consistent formulation was given by Roos and Taylor,[11] leading to the complete active space self-consistent field (CASSCF) approach. A schematic representation of the previous discussion and a comparison to HF method and to the multi reference perturbation theory approach (which is discusses in firthcoming sections) is presented in Figure 1.
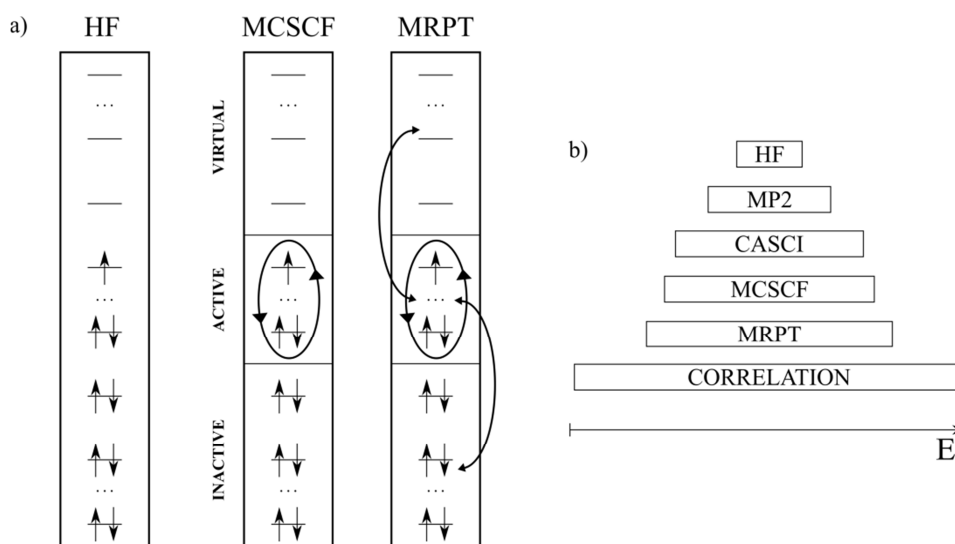
Figure 1. a) Comparison of the orbital distribution in HF methods and multi reference approaches, which introduce correlation either through variation (MCSCF) or perturbation (MRPT). In MCSCF (and in MRCI) the electronic correlation is accounted within a CAS space. In MRPT, on top of the CAS space, excitations coming from outside are accounted for. b) Scheme indicating that the common goal of all methods is describing properly the electronic correlation. Sizes do not indicate proportionality.

2.1.3.2. Difference Dedicated Configuration Interaction.

In a similar manner as for the single determinant formulation one can expand the wave function in terms of excited Slater determinants (eqn (48)) referred to a zero[th] order HF wave function, in multi reference approaches the wave function can be expanded in terms of excited CSF where the zero[th] order function is no longer a single determinant, but a MCSCF function.

As in the case of eqn (48), the excitations to the zero[th] order function are normally truncated to the second order, leading to the singles-doubles MRCI. These excitations might be classified according to what they generate;[12] either a hole or a particle, as indicated in Figure 2. These singles and doubles excitations are performed on top of the all-orders excitations inside the CAS, and account for the so-called dynamic correlation.
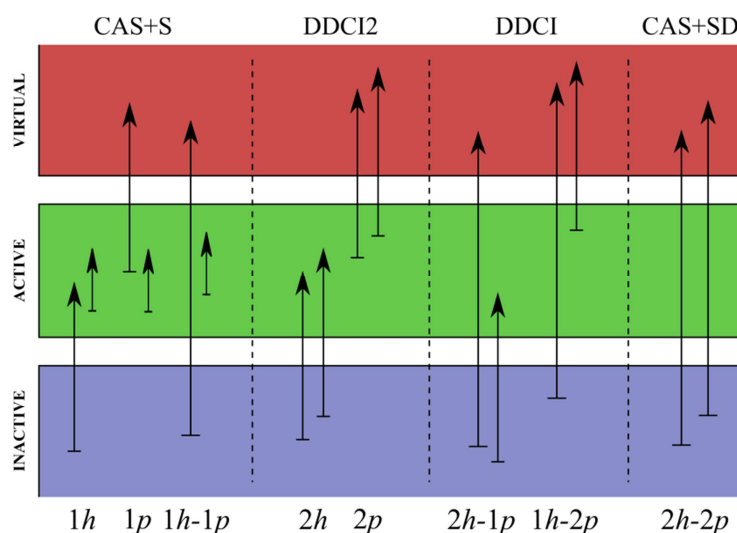
Figure 2. Classes of excitations to be added (from left to right) to the CAS space to generate the various multireference CI spaces according to singles-doubles CI (MR-SDCI) following the number of holes (*h*) and particles (*p*) created in the inactive and virtual orbitals, respectively. This figure comes from Figure 10 in[12].

An exhaustive explanation of the physical contributions brought by each of the excitations is provided in the review by Malrieu *et al.*, from which Figure 2 is extracted. Normally, a calculation with a large enough CAS plus simples and doubles is considered as a reference calculation.

However, to account for dynamic correlation, one can make use of some simplifications that allow neglecting particular excitations, because they bring the same energetic correction to the magnetic states of interests that are being studied, and

therefore when compared, the correction is cancelled. This is precisely the idea behind the difference dedicated configuration interaction (DDCI) method,[12,13] based on the early observation that many terms in the nth-order correction to the wave function and energy are the same for ground and excited states.[14] The computational application of this method implies working with the same set of orbitals for all magnetic states, because otherwise the energetic cancellations do not occur.

2.1.3.3. Multi-Reference Perturbation Theory.

By analogy to the MP2 discussion, one can introduce corrections to the zeroth order wave function by means of perturbation theory, being the reference function a multi configurational one, as for instance a CASSCF wave function.

There are two main schemes on multi-references perturbation theory, depending on whether it is a contracted or uncontracted scheme. Contracted stands for situations in which the perturbation vectors are linear combinations of single determinants, the ratio of which is imposed by the variational solution of the reference wave function. Among them are the CASPT2[15–17] and NEVPT2[18–21] methods. On the other hand, in uncontracted methods such as multi reference Møller-Plesset (MRMP),[22–24] all singly and doubly excited determinants obtained from each of the determinants in the reference wave function are considered.

2.2. Density Functional-Based Methods.
2.2.1. Density Functional Theory.

Density functional theory (DFT) is an alternative approach for the description of the electronic structure of a *N*-electron system. The foundations of this theory lay in the Hohenberg and Kohn[25] theorems, stating that the ground-state electronic energy is entirely determined by the first-order electron density, which is the square of the wave function integrated over *N-1* electron coordinates. This is a quantity that depends only on three coordinates, independently of the number of electrons.

The first theorem has its origins in the Thomas-Fermi electron gas model.[26,27] This model states that for a system consisting of uniformly distributed electrons under the influence of a nuclear field, the properties of the ground state are expressed as a

function of electron density. Further improvements where brought by Dirac[28,29] and Bloch,[30] resulting in the Thomas-Fermi-Dirac model. Based on these early works, the first theorem of Hohenberg and Kohn states that *"The external potential $V_{ext}(\mathbf{r})$ of a nondegenerate electronic state is (to within a constant) a unique functional of the electron density; since, in turn $V_{ext}(\mathbf{r})$ fixes the Hamiltonian, we see that the full many particle ground state is a unique functional of $\rho(\mathbf{r})$."* Therefore, $\rho(\mathbf{r})$ determines both the Hamiltonian and the wave function of the system which translates into knowing every expectation value of any observable of the ground sate. Defining the Hamiltonian as:

$$\hat{H} = \hat{F}_{HK} + \hat{V}_{ext} \tag{67}$$

the energy is expressed as a functional of the electron density

$$E_v[\rho] = F_{HK}[\rho] + \int \rho(r)\hat{V}_{ext}(r)dr \tag{68}$$

where $F_{HK}[\rho] = T[\rho] + V_{ee}[\rho]$ is the Hohenberg-Kohn functional (also known as universal functional) and represents the sum of the potential-independent electronic terms constituted by the kinetic energy $T[\rho]$ and electron-electron repulsion $V_{ee}[\rho]$.

The second theorem takes advantage of the variational principle establishing a lower bond for $E_v[\rho]$ which indeed is the energy of the ground state E_0. It states that *"for a trial density $\rho(\mathbf{r})$ such that $\rho(\mathbf{r}) \geq 0$ and $\int \rho(r)dr \geq N$:*

$$E_0 \leq E_v[\rho] \tag{69}$$

where $E_v[\rho]$ is the energy functional"

Stated in a reversed manner, if the trial density is the one corresponding to the ground state $\rho_0(\mathbf{r})$, the obtained energy is also the energy of the ground state. Thus, to obtain the exact ground state density, it is necessary to minimize the density with respect to the energy $\delta E_v[\rho]/\delta\rho = 0$.

The two Hohenberg and Kohn theorems served as the foundation of modern density functional theory (DFT). However, they do not provide the expression for $F_{HK}[\rho]$ universal functional. Kohn and Sham proposed a similar strategy to HF method, based on a systems of non-interacting electrons.[31] The ansatz proposed by Kohn and Sham assumes that the ground state of the original interacting system is that of some chosen

virtual non-interacting system, which can be exactly soluble (by numerical means) and with all the many-body terms incorporated into an exchange-correlation functional of the density. By solving the equations one can find the ground state density and energy of the original interacting system with the accuracy limited by the approximations in the exchange-correlation functional.

Within this approximation, the ground state is assumed to be a single Slater determinant $\Psi_{KS} = det\{\varphi_i\}$ where φ_i are the eigenfunctions of the non-interacting Hamiltonian containing only single electron terms:

$$\hat{h}_{KS}(r) = -\frac{1}{2}\nabla^2 + v_{KS}(r) \tag{70}$$

Where $v_{KS}(r)$ is the external potential. Thus, the energy can be expressed as

$$E[\rho] = F_{HK}[\rho] + V_{Ne}[\rho] \tag{71}$$

where $V_{Ne}[\rho]$ is the electron-nuclei potential interaction and $F_{HK}[\rho]$ is the Hohenberg-Kohn functional, expressed as:

$$F_{HK}[\rho] = T_g[\rho] + J_g[\rho] + E_{xc}[\rho] \tag{72}$$

In this expression, $T_g[\rho]$ is is the kinetic energy of a non-interacting gas of density, $J_g[\rho]$ is the classical coulombic energy and $E_{xc}[\rho]$ is the exchange-correlation energy, which expression is:

$$E_{xc}[\rho] = \left(T[\rho] - T_g[\rho]\right) + \left(V_{ee}[\rho] - J[\rho]\right) \tag{73}$$

$E_{xc}[\rho]$ accounts for the difference between the interacting description and the non-interacting description of a many-electron system. The first term is the difference between the kinetic energies of the interacting and non-interacting systems, while the second term is the correction on the total electron interaction energy and the coulombic electron-electron repulsion. Given that the $E_{xc}[\rho]$ is known, the exact ground state energy and density of the many-body electron problem could be calculated exactly. However, the exact expression of the correlation-exchange functional is not known, and therefore has to be approximated. Usually, $E_{xc}[\rho]$ is also expressed as a sum of the exchange and correlation functionals $E_{xc}[\rho] = E_C[\rho] + E_X[\rho]$. Several modifications and improvements can be added to each of the two terms, which explains the amount of

different functionals available in the literature. Currently, DFT has become a widespread tool.[32]

2.2.2. Exchange-Correlation Functionals.

There are several strategies to approximate $E_{xc}[\rho]$. The most common ones are the local density approximation (LDA), the generalized gradient approximation (GGA), the hybrid functionals and the range-separated functionals.

LDA is based on the homogeneous electrons gas density, thus assuming that in every point of the space, $E_{xc}[\rho]$ depends only on the local density ρ

$$E_{xc}^{LDA}[\rho] = \int \varepsilon_{LDA}(\rho)dr \qquad (74)$$

where $\varepsilon_{LDA}(\rho)$ is given by the Dirac Formula.

GGA introduces an additional dependence referred to the gradient of the density, resulting in the following expression of the $E_{xc}[\rho]$

$$E_{xc}^{GGA}[\rho] = \int \varepsilon_{GGA}(\rho, \nabla\rho)dr \qquad (75)$$

The gradient-dependant corrections can affect both the correlation and/or the exchange terms, leading to numerous functionals which generally attempt to reproduce experimental results. The most common one for molecular systems within this approach is the PBE functional.[33] An important improvement was brought by the inclusion of an additional dependence of the $E_{xc}[\rho]$ on the Laplacian of the density, leading to the meta-GGA approaches. Therefore, the expression for the $E_{xc}[\rho]$ is

$$E_{xc}^{mGGA}[\rho] = \int \varepsilon_{mGGA}(\rho, \nabla\rho, \nabla^2\rho)dr \qquad (76)$$

The definition of m-GGA functionals may also include semi-empirical parameters and the dependence on the Laplacian can be introduced either in the exchange term, the correlation term, or to both. This results in a variety of functionals, as for instance the M06L.[34]

Hybrid functionals: This strategy incorporates a given amount of exact exchange, as defined within HF theory (eqn(38)) with exchange and correlation obtained by empirically or by *ab initio* calculations. The most popular hybrid functional, which is

also the most commonly used along this thesis, is the three-parameter B3LYP functional.[35] It is defined as follows: for the exchange part, a mixture of 80% of LDA exchange with 20% of HF exchange (with an amount of Becke's correction ΔE_x^{B88} for the exchange part); for the correlation part, the mixing involves 19% of the Vosko-Wilk-Nusair functional with 81% of Lee-Yang-Par correlation, resulting in

$$E_{xc}^{B3LYP} = 0.8E_x^{LDA} + 0.2E_x^{HF} + 0.8\Delta E_x^{B88} + 0.19E_c^{VWN} + 0.81E_c^{LYP} \qquad (77)$$

Another important hybrid functional is the PBE0, which mixes 25% of exact (HF) exchange with 75% of PBE exchange, while describing the correlation solely with PBE

$$E_{xc}^{PBE0} = 0.25E_x^{HF} + 0.75E_x^{PBE} + E_c^{PBE} \qquad (78)$$

The analysis of how short- and long-range interactions decay,[36,37] unveiled two major deficiencies of hybrid functionals with uniform mixing of Fock exchange when applied to solids and molecules. For the former case, the nonlocal exchange interaction has an unphysical and extremely slow spatial decay in metallic systems. For molecules, the asymptotic decay of the exchange potential is incorrectly described since the exact exchange potential decays asymptotically as $-1/r$ while that of a hybrid functional with a fraction c of nonlocal exchange decays as a $-c/r$, which might affect the description of properties such as Rydberg excitations and polarizabilities of long chains. For magnetic properties, it is known that B3LYP tends to overestimate the calculated values of the exchange coupling constants.

Range separated functionals: The main idea behind this strategy is smoothing out the inconvenient physical/numerical behavior of the exact exchange in a given range by defining a way to switch on/off Fock exchange (in the exchange functional) through a given radius used to discriminate the short- and long-range electron-electron interactions. In order to do so, one can define a Gauss-type smooth partitioning function that depends on the value $u = |\mathbf{r}_1 - \mathbf{r}_2|$

$$\text{erf}(\omega u) = \frac{2}{\sqrt{\pi}} \int_0^{\omega|\mathbf{r}_1 - \mathbf{r}_2|} e^{-t^2} dt \qquad (79)$$

and its complementary error function

$$\text{erfc}(\omega u) = 1 - \text{erf}(\omega u) = \frac{2}{\sqrt{\pi}} \int_{\omega|\mathbf{r}_1 - \mathbf{r}_2|}^{\infty} e^{-t^2} dt \qquad (80)$$

By defining

$$\frac{1}{u} = \frac{\text{erfc}(\omega u)}{u} + \frac{\text{erf}(\omega u)}{u} \tag{81}$$

it is possible to switch on a given percent of the Fock exchange in one or the other domain of u values. Heyd *et al.*[38,39] proposed a short-range corrected hybrid functional (HSE) by modifying the hybrid PBE functional as follows

$$E_{xc}^{HSE}(\omega) = aE_x^{SR-HF}(\omega) + (1-a)E_x^{SR-PBE}(\omega) + E_x^{LR-PBE}(\omega) + E_c^{PBE}(\omega) \tag{82}$$

where the hybrid functional is switched on at short electron-electron distances only, whereas the PBE GGA functional is used at long electron-electron distances. A long-range separated hybrid functional of special interest for the purpose of this thesis, since it aims to restore the proper asymptotic limit in molecules, was proposed by Vydrov and Scuseria.[40] It is the so-called LC$-\omega$PBE functional and is defined as:

$$E_{xc}^{\text{LC}-\omega\text{PBE}}(\omega) = E_x^{LR-HF}(\omega) + E_x^{SR-PBE}(\omega) + E_c^{PBE} \tag{83}$$

The performance of HSE and LC$-\omega$PBE functionals for the prediction of magnetic interactions in a variety of compounds, ranging from localized binuclear Cu(II) complexes to organic diradicals was investigated.[41] It was found that range-separated functionals performed better than B3LYP hybrid functional.

2.2.3. Long-Range Interactions: Empirical Dispersion Correction.

The performance of standard density functional methods, where no special corrections for dispersion effects are included, in describing long range interactions is known to be poor.[42–45] Long range interactions are of importance in large systems, as for instance biomolecules and nanoparticles, where several different regions are susceptible to distinct London dispersion interactions.[46]

Particularly, in $\pi-$conjugated interacting systems the inclusion of dispersion corrections is crucial to obtain an accurate description. As a matter of fact, for a benzene dimer sandwiched face-to-face with D_{6h} symmetry, CCSD(T) calculations describe a minimum in the potential energy at a distance of ~3.9 Å showing a stabilization due to interaction energy of ~1.65 Kcal/mol;[47] however, both B3LYP and PBE provide

repulsive interaction energies along the same potential energy surface.[48] This makes mandatory the addition of extra terms accounting for dispersion corrections when using standard DFT methods.

Following this reasoning, and based on an idea previously proposed for Hartree-Fock calculations,[49,50] Grimme proposed a general empirical dispersion correction for density functional calculations[51] which was further extended to more chemical elements and functionals.[52] The dispersion correction is simply add to the Kohn-Sham energy, resulting in an expression for the total energy

$$E_{DFT-D} = E_{KS-DFT} + E_{disp} \tag{84}$$

where E_{KS-DFT} is the usual self-consistent Kohn–Sham energy as obtained from the chosen functional and E_{disp} is an empirical dispersion correction with an expression

$$E_{disp} = -s_6 \sum_{i=1}^{N_{at}-1} \sum_{j=i+1}^{N_{at}} \frac{C_6^{ij}}{R_{ij}^6} f_{dmp}(R_{ij}) \tag{85}$$

N_{at} stands for the number of atoms, C_6^{ij} is the dispersion coefficient for atom pair ij, s_6 refers to a global scaling factor that depends on the density functional used and R_{ij}^6 denotes the interatomic distance. It is worth noting that it is to the sixth power, as is characteristic of the long range interactions. In order to avoid near-singularities for small R, a damping function f_{dmp} is necessary, which is defined as

$$f_{dmp}(R_{ij}) = \frac{1}{1 + e^{-d(R_{ij}/R_r - 1)}} \tag{86}$$

where R_r is the sum of atomic van der Waals radii. A $d = 20$ value is employed in the original paper.[52] Finally, the interatomic parameters C_6^{ij} are calculated as the geometric mean of the individual atomic values C_6^i, which are empirically obtained[52]

$$C_6^{ij} = \sqrt{C_6^i \cdot C_6^j} \tag{87}$$

For the particular purposes of this thesis, especially for the results presented in Chapter 4, the inclusion of dispersion correction terms has proved to be critical for the correct description of structures in extended systems.

2.3. Remarks on the Theoretical Description of Magnetism in Periodic Systems.

2.3.1. General Considerations.

A crystal (periodic system in general) is characterized by an ordered repetition of a structural element or motif, which may be either a single atom or a group of atoms. This repetition can be described through a symmetry operator, which allows treating the whole system considering only the irreducible structural element, also known as the unit cell. The infinite array in which the repeated units of the crystal are arranged is specified by the Bravais lattice.[53] This lattice consists of all points with position vectors $\mathbf{R}$ of the form

$$\mathbf{R} = n_1\mathbf{a}_1 + n_2\mathbf{a}_2 + n_3\mathbf{a}_3 \tag{88}$$

where $\mathbf{a}_1$, $\mathbf{a}_2$ and $\mathbf{a}_3$ are the primitive vectors and span the lattice, and n_1, n_2 and n_3 correspond to the elemental translations, which range through all integer values. Thus, the position of the infinite number of translationally symmetric atoms in the lattice is given by $\sum_{i=1}^{3} x_{s,i} a_i$ where $x_{s,i}$ are the atomic fractional coordinates

Consider a set of points $\mathbf{R}$ constituting a Bravais lattice and a plane wave $e^{i\mathbf{k}-r}$. The set of all wave vectors $\mathbf{K}$ that yield planes waves with the periodicity of a given Bravais lattice is its reciprocal lattice, also known as momentum space or k-space. Analitically, $\mathbf{K}$ belongs to the reciprocal lattice of a Bravais lattice of points $\mathbf{R}$ provided that the relations

$$e^{i\mathbf{K}\cdot(\mathbf{r}+\mathbf{R})} = e^{i\mathbf{K}\cdot r} \qquad\qquad e^{i\mathbf{K}\cdot(\mathbf{R})} = 1 \tag{89}$$

hold for any $\mathbf{r}$ and all $\mathbf{R}$ in the Bravais lattice.

The reciprocal lattice is mathematical construction that simplifies the description of the properties of periodic crystalline lattices, and its use is very convenient for performing analytic studies of periodic systems. Each crystalline lattice $A = \{\mathbf{a}_1, \mathbf{a}_2, \mathbf{a}_3\}$ has its corresponding reciprocal lattice $B = \{\mathbf{b}_1, \mathbf{b}_2, \mathbf{b}_3\}$ satisfying

$$\mathbf{b}_i = 2\pi \frac{\mathbf{a}_j \times \mathbf{a}_k}{\mathbf{a}_i \cdot (\mathbf{a}_j \times \mathbf{a}_k)} \qquad \forall_{i,j,k} \in \{1,2,3\} \text{ and } \mathbf{a}_i \cdot \mathbf{b}_j = 2\pi\delta_{i,j} \tag{90}$$

This allows writing any vector $\mathbf{k}$ as a linear combination of the $\mathbf{b}_i$

$$\mathbf{k} = k_1\mathbf{b}_1 + k_2\mathbf{b}_2 + k_3\mathbf{b}_3 \tag{91}$$

From here it follows that

$$\mathbf{k} \cdot \mathbf{R} = 2\pi(k_1 n_1 + k_2 n_2 + k_3 n_3) \tag{92}$$

For $e^{i\mathbf{K} \cdot (\mathbf{R})} = 1$ to hold (eqn(89)), $\mathbf{k} \cdot \mathbf{R}$ must be 2π times an integer for any choices of the integers n_i what implies that k_i have to be integers. These particularities on the set of $\mathbf{k}$ vectors indicate the possibility of describing periodic systems using plane waves and the reciprocal space, as stated by Bloch.

The description of the wave function of a *N*-electron system subject to periodic conditions is based on the Bloch theorem.[30] This theorem has helped establishing the theoretical framework for the analysis of periodic systems using the reciprocal space. It takes advantage of the periodicity of the potential throughout the crystal, which permits ensuring that, for a given position in the lattice, the properties therein defined will be the same as in any other equivalent position throughout the whole lattice. In other words, it is enough to consider only the first Brillouin zone to reproduce the properties of the entire lattice.

Given that the ions in a perfect crystal are arranged in a regular periodic way, the associated potential $U(\mathbf{r})$ must also have the periodicity of the underlying Bravais lattice

$$U(\mathbf{r} + \mathbf{R}) = U(\mathbf{r}) \tag{93}$$

Thus, the Schrödinger equation that must be solved involves a single electron Hamiltonian

$$H\psi = \left(-\frac{h^2}{2m}\nabla^2 + U(\mathbf{r})\right)\psi = \varepsilon\psi \tag{94}$$

In this situation, Bloch's theorem states that the eigenstates ψ of the one-electron Hamiltonian (as defined in eqn(94) with the condition in eqn(93)) for all $\mathbf{R}$ in a Bravais lattice, can be chosen to have the form of a plane wave times a function with the preriodicity of the Bravais lattice

$$\psi_{n\mathbf{k}}(\mathbf{r}) = e^{i\mathbf{k} \cdot \mathbf{r}} u_{n\mathbf{k}}(\mathbf{r}) \tag{95}$$

where $u_{n\mathbf{k}}(\mathbf{r} + \mathbf{R}) = u_{n\mathbf{k}}(\mathbf{r})$ for all $\mathbf{R}$ in Bravail lattice. Alternatively, Bloch's theorem can be stated as: the eigenstates of H can be chosen so that associated with each ψ is a wave vector $\mathbf{k}$ such that

$$\psi(\mathbf{r} + \mathbf{R}) = e^{i\mathbf{k}\cdot\mathbf{R}}\psi(\mathbf{r}) \qquad (96)$$

for every Bravais lattice. The energy of the periodic system is then calculated as the average of the energy of all k-points considered. Because there is an infinite number of k points in the Brillouin zone, the wave function is calculated for only a grid of points that is sufficiently dense to ensure that accurate enough averages are obtained

Bloch functions are those for which the Bloch theorem is valid and are described as eigenfunctions of the translation operators of the lattice. Bloch functions are eigenfunctions of the Hamiltonian of a periodic system because the wave function must have the same symmetry properties as the lattice ($\widehat{H}$ must commute with the translation operators of the lattice). Therefore, the periodicity of the lattice determines the properties of the crystal.

2.3.2. Crystal Program.

All periodic calculation performed in this thesis have been carried out using CRYSTAL09 program.[54,55] The CRYSTAL program computes the electronic structure of periodic systems within Hartree Fock, density functional or various hybrid approximations, and expresses the Bloch functions of the periodic systems as linear combinations of atom centred Gaussian functions. These serve to define the crystalline orbitals, from which all one-electron properties are calculated, such as population analysis, band structure or density of states.

All performed calculations are spin-unrestricted, where the number of unpaired electrons in the cell is fixed, through the keyword SPINLOCK.

2.3.3. Extraction of Magnetic Interaction in Simple 1D and 2D Examples.

This section aims to exemplify the extraction of the most relevant magnetic exchange interactions in two simple extended cases: a linear chain and a planar network of arranged spins.

The magnetic interactions are assumed to be isotropic, localized and well described with an Ising Hamiltonian,[56] which is expressed as
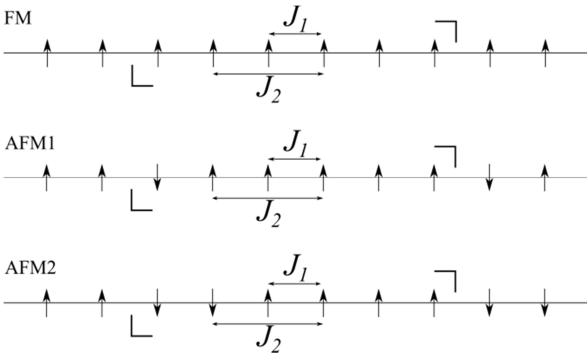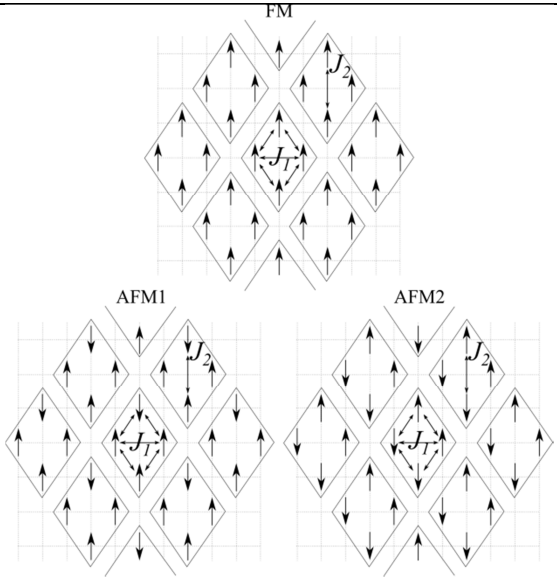
$$\hat{H}^{Ising} = - \sum_{<i,j>} J_{ij} \cdot \hat{S}_i^z \cdot \hat{S}_j^z \tag{97}$$

where J_{ij} is the exchange coupling constant between centres i and j and the $\langle i,j \rangle$ symbol indicates that the sum refers to nearest neighbour interactions only. $\hat{S}_i^z$ is the z-component of the spin operator. If this operator acts on a α spin (spin-up), the expected value is $+1/2$. If the operator acts on a β spin (spin-down), the expected value is $-1/2$. A deeper discussion about the model spin Hamiltonians is provided in Chapter 3, so here the discussion is restricted to show how to apply the Ising Hamiltonian to periodic systems to extract the J_{ij} values.

The number of exchange coupling constant relevant for defining the low-lying magnetic solutions depends on the system under study. One has to make sure to count with the necessary solutions that allow solving the system of equations for all important exchange coupling constants; that is, if there are *N* relevant exchange coupling constant, it is required to have (*N*+1) different solutions that yield a set of *N* linearly independent equations, at least. The parameter that allows defining the convenient amount of solutions is the magnetic cell. The unit cell is the most basic repeating structure needed to replicate the nuclear coordinates in an ordered crystal, but it might not be sufficient to replicate the magnetic order of interest. Then, by discarding some spatial symmetry operations, it is possible to define a larger cell containing the sufficient number of magnetic centres to describe the magnetic solutions of interest. Once the magnetic cell is defined, the different magnetic solutions are defined by considering successive spin-reversals in each of the magnetic centres. Thus, the ferromagnetic solution (FM) displays all of the magnetic centres with the highest *S* value and the different antiferromagnetic solutions (AFM$_i$ $i = 1, N - 1$) represent combinations of all possible *S* values. Additionally, being able to define different magnetic cells allows checking whether the extracted exchange coupling values are consistent.

Scheme 1 introduces two cases that serve as examples to extract the magnetic interactions in a periodic system. Before going into detail, it is convenient to address some common aspects. Since the magnetic interaction involves pairs of neighbours, those interacting inside the magnetic cell contribute with one exchange coupling

constant, while those interactions crossing the magnetic cell contribute with half the exchange coupling constant. If the interaction is between centres of the same spin, the sign of the exchange coupling constant is negative, while if different spin centres are involved, the sign becomes positive. In order to justify this consider two electrons (A and B) with spin-up interacting. According to eqn (97), their interaction is described as $\hat{H}^{Ising} = -J\hat{S}_A^z \cdot \hat{S}_B^z = -J \cdot 1/2 \cdot 1/2 = -J/4$. Similarly, if the A and B electrons have spin-down, their interaction is described as $\hat{H}^{Ising} = -J\hat{S}_A^z \cdot \hat{S}_B^z = -J \cdot (-1/2) \cdot (-1/2) = -J/4$. Finally, if electrons A and B have different spin, the sign of the interaction is reversed $\hat{H}^{Ising} = -J\hat{S}_A^z \cdot \hat{S}_B^z = -J \cdot (-1/2) \cdot 1/2 = +J/4$.

	1 dimensional		2 dimensional	
	Energy	$\Delta E_{\text{FM-AFM}}$	Energy	$\Delta E_{\text{FM-AFM}}$
FM	$-^6/_4 (J_1 + J_2)$		$-3(J_1 + J_2)$	
AFM1	$-^1/_2 (J_1 + J_2)$	$-J_1 - J_2$	0	$-3(J_1 + J_2)$
AFM2	$^1/_2 (-J_1 + J_2)$	$-J_1 - 2J_2$	$J_1 + J_2$	$-4(J_1 + J_2)$

Scheme 1

The leftmost case in Scheme 1 is a simple linear arrangement of equally distanced $S = 1/2$ magnetic centres. By choice, the magnetic cell presents six magnetic centres, as indicated by the brackets. Assuming that the most relevant magnetic interactions are those involving nearest (J_1) and second-nearest (J_2) neighbours only, three magnetic solutions are required in order to have two energetic differences that provide enough equations. Those solutions are named FM, AFM$_1$ and AFM$_2$; FM corresponds to the

high-spin case (all magnetic centres are forced to have the same spin) and AFM_1 and AFM_2 present one and two spin-down respectively. As an example, the calculation of the energy expression for the FM case is inspected in more detail. Following these arguments, the rest of the expressions are easy to obtain. Thus, there are 5 nearest neighbours interactions inside the magnetic cell and two (one from the left and one from the right extremes, contributing half each) outside the cell. Since all the spins are up in the FM solution, it results in $-6J_1 \left(\frac{1}{2}\right)^2$. For the second neighbour's interactions, there are 4 inside the magnetic cell and 4 more (which correspond to 2) outside the magnetic cell. Again, given that all centres have the same spin, it results in $-6J_2 \left(\frac{1}{2}\right)^2$. The sum of these two terms corresponds to $-6/_4 (J_1 + J_2)$. Following this reasoning, the expression for the AFM_1 and AFM_2 in Scheme 1 are easy to check. The only difference is that those interactions involving electrons of different spin imply a reversal of the magnetic coupling constant sign. One is left with two linearly independent energy differences expressions. Then, by computing these solutions within the CRYSTAL program, the actual energetic values can be obtained and the set of equations solved.

For the two dimensional case, the situation is a bit more complex because there are more interactions involved, but the reasoning is the same. Here, and also by choice, inside the magnetic cell there are 4 $S = 1/2$ magnetic centres. In total, there are 19 nearest neighbours (J_1) (5 inside and 14 outside) and 23 second-nearest neighbours (J_2) (1 inside and 22 outside). Within this magnetic cell, there are three different magnetic solutions, which would be enough for obtaining two magnetic coupling constants. However, since in AFM_1 all magnetic interactions vanish, the two energy differences are linearly dependent (Scheme 1) and cannot be used to extract both J_1 and J_2. This illustrates an example where, if there are no arguments for neglecting J_2 and simplifying the scheme, it would be required to define a different magnetic cell.

This concludes the chapter devoted to present and discuss the theoretical background behind each of the computational method used.

(1)   Szabo, A.; Ostlund, N. S. *Modern Quantum Chemistry: Introduction to Advanced Electronic Structure Theory*; Dover Publications, INC: Mineola, New York, 1989.

(2)   Born, M.; Oppenheimer, R. Zur Quantentheorie Der Molekeln. *Ann. Phys.* **1927**, *389* (20), 457–484.

(3)   Wilson, S. *Electron Correlation in Molecules*; Dover Publications, INC: New York, 1984.

(4)   Valeev, E. F.; Sherrill, C. D. The Diagonal Born–Oppenheimer Correction beyond the Hartree–Fock Approximation. *J. Chem. Phys.* **2003**, *118* (9), 3921.

(5)   Coulson, C. A.; Rushbrooke, S. No Title. *Proc. Camb. Phil. Soc.* **1940**, *36*, 193.

(6)   Gutman, I.; Polansky, O. E. *Mathematical Concepts in Organic Chemistry*; Springer-Verlag: New York, 1986.

(7)   Pauncz, R. *Spin Eigenfunctions*; Springer US: Boston, MA, 1979.

(8)   Roothaan, C. C. J. New Developments in Molecular Orbital Theory. *Rev. Mod. Phys.* **1951**, *23* (2), 69–89.

(9)   Hirschfelder, J. O.; Brown, W. B.; Epstein, S. T. Recent Developments in Perturbation Theory. *Adv. Quantum Chem.* **1964**, *1*, 255–374.

(10)   Møller, C.; Plesset, M. S. Note on an Approximation Treatment for Many-Electron Systems. *Phys. Rev.* **1934**, *46* (7), 618–622.

(11)   Roos, B. O.; Taylor, P. R.; Si≑gbahn, P. E. M. A Complete Active Space SCF Method (CASSCF) Using a Density Matrix Formulated Super-CI Approach. *Chem. Phys.* **1980**, *48* (2), 157–173.

(12)   Malrieu, J. P.; Caballol, R.; Calzado, C. J.; de Graaf, C.; Guihéry, N. Magnetic Interactions in Molecules and Highly Correlated Materials: Physical Content, Analytical Derivation, and Rigorous Extraction of Magnetic Hamiltonians. *Chem. Rev.* **2014**, *114* (1), 429–492.

(13)   Miralles, J.; Castell, O.; Caballol, R.; Malrieu, J.-P. Specific CI Calculation of Energy Differences: Transition Energies and Bond Energies. *Chem. Phys.* **1993**, *172* (1), 33–43.

(14)   Malrieu, J. P. Cancellations Occurring in the Calculation of Transition Energies by a Perturbation Development of Configuration Interaction Matrices. *J. Chem. Phys.* **1967**, *47* (11), 4555.

(15)   Roos, B. O.; Linse, P.; Siegbahn, P. E. M.; Blomberg, M. R. A. A Simple Method for the Evaluation of the Second-Order-Perturbation Energy from External Double-Excitations with a CASSCF Reference Wavefunction. *Chem. Phys.* **1982**, *66* (1-2), 197–207.

(16) Andersson, K.; Malmqvist, P. A.; Roos, B. O.; Sadlej, A. J.; Wolinski, K.
      Second-Order Perturbation Theory with a CASSCF Reference Function. *J. Phys.
      Chem.* **1990**, *94* (14), 5483–5488.

(17) Andersson, K.; Malmqvist, P.-A.; Roos, B. O. Second-Order Perturbation Theory
      with a Complete Active Space Self-Consistent Field Reference Function. *J.
      Chem. Phys.* **1992**, *96* (2), 1218.

(18) Angeli, C.; Cimiraglia, R.; Evangelisti, S.; Leininger, T.; Malrieu, J.-P.
      Introduction of N-Electron Valence States for Multireference Perturbation
      Theory. *J. Chem. Phys.* **2001**, *114* (23), 10252.

(19) Angeli, C.; Cimiraglia, R.; Malrieu, J.-P. N -Electron Valence State Perturbation
      Theory : A Fast Implementation of the Strongly Contracted Variant. *Chem. Phys.
      Lett.* **2001**, *350* (3-4), 297–305.

(20) Angeli, C.; Cimiraglia, R.; Malrieu, J.-P. N-Electron Valence State Perturbation
      Theory: A Spinless Formulation and an Efficient Implementation of the Strongly
      Contracted and of the Partially Contracted Variants. *J. Chem. Phys.* **2002**, *117*
      (20), 9138.

(21) Angeli, C.; Pastore, M.; Cimiraglia, R. New Perspectives in Multireference
      Perturbation Theory: The N-Electron Valence State Approach. *Theor. Chem.
      Acc.* **2006**, *117* (5-6), 743–754.

(22) Hirao, K. Multireference Møller—Plesset Method. *Chem. Phys. Lett.* **1992**, *190*
      (3-4), 374–380.

(23) Hirao, K. Multireference Møller-Plesset Perturbation Treatment of Potential
      Energy Curve of N2. *Int. J. Quantum Chem.* **1992**, *44* (S26), 517–526.

(24) Hirao, K. Multireference Møller—Plesset Perturbation Theory for High-Spin
      Open-Shell Systems. *Chem. Phys. Lett.* **1992**, *196* (5), 397–403.

(25) Hohenberg, P. Inhomogeneous Electron Gas. *Phys. Rev.* **1964**, *136* (3B), B864–
      B871.

(26) Thomas, L. H. The Calculation of Atomic Fields. *Proc. Camb. Phil. Soc.* **1927**,
      23 (542-548).

(27) Fermi, E. Eine Statistische Methode Zur Bestimmung Einiger Eigenschaften Des
      Atoms Und Ihre Anwendung Auf Die Theorie Des Periodischen Systems Der
      Elemente. *Zeitschrift für Phys.* **1928**, *48*, 73–79.

(28) Dirac, P. A. M. Note on the Exchange Phenomena in the Thomas Atom. *Proc.
      Camb. Phil. Soc.* **1930**, *26*, 545–555.

(29) Dirac, P. A. M. The Quantum Theory of the Electron. *Proc. R. Soc. A* **1928**, *117*,
      610–623.

(30) Bloch, F. Bemerkung Zur Elektronentheorie Des Ferromagnetismus Und Der Elektrischen Leitfähigkeit. *Zeitschrift für Phys.* **1929**, *57* (7-8), 545–555.

(31) Kohn, W.; Sham, L. J. Self-Consistent Equations Including Exchange and Correlation Effects. *Phys. Rev.* **1965**, *140* (4A), A1133–A1138.

(32) Jones, R. O. Density Functional Theory: Its Origins, Rise to Prominence, and Future. *Rev. Mod. Phys.* **2015**, *87* (3), 897–923.

(33) Perdew, J. P.; Burke, K.; Ernzerhof, M. Generalized Gradient Approximation Made Simple. *Phys. Rev. Lett.* **1996**, *77* (18), 3865–3868.

(34) Zhao, Y.; Schultz, N. E.; Truhlar, D. G. Exchange-Correlation Functional with Broad Accuracy for Metallic and Nonmetallic Compounds, Kinetics, and Noncovalent Interactions. *J. Chem. Phys.* **2005**, *123* (16), 161103.

(35) Becke, a D. Density Functional Thermochemistry. III. The Role of Exact Exchange 98:5648-52. *J Chem Phys* **1993**, *103* (3-4), 361–363.

(36) Henderson, T. M.; Izmaylov, A. F.; Scuseria, G. E.; Savin, A. The Importance of Middle-Range Hartree-Fock-Type Exchange for Hybrid Density Functionals. *J. Chem. Phys.* **2007**, *127* (22), 221103.

(37) Della Sala, F.; Görling, A. Asymptotic Behavior of the Kohn-Sham Exchange Potential. *Phys. Rev. Lett.* **2002**, *89* (3), 033003.

(38) Heyd, J.; Scuseria, G. E.; Ernzerhof, M. Hybrid Functionals Based on a Screened Coulomb Potential. *J. Chem. Phys.* **2003**, *118* (18), 8207.

(39) Heyd, J.; Scuseria, G. E.; Ernzerhof, M. Erratum: "Hybrid Functionals Based on a Screened Coulomb Potential" [J. Chem. Phys. 118, 8207 (2003)]. *J. Chem. Phys.* **2006**, *124* (21), 219906.

(40) Vydrov, O. A.; Scuseria, G. E. Assessment of a Long-Range Corrected Hybrid Functional. *J. Chem. Phys.* **2006**, *125* (23), 234109.

(41) Rivero, P.; Moreira, I. de P. R.; Illas, F.; Scuseria, G. E. Reliability of Range-Separated Hybrid Functionals for Describing Magnetic Coupling in Molecular Systems. *J. Chem. Phys.* **2008**, *129* (18), 184110.

(42) Kristyán, S.; Pulay, P. Can (semi)local Density Functional Theory Account for the London Dispersion Forces? *Chem. Phys. Lett.* **1994**, *229* (3), 175–180.

(43) Hobza, P.; Sponer, J.; Reschel, T. Density Functional Theory and Molecular Clusters. *J. Comput. Chem.* **1995**, *16* (11), 1315–1325.

(44) Pérez-Jordá, J.; Becke, A. D. A Density-Functional Study of van Der Waals Forces: Rare Gas Diatomics. *Chem. Phys. Lett.* **1995**, *233* (1-2), 134–137.

(45)   Pérez-Jordá, J. M.; San-Fabián, E.; Pérez-Jiménez, A. J. Density-Functional Study of van Der Waals Forces on Rare-Gas Diatomics: Hartree–Fock Exchange. *J. Chem. Phys.* **1999**, *110* (4), 1916.

(46)   Stone, A. *The Theory of Intermolecular Forces*, 2nd Ed.; Oxford University Press: Oxford, 2013.

(47)   Sherrill, C. D.; Takatani, T.; Hohenstein, E. G. An Assessment of Theoretical Methods for Nonbonded Interactions: Comparison to Complete Basis Set Limit Coupled-Cluster Potential Energy Curves for the Benzene Dimer, the Methane Dimer, Benzene−Methane, and Benzene−H2S. *J. Phys. Chem. A* **2009**, *113* (38), 10146–10159.

(48)   Grimme, S. Density Functional Theory with London Dispersion Corrections. *Wiley Interdiscip. Rev. Comput. Mol. Sci.* **2011**, *1* (2), 211–228.

(49)   Hepburn, J.; Scoles, G.; Penco, R. A Simple but Reliable Method for the Prediction of Intermolecular Potentials. *Chem. Phys. Lett.* **1975**, *36* (4), 451–456.

(50)   Ahlrichs, R.; Penco, R.; Scoles, G. Intermolecular Forces in Simple Systems. *Chem. Phys.* **1977**, *19* (2), 119–130.

(51)   Grimme, S. Accurate Description of van Der Waals Complexes by Density Functional Theory Including Empirical Corrections. *J. Comput. Chem.* **2004**, *25* (12), 1463–1473.

(52)   Grimme, S. Semiempirical GGA-Type Density Functional Constructed with a Long-Range Dispersion Correction. *J. Comput. Chem.* **2006**, *27* (15), 1787–1799.

(53)   Ashcroft, N. W. Mermin, N. D. *Ashcroft & Mermin*; Saunders College Publishing: New York, 1976.

(54)   Dovesi, R.; Orlando, R.; Civalleri, B. CRYSTAL: A Computational Tool for the Ab Initio Study of the Electronic Properties of Crystals. *Z. Krist.* **2005**, *220*, 571–573.

(55)   Dovesi, R.; Saunders, V. R.; Roetti, C.; Orlando, R.; Zicovich-Wilson, C. M.; Pascale, F.; Civalleri, B.; Doll, K.; Harrison, N. M.; Bush, I. J.; et al. CRYSTAL09 User's Manual. *University of Torino*. Torino 2009.

(56)   Ising, E. Beitrag Zur Theorie Des Ferromagnetismus. *Zeitschrift für Phys.* **1925**, *31* (1), 253–258.

Consistent Mapping Approaches for an Accurate Extraction of Magnetic Exchange Interactions in Heterobinuclear and Trinuclear Coordination Complexes.

3.1. Introduction.

Molecular magnetism has experienced a remarkable success due to achievements in coordination chemistry, allowing for the creation of a vast library of magnetic compounds.[1,2] The employed metallic centres expand throughout the whole periodic table, ranging from transition metal ions to lanthanides and actinides. For the ligands, the same variability on the number and nature of the coordinating atoms is found. As a consequence of such large collection of compounds, diverse magnetic behaviours have been observed, as for instance bistability, single molecular magnets (SMMs), zero-field splitting, spin crossover and magnetic anisotropy among others.[1,3] At the basis of this success lies the capacity of establishing magneto-structural relationships, which depend critically on the information obtained through single-crystal X-ray diffraction. Normally, the recorded magnetic data depend on the temperature at which the samples were measured and ideally this dependence can be tracked down by relating it to structural changes in the single crystal. Structural freedom in these compounds generally affects distances and angles between well-defined molecular units in the crystal packing. In a way, this lies between what is observed for ionic solids, which experience rather abrupt phase transitions affecting large areas of the solid as a whole, and purely organic compounds, where the impact of structural freedom might also affect each of the molecular entities individually. In this sense, and from a general perspective, coordination compounds offer important advantages for studying magnetic properties theoretically. They present an almost fixed molecular structure over a range of temperatures and magnetic orbitals largely localized in the metallic centres. As a result, the number of parameters that can affect the observed magnetic properties is reduced, which converts them in an appropriate framework to apply electronic structure methods. As an early indication, chapter 4 goes a step further and deals with organic polyradicals showing a higher degree of complexity, presenting larger delocalization of the magnetic orbitals over a π-conjugated system and inherent structural flexibility.

An accurate theoretical description of the electronic structure in coordination magnetic compounds is prior to extracting the most relevant exchange coupling constants. Knowledge on these couplings values allows for establishing magneto-structural relationships, which helps in the design of architectures with enhanced properties. Due to the nature of the low-lying energetic states in these sort of systems,

their theoretical description requires accounting for static and dynamic electronic correlation. Ideally, one would aim at treating the electronic structure with the high accuracy attained with multi-reference wave function-based methods, such as CASSCF, CASPT2 or MRCI methodologies, at the computational cost of single determinant approaches, as DFT-based methods. That is precisely the goal of the mapping approach.

This chapter deals with the mapping approach and effective Hamiltonian theory for an accurate extraction of the relevant magnetic exchange interactions, in some coordination compounds of increasing complexity. The chapter is divided as follows: In section 3.2 the concept of mapping approach is revised, both when using spin adapted and broken symmetry (BS) solutions. The standard mapping approach, originally proposed by Noodleman,[4-6] aims at bringing together both solutions, by recovering the energy and wave function of the spin adapted functions by means of broken symmetry solutions. This approach has proved to be a very efficient strategy,[7] but it requires the use of a spin projector in order to relate the spin adapted and the BS solutions. As it will be discussed, the mapping approach presents two weak points, which will be respectively treated in papers #3.1 and #3.2. Paper #3.1 studies a family of heterodinuclear complexes with $S_1 = 1; S_2 = 1/2$ localized moments in centres 1 and 2, and paper #3.2 moves to a general three-centre three-electron case, where no symmetry operation relates the magnetic centres, which is exemplified by a trinuclear Cu(II) complex with $S_1 = S_2 = S_3 = 1/2$ localized moments. In section 3.3, effective Hamiltonian theory is briefly discussed and presented as the rigorous and accurate manner for extracting exchange coupling constants. Due to its complex mathematical structure and the need for a customized development for each particular situation, it cannot be applied as a routine computational strategy. However, it serves to validate the computationally cheaper approach proposed in paper #3.2. Finally, section 3.4 introduces the mentioned papers and section 3.5 summarizes and discusses the presented results.

3.2. Mapping Approach.

The mapping approach appears as an accurate and computationally efficient manner of extracting magnetic exchange interactions in transition metal complexes, organic radicals and periodic systems.[8] For a given magnetic problem, it consists of describing the energy and electronic distribution of the pure spin states by means of broken symmetry solutions using a spin projector.

In a general sense, the mapping approach relies on a one-to-one correspondence between three energetic spectra, one being the exact and the other two being spin model Hamiltonians. This is schematically depicted in Scheme 1. First, it takes advantage of the fact that both the exact, non-relativistic, time independent Hamiltonian and the
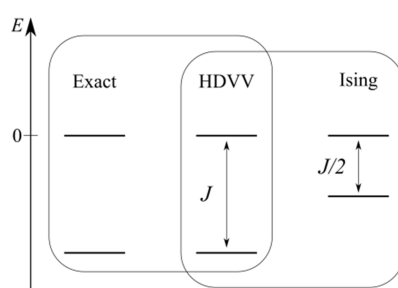
Scheme 1. Representation of the idea behind the mapping approach.

Heisenberg-Dirac-van Vleck (HDVV) spin Hamiltonian, commute with the total spin operator (see section 2.1.1.3 of chapter 2). This means that there exists a set of functions which are eigenfunctions of both Hamiltonians. And second, it exploits the correspondence between the HDVV spectra and the eigenfunctions of the Ising Hamiltonian, which can be assigned to BS solutions, as originally developed by Noodleman[4–6]. Then, the main goal is to univocally match the three spectra, which will allow for an accurate theoretical extraction of the magnetic interaction based on *ab-initio* methods.

The following two sub-sections aim at explaining each of the mentioned correspondences, respectively.

3.2.1. Mapping Approach Based on spin Adapted Wave Functions. HDVV Hamiltonian.

Spin adapted wave functions are eigenfunctions of the phenomenological (HDVV) spin Hamiltonian. This Hamiltonian[9–11] describes the isotropic interaction between localized magnetic moments $\boldsymbol{S}_i$ and $\boldsymbol{S}_j$ as

$$\widehat{H}^{HDVV} = -\sum_{\langle i,j \rangle} J_{ij} \widehat{\boldsymbol{S}}_i \cdot \widehat{\boldsymbol{S}}_j \tag{1}$$

where J_{ij} is the exchange coupling constant between the $\widehat{\boldsymbol{S}}_i$ and $\widehat{\boldsymbol{S}}_j$ localized spin moments and the $\langle i,j \rangle$ symbol indicates that the sum refers to nearest neighbour interactions only. According to the adopted definition in eqn (1), a positive value of the exchange coupling constant J_{ij} corresponds to ferromagnetic interactions, while negative values describe an antiferromagnetic interaction (parallel and antiparallel spins alignments respectively). The number, sign and magnitude of the most relevant J_{ij} determine the low-energy spectrum of the problem and consequently the magnetic ordering of the system. It is worth noting that spin adapted wave functions are also eigenfunctions of the total squared spin operator $\hat{S}^2 = \widehat{\boldsymbol{S}}_x \cdot \widehat{\boldsymbol{S}}_x + \widehat{\boldsymbol{S}}_y \cdot \widehat{\boldsymbol{S}}_y + \widehat{\boldsymbol{S}}_z \cdot \widehat{\boldsymbol{S}}_z$, given that $\left[\widehat{H}^{HDVV}, \hat{S}^2\right] = 0$.

Before going into detail with the description of the mapping approach using spin adapted wave functions, and the corresponding energetic distribution of the magnetic states, it is worth addressing in few words how the different spin operators work. This will be helpful for the discussion of forthcoming sections. Consider $|j, m\rangle$ as the eigenfunctions of angular momentum operator with j and m as eigenvalues. Being $\hat{\jmath}_+$ and $\hat{\jmath}_-$ the associated ladder operators, expressed as a function of the Cartesian operators as

$$\hat{\jmath}_+ = \hat{\jmath}_x + i\hat{\jmath}_y \tag{2.1}$$
$$\hat{\jmath}_- = \hat{\jmath}_x - i\hat{\jmath}_y \tag{2.2}$$

the action on the spin functions writes as:

$$\langle j, m | \hat{\jmath}^2 | j', m' \rangle = j(j+1)\delta_{jj'}\delta_{mm'} \tag{2.3}$$
$$\langle j, m | \hat{\jmath}_z | j', m' \rangle = m\delta_{jj'}\delta_{mm'} \tag{2.4}$$
$$\langle j, m | \hat{\jmath}_\pm | j', m' \rangle = [j(j+1) - m'(m' \pm 1)]^{1/2}\delta_{jj'}\delta_{mm' \pm 1} \tag{2.5}$$

Now, for the simplest case of one unpaired electron, the possible spin functions are $|1/2, \alpha\rangle$ and $|1/2, \beta\rangle$. The different spin operators applied to these spin functions have the following effect:

$$\hat{S}^2|1/2, \alpha\rangle = 3/4\,|1/2, \alpha\rangle \tag{2.6}$$
$$\hat{S}^2|1/2, \beta\rangle = 3/4\,|1/2, \beta\rangle \tag{2.7}$$

$$\hat{S}_z|1/2, \alpha\rangle = 1/2\,|1/2, \alpha\rangle \tag{2.8}$$
$$\hat{S}_z|1/2, \beta\rangle = -1/2\,|1/2, \beta\rangle \tag{2.9}$$

$$\hat{S}_+|1/2, \alpha\rangle \equiv 0 \tag{2.10}$$
$$\hat{S}_+|1/2, \beta\rangle \equiv [1/2 \cdot 3/2 - (-1/2) \cdot 1/2]^{1/2}\,|1/2, \alpha\rangle = |1/2, \alpha\rangle \tag{2.11}$$
$$\hat{S}_-|1/2, \beta\rangle \equiv 0 \tag{2.12}$$
$$\hat{S}_-|1/2, \alpha\rangle \equiv [1/2 \cdot 3/2 - 1/2 \cdot (-1/2)]^{1/2}\,|1/2, \beta\rangle = |1/2, \beta\rangle \tag{2.13}$$

Spin adapted functions are eigenfunctions of $\hat{S}^2$ and $\hat{S}_z$ operators, but not of the spin ladder operators, because in the latter case, the application of the operator over the functions does not yield a constant times the same function. These conclusions are valid for any system with given N magnetic centres bearing any S value. Now, after these considerations, HDVV Hamiltonian can be rewritten in the form

$$\hat{H}^{HDVV} = -\sum_{\langle i,j \rangle} J_{ij}\hat{\boldsymbol{S}}_i \cdot \hat{\boldsymbol{S}}_j$$

$$= -\sum_{\langle i,j \rangle} J(1/2\left[\hat{S}_{i+}\hat{S}_{j-} + \hat{S}_{i-}\hat{S}_{j+}\right] + \hat{S}_i^z \cdot \hat{S}_j^z \tag{3}$$

In order to exemplify the strength of this approach for extracting exchange coupling constants, let's consider two cases of increasing complexity. Those are systems with two magnetic centres (1 and 2) bearing localized spin moments in each centre ranging from $S_1 = S_2 = 1/2$ to $S_1 = S_2 = 1$ and a general three centres case with $S_1 = S_2 = S_3 = 1/2$. Experimentally, access to magnetic information of related systems is granted by coordination chemistry, owing to the numerous Cu(II) and Ni(II) reported complexes that can be described within the mentioned model Hamiltonian.

For these two centres cases, the HDVV Hamiltonian takes the form

$$\hat{H}^{HDVV} = -J\hat{\boldsymbol{S}}_1 \cdot \hat{\boldsymbol{S}}_2$$

$$= -J\{1/2\left[\hat{S}_{1+}\hat{S}_{2-} + \hat{S}_{1-}\hat{S}_{2+}\right] + \hat{S}_1^z \cdot \hat{S}_2^z\} \tag{4}$$

- $S_1 = S_2 = 1/2$ Dimers

The spin adapted states resulting from two interacting magnetic centres with $S = 1/2$ each site in a 1-2 topology, are combinations of $|\alpha\beta\rangle$ and $|\beta\alpha\rangle$ basis functions. They are obtained after diagonalization of the $S_z = 0$ subspace in the matrix representation of the HDVV Hamiltonian. However, for completeness the matrix elements arising from the $S_z = \pm 1$ subspace are also shown, obtained following eqn (2.6-13).

$$\langle\alpha\alpha|\hat{H}^{HDVV}|\alpha\alpha\rangle = \langle\alpha\alpha|\{-J[1/2\,(|0\rangle + |0\rangle) + 1/4\,|\alpha\alpha\rangle]\}$$
$$= \langle\alpha\alpha|\{-J[1/4\,|\alpha\alpha\rangle]\} = \langle\beta\beta|\hat{H}^{HDVV}|\beta\beta\rangle = {}^{-J}\!/_4 \qquad (5)$$

$$\langle\alpha\beta|\hat{H}^{HDVV}|\alpha\beta\rangle = \langle\alpha\beta|\{-J[1/2\,(|0\rangle + |\beta\alpha\rangle) - 1/4\,|\alpha\beta\rangle]\}$$
$$= \langle\alpha\beta|\{-J/2 \cdot |\beta\alpha\rangle + 1/4\,|\alpha\beta\rangle\} = {}^{J}\!/_4 \qquad (6)$$

$$\langle\beta\alpha|\hat{H}^{HDVV}|\alpha\beta\rangle = \langle\beta\alpha|\{-J[1/2\,(|0\rangle + |\beta\alpha\rangle) - 1/4\,|\alpha\beta\rangle]\}$$
$$= \langle\beta\alpha|\{-J/2 \cdot |\beta\alpha\rangle + 1/4\,|\alpha\beta\rangle\} = {}^{-J}\!/_2 \qquad (7)$$

$$\langle\alpha\beta|\hat{H}^{HDVV}|\beta\alpha\rangle = \langle\alpha\beta|\{-J[1/2\,(|\alpha\beta\rangle + |0\rangle) - 1/4\,|\beta\alpha\rangle]\}$$
$$= \langle\alpha\beta|\{-J/2 \cdot |\alpha\beta\rangle + 1/4\,|\beta\alpha\rangle\} = {}^{-J}\!/_2 \qquad (8)$$

$$\langle\beta\alpha|\hat{H}^{HDVV}|\beta\alpha\rangle = \langle\beta\alpha|\{-J[1/2\,(|\alpha\beta\rangle + |0\rangle) - 1/4\,|\beta\alpha\rangle]\}$$
$$= \langle\beta\alpha|\{-J/2 \cdot |\alpha\beta\rangle + 1/4\,|\beta\alpha\rangle\} = {}^{J}\!/_4 \qquad (9)$$

which results in the following symmetric matrix representation,

$\hat{H}^{HDVV}$	$|\alpha\alpha\rangle$	$|\alpha\beta\rangle$	$|\beta\alpha\rangle$	$|\beta\beta\rangle$
$\langle\alpha\alpha|$	$-J/4$	0	0	0
$\langle\alpha\beta|$		$J/4$	$-J/2$	0
$\langle\beta\alpha|$			$J/4$	0
$\langle\beta\beta|$				$-J/4$

Table 1. Matrix elements corresponding to the HDVV Hamiltonian on the chosen basis set. The inner rectangle represents the $S_z = 0$ sub block.

By diagonalizing the $S_z = 0$ sub block of the matrix, one gets the corresponding eigenvalues and eigenvectors $|S, S_z\rangle$, which are associated to the spin adapted wave functions. Thus, the singlet ($S = 0$) wave function is written as,

$$|0,0\rangle = \frac{1}{\sqrt{2}}\{|\alpha\beta\rangle - |\beta\alpha\rangle\} \tag{10}$$

and the triplet ($S = 1$) takes the form

$$|1, +1\rangle = |\alpha\alpha\rangle \tag{11.1}$$

$$|1, -1\rangle = |\beta\beta\rangle \tag{11.2}$$

$$|1,0\rangle = \frac{1}{\sqrt{2}}\{|\alpha\beta\rangle + |\beta\alpha\rangle\} \tag{11.3}$$

where $|1, +1\rangle$ and $|1, -1\rangle$ are the $S_z = 1$ and $S_z = -1$ components, repectively. Now, the corresponding eigenvalues can be obtained by simply applying the HDVV Hamiltonian to the spin adapted functions, first to the three components of the triplet state,

$$\hat{H}^{HDVV}|1,0\rangle = -J\{1/2\left[\hat{S}_{1+}\hat{S}_{2-} + \hat{S}_{1-}\hat{S}_{2+}\right] + \hat{S}_1^z \cdot \hat{S}_2^z\}\frac{1}{\sqrt{2}}\{|\alpha\beta\rangle + |\beta\alpha\rangle\}$$

$$= \frac{-J}{\sqrt{2}}[1/2\,(|0\rangle + |\beta\alpha\rangle + |\alpha\beta\rangle + |0\rangle) - 1/4\,|\alpha\beta\rangle - 1/4\,|\beta\alpha\rangle]$$

$$= \frac{-J}{4}\frac{1}{\sqrt{2}}\{|\alpha\beta\rangle + |\beta\alpha\rangle\} = \frac{-J}{4}|1,0\rangle \tag{12}$$

$$\hat{H}^{HDVV}|1, +1\rangle = -J\{1/2\left[\hat{S}_{1+}\hat{S}_{2-} + \hat{S}_{1-}\hat{S}_{2+}\right] + \hat{S}_1^z \cdot \hat{S}_2^z\}|\alpha\alpha\rangle$$

$$= -J[1/2\,(|0\rangle + |0\rangle) + 1/4\,|\alpha\alpha\rangle] = \frac{-J}{4}|\alpha\alpha\rangle \tag{13}$$

$$\hat{H}^{HDVV}|1, -1\rangle = -J\{1/2\left[\hat{S}_{1+}\hat{S}_{2-} + \hat{S}_{1-}\hat{S}_{2+}\right] + \hat{S}_1^z \cdot \hat{S}_2^z\}|\beta\beta\rangle$$

$$= -J[1/2\,(|0\rangle + |0\rangle) + 1/4\,|\beta\beta\rangle] = \frac{-J}{4}|\beta\beta\rangle \tag{14}$$

and then the singlet state.

$$\hat{H}^{HDVV}|0,0\rangle = -J\{1/2\left[\hat{S}_{1+}\hat{S}_{2-} + \hat{S}_{1-}\hat{S}_{2+}\right] + \hat{S}_1^z \cdot \hat{S}_2^z\}\frac{1}{\sqrt{2}}\{|\alpha\beta\rangle - |\beta\alpha\rangle\}$$

$$= \frac{-J}{\sqrt{2}} [1/2\, (|0\rangle + |\beta\alpha\rangle - |\alpha\beta\rangle - |0\rangle) - 1/4\, |\alpha\beta\rangle + 1/4\, |\beta\alpha\rangle]$$

$$= \frac{3J}{4} \frac{1}{\sqrt{2}} \{|\alpha\beta\rangle - |\beta\alpha\rangle\} = \frac{3J}{4} |0,0\rangle \tag{15}$$

Thus, the eigenvalues for the triplet and singlet states are $-J/4$ and $3J/4$ respectively. Their difference yield the well-known expression for singlet-triplet gap[8,12]

$$E_S - E_T = 3J/4 - (-J/4) = J \tag{16}$$

Wave function-based calculations on $S_1 = S_2 = 1/2$ Cu(II) dinuclear complexes, where the magnetic interaction has been accurately extracted by experiment, have made possible the decomposition of the J value in its fundamental physical contributions.[13,14] These calculations will not be commented, and only the main conclusion will be highlighted here. Basically, the three main components are the ferromagnetic direct exchange between the magnetic orbitals, the antiferromagnetic kinetic exchange (or superexchange) provided by the intersite delocalization of the magnetic electrons, and the polarization of the nonmagnetic electrons in the doubly occupied orbitals.

- $S_1 = S_2 = 1$ dimers.

Now, one can apply the same procedure to the situation where $S_1 = S_2 = 1$ interact. There are one quintet, one triplet and one singlet pure spin states. With an additional restriction about maintaining always the local triplet in each of the centres, and written in the basis set arising from the direct product of local triplet functions ($|1, +1\rangle$, $1, -1\rangle$ and $1,0\rangle$) pure spin states expressed as

$$|2,0\rangle = \frac{1}{\sqrt{6}} \{|1,1; 1,-1\rangle + 2|1,0; 1,0\rangle + |1,-1; 1,1\rangle\} \tag{17.1}$$

$$|2,1\rangle = \frac{1}{\sqrt{2}} \{|1,1; 1,0\rangle + |1,0; 1,1\rangle\} \tag{17.2}$$

$$|2,-1\rangle = \frac{1}{\sqrt{2}} \{|1,-1; 1,0\rangle + |1,0; 1,-1\rangle\} \tag{17.3}$$

$$|2,2\rangle = |1,1; 1,1\rangle \tag{17.4}$$

$$|2,-2\rangle = |1,-1; 1,-1\rangle \tag{17.5}$$

$$|1,0\rangle = \frac{1}{\sqrt{2}} \{|1,1; 1,-1\rangle - |1,-1; 1,1\rangle\} \tag{17.6}$$

$$|1,1\rangle = \frac{1}{\sqrt{2}}\{|1,1;1,0\rangle - |1,0;1,1\rangle\} \qquad (17.7)$$

$$|1,-1\rangle = \frac{1}{\sqrt{2}}\{|1,-1;1,0\rangle - |1,0;1,-1\rangle\} \qquad (17.8)$$

$$|0,0\rangle = \frac{1}{\sqrt{3}}\{|1,1;1,-1\rangle - |1,0;1,0\rangle + |1,-1;1,1\rangle\} \qquad (17.9)$$

The corresponding eigenvalues of the quintet, triples and singlet states are, respectively, $-J, J$ and $2J,$[8] which result in the following energy differences:

$$E_S - E_Q = 2J - (-J) = 3J \qquad (18.1)$$
$$E_S - E_T = 2J - (J) = J \qquad (18.2)$$

At variance with the singlet-triplet case, the additional equation in the $S_1 = S_2 = 1$ case allows to check the consistency of the results, provided that the different states have been calculated with sufficient accuracy.

- Homonuclear Dimers with any S.

The generalization of the above discussion for any two centres case was provided by Landé. It is known as Landé rule and it states that for given any two identical particles with total spin S_i, the energy difference between the different $2S + 1$ multiplets is:

$$E(S-1) - E(S) = JS \qquad (19)$$

The underlying problem is then to ensure an accurate calculation of the different low-lying states of a given dinuclear complex as a strategy to correctly extract the magnetic interactions. This is a particularly delicate issue for large systems, and is specifically treated in paper #3.1, where a family of different heterodinuclear complexes is investigated using a variety of wave function-based methods.

Despite the valuable theoretical efforts for generalizing the two centres problems, they only represent a reduced amount of the real reported cases. There are numerous examples of polynuclear coordination compounds with very interesting properties, as for instance the well-known Mn_{12}-acetate. It is then desirable to go a step further from the two centres case in the description of magnetic interactions using pure spin states.

However, there is an evident flaw for the generalization of this approach, namely cases where the number of pure spin states is not enough to extract all relevant magnetic interactions. This issue has been investigated in paper #3.2 and is exemplified by a trinuclear Cu(II) complex with three interacting $S_1 = 1/2$; $S_2 = 1/2$; $S_3 = 1/2$ localized moments where no symmetry operation relates the magnetic centres, resulting in one quartet and two doublet pure spin states. The lack of symmetry implies that all three two-body magnetic interactions are relevant to define the low-lying HDVV energy spectrum, but only two energy differences between the quartet and two doublet pure spin states are available. In order to solve that, one can make use of the correspondence between the diagonal elements of the HDVV and Ising matrix representations. In order to make a more precise point, a discussion on how to construct the spin adapted wave functions for such case is given.

- $S_1 = S_2 = S_3 = 1/2$ Trimers.

For a general three-electrons in three centres case arranged as depicted in Figure 1
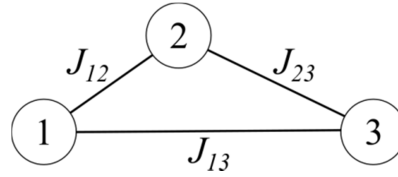
Figure 1. Schematic representation of a general three-electrons in three centres case.

where no symmetry operation relates any of the centres, there are three different magnetic coupling constants and the HDVV Hamiltonian is written as

$$\widehat{H}^{HDVV} = -\sum_{\langle i,j \rangle} J_{ij}\widehat{S}_i \cdot \widehat{S}_j$$

$$= -J_{12}\widehat{S}_1 \cdot \widehat{S}_2 - J_{23}\widehat{S}_2 \cdot \widehat{S}_3 - J_{13}\widehat{S}_1 \cdot \widehat{S}_3 \qquad (20)$$

In the same manner we used $|\alpha\beta\rangle$ and $|\beta\alpha\rangle$ functions in the dimer case, in this situation the pure spin wave functions are obtained as linear combinations of the $|\alpha\alpha\beta\rangle$, $|\alpha\beta\alpha\rangle$ and $|\beta\alpha\alpha\rangle$ functions in a 1-2-3 topology. The number of spin adapted wave functions and the magnitude of the coefficients of the linear combination are obtained after diagonalizing the HDVV matrix representation on this basis. Again, the matrix elements are obtained following eqn (2.6-2.13).

$$\langle\alpha\alpha\alpha|\hat{H}^{HDVV}|\alpha\alpha\alpha\rangle = \langle\alpha\alpha\alpha|\{-J_{12}[1/2\,(|0\rangle + |0\rangle) + 1/4\,|\alpha\alpha\alpha\rangle]$$

$$-J_{23}[1/2\,(|0\rangle + |0\rangle) + 1/4\,|\alpha\alpha\alpha\rangle] - J_{13}[1/2\,(|0\rangle + |0\rangle) + 1/4\,|\alpha\alpha\alpha\rangle]\}$$

$$= \langle\alpha\alpha\alpha|\{\left(-J_{12}/4 - J_{23}/4 - J_{13}/4\right)|\alpha\alpha\alpha\rangle\}$$

$$= -\,^{1}/_{4}\,[J_{12} + J_{23} + J_{13}] \tag{21}$$

$$\langle\alpha\alpha\beta|\hat{H}^{HDVV}|\alpha\alpha\alpha\rangle = \langle\alpha\beta\alpha|\hat{H}^{HDVV}|\alpha\alpha\alpha\rangle = \langle\beta\alpha\alpha|\hat{H}^{HDVV}|\alpha\alpha\alpha\rangle = 0 \tag{22}$$

$$\langle\alpha\alpha\beta|\hat{H}^{HDVV}|\alpha\alpha\beta\rangle = \langle\alpha\alpha\beta|\{-J_{12}[1/2\,(|0\rangle + |0\rangle) + 1/4\,|\alpha\alpha\beta\rangle]$$

$$-J_{23}[1/2\,(|0\rangle + |\alpha\beta\alpha\rangle) - 1/4\,|\alpha\alpha\beta\rangle] - J_{13}[1/2\,(|0\rangle + |\beta\alpha\alpha\rangle) - 1/4\,|\alpha\alpha\beta\rangle]\}$$

$$= \langle\alpha\alpha\beta|\{-J_{23}/2\,|\alpha\beta\alpha\rangle - J_{13}/2\,|\beta\alpha\alpha\rangle - J_{12}/4\,|\alpha\alpha\beta\rangle + J_{23}/4\,|\alpha\alpha\beta\rangle + J_{13}/4\,|\alpha\alpha\beta\rangle\}$$

$$= \,^{1}/_{4}\,[-J_{12} + J_{23} + J_{13}] \tag{23}$$

$$\langle\alpha\beta\alpha|\hat{H}^{HDVV}|\alpha\alpha\beta\rangle = \langle\alpha\beta\alpha|\{\cdots\}$$

$$= \langle\alpha\beta\alpha|\{-J_{23}/2\,|\alpha\beta\alpha\rangle - J_{13}/2\,|\beta\alpha\alpha\rangle - J_{12}/4\,|\alpha\alpha\beta\rangle + J_{23}/4\,|\alpha\alpha\beta\rangle + J_{13}/4\,|\alpha\alpha\beta\rangle\}$$

$$= -\,^{J_{23}}/_{2} \tag{24}$$

$$\langle\beta\alpha\alpha|\hat{H}^{HDVV}|\alpha\alpha\beta\rangle = \langle\beta\alpha\alpha|\{\cdots\}$$

$$= \langle\beta\alpha\alpha|\{-J_{23}/2\,|\alpha\beta\alpha\rangle - J_{13}/2\,|\beta\alpha\alpha\rangle - J_{12}/4\,|\alpha\alpha\beta\rangle + J_{23}/4\,|\alpha\alpha\beta\rangle + J_{13}/4\,|\alpha\alpha\beta\rangle\}$$

$$= -\,^{J_{13}}/_{2} \tag{25}$$

$$\langle\alpha\beta\alpha|\hat{H}^{HDVV}|\alpha\beta\alpha\rangle = \langle\alpha\beta\alpha|\{-J_{12}[1/2\,(|0\rangle + |\beta\alpha\alpha\rangle) - 1/4\,|\alpha\beta\alpha\rangle]$$

$$-J_{23}[1/2\,(|\alpha\alpha\beta\rangle + |0\rangle) - 1/4\,|\alpha\beta\alpha\rangle] - J_{13}[1/2\,(|0\rangle + |0\rangle) + 1/4\,|\alpha\beta\alpha\rangle]\}$$

$$= \langle\alpha\beta\alpha|\{-J_{12}/2\,|\beta\alpha\alpha\rangle - J_{23}/2\,|\alpha\alpha\beta\rangle + J_{12}/4\,|\alpha\beta\alpha\rangle + J_{23}/4\,|\alpha\beta\alpha\rangle - J_{13}/4\,|\alpha\beta\alpha\rangle\}$$

$$= \,^{1}/_{4}\,[J_{12} + J_{23} - J_{13}] \tag{26}$$

$$\langle\alpha\alpha\beta|\hat{H}^{HDVV}|\alpha\beta\alpha\rangle = \langle\alpha\alpha\beta|\{\cdots\}$$

$$= \langle\alpha\alpha\beta|\{-J_{12}/2\,|\beta\alpha\alpha\rangle - J_{23}/2\,|\alpha\alpha\beta\rangle + J_{12}/4\,|\alpha\beta\alpha\rangle + J_{23}/4\,|\alpha\beta\alpha\rangle - J_{13}/4\,|\alpha\beta\alpha\rangle\}$$

$$= -\,^{J_{23}}/_{2} \tag{27}$$

$\langle\beta\alpha\alpha|\hat{H}^{HDVV}|\alpha\beta\alpha\rangle = \langle\beta\alpha\alpha|\{\cdots\}$

$= \langle\beta\alpha\alpha|\{-J_{12}/2\,|\beta\alpha\alpha\rangle - J_{23}/2\,|\alpha\alpha\beta\rangle + J_{12}/4\,|\alpha\beta\alpha\rangle + J_{23}/4\,|\alpha\beta\alpha\rangle - J_{13}/4\,|\alpha\beta\alpha\rangle\}$

$$= -J_{12}/_{2} \qquad\qquad (28)$$

$\langle\beta\alpha\alpha|\hat{H}^{HDVV}|\beta\alpha\alpha\rangle = \langle\beta\alpha\alpha|\{-J_{12}[1/2\,(|\alpha\beta\alpha\rangle + |0\rangle) - 1/4\,|\beta\alpha\alpha\rangle]$

$-J_{23}[1/2\,(|0\rangle + |0\rangle) + 1/4\,|\beta\alpha\alpha\rangle] - J_{13}[1/2\,(|\alpha\alpha\beta\rangle + |0\rangle) - 1/4\,|\beta\alpha\alpha\rangle]\}$

$= \langle\beta\alpha\alpha|\{-J_{12}/2\,|\alpha\beta\alpha\rangle - J_{13}/2\,|\alpha\alpha\beta\rangle + J_{12}/4\,|\beta\alpha\alpha\rangle - J_{23}/4\,|\beta\alpha\alpha\rangle + J_{13}/4\,|\beta\alpha\alpha\rangle\}$

$$= {}^{1}/_{4}\,[J_{12} - J_{23} + J_{13}] \qquad\qquad (29)$$

$\langle\alpha\alpha\beta|\hat{H}^{HDVV}|\beta\alpha\alpha\rangle = \langle\alpha\alpha\beta|\{\cdots\}$

$= \langle\alpha\alpha\beta|\{-J_{12}/2\,|\alpha\beta\alpha\rangle - J_{13}/2\,|\alpha\alpha\beta\rangle + J_{12}/4\,|\beta\alpha\alpha\rangle - J_{23}/4\,|\beta\alpha\alpha\rangle + J_{13}/4\,|\beta\alpha\alpha\rangle\}$

$$= -J_{13}/_{2} \qquad\qquad (30)$$

$\langle\alpha\beta\alpha|\hat{H}^{HDVV}|\beta\alpha\alpha\rangle = \langle\alpha\beta\alpha|\{\cdots\}$

$= \langle\alpha\beta\alpha|\{-J_{12}/2\,|\alpha\beta\alpha\rangle - J_{13}/2\,|\alpha\alpha\beta\rangle + J_{12}/4\,|\beta\alpha\alpha\rangle - J_{23}/4\,|\beta\alpha\alpha\rangle + J_{13}/4\,|\beta\alpha\alpha\rangle\}$

$$= -J_{12}/_{2} \qquad\qquad (31)$$

which results in the following matrix representation

$\hat{H}^{HDVV}$	$|\alpha\alpha\alpha\rangle$	$|\alpha\alpha\beta\rangle$	$|\alpha\beta\alpha\rangle$	$|\beta\alpha\alpha\rangle$
$\langle\alpha\alpha\alpha|$	$-\dfrac{1}{4}(J_{12} + J_{23} + J_{13})$	0	0	0
$\langle\alpha\alpha\beta|$		$\dfrac{1}{4}(-J_{12} + J_{23} + J_{13})$	$-{}^{1}/_{2}\cdot J_{23}$	$-{}^{1}/_{2}\cdot J_{13}$
$\langle\alpha\beta\alpha|$			$\dfrac{1}{4}(J_{12} + J_{23} - J_{13})$	$-{}^{1}/_{2}\cdot J_{12}$
$\langle\beta\alpha\alpha|$				$\dfrac{1}{4}(J_{12} - J_{23} + J_{13})$

Table 2. Matrix elements corresponding to the HDVV Hamiltonian on the chosen basis set. The inner rectangle represents the $S_z = 1/2$ sub block

After diagonalization of the low S_z sub block, one obtains the three spin-adapted eigenfunctions (one quartet and two doublets) describing the low energy spectrum.[15]

$$|Q\rangle = |3/2, 3/2\rangle = 3^{-1/2}(|\alpha\alpha\beta\rangle + |\alpha\beta\alpha\rangle + |\beta\alpha\alpha\rangle) \tag{32}$$

$$|D_1\rangle = |1/2, 1/2\rangle = 2^{-1/2}(|\alpha\alpha\beta\rangle - |\alpha\beta\alpha\rangle) \tag{33}$$

$$|D_2\rangle = |1/2, 1/2\rangle = 6^{-1/2}(|\alpha\alpha\beta\rangle + |\alpha\beta\alpha\rangle - 2 \cdot |\beta\alpha\alpha\rangle) \tag{34}$$

The corresponding eigenvalues are obtained by evaluating the wavefunction with HDVV Hamilonian, resulting in

$$E_Q = -1/4 \cdot (J_{12} + J_{13} + J_{23}) \tag{35}$$
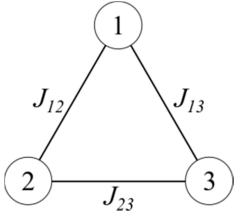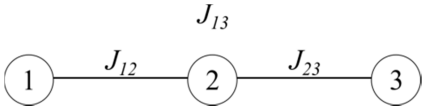
$$E_{D_1} = 1/4 \cdot (J_{12} + J_{13} + J_{23}) - ^1/_2 \cdot X \tag{36}$$

$$E_{D_2} = 1/4 \cdot (J_{12} + J_{13} + J_{23}) + ^1/_2 \cdot X \tag{37}$$

$$X = (J_{12}^2 + J_{13}^2 + J_{23}^2 - J_{12} \cdot J_{13} - J_{12} \cdot J_{23} - J_{13} \cdot J_{23})^{1/2} \tag{38}$$

Here, the problem of the mapping using spin adapted functions, becomes evident since there are three different magnetic interactions, but only two energy differences to solve the spectrum. Normally, to simplify the spectrum, one can either neglect one of the coupling constants based on distances between the magnetic centres or make use of the symmetry of the problem (if any) to establish relationships among the coupling constants. Scheme 2 exemplifies these simplifications presenting the problem of three-centres three-electrons arranged in an equidistant linear way and in an equilateral triangle. In the equilateral case, all three coupling constants become equal, the doublet states become degenerate, and the spectrum consists of only one energetic difference. In the linear case, assuming it is centre-symmetrical, the coupling constants between the two closest neighbours are equal and the external vanishes. In this case, there are two linearly independent equations as a function of the same parameter J which allows for checking the consistency of the spectrum, provided that the energy differences have been calculated with enough accuracy.

Finally, paper #3.2 investigates this problem in a system where none of these assumptions can be made and proposes a solution which is further verified by comparison to the experiments and by means of effective Hamiltonian theory in section 3.3

equilateral	linear

$$J_{12} = J_{23} = J_{13} = J$$

$$J_{12} = J_{23} = J; J_{13} = 0$$

$$X = 0$$

$$X = J$$

$$E_Q = -\frac{3}{4} \cdot J$$

$$E_Q = -\frac{1}{2} \cdot J$$

$$E_{D_1} = E_{D_2} = E_D = \frac{3}{4} \cdot J$$

$$E_{D_1} = 0 \; ; E_{D_2} = J$$

$$E_Q - E_D = -\frac{3}{2} \cdot J$$

$$E_Q - E_{D_1} = -\frac{1}{2} \cdot J \; ; E_Q - E_{D_2} = -\frac{3}{2} \cdot J$$

Scheme 2. Equilateral and linear arrangement of three electrons in three centres and the resulting simplified energy expressions.

3.2.2. Mapping Approach Based on Broken Symmetry Solutions. Ising Hamiltonian.

Broken symmetry (BS) solutions, within the spin polarized formalism, are single Slater determinant solutions to the non-relativistic, time independent Schrodinger equation constructed with two sets of spin orbitals, one for α and another for β electrons. Within the Hartree Fock (UHF) methods, BS determinants are used to approach the N-electron wave function. Similarly, in the Kohn–Sham implementation of DFT, BS solutions are used to describe the density of the N non-interacting electrons. As a consequence of the single determinant nature, the broken symmetry functions used to approach the low-spin electronic states are not eigenfunctions of the square total spin operator. A schematic representation on the shape of a BS solution is given in Scheme 3.
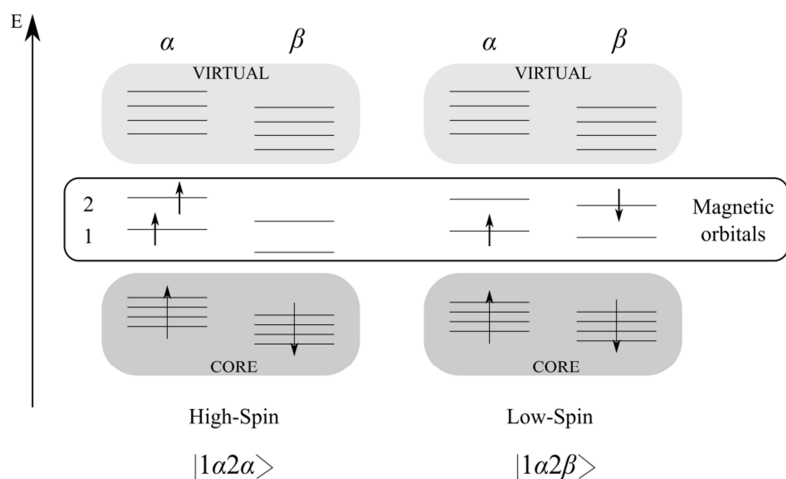
Scheme 3. Comparative representation of the high-spin and broken symmetry solutions in a two-centres two-electrons problem. Note that the unrestricted formulation implies different energies for α and β orbitals.

Section 3.2.2 deals with the second type of mapping approach discussed in the introduction of section 3.2, i.e., the mapping between spin adapted wavefunctions and broken symmetry solutions, or in other words, HDVV and Ising spectra. It has already been shown (section 3.2.1) how to construct the pure spin functions of a system by means of the HDVV Hamiltonian. The Ising Hamiltonian[16] results from neglecting the ladder operator terms in eqn (3) and retaining the *z*-component of **S** (i.e. the diagonal term of HDVV). Therefore, for a given system, it is given by

$$\hat{H}^{Ising} = -\sum_{\langle i,j \rangle} J_{ij} \hat{S}_i^z \hat{S}_j^z \tag{39}$$

The forthcoming sections are divided as follows: First, (section 3.2.2.1) briefly discusses the method employed by Noodleman,[4–6] which can be considered as the standard mapping approach. Due to the inherent spin contamination problems derived from the use of BS solutions, section 3.2.2.2. will introduce strategies to alleviate this issue. Finally, section 3.2.2.3. will present an alternative mapping approach to the one used by Noodleman, as a proposal for avoiding spin projectors.

3.2.2.1. Noodleman's Method.

The use of BS solutions applied to the extraction of magnetic coupling constants was first proposed by Noodleman.[4–6] However, this approximation had been employed previously by Bagus and Benett[17] and by Ziegler, Rauk and Baerends[18] for studying open-shell singlets within the the SCF-Xα and DFT-Xα theories, respectively. Later on

Yamaguchi et al. carried out an extensive analysis of magnetic coupling based on the UHF approximation.[19,20]

Noodleman's method applies to the study of magnetic interaction using BS solutions. It is based on expressing both the energy and the wavefunction of the spin adapted solutions by means of broken symmetry solutions. The advantage of this technique is that it allows one to extract the magnetic exchange interactions from single determinant calculations as if pure spin solutions were computed instead. In order to do so, it is required to define a spin projector. One starts with an unrestricted single determinant self-consistent field (SCF) solution to approach the high-pin solution. From these orbitals and density, the solution with the lowest S_z of the system is calculated, forcing a rupture in spatial and spin symmetry of the magnetic orbitals. This results in solutions in which the spin densities are localized antiparallel in each of the magnetic centres. The associated wave function is not an eigenfunction of the square spin operator of the system, but it can be related to the pure low-spin function by means of spin projector.

Consider again the illustrative example of two magnetic centres with two unpaired electrons in magnetic orbitals 1 and 2. The high-spin function is well defined, and takes the form $|\alpha\alpha\rangle$ as in eqns (11.1, 11.2). The corresponding BS functions $|\alpha\beta\rangle$ and $|\beta\alpha\rangle$ are the same that have been used in eqn (6-9) and are depicted in Scheme 3. For a $S_1 = S_2 = 1/2$ dimer case, Noodleman obtained an expression for the magnetic coupling constant the same using BS, through the spin projection

$$J = \frac{2(E_{BS} - E_{FM})}{1 + S_{ab}^2} \tag{40}$$

where S_{ab}^2 is the overlap integral between the magnetic orbitals in the BS solution and E_{FM} and E_{BS} are the energies of the high-spin and broken symmetry state, respectively. The spin projector appears obvious when comparing eqn (16) and eqn (40) $[J = E_S - E_T \equiv 2(E_{BS} - E_{FM})/(1 + S_{ab}^2)]$. However, such concept is exposed to at least two problematics. The first concerns the univocal existence of a spin projector, which is investigated in paper #3.1 for a family of heterodinuclear complexes. The second one is the implicit assumption that the magnetic coupling constant of the HDVV and Ising models is the same, which is not necessarily true. As an alternative to the use of spin projection, one could map the expectation energy values of the Ising eigenfunctions as

evaluated with the HDDV Hamiltonian,[7] given that the diagonal elements of their matrix representations are the same. This is investigated in paper #3.2 and explained in more detail in section 3.2.2.3. But before that, let's consider another implicit problem to the use of BS solutions, the spin contamination.

3.2.2.2. Spin Contamination in Broken Symmetry Approach.

An additional problem related to the use of broken symmetry solutions arises from spin contamination. Again, it is because the single determinants used to approximate the low spin states are not eigenfunctions of the S^2 spin operator, and a mixing with higher states occurs. For instance, when calculating a triplet state by means of a BS solution, it is possible that higher order spin states mix, like a quintet ($S_z = 1$ component). A well-known approach to that problem was a decontamination scheme proposed by Yamaguchi et al.[19,20] For the two-electrons two-centres case and assuming a strong localized character of the unpaired electrons ($S_{ab}^2 = 0$ in eqn (40)), one has

$$J = E_S - E_T = \frac{2(E_{BS} - E_T)}{\langle S^2 \rangle_T - \langle S^2 \rangle_{BS}} \tag{41}$$

This approach has been extensively applied with successful results to a variety of situations. The computed $\langle S^2 \rangle_T$ is expected to be around 2, and $\langle S^2 \rangle_{BS}$ around 1. Thus, if no spin contamination occurs, i.e. there is no relevant mixing with higher order spin states, eqn (41) converts into eqn (40). However, it is clear that if the assumption on the orbital overlap $S_{ab}^2 = 0$ does not hold, the applicability of eqn (41) is no longer ensured. In fact, for considerably delocalized systems where the magnetic orbitals share large regions of space, as for instance organic diradicals, it is known that eqn (40) leads to inaccurate results. This is due to large deviations from 1 of the computed $\langle S^2 \rangle_{BS}$.

Looking for an improvement to Yamaguchi's formula, several works have aimed to differentiate and assess the contributions of direct exchange, kinetic exchange and core polarization to the magnetic coupling, which are accurately extracted by wave function-based methods,[13,14] by means of BS density functional theory approach. Particularly, Coulaud et al.[21] proposed a decomposition scheme leading to additive contributions of the mentioned direct and kinetic exchange and core polarization. They access the terms independently. Thus, the direct exchange is obtained from restricted DFT calculations; the extraction of the kinetic exchange requires starting from the restricted orbital set and

relaxing only the magnetic orbitals (singly occupied); finally, the spin polarization is achieved by relaxing only the core orbitals (doubly occupied). In here, "relax" means that only certain orbitals (either singly or doubly occupied) are optimized, keeping constant the coefficients of the other set of orbitals. However, a year later, some of the original authors identified a deficiency of the decomposition scheme previously commented and proposed a more general scheme. [22] The problem with the original proposal is that for cases in which the core polarization contribution to the coupling constant value is large, the decomposition scheme can no longer be considered as additive. The latter approach, based on similar partially relaxed/partially frozen DFT calculations, constitutes an almost additive decomposition scheme which provides an unambiguous manner to distinguish the contributions of the different effects, and to evaluate their relative amplitudes on defining the magnetic coupling constant, arising from single determinant BS solutions. More recently, Ferré, Guihéry and Malrieu[23] used this decomposition scheme to prove that whenever the spin polarization of the core orbitals is large, Yamaguchi's formula does not hold. Moreover, they provide a spin-decontamination method to properly account for this situation when describing the triplet-singlet gap on a two-centre two-electron problem. It is based on using a BS solution calculated with the appropriate relaxation of the core orbitals.

3.2.2.3. Mapping Without Spin Projector: Expectation Values.

As mentioned, using the standard mapping approach based on Noodleman method is exposed to two sources of problems. The first one is that there is no reason why the spin projector is always definable, and the second is that it assumes that the magnetic coupling constants of the HDVV and Ising models are the same.

The argument for the first concern is exemplified in cases where the pure spin wave functions of low S_z are expressed as linear combinations of single determinants that cannot be described by BS solutions. In other words, cases where no combination of BS solutions can recover the pure spin states. Particularly, heterodinuclear complexes with $S_1 = 1; S_2 = 1/2$ localized moments represent examples of this kind. It is worth saying that centre 1 always presents a local triplet, because the energetic cost to produce a singlet is well above magnetic energy range. Consider the spin adapted and BS wave functions resulting from the mentioned case, as indicated in Scheme 4.

		Spin adapted	BS
$S_a=1$	$S_b=1/2$	$\lvert Q, \tfrac{1}{2}\rangle = \tfrac{1}{\sqrt{3}}\left(\lvert a_1 a_2 \bar{b}_1\rangle + \lvert a_1 \bar{a}_2 b_1\rangle + \lvert \bar{a}_1 a_2 b_1\rangle\right)$	$\lvert a_1 a_2 b_1\rangle$
		$\lvert D, \tfrac{1}{2}\rangle = \tfrac{2}{\sqrt{3}}\lvert a_1 a_2 \bar{b}_1\rangle - \tfrac{1}{\sqrt{6}}\left(\lvert a_1 \bar{a}_2 b_1\rangle + \lvert \bar{a}_1 a_2 b_1\rangle\right)$	$\lvert a_1 a_2 \bar{b}_1\rangle;$ $\lvert \bar{a}_1 \bar{a}_2 b_1\rangle$

Scheme 4. Schematic representation of a heterodinuclear case with a local triplet and a doublet on centre *a* and *b* respectively. The spin adapted and broken symmetry solutions are also shown.

We restrict the discussion to the $S_z = +1/2$ components for the spin adapted wave functions. Note that the pure doublet state $\lvert D, \tfrac{1}{2}\rangle$ is expressed as a linear combination of three single determinants, two of which break the local triplet in centre *A*. However, the BS solutions must respect the local triplet in *A*. Thus, it is not possible to express the pure doublet state $\lvert D, \tfrac{1}{2}\rangle$ as a combination of BS solutions, which implies that there is not a univocal way of defining the spin projector. Alternatively, and to overcome this problem, one could make use of the expectation value of the square total spin operator to know which BS solution should be used to define the appropriate exchange coupling constant. This issue is more deeply investigated in paper #3.1.

Now, consider the second weak point of the standard mapping approach, which is assuming equal the *J* values given by the HDVV and Ising model Hamiltonians. Taken together with the fact that it is not always possible to define a spin projector, the proposal of an alternative mapping approach becomes desirable. This proposal is based on the fact that the diagonal elements of the HDVV and Ising Hamiltonians are the same, thus allowing for a direct mapping between the energy of the BS solutions and the energy expectation values of the BS functions evaluated with the HDDV Hamiltonian. As a result, the *J* value from HDVV and Ising Hamiltonians are not assumed to be the same which makes unnecessary the use of a spin projector. The forthcoming discussion aims to clarify this point by using the examples developed in section 3.2.1, i.e., $S_1 = S_2 = 1/2$ dimers and $S_1 = S_2 = S_3 = 1/2$ trimers.

- $S_1 = S_2 = 1/2$ Dimers.

The broken symmetry solutions resulting from two interacting magnetic centres with $S = 1/2$ on each site, are single determinants of the type $\lvert \alpha\alpha\rangle$ for the high-spin state and $\lvert \alpha\beta\rangle$ and $\lvert \beta\alpha\rangle$ for the low-spin state, whit a 1-2 topology. Combination of

these functions result in the spin adapted wavefunctions. Now, as done for the HDVV matrix, the Ising Hamiltonian is defined as

$$\hat{H}^{Ising} = -J\hat{S}_1^z\hat{S}_2^z \tag{42}$$

which results in the following matrix elements.

$$\langle\alpha\alpha|\hat{H}^{Ising}|\alpha\alpha\rangle = \langle\alpha\alpha|\{-J(1/4\,|\alpha\alpha\rangle)\} = {}^{-J}\!/_4 \tag{43}$$

$$\langle\alpha\beta|\hat{H}^{Ising}|\alpha\beta\rangle = \langle\alpha\beta|\{-J(-1/4\,|\alpha\beta\rangle)\} = {}^{J}\!/_4 \tag{44}$$

$$\langle\alpha\beta|\hat{H}^{Ising}|\beta\alpha\rangle = \langle\alpha\beta|\{-J(-1/4\,|\beta\alpha\rangle)\} = 0 \tag{45}$$

$$\langle\beta\alpha|\hat{H}^{Ising}|\alpha\beta\rangle = \langle\beta\alpha|\{-J(-1/4\,|\alpha\beta\rangle)\} = 0 \tag{46}$$

$$\langle\beta\alpha|\hat{H}^{Ising}|\beta\alpha\rangle = \langle\beta\alpha|\{-J(-1/4\,|\beta\alpha\rangle)\} = {}^{J}\!/_4 \tag{47}$$

Finally, one obtains the corresponding matrix matrix representation,

$\hat{H}^{Ising}$	$\lvert\alpha\alpha\rangle$	$\lvert\alpha\beta\rangle$	$\lvert\beta\alpha\rangle$	$\lvert\beta\beta\rangle$
$\langle\alpha\alpha\rvert$	$-J/4$	0	0	0
$\langle\alpha\beta\rvert$		$J/4$	0	0
$\langle\beta\alpha\rvert$			$J/4$	0
$\langle\beta\beta\rvert$				$-J/4$

Table 3. Matrix elements corresponding to the Ising spin Hamiltonian on the chosen basis set. The inner rectangle represents the $S_z = 0$ sub block. This respresentation is to be compared with Table 1.

By comparing the matrix representation of Table 3 with the one obtained on the same basis for the HDVV Hamiltonian in Table 1, it becomes evident that the Ising representation is equivalent to HDVV, with the off-diagonal elements equal to zero. Also, note that from eqns (43-47), one can obtain:

$$J = 2(E_{|\alpha\beta\rangle} - E_{|\alpha\alpha\rangle}) = 2(E_{BS} - E_{|\alpha\alpha\rangle}) \tag{48}$$

which is eqn (40) in the limit where $S_{ab}^2 = 0$. A schematic summary of the discussed results is presented in Figure 2.
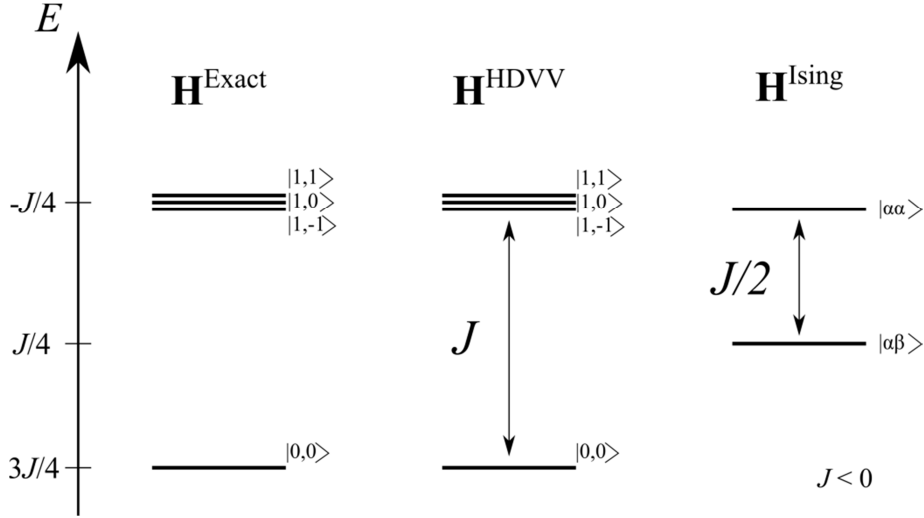
Figure 2. Diagram of the mapping approach for two centres with $S = 1/2$, interacting antiferromagnetically ($J < 0$).

- $S_1 = S_2 = S_3 = 1/2$ trimers.

The Ising Hamiltonian for this case in a 1-2-3 topology is expressed as:

$$\hat{H}^{Ising} = -\sum_{\langle i,j \rangle} J_{ij} \hat{S}_i^z \hat{S}_j^z = -J_{12} \hat{S}_1^z \hat{S}_2^z - J_{23} \hat{S}_2^z \hat{S}_3^z - J_{13} \hat{S}_1^z \hat{S}_3^z \tag{49}$$

Which, written in the same basis set as the corresponding HDVV Hamiltonian, results in the following matrix elements.

$$\langle \alpha\alpha\alpha | \hat{H}^{Ising} | \alpha\alpha\alpha \rangle = \langle \alpha\alpha\alpha | \{ -J_{12}(1/4 \, |\alpha\alpha\alpha\rangle) - J_{23}(1/4 \, |\alpha\alpha\alpha\rangle) - J_{13}(1/4 \, |\alpha\alpha\alpha\rangle)$$

$$= -{}^{1}\!/_{4} \, [J_{12} + J_{23} + J_{13}] \tag{50}$$

$$\langle \alpha\alpha\beta | \hat{H}^{Ising} | \alpha\alpha\alpha \rangle = \langle \alpha\beta\alpha | \hat{H}^{Ising} | \alpha\alpha\alpha \rangle = \langle \beta\alpha\alpha | \hat{H}^{Ising} | \alpha\alpha\alpha \rangle = 0 \tag{51}$$

$$\langle \alpha\alpha\beta | \hat{H}^{Ising} | \alpha\alpha\beta \rangle = \langle \alpha\alpha\beta | \{ -J_{12}(1/4 \, |\alpha\alpha\beta\rangle) - J_{23}(-1/4 \, |\alpha\alpha\beta\rangle) - J_{13}(-1/4 \, |\alpha\alpha\beta\rangle)$$

$$= {}^{1}\!/_{4} \, [-J_{12} + J_{23} + J_{13}] \tag{52}$$

$$\langle \alpha\beta\alpha | \hat{H}^{Ising} | \alpha\alpha\beta \rangle = \langle \alpha\beta\alpha | \{ -J_{12}(1/4 \, |\alpha\alpha\beta\rangle) - J_{23}(-1/4 \, |\alpha\alpha\beta\rangle) - J_{13}(-1/4 \, |\alpha\alpha\beta\rangle)$$

$$= 0 \tag{53}$$

$$\langle\beta\alpha\alpha|\hat{H}^{Ising}|\alpha\alpha\beta\rangle = \langle\beta\alpha\alpha|\{-J_{12}(1/4\,|\alpha\alpha\beta\rangle)-J_{23}(-1/4\,|\alpha\alpha\beta\rangle)-J_{13}(-1/4\,|\alpha\alpha\beta\rangle)$$

$$= 0 \qquad\qquad (54)$$

$$\langle\alpha\beta\alpha|\hat{H}^{Ising}|\alpha\beta\alpha\rangle = \langle\alpha\beta\alpha|\{-J_{12}(-1/4\,|\alpha\beta\alpha\rangle)-J_{23}(-1/4\,|\alpha\beta\alpha\rangle)-J_{13}(1/4\,|\alpha\beta\alpha\rangle)$$

$$= {}^1\!/_4\,[J_{12}+J_{23}-J_{13}] \qquad\qquad (55)$$

$$\langle\beta\alpha\alpha|\hat{H}^{Ising}|\alpha\beta\alpha\rangle = \langle\beta\alpha\alpha|\{-J_{12}(-1/4\,|\alpha\beta\alpha\rangle)-J_{23}(-1/4\,|\alpha\beta\alpha\rangle)-J_{13}(1/4\,|\alpha\beta\alpha\rangle)$$

$$= 0 \qquad\qquad (56)$$

$$\langle\beta\alpha\alpha|\hat{H}^{Ising}|\beta\alpha\alpha\rangle = \langle\beta\alpha\alpha|\{-J_{12}(-1/4\,|\beta\alpha\alpha\rangle)-J_{23}(1/4\,|\beta\alpha\alpha\rangle)-J_{13}(1/4\,|\beta\alpha\alpha\rangle)$$

$$= {}^1\!/_4\,[J_{12}-J_{23}+J_{13}] \qquad\qquad (57)$$

what leads to the following matrix representation

$\hat{H}^{Ising}$	$|\alpha\alpha\alpha\rangle$	$|\alpha\alpha\beta\rangle$	$|\alpha\beta\alpha\rangle$	$|\beta\alpha\alpha\rangle$
$\langle\alpha\alpha\alpha|$	$-\dfrac{1}{4}(J_{12}+J_{23}+J_{13})$	0	0	0
$\langle\alpha\alpha\beta|$		$\dfrac{1}{4}(-J_{12}+J_{23}+J_{13})$	0	0
$\langle\alpha\beta\alpha|$			$\dfrac{1}{4}(J_{12}+J_{23}-J_{13})$	0
$\langle\beta\alpha\alpha|$				$\dfrac{1}{4}(J_{12}-J_{23}+J_{13})$

Table 4. Matrix elements corresponding to the Ising Hamiltonian on the chosen basis set. The inner rectangle represents the $S_z = 1/2$ sub block. This representation is to be compared with Table 2.

A comparison of the matrix elements included in Table 2 and Table 4 demonstrates the equivalence between the diagonal terms of HDVV and Ising Hamiltonian, as in the dimer case previously discussed. This correspondence allows proposing a different mapping approach that does not require using a spin projector, based on the expectation values of Ising eigenfunctions evaluated with the HDVV Hamiltonian. The application of this approach is, however, limited to cases where the off-diagonal terms do not deviate too much from zero, or in other words, there is not a significant mixing of states. Nevertheless, if that is the case, it implies that the HDVV is not an appropriate model for the problem, since the magnetic centres cannot be associated to localized moments.

A summary of the discussed results is presented in Figure 3.
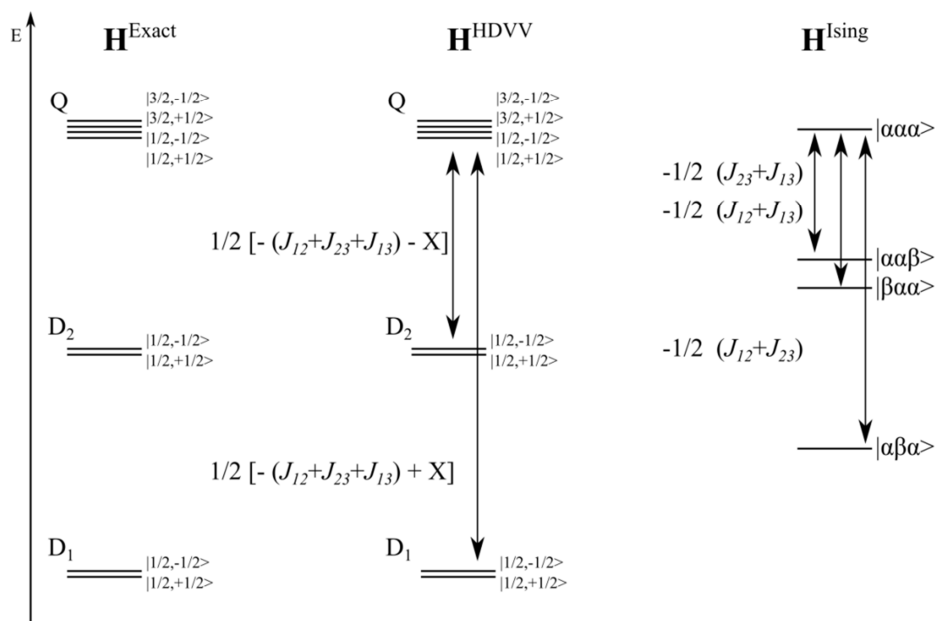
Figure 3. Diagram of the mapping approach for three centres with $S = 1/2$, interacting antiferromagnetically ($J < 0$).

In summary, this section has presented some weak point of the standard mapping approach originally developed by Noodleman,[4–6] and proposed, based on previous works on the group,[8] an extension of an alternative formulation. This alternative approach proposes to directly map the energy of the BS solutions into the energy expectation values of BS functions of the HDVV Hamiltonian. The difference with the standard mapping approach is that it does not require using a spin projector, because it does not aim to describe the wave function of the pure spin solutions by means of BS solutions. This is advantageous because as it has been demonstrated (see section 3.2.2.3 and Scheme 4), the spin projector cannot always be defined.

In paper #3.2 this proposal is applied to a general three-centre three-electron problem, from which experimental data is available, and it is therefore possible to check the validity of the approach. However, not always there is experimental data available to compare with, which makes necessary the validation of the proposal by other means. This is the purpose of the next section, where effective Hamiltonian theory is exemplified on very simple model systems based on helium and hydrogen atoms, and further applied to the trinuclear case of paper #3.2 and to a purely organic triradical, of relevance for chapter 4.

3.3. Effective Hamiltonian Theory Applied to the 3 Electrons 3 Centres Problem.

In order to extract the three relevant magnetic coupling constants in the general 3 electrons in 3 centres case from *ab initio* wave function approaches, we need to provide and additional equation to complement the two energy differences derived from the spectrum of the magnetic states. A useful theoretical tool to extract this additional information from the wave functions of the magnetic states is provided by the effective Hamiltonian theory. This theory offers a rigorous mathematical scheme to reduce the electronic Hamiltonian to a spin Hamiltonian of the HDVV type by means of projection techniques. The utility of the effective Hamiltonians relies in their interpretative power of a very complex problem (the full electronic problem) by means of a projection in a suitable reduced subspace that provides the essential interpretative VB forms. However, the effective Hamiltonian theory also provides a tool to extract additional information from the wave function that is not directly accessible from the energy spectrum. Here, we extend the previous applications developed in our group to construct an effective spin Hamiltonian to describe the general 3 electrons in 3 centres case. Effective Hamiltonians can be seen as a particular case of model Hamiltonians that can be constructed by well-defined mathematical techniques to reduce the information included in the electronic wave function by projection on a suitable VB model space. This reduction has been shown to be useful to treat spin systems. Here we have constructed an effective spin Hamiltonian following Durand and Malrieu[24] and previous applications in our group.[25]

To this end, we have considered a simple magnetic system that provides a suitable model to construct this interpretative tool. In particular, we have considered the linear symmetrical H--He--H--He--H system (d(H--He)= 2.0 Å) and the distorted linear H-He-H--He--H system (d(H-He)$_{short}$= 1.625 Å, d(H--He)$_{long}$=2.0 Å) at this fixed geometry. In both cases we use a localised set of molecular orbitals obtained by the Pipek-Mezey localization of the ROHF orbitals of the quartet state and 6-31G**[26] basis set for H and 6-31G for He. The exact energies of the magnetic states have been calculated at the FCI level using the determinant approach implemented in GAMESS12.[27] We have also considered two larger systems of interest for this thesis: a) a Cu(II) asymmetric trinuclear complex (the same complex as the one described in paper #3.2) and b) a prototypic odd alternant organic triradical derived from *m*-xylylene (see paper #4.1 in

chapter 4 for the *m*-xylylene and the discussion after paper #4.3 in chapter 4 for the prototypic triradical). For the Cu(II) asymmetric trinuclear molecular complex, construction of the effective Hamiltonian has been performed at the same geometry and with the same computational parameters for the DDCI[28] calculation (basis set, frozen and deleted orbitals), as explained in paper #3.2. For the organic triradical, the effective Hamiltonian has been constructed at the molecular geometry denoted as 1 in Table 4.3.3, to be found in the discussion after paper #4.3 in chapter 4. DDCI calculations at this geometry are performed using the 6-311G**[26] standard basis set for both carbon and hydrogen atoms, the localization scheme from the CASDI program,[29] freezing 21 and deleting 150 orbitals (which results in ~87 million determinants)

The calculations on the trinuclear Cu(II) complex and the triradical PAH were carried out using to the MOLCAS7.6 package[30] which was also interfaced with the CASDI code[29] for the DDCI calculations.[28]

It is evident from the expression of the wave functions that in all cases the model space is defined by the neutral VB forms of the CAS(3,3) using the open shell localised orbitals which are the most important contributions of the three lowest energy magnetic states of the systems.

Now, let us now consider the construction of the effective Hamiltonian targeting the spin space determining the low-lying energy spectrum, which is the model space. There are two main ways of constructing an effective Hamiltonian; the one developed Bloch[31] which leads to a non-Hermitian representation, and the one proposed by des Cloizeaux[32] that solves this problem and for our purposes is the most convenient one. Basically, the construction of the effective Hamiltonian implies the projection of the exact non-relativistic electronic Hamiltonian onto a *N*-dimensional model space *S* containing the information that interests us. This theory ensures that there exists a correspondence between the eigenvalues of the exact Hamiltonian and the effective Hamiltonian ones, and that the eigenfunctions of the exact Hamiltonian coincide with their projection onto the model space. The validity and robustness of this theory when applied to molecular magnetism and highly correlated materials has been recently reviewed by Malrieu *et al.*[12] Let E_m and φ_m be the energy and the corresponding eigenfunction of state *m*. Then:

$$\hat{H}\varphi_m = E_m\varphi_m \qquad (58)$$

We can then define a projector targeting the model space *S* as:

$$\hat{P}_S = \sum_{I \in S}^{N} |I\rangle\langle I| \tag{59}$$

where $\{|I\rangle\}$ is an orthonormal basis of the space of dimension *N*. In our case, it is constituted by the determinants that span the Heisenberg Hamiltonian $|\alpha\alpha\beta\rangle$, $|\alpha\beta\alpha\rangle$ and $|\beta\alpha\alpha\rangle$. Thus, it can be defined an Effective Hamiltonian such that:

$$\hat{H}^{eff}\varphi_{S,m} = E_m\varphi_{S,m} \tag{60}$$

being:

$$\varphi_{S,m} = \hat{P}_S\varphi_m \tag{61}$$

The basis set in which $\varphi_{S,m}$ is written is not necessarily orthonormal. Hence, the overlap matrix between the states in this basis set, *S*

$$S_{m,q} = \langle\varphi_{S,m}|\varphi_{S,q}\rangle \tag{62}$$

should be taken into account for the transformations. An orthonormalization procedure is used to simplify the expression of the effective Hamiltonian and, for instance, the Löwdin procedure

$$\bar{\varphi}_{S,m} = S_{m,q}^{-1/2}\varphi_{S,m} \tag{63}$$

provides a convenient symmetric orthogonalization, as suggested by des Cloizeaux. Thus, making use of the spectral decomposition of the Hamiltonian, it is possible to construct its matrix representation in the space of neutral determinants; its elements are expressed as:

$$H_{I,J}^{eff} = \sum_{m=1}^{N} \langle I|\bar{\varphi}_{S,m}\rangle E_m\langle\bar{\varphi}_{S,m}|J\rangle \tag{64}$$

The elements of this matrix can now be directly compared to the elements of the Heisenberg Hamiltonian, given that they are written in the same basis. Moreover, this also represents a rigorous manner to validate the strategy for recovering the mapping procedure in systems with three electrons in three centers.

Now, let us turn to the application of the effective Hamiltonian theory described to the particular systems considered above. For the linear symmetrical H_2--He--H_1--He--H_3 model system (d(H-He)= 2.0 Å) the FCI magnetic states projected on the neutral determinants of the CAS(3,3) in local orbitals have the following energies and components:

	D_1	D_2	Q
$\Delta E (cm^{-1})$	-80.898	-26.979	0.0
$\langle \alpha\alpha\beta \|$	-0.406208	0.703842	-0.574795
$\langle \alpha\beta\alpha \|$	-0.406208	-0.703842	-0.574795
$\langle \beta\alpha\alpha \|$	0.812416	0.000000	-0.574795
$\sum_{I \in CAS} c_I^2$	0.99112	0.99115	0.99117
$\sum_{I \in N} c_I^2$	0.99002	0.99079	0.99117

Table 5

From these values, the matrix elements (in cm^{-1}) of the effective Hamiltonian obtained using eqn (64) and orthonormalized projections of the magnetic states on the model VB space is as follows:

$\widehat{H}^{eff}$	$\|\alpha\alpha\beta\rangle$	$\|\alpha\beta\alpha\rangle$	$\|\beta\alpha\alpha\rangle$
$\langle \alpha\alpha\beta \|$	-26.972	0.006	26.966
$\langle \alpha\beta\alpha \|$	0.006	-26.972	26.966
$\langle \beta\alpha\alpha \|$	26.966	26.966	-53.932

Table 6

Comparison of the matrix elements of the effective Hamiltonian thus constructed and the expression of the representation of the Heisenberg Hamiltonian shown in Table 2 provides the expected values for this (2)--(1)--(3) symmetric system $J_{12} = J_{13} = -2 \cdot (H^{eff})_{1,3} = -2 \cdot (H^{eff})_{2,3} = -53.932 \ cm^{-1}$ and $J_{23} = -2 \cdot (H^{eff})_{1,2} = -0.012 \ cm^{-1}$. These values are almost identical to those that can be extracted directly from the energy differences obtained from the magnetic spectrum. In this symmetric case we have enough equations to extract the relevant $J_{12} = J_{13} = J$ and $J_{23} = J'$ values.

Now we turn to the asymmetric case where this procedure will provide the additional equation to extract the three $J_{12} \neq J_{13} \neq J_{23}$ coupling constants.

The results for the linear asymmetrical H_2-He-H_1--He--H_3 asymmetric (d(H-He)$_{short}$= 1.625 Å, d(H--He)$_{long}$=2.0 Å) the FCI magnetic states projected on the neutral determinants of the CAS(3,3) in local orbitals have the following energies and components:

	D_1	D_2	Q
$\Delta E(cm^{-1})$	-529.168	-41.959	0.0
$\langle \alpha\alpha\beta |$	-0.041316	0.811441	-0.574696
$\langle \alpha\beta\alpha |$	-0.679604	-0.441623	-0.574696
$\langle \beta\alpha\alpha |$	0.720920	-0.369817	-0.574696
$\sum_{I \in CAS} c_I^2$	0.99045	0.99080	0.99083
$\sum_{I \in N} c_I^2$	0.98329	0.99023	0.99083

Table 7

From these values, the matrix elements (in cm^{-1}) of the effective Hamiltonian obtained using eqn (64) and orthonormalized projections of the magnetic states on the model VB space is as follows:

$\hat{H}^{eff}$	$|\alpha\alpha\beta\rangle$	$|\alpha\beta\alpha\rangle$	$|\beta\alpha\alpha\rangle$
$\langle \alpha\alpha\beta |$	-28.818	0.074	28.745
$\langle \alpha\beta\alpha |$	0.074	-256.819	256.745
$\langle \beta\alpha\alpha |$	28.745	256.745	-285.490

Table 8

In this case, comparison of the matrix elements of the effective Hamiltonian thus constructed and the expression of the representation of the Heisenberg Hamiltonian shown in Table 2 provides an additional equation to extract J_{23} for this (2)-(1)--(3) asymmetric system: $J_{12} = -2 \cdot (H^{eff})_{2,3} = -513.490 \, cm^{-1}$, $J_{13} = -2 \cdot (H^{eff})_{1,3} = -57.489 \, cm^{-1}$ and $J_{23} = -2 \cdot (H^{eff})_{1,2} = -0.147 \, cm^{-1}$. In this case, if the assumption of symmetry is used to extract an average J value from the energy spectrum,

the large difference between J_{12} and J_{13} values leads to an unphysical J_{23} value. This example shows how important is the utility of the effective Hamiltonian in this case.

In the case of the trinuclear Cu(II) complex, HAKKEJ, the DDCI magnetic states projected on the neutral determinants of the CAS(3,3) in localised orbitals in the (1)-(2)-(3) topology have the following energies and components:

	D_1	D_2	Q
$\Delta E(cm^{-1})$	-317.773	-105.919	0.000
$\langle\alpha\alpha\beta\|$	-0.041316	0.811441	-0.574696
$\langle\alpha\beta\alpha\|$	-0.679604	-0.441623	-0.574696
$\langle\beta\alpha\alpha\|$	0.720920	-0.369817	-0.574696
$\sum_{I\in CAS} c_I^2$	0.86010	0.86248	0.86397
$\sum_{I\in N} c_I^2$	0.81888	0.84840	0.86397

Table 9

From these values, the matrix elements (in cm^{-1}) of the effective Hamiltonian obtained using eqn (64) on the model VB space is as follows:

$\widehat{H}^{eff}$	$\|\alpha\alpha\beta\rangle$	$\|\alpha\beta\alpha\rangle$	$\|\beta\alpha\alpha\rangle$
$\langle\alpha\alpha\beta\|$	-113.734	113.204	0.511
$\langle\alpha\beta\alpha\|$	113.204	-211.300	98.108
$\langle\beta\alpha\alpha\|$	0.511	98.108	-98.613

Table 10

Again, a comparison of the matrix elements of the effective Hamiltonian thus constructed and the expression of the representation of the Heisenberg Hamiltonian shown in Table 2 provides all the J values for the (1)-(2)-(3) topology: $J_{12} = -2 \cdot (H^{eff})_{2,3} = -196.217 \ cm^{-1}$, $J_{13} = -2 \cdot (H^{eff})_{1,3} = -1.022 \ cm^{-1}$ and $J_{23} = -2 \cdot (H^{eff})_{1,2} = -226.409 \ cm^{-1}$. These values are in line with the observed Cu-Cu distances in the molecule. Moreover, these ab initio estimates of the relevant magnetic coupling constants provide a value of $J_{12}/J_{23} = 0.867$ that is in good agreement with the corresponding hybrid DFT values around 0.90 (see Table 2 of paper #3.2).

However, if the assumption of symmetry is used to extract an average J value from the energy spectrum as used in the experimental fitting of the magnetic susceptibility *vs.* T curves, the large difference between J_{12} and J_{23} values may lead to an unphysical J_{13} value.

Finally, let us turn our attention to the organic triradical. For this system the DDCI magnetic states projected on the neutral determinants of the CAS(3,3) constructed with localised p orbitals on the radical centres in the (1)-(2)-(3) topology have the following energies and components:

	D_1	D_2	Q
$\Delta E(cm^{-1})$	2431.46004493	788.80209430	0.00000000
$\langle\alpha\alpha\beta\|$	-0.6508127	-0.4457024	0.5580807
$\langle\alpha\beta\alpha\|$	0.0617992	-0.7876415	-0.558082
$\langle\beta\alpha\alpha\|$	0.7125919	-0.341919	0.5580924
$\sum_{I\in CAS} c_I^2$	0.93531	0.93638	0.93438
$\sum_{I\in N} c_I^2$	0.93516	0.93594	0.93437

Table 11

The matrix elements (in cm^{-1}) of the effective Hamiltonian obtained using eqn (64) on this model VB space is as follows:

$\hat{H}^{eff}$	$\|\alpha\alpha\beta\rangle$	$\|\alpha\beta\alpha\rangle$	$\|\beta\alpha\alpha\rangle$
$\langle\alpha\alpha\beta\|$	874.528	-879.065	4.539
$\langle\alpha\beta\alpha\|$	-879.065	1614.680	-735.603
$\langle\beta\alpha\alpha\|$	4.539	-735.603	731.050

Table 12

In this case, the extracted J values for the (1)-(2)-(3) topology are as follows: $J_{12} = -2 \cdot (H^{eff})_{2,3} = -1471.206 \ cm^{-1}$ (182.41 meV), $J_{13} = -2 \cdot (H^{eff})_{1,3} = -9.079 \ cm^{-1}$ (-1.13 meV) and $J_{23} = -2 \cdot (H^{eff})_{1,2} = -1758.130 \ cm^{-1}$ (217.98 meV). These values are in line with the reported values obtained using BS approach as reported in Table 4.3.3, to be found in the discussion after paper #4.3 in chapter 4.

However, as compared with the trinuclear Cu(II) case, these ab initio estimates of the relevant magnetic coupling constants provide a value of $J_{12}/J_{23}=0.837$ that is significantly larger than the corresponding hybrid DFT value around 0.70 suggesting that some larger delocalisation is present in some BS solutions (the asymmetric $|\alpha\alpha\beta\rangle$ solution). This effect has a larger effect on the value of J_{13} which is overestimated by almost one order of magnitude. The precise numerical relation between the different magnetic coupling constants in complex magnetic systems is important since the subtle interplay between the dominant and the less intense but more frequent (i.e.: larger number of pairs) is responsible of magnetic structure and properties of the system.

REFERENCES

(1)   Kahn, O. *Molecular Magnetism*; VCH: New York, 1993.

(2)   Gatteschi, D.; Sessoli, R.; Villain, J. *Molecular Nanomagnets*; Oxford University Press: Oxford, 2006.

(3)   Carlin, R. L. *Magnetochemistry*; Springer-Verlag, 1986.

(4)   Noodleman, L. Valence Bond Description of Antiferromagnetic Coupling in Transition Metal Dimers. *J. Chem. Phys.* **1981**, *74*, 5737–5743.

(5)   Noodleman, L.; Davidson, E. R. Ligand Spin Polarization and Antiferromagnetic Coupling in Transition Metal Dimers. *Chem. Phys.* **1986**, *109* (1), 131–143.

(6)   Noodleman, L.; Peng, C. Y.; Case, D. A.; Mouesca, J.-M. Orbital Interactions, Electron Delocalization and Spin Coupling in Iron-Sulfur Clusters. *Coord. Chem. Rev.* **1995**, *144*, 199–244.

(7)   Caballol, R.; Castell, O.; Illas, F.; Moreira, I. de P. R.; Malrieu, J. P. Remarks on the Proper Use of the Broken Symmetry Approach to Magnetic Coupling. *J. Phys. Chem. A* **1997**, *101* (42), 7860–7866.

(8)   Moreira, I. de P. R.; Illas, F. A Unified View of the Theoretical Description of Magnetic Coupling in Molecular Chemistry and Solid State Physics. *Phys. Chem. Chem. Phys.* **2006**, *8* (14), 1645–1659.

(9)   Heisenberg, W. Zur Theorie Des Ferromagnetismus. *Zeitschrift für Phys.* **1928**, *49* (9-10), 619–636.

(10)   Dirac, P. A. M. *The Principles of Quantum Mechanics*; Clarendon Press: Oxford, 1958.

(11)   Van Vleck, J. H. *The Theory of Electric and Magnetic Susceptibilities*; Oxford University Press: Oxford, 1932.

(12)   Malrieu, J. P.; Caballol, R.; Calzado, C. J.; De Graaf, C.; Guihéry, N. Magnetic Interactions in Molecules and Highly Correlated Materials: Physical Content, Analytical Derivation, and Rigorous Extraction of Magnetic Hamiltonians. *Chem. Rev.* **2014**, *114*, 429–492.

(13)   Calzado, C. J.; Cabrero, J.; Malrieu, J. P.; Caballol, R. Analysis of the Magnetic Coupling in Binuclear Complexes. I. Physics of the Coupling. *J. Chem. Phys.* **2002**, *116*, 2728–2747.

(14)   Calzado, C. J.; Angeli, C.; Taratiel, D.; Caballol, R.; Malrieu, J. P. Analysis of the Magnetic Coupling in Binuclear Systems. III. The Role of the Ligand to Metal Charge Transfer Excitations Revisited. *J. Chem. Phys.* **2009**, *131* (4), 044327–044500.

(15)   Sinn, E. Magnetic Exchange in Polynuclear Metal Complexes. *Coord. Chem. Rev.* **1970**, *5* (3), 313–347.

(16)   Ising, E. Beitrag Zur Theorie Des Ferromagnetismus. *Zeitschrift für Phys.* **1925**, *31* (1), 253–258.

(17)   Bagus, P. S.; Bennett, B. I. Singlet-Triplet Splittings as Obtained from the Xα-Scattered Wave Method: A Theoretical Analysis. *Int. J. Quantum Chem.* **1975**, *9* (1), 143–148.

(18)   Ziegler, T.; Rauk, A.; Baerends, E. J. On the Calculation of Multiplet Energies by the Hartree-Fock-Slater Method. *Theor. Chim. Acta* **1977**, *43* (3), 261–271.

(19)   Yamaguchi, K.; Tsunekawa, T.; Toyoda, Y.; Fueno, T. Ab Initio Molecular Orbital Calculations of Effective Exchange Integrals between Transition Metal Ions. *Chem. Phys. Lett.* **1988**, *143* (4), 371–376.

(20)   Yamaguchi, K.; Fueno, T.; Ueyama, N.; Nakamura, A.; Ozaki, M. Antiferromagnetic Spin Couplings between Iron Ions in Iron—sulfur Clusters. A Localized Picture by the Spin Vector Model. *Chem. Phys. Lett.* **1989**, *164* (2-3), 210–216.

(21)   Coulaud, E.; Guihéry, N.; Malrieu, J. P.; Hagebaum-Reignier, D.; Siri, D.; Ferré, N. Analysis of the Physical Contributions to Magnetic Couplings in Broken Symmetry Density Functional Theory Approach. *J. Chem. Phys.* **2012**, *137*, 114106–2.

(22)   Coulaud, E.; Malrieu, J. P.; Guihéry, N.; Ferré, N. Additive Decomposition of the Physical Components of the Magnetic Coupling from Broken Symmetry Density Functional Theory Calculations. *J. Chem. Theory Comput.* **2013**, *9*, 3429–3436.

(23)   Ferré, N.; Guihéry, N.; Malrieu, J.-P. Spin Decontamination of Broken-Symmetry Density Functional Theory Calculations: Deeper Insight and New Formulations. *Phys. Chem. Chem. Phys.* **2015**, *17* (22), 14375–14382.

(24)   Durand, P.; Malrieu, J.-P. *Effective Hamiltonians and Pseudo-Operators as Tools for Rigorous Modelling*; Lawley, K. P., Ed.; Advances in Chemical Physics: Ab Initio Methods in Quantum Chemistry Part I; John Wiley & Sons, Inc.: New York, 1987; Vol. 67.

(25)   Moreira de P. R., I. Modelos Mecanicocuánticos Para La Determinación Precisa de Constantes de Acoplamiento Magnético En Sólidos Iónicos, Univesitat de Barcelona, 2001.

(26)   Ditchfield, R. Self-Consistent Molecular-Orbital Methods. IX. An Extended Gaussian-Type Basis for Molecular-Orbital Studies of Organic Molecules. *J. Chem. Phys.* **1971**, *54* (2), 724.

(27)   Schmidt, M. W.; Baldridge, K. K.; Boatz, J. A.; Elbert, S. T.; Gordon, M. S.; Jensen, J. H.; Koseki, S.; Matsunaga, N.; Nguyen, K. A.; Su, S.; et al. General Atomic and Molecular Electronic Structure System. *J. Comput. Chem.* **1993**, *14* (11), 1347–1363.

(28)   Miralles, J.; Castell, O.; Caballol, R.; Malrieu, J.-P. Specific CI Calculation of Energy Differences: Transition Energies and Bond Energies. *Chem. Phys.* **1993**, *172* (1), 33–43.

(29)   Ben Amor, N.; Maynau, D. Size-Consistent Self-Consistent Configuration Interaction from a Complete Active Space. *Chem. Phys. Lett.* **1998**, *286* (3-4), 211–220.

(30)   Aquilante, F.; De Vico, L.; Ferré, N.; Ghigo, G.; Malmqvist, P.-Å.; Neogrády, P.; Pedersen, T. B.; Pitoňák, M.; Reiher, M.; Roos, B. O.; et al. MOLCAS 7: The Next Generation. *J. Comput. Chem.* **2010**, *31* (1), 224–247.

(31)   Bloch, C. Sur La Théorie Des Perturbations Des États Liés. *Nucl. Phys.* **1958**, *6*, 329–347.

(32)   Des Cloizeaux, J. Extension D'une Formule de Lagrange À Des Problèmes de Valeurs Propres. *Nucl. Phys.* **1960**, *20*, 321–346.

3.4. Publications.

This section presents the work developed during this thesis concerning the accurate theoretical extraction of magnetic exchange interactions in complex systems. The contribution is presented in two works that have been partially explained throughout the previous discussion. Both are published.

The two papers use the crystal structure of coordination compounds to extract the relevant magnetic interactions by means of the mapping approach, although each of them deals with different aspects of the formulation. Paper #3.1 focuses the attention on a family of heterodinuclear complexes and finds that in some cases the spin projector, which links the Heisenberg and Ising energetic spectra, cannot be defined. Paper #3.2 studies a general trinuclear Cu(II) complex, where no symmetry operator relates the magnetic centres. Here, the problem with the mapping approach is not on the definition of the spin projector, but rather on the Heisenberg spectrum itself, since it does not offer enough energy differences to extract all relevant magnetic interactions. Both works served to identify some deficiencies of the mapping approach proposed by Nooddleman,[4–6] which, following previous studies on our group,[8] led to the proposal of an alternative mapping approach, and to its application and validation on three electrons three centres problem.

3.4.1.   Paper #3.1.

Spin Adapted versus Broken Symmetry Approaches in the Description of Magnetic Coupling in Heterodinuclear Complexes.

Spin Adapted versus Broken Symmetry Approaches in the Description of Magnetic Coupling in Heterodinuclear Complexes

Ramon Costa,[†,‡] Rosendo Valero,[§] Daniel Reta Mañeru,[†,∥] Ibério de P. R. Moreira,[†,∥] and Francesc Illas*[,†,∥]

[†]Institut de Química Teòrica i Computacional (IQTCUB), [‡]Departament de Química Inorgànica, and [∥]Departament de Química Física, Universitat de Barcelona, C/Martí i Franquès 1, E-08028 Barcelona, Spain

[§]Center for Superfunctional Materials, Department of Chemistry, School of Natural Science, Ulsan National Institute of Science and Technology (UNIST), UNIST-gil 50, Ulsan 689-798, Korea

ⓢ *Supporting Information*

ABSTRACT: The performance of a series of wave function and density functional theory based methods in predicting the magnetic coupling constant of a family of heterodinuclear magnetic complexes has been studied. For the former, the accuracy is similar to other simple cases involving homodinuclear complexes, the main limitation being a sufficient inclusion of dynamical correlation effects. Nevertheless, these series of calculations provide an appropriate benchmark for density functional theory based methods. Here, the usual broken symmetry approach provides a convenient framework to predict the magnetic coupling constants but requires deriving the appropriate mapping. At variance with simple dinuclear complexes, spin projection based techniques cannot recover the corresponding (approximate) spin adapted solution. Present results also show that current implementation of spin flip techniques leads to unphysical results.
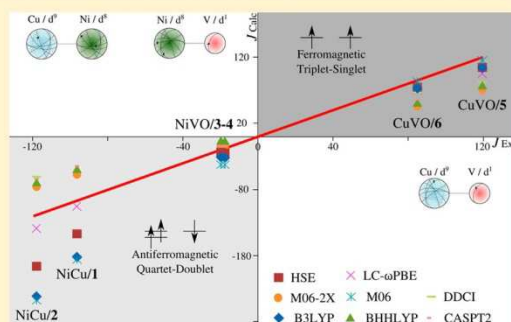
1. INTRODUCTION

One of the most active areas in contemporary coordination chemistry is the research on molecular magnetism triggered by the possibility to build nanoscale magnetic devices.[1] From a fundamental point of view, this field of research focuses on the study of the exchange coupling interactions between unpaired electrons associated with different metal centers that produce nonmetallic materials with new magnetic properties.[2] Many efforts have been devoted to the preparation, characterization, and study of such polynuclear complexes with the aim of understanding and controlling their magnetic and electronic properties in order to prepare new materials with applications in electronic and optical devices.[3]

Progress in this field has been based in establishing magnetostructural correlations for simple systems, paying attention to the nature and oxidation state of the transition metal centers (including the lanthanides), their coordination geometry, and the kind and disposition of the bridging ligands.[4,5] After analyzing the wide variety of magnetic compounds obtained so far, it has been possible to design and synthesize more complex and efficient systems. Nevertheless, most of the major improvements such as single molecule magnets (SMMs) have been largely achieved through empirical work.[6] SMMs are metal–organic molecular compounds that show superparamagnetism below a certain "blocking" temperature at the molecular scale.[7] These systems do not show, in general, collective long-range magnetic order

(i.e., negligible intermolecular magnetic coupling) and the molecular elements consist of a few magnetic centers showing zero-field splitting (ZFS) that provokes a strong anisotropy and significant intramolecular exchange interactions.

From a structural point of view, molecular based magnets are solids formed by molecular building blocks that exhibit ferro-, antiferro-, or ferrimagnetism due to intermolecular interactions between more or less localized magnetic moments. The main difference between these compounds and the standard ferro- or ferrimagnets is related to their low-energy synthesis from wet chemistry (precipitation/crystallization versus metallurgical or electroplating processes) that allows for a series of combinations of different molecular blocks to produce materials with tailored electric, optic, and magnetic properties.[7] These can be purely organic molecular materials or, most commonly, inorganic or organometallic molecular materials. Finally, it is worth pointing out that purely organic diradicals and polyradicals raised considerable interest because of their possible application in magnetic technologies.[8,9]

Because of their relative simplicity, binuclear Cu(II) complexes have been the focus in the initial development in molecular magnetism. In these systems, each metallic center contributes to the electronic structure with one unpaired electron localized essentially in one 3d orbital and relativistic

effects are almost negligible. Nevertheless, these simple systems exhibit a broad range of magnetic couplings which go from strong ferro- to strong antiferromagnetic, a behavior which can be tuned thanks to a variety of structural features involving coordination geometries, and use of different terminal and bridging ligands. This has permitted to go from mostly empirical[4] to rational magnetostructural correlations[10] and provided a convenient data set[11] to test the accuracy of different types of theoretical methods, either a wave function based on density functional theory (DFT),[12,13] appropriate calculations through exploration of the low-energy electronic states of different multiplicity, or making use of an appropriate mapping. In the case of DFT based methods, this often implies using a broken symmetry solution, and appropriate mappings to spin eigenfunctions have been proposed,[14,15] as reviewed in some detail in following text.

The simplicity of the mapping procedures encountered in the case of dinuclear Cu(II) complexes makes it easy to directly extrapolate to other cases, as in the cases involving two Ni(II) centers.[12] However, little is known about the validity of these, in principle, simple procedures for use with more complicated cases such as those involving heteronuclear complexes with two or more different metal atoms. In the present work, we use mixed Cu–V and Ni–Cu dinuclear complexes to explore the different possible approaches to predict magnetic coupling in these systems. In particular, we focus on methods involving spin eigenfunctions either at the wave function or DFT levels and, in the latter, we analyze broken symmetry solutions and propose pertinent mappings.

2. GENERAL THEORETICAL FRAMEWORK

For many molecular and extended magnetic systems, the magnetic moments are well-localized on a given atom or group of atoms, referred to as magnetic centers or magnetic sites.[16] A simple model to represent the low-energy spectrum of this kind of systems consists of assigning a given effective magnetic moment, S_i, to each magnetic center and making use of a suitable spin Hamiltonian. The possible values of S_i depend on the actual electronic configuration of the magnetic center. Hence, the d^8 configuration of Ni^{2+} in NiO or $KNiF_3$ corresponds to an effective magnetic moment of $S_{Ni} = 1$, whereas in the case of Cu dinuclear complexes $S_{Cu} = 1/2$.[17,18] The physical description of magnetic coupling, or exchange coupling as it is also often termed, in a broad class of chemical compounds including organic biradicals, inorganic complexes, and ionic solids is based on the use of the well-known phenomenological Heisenberg–Dirac–van Vleck (HDVV) Hamiltonian[17,18] as in eq 1. This Hamiltonian describes the isotropic interaction between localized magnetic moments S_i and S_j as

$$\hat{H}^{HDVV} = -\sum_{\langle i,j \rangle} J_{ij} \hat{\mathbf{S}}_i \cdot \hat{\mathbf{S}}_j \tag{1}$$

where J_{ij} constants give the magnitude and type of interaction between S_i and S_j localized spin moments and the $\langle i,j \rangle$ symbol indicates that the sum extends to nearest-neighbor interactions only. It is worth pointing out that the magnetic interactions in the HDVV Hamiltonian are of a purely (relativistic) quantum mechanical nature and, in general, much stronger than classical interactions between magnetic dipoles. In eq 1, a positive value of J_{ij} corresponds to a ferromagnetic interaction thus favoring a situation with parallel spins. The set $\{J_{ij}\}$ of parameters (their

number and magnitude) defining the HDVV Hamiltonian characterizes the magnetic ordering of the system and permits one to describe the lowest part of the excitation spectra of magnetic systems. The sign and magnitude of the relevant (i.e., large enough) J_{ij} parameters result from the particular electronic structure that, at the same time, determines the stable molecular or crystal structure of the system. Hence, the magnetic order and the crystal structure of the system are consequences of the actual electronic distribution. Nevertheless, one must advert that in some cases a general spin Hamiltonian containing additional terms may be needed.[19]

The approach described previously may seem an empirical one, but there is overwhelming evidence that the HDVV Hamiltonian appropriately describes the low-energy spectrum of magnetic systems which, in turn, represents a fundamental input for the design and preparation of new compounds with tailored magnetic properties. Clearly, understanding and predicting the $\{J_{ij}\}$ set is of paramount importance. Usually, this set of J_{ij} parameters is extracted from experimental measurements such as magnetic susceptibility curves, heat capacity curves, or neutron diffraction experiments and assumes a given form of the spin Hamiltonian. In this way, trial and error procedures are commonly used to fit results and intuition is invoked to choose the relevant interactions.

To avoid an excess of serendipity and to provide unbiased predictions about the relative importance of the different terms, accurate theoretical studies are needed. Here, it is important to point out that theoretical studies based on ab initio methods of electronic structure or on DFT play a very important role, although they also suffer from some limitations, as commented on later. Rigorously speaking, a fully relativistic formalism should be employed. However, the complexity of the n-electron relativistic problem does not permit one to carry out the required calculations for the systems of interest. Still, one can use the nonrelativistic Hamiltonian and handle magnetic interactions through a proper introduction of spin coordinates and spin symmetry, although the price to be paid is that anisotropy, Dzyaloshinskii–Moriya, spin canting, and similar effects cannot be taken into account.[19] To establish an appropriate link between predictions from the HDVV and from accurate calculations, the low-energy spectrum obtained from both approaches needs to be mapped, thus giving rise to a direct way to extract the exchange couplings, although in some cases the low-energy spectrum is not enough and effective Hamiltonian theory must be invoked.[13]

The focus of the present work is precisely on the theoretical prediction of magnetic coupling in inorganic complexes with localized magnetic moments where magnetic coupling usually results from electron–electron correlation effects.[18–21] Nonetheless, it is fair to acknowledge the few efforts toward an ab initio description of magnetic coupling including spin–orbit effects.[22] This field has been studied in detail by various authors, and a recent review is available.[13] The novelty here is in the heteronuclear nature of the magnetic complexes which, as stated in the previous section, introduces nontrivial aspects on the usual mapping procedure,[12] as described in the next section.

3. STRUCTURAL AND MAGNETIC PARAMETERS OF THE SYSTEMS STUDIED

Two antiferromagnetic Cu(II)–Ni(II) systems with CCDC references PAJZAB (compound **1**) and PAJZEF (compound **2**) have been selected.[23] These antiferromagnetic complexes show

different coordination on the nickel atom, a 6-fold coordinate for the former and a distorted-TBP 5-fold coordinate for the latter, but with the same oxamato bridging ligand and a similar square-planar environment for the Cu(II) ion. The experimentally reported values are $J(\text{PAJZAB}) = -96.3 \text{ cm}^{-1}$ and $J(\text{PAJZEF}) = -117.8 \text{ cm}^{-1}$. We also selected two $VO^{IV}Ni^{II}$ systems, WIXFOZ (compound **3**) and WIXFUF (compound **4**),[24] which are electronically equivalent to the Cu(II)−Ni(II) ones and of an antiferromagnetic nature, but here one metal is placed at the beginning of the first transition series and the other at the end, in such a way that the magnetic orbitals are very different in energy. The experimental values are $J(\text{WIXFOZ}) = -17.8 \text{ cm}^{-1}$ and $J(\text{WIXFUF}) = -20.0 \text{ cm}^{-1}$.

Finally, we choose two VO(IV)−Cu(II) systems, BIGFAY[25] and PUSJOC,[26] electronically equivalent to Cu(II) binuclears, and both moderately ferromagnetic. As in the preceding systems, the magnetic orbitals are again well-separated in energy. The BIGFAY complex (compound **5**) consists of two ions inside parallel square-pyramidal environments favored by a Schiff-base bichelating ligand providing two phenoxo-type bridges. The PUSJOC complex cation (compound **6**) contains both ions in a hexacoordinated environment inside a macrocyclic ligand with similar phenoxo bridges plus a μ_2-O,O'-acetato. The experimental coupling constants are $J(\text{BIG-FAY}) = 118 \text{ cm}^{-1}$ and $J(\text{PUSJOC}) = 85 \text{ cm}^{-1}$.

The relevant information regarding these compounds is summarized in Table 1.

Table 1. Cambridge Crystallographic Data Base (CCDB) Names, Experimental J Values (cm^{-1}), and Reference of the Molecular Systems Studied

complex	CCDB name	J	ref
1	PAJZAB	−96.3	23
2	PAJZEF	−117.8	23
3	WIXFOZ	−17.8	24
4	WIXFUF	−20.0	24
5	BIGFAY	118	25
6	PUSJOC	85	26

4. EXTENDING THE MAPPING APPROACH TO HETERODINUCLEAR COMPLEXES

a. Case of Spin Eigenfunctions. For a Cu(II)−Cu(II) system, the two unpaired electrons can couple in either a triplet state (parallel alignment) or a singlet state (antiparallel alignment). The relative disposition and energy difference between both states determines the ground state. Hence, a ferromagnetic coupling results in a triplet (T) ground state whereas antiferromagnetic coupling results in singlet (S) ground state. In this simple case, the singlet−triplet gap directly determines the J coupling constant (positive or negative, respectively) in the simple HDVV spin Hamiltonian involving now two magnetic centers only

$$\hat{H}^{\text{HDVV}} = -J\hat{\mathbf{S}}_1 \cdot \hat{\mathbf{S}}_2 \tag{2}$$

with $S_1 = S_2 = 1/2$ and $J = E(S) - E(T)$.[12]

With a similar reasoning, it turns out that for a Ni(II)−Ni(II) (octahedral) system, the two unpaired electrons per center couple in a local triplet state leading to effective $S_1 = S_2 = 1$ magnetic centers. Now S_1 and S_2 can couple into a quintet (Q), a triplet (T), or a singlet (S) state. Depending on the nature of

the ground state (Q or S), one gets ferromagnetic or antiferromagnetic coupling. Again, the coupling constant J (positive or negative for ferro- and antiferromagnetic coupling, respectively) defining the two-center HDVV spin Hamiltonian as in eq 2, but with $S_1 = S_2 = 1$, is related to the energy difference between spin states, so that $J = E(S) - E(T)$ and $2J = E(T) - E(Q)$ providing, in addition, a way to check that the low-energy spectrum is described by the HDVV spin Hamiltonian.

In a general case involving dinuclear complexes with S_1 and S_2 localized spins, one can easily show that, taking $S_1 \geq S_2$, the possible values for total S range from $(S_1 + S_2)$ down to $(S_1 - S_2)$ and that

$$E(S) - E(S - 1) = (2S + 1)J \tag{3}$$

which is the well-known Landé rule. For Cu(II)−Ni(II) compounds, where $S_1 = 1/2$ and $S_2 = 1$, one simply gets

$$E(Q) - E(D) = -3J/2 \tag{4}$$

which also holds for the case of VO(IV)−Ni(II) complexes, magnetically equivalent to Cu(II)−Ni(II). Finally, for the VO(IV)−Cu(II) complexes, magnetically equivalent to Cu-(II)−Cu(II), the singlet−triplet energy difference gives directly J (see Figure 1).

The preceding discussion provides the basis for extracting the J coupling constant from appropriate theoretical calculation of the energy of the different spin states of the system. Clearly, calculations should be accurate enough to resolve small energy differences typically within or below the wavenumber range. Moreover, one must realize that, even if the highest multiplicity state can be expressed by a single determinant wave function, the low spin states involve necessarily a multideterminantal description which often involves more than one configuration state function. Rigorously speaking, multiconfigurational methods are required to describe these electronic states, and, in addition, electron correlation effects are essential to accurately estimate not only the total energy but the total energy differences. For small and medium size systems, this type of calculations can be carried out as described later on.

We now briefly introduce the minimum multiconfiguration form of the relevant electronic states. To this end, we assume that a localized basis set is used with orbitals a_1 and a_2 in center a with local $S_a = 1$ and b_1 in center b with local $S_b = 1/2$. The high spin components of the quartet state can be described as

$$\left| Q, \frac{3}{2} \right\rangle = |a_1 a_2 b_1\rangle \tag{5}$$

or

$$\left| Q, -\frac{3}{2} \right\rangle = |\bar{a}_1 \bar{a}_2 \bar{b}_1\rangle \tag{6}$$

where, as usual, a and $\bar{a}$ denote α and β spin−orbitals, respectively. Similarly, the low spin components of the quartet state are

$$\left| Q, \frac{1}{2} \right\rangle = \frac{1}{\sqrt{3}} \left(|a_1 a_2 \bar{b}_1\rangle + |a_1 \bar{a}_2 b_1\rangle + |\bar{a}_1 a_2 b_1\rangle \right) \tag{7}$$

$$\left| Q, -\frac{1}{2} \right\rangle = \frac{1}{\sqrt{3}} \left(|a_1 \bar{a}_2 \bar{b}_1\rangle + |\bar{a}_1 a_2 \bar{b}_1\rangle + |\bar{a}_1 \bar{a}_2 b_1\rangle \right) \tag{8}$$

and those of the doublet can be written as
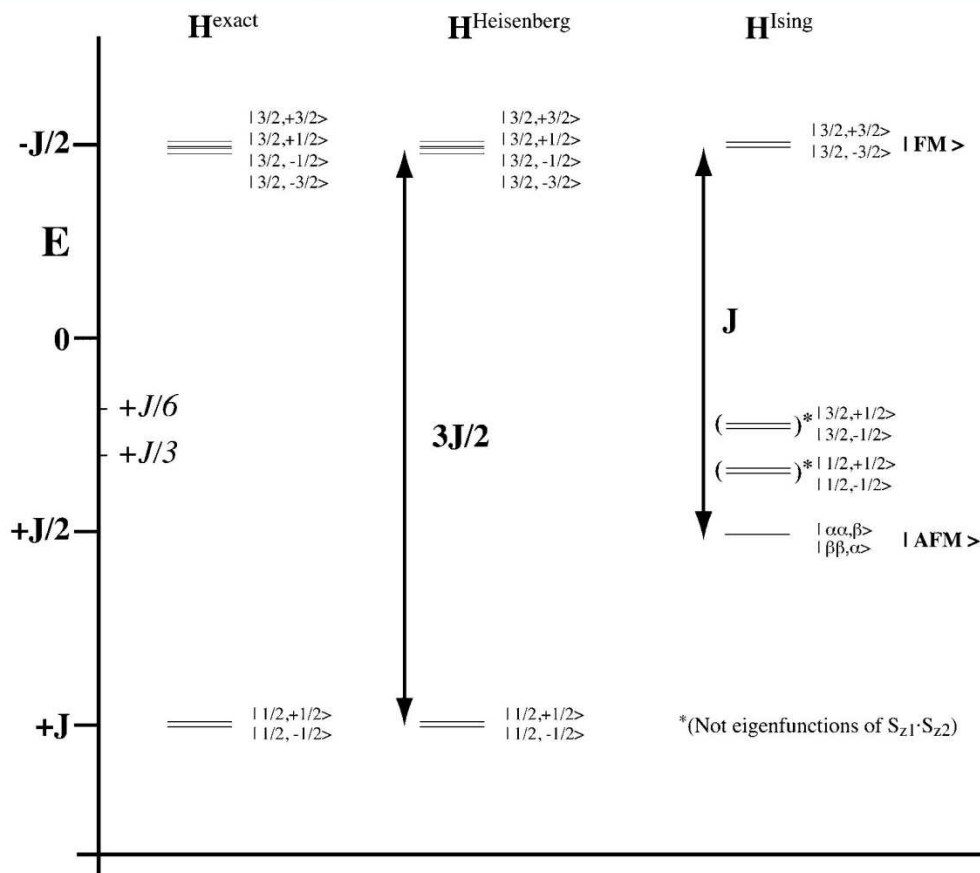
Figure 1. Energy diagram for the eigenstates of the exact, Heisenberg, and Ising model Hamiltonians for a system of local $S_1 = 1$ and $S_2 = 1/2$ interacting spin states with $J < 0$. The states in parentheses indicate that these particular eigenstates of the Heisenberg Hamiltonian are not eigenfunctions of the Ising Hamiltonian and their energy is just an expectation value.

$$\left| D, \frac{1}{2} \right\rangle = \sqrt{\frac{2}{3}} |a_1 a_2 \bar{b}_1\rangle - \frac{1}{\sqrt{6}} (|a_1 \bar{a}_2 b_1\rangle + |\bar{a}_1 a_2 b_1\rangle) \quad (9)$$

$$\left| D, -\frac{1}{2} \right\rangle = \frac{1}{\sqrt{6}} (|a_1 \bar{a}_2 \bar{b}_1\rangle + |\bar{a}_1 a_2 \bar{b}_1\rangle) - \sqrt{\frac{2}{3}} |\bar{a}_1 \bar{a}_2 b_1\rangle \quad (10)$$

From eqs 7–10, it is clear that the doublet states and the $S_z = \pm 1/2$ components of the quartet state include forms that break the local triplet in the $S_a = 1$ center, for instance $|a_1 \bar{a}_2 \bar{b}_1\rangle$, $|\bar{a}_1 a_2 \bar{b}_1\rangle$, $|a_1 \bar{a}_2 b_1\rangle$ and $|\bar{a}_1 a_2 b_1\rangle$. In the following we will show that this fact introduces difficulties in defining the proper mapping to derive the J value from broken symmetry solutions.

b. Case of Broken Symmetry Solutions. For very large systems, explicitly correlated wave function based methods may become unfeasible. Here, one can rely on standard DFT based methods which have proven to provide accurate predictions.[11,12] Note, however, that these methods are single determinant in nature and the description of the low spin states often involves the use of a broken symmetry (BS) solution. In spite of initial claims that the BS solution approaches the energy of the low spin state, it has been shown that this is not the case,[12,27] and appropriate mappings are required. This can be easily achieved by realizing that DFT calculated energies are related to the diagonal matrix elements

of the HDVV Hamiltonian and mapping to expectation values rather than to the energy of each spin state. This is consistent with the use of the Ising Hamiltonian, a special case of the HDVV involving diagonal terms only. However, the mapping in terms of expectation values does not require assuming that the J values in both spin Hamiltonians are the same. For Cu dinuclear complexes, J is simply obtained as

$$J = E(S) - E(T) = 2[E(BS) - E(T)] \quad (11)$$

whereas in the general case one gets

$$J = [E(BS) - E(HS)]/2S_1 S_2 \quad (12)$$

where HS simply stands for the high spin state. To take into account the inherent spin contamination of the BS solution, Yamaguchi et al.[28−30] introduced the expectation value of the square of the total spin operator for the HS and BS solutions.

$$J = \frac{E(BS) - E(HS)}{2(\langle S^2 \rangle_{HS} - \langle S^2 \rangle_{BS})} \quad (13)$$

In the cases considered so far, the energy of the low spin states is directly achievable from the appropriate mapping; see for instance Figures 1 and 2 in ref 15. The situation is less clear in the case of heterodinuclear complexes such as those where $S_1 = 1/2$ and $S_2 = 1$ described in the previous section. Obviously,

the description of the high spin state, a quartet (Q) for Cu(II)−Ni(II) and VO(IV)−Ni(II) and a triplet (T) for VO(IV)−Cu(II), poses no problems. However, the situation is less clear for the corresponding low spin states (doublet or open shell singlet, respectively). For the Cu(II)−VO(IV) ferromagnetic systems, the first excited state corresponds to an open shell singlet that we propose to describe by means of a suitable $S_z = 0$ BS solution (here denoted SBS). Here the mapping is as in eq 11, which can be written as

$$J = 2[E(SBS) - E(T)] \qquad (14)$$

For the antiferromagnetic Ni(II)−Cu(II) and Ni(II)−VO(IV) complexes, the quadruplet state corresponds to the first excitation, and the ground state is a multideterminantal doublet where two electrons in the Ni(II) ion remain unpaired and parallel, and in opposite alignment with the unpaired electron of the Cu(II) or VO(IV) moieties. Here, one finds several BS solutions as shown schematically in Figure 1. Note, in addition, that some of the BS solutions are not eigenfunctions of the Ising spin Hamiltonian and, hence, they cannot be compared to the diagonal elements of the HDVV Hamiltonian. This means that these BS solutions cannot be used in the mapping procedure to extract the magnetic coupling constant and one must warn that their use is likely to lead to unphysical results. To solve the puzzle and find the appropriate mapping, one can make use of the information provided by the spin eigenstates in eqs 5−10. Note that from the multiple possible broken symmetry solutions, two cases with $S_z = \pm 1/2$ exist maintaining the local spin on center a as $S_a = 1$. These are $|BS_1\rangle$ and $|BS_2\rangle$ which are closely related to the $|a_1 a_2 \overline{b_1}\rangle$ and $|\overline{a_1} \overline{a_2} b_1\rangle$ determinants introduced earlier, provided the spatial part of the α and β spin−orbitals are not too different. Obviously, the high spin state solutions are suitable representations of the $|a_1 a_2 b_1\rangle$ and $|\overline{a_1} \overline{a_2} \overline{b_1}\rangle$ determinants. Now, note that the $|BS_1\rangle$ and $|BS_2\rangle$ solutions are combinations of the $|D, \pm 1/2\rangle$ and $|Q, \pm 1/2\rangle$ wave functions

$$|BS_1\rangle = 1/\sqrt{3}(|Q, 1/2\rangle + \sqrt{2}|D, 1/2\rangle) \qquad (15)$$

$$|BS_2\rangle = 1/\sqrt{3}(|Q, -1/2\rangle - \sqrt{2}|D, -1/2\rangle) \qquad (16)$$

which is reminiscent of the simple singlet−triplet case where, except for spin contaminations, the broken symmetry solution is a mixture of singlet and triplet states.[14] Now, the expectation value of the $|BS_1\rangle$ and $|BS_2\rangle$ solutions for the HDVV Hamiltonian can be easily derived as

$$\langle BS_1|HDVV|BS_1\rangle = 1/3[E(Q) + 2E(D)]$$
$$= 1/3(-J/2 + 2J)$$
$$= J/2 \qquad (17)$$

$$\langle BS_2|HDVV|BS_2\rangle = \langle BS_1|HDVV|BS_1\rangle \qquad (18)$$

whereas for the high spin state one has

$$\langle HS|HDVV|HS\rangle = -J/2 \qquad (19)$$

Note, assuming that the square of the total spin operator can be computed from the Kohn−Sham density, one also has

$$\langle S^2\rangle_{BS_1} = 1/3(\langle S^2\rangle_Q + 2\langle S^2\rangle_D) = 1.75 \qquad (20)$$

$$\langle S^2\rangle_{HS_1} = \langle S^2\rangle_Q = 3.75 \qquad (21)$$

From the preceding discussion it is clear that any possible combination of $|BS_1\rangle$ and $|BS_2\rangle$ does not contain any term violating the local triplet $S_a = 1$ on the a center; those components exactly cancel but they are necessary to define the spin states as in eqs 9 and 10. Consequently, it is not possible to univocally define an appropriate spin projector to reconstruct the doublet state from the BS solutions. It is worth pointing out that this is at variance with the homonuclear cases where spin projection reconstructs the appropriate spin state. Figure 1 summarizes the preceding main conclusions and illustrates that, in practice, one can simply use

$$J = E(SBS) - E(Q) \qquad (22)$$

where SBS stands for suitable $S_z = 1/2$ BS solution and Q for the high spin solution representing the quartet state. Finally, note that some of the problems encountered in deriving the preceding mappings for the heterodinuclear complexes were already identified in the case of Ni(II)−Ni(II) complexes, where multiple BS solutions exist, some of which do not have physical meaning.[12,15] An important difference between Ni(II)−Ni(II) and heteronuclear systems exists. In the first case, the two possible antiferromagnetic BS solutions (i.e., $|a_1 a_2 \overline{b_1} \overline{b_2}\rangle$ and $|\overline{a_1} \overline{a_2} b_1 b_2\rangle$) are degenerate with respect to the Ising Hamiltonian, and, consequently, the two corresponding diagonal elements of the HDVV Hamiltonian are also identical. Therefore, they can be combined, and one of the combinations recovers the symmetry of one of the three spin states, the triplet one. The absence of symmetry in the heterodinuclear complexes breaks this degeneracy, and it is not possible to combine BS solutions to reconstruct a spin state. Nevertheless, an appropriate mapping can be found as previously described and illustrated in Figure 1.

5. COMPUTATIONAL DETAILS

Explicitly correlated wave function and DFT methods have been used to obtain the appropriate energy values to be used in the corresponding mapping. In the first case, we used a variety of methods of increasing accuracy, starting with the CASSCF wave function[31] as a reference to second-order perturbation, introduced through the well-known CASPT2[32−34] procedure, and to variational multireference configuration interaction (MRCI) calculations using the difference dedicated configuration interaction (DDCI)[35] method. To complete the study, a series of hybrid DFT calculations have been carried out to extract the magnetic coupling constants with state-of-the-art exchange-correlation functionals. A number of such exchange-correlation potentials have been used, starting with the popular B3LYP hybrid,[36,37] the BHHLYP (or BHandHLYP)[38] one, and including the M06 and M06-2X meta hybrid functionals of Zhao and Truhlar[39−41] and the short-range HSE[42] and long-range LC-ωPBE[43] range-separated functionals with the standard value of the range separation parameter (ω). Note that the selected functionals incorporate different amounts of Fock exchange: 20% for B3LYP, 27% for M06, 50% for BHandHLYP, and 54% for M06-2X. In all cases, the DFT calculations were carried out within the spin-polarized (unrestricted) formalism based on a single determinant, and high spin and BS solutions were considered. In order to avoid the problems encountered when dealing with BS solutions, calculations have also been carried out with the time-dependent DFT (TDDFT)[44−47] in its spin flip variant.[48−50] Previous work on Cu dinuclear complexes[27] has shown that, for a given

functional, spin flip TDDFT calculated magnetic coupling constants are consistent with those obtained from the appropriate mapping (spin projection). We anticipate, however, that this method encounters severe problems when aiming at obtaining the singlet−triplet and doublet−quartet splitting of the present heterodinuclear systems, thus hampering the prediction of the corresponding magnetic couplings. It is worth pointing out that some alternative methods have been proposed to calculate exchange couplings, such as the variation of constrained DFT[51] based on the use of coupled-perturbed Kohn−Sham equations as proposed by Phillips and Peralta.[52] However, to our knowledge, this method has not been used in heteronuclear systems. It would be interesting to see if it can reproduce the exchange couplings in this case, where spin flip TDDFT fails to give physical results.

The wave function and DFT calculations were carried out using suitable Gaussian-type orbitals (GTO) basis sets. For nonmetal atoms, the all electron standard 6-31G(d) basis set has been selected. For the metallic centers, we used either all electron (AE) or effective core potential (ECP) bases. In the first case, we used the rather large standard basis set GTO 6-3111+G for V, Ni, and Cu. From a technical point of view one must mention that in the calculations with the Gaussian code this basis was entered manually since otherwise the results obtained correspond actually to the 6-311G basis. For the calculations where the metal innermost electrons are described through an ECP, we used the extended standard LANL2TZ small core basis, which allows one to take scalar relativistic effects into account. The basis sets chosen were the same as in previous works[11,53,54] except for the computationally expensive NiVO (compound 4), where the polarization functions of the light atoms basis set have been removed leading simply to a 6-31G basis set.

To make DDCI calculations feasible, we used 6-31G for C and H, 6-31G(d) for O and N, and all electron 6-3111+G for metal atoms. It was proven that there is no important deviation in doing so at CASSCF level. For compound 2 CASSCF(3,3) with 6-31G(d) yields a $J = -13.1$ (638 basis functions) and $J = -12.9$ (518 basis functions) with 6-31G for H, C. For compound 5 CASSCF(3,3) with 6-31G(d) yields $J = 30.8$ (516 basis functions) and $J = 31.4$ (421 basis functions) with 6-31G for H, C. For compound 6 CASSCF(3,3) with 6-31G(d) yields a $J = 23.4$ (678 basis functions) and $J = 23.5$ (543 basis functions) with 6-31G for H, C. More details can be found in Table S11 (Supporting Information).

For the CASSCF calculations, two types of active space were defined, a minimal one including the magnetic orbitals only and one including molecular orbitals centered on the bridging ligands. For the singlet−triplet systems this leads to a two-electron-in-two-orbitals active space (CASSCF(2,2)), whereas for the doublet−quartet systems one has a three-electron-in-three-orbitals active space (CASSCF(3,3)). The second type of active space involves CASSCF(12,12) and CASSCF(13,13) for singlet−triplet systems and for doublet−quartet systems, respectively, and were essentially carried out to verify that the minimal CAS description is physically meaningful (see Tables S1−S4 of the Supporting Information). In this respect, care was taken to ensure that all of the MOs in the active space are equivalent when using both LANL2TZ and AE 6-3111+G basis sets for the metal atoms. To avoid intruder states in the CASPT2 treatment, an imaginary level shift[55] of 0.2 au has been applied. In the most recent version of CASPT2, the zero-order Fock operator is modified with a so-called IPEA shift.[56]

In the present work, and following previous research on magnetic systems,[57] this shift has been removed. Finally, to reduce the computational burden, we have applied the Cholesky decomposition to the two-electron integrals[58,59] with the default threshold of 10^{-4}.

MRCI calculations using the difference dedicated configuration DDCI method[35] have been carried out, starting from minimal CASSCF as the reference state. The DDCI leads to a configuration interaction expansion which is a subset of the full MRSDCI, neglecting the 2h−2p (h = hole; p = particle) excitations involving orbitals out of the CAS, which at second order of perturbation theory equally contribute to the two states, provided the same set of molecular orbitals is used.[60] Both DDCI2 and DDCI methods, including two and three degrees of freedom for excitations out of the CAS, respectively, have been used. In the case of the doublet−quartet systems (compounds 2 and 3), the DDCI calculations have been carried out with the orbital set optimized for the quartet state. In the case of the singlet−triplet systems (compounds 5 and 6), the DDCI calculations were carried out with three different sets of orbitals, those of the singlet, triplet, and the state specific (SS) ones. The large size of the molecules studied required a reduction in the active electrons and virtual orbitals to produce tractable DDCI spaces of the order of 10^8-10^9 determinants. Thus, for compound 2 we explicitly treat 211 electrons in 317 orbitals; for compound 3, 238 electrons in 320 orbitals; and for compounds 5 and 6, 166 electrons in 274 orbital and 220 electrons in 338 orbitals, respectively. Additional information can be found in the Supporting Information.

All calculations were performed on the crystallographic structures of the isolated heterodimetallic complexes (cationic or neutral) in vacuo, in order to prevent mixing structural and electronic effects and avoid introducing errors in the magnetic coupling constants arising from errors in the structure optimization. For structures 1 (PAJZAB) and 2 (PAJZEF), it was necessary to previously optimize the disordered atoms ($C_3H_6NH_2$ and CH_3 moieties, respectively) together with the "lost" hydrogen atoms, using the B3LYP method on the quartet state.

The DFT based calculations have been carried out using the Gaussian 09 suite of programs.[61] The electronic structure packages Q-Chem 3.2[62] and GAMESS[63,64] were used for the SF-TDDFT calculations. Q-Chem 3.2 allows one to use only unrestricted reference states, whereas GAMESS can employ both restricted and unrestricted reference states. MOLCAS 7.8[65] was used to perform the CASPT2 calculations. Finally, DDCI calculations were carried out using the CASDI code[66] interfaced to the MOLCAS 7.6 package[65] which provided the CASSCF reference wave functions.

6. RESULTS AND DISCUSSION

a. Results from CASSCF/CASPT2 Calculations.
For the singlet−triplet cases, the minimal (2,2) active space was completed with molecular orbitals centered on the ligands up to a (12,12) size. It is interesting to underline the character of those orbitals. For CuVO containing compounds 5 and 6, besides the magnetic orbitals, there are two π molecular orbitals (MOs) with contribution in the oxygen atoms between the metallic centers, three MOs that form the V−O bond, and the corresponding five antibonding MOs. For the doublet−quartet cases in compounds 1−4, the minimal (3,3) active space was completed with molecular orbitals centered on the ligands up to a (13,13) size. For compounds 3 and 4, the additional MOs

Table 2. Calculated ab Initio J Values (cm^{-1}) of the Molecular Systems Studied[a]

| M$_1$M$_2$/compd | CASPT2 | | method | DDCI | | J_{exp} |
| | | | | DDCI2 | DDCI | |
	LANL2	AE	orbitals/CAS	AE	AE	
NiCu/**1**	−49.5	−45.2				−96.3
NiCu/**2**	−68.9	−62.3	Q/3,3	−23.5	−61.1	−117.8
NiVO/**3**	−15.9	−16.2	Q/3,3	−10.1	−16.8	−17.8
NiVO/**4**	−15.7	−15.2				−20.0
CuVO/**5**	71.8	65.0	T/2,2	39.9	81.1	118
			T/4,4	40.1	73.6	
			S/4,4		72.1	
			SS/4,4		83.3	
CuVO/**6**	55.5	49.6	T/2,2	22.6	60.4	85
			S/2,2		59.4	
			SS/2,2		66.8	

[a] M$_1$M$_2$ specifies the couple of magnetic centers; LANL2 and AE stand for calculations carried out with effective core potentials or all electron, respectively. The CASPT2 calculations use the minimal (3,3) or (2,2) active space. The basis sets are as specified in the text; note that in the DDCI calculations C and H atoms are described with a standards 6-31G basis set. S,T, D, Q, or state specific (SS) indicates the orbital set used to carry out the DDCI2 and DDCI calculations.
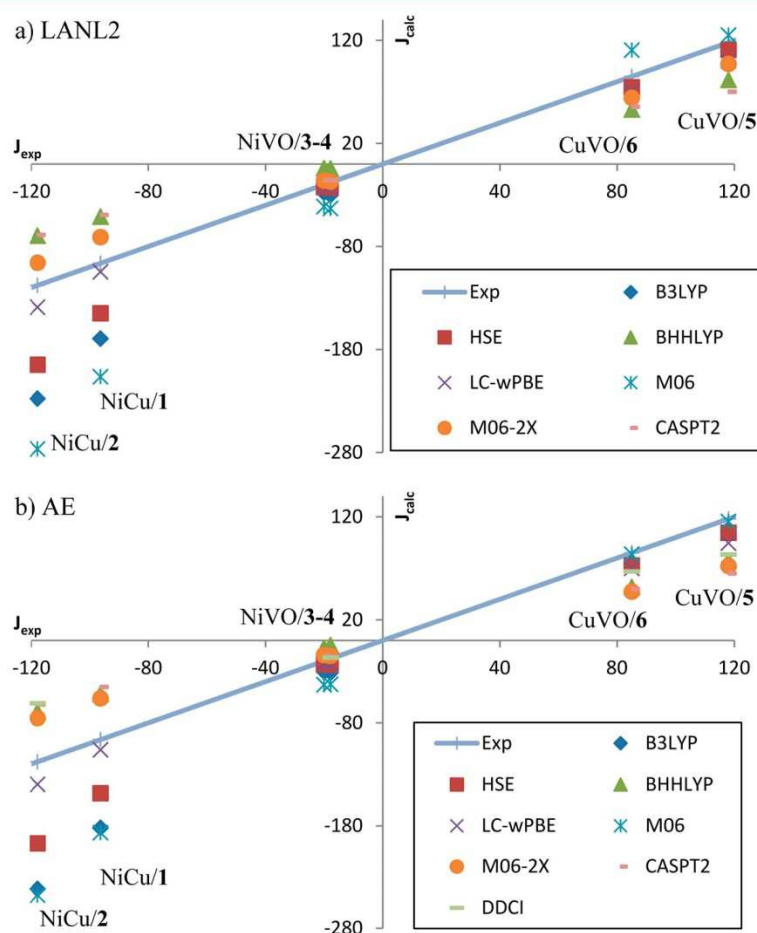
Figure 2. Schematic representation of the deviation from experiment of DFT and CASPT2 results based on the use of a broken symmetry approach, as discussed in section 6.c. The straight line indicates the perfect correlation between experimental and calculated J values (cm^{-1}) to guide the eye. Panel a presents the results using LANL2 pseudopotential for the description of the metallic center; panel b, for the all electron description including both CASPT2 and DDCI results.
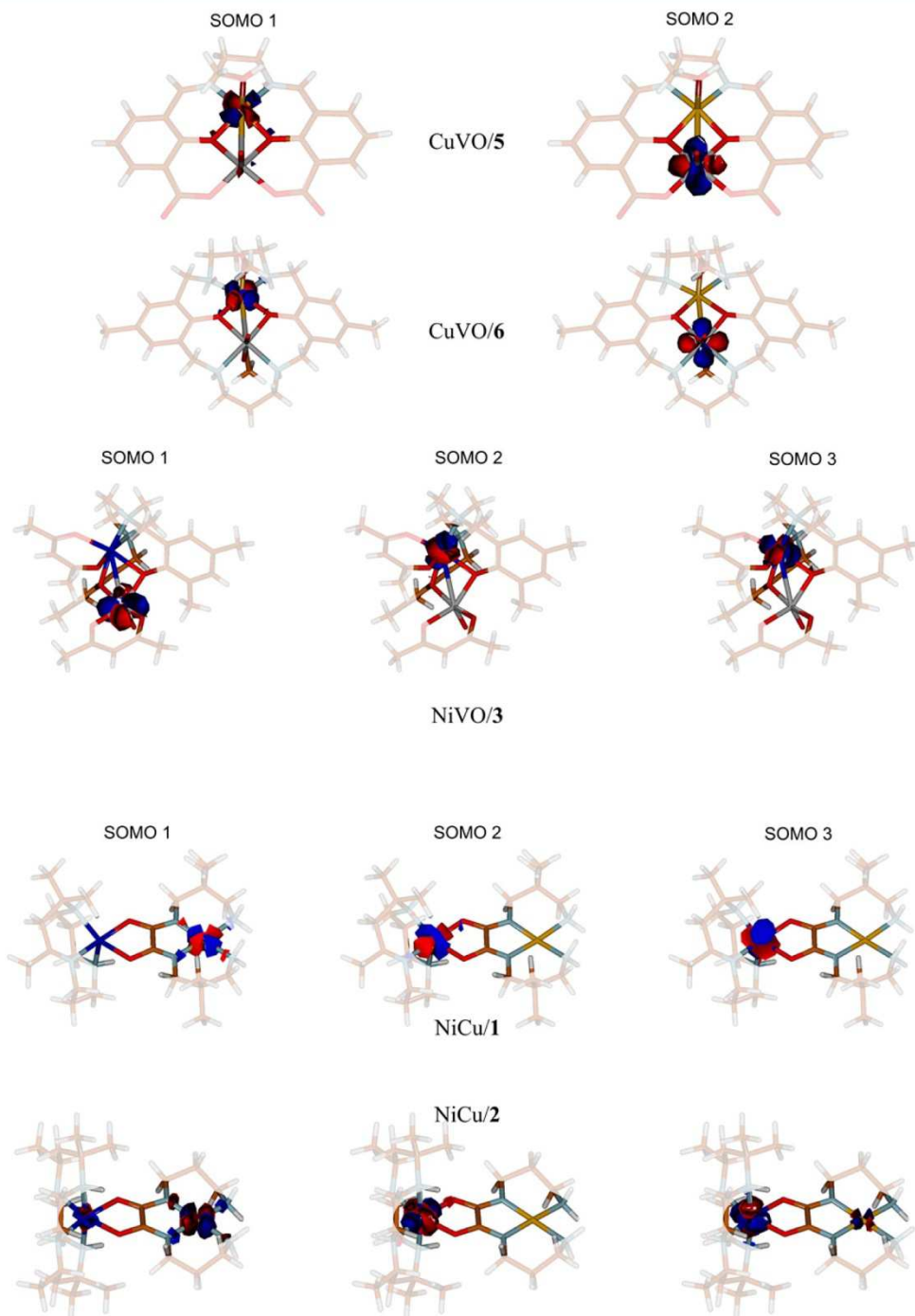
Figure 3. Contour plots of the relevant magnetic orbitals of compounds **1−3**, **5**, and **6** taken from the CASSCF high spin state wave function.

are completely analogous to those previously described for the CuVO systems **5** and **6**, namely, three of σ type with respect to the plane of the ligands and two of π type with the correlating five antibonding MOs.

At the CASSCF level, the magnetic coupling constants calculated with the minimal and extended active spaces are almost identical indicating (Tables S1−S5 in the Supporting

Information) that the former contains the physically meaningful orbitals. Consequently, CASPT2 calculations presented in Table 2 correspond to the minimal CAS; CASPT2 calculations for the more extended CAS are presented in Table S2 of the Supporting Information. From Table 2 it is clear that, with a minimal active space, CASPT2 is only capable of providing qualitatively correct results and it underestimates the value of

the magnetic coupling for both ferromagnetic and antiferromagnetic complexes, in line with previous work.[13] Results from CASPT2 on top of the extended CAS (Table S2 of the Supporting Information) do not improve the description indicating the need to go beyond second-order perturbation theory and justify carrying out the computationally demanding DDCI calculations described later. Overall, the calculated J values are slightly better when LANL2TZ is used for the metals, as compared with the all electron 6-3111+G basis set. Exceptions are **3** and **4**, for which CASPT2 and experiment are in good agreement.

The recovery of, in general, a fraction of magnetic coupling only with CASPT2, and their underestimate, are well-known.[55,67] An essential limitation of the method is that the computational cost rises steeply with the size of the CASSCF active space. Furthermore, both the present report and previous work have shown that CASPT2 prediction of magnetic couplings strongly depends on several technical parameters. In the version of CASPT2 we have employed, namely, the one implemented in the MOLCAS 7.8 package,[63] the default zero-order Hamiltonian contains the so-called IPEA shift (see Computational Methods). The purpose of this shift is to balance the description of closed and open shell systems. In the present study and following previous work,[65] we set this shift to zero. The standard value of this shift (0.25 au) gave the wrong ground state for CuVO. In the literature, widely different values of the IPEA shift have been employed, ranging from zero to 0.70 au.[68−72] Also in CASPT2, the presence of intruder states forces one to either increase the size of the active space, which is not always possible or convenient, or to introduce a level shift. Using a value of the imaginary level shift of 0.20 au, all obtained magnetic couplings are reasonable, and we have adopted that value. However, an important uncertainty remains, namely, whether the heteronuclear systems considered can be described with the Heisenberg Hamiltonian. The present systems, with a total of two or three magnetic electrons, only produce two electronic states and an energy difference, which can always be related to a value of J. For systems such that several magnetic electronic states are possible, it has been found that CASPT2 does not fulfill the Landé interval rule,[65] as it should for a complex well-described by the Heisenberg Hamiltonian. This problem is likely to be due to the use of different orbitals for each state, as reported earlier for Fe dinuclear complexes.[73] The logic is that each set of orbitals spans a different effective Hamiltonian and, hence, there is no one-to-one mapping. This problem could be ignored at a pragmatic level choosing the two electronic states that give the best value of J, but of course this cannot be regarded as satisfactory at a theoretical level.

From all of the preceding discussion, one can conclude that the CASPT2 method, at least in its current form, is not suitable for the study of magnetic systems. CASPT2 can describe relatively simple systems at a qualitative level, but a quantitative prediction is not possible, since there are at present too many uncertainties for its application to general magnetic systems.

b. Results from DDCI Calculations. To further confirm that the shortcomings of the CASPT2 method arise from the neglect of important dynamical correlation effects, DDCI calculations have been carried out for those compounds where molecular size is not excessive, as reported in Table 2. A schematic representation of the results can be found in Figure 2. For the singlet–triplet systems **2** and **3**, DDCI results are close to those obtained with the CASPT2 approach. For

compound **3** both methods predict results in very good agreement with experiment. However, for compound **2** both CASPT2 and DDCI results considerably underestimate the experimental magnetic coupling constant. The reason is likely to be due to the contribution of bridging ligands to the differential correlation effects. This is corroborated by the orbital contours in Figure 3 showing a considerable delocalization of the active orbitals beyond the magnetic centers. For compounds **5** and **6**, DDCI represents a significant improvement over CASPT2, although the DDCI calculated magnetic coupling constants still underestimate the experimental values.

The conclusion from these very demanding calculations is that, for real systems with bulky ligands and different magnetic centers, electronic correlation effects are very important and not recovered by excitation out of the minimal CAS implying that higher excitations still play a role. Note also that some of the DDCI calculations required neglecting excitation from/to some core and virtual orbitals. Enlarging the CAS is certainly possible, but the resulting DDCI expansion is too large to be handled.

In addition one has to point out that, compared to homobimetallic systems, heterobimetallic complexes have some peculiarities. For instance, in a very recent report, several homo- and heterobimetallic complexes of divalent first-row transition metal atoms (Mn, Fe, and Co) with a direct bonding between the metals were synthesized and their properties compared.[74] All of the complexes are antiferromagnetic, but the di-iron complex is different from the rest in that it contains a metal−metal single bond and a septet ground state. In contrast, the other complexes have weak metal−metal interactions and much lower spin states. Also, in recent reports it has been shown that heterobimetallic systems in their singlet states have particularly large values of second hyperpolarizabilities, in turn giving rise to large third-order nonlinear optical (NLO) effects. This finding has been attributed to the contribution of electrons with an intermediate diradical character, and it is more marked in heterobimetallic systems due to charge asymmetry effects.[75,76]

c. Results from Spin Flip TDDFT Calculations. To test the performance of the SF-TDDFT method, calculations were carried out for the M06, BHHLYP, and M06-2X functionals only. For the singlet−triplet cases, an approximately correct spin state is obtained with the BHHLYP functional. For the CuVO complex **5**, using the LANL2DZ basis functions for the metallic ions and an unrestricted reference, we obtain $\langle \hat{S}^2 \rangle = 1.96$ and 0.13 for the approximate triplet and singlet states, respectively. The predicted magnetic coupling of $J = 81 \text{ cm}^{-1}$ is in agreement with the BS results presented later using the same functional but too small compared to experiment. Moreover, for the CuVO complex **6**, using the all electron basis sets for the metals and an unrestricted reference, we obtain $\langle \hat{S}^2 \rangle = 1.86$ and 0.29, and a magnetic coupling of $J = 65 \text{ cm}^{-1}$. Interestingly, better spin adaptation is obtained with unrestricted references as compared to restricted references. So far, results are in agreement with previous work in homodinuclear compounds.[27]

The situation is completely different for the doublet−quartet cases. In fact, for compounds **3** and **4**, we obtain values of $\langle \hat{S}^2 \rangle$ very far from the expected values of 0.75 and 3.75 for the doublet and quartet, respectively. Thus, the obtained values of $\langle \hat{S}^2 \rangle$ are 1.75 and 2.75 for the lowest two spin flip states. Note

that the expectation value for the doublet corresponds to the SBS, as defined in section 4.b, which is clear evidence that the spin flip approach for the doublet state actually describes a mixture of doublet and quartet states. As a consequence, in these cases it is not possible to estimate the values of magnetic coupling from SF-TDDFT, at least with the current implementations where all excitations are allowed.

The reason for the large deviation is the presence of single excitations that destroy the high spin coupling in the Ni atom, thus mixing local singlet and triplet states. In conclusion, SF-TDDFT is not capable of providing a uniformly correct description of the six heteronuclear complexes studied. Whereas an approximately correct spin adaptation and good values of J are obtained for the singlet–triplet cases, for the doublet–quartet cases the values of $\langle \hat{S}^2 \rangle$ and the magnetic couplings are far from the experiment even in the most favorable cases. Apparently, whether one obtains well-spin-adapted solutions depends very sensitively on the density functional and on its percentage of exact exchange. This is in contrast to the case of homonuclear complexes, where good results can be obtained with a single density functional for a range of complexes.[27,77]

d. Results from DFT Calculations with the BS Approach. The last inspection concerns the monodeterminantal description of the compounds by means of broken symmetry approach. Taking into account the problematic discussed in section 4.b. results are summarized in Table 3 and schematically depicted in Figure 2. Additional information regarding for instance $\langle \hat{S}^2 \rangle$ values can be found in the Supporting Information (Tables S5–S10).

A first thing to notice is the strong dependence on the chosen functional. Taking compound **1** as an example, the deviation with respect to the experimental value ranges from +94% for the M06 and B3LYP functionals to −46% for BHHLYP. The dependence in the functional can also be observed in Tables 4 and 5 reporting the spin density on the metallic centers as predicted by the DFT methods used although a correlation between the trends in calculated J values and spin densities does not seem to exist. The tables report results from the all electron series of calculations although very similar values are obtained when describing the core electrons by ECPs. Among all of the functionals, the long-range corrected LC-ωPBE potential comparatively gives the best results for all compounds. Among the compounds, as depicted in Figure 2, there are two families: the ferromagnetic one where the energetic difference is between singlet–triplet states (CuVO/ **5**−**6**) and the antiferromagnetic one presenting compounds with a doublet electronic state as ground state (NiCu/**1**−**2**, NiVO/**3**−**4**). There is a general underestimation of the coupling constant in the first family while the opposite stands for the antiferromagnetic compounds. Compounds **1** and **2** are poorly described by the majority of functionals, presenting the biggest deviations in the case of the B3LYP, HSE, and M06 hybrid functionals, as represented in the leftmost values in Figure 2. The reason behind the different agreement with respect to experimental values for compounds **1**−**2** and **3**−**4** might be the large difference in distance between the two metallic centers and the different chemical nature of the bridge, the π system of the oxamato bridge in **1**−**2** as opposed to the μ-O bridges in **3**−**4** (see Figure 3).

Moreover, for the M06 and M06-2X hybrid functionals there is a considerable impact depending on how the metallic center

Table 3. Calculated DFT J Values (cm^{-1}) of the Molecular Systems Studied Using the Broken Symmetry Approach[a]

	B3LYP		HSE		BHHLYP		LC-ωPBE		M06		M06-2X		J_{exp}/cm^{-1}
M_1M_2/compd	LANL2	AE	LANL2	AE	LANL2	AE	LANL2	AE	LANL2	AE	LANL2	AE	
NiCu/**1**	−169.50	−182.01	−144.86	−148.03	−51.17	−52.06	−104.52	−106.16	−206.42	−186.50	−70.97	−56.21	−96.3
NiCu/**2**	−227.74	−241.78	−194.89	−197.07	−69.53	−69.29	−138.97	−139.67	−276.62	−247.71	−95.82	−75.41	−117.8
NiVO/**3**	−30.1	−31.3	−23.1	−23.6	−4.4	−4.6	−22.3	−22.7	−43.1	−42.5	−17.1	−14.9	−17.8
NiVO/**4**	−27.9	−30.2	−22.3	−23.3	−4.2	−7.3	−21.8	−22.5	−41.3	−43.0	−16.0	−14.2	−20.0
CuVO/**5**	+108.0	+106.6	+110.8	+104.5	+81.5	+77.6	+100.3	+94.5	+125.2	+115.4	+97.2	+72.4	118
CuVO/**6**	+74.3	+75.6	+74.5	+72.7	+52.8	+51.9	+71.0	+70.0	+110.6	+83.8	+64.4	+47.4	85

[a]LANL2 and AE stand for calculation with effective core potentials and all electron, respectively.

Table 4. Spin Density on the Metallic Centers of NiCu Compounds 1 and 2 As Predicted by the Different Computational Methods Used with the Broken Symmetry Approach[a]

| | compd **1** | | | | compd **2** | | | |
| | Ni(II) | | Cu (II) | | Ni(II) | | Cu(II) | |
method	HS	BS	HS	BS	HS	BS	HS	BS
BHandHLYP	1.81	1.81	0.75	−0.75	1.81	1.81	0.74	−0.74
B3LYP	1.67	1.67	0.60	−0.60	1.67	1.67	0.60	−0.59
HSEh1PBE	1.71	1.71	0.63	−0.63	1.71	1.71	0.62	−0.62
LC-wPBE	1.71	1.71	0.64	−0.64	1.71	1.71	0.63	−0.63
M06	1.69	1.68	0.61	−0.61	1.69	1.69	0.60	−0.60
M062x	1.80	1.80	0.76	−0.75	1.80	1.80	0.75	−0.75

[a]Reported values correspond to the series of all electron calculations. HS and BS stand for the high spin and broken symmetry solutions, respectively.

Table 5. Spin Density on the Metallic Centers of NiVO Compounds 3 and 4 and CuVO Compounds 5 and 6 As Predicted by the Different Computational Methods Used with the Broken Symmetry Approach[a]

| | compd **3** | | | | compd **4** | | | | compd **5** | | | | compd **6** | | | |
| | VO(II) | | Ni(II) | | VO(II) | | Ni(II) | | VO(II) | | Cu(II) | | VO(II) | | Cu(II) | |
method	HS	BS	HS	BS	HS	BS	HS	BS	HS	BS	HS	BS	HS	BS	HS	BS
BHandHLYP	1.22	−1.23	1.82	1.82	1.22	−1.22	1.82	1.81	1.17	−1.17	0.79	0.79	1.31	1.31	0.84	−0.84
B3LYP	1.13	−1.13	1.69	1.67	1.12	−1.13	1.69	1.68	1.09	−1.08	0.65	0.65	1.18	1.18	0.70	−0.70
HSEh1PBE	1.16	−1.16	1.72	1.72	1.15	−1.15	1.72	1.72	1.11	−1.11	0.68	0.68	1.22	1.22	0.73	−0.73
LC-wPBE	1.16	−1.16	1.73	1.72	1.15	−1.16	1.72	1.72	1.11	−1.11	0.69	0.69	1.22	1.22	0.74	−0.74
M06	1.24	−1.24	1.71	1.70	1.23	−1.24	1.70	1.70	1.18	−1.17	0.66	0.66	1.32	1.32	0.71	−0.71
M062x	1.21	−1.21	1.81	1.80	1.21	−1.21	1.81	1.80	1.16	−1.16	0.79	0.79	1.28	1.28	0.83	−0.84

[a]Reported values correspond to the series of all electron calculations. HS and BS stand for the high spin and broken symmetry solutions, respectively.

is described, i.e., using an effective core potential or an all electron basis set. This is not observed for the rest of the methods, as indicated by Figure 2. As previously reported,[52] this is an indication of a pathology present in these functionals. It could also be argued that the ECPs obtained through the Hartree–Fock formalism are not appropriate to describe the M06 cores although this remains to be proven.

7. CONCLUSION

In this work we have investigated magnetic coupling in several heterodinuclear complexes by means of a variety of DFT and wave function based methods. In each case, appropriate mappings are presented enabling one to extract the magnetic coupling constant from total energy differences, provided the correct solutions are used. This is a particularly delicate issue when using DFT based methods within the BS approach. In fact, the current implementation of spin flip DFT appears to be useless in the case of NiCu and NiVO compounds since the excitations involved break the local triplet in Ni resulting in severe spin contamination thus hindering the use of mapping approaches. On the other hand, the use of a broken symmetry approach requires careful analysis, especially in the case of doublet states. This is because, in this case, it is not possible to define a spin projector allowing one to reconstruct the pure doublet state from the BS solutions. However, a mapping procedure using the expectation values of the Heisenberg Hamiltonian with an appropriate BS determinant provides a consistent relationship to derive J values from BS solutions. Note, however, that obtaining corresponding solutions with the appropriate d orbital occupancy is not always straightforward.

Regarding the predicted values, a large dispersion of the calculated results exists. Apart from the well-known depend-

ence of the calculated results with respect to the exchange-correlation functional,[12] the DFT based methods tend to overestimate (in absolute value) antiferromagnetic interactions and to underestimate ferromagnetic ones. Nevertheless, qualitative values are obtained and regular trends are always observed. Interestingly, the best results are obtained with LC-ωPBE functional, in agreement with previous work for Cu-dinuclear complexes,[51,78] and the worst correspond to M06 and B3LYP methods. Note, however, the LC-ωPBE does not perform so well in organic diradical whereas the opposite holds for M06 and, especially, M06-2X.[79]

The explicitly correlated CASPT2 and DDCI wave function based methods show accuracy similar to the best DFT approach although both tend to underestimate (in absolute value) antiferromagnetic and ferromagnetic interactions. This is, in part, related to the use of minimal CAS containing the magnetic orbitals only. Nevertheless, DDCI and CASPT2 results show a balanced behavior over the whole range of J values.

Compounds **3** and **4** containing the NiVO magnetic centers are homogeneously well described by most of the methods whereas, despite belonging to the antiferromagnetic family with quartet–doublet magnetic states, compounds **1** and **2** containing NiCu present the largest deviations and dispersion. The differential behavior in these four compounds can be ascribed to the different nature of the ligands bridging the metallic centers. Compounds **5** and **6** are both ferromagnetic, the magnetic coupling constant, involving a singlet–triplet energy difference, is homogeneously described by all of the methods, although always underestimated.

To summarize, magnetic coupling in heteronuclear complexes can be predicted from accurate total energy differences.

In the case of using wave function based methods the procedure and the performance is as in other dinuclear complexes. However, when using DFT based methods, the lack of left—right symmetry in the metallic center has important consequences and special care is needed on selecting the appropriate broken symmetry solutions and on using the appropriate mapping.

■ ASSOCIATED CONTENT

Ⓢ Supporting Information

Tables listing energies and coupling constants for triplet/singlet cases, Mulliken spin densities on the transition metal atoms, and details about the number of electrons. This material is available free of charge via the Internet at http://pubs.acs.org.

■ AUTHOR INFORMATION

Corresponding Author

*E-mail: francesc.illas@ub.edu.

Notes

The authors declare no competing financial interest.

■ ACKNOWLEDGMENTS

■ REFERENCES

(1) Caneschi, A.; Gatteschi, D.; Sessoli, R.; Rey, P. Toward Molecular Magnets—The Metal—Radical Approach. *Acc. Chem. Res.* **1989**, *22*, 392—398.

(2) Christou, G.; Gatteschi, D.; Hendrickson, D. N.; Sessoli, R. Single-Molecule Magnets. *MRS Bull.* **2000**, *25*, 66—71.

(3) Alivisatos, A. P.; Barbara, P. F.; Castleman, A. W.; Chang, J.; Dixon, D. A.; Klein, M. L.; McLendon, G. L.; Miller, J. S.; Ratner, M. A.; Rossky, P. J.; Stupp, S. I.; Thompson, M. E. From molecules to materials: Current trends and future directions. *Adv. Mater.* **1998**, *10*, 1297—1336.

(4) Ribas, J.; Escuer, A.; Monfort, M.; Vicente, R.; Cortes, R.; Lezama, L.; Rojo, T. Polynuclear Ni-II and Mn-II Azido Bridging Complexes. Structural Trends and Magnetic Behavior. *Coord. Chem. Rev.* **1999**, *193—195*, 1027—1068.

(5) Milios, C. J.; Inglis, R.; Vinslava, A.; Bagai, R.; Wernsdorfer, W.; Parsons, S.; Perlepes, S. P.; Christou, G.; Brechin, E. K. Toward a Magnetostructural Correlation for a Family of Mn₆SMMs. *J. Am. Chem. Soc.* **2007**, *129*, 12505—12511.

(6) Gatteschi, D.; Sessoli, R. Quantum Tunneling of Magnetization and Related Phenomena in Molecular Materials. *Angew. Chem., Int. Ed.* **2003**, *42*, 268—297.

(7) A general review of the different classes of molecular magnetic materials is provided in the "molecule-based magnets" special issue of *MRS Bull.* **2000**, *25* (11).

(8) Rajca, A. Organic Diradicals and Polyradicals: From Spin Coupling to Magnetism? *Chem. Rev.* **1994**, *94*, 871—893.

(9) Iwamura, H.; Koga, N. Studies of Organic Di-, Oligo-, and Polyradicals by Means of Their Bulk Magnetic Properties. *Acc. Chem. Res.* **1993**, *26*, 346—351.

(10) Ruiz, E.; Alemany, P.; Alvarez, S.; Cano, J. Toward the Prediction of Magnetic Coupling in Molecular Systems: Hydroxo- and Alkoxo-Bridged Cu(II) Binuclear Complexes. *J. Am. Chem. Soc.* **1997**, *119*, 1297—1303.

(11) Valero, R.; Costa, R.; Moreira, I. de P. R.; Truhlar, D. G.; Illas, F. Performance of the M06 Family of Exchange-Correlation Functionals for Predicting Magnetic Coupling in Organic and Inorganic Molecules. *J. Chem. Phys.* **2008**, *128*, No. 114103.

(12) Moreira, I. de P. R.; Illas, F. A Unified View of the Theoretical Description of Magnetic Coupling in Molecular Chemistry and Solid State Physics. *Phys. Chem. Chem. Phys.* **2006**, *8*, 1645—1659.

(13) Malrieu, J. P.; Caballol, R.; Calzado, C. J.; de Graaf, C.; Guihéry, N. Magnetic Interactions in Molecules and Highly Correlated Materials: Physical Content, Analytical Derivation, and Rigorous Extraction of Magnetic Hamiltonians. *Chem. Rev.* **2014**, *114*, 429—492.

(14) Caballol, R.; Castell, O.; Illas, F.; Malrieu, J. P.; Moreira, I. de P. R. Remarks on the Proper Use of the Broken Symmetry Approachto Magnetic Coupling. *J. Phys. Chem. A* **1997**, *101*, 7860—7866.

(15) Illas, F.; Moreira, I. de P. R.; de Graaf, C.; Barone, V. Magnetic Coupling in Biradicals, Binuclear Complexes and Wide Gap Insulators: A Survey of Ab Initio Wave Function and Density Functional Theory Approaches. *Theor. Chem. Acc.* **2000**, *104*, 265—272.

(16) Neese, F. Prediction of Molecular Properties and Molecular Spectroscopy with Density Functional Theory: From Fundamental Theory to Exchange-Coupling. *Coord. Chem. Rev.* **2009**, *253*, 526—563.

(17) de Jongh, L. J.; Miedema, A. R. Experiments on Simple Magnetic Model Systems. *Adv. Phys.* **2001**, *50*, 947—1170 (Reprinted from *Advances in Physics*, Vol. 23, 1974).

(18) Mattis, D. C. *The Theory of Magnetism*, Springer Series in Solid-State Sciences, Vols. *17* and 55; Springer-Verlag: Berlin, 1985.

(19) Yosida, K. *Theory of Magnetism*, Springer Series in Solid-State Sciences, Vol. *122*; Springer-Verlag, Berlin, 1996.

(20) Moreira, I. de P. R.; Illas, F.; Calzado, C. J.; Sanz, J. F.; Malrieu, J. P.; Ben Amor, N.; Maynau, D. Local Character of Magnetic Coupling in Ionic Solids. *Phys. Rev. B* **1999**, *59*, R6593—R6596.

(21) Muñoz, D.; Moreira, I. de P. R.; Illas, F. Accurate Prediction of Large Antiferromagnetic Interactions in High-Tc HgBa₂Caₙ₋₁CuₙO₂ₙ₊₂₊δ (n=2,3) Superconductor Parent Compounds. *Phys. Rev. Lett.* **2000**, *84*, 1579—1582.

(22) Fink, K.; Wang, C.; Staemmler, V. Superexchange and Spin—Orbit Coupling in Chlorine-Bridged Binuclear Cobalt(II) Complexes. *Inorg. Chem.* **1999**, *38*, 3847—3856.

(23) Escuer, A.; Vicente, R.; Ribas, J.; Costa, R.; Solans, X. New Nickel(II)—Copper(II) Heterodinuclear Complexes with Hexa- and Pentacoordinated Nickel(II) Ions. Magnetostructural Correlations. *Inorg. Chem.* **1992**, *31*, 2627—2633.

(24) Mandal, D.; Chatterjee, B. P.; Ganguly, R.; Tiekink, E. R. T.; Clérac, R.; Chaudhury, M. Tetra- and Dinuclear Nickel(II)—Vanadium(IV/V) Heterometal Complexes of a Phenol-Based N₂O₂ Ligand: Synthesis, Structures, and Magnetic and Redox Properties. *Inorg. Chem.* **2008**, *47*, 584—591.

(25) Kahn, O.; Galy, J.; Journaux, Y.; Jaud, J.; Morgenstern-Badarau, I. Synthesis, Crystal Structure and Molecular Conformations, and Magnetic Properties of a Copper-Vanadyl (CuII-VOII) Heterobinuclear Complex: Interaction between Orthogonal Magnetic Orbitals. *J. Am. Chem. Soc.* **1982**, *104*, 2165—2176.

(26) Mohanta, S.; Nanda, K. K.; Thompson, L. K.; Flörke, U.; Nag, K. Spin Exchange Coupling in Heterobimetallic MᴵᴵVᴵ�V O (M = Cu, Ni, Co, Fe, Mn) Macrocyclic Complexes. Synthesis, Structure, and Properties. *Inorg. Chem.* **1998**, *37*, 1465—1472.

(27) Valero, R.; Illas, F.; Truhlar, D. G. Magnetic Coupling in Transition Metal Binuclear Complexes by Spin-Flip Time-Dependent Density Functional Theory. *J. Chem. Theory Comput.* **2011**, *7*, 3523—3531.

(28) Yamaguchi, K.; Takahara, Y.; Fueno, T.; Nasu, K. Ab Initio MO Calculations of Effective Exchange Integrals between Transition-Metal Ions via Oxygen Dianions: Nature of the Copper-Oxygen Bonds and Superconductivity. *Jpn. J. Appl. Phys.* **1987**, *26*, No. L1362.

(29) Yamaguchi, K.; Jensen, F.; Dorigo, A.; Houk, K. N. A Spin Correction Procedure for Unrestricted Hartree-Fock and Møller-Plesset Wave Functions for Singlet Diradicals and Polyradicals. *Chem. Phys. Lett.* **1988**, *149*, 537—542.

(30) Yamaguchi, K.; Takahara, Y.; Fueno, T.; Houk, K. N. Extended Hartree-Fock (EHF) Theory of Chemical-Reactions 3. Projected Moller-Plesset (PMP) Perturbation Wavefunctions for Transition

Article

Structures of Organic-Reactions. *Theoret. Chim. Acta* **1988**, *73*, 337–364.

(31) Roos, B. O.; Taylor, P. R.; Siegbahn, P. E. M. A complete active space SCF method (CASSCF) using a density matrix formulated super-CI approach. *Chem. Phys.* **1980**, *48*, 157–173.

(32) Andersson, K.; Malmqvist, P.-Å.; Roos, B. O.; Sadlej, A. J.; Wolinski, K. Second-Order Perturbation Theory with a CASSCF Reference Function. *J. Phys. Chem.* **1990**, *94*, 5483–5488.

(33) Andersson, K.; Malmqvist, P.-Å.; Roos, B. O. Second-order perturbation theory with a complete active space self-consistent field reference function. *J. Chem. Phys.* **1992**, *96*, 1218–1226.

(34) de Graaf, C.; Sousa, C.; Moreira, I.; de, P. R.; Illas, F. Multiconfigurational Perturbation Theory: An Efficient Tool to Predict Magnetic Coupling Parameters in Biradicals, Molecular Complexes, and Ionic Insulators. *J. Phys. Chem. A* **2001**, *105*, 11371–11378.

(35) Miralles, J.; Castell, O.; Caballol, R.; Malrieu, J. P. Specific CI Calculation of Energy Differences: Transition Energies and Bond Energies. *Chem. Phys.* **1993**, *172*, 33–43.

(36) Becke, A. D. Density-Functional Thermochemistry. III. The Role of Exact Exchange. *J. Chem. Phys.* **1993**, *98*, 5648–5652.

(37) Stephens, P. J.; Devlin, F. J.; Chabalowski, C. F.; Frisch, M. J. Ab Initio Calculation of Vibrational Absorption and Circular Dichroism Spectra Using Density Functional Force Fields. *J. Phys. Chem.* **1994**, *98*, 11623–11627.

(38) Becke, A. D. A New Mixing of Hartree–Fock and Local Density-Functional Theories. *J. Chem. Phys.* **1993**, *98*, No. 1372.

(39) Zhao, Y.; Truhlar, D. G. A New Local Density Functional for Main-Group Thermochemistry, Transition Metal Bonding, Thermochemical Kinetics, and Noncovalent Interactions. *J. Chem. Phys.* **2006**, *125*, 194101–194118.

(40) Zhao, Y.; Truhlar, D. G. Density Functional for Spectroscopy: No Long-Range Self-Interaction Error, Good Performance for Rydberg and Charge-Transfer States, and Better Performance on Average than B3LYP for Ground States. *J. Phys. Chem. A* **2006**, *110*, 13126–13130.

(41) Zhao, Y.; Truhlar, D. G. The M06 Suite of Density Functionals for Main Group Thermochemistry, Thermochemical Kinetics, Noncovalent Interactions, Excited States, and Transition Elements: Two New Functionals and Systematic Testing of Four M06-Class Functionals and 12 Other Functionals. *Theor. Chem. Acc.* **2008**, *120*, 215–241.

(42) Heyd, J.; Scuseria, G. E.; Ernzerhof, M. Hybrid Functionals Based on a Screened Coulomb Potential. *J. Chem. Phys.* **2003**, *518*, No. 8207; Erratum: "Hybrid Functionals Based on a Screened Coulomb Potential". **2006**, *124*, No. 219906(E).

(43) Vydrov, O. A.; Scuseria, G. E. Assessment of a Long-Range Corrected Hybrid Functional. *J. Chem. Phys.* **2006**, *125*, 234109–234119.

(44) Runge, E.; Gross, E. K. U. Density-Functional Theory for Time-Dependent Systems. *Phys. Rev. Lett.* **1984**, *52*, 997–1000.

(45) Casida, M. E. In *Time-Dependent Density-Functional Response Theory for Molecules*; Chong, D. P., Ed.; World Scientific: Singapore, 1995; Vol. *1*, pp 155–192.

(46) Bauernschmitt, R.; Ahlrichs, R. Treatment of Electronic Excitations within the Adiabatic Approximation of Time Dependent Density Functional Theory. *Chem. Phys. Lett.* **1996**, *256*, 454–464.

(47) Stratmann, R. E.; Scuseria, G. E.; Frisch, M. J. An Efficient Implementation of Time-Dependent Density-Functional Theory for the Calculation of Excitation Energies of Large Molecules. *J. Chem. Phys.* **1998**, *109*, 8218–8224.

(48) Shao, Y.; Head-Gordon, M.; Krylov, A. I. The Spin–Flip Approach within Time-Dependent Density Functional Theory: Theory and Applications to Diradicals. *J. Chem. Phys.* **2003**, *118*, 4807–4818.

(49) Hirata, S.; Head-Gordon, M. Time-Dependent Density Functional Theory within the Tamm–Dancoff Approximation. *Chem. Phys. Lett.* **1999**, *314*, 291–299.

(50) Zhekova, H.; Seth, M.; Ziegler, T. Introduction of a New Theory for the Calculation of Magnetic Coupling Based on Spin–Flip Constricted Variational Density Functional Theory. Application to Trinuclear Copper Complexes which Model the Native Intermediate in Multicopper Oxidases. *J. Chem. Theory Comput.* **2011**, *7*, 1858–1866.

(51) Rudra, I.; Wu, Q.; van Voorhis, T. Accurate magnetic exchange couplings in transition-metal complexes from constrained density-functional theory. *J. Chem. Phys.* **2006**, *124*, No. 024106.

(52) Phillips, J. J.; Peralta, J. E. Magnetic exchange couplings from constrained density functional theory: An efficient approach utilizing analytic derivatives. *J. Chem. Phys.* **2011**, *135*, No. 084108.

(53) Costa, R.; Moreira, I. de P. R.; Youngme, S.; Siriwong, K.; Wannarit, N.; Illas, F. Towards the Design of Ferromagnetic Molecular Complexes: Magnetostructural Correlations in Ferromagnetic Triply-Bridged Dinuclear Cu(II) Compounds Containing Carboxylato and Hydroxo Bridges. *Inorg. Chem.* **2010**, *49*, 285–294.

(54) Wannarit, N.; Pakawatchai, Ch.; Mutikainen, I.; Costa, R.; Moreira, I. de P. R.; Youngme, S.; Illas, F. Hetero Triply-Bridged Dinuclear Copper(II) Compounds with Ferromagnetic Coupling: A Challenge for Current Density Functionals. *Phys. Chem. Chem. Phys.* **2013**, *15*, 1966–1975.

(55) Forsberg, N.; Malmqvist, P.-Å. Multiconfiguration Perturbation Theory with Imaginary Level Shift. *Chem. Phys. Lett.* **1997**, *274*, 196–204.

(56) Ghigo, G.; Roos, B. O.; Malmqvist, P.-Å. A Modified Definition of the Zeroth-Order Hamiltonian in Multiconfigurational Perturbation Theory (CASPT2). *Chem. Phys. Lett.* **2004**, *396*, 142–149.

(57) Queralt, N.; Taratiel, D.; de Graaf, C.; Caballol, R.; Cimiraglia, R.; Angeli, C. On the Applicability of Multireference Second-Order Perturbation Theory to Study Weak Magnetic Coupling in Molecular Complexes. *J. Comput. Chem.* **2008**, *29*, 994–1003.

(58) Koch, H.; Sánchez de Merás, A. M. J.; Pedersen, T. B. Reduced Scaling in Electronic Structure Calculations using Cholesky Decompositions. *J. Chem. Phys.* **2003**, *118*, 9481–9484.

(59) Pedersen, T. B.; Sánchez de Merás, A. M. J.; Koch, H. Polarizability and Optical Rotation Calculated from the Approximate Coupled Cluster Singles and Doubles CC2 Linear Response Theory Using Cholesky Decompositions. *J. Chem. Phys.* **2004**, *120*, 8887–8897.

(60) Malrieu, J. P. Cancellations Occurring in the Calculation of Transition Energies by a Perturbation Development of Configuration Interaction Matrices. *J. Chem. Phys.* **1967**, *47* (11), 4555.

(61) Frisch, M. J.; Trucks, G. W.; et al. *Gaussian 09*, Revision A.1; Gaussian: Wallingford, CT, USA, 2009.

(62) Shao, Y.; Fusti-Molnar, L.; et al. Advances in Methods and Algorithms in a Modern Quantum Chemistry Program Package. *Phys. Chem. Chem. Phys.* **2006**, *8*, 3172–3191.

(63) Schmidt, M. W.; Baldridge, K. K.; Boatz, J. A.; Elbert, S. T.; Gordon, M. S.; Jensen, J. H.; Koseki, S.; Matsunaga, N.; Nguyen, K. A.; Su, S. J.; Windus, T. L.; Dupuis, M.; Montgomery, J. A., Jr. General Atomic and Molecular Electronic Structure System. *J. Comput. Chem.* **1993**, *14*, 1347–1363.

(64) Gordon, M. S.; Schmidt, M. W. In *Theory and Applications of Computational Chemistry: The First Forty Years*; Dykstra, C. E., Frenking, G., Kim, K. S., Scuseria, G. E., Eds.; Elsevier: Amsterdam, The Netherlands, 2005; Chapter 41, pp 1167–1189.

(65) Aquilante, F.; De Vico, L.; Ferré, N.; Ghigo, G.; Malmqvist, P.-Å.; Neogrady, P.; Pedersen, T. B.; Pitonák, M.; Reiher, M.; Roos, B. O.; Serrano-Andrés, L.; Urban, M.; Veryazov, V.; Lindh, R. MOLCAS 7: The Next Generation. *J. Comput. Chem.* **2010**, *31*, 224–247.

(66) Ben Amor, N.; Maynau, D. Size-Consistent Self-Consistent Configuration Interaction from a Complete Active Space. *Chem. Phys. Lett.* **1998**, *286*, 211–220 (CASDI program: Package developed at the Laboratoire de Chimie et Physique Quantiques, Université Paul Sabatier, Toulouse (France))..

(67) Negodaev, I; de Graaf, C.; Caballol, R.; Lukov, V. V. On the Magnetic Coupling in Asymmetric Bridged Cu(II) Dinuclear

Complexes: The Influence of Substitutions on the Carboxylato Group. *Inorg. Chim. Acta* **2011**, *375*, 166−172.

(68) Kepenekian, M.; Robert, V.; Le Guennic, B. What Zeroth-Order Hamiltonian for CASPT2 Adiabatic Energetics of Fe(II)N$_6$ Architectures? *J. Chem. Phys.* **2009**, *131* (114702), 1−8.

(69) Vancoillie, S.; Rulíšek, L.; Neese, F.; Pierloot, K. Theoretical Description of the Structure and Magnetic Properties of Nitroxide−Cu(II)−Nitroxide Spin Triads by Means of Multiconfigurational ab Initio Calculations. *J. Phys. Chem. A* **2009**, *113*, 6149−6157.

(70) Bonnet, M.-L.; Robert, V.; Tsuchiizu, M.; Omori, Y.; Suzumura, Y. Intramolecular Charge Ordering in the Multi Molecular Orbital System (TTM-TTP)I$_3$. *J. Chem. Phys.* **2010**, *132* (214705), 1−6.

(71) Ma, Y.; Bandeira, N. A. G.; Robert, V.; Gao, E.-Q. Experimental and Theoretical Studies on the Magnetic Properties of Manganese(II) Compounds with Mixed Isocyanate and Carboxylate Bridges. *Chem.—Eur. J.* **2011**, *17*, 1988−1998.

(72) Daku, L. M. L.; Aquilante, F.; Robinson, T. W.; Hauser, A. Accurate Spin-State Energetics of Transition Metal Complexes. 1. CCSD(T), CASPT2, and DFT Study of [M(NCH)$_6$]$^{2+}$ (M = Fe, Co). *J. Chem. Theory Comput.* **2012**, *8*, 4216−4231.

(73) Mödl, M.; Povill, A.; Rubio, J.; Illas, F. Ab Initio Study of the Magnetic Coupling in Na$_6$Fe$_2$S$_6$. *J. Phys. Chem. A* **1997**, *101*, 1526−1531.

(74) Tereniak, S. J.; Carlson, L. K.; Clouston, L. J.; Young, V. G., Jr.; Bill, E.; Maurice, R.; Chen, Y.-S.; Kim, H. J.; Gagliardi, L.; Lu, C. C. Role of the Metal in the Bonding and Properties of Bimetallic Complexes Involving Manganese, Iron, and Cobalt. *J. Am. Chem. Soc.* **2014**, *136*, 1842−1855.

(75) Fukui, H.; Inoue, Y.; Yamada, T.; Ito, S.; Shigeta, Y.; Kishi, R.; Champagne, B.; Nakano, M. Enhancement of the Third-Order Nonlinear Optical Properties in Open-Shell Singlet Transition-Metal Dinuclear Systems: Effects of the Group, of the Period, and of the Charge of the Metal Atom. *J. Phys. Chem. A* **2012**, *116*, 5501−5509.

(76) Yamada, T.; Inoue, Y.; Champagne, B.; Nakano, M. Theoretical Study on the Diradical Characters and Third-Order Nonlinear Optical Properties of Transition-Metal Heterodinuclear Systems. *Chem. Phys. Lett.* **2013**, *579*, 73−77.

(77) Zhekova, H.; Seth, M.; Ziegler, T. Introduction of a New Theory for the Calculation of Magnetic Coupling Based on Spin−Flip Constricted Variational Density Functional Theory. Application to Trinuclear Copper Complexes which Model the Native Intermediate in Multicopper Oxidases. *J. Chem. Theory Comput.* **2011**, *7*, 1858−1866.

(78) Rivero, P.; Moreira, I. de P. R.; Illas, F.; Scuseria, G. E. Reliability of Range Separated Hybrids Functionals in Describing Magnetic Coupling in Molecular Systems. *J. Chem. Phys.* **2008**, *129*, 184110−184117.

(79) Reta Mañeru, D.; Pal, K. P.; Moreira, I. de P. R.; Datta, S. N.; Illas, F. The Triplet-Singlet Gap in the *m*-Xylylene Radical: A Not So Simple One. *J. Chem. Theory Comput.* **2014**, *10*, 335−345.

3.4.2.   Paper #3.2.

Handling Magnetic Coupling in Trinuclear Cu(II) Complexes.

Handling Magnetic Coupling in Trinuclear Cu(II) Complexes

Daniel Reta Mañeru,[†] Ramon Costa,[‡] Meritxell Guix Márquez,[‡] Ibério de P. R. Moreira,[†] and Francesc Illas*,[†]

[†]Departament de Química Física & Institut de Química Teòrica i Computacional (IQTCUB), Universitat de Barcelona, C/Martí i Franquès 1, 08028 Barcelona, Spain

[‡]Departament de Química Inorgànica & Institut de Química Teòrica i Computacional (IQTCUB), Universitat de Barcelona, C/Martí i Franquès 1, 08028 Barcelona, Spain

ABSTRACT: The problem of deriving three different two-body magnetic couplings in three electrons/three centers in a general geometric arrangement is investigated using the trinuclear Cu(II) HAKKEJ complex as a real case example. In these systems, one quartet and two doublet low lying electronic states exist, which define the magnetic spectra. However, the two possible linearly independent energy differences do not provide enough information to extract the three magnetic coupling constants. Here, we show how to obtain these parameters without making any assumption on the symmetry of the system from a combination of density functional- and wave function-based calculations. The density functional calculations explore various broken symmetry solutions and relate the corresponding energy to the expectation value of the Heisenberg Hamiltonian. This allows one to obtain all magnetic couplings, although their magnitude strongly depends on the exchange–correlation functional. Interestingly, a constant ratio between the magnetic coupling constants along a series of investigated functionals is found. This provides an additional equation to be used when relying on energy differences between spin states, which in turn allow solving the Heisenberg spectrum. The magnetic couplings thus obtained are compared to the experiment. Implications for the appropriate interpretation of the experiment and for the study of more complex systems are discussed.
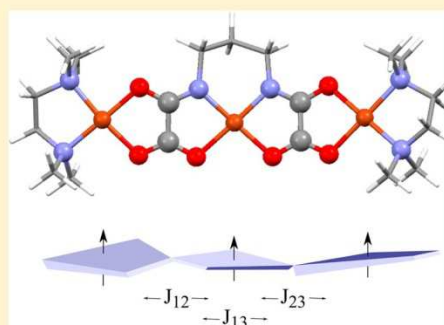
1. INTRODUCTION

The theoretical study of magnetic interactions on transition metal complexes has deserved copious attention during the past decades.[1−5] The crucial goals have been to understand the dependence of the magnetic properties on the structural parameters and the accurate prediction of the magnetic coupling constants. These are not simple tasks due to the complex nature of the magnetic interactions involving electronic states in a very narrow range of energy. Nevertheless, the investigation of the magnetic coupling mechanism in terms of electronic interactions[3−5] provides the way to analyze the magnetic properties and their structural correlations. These constitute valuable and useful tools to design novel molecular and extended magnetic materials with potential technological applications.

The relative simplicity and wide structural diversity of Cu(II) dinuclear complexes makes them ideal systems for the study of magnetic properties either from experiment[1] or theory.[3−5] Not surprisingly, the structural and magnetic properties and the details of their electronic structure have been determined in detail. It is nowadays well established that these systems can be described in terms of a Heisenberg (more properly Heisenberg–Dirac–Van Vleck or HDVV) Hamiltonian with one S = 1/2 spin moment per Cu(II) center. It is important to point out that the spin moments arise from the d^9 electronic configuration of the Cu(II) center. Hence, there is one electron per magnetic center strongly localized on a single atomic-like magnetic molecular orbital. However, the coordination around the magnetic center quenches the orbital angular momentum and, consequently, spin–orbit effects can be neglected. The two S = 1/2 spin moments couple in one triplet (T with total magnetic spin S = 1) and one singlet (S with total magnetic spin S = 0) states. The ordering and energy separation between these two spin states determine the sign and magnitude of the exchange coupling constant J defining the Heisenberg Hamiltonian. The magnitude of the J value can be extracted from experimental data concerning magnetic susceptibility versus temperature and making use of the Bleaney–Bowers equation[6] relating the product of the molar susceptibility and temperature ($\chi_M T$) to temperature. Alternatively, J can be predicted from theoretical calculations as the energy difference between the two low-lying triplet and singlet spin states. This is the basis of the mapping procedure as described in detail in the review paper by some of us.[4]

Due to the special features of dinuclear copper(II) complexes commented on above, these systems have been extensively studied by means of ab initio methods, either from accurate wave function-based methods[7−10] or advanced density functionals[11−15] and provide a convenient open-shell database[13] to

check the accuracy of further developments. The former allow for a deep understanding of the physical mechanisms behind magnetic coupling[5,16−18] whereas the latter open the door to the study of magnetic coupling in larger systems.[19] For these homodinuclear complexes and as a result of these efforts, the extraction of the magnetic coupling constants by means of wave function and/or density functional theory (DFT)-based methods, together with the appropriate mapping are well defined and established.[12,20] The mapping approach has also been recently used to investigate magnetic coupling in a variety of heterodinuclear complexes.[21]

Unfortunately, the usual mapping approach may fail when considering systems involving more than two magnetic centers. More specifically, the mapping approach cannot be applied when the number of pure spin states—eigenfunctions of the square of the total spin operator and of its z-component—leads to a number of linear independent energy differences smaller than the number of two-body magnetic couplings. This limitation comes from the specific nature of the system of interest and even knowing the exact solution, either via wave function-based methods or through the exact universal functional will not provide a solution, and other alternative approaches are needed as discussed below. Let us simply consider the case of a trinuclear Cu(II) complex. Following the line of reasoning described above, there are three $S = 1/2$ spin moments well localized in each center and coupled to two doublet (D_1 and D_2) and one quartet (Q) states. For a trinuclear complex, the most general form of the Heisenberg Hamiltonian with two-body interactions only involves three magnetic coupling constants (J_{12}, J_{13}, and J_{23}, where 1, 2, and 3 correspond to each magnetic center in a 1−2−3 topology). The three electronic states lead to two linear independent equations regarding the energy difference involving the D_1, D_2, and Q electronic states. Therefore, from the low lying energy spectrum, it is not possible to determine the three magnetic coupling constants. This problem also affects the fitting of experimental data, which requires some initial physically meaningful guess and depending on the particular choice, it is possible to come out with different sets of coupling constants that equally represent the experimental magnetic susceptibility versus temperature curve. To avoid this problem it is customary to neglect some of the terms or to rely on symmetry. In the case of strictly symmetric systems in which a symmetry element relates two of the magnetic centers (1 and 3) and passes across the third one (2), one can safely state that $J_{12} = J_{23} = J$ with a concomitant simplification of the spectrum arising from the corresponding Heisenberg. In this case, the energy spectrum becomes much simpler. Assuming an antiferromagnetic D_1 ground state where energy is arbitrarily set to zero, the energy of D_2 is $−J+J_{13}$ and that of Q is $−3J/2$. In this case, the two magnetic coupling constants of interest are again determined univocally from energy differences. The recently reported two trinuclear linear complexes $[Cu(II)_3(L)_2](BF_4)_2$ and $[Ni(II)_3(L)_2(MeOH)_4](BF_4)_2$ supported by the $L^{2−}$ multidentate ligand derived from $H_2L = 5,5′$-pyridyl-3,3′-bi-1H-pyrazole constitute paradigmatic examples of real centrosymmetric systems.[22] For pseudosymmetric systems, the common approach used by magnetochemists to derive the magnetic couplings from the magnetic susceptibility versus temperature curves is simply to ignore deviations from symmetry. Often, a further simplification is added for linear systems where terminal centers 1 and 3 are far enough and not directly connected by any bridging ligand, which consist simply in neglecting J_{13} even

if there is no physical justification. Although these simplifications facilitate the fitting procedure and give an accurate enough estimate of the sign and magnitude of the most intense coupling constants, the information regarding to which extent the $J_{12} = J_{23}$ and $J_{13} = 0$ hypothesis hold is lost.

In the case of the theoretical prediction of magnetic coupling constants, a general and elegant alternative to the use of symmetry constraints consists in the ab initio derivation of the effective spin Hamiltonian and to extract the coupling constants from the pertinent matrix elements. Effective Hamiltonians provide a powerful tool described in detail in the review paper of Malrieu et al.[5] and is used, among other applications, to derive the magnetic coupling constants in systems with two unpaired electrons per magnetic site.[23] The derivation of effective Hamiltonians in more complicated cases has been recently reported from spin−flip methods.[24] This procedure also allows one to recover pure spin states, but again, in the present case the information arising from the pure spin states is insufficient to determine the three coupling constants. Nevertheless, the derivation of the effective Hamiltonian is far from being routine; it requires obtaining complex matrix elements and a general computer code does not yet exist. In the present paper, we use a theoretical approach that combines wave function- and DFT-based calculations; the latter exploits the existence of many broken symmetry solution and is based in the seminal work of Noodleman aimed to extract two-body magnetic constants in a number of transition metal dimers.[25−27] However, the present strategy involves a subtle difference. In the original work of Noodleman,[25] and in most of the subsequent applications (see refs 2−4 and references therein), the idea is to approximate the energy of the pure spin states from the energy of the broken symmetry solutions by appropriate spin projection. This is the case even in complex systems such as those involving several magnetic centers as in tetranuclear iron−sulfur clusters[28] and also applies to the spin−flip techniques commented on above.[24] Here, following a proposal by some of us,[4] we will make use directly of the energy of the broken symmetry solutions—without spin projection—and appropriately map them into the expectation value of the energy of the corresponding broken symmetry solutions of the HDVV Hamiltonian. To illustrate the overall procedure while preserving the simplicity as much as possible, we have chosen to study a linear trinuclear pseudosymmetric system, whose structure consists of a central Cu(II) ion coordinated to two identical bridging ligands that connect it to two equal Cu(II)-terminal ligand fragments as described in detail in Section 3.

2. RECOVERING THE HEISENBERG PICTURE FROM BROKEN SYMMETRY SOLUTIONS

To illustrate the main ideas behind the mapping approach used in the present work, we recall that for a system with three $S = 1/2$ magnetic centers in a 1−2−3 asymmetrical topology, the low energy spectrum is well described by a HDVV Hamiltonian.

$$\hat{H}^{HDVV} = -\sum_{<i,j>} J_{ij} \cdot \hat{S}_i \cdot \hat{S}_j$$

$$= -J_{12} \cdot \hat{S}_1 \cdot \hat{S}_2 - J_{23} \cdot \hat{S}_2 \cdot \hat{S}_3 - J_{13} \cdot \hat{S}_1 \cdot \hat{S}_3 \qquad (1)$$

In the most general case, this spectrum involves the D_1, D_2, and Q states described in the Introduction. These states can be expressed as a linear combination of the $|\alpha\alpha\beta\rangle$, $|\alpha\beta\alpha\rangle$, and $|\beta\alpha\alpha\rangle$ basis set elements, which are eigenfucntions of the z-

component of the total spin; the +1/2 component is chosen for convenience. By diagonalizing the matrix representation of the HDVV Hamiltonain in the above-mentioned basis set, one obtains,[29]

$$|D_1\rangle = 2^{-1/2}(|\alpha\alpha\beta\rangle - |\alpha\beta\alpha\rangle) \tag{2}$$

$$|D_2\rangle = 6^{-1/2}(|\alpha\alpha\beta\rangle + |\alpha\beta\alpha\rangle - 2\cdot|\beta\alpha\alpha\rangle) \tag{3}$$

$$|Q\rangle = 3^{-1/2}(|\alpha\alpha\beta\rangle + |\alpha\beta\alpha\rangle + |\beta\alpha\alpha\rangle) \tag{4}$$

and the corresponding eigenvalues are

$$E_{D_1} = 1/4\cdot(J_{12} + J_{13} + J_{23}) - 1/2\cdot X \tag{5}$$

$$E_{D_2} = 1/4\cdot(J_{12} + J_{13} + J_{23}) + 1/2\cdot X \tag{6}$$

$$E_Q = -1/4\cdot(J_{12} + J_{13} + J_{23}) \tag{7}$$

with

$$X = (J_{12}^2 + J_{13}^2 + J_{23}^2 - J_{12}\cdot J_{13} - J_{12}\cdot J_{23} - J_{13}\cdot J_{23})^{1/2} \tag{8}$$

from which the following expressions for the energy differences are obtained.

$$E_Q - E_{D_1} = 1/2\cdot(-(J_{12} + J_{13} + J_{23}) + X) \tag{9}$$

$$E_Q - E_{D_2} = 1/2\cdot(-(J_{12} + J_{13} + J_{23}) - X) \tag{10}$$

Note that these expressions, derived from the original work by Sinn,[29] hold in the case that the low-spin eigenstates are the ground states. For a system with the quartet state as the ground state, one would simply have

$$E_Q - E_{D_1} = 1/2\cdot(-(J_{12} + J_{13} + J_{23}) - X) \tag{9'}$$

$$E_Q - E_{D_2} = 1/2\cdot(-(J_{12} + J_{13} + J_{23}) + X) \tag{10'}$$

In the absence of further assumptions, these equations do not provide enough information to extract the three magnetic coupling constants. Note in passing by that the exact and HDVV Hamiltonians both commute with the square of the total spin and, obviously, with the z-component of the total spin operators. Hence, the eigenfunction in eqs 2–4 are spin eigenfunctions. The exact solutions are also spin eigenfunctions, and there is a one to one correspondence between these two sets. References 4 and 20 show examples of the application of the mapping approach issued from the original works of Noodleman[25–28] to binuclear complexes and applied here to the case of trinuclear systems. The mapping is clearly illustrated in Figure 1 and, in the present case, evidence that it does not allow one to extract the three magnetic coupling constants from energy differences involving pure spin states only (see also eqs 9 and 10).

Let us now consider the Ising Hamiltonian involving only the z-component of the spin operators in eq 1

$$\hat{H}^{Ising} = -\sum_{<i,j>} J_{ij}\cdot \hat{S}_i^z\cdot\hat{S}_j^z$$

$$= -J_{12}\cdot\hat{S}_1^z\cdot\hat{S}_2^z - J_{23}\cdot\hat{S}_2^z\cdot\hat{S}_3^z - J_{13}\cdot\hat{S}_1^z\cdot\hat{S}_3^z \tag{11}$$

It is easy to show that $|\alpha\alpha\beta\rangle$, $|\alpha\beta\alpha\rangle$, and $|\beta\alpha\alpha\rangle$ basis set elements used to represent the HDVV eigenfunctions are already eigenfunctions of the Ising Hamiltonian; the corresponding values are given in eqs 12–14.
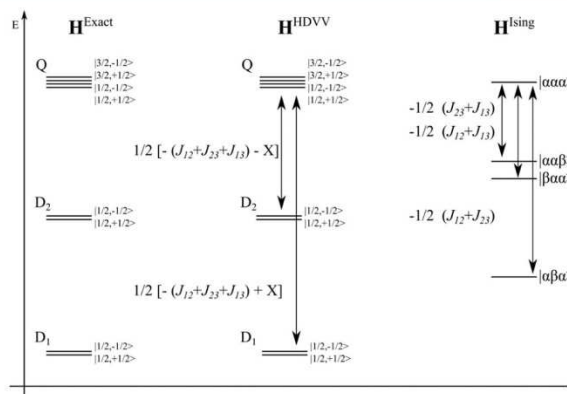

Figure 1. Schematic representation of the low lying spectrum of the exact, HDVV, and Ising Hamiltonians with X defined in eq 8. Note that in the case of the exact and HDVV Hamiltonians, the corresponding eigenfunctions (cf. eqs 2–4) are also spin eigenfunctions. Note that $X = (J_{12}^2 + J_{13}^2 + J_{23}^2 - J_{12}\cdot J_{13} - J_{12}\cdot J_{23} - J_{13}\cdot J_{23})^{1/2}$ as in eq 8.

$$E_{\alpha\alpha\beta}^{Ising} = 1/4\cdot(-J_{12} + J_{13} + J_{23}) \tag{12}$$

$$E_{\alpha\beta\alpha}^{Ising} = 1/4\cdot(J_{12} - J_{13} + J_{23}) \tag{13}$$

$$E_{\beta\alpha\alpha}^{Ising} = 1/4\cdot(J_{12} + J_{13} - J_{23}) \tag{14}$$

For completeness, it is convenient to consider also the high $|\alpha\alpha\alpha\rangle$ spin function, which in this case is also eigenfunction of the HDVV Hamiltonian, and the eigenvalues for HDVV and Ising Hamiltonians coincide.

$$E_{\alpha\alpha\alpha}^{Ising} = -1/4\cdot(J_{12} + J_{13} + J_{23}) = E_Q \tag{15}$$

The same result is obviously obtained if one uses the appropriate combination of the $|\alpha\alpha\beta\rangle$, $|\alpha\beta\alpha\rangle$, and $|\beta\alpha\alpha\rangle$ basis set elements given in eq 4, which corresponds to the $M_S = 1/2$ component of the Q spin state. Interestingly, with the $|\alpha\alpha\beta\rangle$, $|\alpha\beta\alpha\rangle$, and $|\beta\alpha\alpha\rangle$ basis set elements, the Ising Hamiltonian has four eigenvalues, four energy levels (Figure 1) and, consequently, three energy differences, which would allow one to extract the three Ising magnetic coupling constants of interest.

$$E_{\alpha\alpha\alpha}^{Ising} - E_{\alpha\alpha\beta}^{Ising} = -1/2\cdot(J_{13} + J_{23}) \tag{16}$$

$$E_{\alpha\alpha\alpha}^{Ising} - E_{\alpha\beta\alpha}^{Ising} = -1/2\cdot(J_{12} + J_{23}) \tag{17}$$

$$E_{\alpha\alpha\alpha}^{Ising} - E_{\beta\alpha\alpha}^{Ising} = -1/2\cdot(J_{12} + J_{13}) \tag{18}$$

Note also that by combining appropriately eqs 16–18, one gets

$$(E_{\alpha\alpha\alpha}^{Ising} - E_{\alpha\alpha\beta}^{Ising}) - (E_{\alpha\alpha\alpha}^{Ising} - E_{\alpha\beta\alpha}^{Ising}) + (E_{\alpha\alpha\alpha}^{Ising} - E_{\beta\alpha\alpha}^{Ising})$$
$$= -J_{13} \tag{19}$$

One may properly argue that the coupling constants thus determined are those of the Ising Hamiltonian and hence do not represent the real system, which is described through the HDVV Hamiltonian. At this point, one must realize that the eigenvalues of the Ising Hamiltonian in eqs 12–15 coincide with the diagonal elements of the matrix representation of the HDVV in the same basis set. Since there is a one to one

correspondence between eigenvalues of the exact and HDVV Hamiltonians (Figure 1), one can safely take the energy expectation value of the exact Hamiltonian within this basis set and make use of the relationships in eqs 16–19. This would require variationally minimizing these energy expectation values, which can be done with an appropriate quantum chemical method. Since, in practice, the basis set elements correspond to single Slater determinants of the broken symmetry type, one can for instance choose an appropriate DFT method. This is not free of problems since magnetic coupling constants computed within the broken symmetry approach and DFT methods are known to strongly depend on the particular choice of the exchange correlation potential.[12–15,30,31] To overcome this difficulty, we suggest one obtains the three coupling constants with a variety of functionals. We will show that while the absolute value of the magnetic coupling constants largely depends on the functional used, the relative values J_{23}/J_{12} and J_{13}/J_{12} are almost constant. Next, one can plug the magnetic coupling constants relationships in the HDVV Hamiltonian spectrum and simplify the expressions of the energetic differences between spin-adapted states, which in turn can be obtained from accurate ab initio wave function-based calculations. In addition, if both relationships are used, the consistency of the overall procedure can be checked because both $E_Q - E_{D_1}$ and $E_Q - E_{D_2}$ in eqs 9 and 10 will depend only on one parameter (i.e., J_{12}). Since the precise numerical value of $E_Q - E_{D_1}$ and $E_Q - E_{D_2}$ is obtained from ab initio calculations, there will be two different estimates of $E_Q - E_{D_1}$ and $E_Q - E_{D_2}$, and in the case of coincidence, one will have confirmed the validity of the present approach. A further check is provided by comparison to available experimental data.

Therefore, the combination of wave function-based methods and of DFT calculations within the broken symmetry approach opens the door to recover the simplicity of the mapping procedure. Note, however, that this mapping does not intend to recover the energy of the pure spin states. It only attempts to provide additional information to extract the full set of magnetic coupling constants from first-principles arguments. The feasibility of the present approach will be further verified by numerical calculations on a real trinuclear linear and no symmetrical Cu(II) system for which experimental values are available, as described in the forthcoming sections.

3. DEFINING A CONVENIENT TEST SYSTEM

To test the feasibility and accuracy of the mapping procedure described in the previous section, we have searched the Cambridge Structural Database (CCDC) for an appropriate linear trinuclear pseudosymmetric system. The structure chosen is derived from the HAKKEJ[32] one in the CCDC; it consists of a central Cu(II) ion coordinated to two identical oxamato bridging units, which is able to transmit moderate antiferromagnetic interactions, connecting two additional Cu(II) ions with terminal ligand fragments. This structure fulfills the requirements that all atoms, included hydrogen, are well defined with an occupancy factor of 1 and that the counterions or water molecules are far enough from the magnetic centers to not affect the magnetic exchange.

The crystal structure of HAKKEJ, represented in Figure 2a, contains a trinuclear core with the central Cu(2) atom coordinated by a ligand formed by two oxamato bridges held together by a propylene chain. The metal ion lies in an almost square-planar environment with a slight tetrahedral distortion.
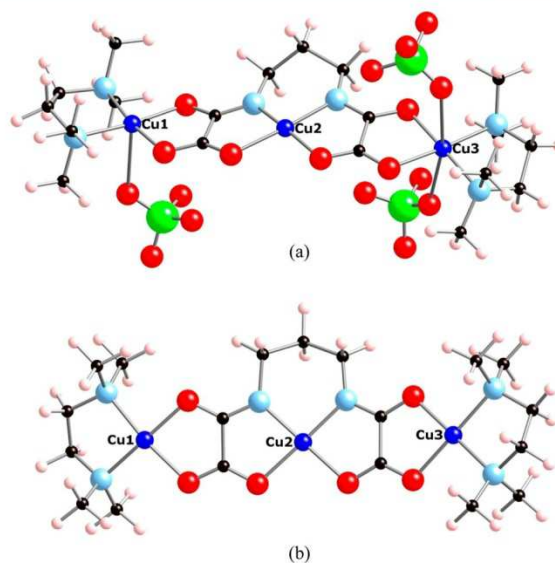

Figure 2. Molecular structure of HAKKEJ (a) and of the reduced model used in the calculations neglecting the perchlorate counterions (b).

The terminal copper atoms are blocked against polymerization by the quelating amine N,N,N',N'-tetrametyletylenediamine (tmen) and linked to the central core through the bridging oxamidate residues. The Cu(1) ion has a 4 + 1 coordination, the basal plane being formed by the two nitrogen atoms from the amine and the two oxygen atoms from the oxamate. The Cu(1) coordination is completed by the apical oxygen atom O(9) from the perchlorate(1) anion at 2.723 Å. Cu(3) lies in a 4 + 2 coordination environment, with a basal plane similar to that described for Cu(1) with the axial positions occupied by the oxygen atoms O(7) and O(11) of perchlorate anions (1) and (2) at 2.587 and 2.875 Å, respectively. Note also that, while, for convenience, the structure depicted in Figure 2a contains three perchlorates anions, the full crystallographic unit cell involves only two; the third one is, in fact, connected to another periodically repeated trinuclear unit. Since the distance from the metal center to the perchlorates is long and the Cu(1) and Cu(3) ions deviate less than 0.11 Å from the mean basal planes, all the magnetic orbitals must be strongly localized inside the copper basal planes. It is thus reasonable to neglect the perchlorate anions when attempting to compute the magnetic states of interest. Therefore, all calculations have been carried out using the resulting trinuclear dicationic fragment in Figure 2b.

In order to compare calculated results to the experiment, it is worth mentioning that the magnetic coupling constant of HAKKEJ was obtained from susceptibility (χ) measurements in the 4.2–300 K range. The experimental data were converted to $\chi_m T$ versus T plots and fitted assuming the Van Vleck expression for the simplified symmetric spin Hamiltonian $H = -J (S_1 S_2 + S_2 S_3)$ and including a Curie–Weiss parameter to take into account the weak intermolecular interactions. The least-squares regression value found for the compound was -379 cm^{-1}. Note that J_{13} has been neglected in the fitting.

An important feature of the model systems chosen in this work is that it can be artificially fragmented into two dinuclear species for which the calculation of the magnetic coupling
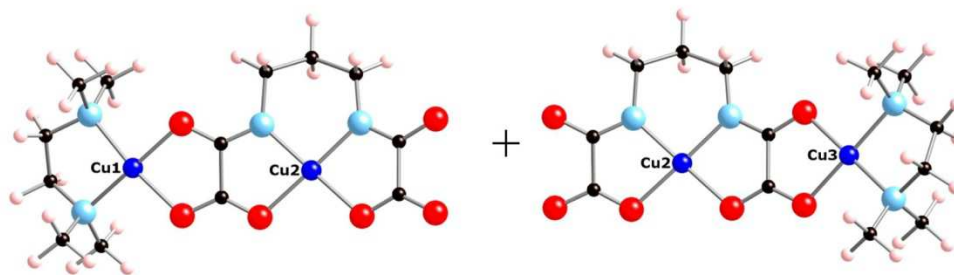
Figure 3. Two model dinuclear neutral molecules constructed from the entire HAKKEJ structure.

constant is more straightforward. The idea behind these new models is to check how similar/different the magnetic coupling constants are and to unequivocally assign the two central-terminal coupling constants J_{12} and J_{23} to the correct magnetic centers. This will provide a rough indirect estimate of the magnetic asymmetry in the trinuclear complex, an important piece of information required to carry out the fitting to experimental data and also regarding the locality of the magnetic interaction. These values will also be compared to those obtained from the general mapping procedure and to the experimental value obtained as indicated above. In order to both obtain suitable dinuclear species that can exist independently while keeping the coordination sphere of the central Cu(II) ion, the fragments have been built preserving the integrity of the whole bridging ligand with appropriate charge compensation. The two artificial neutral moieties thus constructed are described in Figure 3. At first sight, these two dinuclear model systems look very similar. However, a close examination of the distances and angles reveals non-negligible differences, which are consistent with the pseudosymmetric structure of HAKKEJ.[32] It is worth pointing out that these hypothetical complexes closely resemble those experimentally described by Ribas et al.[33]

4. COMPUTATIONAL DETAILS

Calculations for the trinuclear model system in Figure 2b have been carried out using a variety of wave function- and DFT-based methods. For simplicity and to avoid complications arising from different atomic structures, all calculations have been carried out using the crystallographic coordinates and with a total charge of +2 to compensate the removing of the perchlorate counteranions.

The DFT calculations have been carried out with the Gaussian 09 suite of programs.[34] Following previous work on dinuclear complexes, the DFT calculations have been performed using the BHandHLYP[35] and the popular B3LYP[36] hybrid functionals, the M06 and M062X hybrid meta-GGA developed by Zhao and Truhlar,[37−39] and the range separated functionals proposed by Scuseria and collaborators; in particular, we used the HSE06 (HSEh1PBE keyword in Gaussian 09) short-range[40,41] and the LC-ωPBE long-range[42] corrected. Note that the selected functionals incorporate different amounts of Fock exchange: 20% for B3LYP, 27% for M06, 50% for BHandHLYP, and 54% for M06-2X. All calculations were carried out within the unrestricted Kohn−Sham formalism and the use of broken symmetry solutions, except for the highest multiplicity. The energy values thus computed have been used to estimate the magnetic coupling constants through eqs 16−18.

For the wave function-based calculations, we used a variety of methods of increasing accuracy, starting with the CASSCF(3,3) wave function[43] as a reference to second order perturbation, introduced either variationally, through multireference configuration interaction (MRCI) calculations using the Difference Dedicated Configuration Interaction (DDCI)[44] or perturbatively. In the last case, second-order perturbation was obtained through the well-known CASPT2[45−47] procedure as well as through Multi Reference Møller−Pleset (MRMP).[48−51] Note that MRMP is sometimes denoted as MCQDPT for Multi-configurational Quasi Degenerate Perturbation Theory. Both MRMP and CASPT2 use the CASSCF wave function as starting zeroth order description. The wave function-based calculations were carried out using the MOLCAS7.6 package,[52] which was also interfaced with the CASDI[53] code for the DDCI calculations. MRMP on top of CASSCF calculations were carried out using the GAMESS13 code.[54,55] It is worth mentioning that the difference between CASPT2 and MRMP perturbation theories lies in the states used to span the first-order wave function. In CASPT2, single and double excitations are applied to the reference wave CASSCF function, while in MRMP, all singly and doubly excited determinants obtained from each of the determinants in the reference wave function are considered. In other words, CASPT2 uses a contracted reference function, whereas MRMP does not. We have carried out these two types of calculations because of the nature of the doublet states here treated, as explained in the forthcoming section. Finally, it is worth pointing out that in order to make the calculations feasible the DDCI values have been carried out considering a subset of orbitals either in the occupied and virtual subspaces chosen from the CASSCF(3,3) solution for the quintet state. Hence, by freezing 70 doubly occupied and deleting 250 virtual orbitals, 187 electrons have been explicitly correlated using 377 orbitals; with these setting the number of determinants included in the DDCI expansion rises to 1.9×10^8, this is quite at the limit of present computational resources. The same expansion was used to determine the energy of the Q, D_1, and D_2 states.

The basis set used for all DFT, CASPT2, and DDCI calculations is the standard 6-311G[56] extended with an f function with exponent of 0.528 for Cu, the 6-31G(p,d)[57] for the H, C, N, and O atoms. For the MRMP calculations, it has been necessary to use a slightly reduced basis set for Cu and H. Thus, the H atoms are described with the 6-31G basis set, and the [Ar]-cores of Cu atoms have been substituted by the LANL2 effective core potential and the valence electrons described with the LANL2DZ basis set[58−60] extended with an f function with exponent of 0.528.

5. NUMERICAL VALIDATION AND DISCUSSION

Let us start by analyzing the hypothetical Cu-dinuclear models. In all calculations, the magnetic interaction between the neighboring Cu(II) ions through the oxamato bridge is predicted to be antiferromagnetic, in agreement with the experiment. However, the J values calculated using the broken symmetry approach appear to exaggeratedly depend on the exchange−correlation potential with values ranging from −258 and −243 cm^{-1}, respectively, at the BHandHLYP level to −2629 and −2359 cm^{-1}, respectively, as predicted by the B3LYP method. In both cases, the calculated values are far from being identical, thus providing a first indication that the J_{12} and J_{23} of the real HAKKEJ trinuclear complex are likely to be similar but also noticeably different. However, the difference between the values predicted by the different methods is clearly too large, much larger than encountered for similar dinuclear complexes,[4,12,13,15] which hinders making use of these results to reach reliable conclusions. A close inspection of the dinuclear models evidence that the neglect of the third Cu(II) magnetic center may induce artifacts in the electronic distribution of the resulting fragments. In order to investigate whether this is the case, a new series of calculations have been launched in which the presence of the third Cu(II) is modeled through a total ion potential (TIP) consisting of a +2 charge and an appropriate total effective core potential.[61] The results are reported in Table 1. This strategy has been efficiently used to provide an adequate

Table 1. Magnetic Coupling Constants of the Dinuclear Model Systems (in cm^{-1}) as Predicted from Different DFT-based Methods[a]

	J_{12}	J_{23}	J_{23}/J_{12}
BHHLYP	−214	−192	0.898
M06-2X	−228	−205	0.900
LC-ωPBE	−443	−399	0.901
HSEH1PBE	−613	−566	0.923
B3LYP	−735	−682	0.928
M06	−754	−699	0.927

[a]The rightmost column reports the J_{23}/J_{12} ratios.

environment to cluster models of high critical temperature superconducting cuprates parent compounds.[62,63] For this new model, calculated values with different functionals differ, as expected, but are all of the order of magnitude of the experimentally derived magnetic coupling constant in HAKKEJ. In these calculations, the spin density is almost completely localized on the Cu atoms, and the expectation value of the square of the total spin operator ($\langle S^2 \rangle$) is ~2.0 for the high spin and ~1.0 for the low spin broken symmetry solution as predictable. Additionally, all the coupling constants of the dinuclear units calculated with the different DFT functionals point to the fact that the antiferromagnetic interactions between the crystallographic Cu(1)−Cu(2) magnetic centers are more intense than for the Cu(2)−Cu(3) ones, indicating that |J_{12}| > |J_{23}| and, more specifically, that irrespective of the functional, $J_{12}/J_{23} \sim$ 0.9 (Table 1). We will come back to this important conclusion later on when discussing the results for the trinuclear complex. Here, let us advance that the $J_{12}/J_{23} \sim$ 0.9 relation also holds when explicitly dealing with the whole molecular structure of HAKKEJ but substituting Cu_1 or Cu_3 by the TIP.

For the trinuclear dication, calculations were carried out for the $|\alpha\alpha\alpha\rangle$ high spin state and for the three $|\alpha\alpha\beta\rangle$, $|\alpha\beta\alpha\rangle$, and

$|\beta\alpha\alpha\rangle$ broken symmetry solutions. In all cases, the electronic ground state corresponds to the $|\alpha\beta\alpha\rangle$ broken symmetry solution, indicating a dominant antiferromagnetic character, in agreement with the experiment. Moreover, the $|\beta\alpha\alpha\rangle$ solution is always slightly more stable than the $|\alpha\alpha\beta\rangle$, which seems to indicate that $J_{12} > J_{23}$ as suggested by the results on the artificially cut dinuclear models. From the mapping procedure (eqs 16−18), it is possible to extract the three magnetic coupling constants which are reported in Table 2. From the

Table 2. Magnetic Coupling Constants of the Trinuclear HAKKEJ Compound (in cm^{-1}) as Predicted from Different DFT-based Methods[a]

	J_{12}	J_{23}	J_{13}	J_{23}/J_{12}	J_{13}/J_{12}
BHHLYP	−211	−190	−0.4	0.899	0.002
M06-2X	−224	−202	−0.5	0.902	0.002
LC-ωPBE	−440	−397	−2	0.903	0.005
HSEH1PBE	−620	−576	−6	0.929	0.010
B3LYP	−750	−700	−10	0.933	0.013
M06	−769	−716	−10	0.932	0.013

[a]The two rightmost columns report two linear independent ratios. The experimental data fitted to a single magnetic coupling constant gives $J = -379$ cm^{-1}.[32]

values reported, one can conclude that $J_{12} > J_{23}$, which has implications in the hypothesis used to extract J from fitting the experimental data. The calculated values are all in the −200 to −700 cm^{-1} range, which are on the order of magnitude of the experimentally derived J value of −379 cm^{-1}. Interestingly, for a given functional, the values reported in Table 2 nicely coincide with those reported in Table 1 and extracted from the dinuclear models including a representation of the third magnetic center. Even more, the results in Table 2 can be reproduced from calculations in HAKKEJ models where each one of the Cu sites is alternatively substituted by the TIP.

Unfortunately, in spite of the coherence of the ratios of the calculated values, these results exhibit a too large dependence with the exchange correlation functional. This is consistent with previous studies[12−15] but at the same time precludes a more accurate prediction. Note, however, that LC-ωPBE provides the best estimate, in agreement with previous works for antiferromagnetic Cu(II) dinuclear complexes.[64] Nevertheless, this functional fails to predict the difference in the magnitude of the magnetic coupling constant in a series of ferromagnetic compounds[65] and also performs quite badly in organic diradicals with high spin ground state.[66]

The exceedingly large dependence of the calculated results with respect to the choice of the exchange−correlation functional and their shortcoming in describing the ferromagnetic description represents a clear limitation of the DFT-based methods. The general trends and magnetostructural correlations are well described, but the magnitude of the magnetic coupling constants is not. To overcome this problem, it is highly desirable to make use of methods of quantum chemistry based on accurate wave functions. However, in the present case, the magnetic coupling constants cannot be extracted from the energy difference (see Section 2) and will need to rely on effective Hamiltonian theory. In order to overcome the tedious procedure required to compute the elements of the effective Hamiltonian matrix representations, one can make use of the additional information in the two rightmost columns of Table 2 reporting the J_{23}/J_{12} and J_{13}/J_{12} ratios for the different DFT

methods. Table 2 shows that while the calculated values of the magnetic coupling constants are strongly dependent on the DFT methods used, J_{23}/J_{12} and J_{13}/J_{12} are much less dependent and, in particular, J_{23}/J_{12} is almost constant. This is for sure the reason behind the success of DFT calculations in describing magnetostructural correlations.[11] Consequently, one can make use of this additional information extracted from the DFT calculations to derive the magnetic coupling constants using energy differences of spin-adapted wave functions. In particular, one could use the J_{23}/J_{12} almost constant value and eqs 9 and 10 to determine the three coupling constants. The resulting set of three equations can be solved numerically, for instance, by using a Newton−Raphson method. Table 3 reports the calculated values of the three magnetic coupling constants at different levels of ab initio wave function theory.

Table 3. Magnetic Coupling Constants of the Trinuclear HAKKEJ Compound (in cm^{-1}) as Predicted from Different Wave Function-based Methods Using eqs 9 and 10 with $J_{23}/J_{12} = 0.9^a$

methods	orbital set	J_{12}	J_{23}	J_{13}
CASSCF(3,3)	SA	−35	−31	2
	SS	−35	−32	2
CASPT2	SA	−181	−163	−129
	SS	−205	−184	−92
MRMP	SA	−161	−144	−33
	SS	−192	−173	11
DDCI	Q	−223	−200	−1

^{a}SA, SS, and Q stand for state average, state specific, and quartet, respectively, and refer to the orbital set used to carry out each set of calculations. The experimental data fitted to a single magnetic coupling constant gives $J = -379$ cm^{-1}.[32]

The analysis of the results in Table 3 provides a number of significant conclusions and also some surprises. The CASSCF-calculated values for J_{12} and J_{23} are, not surprisingly, too small with respect to the experimental estimate, but the J_{13} value is correctly predicted to be much smaller. Moreover, the CASSCF-calculated values are only slightly sensitive to the choice of the orbital set; calculations with state average or state specific CASSCF orbital lead to almost the same set of results. These results follow the trends described in previous works for dinuclear complexes;[5,8] the underestimation of the magnetic coupling constants being due to the lack of dynamical correlation in the CASSCF wave function. Including dynamical correlation through the CASPT2 method improves the prediction of J_{12} and J_{23} values, which are now considerably larger although still represent ∼50% of the experimental estimate (-379 cm^{-1}) only. The dependence of the results on the orbital set used in the CASPT2 calculations is moderate and also follows the expected trends. However, the CASPT2 estimate for J_{13} appears to be exceedingly large and can only be interpreted as an artifact arising from the contracted nature of the method. This is confirmed by the MRMP calculations, which predict similar values for J_{12} and J_{23} but a much smaller J_{13} value. Note also that this latter value is largely affected by the orbitals set used to include the second order perturbation, which indicates the delicate interplay between the three magnetic coupling constants and, correspondingly, the need for an accurate estimate of the energy differences involved. This is further verified by the DDCI calculations predicting J_{12} and J_{23} values of ∼60% of the experimental value (-379 cm^{-1}) and

an almost negligible J_{13} value, as expected from the large distance between Cu(1) and Cu(3). The calculated J_{12} and J_{23} values are still too small, but this can be attributed to the limited basis set and to the truncation of the orbital space used to carry out the DDCI calculations.

The conclusion from the set of explicitly correlated calculations coupled to the DFT results is that it is possible to obtain a reasonable, necessarily underestimated, prediction of the three magnetic coupling constants by making use of energy differences between spin states and of the DFT J_{23}/J_{12} ratio. The calculations consistently envisage that J_{12} and J_{23} are different and that J_{13} is significantly smaller than J_{12} and J_{23} but not zero. In the next section, we will discuss the implications of these results in the estimation of the coupling constants from fitting to the experimental magnetic susceptibility curves.

Before closing this part, it would be interesting to further validate the present approach by noticing that one can make use of both J_{23}/J_{12} and J_{13}/J_{12} DFT ratios in Table 2 to express the energy differences in eqs 9 and 10 as a function of J_{12}. Thus, one gets

$$E_Q - E_{D1} = A \cdot J_{12} \tag{20}$$

$$E_Q - E_{D2} = B \cdot J_{12} \tag{21}$$

allowing one to obtain the same J_{12} coupling constant from two independent equations where the A and B parameters are determined by the choice of J_{23}/J_{12} and J_{13}/J_{12}. Now one can substitute the energy differences on the left-hand side of eqs 20 and 21 with the corresponding CASSCF, CASPT2, MRMP, and DDCI numerical values. The closer the J_{12} computed from eqs 20 and 21 is, the better the description of the Heisenberg spectrum by the method of choice is. It is worth pointing out that while J_{23}/J_{12} is almost constant and equal to 0.9, J_{13}/J_{12} varies between 0.002 for M06-2X (and BHHLYP) and 0.013 for B3LYP (and M06). However, in spite of the large variation in J_{13}/J_{12}, the A and B values exhibit a small variation as reported in the caption of Table 4. Indeed, values reported in Table 4 confirm the validity of using the DFT obtained ratios to derive the magnetic coupling constants from two accurate enough energy differences. The DDCI entry in Table 4 clearly confirms this claim. Note, however, that the CASPT2 entry in Table 4 reports quite different values for J_{12} when obtained from eq 20 or 21. This seems to indicate that the different

Table 4. Calculated Values of J_{12} As Obtained from Eqs 20 and 21 with $A = -1.45$ and $B = -0.5$ (B3LYP) and $A = -1.43$ and $B = -0.48$ (M06-2X) As Obtained from Values in Table 1^a

method	orbital set	J_{12}			
		A and *B* from B3LYP		*A* and *B* from M06-2x	
		eq 20	eq 21	eq 20	eq 21
CASSCF	SS	−35	−31	−35	−32
	SA	−34	−29	−35	−30
CASPT2	SS	−202	−379	−205	−396
	SA	−179	−429	−181	−449
MRMP	SS	−189	−160	−192	−168
	SA	−159	−221	−162	−231
DDCI	Q	−219	−213	−222	−223

^{a}SA, SS, and Q stand for state average, state specific, and quartet, respectively, and refer to the orbital set used to carry out each set of calculations.

states are not equally described by the CASPT2 methods, which can be attributed to the contracted nature of the zero-order wave function. In fact, the MRMP methods predicts results which are more consistent than CASPT2 although less reliable than those predicted from DDCI

6. IMPLICATIONS FOR EXPERIMENTALLY DERIVED COUPLING CONSTANTS

The fact that all methods, DFT- and wave function-based, consistently predict different values for J_{12} and J_{23} indicates that, in this case, the assumption of symmetry does not hold. This is also clear from the calculations on the models using the corresponding dinuclear fragments as discussed above. Likewise, it also appears that the assumption of $J_{13} = 0$ may not be rigorously justified. In order to investigate the possible consequences on the values derived from fitting to the experimental magnetic susceptibility ($\chi_m T$) versus temperature curves some considerations need to be discussed. Clearly, different sets of J_{12}, J_{23}, and J_{13} values can be derived providing a statistically meaningful fit to the $\chi_M T$ versus T values obtained from the Bleaney–Bowers equation.[6] This is surely one of the reasons behind the hypothesis in the experimental work leading to a single magnetic coupling for this system. However, the possibility to derive a set of parameters purely from first-principles-based calculations provides an unbiased way to choose one set of parameters. This strategy was successfully used[67] some years ago to derive the dominant magnetic couplings of the Li_2CuO_2 chain compounds for which different proposals were reported with up to seven parameters included in the original fitting. The simulation with the ab initio-derived parameters was in agreement with experiment and provided a physically meaningful, unbiased picture of magnetic interactions in this chain compound.

To further illustrate procedure, the following strategy is used. In the first step, the $\chi_M T$ versus T values are obtained from the Bleaney–Bowers equation[6] assuming the calculated (DDCI or LC-ωPBE) values for J_{12}, J_{23}, and J_{13}. In the second step, a fitting procedure is used to obtain a single value for the magnetic coupling constant assuming symmetry ($J_{12} = J_{23}$) and $J_{13} = 0$. The different sets of results are reported in Figure 4,
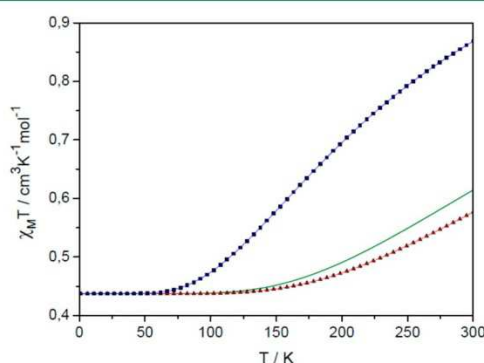

Figure 4. Molar susceptibility times temperature ($\chi_M T$) versus temperature (T) plots obtained from the Bleaney–Bowers equation using DDCI or LC-ωPBE calculated values for J_{12}, J_{23}, and J_{13} (squares and triangles, respectively). A fitting to these simulated curves employing just one magnetic coupling constant are also provide (blue and red lines, respectively). The curve fitting experimental data of ref 32 is included for comparison (green curve).

where the green line shows the $\chi_m T$ versus T values corresponding to the simulation of the original experimental data to a single J value of -379 cm^{-1} and excluding the Curie–Weiss parameter for the intermolecular interactions affecting the very low-temperature data used in ref 32. The squares correspond to the simulation of the $\chi_m T$ versus T values arising from the three DDCI magnetic coupling constants, and the triangles correspond to the simulation obtained when using the three LC-ωPBE values for the magnetic coupling constants. The blue and red curves show, respectively, the best fit of the DDCI and LC-ωPBE simulated $\chi_m T$ versus T values using a single J value. In the case of the DDCI curve, this corresponds to a J of -208.1 cm^{-1}, which is far from the experimental estimate. However, in the case of the LC-ωPBE curve a value of -418.9 cm^{-1} is obtained, which is in good agreement with experiment.

From Figure 4, it is clear that the experimental $\chi_M T$ versus T curve and the ones obtained from DDCI- or LC-ωPBE-calculated J_{12}, $J_{2,3}$ and J_{13} values can be accurately fitted with just one J parameter with a value intermediate between J_{12} and J_{23}. This is not surprising since fitting procedures are known to exhibit multiple solutions. The important conclusion is, however, that without theoretical information one can at most obtain the order of magnitude of the magnetic interaction but at the cost of losing the fine details concerning the difference between J_{12} and J_{23} and the magnitude of J_{13}. However, with appropriate input from calculations, it is possible to gain a deeper insight into the underlying magnetic interactions.

The DDCI-calculated values are clearly too small, which as commented on above is not surprising and comes from the limitations in the DDCI expansion resulting in a limited description of differential electronic correlation effects. Now, for the particular systems studied in the present work, using the experimental information that the dominant magnetic coupling constants are about -400 cm^{-1}, one can come back to the DFT results in Table 2 to obtain a more accurate picture. The calculated DFT magnetic coupling constants depend strongly on the choice of the functional, but the ones predicted by the LC-ωPBE method are precisely in the range of the experimental value. Hence, one can safely take this set of results as a reasonable prediction. Clearly, taking $J_{12} = -440$ cm^{-1}, $J_{23} = -397$ cm^{-1}, and $J_{13} = -2$ cm^{-1} leads to the $\chi_M T$ versus T curve (triangles sequence, Figure 4) close to the experimental one (simulated green curve, Figure 4). We must insist on the fact that these data can be fitted with a single J value of -418.9 cm^{-1} (red curve, Figure 4), which is close enough to the experimentally reported value.

7. CONCLUSIONS

In the case of binuclear complexes, deriving magnetic coupling constants from ab initio calculations is straightforward and well established.[2−5] However, difficulties are present when handling more complicated systems such as heterodinuclear complexes, as discussed in a recent work.[21] The case of trinuclear complexes introduces a different type of difficulty since the number of pure spin states does not offer sufficient information to extract the different magnetic coupling constants from the corresponding energy differences and one is thus bound to use effective Hamiltonian theory,[5] which while elegant and robust is difficult to use by nonspecialists and requires a considerable computational effort.

The existence of a larger number of broken symmetry states seems to offer a way out since the required energy differences can be written. However, in that case, one maps expectation values of the exact and HDVV Hamiltonian obtained from the different broken symmetry solutions. This is at variance of the usual mapping involving the energy of the pure spin states and the eigenvalues of the HDVV Hamiltonian. Still, the mapping involving expectation values and broken symmetry solutions is robust, and the only problem comes from the too large dependence on the calculated results with the form of the exchange−correlation potential used to compute the energy of the different broken symmetry solutions. At this point, one needs either information from experiment or from ab initio wave function-based calculations. In this work, we have shown that while the calculated magnetic coupling constants depend on the DFT method used, the ratio between the different magnetic coupling constants is almost constant. This is surely the reason behind the success of DFT in predicting magnetostructural relationships.[3] This almost constant ratio between different coupling constants provides extra information to derive the magnetic coupling constants from energy differences between spin states. In this way, one would combine ab initio wave function energy differences (e.g., obtained from DDCI calculations) between the pure spin states and the DFT-derived ratio leading to a convenient approach.[4]

The three magnetic couplings of the trinuclear HAKKEJ complex constants have been obtained, and the results consistently show that the two dominant coupling constants are not equal and that the smallest one is not zero. However, the magnetic coupling constants thus obtained are smaller than the single value obtained from the experiment assuming symmetry and neglecting one of the couplings. The underestimation of the magnetic coupling constants comes from the limited inclusion of electronic correlation probably due to the necessary truncation of the orbital space.

Interestingly, the values obtained with the LC-ωPBE functional are in the range of the experimental value commented on above, which suggest that the three magnetic coupling constants derived from the broken symmetry calculations provide a reliable estimate. The values thus obtained also indicate that the two dominant coupling constants are significantly different and that the smallest one is almost negligible but not zero. This result has implications for the interpretation of the experimental $\chi_M T$ versus T curve. The simulations in the present work show that it is well possible to successfully fit the $\chi_M T$ versus T curve corresponding to a system with three different and well-defined magnetic coupling constants with a single one. The information thus obtained is just an average, and the details of the magnetic interactions are lost. Using the calculated values to guide the fitting will provide a much deeper insight in the details of the magnetic system. The strategy suggested in the present work regarding the representation of different magnetic centers by appropriate total ion potentials can be extended to more complicated systems in a quite straightforward way.

■ AUTHOR INFORMATION

Corresponding Author

*E-mail: francesc.illas@ub.edu.

Notes

The authors declare no competing financial interest.

■ REFERENCES

(1) Kahn, O. *Molecular Magnetism*; VCH: New York, 1993.

(2) Datta, S. N.; Trindle, C. O.; Illas, F. *Theoretical and Computational Aspects of Magnetic Organic Molecules*; Imperial College Press: London, 2014.

(3) Ciofini, I.; Daul, C. A. DFT calculations of molecular magnetic properties of coordination compounds. *Coord. Chem. Rev.* **2003**, *238−239*, 187−209.

(4) Moreira, I. de P. R.; Illas, F. A Unified View of the Theoretical Description of Magnetic Coupling in Molecular Chemistry and Solid State Physics. *Phys. Chem. Chem. Phys.* **2006**, *8*, 1645−1659.

(5) Malrieu, J. P.; Caballol, R.; Calzado, C. J.; de Graaf, C.; Guihery, N. Magnetic Interactions in Molecules and Highly Correlated Materials: Physical Content, Analytical Derivation, and Rigorous Extraction of Magnetic Hamiltonians. *Chem. Rev.* **2014**, *114*, 429−492.

(6) Bleaney, B.; Bowers, K. D. Anomalous Paramagnetism of Copper Acetate. *Proc. R. Soc. London, Ser. A* **1952**, *214*, 451−465.

(7) Miralles, J.; Castell, O.; Caballol, R.; Malrieu, J. P. Specific CI Calculation of Energy Differences: Transition Energies and Bond Energies. *Chem. Phys.* **1993**, *172*, 33−43.

(8) Graaf, C. de; Sousa, C.; Moreira, I. de P. R.; Illas, F. Multiconfigurational perturbation theory, an efficient tool to predict magnetic coupling parameters in biradicals, molecular complexes and ionic insulators. *J. Phys. Chem. A* **2001**, *105*, 11371−11378.

(9) Negodaev, I.; Queralt, N.; Caballol, R.; Graaf, C. de Theoretical Study of the Magnetic Exchange Interaction in Catena-mu-Tris-[oxalato(2-)-O-1,O-2;O-3,O-4]-Dicopper Complex with Interlocked Helical Chains. *Chem. Phys.* **2011**, *379*, 109−115.

(10) Negodaev, I.; de Graaf, C.; Caballol, R.; Lukov, V. V. On the Magnetic Coupling in Asymmetric Bridged Cu(II) Dinuclear Complexes: The Influence of Substitutions on the Carboxylato Group. *Inorg. Chim. Acta* **2011**, *375*, 166−172.

(11) Ruiz, E.; Alemany, P.; Alvarez, S.; Cano, J. Toward the Prediction of Magnetic Coupling in Molecular Systems: Hydroxo- and Alkoxo-bridged Cu(II) Binuclear Complexes. *J. Am. Chem. Soc.* **1997**, *119*, 1297−1303.

(12) Caballol, R.; Castell, O.; Illas, F.; Malrieu, J. P.; Moreira, I. de P. R. Remarks on the Proper Use of the Broken Symmetry Approachto Magnetic Coupling. *J. Phys. Chem. A* **1997**, *101*, 7860−7866.

(13) Valero, R.; Costa, R.; Moreira, I. de P. R.; Truhlar, D. G.; Illas, F. Performance of the M06 Family of Exchange-Correlation Functionals for Predicting Magnetic Coupling in Organic and Inorganic Molecules. *J. Chem. Phys.* **2008**, *128*, 114103.

(14) Rivero, P.; Moreira, I. de P. R.; Illas, F.; Scuseria, G. E. Reliability of range separated hybrids functionals in describing magnetic coupling in molecular systems. *J. Chem. Phys.* **2008**, *129*, 184110.

(15) Costa, R.; Moreira, I de P. R.; Youngme, S.; Siriwong, K.; Wannarit, N.; Illas, F. Toward the Design of Ferromagnetic Molecular Complexes: Magnetostructural Correlations in Ferromagnetic Triply Bridged Dinuclear Cu(II) Compounds Containing carboxylato and Hydroxo Bridges. *Inorg. Chem.* **2010**, *49*, 285−294.

(16) Calzado, C. J.; Cabrero, J.; Malrieu, J. P.; Caballol, R. Analysis of the Magnetic Coupling in Binuclear Complexes. I. Physics of the Coupling. *J. Chem. Phys.* **2002**, *116*, 2728−2747.

(17) Calzado, C. J.; Cabrero, J.; Malrieu, J. P.; Caballol, R. Analysis of the Magnetic Coupling in Binuclear Complexes. II. Derivation of Valence Effective Hamiltonians from ab initio CI and DFT Calculations. *J. Chem. Phys.* **2002**, *116*, 3985−3999.

(18) Calzado, C. J.; Angeli, C.; Taratiel, D.; Caballol, R.; Malrieu, J. P. Analysis of the Magnetic Coupling in Binuclear Systems. III. The Role of the Ligand to Metal Charge Transfer Excitations Revisited. *J. Chem. Phys.* **2009**, *131*, 044327.

(19) Neese, F. Prediction of Molecular Properties and Molecular Spectroscopy with Density Functional Theory: From Fundamental Theory to Exchange-Coupling. *Coord. Chem. Rev.* **2009**, *253*, 526–563.

(20) Illas, F.; Moreira, I de P. R.; de Graaf, C.; Barone, V. Magnetic Coupling in Biradicals, Binuclear Complexes and Wide Gap Insulators: A Survey of Ab Initio Wave Function and Density Functional Theory Approaches. *Theor. Chem. Acc.* **2000**, *104*, 265–272.

(21) Costa, R.; Valero, R.; Mañeru, D. R.; Moreira, I. de P. R.; Illas, F. Spin Adapted versus Broken Symmetry Approaches in the Description of Magnetic Coupling in Heterodinuclear Complexes. *J. Chem. Theory Comput.* **2015**, *11*, 1006–1019.

(22) Terashima, S.; Newton, G. N.; Shiga, T.; Oshio, H. Planar Trinuclear Complexes with Linear Arrays of Metal Ions. *Inorg. Chem. Front.* **2015**, *2*, 125–128.

(23) Moreira, I. de P. R.; Suaud, N.; Guihéry, N.; Malrieu, J. P.; Caballol, R.; Bofill, J. M.; Illas, F. Derivation of spin Hamiltonians from the exact Hamiltonian: Application to systems with two unpaired electrons per magnetic site. *Phys. Rev. B: Condens. Matter Mater. Phys.* **2002**, *66*, 134430.

(24) Mayhall, N. J.; Head-Gordon, M. Computational Quantum Chemistry for Multiple-Site Heisenberg Spin Couplings Made Simple: Still Only One Spin–Flip Required. *J. Phys. Chem. Lett.* **2015**, *6*, 1982–1988.

(25) Noodleman, L. Valence Bond Description of Anti-Ferromagnetic Coupling in Transition-Metal Dimers. *J. Chem. Phys.* **1981**, *74*, 5737.

(26) Noodleman, L.; Davidson, E. R. Ligand Spin Polarization and Antiferromagnetic Coupling in Transition-Metal Dimers. *Chem. Phys.* **1986**, *109*, 131.

(27) Noodleman, L.; Peng, C. Y.; Case, D. A.; Mouesca, J. M. Orbital Interactions, Electron Delocalization and Spin Coupling in Iron-Sulfur Clusters. *Coord. Chem. Rev.* **1995**, *144*, 199.

(28) Mouesca, J. M.; Noodleman, L.; Case, D. A. Density-Functional Calculations of Spin Coupling in $[Fe_4s_4]^{3+}$ Clusters. *Int. J. Quantum Chem.* **1995**, *56*, 95.

(29) Sinn, E. Magnetic Exchange in Polynuclear Metal Complexes. *Coord. Chem. Rev.* **1970**, *5*, 313–347.

(30) Martin, R. L.; Illas, F. Antiferromagnetic Exchange Interactions from Hybrid Density Functional Theory. *Phys. Rev. Lett.* **1997**, *79*, 1539–1542.

(31) Illas, F.; Martin, R. L. Magnetic coupling in ionic solids studied by density functional theory. *J. Chem. Phys.* **1998**, *108*, 2519–2527.

(32) Costa, R.; Garcia, A.; Ribas, J.; Mallah, T.; Journaux, Y.; Sletten, J.; Solans, X.; Rodriguez, V. Tailored Magnetic Properties in Trinuclear Copper(II) Complexes: Synthesis, Structure, and Magnetic Properties of Complexes Derived from [1,3-propanediylbis-(oxamato)]cuprate(II) ([Cu(pba)]$^{2-}$). *Inorg. Chem.* **1993**, *32*, 3733–3742.

(33) Ribas, J.; Garcia, A.; Costa, R.; Monfort, M.; Alvarez, S.; Zanchini, C.; Solans, X.; Domenech, M. V. Dinuclear Complexes of Copper(II) Derived from (1,3-Propanediylbis(Oxamato))Cuprate(II): Magneto-Structural Correlations. *Inorg. Chem.* **1991**, *30*, 841–845.

(34) Frisch, M. J.; Trucks, G. W; et al. *Gaussian 09*, Revision A.1; Gaussian, Inc.: Wallingford, CT, 2009.

(35) Becke, A. D. A New Mixing of Hartree–Fock and Local Density-Functional Theories. *J. Chem. Phys.* **1993**, *98*, 1372.

(36) Becke, A. D. Density-Functional Thermochemistry. III. The Role of Exact Exchange. *J. Chem. Phys.* **1993**, *98*, 5648–5652.

(37) Zhao, Y.; Truhlar, D. G. A New Local Density Functional for Main-Group Thermochemistry, Transition Metal Bonding, Thermochemical Kinetics, and Noncovalent Interactions. *J. Chem. Phys.* **2006**, *125*, 194101–194118.

(38) Zhao, Y.; Truhlar, D. G. Density Functional for Spectroscopy: No Long-Range Self-Interaction Error, Good Performance for Rydberg and Charge-Transfer States, and Better Performance on Average than B3LYP for Ground States. *J. Phys. Chem. A* **2006**, *110*, 13126–13130.

(39) Zhao, Y.; Truhlar, D. G. The M06 Suite of Density Functionals for Main Group Thermochemistry, Thermochemical Kinetics, Non-

covalent Interactions, Excited States, and Transition Elements: Two New Functionals and Systematic Testing of four M06-class Functionals and 12 other Functionals. *Theor. Chem. Acc.* **2008**, *120*, 215–241.

(40) Heyd, J.; Scuseria, G. E.; Ernzerhof, M. Hybrid Functionals Based on a Screened Coulomb Potential. *J. Chem. Phys.* **2003**, *118*, 8207; *J. Chem. Phys.* **2006**, *124*, 219906.

(41) Heyd, J.; Scuseria, G. E. Assessment and Validation of a Screened Coulomb Hybrid Density Functional. *J. Chem. Phys.* **2004**, *120*, 7274–7280.

(42) Vydrov, O. A.; Scuseria, G. E. Assesment of a Long-Range Corrected Hybrid Functional. *J. Chem. Phys.* **2006**, *125*, 234109–234119.

(43) Roos, B. O.; Taylor, P. R.; Siegbahn, P. E. M. A complete active space SCF method (CASSCF) using a density matrix formulated super-CI approach. *Chem. Phys.* **1980**, *48*, 157–173.

(44) Miralles, J.; Castell, O.; Caballol, R.; Malrieu, J. P. Specific CI Calculation of Energy Differences: Transition Energies and Bond Energies. *Chem. Phys.* **1993**, *172*, 33–43.

(45) Andersson, K.; Malmqvist, P.-Å.; Roos, B. O.; Sadlej, A. J.; Wolinski, K. Second-Order Perturbation Theory with a CASSCF Reference Function. *J. Phys. Chem.* **1990**, *94*, 5483–5488.

(46) Andersson, K.; Malmqvist, P.-Å.; Roos, B. O. *J. Chem. Phys.* **1992**, *96*, 1218–1226.

(47) Graaf, C. de; Sousa, C.; Moreira, I. de P. R.; Illas, F. Multiconfigurational Perturbation Theory: An Efficient Tool to Predict Magnetic Coupling Parameters in Biradicals, Molecular Complexes, and Ionic Insulators. *J. Phys. Chem. A* **2001**, *105*, 11371–11378.

(48) Hirao, K. Multireference Møller–Plesset Perturbation Treatment of Potential Energy Curve of N2. *Int. J. Quantum Chem.* **1992**, *44*, 517–526.

(49) Hirao, K. Multireference Møller-Plesset Method. *Chem. Phys. Lett.* **1992**, *190*, 374–380.

(50) Hirao, K. Multireference Møller-Plesset Perturbation Theory for High-Spin Open-Shell Systems. *Chem. Phys. Lett.* **1992**, *196*, 397–403.

(51) Hirao, K. State-Specific Multireference Møller—Plesset Perturbation Treatment for Singlet and Triplet Excited States, Ionized States and Electron Attached States of H$_2$O. *Chem. Phys. Lett.* **1993**, *201*, 59–66.

(52) Aquilante, F.; de Vico, L.; Ferre, N.; Ghigo, G.; Malmqvist, P.-A.; Pedersen, T.; Pitonak, M.; Reiher, M.; Roos, B. O.; Serrano Andres, L.; Urban, M.; Veryazov, V.; Lindh, R. Software News and Update MOLCAS 7: The Next Generation. *J. Comput. Chem.* **2010**, *31*, 224–247.

(53) Ben Amor, N.; Maynau, D. CASDI program: Package developed at the Laboratoire de Chimie et Physique Quantiques, Université Paul Sabatier, Toulouse (France). *Chem. Phys. Lett.* **1998**, *286*, 211.

(54) Schmidt, M. W.; Baldridge, K. K.; Boatz, J. A.; Elbert, S. T.; Gordon, M. S.; Jensen, J. H.; Koseki, N.; Matsunaga, K.; Nguyen, A.; Su, S.; Windus, T. L.; Dupuis, M. J.; Montgomery, A. General Atomic and Molecular Electronic Structure System. *J. Comput. Chem.* **1993**, *14*, 1347–1363.

(55) Gordon, M. S.; Schmidt, M. W. Advances in Electronic Structure Theory: GAMESS a Decade Later. In *Theory and Applications of Computational Chemistry: the First Forty Years*; Dykstra, C. E., Frenking, G., Kim, K. S., Scuseria, G. E., Eds.; Elsevier: Amsterdam, 2005; pp 1167–1189.

(56) Hehre, W. J.; Ditchfield, R.; Pople, J. A. Self-Consistent Molecular Orbital Methods. XII. Further Extensions of Gaussian-Type Basis Sets for Use in Molecular Orbital Studies of Organic Molecules. *J. Chem. Phys.* **1972**, *56*, 2257–2261.

(57) Ditchfield, R.; Hehre, W. J.; Pople, J. A. Self-Consistent Molecular-Orbital Methods. IX. An Extended Gaussian-Type Basis for Molecular-Orbital Studies of Organic Molecules. *J. Chem. Phys.* **1971**, *54*, 724–728.

(58) Hay, P. J.; Wadt, W. R. Ab Initio Effective Core Potentials for Molecular Calculations. Potentials for the Transition Metal Atoms Sc to Hg. *J. Chem. Phys.* **1985**, *82*, 270–283.

Article

(59) Hay, P. J.; Wadt, W. R. Ab Initio Effective Core Potentials for Molecular Calculations. Potentials for Main Group Elements Na to Bi. *J. Chem. Phys.* **1985**, *82*, 284−298.

(60) Hay, P. J.; Wadt, W. R. Ab Initio Effective Core Potentials for Molecular Calculations. Potentials for K to Au Including the Outermost Core Orbitals. *J. Chem. Phys.* **1985**, *82*, 299−310.

(61) Martin, R. L. Cluster studies of La_2CuO_4: A mapping onto the Pariser−Parr−Pople (PPP) model. *J. Chem. Phys.* **1993**, *98*, 8691−8697.

(62) Muñoz, D.; Moreira, I. de P. R.; Illas, F. Accurate prediction of large antiferromagnetic interactions in High-T_c $HgBa_2Ca_{n-1}Cu_nO_{2n+2+\delta}$ (n=2,3) superconductor parent compounds. *Phys. Rev. Lett.* **2000**, *84*, 1579−1582.

(63) Moreira, I. de P. R.; Calzado, C. J.; Malrieu, J. P.; Illas, F. Four-body spin terms in High-T_c cuprates. *Phys. Rev. Lett.* **2006**, *96*, 087003.

(64) Wannarit, N.; Siriwong, K.; Chaichit, N.; Youngme, S.; Costa, R.; Moreira, I. de P. R.; Illas, F. A New Series of Triply-Bridged Dinuclear Cu(II) Compounds: Synthesis, Crystal Structure, Magnetic Properties and Theoretical Study. *Inorg. Chem.* **2011**, *50*, 10648−10659.

(65) Wannarit, N.; Pakawatchai, Ch.; Mutikainen, I.; Costa, R.; Moreira, I. de P. R.; Youngme, S.; Illas, F. Hetero Triply-Bridged Dinuclear Copper(II) Compounds with Ferromagnetic Coupling: A Challenge for Current Density Functionals. *Phys. Chem. Chem. Phys.* **2013**, *15*, 1966−1975.

(66) Reta Mañeru, D.; Pal, A. K.; Moreira, I. de P. R.; Datta, S. N.; Illas, F. The Triplet-Singlet Gap in the m-Xylylene Radical: a not so Simple One. *J. Chem. Theory Comput.* **2014**, *10*, 335−345.

(67) de Graaf, C.; Moreira, I. de P. R.; Illas, F.; Iglesias, O.; Labarta. The magnetic structure of Li_2CuO_2: from ab initio calculations to macroscopic simulations. A. *Phys. Rev. B: Condens. Matter Mater. Phys.* **2002**, *66*, 014448.

3.5. Summary and Discussion of Results.

The work here presented has dealt with the accurate calculation of magnetic interactions in coordination complexes, ranging from heterodinuclear to homotrinuclear compounds. The availability of crystal structures reduces the problem to only the electronic structure and the metallic nature of magnetic centres fulfils the assumption about local spins made by the spin Hamiltonians employed. This makes these systems ideal to develop and define robust approaches for the extraction of magnetic interactions. Additionally, these approaches can be further applied to organic interacting radicals where the magnetic centres are much more delocalized and on top of the electronic problem there is the structural flexibility, as investigated in chapter 4, which constitutes another test to check their validity.

The structure of the chapter has aimed to present the ideas behind the mapping approach, by specifying each of the aspects with which it deals. In a general sense, the mapping approach relies on a one-to-one correspondence between three energetic spectra, one arising from the exact, non-relativistic, time-independent Hamiltonian and two from the spin model HDVV and Ising Hamiltonians. In the standard formulation it requires a spin projector that relates the energy and electronic distribution of the pure spin states by means of broken symmetry solutions. From the energy differences of these states, one can extract the magnetic coupling constants. Therefore, implicit in the mapping approach there are two requirements- first, the possibility of defining a spin projector, and second, counting with a sufficient number of energy differences to extract all relevant magnetic interactions. However, these requirements are not always fulfilled, and therefore alternative formulations of the mapping approach are needed. Thus, section 3.2.1. focuses on the description of pure spin states and introduces the three-electron three-centre problem, where the HDVV Hamiltonian does not provide enough equations to extract the three coupling constants (see eqns(32-38)). Section 3.2.2 concentrates on broken symmetry solutions, which corresponds to the Ising representation, and by developing the same examples as in section 3.2.1. manifests a relation between the diagonal elements of the HDVV and Ising matrix elements (compare Table 1 with Table 3 and Table 2 with Table 4). This is at the basis of an alternative formulation to the mapping approach, originally proposed in previous work on the group for dimer cases,[8] and extended here to a general three-centre three electron

case. Finally, in section 3.3 the basic ideas of effective Hamiltonian theory are presented, and used to validate our proposal.

Paper #3.1 studies a family of heterodinuclear coordination compounds that include copper vanadium (Cu-V), nickel vanadium (Ni-V) and copper nickel (Cu-Ni) dimer complexes with a variety of computational methods, ranging from wave function to density functional (including spin-flip techniques) based methods. All of them represent a a step further in the homodinuclear standard models used to describe magnetic interaction.[8,12–14] For the Cu-V case, which is a two-centre two-electron problem, the performance of the various computational techniques yields magnetic coupling constants that are in good agreement with experiment, although generally underestimated and with a noticeable dependence on the density functional used. This is also seen for the simpler case of dinuclear Cu(II) complexes, which indicates that the different nature of the d electrons (d^9 for Cu(II) and d1 for V) does not introduce major differences in the theoretical description of coupling constant values. The four compounds formed by the Ni-V and Cu-Ni couples are examples of a $S = 1$ (Ni(II)) and a $S = 1/2$ (Cu(II) or V) interacting centres and represent a local triplet interacting with a local doublet. Interestingly, the standard mapping approach[4–6] cannot be applied here because one cannot define a spin projector (see Scheme 4 and discussion therein). However, a mapping procedure using the expectation values of the Heisenberg Hamiltonian with an appropriate BS determinant provides a consistent relationship to derive the coupling constant value from BS solutions.

Paper #3.2 studies a homotrinuclear Cu(II) compound where no symmetry operation relates the magnetic centres. At variance with paper #3.1, the problem on the mapping approach here arises because the system does not present enough pure spin states to extract all relevant magnetic interactions. Normally, a solution to this consists of neglecting one of the coupling constants or assuming certain symmetries that force equivalence between the magnetic centres, which simplifies the spectrum of the model Hamiltonian (see Scheme 2). However, as in the studied case in paper #3.2, these simplifications might not be applicable to the system, which demands alternative strategies that allow for an accurate extraction of all relevant coupling constants. Based on the equivalence of the diagonal elements of the HDVV and Ising matrix representations, one can use the energy of the corresponding broken symmetry solutions and map them into the expectation value of the energy of the corresponding broken

symmetry solutions of the HDVV Hamiltonian. This approach is validated by comparison of the calculated and experimentally obtained values. Whenever the system is of a Heisenberg type, this alternative formulation is expected to work well, because that would imply that there is no considerable mixing of the states, that the spin moments are local and interaction among pairs is isotropic. Moreover, despite the diverse values for the coupling constants obtained from different functionals, the relationship between the values remains almost constant. Additionally, paper #3.2 finds that by substituting one the magnetic centres by a total ion potential, which reduces the problem to two triplet-singlet energy differences[8] to extract the two magnetic coupling constants. The calculated values are close to the extracted constants in the whole molecule. This might result in an effective strategy to study magnetic interaction in larger polynuclear complexes, by artificially reducing the system to simple units. The success of this oversimplified strategy is an indication of the locality of the magnetic interaction between magnetic centres. The fact of removing one of the magnetic centres (as long as the electrostatic potential left is well-treated) does not affect either the magnitude or the sign of the rest of magnetic interactions. This is further confirmed by effective Hamiltonian theory, since the relationship found for the magnetic coupling constants, as predicted by DFT-based calculations and the effective Hamiltonian, is similar.

To conclude, this chapter uses the mapping approach as a general and accurate manner for extracting magnetic interactions in complex systems. By pointing out two main deficiencies that make the standard mapping approach[4–6] not applicable to certain systems, and following previous work,[8] we propose an alternative approach and apply it to three-centre three-electron problem. This approach is further verified by comparison to experiment and by means of effective Hamiltonian theory.

Theoretical Study of High-Spin Ground State Odd Alternant Hydrocarbons

4.1. Introduction.

As shown in Chapter 1, magnetic properties in organic systems arise from a variety of different processes. However, a common feature is that the dominant exchange coupling between radical centres can always be classified either as a through-space or through-bond type interaction. One of the parameters that define the robustness of the magnetic properties in any material is the Curie temperature (T_C). It is the temperature above which ferromagnetic behaviour is lost, leading to a paramagnetic response. In general, organic compounds showing through-space interacting radicals, such as nitroxides or charge transfer salts, present very low T_C, as a result of the associated weak exchange interactions. On the contrary, π-conjugated neutral molecular compounds with a large number of radical centres interacting through-bond usually show stronger ferro- or antiferromagnetic interaction between the radical centres and are generally seen as good candidates for materials with relatively high T_C, owing to the strong exchange coupling. That will be the case given that a particular set of conditions are fulfilled.

Thus, this chapter aims at several goals. First, to present and justify those conditions, which translate into alternant non-Kekulé polycyclic hydrocarbons with non-disjoint singly occupied molecular orbitals (SOMOs). Second, to introduce and discuss different ways of assembling these molecular units for achieving extended polyradical systems, in order to promote chemical stability of the radical-bearing centres and robust ferromagnetic properties over a wide range of temperatures. To this end, a careful treatment of structural features (normally overlooked in the literature), derived from the inherent flexibility of the molecules, needs to be addressed. Finally, this chapter also serves to present and contextualize part of the work developed in this thesis as an attempt to move forward in this field of organic magnetism.

Following this line of reasoning, the structure of this chapter is as follows: Section 4.2 provides the arguments that justify why odd alternant hydrocarbons are considered the most promising molecular building blocks for obtaining very high-spin ground state π-conjugated polyradical systems. It will deal first with the theoretical works that rationalized the appearance of open-shell states in these neutral organic molecules with an even number of electrons (sections 4.2.1-4.2.3). Then, the validity of these topological rules is confirmed on a selection of experimentally characterized molecules.

This discussion also highlights the importance of providing effective manners to stabilize the radical centres when growing towards a polyradical, either promoting steric protection or introducing large delocalization of the unpaired electrons. Finally, this section ends with a discussion on the different coupling schemes to assemble the open-shell building blocks. In particular, the experimental work developed by Rajca is ubiquitous along the discussion, since his research is the closest approach to a purely organic magnetism up to date. The interplay between topological arguments and connectivity of the building blocks is crucial to rationalize different observed phenomena and provide strategies to investigate new materials/molecules with improved magnetic properties.

Section 4.3 presents the different works related to the subject of organic magnetism developed during the thesis. It consists of six works ranging from the most basic constituent in all discussed architectures, i.e. the *m*-xylylene (paper #4.1), to polymeric systems in one and two dimensions (papers #4.5 and #4.6 respectively). Paper #4.2 investigates the role of 1,3-phenylene unit as a strong ferromagnetic coupler; paper #4.3 studies the effect of structural flexibility on the ordering of electronic states of some organic diradicals; and paper #4.4 is a joint experimental and theoretical work dealing with the applicability of individual organic radicals as candidates for single molecule devices. In all cases, the discussion presents two sides. First, a proper treatment of the electronic structure for the description of magnetic properties, and second, a discussion on the structural features, which due to the inherent structural flexibility, play a significant role at variance with the systems presented in chapter 3.

Section 4.4 presents a summary and a discussion on the the presented work.

4.2. Ensuring High-Spin Ground States. Intramolecular Ferromagnetism.

A typical organic molecule is always thought as a closed-shell system where all electrons are paired forming bonding molecular orbitals (MOs) and, therefore, no permanent magnetic moment is expected. Hence, the expected response of the system is diamagnetism. In general, the term radical (unpaired electron) in organic molecules is associated with an odd number of electrons, which implies an excess of one electron spin and the subsequent permanent magnetic moment. However, there exist molecules

which, even with an even number of electrons, unpaired electrons related to nearly degenerate non-bonding molecular orbitals (NBMOs) are present. Diradicals represent a very widely studied molecules.[1,2] That sort of molecules has been central to the development of purely organic magnetism in the last decades, since they constitute some of the basic building block, and is at the heart of this thesis, structuring the discussion all along. Thus, this section aims to explain the reasons behind the appearance of open-shell states in these neutral radical species showing a significant chemical stability, which affords its use as building blocks in extended polyradical systems. Moreover, these arguments provide a set of rules to rationalize the problem, tentatively discarding possible molecular candidates together with a roadmap for moving forward in the development of purely organic magnetism. These rules rely on topological arguments to discuss the ground state spin preference of planar hydrocarbon molecules.

4.2.1. Electronic Structure Considerations for Stabilizing Open-Shell States.

In searching for organic ferromagnetism and the subsequent applications, the first element to consider is the basic molecular units to be used in constructing the desired material. Ideally, and as a rough approximation, the unit would promote a strong enough ferromagnetic coupling so as to ensure no crossing of states in a wide range of temperatures. Then, by covalently adding up basic units, the behaviour of the polyradical system would be expected to show similar characteristics, making it ferromagnetic in the same range of temperatures as the basic constituent.

For a qualitative and conceptual explanation of the particular conditions that a system must fulfil to possess high-spin states preferentially stabilized, two electrons in two orbitals appear as an ideal case study. The discussion will serve, to a first approximation, to provide arguments on the preferential spin state of the system, based on two simple concepts: the orbital overlap and the exchange integral between the orbitals with unpaired electrons. What concerns us here is the electronic problem. In order to calculate the stationary quantum states of a given system of electrons and nuclei, it is necessary to solve the non-relativistic, time-independent Schrodinger equation:

$$\hat{H}\Psi = E\Psi \tag{1}$$

where $\hat{H}$ is the Hamiltonian operator associated to the system, E is the energy of a given stationary state and Ψ the wave function describing it. As a first approximation, we assume that, given the different mass between the electrons and nuclei, the description of their motion can be separated. This is the Born-Oppenheimer approximation,[3] as explained in chapter 2, section 2.1.1. Since only light atoms of 1st and 2nd row are discussed, relativistic effects are discarded, except for the spin, which is introduced through the antisymmetry principle in the wave function. Then, the electronic Hamiltonian for a system formed by M nuclei and N electrons is written as

$$H_{elec} = -\sum_{i=1}^{N}\frac{1}{2}\nabla_i^2 - \sum_{i=1}^{N}\sum_{A=1}^{M}\frac{Z_A}{r_{iA}} + \sum_{i=1}^{N}\sum_{j>i}^{N}\frac{1}{r_{ij}} \tag{2}$$

where Z_A is the atomic number of nucleus A, ∇_i^2 is the Laplacian operator involving differentiation with respect to the coordinates of the ith electron, r_{iA} is the distance between the ith electron and the Ath nucleus and r_{ij} is the distance between the ith and j^{th} electron.

Now, let two electrons be in two spin orbitals ψ_1 and ψ_2, which represents the case of a diradical. There are six different manners of arranging the two electrons in the two spin orbitals. Two correspond to the closhed-shell singlet (the electrons have opposite spin being in the same orbital). The one with the two electrons in orbital ψ_1 is taken as the reference and will serve to construct the rest by mono and double excitations.

$$|\Psi_0> = |\psi_1\bar{\psi}_1> = 2^{-1/2}[\psi_1(1)\psi_1(2)](\alpha(1)\beta(2) - \beta(1)\alpha(2)) \tag{3.a}$$

$$|\Psi_{1\bar{1}}^{2\bar{2}}> = |2\bar{2}> = 2^{-1/2}[\psi_2(1)\psi_2(2)](\alpha(1)\beta(2) - \beta(1)\alpha(2)) \tag{3.b}$$

The following two correspond to the $S_z = \pm 1$ component of the triplet state (the electrons have the same spin being each in different orbital);

$$|\Psi_1^{\bar{2}}> = |2\bar{1}> = -2^{-1/2}[\psi_1(1)\psi_2(2) - \psi_2(1)\psi_1(2)]\beta(1)\beta(2) \tag{4.a}$$

$$|\Psi_{\bar{1}}^{2}> = |12> = -2^{-1/2}[\psi_1(1)\psi_2(2) - \psi_2(1)\psi_1(2)]\alpha(1)\alpha(2) \tag{4.b}$$

and remaining two corresponding to the electrons having opposite spin being in different orbitals (open-shell singlet).

$$|\Psi_1^2> = |2\bar{1}> \tag{5.a}$$

$$\left|\Psi_{\bar{1}}^{\bar{2}}\right> = \left|1\bar{2}\right>$$
(5.b)

These configurations are not eigenfunctions of the S^2 operator (see chapter 2) but, by taking the appropriate linear combinations, they can become spin-adapted. In particular, the singlet spin-adapted configuration is

$$
\begin{aligned}
\left|{}^1\Psi_1^2\right> &= 2^{-1/2}\left(\left|\Psi_{\bar{1}}^{\bar{2}}\right> + \left|\Psi_1^2\right>\right) \\
&= \frac{1}{2}[\psi_1(1)\psi_2(2) + \psi_1(2)\psi_2(1)](\alpha(1)\beta(2) - \beta(1)\alpha(2))
\end{aligned}
$$
(6)

and the triplet spin-adapted configuration is

$$
\begin{aligned}
\left|{}^3\Psi_1^2\right> &= 2^{-1/2}\left(\left|\Psi_{\bar{1}}^{\bar{2}}\right> - \left|\Psi_1^2\right>\right) \\
&= \frac{1}{2}[\psi_1(1)\psi_2(2) - \psi_1(2)\psi_2(1)](\alpha(1)\beta(2) + \beta(1)\alpha(2))
\end{aligned}
$$
(7)

By calculating the energy of these two spin-adapted configurations, expressed in terms of single electron operators (see chapter 2 section 2.1.2) it is obtained that,

$$\left<{}^1\Psi_1^2\middle|H\middle|{}^1\Psi_1^2\right> = h_{11} + h_{22} + J_{12} + K_{12}$$
(8)

$$\left<{}^3\Psi_1^2\middle|H\middle|{}^3\Psi_1^2\right> = h_{11} + h_{22} + J_{12} - K_{12}$$
(9)

where h_{11} and h_{22} are the one-electron contributions, due to the kinetic energy and nuclear attraction for occupying orbital 1 and 2 respectively. J_{12} is a two-electron integral, normally referred to as coulomb integral, and represents the classical Coulombic repulsion between the charges of electron 1 and 2. It writes as

$$J_{12} = \int d\boldsymbol{r}_1\, d\boldsymbol{r}_2 |\psi_1(\boldsymbol{r}_1)|^2 r_{12}^{-1} |\psi_2(\boldsymbol{r}_2)|^2$$
(10)

K_{12} is also a two-electron integral, called exchange integral, and it does not have a classical interpretation. It writes as

$$K_{12} = \int d\boldsymbol{r}_1\, d\boldsymbol{r}_2 \psi_1^*(\boldsymbol{r}_1)\psi_2(\boldsymbol{r}_1) r_{12}^{-1} \psi_2^*(\boldsymbol{r}_2)\psi_1(\boldsymbol{r}_2)$$
(11)

Both coulomb and exchange integrals are positive, which implies that if the orbitals for both states are equal or similar, the triplet state is more stable than the singlet state by an amount of two times the exchange integral.

$$\left\langle\,^{3}\Psi_{1}^{2}\big|H\big|\,^{3}\Psi_{1}^{2}\right\rangle - \left\langle\,^{1}\Psi_{1}^{2}\big|H\big|\,^{1}\Psi_{1}^{2}\right\rangle = -2K_{12} \tag{12}$$

Given the importance of this term in defining, to a first order, the relative energetic position of the spin-states, few more words are needed. First, in order to clarify the origin and nature of the exchange integral, consider the Hartree product approximation to the wavefunction, which is a simple product of spin orbital wave functions for each electron, in the form $\Psi^{HP}(x_1, x_2, \dots, x_N) = \chi_i(x_1)\chi_j(x_2)\dots\chi_k(x_N)$. It is an uncorrelated wave function because the simultaneous probability of finding electron-one in the volume element dx_1, electron-two in dx_2, etc., is equal to the product of probabilities of finding electron-one in dx_1, times the probability of finding electron-two in dx_2, etc. Consequently, this approximation does not account for the indistinguishability of the electrons. If Hartree products are used to calculate the energies of two electrons with spin-up or down against two electrons with opposite spins each, they will be found to be degenerate, and only coulomb-type two electron integrals appear. It is then clear that the exchange integral arises when accounting for the indistinguishability of electrons, which is achieved when using a wave function that fulfils the antisymmetry principle. As a consequence, the exchange integral is a manifestation of the correlation between electrons of the same spin, even at a monodeterminantal approximation to the wave function. Second, for an explicit discussion on the interpretation of the exchange integral, consider the associated operator and its application to the spin orbital ψ_1

$$\hat{K}_2(1)\psi_1(1) = \left[\int dx_2 \psi_2^*(2) r_{12}^{-1}\psi_1(2)\right]\psi_2(1) \tag{13}$$

The application of $\hat{K}_2(1)$ on $\psi_1(1)$ depends on the value of ψ_1 in all space, not only at x_1, which is the reason for considering the exchange operator as a nonlocal operator; it does not exist a simple potential $K_2(1)$ uniquely defined at a local point in space x_1.

From the previous discussion it is evident that the larger the exchange integral, the larger the energetic gap between the singlet and triplet states. Given that it is defined throughout the space, the larger the regions where orbitals are defined, the larger the value for the exchange integral. At this point is where the interplay between the exchange integral and the orbital overlap for the discussion of spin preference becomes evident. The overlap integral between orbitals ψ_1 and ψ_2 is defined as follows:

$$S_{12} = \int \psi_1^* \psi_2 \, dV \tag{14}$$

Thus, the larger the region of space in which the two orbitals are defined, the larger the value of the overlap integral, as in the case of the exchange integral. However, they introduce opposite effects. While a greater K_{12} value stabilizes the triplet state (eqn(12)), a larger S_{12} value implies an enlarged highest occupied to lowest unoccupied molecular orbital (HOMO-LUMO) gap, what favours the pairing of the electrons. Then, to a first approximation, to ensure the stabilization of the triplet state it is required a close-to zero overlap between the orbitals and at the same time, a large region of space shared by the two unpaired electrons.

In a general sense, magnetism arises when the orbital overlap (eqn14) is small, which avoids pairing of the electrons, and the exchange integral (eqn11) is large, favouring open-shell states. There are different manners to achieve a favourable balance of the exchange integral with respect to the orbital overlap, resulting in a preference for high-spin ground states. One is ensuring orthogonal orbitals ($S_{12} = 0$ by definition and Hund's rule applies) and another promoting a balance between through-bond and through-space magnetic interactions in localized radicals[4,5]. Another way, which is the adopted strategy in this thesis, is based on fully conjugated π-systems with certain topologies that ensure a degenerate and orthogonal character of the non-bonding molecular orbitals (NBMOs), promoting an almost zero orbital overlap while maximizing the exchange integral. This strategy is at the core of the chapter and helps to introduce the particular requirements of the molecular architectures here studied.

4.2.1.1. Atomic Centres: The Hund's Rule.

The most straightforward way for such favourable interplay between the exchange and orbital overlap integral occurs when the system presents orthogonal orbitals, as in simple atoms and carbenes. Here, the orthogonality ensures a zero orbital overlap. On the other hand, since the orbitals are defined over the same centre, there are regions of space where the electrons can interact (i.e. large exchange integral). On the basis of this argument, the high-spin ground state of carbenes or of the *3d-* and *4f-*atomic orbitals on the transition and lanthanide metal atoms is explained. This argument can be extended and applied to more general cases, passing from a situation in which the orthogonal orbitals are defined over the same centre, to a multicentre system. In such case, the

crucial point would then be to ensure a proper orthogonality of the atomic orbitals bearing the unpaired electrons, and as it will be discussed in the forthcoming sections, topology is the key parameter to help defining such restrictions. Therefore, Hund's rule by itself is not a sufficient argument in searching for high-spin ground state molecules and further consideration have to be made as discussed in more detail in section 4.2.2 and 4.2.3.

4.2.1.2. Localized Biradicals. Through-Space and Through-Bond Interactions.

A second manner of enlarging the exchange integral while minimizing the orbital overlap is the introduction of a unit that links the unpaired electrons through a covalent bond. In here, at variance with the two orbitals being defined over the same centre, the unpaired electrons are localized in different centres. The subsequent phenomena can be successfully described in terms of orbital interactions through-space and/or through-bond. In solid-state chemistry, this corresponds to the superexchange mechanism introduced by Anderson[6,7] in order to explain the appearance of antiferromagnetism, which was further treated by Hay, Thibeault and Hoffmann.[8] In organic molecules, the first mention to a through-bond interaction is found in the work by Hoffman[9,10] describing trimethylene, which was later extended by Dougherty et al[4,5] for the case of localized biradicals.

The treatment that Hay, Thibeault and Hoffmann[8] and Goldberg and Dougherty[4] perform is similar. In each work the orbitals are transformed in order to get a general valence bond description. A detailed development of the procedure followed can be found in the mentioned references; here, only the main conclusions will be discussed, since it provides the necessary arguments to later introduce the particular structural features of the molecules that are at the core of this thesis. Both works describe the magnetic interactions of two localized unpaired electrons and provide expressions for the singlet-triplet energy gap expressed in terms of electronic integrals, as two opposing terms. The conclusions obtained are therefore equivalent, despite the different nature of the spin-bearing centres, being in one case copper d^9 atoms and in the other radical sp^2 atoms. An important success of these models is that they provide structural arguments for the design of molecules with a preferential triplet spin state. This is clearly seen inspecting the equation that Hay, Thibeault and Hoffmann[8] provide for the singlet-triplet energy gap:

$$E_S - E_T = J = 2K_{ab} - \frac{(\varepsilon_1 - \varepsilon_2)^2}{J_{aa} - J_{bb}} \tag{15}$$

where ε corresponds to the one-electron energy corresponding to the mono occupied orbital and J_{aa} and K_{ab} correspond to the coulomb and exchange integrals respectively. It is worth saying that this expression can be seen as a generalization of equation (12), and defines more specifically the previous discussion about the interplay between the exchange integral and the orbital overlap, as denoted by the two opposing terms. The term $\varepsilon_1 - \varepsilon_2$ clearly relates to the orbital overlap; a large $\varepsilon_1 - \varepsilon_2$ difference will make the rightmost term in eq. 15 greater than the exchange integral, resulting in a stabilization of the singlet state ($E_S - E_T < 0$). Similarly, a large overlap will increase the energetic difference between the resulting HOMO-LUMO orbitals, favouring the singlet state. Contrarily, if the mono occupied orbitals are degenerate, i.e. $\varepsilon_1 = \varepsilon_2$, the rightmost term in eq. 15 vanishes and the triplet state is two times the exchange integral more stable. The discussed picture is also similarly derived from the treatment that Goldberg and Dougherty[4] perform. The expression that they provide is less compact, but essentially holds the same conclusions. The expression for the singlet-triplet energy gap that they find is

$$\Delta E_{S-T} = \frac{2K_{lr}}{(1 - S_{lr}^4)} - \frac{(-4S_{lr}h_{lr} + 2S_{lr}^2 h + 2S_{lr}^2 h_{rr} + 2S_{lr}^2 J_{lr})}{(1 - S_{lr}^4)} \tag{16}$$

where h, J and K are, respectively, the one-electron, Coulomb and exchange integrals over the general valence bond orbitals. S_{lr} is the general valence bond pair overlap. There is a clear correspondence between this expression and the one given by Hay, Thibeault and Hoffmann,[8] although here the role of the orbital overlap appears explicitly, through S_{lr}. As concluded previously, a large overlap between the orbitals indicate a bonding interaction, leading to a preference for the singlet state. Interestingly, Goldberg and Dougherty separate the nature of the problem into an additional opposing relationship between through-space and through-bond interactions. They conclude that for a stabilization of the triplet state to happen in this sort of localized biradicals, specific and quite restrictive conditions must be fulfilled. Particularly,[4] "*only when the through-bond and through-space effects nearly balance one another and the non-bonding molecular orbitals (NBMOs) are nearly degenerate does a triplet ground state result*". This is a direct consequence of the features of localized radicals, and hinders

their use to effectively achieve extended polyradical systems, where the different conformations and interactions might make the degeneracy of the NBMOs not an easy parameter to control.

Taken together, the previous discussion exemplifies how a proper control of the orbital overlap and the exchange integral affords a preferential stabilization of the triplet state with respect to the open shell singlet state. Such control is dictated by the particularities of the system under study; thus, the triplet state in a carbene is an expression of Hund's rules and in localized diradicals is the consequence of the equilibrated through-bond and through-space interactions. However, for the purpose of obtaining a high-spin ground state molecule with many unpaired electrons interacting ferromagnetically, these two strategies are inappropriate due to the limited number of interacting spins.

It would be then convenient to count with strategies that afford open-shell ground states due to a favourable balance between the exchange integral (eqn. 11) and the orbital overlap (eqn. 14) while offering the possibility for many spins to interact. The most efficient manner is by introducing π-conjugation, which allows a large delocalization and consequently interaction of the unpaired electrons throughout the π-system.

4.2.1.3. Promoting Delocalization: π-Conjugation.

For the upcoming discussion it is appropriate to explicitly define the most relevant concepts, such as conjugation and delocalization.

Conjugated system (conjugation): A conjugated system is a molecular entity whose structure may be represented as a system of alternating single and multiple bonds: e.g. $CH_2=CH–CH=CH_2$. In such systems, conjugation is the interaction of one π-orbital with another across an intervening σ-bond in such structures.

Delocalization: A quantum mechanical concept most usually applied in organic chemistry to describe the π-bonding in a conjugated system. This bonding is not localized between two atoms: instead, each link has a 'fractional double bond character' or bond order. There is a corresponding 'delocalization energy', identifiable with the stabilization of the system compared with a hypothetical alternative in which formal (localized) single and double bonds are present. The effects are particularly evident in aromatic.

Aromaticity: A cyclically conjugated molecular entity with a stability (due to delocalization) significantly greater than that of a hypothetical localized structure (e.g.

Kekulé structure) is said to possess aromatic character. If the structure is of higher energy (less stable) than such a hypothetical classical structure, the molecular entity is 'antiaromatic'.

From a qualitative point of view, the introduction of conjugation delocalizes the spatial areas where the orbitals hosting the unpaired electrons are defined. This implies that there are larger regions where the electrons interact. If no further restrictions apply, the orbital overlap (eqn. 14) will overcome the direct exchange integral (eqn. 11) resulting in bonding interaction, which would suppress any interesting magnetic property.

Fortunately, by topological arguments it is possible to define π–orbitals that, while defined over the same regions of space, are degenerate and orthogonal, which penalizes orbital overlap and enhances direct exchange integral. These topological arguments translate into very specific characteristics of the conjugated system, restricting the molecular candidates to alternant non-kekulé polycyclic hydrocarbons with non-disjoint singly occupied molecular orbitals (SOMOs). By construction, the degeneracy is fixed (through the topology), and the discussion on spin state preference reduces to terms related to the exchange integral. The purpose of the forthcoming sections is the explanation of each of these terms, together with the discussion of experimental and theoretical efforts that targeted such specific molecules as candidates for the development of extended polyradical systems.

4.2.2. Topology.

Topological arguments are of paramount importance because they allow a simplification of the electronic problem and provide valuable predictions. Particularly, in π–conjugated planar systems, one can divide the orbitals with local σ and π symmetry and treat them separately. For the vast majority of properties related to the low-lying energy states in a conjugated molecule, the associated phenomena are governed by valence electrons located in π orbitals.

This section discusses the theoretical works that settled the basis of spin preference based on topological arguments. Particularly, those are the works by Longuet-Higgins[11], Ovchinnikov[12] and Lieb.[13–15] The discussion of what they propose allows introducing explicitly the arguments for the choice of alternant non-kekulé hydrocarbons in the broader category of alternant non-kekulé hydrocarbons with non-disjoint singly

occupied molecular orbitals (SOMOs) molecules studied in the present thesis. Then, this section can be regarded as a preliminary step defining the most basic elements which helped into the development of purely organic magnetism and that are common to all structures discussed from now on. Before going in further detail, it is convenient to define the different terms that will be used.

Hydrocarbon: Compound consisting of carbon and hydrogen atoms only.

Alternant: A conjugated system of π electrons is termed alternant if its atoms can be divided into two sets (starred, not-starred) so that no atom of one set is directly linked to other atom of the same set. Even hydrocarbons refer to systems with the same number of starred and not-starred, while odd hydrocarbon present different number of atoms belonging to each subset.

Alternancy symmetry: A topological property of the molecular graphs of alternant hydrocarbons. A consequence of this property is the symmetrical arrangement of the energy levels of bonding and antibonding Hückel MOs relative to the level of a nonbonding orbital.

Non-Kekulé molecule: Molecules that are fully conjugated, but each of whose Kekulé structures contains at least two atoms that are not π-bonded.

In a broad sense, the three mentioned works deal with the theoretical prediction of the electronic configuration in the ground state of a given alternant lattice of electrons. The alternant condition is crucial since it introduces the necessary restrictions in terms of the allowed interactions that account for the obtained properties. Where Longuet-Higgins relies on molecular orbitals theory, Ovchinnikov applies general valence bond, overcoming some inconsistencies of the former. Lieb's work brings the most general approach analysing the problem in terms of Hubbard Hamiltonian, but in essence Ovchinnikov's (mostly applied in polycyclic AHs) and Lieb's (used in solid-state physics) formulations are equivalent. For a deeper insight, the different works will be briefly reviewed.

4.2.2.1. Predicting the Number of Unpaired Electrons: Longuet-Higgins Analysis.[11]

This work deals with unsaturated hydrocarbons in which all the carbon and hydrogen atoms lie in one plane and each carbon atom possesses a sp^2 hybridization. The main purpose of the inspection is to determine the number of unpaired electrons in the ground state of such alternant hydrocarbons (AHs), using the linear combination of atomic orbitals (LCAO) approximation to describe the resulting π orbitals. The starting point of the argumentation is that in an AH with N carbon atoms, there will be N π

molecular orbitals, out of which *M* will have non-zero binding energy and will appear in pairs with opposite energies, as stated in Coulson and Rushbrooke pairing theorem.[16] The ones with negative energy correspond to bonding orbitals and will consecutively host pairs of electrons. Therefore, there are *N-2M* π orbitals of zero energy which cannot mix. By applying Hund's rule is then stated that in the most stable configuration there will be, at least, as many unpaired electrons as zero-energy molecular orbitals. In a more general sense, the conclusion of this work can be expressed as

$$Number_{unpaired\ electrons} = N - 2T \qquad (17)$$

where *N* is the number of carbon atoms and *T* is the maximum number of double bonds (a triple bond being counted as two double bonds) occurring in any resonance structure in a given alternant hydrocarbon. This number happens to coincide with the number of carbon atoms without double bonds in any of the resonant structures. Obviously, the number of unpaired electrons is the same as the number of non-bonding molecular orbitals (NBMOs).

Despite the approximations of this approach, which is based on simple Hückel model, it counts with numerous examples that proof its convenience. As a matter of fact, consider the *m*-xylylene diradical as indicated in Figure 1. Note that the number of double bonds in any resonant structure is three, which together with the eight carbon atoms, result in the prediction of two unpaired electrons. The electronic structure of *m*-xylylene was experimentally investigated by negative ion photoemission electron spectroscopy and indeed was found to possess a ground state with two unpaired electrons interacting ferromagnetically,[17] well below in energy (~9.6 Kcal/mol) from the closest excites state. However, it is worth saying that Longuet-Higgins work does not provide any information on how the unpaired electrons interact (either ferro- or antiferromagnetically) and that the predictions derived from the model are not always accurate, as it will be explicitly treated in section 4.2.4. Ovchinnikov and Lieb treatment correct some of these deficiencies.
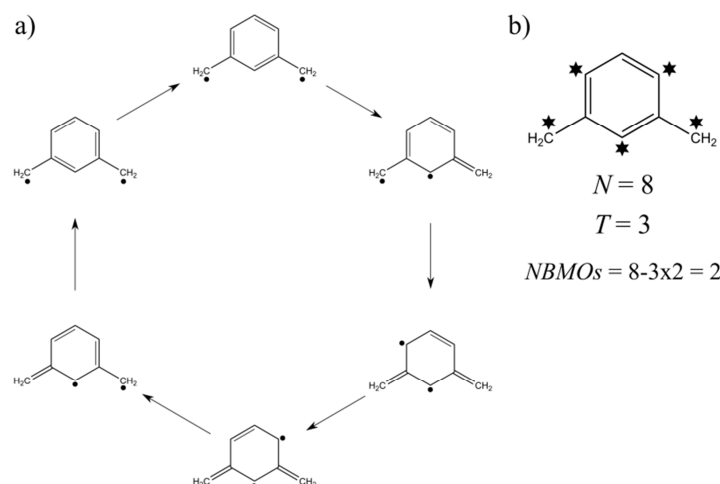
Figure 1. *m*-xylylene diradical. a) resonant forms involved in the stabilization of the unpaired electrons. b) alternant character of the molecule and number of unpaired electrons as predicted by Longuet-Higgins.

4.2.2.2. Predicting Ground State Multiplicity: Ovchinnikov[12] and Lieb[13–15] Analysis.

Any model aiming to explain the interactions of N fermions in a given lattice, should correctly predict the multiplicity of the ground state in the resulting arrangement. On top of that, the issue of degeneracy appears as paramount because it is the way of ensuring uniqueness of the ground state. This is precisely the goal of the works discussed here. Let's first consider Ovchinnikov's development in alternant hydrocarbons, since it can be seen as a particular case of the more general Lieb's theorem for bipartite lattices. Bipartite lattice is equivalent to alternant lattice.

Ovchinnikov introduces the problem of an odd alternant lattice in which the number of starred carbon atoms (n_{A^*}) is different to the number of non-starred ones (n_A). The spin Hamiltonian that is used throughout his work is the standard Heisenberg-Dirac-Van Vleck spin Hamiltonian (see chapter 3, section 3.2.1) considering two-body interactions through nearest neighbours. It writes as

$$H' = \frac{1}{2} \sum_{l,l'} J_{l,l'}^{(1)} (S_l^+ S_{l'}^- + S_{l'}^+ S_l^-) + \sum_{l,l'} J_{l,l'}^{(2)} S_l^z S_{l'}^z \tag{18}$$

where S_l^+ acts on site l by increasing ½ the spin value, $S_{l'}^-$ acts on site l' by decreasing ½ the spin value, and S_l^z is the projection in the z axis of the spin value (1/2 for spin-up and -1/2 for spin down). Then, by definition, it is imposed that all two-body terms are

positive ($J_{l,l'}^{(1)}$ and $J_{l,l'}^{(2)}$ are fixed >0), implying an antiferromagnetic interaction between neighbouring sites. The sign of the left-most sum will always be positive, since the spin operators S_l^+ and $S_{l'}^-$ do not change the sign of the exchange integral $J_{l,l'}^{(1)}$. It follows that for obtaining the lowest state energy, it is necessary to minimize the right-most sum. That is achieved if the sign of all $J_{l,l'}^{(2)}$ are negative, which is the case only when all n_{A^*} atoms have $S_l^z = {}^1/_2$ and all n_A atoms have $S_l^z = -{}^1/_2$. Consequently, the total spin of such state is positive and equals:

$$S = \frac{|n_{A^*} - n_A|}{2} \tag{19}$$

What is left is to ensure that the found lowest state is non-degenerate, which is obtained following the reasoning of Lieb, Schultz and Mattis,[13] but will not be explained here.

On the other hand, Lieb[15] adopts a more general approach making use of the Hubbard model. Again, the characteristic that defines the rest of the properties is the bipartite character of the chosen lattice, where $|B|$ ($|A|$) is the number of sites in the B (A) sub lattice and N is the number of electrons. The Hubbard model on a finite lattice Λ is defined by the Hamiltonian

$$H = \sum_{\sigma} \sum_{x,y \in \Lambda} t_{xy} c_{x\sigma}^\dagger c_{y\sigma} + \sum_{x \in \Lambda} U_x n_{x\uparrow} n_{x\downarrow} \tag{20}$$

where U_x is the on-site repulsion energy, the operators $c_{x\uparrow}$ and $c_{x\downarrow}$ and their adjoints $c_{x\sigma}^\dagger$ satisfy the fermion anticommutation relations $\{c_{x\sigma}^\dagger, c_{y\tau}\} = \delta_{xy}\delta_{\sigma\tau}$ and $\{c_{x\sigma}, c_{y\tau}\} = 0$. The hopping matrix elements t_{xy} are real and satisfy $t_{xy} = t_{yx}$. They can be interpreted as overlap matrix elements of real operators in real, localized orbitals. Given a bipartite lattice Λ, $t_{xy} = 0$ for all $x \in A$ and $y \in A$ or $x \in B$ and $x \in B$. The aim is then to study the ground state of H for a given N. According to the sign of U_x, Lieb presents two theorems. The first theorem addresses the case in which $U_x \leq 0$ for every x (attractive case) and N is even. Then, it is stated that among the ground states of H there is one with spin multiplicity $S = 0$, which, if $U_x < 0$ for every x, is unique. The second theorem considers the case in which $U_x > 0$ for every x (repulsive case), N is even and $|B| \geq |A|$. Then, it is stated that the ground state of H is unique and has spin multiplicity

$$S = \frac{1}{2}(|B| - |A|) \tag{21}$$

This expression is equivalent to the one provided by Ovchinnikov[12] as shown in Eq. (19).

Taken together, these arguments provide a first approximation for the prediction of ground state multiplicity in alternant hydrocarbons, and allow for a choice of the building blocks to be used in the construction of extended polyradicals. Figure 2

	connectivity		number SOMOs	multiplicity
ortho			$N=8$ $T=4$ $8 - 4 \times 2 = 0$	$|A|=4$ $|B|=4$ $S = 1/2 \times (4 - 4) = 0$
meta		No possible Kekulé structure	$N=8$ $T=3$ $8 - 3 \times 2 = 2$	$|A|=5$ $|B|=3$ $S = 1/2 \times (5 - 3) = 1$
para			$N=8$ $T=4$ $8 - 4 \times 2 = 0$	$|A|=4$ $|B|=4$ $S = 1/2 \times (4 - 4) = 0$

Figure 2. Schematic representation of the three different manners (coupling units) of connecting two unpaired electrons through a six-membered ring. 1,3-phenylene unit promotes a ferromagnetic coupling.

schematically presents the three different manners of connecting two unpaired electrons through a six- membered aromatic ring and indicates that only through a *meta* connection a high-spin character of the ground state is predicted. Experimentally,[18–21] much effort has been devoted to this particular issue, leading to a general accepted conclusion: If the spin density in the six-membered ring unit is not affected by large steric hindrance, a *meta* or *1,3*-phenylene connection leads to ferromagnetic interaction between unpaired electrons.

Finally, in order to close the selection of theoretical works dealing with topological arguments for the magnetic description of conjugated hydrocarbon systems, it is important to mention the exhaustive treatment carried out by Maynau and Malrieu.[22,23] They propose and apply a method, based on a valence bond effective Hamiltonian

parametrized by means of ab-initio calculations, to inspect how neutral determinants interact with higher-order excitations and which is the associated contribution to the energy. It is worth mentioning that all discussed theoretical works assume perfect planarity of the systems, allowing for a strict σ−π separation. However, in real case examples, this is an exception rather than a rule, given the structural flexibility of the covalent organic bonds. In fact, as far as theoretical calculations based on ab-initio methods for the prediction of magnetic coupling constants in this sort of compounds are concerned, molecular conformation has very rarely been taken into account. Precisely, one of the objectives of this thesis is to take advantage of such flexibility to provide new arguments on the stability and magnetic interactions of related compounds.

Finally, and as an early indication of the forthcoming discussion, it is worth saying that if a chemical stabilization of the radical centres is not addressed, the prediction of the ground state multiplicity becomes secondary because the high reactivity of such exposed centres would immediately destroy any property of interest. Therefore, the possibility of sterically protecting the radical centre becomes crucial. For instance, in the *m*-xylylene diradical, substitution of Hydrogen atoms for phenyl rings at each of the radical centres leads to the Schlenk diradical, which might be seen as two Gomberg's monoradicals. These are three very reactive species. However, for the latter case, a further substitution of Hydrogen atoms by Chlorine atoms, results in the perchlorotriphenylmethyl (PTM) radical, known as one of the most stable organic radicals.

In conclusion, the choice of these architectures to achieve extended polyradical systems allows ensuring the ground state multiplicity through topological arguments and a chemical stabilization of the radical centre through steric protection.

4.2.3. Ordering of Low-lying Electronic States: Disjoint *vs* Non-Disjoint SOMOs.

The previous sections have consecutively introduced each of the concepts and reasons that provide arguments for using alternant non-Kekulé polycyclic hydrocarbons for achieving high-spin ground state purely organic compounds. The underlying reasoning was promoting a large exchange integral while minimizing the orbital overlap. This section will be devoted to the last characteristic of the molecules that have been used in this thesis for the design of extended polyradicals, i.e., non-disjoint singly occupied molecular orbitals (SOMOs). The rationalization of the problem in terms of

disjoint and non-disjoint molecular orbitals permits the correct prediction of the ground state multiplicity in compounds where pure topological arguments could be misleading.

This section will deal entirely with the work of Borden and Davidson,[24] who were the first making use of the non-disjoint *vs* disjoint character of singly occupied molecular orbitals (SOMOs) to explain the electronic nature of some conjugated alternant hydrocarbon (AH) diradicals. As explicitly pointed out in the work, the interest of the authors derive from the investigation of the electronic structure in trimethylenemethane (TMM), where a conformational change is concomitant to a change of the ground state. This is a first indication of the subtleties of this sort of molecules where a shortcut in the π system has large implications on the electronic structure. This particular issue will be further investigated in the forthcoming sections.

The most straightforward message of the work is that the classification of alternant hydrocarbons depending on whether their non-bonding Hückel orbitals (NBMOs) can be confined to disjoints sets of atoms or not, allows for an accurate prediction of both the ground state of the system and the character of the triplet and singlet open shell wave functions. Basically, for an even alternant hydrocarbon, it will always be possible to define disjoints SOMOs, resulting in a triplet and singlet open shell states almost degenerate. On the other hand, for and odd alternant hydrocarbon, it is possible to construct the corresponding SOMOs which will be non-disjoint and defined uniquely over the starred atoms. As a consequence, the triplet state will be more stable than the open shell singlet. This conclusion is reminiscent of the discussion concerning eq. (12). However, it always exist the possibility of carrying out a further localization of these SOMOs in different atoms belonging to the same starred subset. If that is the case, the triplet and open shell singlet would be degenerate again. An important conclusion of this work is that it provides the way of checking if this additional localization can be performed. This will occur when a diradical can be analysed as resulting from union of two odd AHs at an inactive carbon (those with a zero coefficient in their NBMO) of each, provided that in one and only one of the odd AH fragments the inactive carbon belongs to the same (starred) set as the active carbons of the NBMO. For a qualitative explanation of the discussion, Figure 3 presents two odd AHs. Those molecules are the
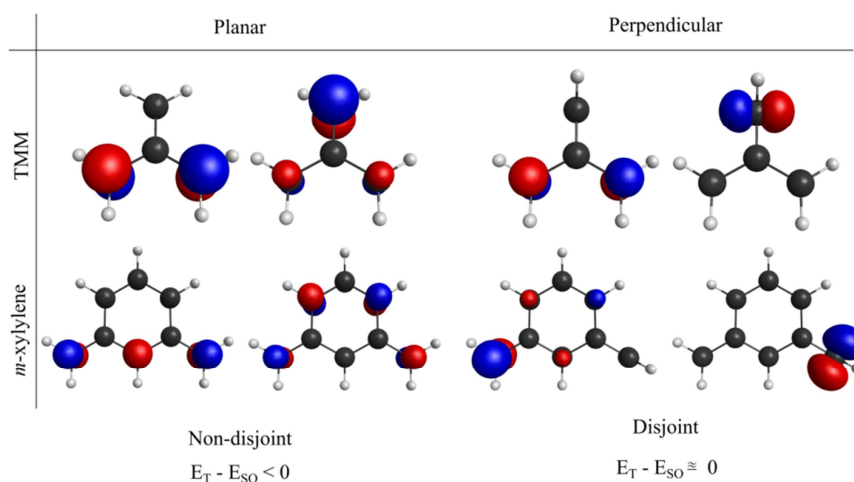
Figure 3. Singly occupied non-bonding MO for TMM and *m*-xylylene in the triplet state, with a total conjugated π-sytem and a disrupted one. The character of the SOMOs and the energetic difference between the triplet and open shell singlet is also indicated.

well-known trimethylenemethane (TMM) and *m*-xylylene. When they are planar, the SOMOs are non-disjoint, resulting in a triplet ground state. However, if there is a disruption of the π system through a rotation of one of the methyl groups, the SOMOs can be confined to different atoms belonging to the same subset, what results in an almost degeneracy of the two electronic states. Obviously, for the design of extended polyradical systems making use of these units as building blocks, those are features to take into account. In fact, an exhaustive study of the conformational freedom of some di- and triradicals derived from the *m*-xylylene, and the impact on the ordering of the electronic states is presented in papers #4.3 and #4.4.

This section has finished introducing the necessary conditions that a given AH must fulfil to ensure a high-spin ground state, and justifies the structures that have been investigated along this chapter of the thesis. Once again, those are alternant non-Kekulé polycyclic hydrocarbons with non-disjoint singly occupied molecular orbitals (SOMOs). As previously discussed, a non-disjoint character of the SOMOs implies an odd alternant hydrocarbon. These requirements provide enough information for making a grounded choice on the most appropriate building block for a hypothetical construction of extended polyradicals. However, those are not concerned with the stabilization of the intrinsically unstable radical centres, and by themselves do not warrantee that the predicted systems are feasible experimentally. Thus, for a reasonable prediction of interesting purely organic magnetic systems, chemical stability arguments must be considered as a pre-requisite, and using persistent radical, which are already

chemically stable, as building blocks appear as a reasonable starting point. Next section presents some of the available persistent organic radicals in the literature aiming at selecting the most promising ones, in terms of chemical stability and possibilities of extension, to construct stable high-spin ground state polyradicals. Additionally, this discussion serves a test for checking the validity of the topological rules.

4.2.4. Experimental Examples of Topological Rules.

This section will present some of the examples of neutral alternant hydrocarbon compounds existing in the literature showing radical character. It aims at providing the experimental counterpart and validation of the theoretical considerations that have been discussed so far.

Figure 4 introduces a series of alternant hydrocarbons that have been characterized as radical species. In the first column, the discussed molecules are divided depending on whether they are even (**1-4**) or odd (**5-13**) hydrocarbons, i.e.; if they possess the same number of atoms belonging to the two subsets (|A|, |B|). Another difference is that despite being depicted as diradicals, for molecules **1-4**, it is possible to write down resonant forms breaking the aromaticity of the six membered rings, pairing the unpaired electrons in the methylene extremes. In molecules **5-13** that is not possible. The second column indicates the total number of carbon atoms (N) and the maximum number of double bonds occurring in any resonance structure (T) together with the number of atoms belonging to the two subsets. This information is used as input for equation (17) and equation (21), for the prediction of the number of non-bonding MOs and ground state multiplicity as discussed in section 2.2, respectively in the third and fourth column. Fifth column indicates the character of the associated singly occupied MOs, as introduced in section 2.3. Finally, the rightmost column compares the ground state of the molecule as predicted theoretically and proved experimentally. Thus, even hydrocarbons present disjoint SOMOs resulting on a triplet and open shell singlet nearly degenerated. On the contrary, odd hydrocarbons present non-disjoint SOMOs and if no further localization to different atoms of the same subset can be made, the triplet state will be around two times the exchange integral more stable than the open shell singlet. Again, at a first approximation, the reason for such differential stabilization is due to the degenerate and orthogonal character of the SOMOs, which is dictated by the alternancy

of the lattice, ensuring an almost zero orbital overlap while maximizing the shared region of space (exchange integral).

First, a close inspection of molecules **1-4** and some works derived from them will be presented. Molecule **1** is the well-known tetramethyleneethane (TME). The ground state of this molecule is subject to controversy, because two experimental independent methodologies provide contradictory conclusions. In one hand, Dowd et al.[25] found that the temperature dependence of the intensity of triplet EPR signal followed the Curie-Weiss law, concluding that the ground state was a triplet. On the other hand, NIPES experiment[26] indicated that the singlet state is 3 Kcal/mol more stable than the triplet. As proposed by Lineberger and Borden,[27] an explanation that would bring together the two experiments would be to assume that the populated triplet states of TME slowly relax to the lower energy state, which is a singlet. Compound **2** is the *para*-quinodimethane (*p*-QDM) or *p*-xylylene, showing a well characterized singlet as the ground state,[28–30] in accordance with the prediction from the topological rules. It is worth noting that the associated 1,4-phenylene is an antiferromagnetic coupling unit (see Figure 2). Molecule **3** is the hypothetical *p*-dimethylene pyrene, predicted to be an open-shell singlet ground state. No experimental evidence on its electronic structure is available. Finally, compound **4** is the well-known Thiele's diradical, showing a singlet as the ground state.[31]. Clearly, even alternant hydrocarbons do not appear as promising candidates as building blocks for achieving polyradicals, but they possess other interesting characteristics. In particular they represent a field to study the interplay between aromatic and radical character, together with a variety of optical properties, due the different nature of the low-lying states. This subtle interplay has been reviewed by Wu et. al.[32] and theoretically investigated by Trinquier and Malrieu,[33] in **2-4** molecules and extended derivatives. Basically, if the energy required to break a double bond, which yields the unpaired electron, is paid back by the concomitant generation of the aromatic six-membered ring, a strong radical character can be expected. The use of quinoidal cores (1,4-phenylene) is the most convenient route for this end. An additional feature of these compounds derives from the role that anti-aromaticity has in stabilizing the triplet excited state, bringing it even closer in energy to the ground state, as investigated by Baird through second order perturbation theory.[34] Baird established that the rules for ground-state aromaticity are reversed in the lowest triplet excited state because *4n* rings
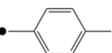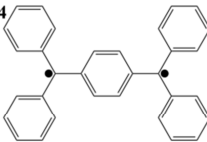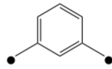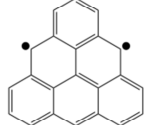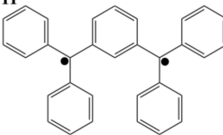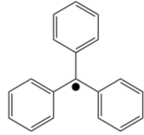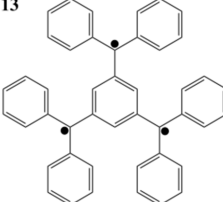
		N ; T |A| ; |B|	NBMOs eq. (17)	S eq. (21)	SOMOs	Ground state Theory Exp.	
1		6 ; 2 3 ; 3	6 - 2x2 = 2	(3 - 3)/2 = 0	Disjoint	S	S
2		8 ; 4 4 ; 4	8 - 2x4 = 0	(4 - 4)/2 = 0	Disjoint	S	S
3		18 ; 9 9 ; 9	18 - 2x9 = 0	(9 - 9)/2 = 0	Disjoint	S	
4		32 ; 16 16 ; 16	32 - 2x16 = 0	(16 - 16)/2 = 0	Disjoint	S	S
5		3 ; 1 2 ; 1	3 - 2x1 = 1	(2 - 1)/2 = 1/2	Non-disjoint	D	D
6		4 ; 1 3 ; 1	4 - 2x1 = 2	(3 - 1)/2 = 1	Non-disjoint	T	T
7		8 ; 3 5 ; 3	8 - 2x3 = 2	(5 - 3)/2 = 1	Disjoint	S	
8		6 ; 2 4 ; 2	6 - 2x2 = 2	(4 - 2)/2 = 1	Non-disjoint	T	T
9		8 ; 3 5 ; 3	8 - 2x3 = 2	(5 - 3)/2 = 1	Non-disjoint	T	T
10		22 ; 10 12 ; 10	22 - 2x10 = 2	(12 - 10)/2 = 1	Non-disjoint	T	T
11		32 ; 15 17 ; 15	32 - 2x15 = 2	(17 - 15)/2 = 1	Non-disjoint	T	T
12		19 ; 9 10 ; 9	19 - 2x9 = 1	(10 - 9)/2 = 1/2	Non-disjoint	D	D
13		45 ; 21 24 ; 21	45 - 2x21 = 3	(24 - 21)/2 = 3/2	Non-disjoint	Q	Q

Figure 4. Selected hydrocarbons with radical character. Molecules **1-4** belong to even hydrocarbon (\|A\|=\|B\|), while **5-13** to odd hydrocarbon (\|A\|≠\|B\|) class. D, S, T and Q stand for doublet, singlet, triplet and quintet, respectively.

display aromatic character whereas *4n+2* rings display antiaromatic character. As a consequence, a variety of electronic states of different nature are accessible in these compounds, making them very interesting to investigate optical properties. Despite not presenting any work dealing with this particular issue in this thesis, this brief discussion is thought to give a more solid form to the whole reasoning.

Now, a more detailed discussion of molecules **5-13** in Figure 4 will be given. The success in designing extended polyradicals from this kind of hydrocarbons will depend on the amount of unpaired electrons that can be coupled ferromagnetically. Molecules **5** and **6** (allyl radical and trimethylenemethane respectively) have been extensively studied, representing case studies for electronic structure theory. Both are associated with very reactive species due to the exposure of the unpaired electrons, preventing any use in a hypothetical extended polyradical. However, the purpose of their inclusion is as examples of the succeful predictions of the topological arguments. Allyl radical is known for presenting one unpaired electron (doublet), and the two unpaired electrons in TMM couple in a triplet state, with an estimated singlet-triplet gap of 13-16 Kcal/mol.[35,36] Molecule **7** is a hypothetical compound as introduced by Borden and Davidson,[24] but serves as an illustrative example of the subtle character of disjoint *vs* non-disjoint character of the SOMOs. Despite being an odd hydrocarbon, an additional localization of the SOMOs to different atoms of the same subset can be performed. Then, the ground state is predicted to be an open-shell singlet state.[24] Molecule **8** and derivatives were investigated by Dougherty et al,[5] who named it as a non-Kekulé benzene and showed that the ground state is a triplet. Covalently assembling these units led to the concept of non-Kekulé acenes as a way of achieving a large number of unpaired electrons. However, within this approach, the resulting interaction between the electrons is a weak antiferromagnetism.[5] By changing the unit that connects the unpaired electrons, a preferential ferromagnetism can be promoted. That is the case of 1.3-phenylene units, as discussed in Section 4.2.2.2. Molecule **9,** also known as *m*-xylylene or MBQDM, is predicted to have a triplet ground state, which is confirmed by NIPES experiments.[17] Unfortunately, as in TMM, MBQDM is a very reactive species due to the accessibility to the exposed radical centres. However, the large triplet-singlet gap (~ 9.6 Kcal/mol) found for this molecule indicate that it is a good candidate for promoting ferromagnetism in extended polyradicals, given that an effective stabilization of the radical centres is achieved. A strategy to do so is the participation of the unpaired

electrons in an extended conjugated π system, which decreases the spin density on the radical centres by promoting several resonant forms that bring a net stabilization. Triangulene **10** represents a case study where this sort of stabilization has been investigated. The first attempts to synthesize triangulene **10** were made by Clar et al. in the fifties, but only polymerized product was achieved.[37] This is an indication of the kinetic instability of the molecule, and lack of sufficient stabilization of the centres. However, additional strategies can be envisioned such as steric protection, leading to the first entirely hydrocarbon triangulene derivative showing a triplet ground state.[38] Following the same reasoning, more recent works have been able to synthesize and characterize similar species.[39] These works demonstrate that the combination of a steric protection together with participation on a π system, results in effective stabilization of the carbon-bearing radical centres. However, using triangulene units for the design of hypothetical polyradicals has an implicit drawback, named the low density of unpaired electrons in the network. For the appearance of a radical centre, many more carbon atoms must be introduced. Molecule **11**, known as Schlenk diradical,[40] represents an alternative manner of stabilizing the radical centres by steric protection and participation on a π system, and additionally, holds the potential of a large density of unpaired electrons in an extended polyradical. It is consider the first organic diradical reported, and it can be seen as a phenyl substituted *m*-xylylene. For this and similar compound, theory and experiment predict a triplet ground state. Additionally, the radical centres can be further stabilized by substituting all hydrogen atoms by chlorine atoms. The ground state keeps being a triplet.[41] Still, Schlenk diradical is not the most basic unit of its kind, but an extension of the first organic monoradical reported: molecule **12** or Gomberg radical.[42] Very interestingly, molecule **12** can be further stabilized as molecule **11**, resulting in perchlorotriphenylmethyl (PTM), one of the most stable organic radicals.[43] The stability of this compound is such that can be deposited over surfaces,[44] coordinate to metal atoms[45] and create porous magnetic materials.[46] Following the same strategy, molecule **13** or Leo triradical,[47] which shows a quartet ground state in solution, can be further stabilized by chlorine substitution. This results in a very stable triradical[48] showing ferromagnetic interaction even at room temperature.

In view of the previous discussion, topological rules can be assumed to be a useful predictive tool on the ground state multiplicity of alternant hydrocarbons. It is worth pointing out that even if these rules were established for perfectly planar cases, where

the $\sigma - \pi$ separation is strictly correct, they also provide accurate predictions for largely distorted geometries. For instance, as mentioned, experimental measurements show that the chlorinated molecule **13** presents a robust quartet ground state, even at room temperature, despite showing two stereoisomers with C_2 and D_3 symmetry that imply large torsion angles. Additionally, and as highlighted throughout the previous discussion, for constructing high-spin ground state polyradicals interacting through-bond, the building block used must also offer effective paths for its extension, and together with that, the possibility of chemically stabilize the exposed radical centre.

4.2.5. Chemical Stability of Radical Centres.

Up to now, theoretical and experimental evidence of possible organic building blocks showing high-spin ground states has been presented. On the basis of chemical stability of the radical centres, derivatives of molecules **9**, **11-13** are selected as candidates to develop the main research of this chapter (papers #4.1-6) for approaching organic magnetism based on odd alternant hydrocarbons compounds. Basically, they are *m*-xylylene and triarylmethyl derivatives. The choice of these building blocks is deliberate because, on top of fulfilling the topological arguments that predict a high-spin ground state, they offer two important features related to stability when used to obtain polyradicals. Those are the multiple manners of assembling them, leading to different magnetic topologies, and the possibility of sterically protecting the radical centres. The latter feature is crucial, because when going to extended systems, topological degeneracy becomes one of the many requirements to achieve high-spin polyradicals. As the molecular dimensionality increases, other questions such as how to promote a strong ferromagnetic interaction in the whole molecule or how to obtain significant magnetic anisotropy barriers, play a significant role. This is tightly related to the shape of the macromolecule, which is determined by how the polyradical is extended. Then, what is left is to ensure an assembly of the building blocks such that diminishes the impact of any possible defects destroying magnetic interactions and ensures robust magnetic properties. That is the aim of the forthcoming section 2.6.

4.2.6. Coupling schemes to obtain π–conjugated high-spin polyradicals.

Before going into detail on the different manners for extending a high-spin polyradical, it is worth to highlight the macroscopic properties that might be of interest in the final product and the most common experimental difficulties found in the

synthetic approaches. Then, the best choice among the different coupling schemes may be guided by the interplay between those two features; the adopted coupling scheme determines the expected macroscopic properties, since they relate to molecular shape, and limits the kind and extent of defects affecting magnetic interaction. This section is largely inspired by Rajca's work.[49]

4.2.6.1. Macroscopic Properties.

The assembly of a large number of high-spin units results in a mesoscopic entity, expected to show macroscopic properties. In principle, by the discussed topological arguments, correctly choosing the topology of the π system of the constituents ensures a high-spin ground state. However, at a macroscopic scale there are other requirements that are equally important in defining interesting magnetic properties, as for instance magnetic anisotropy barriers. The appearance of magnetic anisotropy implies an energy barrier (E_A) which must be overcome for rotating the magnetization vector along the easy axis. There are two primary sources contributing to the magnetic anisotropy barrier in magnetic materials: spin-orbit coupling and dipole-dipole interactions. It is known that for metal-free, carbon-based π conjugated systems, spin-orbit coupling is negligible, as observed by Rajca when comparing the small deviation in the g-factors of these species with respect to the g-factor of a free electron.[50] Therefore, in these compounds, classical dipole-dipole interactions within the macromolecule are the main contributor to the shape of anisotropy barrier, which expressed in units of temperature takes the form of Equation (22).

$$E_A/k_B = 0.5NVM_{sat}^2/k_B \qquad (22)$$

k_B is the Boltzmann constant, N a shape factor related to the demagnetisation factor ($0 \leq N \leq 2\Pi$ with $N = 0$ for a sphere and $N = 2\Pi$ for an infinite rod), V is the volume of the macromolecule and M_{sat} the magnetization at saturation. Taking as an example a polyarylmethyl polyradical with an elongated ellipsoidal shape, 200 ferromagnetically coupled spins are required to approach a barrier of 2 K ($N = 3$).[49] Thus, the barriers for coherent rotation of magnetization may be related to the molecular shape of the polyradicals and its spin density, being especially large in elongated shapes. Such approach could provide blocked superparamagnets below certain temperature, similar to magnetic metal-based particles or coordination chemistry crystals. Figure 5 exemplifies

the previous discussion on a single domain particle, showing the dependence of the energy (E) with respect to the angle (θ) between the magnetisation vector (M) and the easy magnetisation axis in the absence of an applied magnetic field.
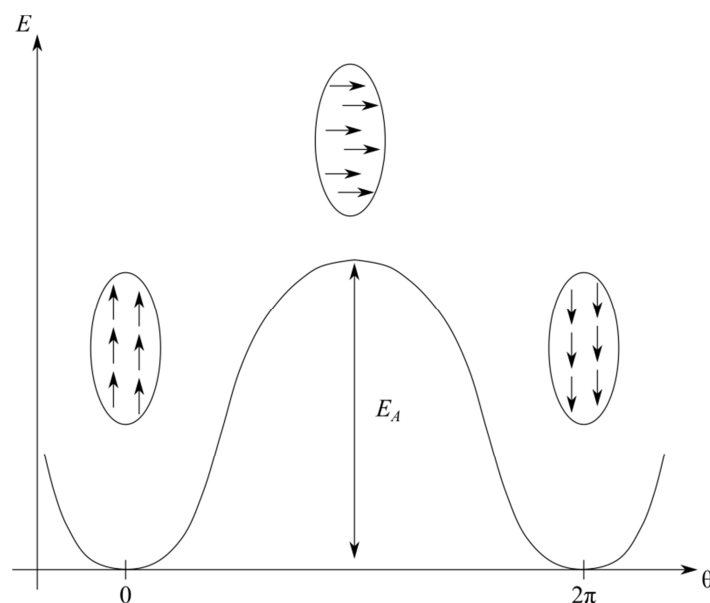

Figure 5. Energy barrier to remagnetisation of a single-domain particle with oblong shape, in the absence of an applied external field.

To summarize, the macroscopic properties of interest in very high-spin polyradicals are tightly related to the shape of the obtained macromolecule, which in turn is dictated by the adopted coupling scheme.

4.2.6.2. Defects.

The most common defects encountered experimentally when synthesizing very high-spin polyradicals based on odd alternant hydrocarbons are out-of-plane torsions and chemical defects. Out-of-plane torsions are due to the intrinsic flexibility of the compounds, whereas chemical defects can be considered as a consequence of the synthetic route, which consists on a carbanionic method and requires from polyethers precursors to generate the radical centres.[49] A scheme on the synthetic method is presented in Figure 6, chapter 1 section *1.3.1.4. Radicals with Unpaired Electron in Carbon Atoms.* These defects range from the incomplete generation of the radical centre to formation of various bonds, such as C−I or C−H at the radical site. The appearance of these problems is ubiquitous, but by properly choosing the coupling scheme there are manners of diminishing their impact on the final magnetic properties.

Figure 6 illustrates the impact of the mentioned defects when occurring in the interior of a dendritic structure as synthesized by Rajca et al.[51] First, the presence of chemical defects, such as the incomplete generation of radical centres from the precursors, might interrupt the ferromagnetic interaction among unpaired electrons and even split the polyradical in different, non-interacting, low S value parts, as depicted in Figure 6 b). However, this drawback is not equally critical for different arrangements. The more paths connect one radical centre, the less is the impact on the appearance of a chemical defect, as depicted in Figure 7. Second, out-of-plane torsions have been investigated in a large number of alkyl-substituted and/or conformationally restrained diradicals, based on diradical **11**.[49]
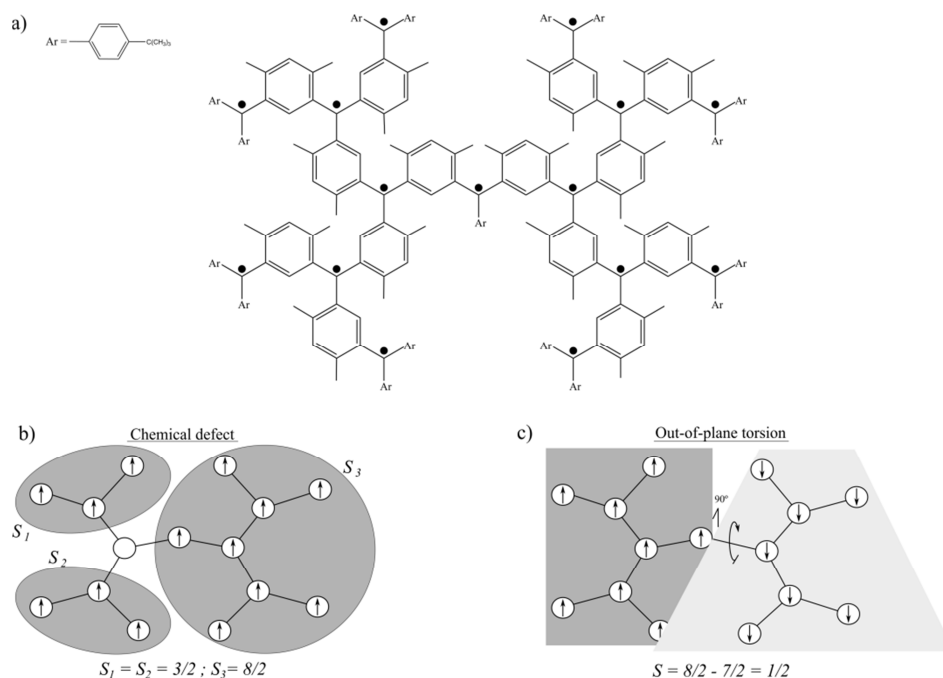

Figure 6. Impact of chemical defects and out-of-plane torsions on a dendtritic pentadecaradical. a) synthesized by Rajca. In b) and c) lines represent ferromagnetic coupling units, empty circles chemical defects and darker (lighter) grey colours indicate spin-up (spin-down) interacting regions.

The conclusion of these works developed throughout decades is that there is a delicate interplay between conformation and exchange coupling, which is affected by the molecular structures, conformations, and the medium. Although in most cases 1,3-phenylene is a robust ferromagnetic coupler, if large out-of-plane twisting happens, it might result in a decrease of the ferromagnetic exchange coupling and even reversal to antiferromagnetic coupling, as exemplified in Figure 6 c).
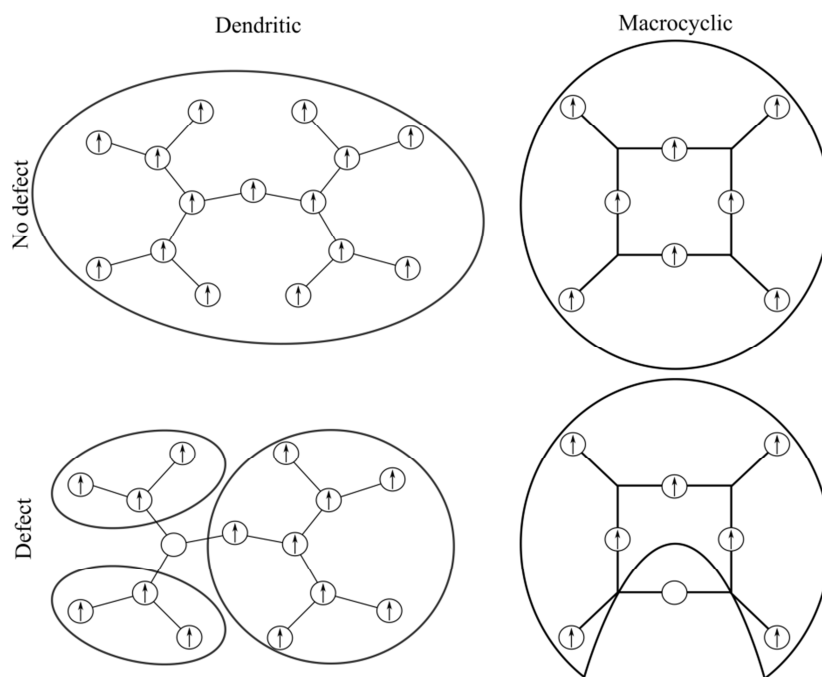
Figure 7. Comparison of a random chemical defect on different assemblies. Solid lines connecting unpaired electrons indicate ferromagnetic interaction and circles define interacting regions.

Then, the design of very high-spin polyradicals from odd alternant hydrocarbons, especially from molecules **9**, **11-13** and derivatives, must deal with this sort of problems. The most effective manner for minimizing the impact is by a proper choice of assembling the units, i.e., the coupling scheme.

4.2.6.3. Coupling schemes.

Up to now it has been discussed the macroscopic magnetic properties that are likely to arise as a consequence of the macromolecule's shape, and the possible defects to be encountered in the synthesis. Given that the pursued goal is the design of polyradicals showing intermolecular robust magnetic interaction among the radical centres, the possibilities for using odd alternant polycyclic hydrocarbons as building blocks are restricted to three limiting coupling schemes, as stated by Rajca.[49] This classification is summarized in Figure 8 and arises from the combination of either ferromagnetic coupling units, like 1,3-phenylene or antiferromagnetic ones, like 1,4-phenylene. The reasons behind the differential preferential spin state in each of the units have been given in the previous sections.

The first coupling scheme is the so-called ferromagnetic scheme. This strategy is based on the existence of a ferromagnetic coupling unit (fCU) connecting the unpaired electrons in an alternant lattice. The ground state multiplicity of the resulting

polyradical is assumed to be $S = n/2$ where n is the number of radical sites. This results from the topological arguments applied to the coupling unit (generally a 1,3-phenylene, Figure 2). Yet, there are two distinct classes of polyradicals that result from this coupling scheme, depending on the arrangement of the radical centres. Class **I** polyradicals present the spin sites within the π-system that mediates the spin-coupling interaction. This results in polymers with the radical centres belonging to the backbone of the repeating unit. The extension to higher order molecules can be done through a linear, star-branched, dendritic or macrocyclic connectivity, as exemplified in Figure 9. Class **II** polyradicals bear the pendant spin centres attached to the π-system. This is the coupling scheme that counts with the largest amount of reported examples, specially Class **I** polyradicals.
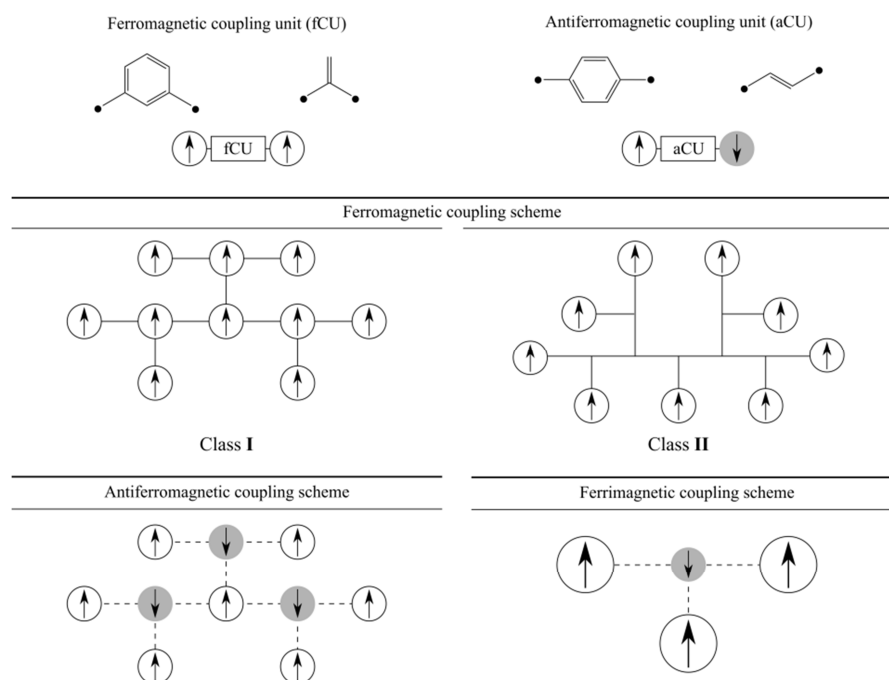
Figure 8. Ferro- and antiferromagnetic coupling units and resulting coupling schemes arising from their combination. Solid lines represent ferromagnetic interaction while dashed ones antiferromagnetic.

The second is the antiferromagnetic coupling scheme, which relies on antiferromagnetic coupling units (aCU) in an alternant lattice. Each spin site bears the same S value, and consequently the appearance of high-spin ground state must come from an uncompensated connectivity that accounts for an uncompensated spin cancelling. In order for that to happen, particular shapes and topologies are required, such as hyper-branched structures.

Finally, the third case is the ferrimagnetic coupling scheme. In here, spin sites are connected through an aCU along an alternate lattice, but each spin site bears a different *S* value. The advantage of this approach is that it leads to uncompensated spin cancelling for most connectivities, ranging from linear to dendritic or macrocyclic.
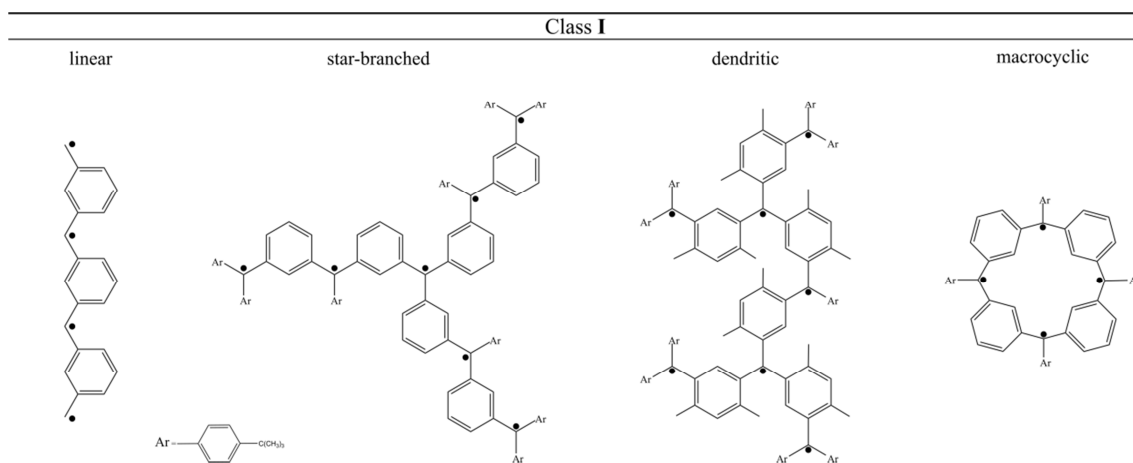

Figure 9. Examples of linear, star-branched, dendritic and macrocyclic connectivities as limiting cases for Class **I** polyradicals.

Now, as a comparative argument, let's briefly mention another type of polyradicals that have discussed in chapter 1: radical polymers. Despite being based on a totally different approach, where no topological arguments on the coupling unit (CU) ensures any particular multiplicity of the ground state, radical polymers could be considered as a complement to the previous classification, especially because of the structural information that can be accessed within this approach. Radical polymers are aliphatic or non-conjugated polymers bearing organic robust radicals as pendant groups per repeating unit. In this approach the interaction of the unpaired electrons is entirely dictated by the adopted conformation, passing from para to diamagnetism.[52–54] This serves as an indication of the importance of secondary structure for defining the magnetic properties.

As mentioned, the amount of reported polyradicals of Class **I** belonging to the ferromagnetic coupling scheme, clearly indicates the success of this strategy. However, most of the reported molecules present relatively low *S* values and none surpasses $S \approx 6$.[49] The reason for that is the large negative impact that chemical defects and out-of-plane torsions have in Class **I** polyradicals. As discussed previously, linear, star-branched and dendritic connectivities are more exposed than a macrocyclic to losing the

magnetic properties if a defect happens, due to fewer alternative paths to spread the magnetic interaction, as shown in Figure 7. In a more concrete manner, this problematic is exemplified comparing two case studies: dendritic architectures with potentially 15 and 31 unpaired electrons showing the same magnetic behaviour as their homologues with only 7 and 10 sites,[51] and a macrocyclic with 14 spin sites and a $S \approx 6$ ground state.[55] Despite the more robust approach based on macrocyclic connectivity, the S value continue to be low.

In addition to changing the connectivities in the coupling scheme to prevent the defects from happening, one can also stabilize the radical centres in order to increase the stability of the polyradical. The most successful strategy within this approach has relied on steric protection of the radical centre, as exemplified by PTM radical, a perchlorinated derivative of molecule **12**. Veciana el al. have devoted special attention to this issue,[41,48,56] arguing that a more stable building block (PTM with respect to purely hydrocarbons polyarylmethyls derivatives used by Rajca) would provide more robust magnetic properties of the extended polyradical. Based on that, they prepared three different strategies for achieving high-spin polyradicals from PTM units. However, only one proved to be efficient for the synthesis of a triradical,[48] while the rest presented such steric congestion due to the Chlorine atoms, that even the precursors were difficult to address.[56] Despite that, one could wonder if with the currently available catalogue of differently substituted PTM radicals, these early attempts might be revisited. Even more so, to take advantage of their stability over surfaces[44] to design two-dimensional ordered magnetic compounds.
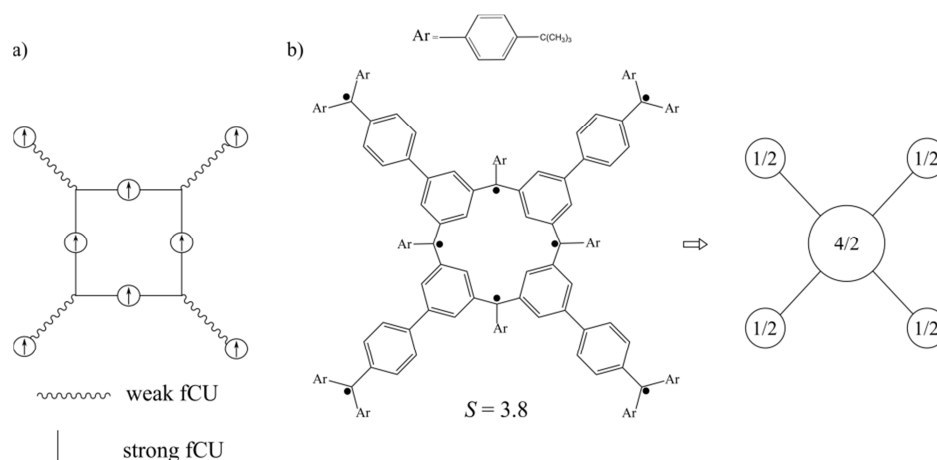

Figure 10. a) Schematic representation of high-spin organic cluster. b) Example of a dendritic-macrocyclic organic spin cluster and its magnetic topology.

With the presented evidences, it is reasonable to conclude that despite much accomplished, ferromagnetic coupling scheme and more specifically Class **I** polyradicals alone, do not stand the chance to achieve very high-spin polyradicals with robust magnetic interactions. Rajca proposed an intermediate between the ferromagnetic and ferrimagnetic coupling schemes as a promising manner of moving forward, introducing the concept of organic spin clusters. The key feature relies on a combination of weak and strong fCU, achieved by means of 3,4′-biphenylene and 1,3-phenylene connectivities respectively, as depicted in Figure 10. Within this strategy, there are three different ways of carrying out the assembly: dendritic-macrocyclic, macrocyclic-macrocyclic and annelated macrocyclic polyradicals. This conceptual advance has led to one of the milestones in this field of research, which is magnetic ordering in a purely organic polymer-based polyradical.[57] However, and despite this enormous success, magnetic ordering is limited to temperatures below 10 K. One could wonder if by other coupling schemes, which induce other type of spatial arrangements of the extended polyradicals, the resulting compound might display more robust magnetic properties.

From a theoretical point of view, there are many relevant works addressing how to extend an organic lattice that shows magnetic properties. Of special interest is the work by Mataga,[58] who suggested possible ferromagnetic lattices, made out of *m*-xylylene and triarylmethyl radicals. Afterwards, Tyutyulkov *et al.*[59–61] and Yoshizawa et. al[62,63] published a series of studies on the electronic structure of linear polyradicals. Of major importance for the purpose of this thesis is the work by Yoshizawa and Hoffman,[63] because it points at the existence of a secondary structure in structurally flexible polyradicals. More recently Trinquier et. al[64,65] have focused their attention on the design of organic magnetic lattices, seeking a high-spin ground state. However, the assumption of planarity in almost all the cases and the little attention paid to the chemical stability of the radical centres, leave plenty of space for improvement.

Altogether, the set of works presented in the forthcoming section, which constitute the largest part of this thesis, aims at providing reliable arguments for achieving robust ferromagnetic properties in purely organic π-conjugated materials. The roadmap to follow is a proper theoretical treatment of the electronic structure of the investigated compounds, an accurate extraction of the relevant magnetic interactions and a careful study of the impact that structural flexibility has on the magnetic properties.

REFERENCES

(1)   Borden, W. T. *Diradicals*; Wiley-Interscience: New York, 1982.

(2)   Abe, M. Diradicals. *Chem. Rev.* **2013**, *113*, 7011–7088.

(3)   Born, M.; Oppenheimer, R. Zur Quantentheorie Der Molekeln. *Ann. Phys.* **1927**, *389* (20), 457–484.

(4)   Goldberg, A. H.; Dougherty, D. A. Effects of through-Bond and through-Space Interactions on Singlet-Triplet Energy Gaps in Localized Biradicals. *J. Am. Chem. Soc.* **1983**, *105* (2), 284–290.

(5)   Dougherty, D. A. Spin Control in Organic Molecules. *Acc. Chem. Res.* **1991**, *24* (3), 88–94.

(6)   Anderson, P. W. Antiferromagnetism. Theory of Superexchange Interaction. *Phys. Rev.* **1950**, *79* (2), 350–356.

(7)   Anderson, P. W. Theory of Magnetic Exchange Interactions:Exchange in Insulators and Semiconductors. *Solid State Phys.* **1963**, *14*, 99–214.

(8)   Hay, P. J.; Thibeault, J. C.; Hoffmann, R. Orbital Interactions in Metal Dimer Complexes. *J. Am. Chem. Soc.* **1975**, *97*, 4884–4899.

(9)   Hoffmann, R. Trimethylene and the Addition of Methylene to Ethylene. *J. Am. Chem. Soc.* **1968**, *90* (6), 1475–1485.

(10)   Hoffmann, R. Interaction of Orbitals through Space and through Bonds. *Acc. Chem. Res.* **1971**, *4* (1), 1–9.

(11)   Longuet-Higgins, H. C. Some Studies in Molecular Orbital Theory I. Resonance Structures and Molecular Orbitals in Unsaturated Hydrocarbons. *J. Chem. Phys.* **1950**, *18* (3), 265.

(12)   Ovchinnikov, A. A. Multiplicity of the Ground State of Large Alternant Organic Molecules with Conjugated Bonds. *Theor. Chim. Acta* **1978**, *47*, 297–304.

(13)   Lieb, E.; Schultz, T.; Mattis, D. Two Soluble Models of an Antiferromagnetic Chain. *Ann. Phys. (N. Y).* **1961**, *16* (3), 407–466.

(14)   Lieb, E.; Mattis, D. Ordering Energy Levels of Interacting Spin Systems. *J. Math. Phys.* **1962**, *3*, 749–751.

(15)   Lieb, E. H. Two Theorems on the Hubbard Model. *Phys. Rev. Lett.* **1989**, *62* (16), 1927–1927.

(16)   Coulson, C. A.; Rushbrooke, S. No Title. *Proc. Camb. Phil. Soc.* **1940**, *36*, 193.

(17)   Wenthold, P. G.; Kim, J. B.; Lineberger, W. C. Photoelectron Spectroscopy of M -Xylylene Anion. *J. Am. Chem. Soc.* **1997**, *119* (16), 1354–1359.

(18)   Teki, Y.; Takui, T.; Itoh, K.; Iwamura, H.; Kobayashi, K. Preparation and ESR Detection of a Ground-State Nonet Hydrocarbon as a Model for One-Dimensional Organic Ferromagnets. *J. Am. Chem. Soc.* **1986**, *108* (9), 2147–2156.

(19)   Jacobs, S. J.; Shultz, D. A.; Jain, R.; Novak, J.; Dougherty, D. A. Evaluation of Potential Ferromagnetic Coupling Units: The bis(TMM) [bis(trimethylenemethane)] Approach to High-Spin Organic Molecules. *J. Am. Chem. Soc.* **1993**, *115* (5), 1744–1753.

(20)   Gallagher, N. M.; Olankitwanit, A.; Rajca, A. High-Spin Organic Molecules. *J. Org. Chem.* **2015**, *80* (1), 1291–1298.

(21)   Rajca, A.; Rajca, S. Alkyl-Substituted Schlenk Hydrocarbon Diradicals with Triplet and Singlet Ground States in Frozen Solutions. *J. Chem. Soc. Perkin Trans. 2* **1998**, No. 5, 1077–1082.

(22)   Malrieu, J. P.; Maynau, D. A Valence Bond Effective Hamiltonian for Neutral States of .pi. Systems. 1. Method. *J. Am. Chem. Soc.* **1982**, *104* (11), 3021–3029.

(23)   Maynau, D.; Malrieu, J. P. A Valence Bond Effective Hamiltonian for the Neutral States of .pi. Systems. 2. Results. *J. Am. Chem. Soc.* **1982**, *104* (11), 3029–3034.

(24)   Borden, W. T.; Davidson, E. R. Effects of Electron Repulsion in Conjugated Hydrocarbon Diradicals. *J. Am. Chem. Soc.* **1977**, *99* (14), 4587–4594.

(25)   Dowd, P.; Chang, W.; Paik, Y. H. Tetramethyleneethane, a Ground-State Triplet. *J. Am. Chem. Soc.* **1986**, *108* (23), 7416–7417.

(26)   Clifford, E. P.; Wenthold, P. G.; Lineberger, W. C.; Ellison, G. B.; Wang, C. X.; Grabowski, J. J.; Vila, F.; Jordan, K. D. Properties of Tetramethyleneethane (TME) as Revealed by Ion Chemistry and Ion Photoelectron Spectroscopy. *J. Chem. Soc. Perkin Trans. 2* **1998**, No. 5, 1015–1022.

(27)   Lineberger, W. C.; Borden, W. T. The Synergy between Qualitative Theory, Quantitative Calculations, and Direct Experiments in Understanding, Calculating, and Measuring the Energy Differences between the Lowest Singlet and Triplet States of Organic Diradicals. *Phys. Chem. Chem. Phys.* **2011**, *13* (25), 11792–11813.

(28)   Errede, L. A.; Hoyt, J. M. The Chemistry of Xylylenes. III. Some Reactions of P-Xylylene That Occur by Free Radical Intermediates 2. *J. Am. Chem. Soc.* **1960**, *82* (2), 436–439.

(29)   Williams, D. J.; Pearson, J. M.; Levy, M. Nuclear Magnetic Resonance Spectra of Quinodimethanes. *J. Am. Chem. Soc.* **1970**, *92* (5), 1436–1438.

(30)   Koenig, T.; Southworth, S. The Helium (He I) Photoelectron Spectrum of 3,7-
        Dimethyl-P-Quinodimethane. A Non-Koopmans Theorem Effect. *J. Am. Chem.
        Soc.* **1977**, *99* (8), 2807–2809.

(31)   Montgomery, L. K.; Huffman, J. C.; Jurczak, E. A.; Grendze, M. P. The
        Molecular Structures of Thiele's and Chichibabin's Hydrocarbons. *J. Am. Chem.
        Soc.* **1986**, *108* (19), 6004–6011.

(32)   Zeng, Z.; Shi, X.; Chi, C.; López Navarrete, J. T.; Casado, J.; Wu, J. Pro-
        Aromatic and Anti-Aromatic Π-Conjugated Molecules: An Irresistible Wish to
        Be Diradicals. *Chem. Soc. Rev.* **2015**, *44*, 6578–6596.

(33)   Trinquier, G.; Malrieu, J.-P. Kekulé versus Lewis: When Aromaticity Prevents
        Electron Pairing and Imposes Polyradical Character. *Chemistry* **2015**, *21* (2),
        814–828.

(34)   Baird, N. C. Quantum Organic Photochemistry. II. Resonance and Aromaticity in
        the Lowest 3.pi..pi.* State of Cyclic Hydrocarbons. *J. Am. Chem. Soc.* **1972**, *94*
        (4), 4941–4948.

(35)   Dowd, P. Tetramethyleneethane. *J. Am. Chem. Soc.* **1970**, *92* (4), 1066–1068.

(36)   Wenthold, P. G.; Hu, J.; Squires, R. R.; Lineberger, W. C. Photoelectron
        Spectroscopy of the Trimethylene- Methane Negative Ion. The Singlet−Triplet
        Splitting of Trimethylenemethane. *J. Am. Chem. Soc.* **1996**, *118* (2), 475–476.

(37)   Clar, E.; Stewart, D. G. Aromatic Hydrocarbons. LXVIII. Triangulene
        Derivatives. Part II 1. *J. Am. Chem. Soc.* **1954**, *76* (13), 3504–3507.

(38)   Inoue, J.; Fukui, K.; Kubo, T.; Nakazawa, S.; Sato, K.; Shiomi, D.; Morita, Y.;
        Yamamoto, K.; Takui, T.; Nakasuji, K. The First Detection of a Clar's
        Hydrocarbon, 2,6,10-Tri- Tert -Butyltriangulene: A Ground-State Triplet of Non-
        Kekulé Polynuclear Benzenoid Hydrocarbon. *J. Am. Chem. Soc.* **2001**, *123* (50),
        12702–12703.

(39)   Li, Y.; Huang, K.-W.; Sun, Z.; Webster, R. D.; Zeng, Z.; Zeng, W.; Chi, C.;
        Furukawa, K.; Wu, J. A Kinetically Blocked 1,14:11,12-Dibenzopentacene: A
        Persistent Triplet Diradical of a Non-Kekulé Polycyclic Benzenoid Hydrocarbon.
        Chem. Sci. **2014**, *5*, 1908.

(40)   Schlenk, W. Brauns, M. No Title. *Ber. Dtsch. Chem. Ges.* **1915**, *48*, 661–669.

(41)   Veciana, J.; Rovira, C.; Crespo, M. I.; Armet, O.; Domingo, V. M.; Palacio, F.
        Stable Polyradicals with High-Spin Ground States. 1. Synthesis, Separation, and
        Magnetic Characterization of the Stereoisomers of 2,4,5,6-Tetrachloro-
        .α.,.α.,.α.',.α.'-Tetrakis(pentachlorophenyl)-M-Xylylene Biradical. *J. Am. Chem.
        Soc.* **1991**, *113* (7), 2552–2561.

(42)   Gomberg, M. An Instance of Trivalent Carbon: Triphenylmethyl. *J. Am. Chem.
        Soc.* **1900**, *22* (11), 757–771.

(43) Ballester, M.; Riera-Figueras, J.; Castaner, J.; Badfa, C.; Monso, J. M. Inert Carbon Free Radicals. I. Perchlorodiphenylmethyl and Perchlorotriphenylmethyl Radical Series. *J. Am. Chem. Soc.* **1971**, *93* (9), 2215–2225.

(44) Mas-Torrent, M.; Crivillers, N.; Rovira, C.; Veciana, J. Attaching Persistent Organic Free Radicals to Surfaces: How and Why. *Chem. Rev.* **2012**, *112*, 2506–2527.

(45) Roques, N.; Domingo, N.; Maspoch, D.; Wurst, K.; Rovira, C.; Tejada, J.; Ruiz-Molina, D.; Veciana, J. Metal-Radical Chains Based on Polychlorotriphenylmethyl Radicals: Synthesis, Structure, and Magnetic Properties. *Inorg. Chem.* **2010**, *49* (9), 3482–3488.

(46) Maspoch, D.; Domingo, N.; Ruiz-Molina, D.; Wurst, K.; Vaughan, G.; Tejada, J.; Rovira, C.; Veciana, J. A Robust Purely Organic Nanoporous Magnet. *Angew. Chemie - Int. Ed.* **2004**, *43*, 1828–1832.

(47) Wilker, W.; Kothe, G.; Zimmermann, H. Über Das Radikal 1,3,5-Benzoltris(diphenylmethyl). Tetramere Und Quartettzustand. *Chem. Ber.* **1975**, *108* (6), 2124–2136.

(48) Veciana, J.; Rovira, C.; Ventosa, N.; Crespo, M. I.; Palacio, F. Stable Polyradicals with High-Spin Ground States. 2. Synthesis and Characterization of a Complete Series of Polyradicals Derived from 2,4,6-Trichloro-.α.,.α.,.α.',.α.',.α.",.α."-Hexakis(pentachlorophenyl)mesitylene with S = 1/2,. *J. Am. Chem. Soc.* **1993**, *115*, 57–64.

(49) Rajca, A. The Physical Organic Chemistry of Very High-Spin Polyradicals. *Adv. Phys. Org. Chem.* **2005**, *40*, 153–199.

(50) Rajca, A. Organic Diradicals and Polyradicals: From Spin Coupling to Magnetism? *Chem. Rev.* **1994**, *94*, 871–893.

(51) Rajca, a; Utamapanya, S. Toward Organic-Synthesis of a Magnetic Particle - Dendritic Polyradicals with 15 and 31 Centers for Unpaired Electrons. *J. Am. Chem. Soc.* **1993**, *115* (9), 10688–10694.

(52) Murata, H.; Miyajima, D.; Nishide, H. A High-Spin and Helical Organic Polymer: Poly{[4-(dianisylaminium)phenyl]acetylene}. *Macromolecules* **2006**, *39* (19), 6331–6335.

(53) Matsuda, K.; Stone, M. T.; Moore, J. S. Helical Pitch of M -Phenylene Ethynylene Foldamers by Double Spin Labeling. *J. Am. Chem. Soc.* **2002**, *124* (40), 11836–11837.

(54) Kaneko, T.; Abe, H.; Teraguchi, M.; Aoki, T. Folding-Induced Through-Space Magnetic Interaction of Poly(1,3-Phenyleneethynylene)-Based Polyradicals. *Macromolecules* **2013**, *46* (7), 2583–2598.

(55)   Rajca, A.; Lu, K.; Rajca, S. High-Spin Polyarylmethyl Polyradical: Fragment of a Macrocyclic 2-Strand Based upon Calix[4]arene Rings. *J. Am. Chem. Soc.* **1997**, *119* (43), 10335–10345.

(56)   Ruiz-Molina, D.; Veciana, J.; Palacio, F.; Rovira, C. Drawbacks Arising from the High Steric Congestion in the Synthesis of New Dendritic Polyalkylaromatic Polyradicals. *J. Org. Chem.* **1997**, *62* (26), 9009–9017.

(57)   Rajca, A.; Wongsriratanakul, J.; Rajca, S. Magnetic Ordering in an Organic Polymer. *Science* **2001**, *294*, 1503–1505.

(58)   Mataga, N. Possible Ferromagnetic States of Some Hypothetical Hydrocarbons. *Theor. Chim. Acta* **1968**, *10* (4), 372–376.

(59)   Tyutyulkov, N.; Schuster, P.; Polansky, O. Band Structure of Nonclassical Polymers. *Theor. Chim. Acta* **1983**, *63* (4), 291–304.

(60)   Tyutyulkov, N.; Polansky, O. E.; Schuster, P.; karabunarliev, S.; Ivanov, C. I. Structure and Properties of Non-Classical Polymers II. Band Structure and Spin Densities. *Theor. Chim. Acta* **1985**, *67* (3), 211–228.

(61)   Tyutyulkov, N. N.; Karabunarliev, S. C. Structure and Properties of Nonclassical Polymers. III. Magnetic Characteristics at Finite Temperatures. *Int. J. Quantum Chem.* **1986**, *29* (5), 1325–1337.

(62)   Yoshizawa, K.; Tanaka, K.; Yamabe, T. Ferromagnetic Coupling through M-Phenylene. Molecular and Crystal Orbital Study. *J. Phys. Chem.* **1994**, *98* (7), 1851–1855.

(63)   Yoshizawa, K.; Hoffmann, R. Potential Linear-Chain Organic Ferromagnets. *Chem. - A Eur. J.* **1995**, *7*, 403–413.

(64)   Trinquier, G.; Suaud, N.; Malrieu, J.-P. Theoretical Design of High-Spin Polycyclic Hydrocarbons. *Chemistry* **2010**, *16* (29), 8762–8772.

(65)   Trinquier, G.; Suaud, N.; Guihéry, N.; Malrieu, J. P. Designing Magnetic Organic Lattices from High-Spin Polycyclic Units. *ChemPhysChem* **2011**, *12*, 3020–3036.

(66)   Malrieu, J. P.; Trinquier, G. A Recipe for Geometry Optimization of Diradicalar Singlet States from Broken-Symmetry Calculations. *J. Phys. Chem. A* **2012**, *116*, 8226–8237.

4.3. Publications.

This section presents the work developed during this thesis within the theoretical and computational description of magnetic interactions in the field of organic magnetism based on odd-alternant hydrocarbon compounds. The contribution is presented in six works; papers #4.1 to #4.3 are already published, papers #4.4 and #4.5 are submitted and paper #4.6 is under preparation for submission.

All of them deal with different aspects related to the discussion presented in section 2, and investigate molecules where the topological arguments justify the electronic structure.

4.3.1.   Paper #4.1.

The Triplet-Singlet Gap in the *m*-xylylene Radical: A Not So Simple One

# The Triplet−Singlet Gap in the *m*-Xylylene Radical: A Not So Simple One

Daniel Reta Mañeru,[†] Arun K. Pal,[‡] Ibério de P. R. Moreira,[†] Sambhu N. Datta,[‡] and Francesc Illas*,[†]

[†]Departament de Química Física & Institut de Química Teòrica i Computacional (IQTCUB), Universitat de Barcelona, C/Martí i Franquès 1, E-08028 Barcelona, Spain

[‡]Department of Chemistry, Indian Institute of Technology, Bombay, Powai, Mumbai 400076, India

S *Supporting Information*

ABSTRACT: *Meta*-benzoquinodimethane (MBQDM) or *m*-xylylene provides a model for larger organic diradicals, the triplet−singlet gap being the key property. In the present work this energy difference has been the object of a systematic study by means of several density functional theory-based methods including B3LYP, M06, M06-2X, HSE and LC-ωPBE potentials and a variety of wave function-based methods such as complete active space self consistent field (CASSCF), Multireference second-order Møller−Plesset (MRMP), difference dedicated configuration interaction (DDCI), and Multireference configuration interaction (MRCI). In each case various basis sets of increasing quality have been explored, and the effect of the molecular geometry is also analyzed. The use of the triplet and broken symmetry (BS) solutions for the corresponding optimized geometries obtained from B3LYP and especially M06-2X functionals provide the value of the adiabatic triplet−singlet gap closer to experiment when compared to the reported value of Wenthold, Kim, and Lineberger, (*J. Am. Chem. Soc.* **1997**, *119*, 1354) and also for the electron affinity. The agreement further improves using the full π-valence CASSCF(8,8) optimized geometry as an attempt to correct for the spin contamination effects on the geometry of the BS state. The CASSCF, MRMP, and MRCI, even with the full π valence CAS(8,8) as reference and relatively large basis set, systematically overestimate the experimental value indicating either that an accurate description must go beyond this level of theory, including σ electrons and higher order polarization functions, or perhaps that the measured value is affected by the experimental conditions.
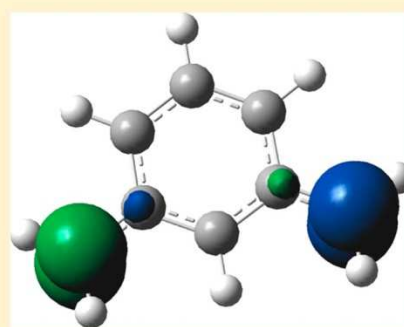
1. INTRODUCTION

Apart from the obvious interest in general organic chemistry,[1] organic diradicals constitute an invaluable set of systems to investigate chemical reactivity and molecular mechanisms.[2] Along the years, several experimental techniques such as matrix isolation[3] and flash photolysis[4,5] allowed the synthesis of these generally short-lived species. Further developments allowed the spectroscopic characterization of diradicals and, in particular, negative ion photoelectron spectroscopy (NIPES) has been shown to be a very useful tool to scrutiny their electronic structure.[6] A second field of interest related to diradicals is their possible application in magnetic technologies.[7,8] Here, the energy difference between low-lying states of different multiplicity, usually singlet and triplet states, becomes the key property and efforts have been made to synthesize diradicals with tuned triplet−singlet gaps and, more specifically, to obtain diradicals with a triplet ground state which can be used in magnetic devices. Most of the organic radicals, diradicals, and polyradicals are highly conjugated systems, in contrast to metal complexes or clusters. For such conjugated species, the Borden−Davidson disjoint SOMO dictum[9] and the spin alternation principle[10,11] in unrestricted SCF calculations[12,13] of Kohn−Sham form have been found to be highly successful in the prediction of triplet ground states. Clearly, the accurate

prediction of triplet−singlet gaps in organic diradicals is of paramount importance.[14−17] Several theoretical methods have been proposed including those based on different density functional theory (DFT)-based method and those based in wave function theory. A brief summary of the different methods and their performance for metal complexes and similar systems can be found in several recent reviews[18,19] and specialized articles.[20]

Among the different known rather stable diradicals, *meta*-benzoquinodimethane (MBQDM) or *m*-xylylene (Scheme 1) has been considered as a benchmark because it is well characterized from experiment. In fact, Platz et al.[21] have synthesized MBQDM and used electron spin resonance (ESR) to provide the first evidence of the triplet character of its electronic ground state. The molecular structure of MBQDM exhibits C_{2v} symmetry and the open-shell orbitals a_1 and b_2 character so that the electronic ground state can be denoted as $^3B_2$. Later on, Wenthold et al.[22] provided an accurate estimate of the electron affinity of this diradical, and their NIPES study has shown that the low-lying electronic states are $^1A_1$ and $^1B_2$, respectively. Note that both electronic states have a strong

Scheme 1. Schematic Representation of the Molecular Structure of *m*-Xylylene[a]
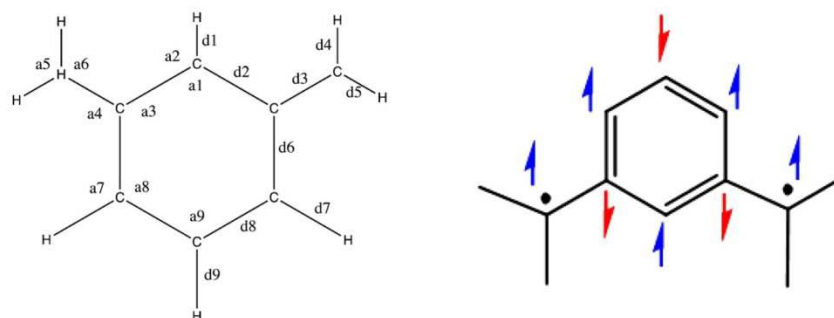
[a]Bond angles and lengths are named. The spin alternation scheme is explicitly illustrated indicating the diradical to be a ground-state triplet.

open-shell character and that the $^1A_1$ cannot be represented by a single closed-shell Slater determinant. The order of the electronic states is well predicted by theoretical arguments and appropriate ab initio calculations.[23] The electronic structure of this and other diradicals has also been reviewed in a recent perspective paper.[24] Note, however, that previous studies using approximate but rather extended configuration interaction wave function in the π space predicted a quite large effect of the quadruple excitations on a single reference,[25] which can be taken as a first indication of the subtleties hidden in the electronic structure of this kind of diradical; we will come back to this point later on.

An additional puzzling aspect with the electronic structure of MBQDM, however, is that photoelectron spectroscopy exhibits an adiabatic character as the spectra display a vibrational fine structure which is also resolved. To understand the experiment is convenient to consider the illumination of a doublet anion by light. The photon has enough energy ($h\nu$) to eject one electron. The remaining neutral species is left in its vibronic states. The energy difference ($h\nu - KE_{max}$), where KE_{max} is the maximum kinetic energy of the electron equals the energy between the neutral molecule and the negative ion, that is, the electron affinity of the neutral species. It transpires that the NIPES spectrum will give the relative energies of the adiabatic ground states with different spin. Because the KE_{max} spectrum shows vibrational structure, the NIPES data can be interpreted for the adiabatic coupling constant, with zero-point vibrational energy correction. This is also consistent with the fact that agreement between experiment and theory is better reproduced by considering adiabatic transitions[23] as explained in detail below. The agreement between experiment and theory is, however, only moderate since the multireference second-order perturbation theory (CASPT2) calculations of Hrovat et al.,[23] using a complete active space self consistent field (CASSCF) reference with eight electrons and eight orbitals, hereafter referred to as CAS(8,8), defining the complete active space, predict an adiabatic triplet–singlet gap of 11.7 kcal mol^{-1} (4092 cm^{-1})—11.0 kcal mol^{-1} or 3850 cm^{-1} after correcting for the zero-point energy (ZPE) using the CASSCF vibrational frequencies—while the experimental value is of 9.6 ± 0.2 kcal mol^{-1} (3358 ± 70 cm^{-1}). The absolute error of 2.1 kcal mol^{-1} or 734 cm^{-1} (492 cm^{-1} if ZPE corrected), while modest in absolute terms, still represents a relative large error of 22%, and one may wonder whether a more accurate value can be obtained by improving the level of theory. For instance, the value reported by Hrovat et al.[23] has been obtained using the geometry optimized of each state at the 6-31G*/CASSCF level

with a CAS(8,8). In principle, the basis set quality can be easily improved which can affect the equilibrium geometry of the two electronic states. It is also convenient to explore the value corresponding to a Franck–Condon transition which would provide information about the effect of geometry relaxation in the excited state. Vertical and adiabatic excitation energies have been reported by Wang and Krylov[26] using the equation of motion spin-flip coupled cluster singles and doubles (EOM-SF-CCSD) method and a larger basis set (6-311G(2d) for C and 6-31G* for H). The reported values are 13.8 kcal mol^{-1} (4839 cm^{-1}) and 11.3 kcal mol^{-1} (3952 cm^{-1}) for the vertical and adiabatic transitions, respectively. In this case, the difference between vertical and adiabatic values is significantly large, 2.5 kcal mol^{-1} or almost 900 cm^{-1}. There is a modest improvement over the CASPT2 values of Hrovat et al.,[23] and an 18% error with respect to experiment still remains.

From a more fundamental point of view, it is also important to note that for a diradical such as MBQDM, one would expect a minimal CAS(2,2) description to be sufficient. This is the case for several organic diradicals and also for Cu dinuclear and similar magnetic inorganic complexes where CASPT2 or DDCI calculations carried out using a minimal CAS(2,2) reference space predict excellent values of the triplet–singlet gap or equivalently of the magnetic coupling constant which happens to be a more appropriate term when the energy difference is very small.[18,27] Very recently Suaud et al.[28] have analyzed this problem in detail and found that the description based on a CAS(2,2) fails for MBQDM. They attribute the failure to the too localized character of the singly occupied orbitals in the CASSCF(2,2) wave function and develop an iterative procedure to improve the orbitals based on natural orbitals. These authors use geometries for singlet and triplet optimized using the EOM-SF-CCSD method as reported by Wang and Krylov.[26] The best value obtained by these authors for the adiabatic triplet–singlet gap restricted to a CAS(2,2) model is 12.4 kcal mol^{-1} (4355 cm^{-1}), comparable to their CASPT2 value of 10.8 kcal mol^{-1} (3790 cm^{-1}) obtained using the EOM-SF-CCSD structures and a CASSCF(8,8) reference. This value is clearly too large, indicating the difficulty to project the physics into the minimal CAS space. The CASPT2 value, obtained using a CASSCF(8,8) reference, a 6-31G** and the geometry from the EOM-SF-CCSD calculations are in better agreement with experiment, the relative error being reduced to 13%.

The discussion above shows evidence of the delicate interplay between, structure, basis set, and description of electron correlation in defining the triplet–singlet gap of

MBQDM which calls for a more systematic study. On the other hand, one must also realize that this type of CASSCF/CASPT2 calculations become rapidly intractable when the size of the molecule increases, even moderately. DFT-based calculations offer a very attractive alternative, and there is abundant literature in related systems indicating that the popular B3LYP and similar hybrid functionals tend to provide values close to the experimental one,[29−37] although the semiempirical flavor of hybrid functionals makes one wonder if the right answer comes from the right reason, a long-standing question in modern electronic structure theory. Nevertheless, the complexity of the electronic structure of MBQDM revealed by the CASPT2 and EOM-SF-CCSD calculations commented above may also appear to be difficult for DFT-based methods. In the present work, we provide a systematic study of the triplet−singlet gap of MBQDM using a variety of wave function- and DFT-based methods covering different types of active spaces and several configuration interaction approaches, various types of basis sets ranging from standard Pople's basis to correlation consistent sets, different exchange−correlation functionals, and carefully exploring the effect of the geometry in the vertical and adiabatic triplet−singlet gap of this not so simple organic diradical.

2. COMPUTATIONAL DETAILS

The triplet−singlet gap of MBQDM has been studied at various levels of theory, including several wave function and DFT methods, as specified in detail below. In these calculations all electrons have been explicitly considered and the corresponding one electron states, molecular or Kohn−Sham, expanded in Gaussian type basis sets of increasing size. Two families of basis sets have been used, the first one follows the well-known approach developed by Pople and co-workers[38,39] which is broadly used in all sorts of applications, and the second one follows the approach of Dunning for correlations consistent basis sets,[40] especially designed to be used in explicitly correlated calculations. For the first set, we start with the 6-31G* double-ζ plus polarization standard basis, the 6-31G** including a polarization in the H atoms,[41] the 6-311G** and 6-311++G** triple-ζ basis plus polarization sets, the latter including also diffuse functions,[42] and the more extended 6-311++G(3df,3pd).[43] For the second one we used the aug-cc-pVDZ and the aug-cc-pVTZ sets.[40,44]

For the DFT-based methods a number of state of the art exchange−correlation potentials have been used starting with the popular B3LYP hybrid method[45] and including the M06 and M06-2X meta hybrid functionals of Zhao and Truhlar[46−48] and the short-range HSE[49] and long-range LC-ωPBE[50] range separated functionals. Note, however, that the standard Kohn−Sham implementation of DFT does not allow treating open-shell systems in a rigorous way[51,52] and some alternative approaches such as restricted ensemble Kohn−Sham (REKS)[53,54] and, more recently, spin flip time-dependent DFT (SF-TDDFT)[55] methods have been proposed and applied to similar problems where the quantity of interest is a triplet−singlet energy difference.[56,57] In the present work we make use of the standard spin unrestricted Kohn−Sham formalism, where a high-spin Kohn−Sham determinant with two unpaired electrons with parallel spin is used to represent the triplet state and a broken symmetry (BS)[58−60] solution is used to obtain the energy of the singlet[61] using the formula proposed by Yamaguchi.[62−64] In this way, the vertical DFT triplet−singlet gap is approximately twice the energy difference between the high spin and the BS solutions. It is also worth pointing out

that, for a given functional, triplet−singlet gaps computed using spin projection are in good agreement with those obtained from the SF-TDDFT methods where spin states are properly represented.[57]

The case of adiabatic transitions requires some additional comments. In fact, it is important that the Yamaguchi's approach is well-defined for a given geometry, either singlet (S), triplet (T) approximated by the high-spin state or BS obtained from the appropriate method. Following Yamaguchi[62−64] one can obtain the vertical triplet−singlet gap (triplet to singlet excitation energy) Δ_{TS}^i (or simply Δ_{vert}) at a given geometry i as

$$\Delta_{TS}^i \equiv \Delta_{vert} = E_{S^i} - E_{T^i} = \frac{2(E_{BS^i} - E_{T^i})}{\langle S_{T^i}^2 \rangle - \langle S_{BS^i}^2 \rangle} \tag{1}$$

where E_{S^i}, E_{T^i} and E_{BS^i} are the energy of the singlet, triplet, and BS solution, respectively, and the superindex "i" is used to indicate the geometry used in the calculations. The denominator contains the expectation value of the square of the total spin operator for the triplet and BS solutions (close to 2.000 and 1.000, respectively) and, again, the superindex indicates the molecular geometry. Obviously, the expectation value of the square of the total spin operator has been obtained from the electron density for the reference Kohn−Sham system. From eq 1 it is possible to not only calculate Δ_{TS}^i but also to estimate the energy of the (decontaminated) open-shell singlet E_{S^i} as

$$E_{S^i} = \frac{2(E_{BS^i} - E_{T^i})}{\langle S_{T^i}^2 \rangle - \langle S_{BS^i}^2 \rangle} + E_{T^i} \tag{2}$$

which is required to obtain the adiabatic triplet−singlet gap Δ_{TS}^{adia} (or simply Δ_{adia}) as

$$\Delta_{TS}^{adia} \equiv \Delta_{adia} = E_{S^i} - E_{T^j} = \frac{2(E_{BS^i} - E_{T^i})}{\langle S_{T^i}^2 \rangle - \langle S_{BS^i}^2 \rangle} + E_{T^i} - E_{T^j} \tag{3}$$

where i and j refer now to the molecular geometry of the singlet, usually taken as that predicted from the BS approach, and of the triplet, respectively. Note, however, that one could use the geometry of the open-shell singlet as predicted by the appropriate method. In the next section we will come back to this point in some more detail. For practical purposes one may approximate eq 3 as

$$\Delta_{TS}^{adia,approx} \equiv \Delta_{apadia} = E_{S^i} - E_{T^j} = \frac{2(E_{BS^i} - E_{T^j})}{\langle S_{T^j}^2 \rangle - \langle S_{BS^i}^2 \rangle} \tag{4}$$

which does not require the calculation of the energy of triplet state at the BS (or singlet) geometry. Note, however, that use of eq 4 may lead to inaccurate values if the geometry of the two states differs significantly.

Finally, a number of explicitly correlated wave function methods have been explored, all starting from a CASSCF reference but with the CAS varying from the minimal (2,2) description to the CAS(8,8) full π valence. Next, dynamical correlation is included through the second-order multireference Møller−Plesset (MRMP) perturbation theory[65−68] and, in some cases, through fully variational multireference single and doubles configuration interaction (MRSDCI). A series of calculations using the difference dedicated configuration interaction (DDCI)[69] method have also been carried out starting from different CAS as reference. The DDCI leads to a

Table 1. Vertical and Adiabatic Triplet–Singlet (Δ_{vert} and Δ_{adia}) Gap of *m*-Xylylene As Predicted from Different DFT-Based Methods Using Basis Sets of Increasing Size[a]

cm^{-1}	6-311++G**			6-31G**			6-31G*		
	Δ_{vert}	Δ_{apadia}	Δ_{adia}	Δ_{vert}	Δ_{apadia}	Δ_{adia}	Δ_{vert}	Δ_{apadia}	Δ_{adia}
B3LYP	4564	4256	4133	4753	4430	4304	4773	4444	4320
M06	5100	4828	4679	5329	4948	4789	5361	4966	4812
M06-2X	4142	3755	3615	4100	3706	3566	4096	3697	3560
HSE	5097	4719	4576	5270	4881	4735	5293	4897	4753
LC-ωPBE	7371	6439	6185	7534	6600	6340	7551	6617	6356

[a]In order to separate geometric effects, all values have been computed using the optimized structure as obtained with the 6-311G** basis set for each method.

Table 2. Total Energy and $<S^2>$, Both in Atomic Units, Vertical and Adiabatic Triplet-Singlet (Δ_{vert} and Δ_{adia}) Gap As Predicted From UB3LYP and UM062X Functionals Using 6-311++G(3df,3pd) Basis Set[a]

system	state/geom	B3LYP		M062X	
		E	$<S^2>$	E	$<S^2>$
	T/T	−309.6905204	2.063121	−309.5325703	2.069032
	BS/T	−309.6796469	1.012419	−309.5226956	1.018404
	Δ_{vert}	4542		4126	
m-xylylene diradical	T/BS	−309.689707	2.060854	−309.5317944	2.064708
	BS/BS	−309.6803489	1.011834	−309.5235966	1.017800
	Δ_{adia}	4127		3607	
m-xylylene anion	D/D	−309.7193305	0.781376	−309.5619826	0.786878

[a]Δ_{vert} and Δ_{adia} values in cm^{-1} are also reported. T = triplet, D = doublet, BS = broken symmetry.

configuration interaction expansion which is a subset of the full MRSDCI, neglecting the 2h–2p (h = hole; p = particle) excitations involving orbitals out of the CAS which at second order of perturbation theory equally contribute to the two states, provided the same set of molecular orbital is used.[70] In the case of CAS(8,8), the resulting MRSDCI expansion is too large to be explicitly treated, and a selection procedure has been carried out based on the weight of the configurations in the CASSCF wave function. Here it is important to point out that DDCI and MRSDCI wave functions, as any truncated CI expansion, suffer from the normalization error, and this may introduce some uncertainty in the calculated excitation energy values. Nevertheless, these methods are often the choice for studies involving excited states, and the accuracy in calculated excitation energies is usually below 500 cm^{-1}.[71−73] Note, however, that in the case of magnetic coupling constants of dinuclear complexes, the values predicted by the DDCI method are often within 50−100 cm^{-1} of the experimental values.[74]

In order to explore the effect of the geometry separately, single point energy calculations have been carried out for the singlet and triplet states at the geometry optimized by different methods either of DFT or wave function type and by employing several of the basis sets described above. Vertical and adiabatic transitions have been obtained, and the pertinent optimized structures, total energy values, and other relevant data are collected in the Supporting Information file.

The DFT-based calculations have been carried out using the Gaussian09 suite of programs;[75] CASSCF and MRMP calculations were run with the GAMESS06 code[76,77] and, finally, DDCI and selected CI calculations were carried out using the CASDI code[78] interfaced to the MOLCAS7.6 package[79] which provided the CASSCF reference wave functions. Here it is important to point out that MRMP has some important differences with the broadly used CASPT2 method[80,81] regarding the states used to span the first-order wave function. In CASPT2, single and double excitations are

applied to the reference wave CASSCF function, while in MRPT all singly and doubly excited determinants obtained from each of the determinants in the reference wave function are considered. In other words, CASPT2 uses a contracted reference function, whereas MRPT does not. The use of a contracted/uncontracted reference may be advantageous depending on the particular case, although there is not a general rule. An alternative, possibly better, option might consist in using the NEVPT2 formalism of Malrieu et al.[82] which uses a different partition of the Hamiltonian which has some formal and practical advantages, it avoids the problem of intruder states although these do not appear here. In any case one must keep in mind that CASPT2, MRMP, and NEVPT2 are second-order approaches and that higher order terms, which can make important contributions, are missing.

3. THE EFFECT OF BASIS SET, GEOMETRY, AND METHOD

In order to separate effects arising from the choice of the method, the choice of the basis set, and the influence of the geometry, a series of calculations have been carried out which use the same geometry with different basis set and a given method or the optimum geometry with different basis sets and different methods. For simplicity, the results of DFT calculations will be described first.

3.1. Influence of the Basis Set and Exchange–Correlation Potential in the DFT-Based Calculations.

First, we explore the effect of the basis set on the calculation of the triplet–singlet gap by taking the geometry optimized for the triplet and BS states for each density functional with the 6-311G** basis set and evaluate the energy with different basis sets. Results in Table 1 for the vertical, approximated adiabatic, and adiabatic triplet–singlet gap (Δ_{vert}, Δ_{apadia}, and Δ_{adia}), respectively, allow one to extract several conclusions. In general the Δ_{apadia} values follow the trends of Δ_{adia} but are less accurate.

Table 3. Vertical and Adiabatic Triplet−Singlet (Δ_{vert} and Δ_{adia}) Gap of *m*-Xylylene As Predicted from Different DFT-Based Methods[a]

cm^{-1}	B3LYP		HSE		M06		M06-2X		$\mu \pm \sigma$	
	Δ_{vert}	Δ_{adia}	Δ_{vert}	Δ_{adia}	Δ_{vert}	Δ_{adia}	Δ_{vert}	Δ_{adia}	Δ_{vert}	Δ_{adia}
B3LYP	4564	4133	4503	4092	4600	3996	4405	4052	4518 ± 74	4068 ± 51
M06	5067	4585	4994	4529	5100	4679	4884	4483	5011 ± 83	4569 ± 73
M06-2X	4324	3726	4255	3665	4370	3718	4142	3615	4273 ± 86	3681 ± 45
HSE	5166	4633	5097	4576	5207	4637	4985	4528	5114 ± 84	4594 ± 45

[a]The values have been obtained from calculations using the 6-311++G** basis set and the optimized structure, either for triplet of singlet, obtained with the 6-311G** basis set for each method. The different columns indicate the origin of the geometry, and the rows report calculated values at the different structures. Mean values (μ) and standard deviation (σ) are provided in the rightmost columns.

Therefore, they are presented in Table 1 for completeness but are not further discussed. The adiabatic (Δ_{adia}) values are always closer to experiment, and the difference between vertical and adiabatic calculated excitations is roughly 400 cm^{-1} rather irrespective of the method and basis used. Likewise, the effect of the density functional is much larger than the effect of the basis set. For instance, for the B3LYP functional the Δ_{vert} value goes from 4564 to 4773 cm^{-1} when decreasing the basis set from 6-311++G** to the much less extended 6-31G*; a change of 200 cm^{-1} that is certainly not negligible. However, the use of M06-2X instead of B3LYP while keeping the 6-311++G** basis set leads to a change of more than 400 cm^{-1}. The change is even larger if one considers the range separated functionals. In this respect, it is surprising to find that the LC-ωPBE performs quite badly, especially because this functional was parametrized for thermochemistry and barrier heights of main group molecules.[50] This functional, however, led to excellent results in the case of the triplet−singlet gap in Cu dinuclear complexes[83] and the superconducting cuprates parent compounds.[84] The LC-ωPBE results will not be commented in the forthcoming sections.

In order to further check the effect of the basis set we comment on the results obtained with the largest set, the 6-311++G(3df,3pd), and with the B3LYP and M06-2X functional as shown in Table 2. The calculated Δ_{adia} values are 4127 and 3607 cm^{-1}, respectively, which correspond to changes of only 6 cm^{-1} (B3LYP) and 8 cm^{-1} (M06-2X) with respect to values computed with the 6-311++G** basis set. Therefore, it is possible to consider the values thus obtained as effectively converged. Note, in addition that while the B3LYP value exhibits a 23% error with respect to experiment, the M06-2X one displays a much smaller error of 7% only, surprisingly better than the more computationally demanding EOM-SF-CCSD calculations and also better than CASPT2 with a CAS(8,8) reference. Clearly, the weakness of the DFT methods is that to a priori predict which of the plethora of available functionals is appropriate for the problem of interest is nearly impossible. However, one may safely rely on the time-tested B3LYP and the more modern M06-2X, at least to get a qualitatively correct guidance.

3.2. Influence of the Geometry in the DFT-Based Calculations. Results in the previous subsection clearly show that the calculated triplet−singlet gap largely depends on the exchange−correlation potential. This is not surprising, as it has been recognized long ago for a variety of magnetic systems, mostly dinuclear complexes or magnetic solids as fluorides or cuprates.[18,57,61] Here, the energy difference between the two states is more in the range of optical excitations, but nonetheless, the main features remain practically the same except for a less localized character of the open-shell orbitals in

MBQDM which has significant implications in the wave function description. In the case of dinuclear complexes or magnetic solids, it is customary to explore the different electronic states of interest at the experimental geometry, which is available from experiment,[57] mainly through X-ray diffraction. In the case of organic diradicals the situation is different since the species are short-lived and structural determination becomes extremely difficult.

Theoretical methods provide an alternative approach to structure determination, even for short-lived species, and most DFT-based methods provide reliable structures.[85] However, the fact that the triplet−singlet gap is so sensitive to the exchange−correlation potential raises questions about whether the molecular structure is a crucial point. This is also relevant to explicitly correlated wave function-based methods for which geometry optimization can be extremely time-consuming. In order to disentangle molecular structure from energy evaluation, we have carried out a series of calculations where, in a first step, the geometry of the triplet and singlet (BS) states of MBQDM is obtained with the different DFT methods used in the present work and using a 6-311G** basis set. In a second step, the energy of the two electronic states is evaluated for each one of the structures determined in the first step using each of the exchange−correlation potential and the results for the triplet−singlet gap reported in Table 3 in a matrix form, where rows report Δ_{vert} and Δ_{adia} predicted by a given potential at geometries predicted by a given method and columns report the values predicted by different potentials at a given geometry. Results arising from the range separated LC-ωPBE functional are not included in Table 3 because the predictions, with values in the 6500−7500 cm^{-1} range, are too far from available experimental data.

From Table 3 it is clear that all explored density functionals lead to optimized geometry structures for the triplet and singlet — as represented by a BS solution — which are relatively close. In fact, the vertical, approximate adiabatic (not shown in Table 3) from eq 4 and adiabatic from eq 3 calculated triplet−singlet gap obtained by using the different optimized structures exhibit a quite small variation of at most 3%. This is an important result because it clearly indicates that the variation with the functional, evident in Tables 1 and 3, does not arise from a difference in the predicted optimized geometry of the triplet and BS states but has its origin in the functional itself. Another important consequence is that choosing a density functional optimized geometry to evaluate the energy by a more sophisticated method such as CASSCF, CASPT2, MRCI, or DDCI can, in principle, be a well justified strategy.

Regarding the point above, it is important to advert that the inherent spin contamination of BS solution may also introduce artifacts in the corresponding optimized geometry. This has

been recently discussed by Malrieu and Trinquier[86] and by Saito and Thiel[87] proposing also different procedures to overcome this problem. The approach of Malrieu and Trinquier[86] consists on an extrapolation of the geometry to obtain a better estimate of the minimum energy of the spin decontaminated singlet, whereas Saito and Thiel[87] develop analytical gradients for the solution from spin projection of the BS solution and found that the structure of the approximate singlet thus obtained has some differences with that of the BS solution. The present B3LYP/6-311G** geometry for the BS solution matches the one of Saito and Thiel[87] up to 0.01 Å, as expected. Interestingly, the CASSCF(8,8)/6-31G* and CASSCF(8,8)/aug-cc-pVTZ optimized geometries for the singlet state are almost identical and also match the one predicted by Saito and Thiel[87] using the AGAP correction on top of the B3LYP/6-311G** geometry for the BS solution. Therefore, one can suggest using the CASSCF(8,8) geometry to obtain an estimate of the effect of spin contamination in the geometry of the BS solution. The results in Table 4 clearly

Table 4. Adiabatic Triplet−Singlet (Δ_{adia}) Gap of *m*-Xylylene As Predicted from Different DFT-Based Methods[a]

	Δ_{adia}	
	geom CASSCF	geom B3LYP
B3LYP	4118	4133
M06	4559	4585
M06-2X	3531	3726
HSE	4530	4633

[a]The values have been obtained from calculations using the 6-311++G** basis set and using either the optimized structures obtained at the CASSCF(8,8)/6-31G* (column geom CASSCF) or B3LYP/6-311G** (column geom B3LYP) levels.

indicate that the changes due to the incorrect geometry of the BS solution are quite small for B3LYP, and M06 indicating that with these functionals, the BS approach predicts structures for the open-shell singlet comparable to those predicted by explicitly correlated wave function methods. Interestingly, significant differences are found for M06-2X and HSE. Therefore, this is an effect to be considered in this type of studies. The Δ_{adia} values calculated by the B3LYP and M06-2X functionals using the CASSCF(8,8) geometry for the open-shell singlet get closer to the experimental value. The variation is, however, small meaning that the use of DFT methods to predict the geometry for subsequent post-Hartree−Fock calculations in this type of systems represents a rather reliable

strategy. In the general case, however, one needs to be aware of possible inaccuracies caused by the artifact in the geometry predicted by the BS approach.

3.3. Influence of Active Space in CASCI, CASSCF, DDCI, and MRSDCI Calculations. From results in previous subsections it is clear that it is desirable to validate the functional chosen which can be done either by comparison to experiment or by accurate ab initio wave function-based calculations. In the present subsection we explore the performance of some of the well-known wave function methods such as CASSCF, DDCI, and MR(SD)CI calculations. In particular, we explore the effect of the active space dimension in the CASSCF calculations and the influence of the orbitals chosen to carry out DDCI and MRSDCI calculations.

Table 5 summarizes results for Δ_{vert} obtained with the several wave function-based methods using different sets of optimized orbitals obtained by means of CASSCF(n,n)/6-31G** ($n = 2$, 4, 6, 8) where $n = 2$ corresponds to the minimal active space and $n = 8$ to the full π valence. These calculations are carried out at the geometry obtained at the CASSCF(8,8)/6-31G* level. Similar results are obtained when using the geometry predicted by CASSCF(8,8)/6-311++G** indicating that the problems described below cannot be attributed to structural effects. In the light of the work by Suaud et al.[28] on the effect of the orbitals we have computed Δ_{vert} with the DDCI2, a variant of DDCI including all single excitation but only double excitations out of the CAS with two degrees of freedom (1h−1p, 2h, or 2p), the full DDCI, and MRSDCI with different sets of orbitals. Thus, the DDCI2, DDCI, and MRSDCI calculations use a complete active space configuration interaction (CASCI) with two electrons in two orbitals—hereafter referred to as CASCI(2,2)—as reference space for the subsequent CI-type calculations but with the natural orbitals obtained from CASSCF calculations using active spaces of increasing size. Moreover, the DDCI2, DDCI, and MRSDCI calculations are repeated using the orbitals corresponding to CASSCF calculations for the triplet, the singlet, or of state-specific type. Here, a caveat is necessary: strictly speaking, the DDCI calculations are fully justified when the same set of orbitals is used for the two states of interest, even though computational experience shows that the effect of the orbitals is most often not so crucial. In the forthcoming discussion we will show that this is not the case for MBDQM.

The first row of Table 5 reports the results of CASCI(n,n) calculations and different sets of orbitals. Note that, except in the case of state-specific results in the rightmost column, this is different from CASSCF since the orbitals of the triplet or of the

Table 5. Vertical Triplet−Singlet (Δ_{vert}) Gap of *m*-Xylylene As Predicted from Different Wave Function-Based Methods Using Orbitals Obtained From CASSCF/6-31G Calculations[a]**

	orbital set used											
	CASSCF for $^3B_2$				CASSCF for $^1A_1$				state-specific CASSCF			
Δ_{vert}	(2,2)	(4,4)	(6,6)	(8,8)	(2,2)	(4,4)	(6,6)	(8,8)	(2,2)	(4,4)	(6,6)	(8,8)
CASCI(n,n)	2643	5363	5061	5885	1119	2012	4441	5266	1632	3291	4757	5576
CASCI(2,2)+S	5823	6214	6283	6288	5122	5276	5530	5617	5903	6598	6824	6918
DDCI2	5364	5612	5620	5582	4835	4957	5150	5582	5612	6288	6480	6567
DDCI	3780	4629	5207	5714	3294	3366	3481	3543	5639	7589	8099	8342
MRSDCI	2511	5012	6825	8541	1299	1452	1764	1942	2300	2775	2218	1916

[a]Except for the CASCI(n,n) values, the orbitals correspond to CASSCF calculations of increasing size but taking the CASCI(2,2) as reference for subsequent calculations. The CASCI results of the first row, however, are consistent with the active space used in the CASSCF calculations. All calculations have been carried out using the CASSCF(8,8)/6-31G** geometry of the triplet state. All values are in cm^{-1}.

Table 6. Vertical and Adiabatic Triplet−Singlet (Δ_{vert} and Δ_{adia}) Gap of *m*-Xylylene As Predicted from Different CASSCF and MRMP Methods with the CAS(8,8)^a

cm^{-1}	B3LYP		HSE		M06		CASSCF		$\mu \pm \sigma$	
	Δ_{vert}	Δ_{adia}	Δ_{vert}	Δ_{adia}	Δ_{vert}	Δ_{adia}	Δ_{vert}	Δ_{adia}	Δ_{vert}	Δ_{adia}
CASSCF	5649	4892	5576	4817	5743	4915	5576	4482	5636 ± 69	4776 ± 174
MRMP	4622	4216	4576	4198	4678	4240	4577	4254	4613 ± 42	4227 ± 22

^{a}The values have been obtained from calculations using the 6-31G** basis set and the optimized structure either for triplet or singlet, obtained with the 6-311G** basis set for the DFT-based methods and 6-31G* for CASSCF. The different columns indicate the origin of the geometry and the rows report calculated values at the different structures. Mean values (μ) and standard deviation (σ) are provided in the rightmost columns.

singlet are used to carry out the CASCI for the two states. The CASCI(n,n) results show that the effect of orbitals is dramatic. The triplet−singlet gap obtained from the orbitals of the triplet is very different from the value obtained from the orbitals of the singlet, and both are different from the result predicted from state-specific orbitals. Moreover, for a given choice of orbitals, the CASCI(n,n) results show a tremendous dependence on the choice of the active space, and only the CASCI(8,8) results arising from the orbitals obtained with CASSCF(8,8) show an onset of minimum stability, although the result still exhibits a large (66%) error with respect to experiment. This implies that dynamical electron correlation plays an essential role and also explains the difficulty to reduce the physics to the CAS(2,2) space evidenced in the recent work of Suaud et al.[28]

Electron correlation effects out of the CAS(2,2) reference space can be accounted for by including the single or single and double excitations out of the Slater determinants defining the CAS. This leads to the CASCI(2,2)+S and MR(SD)CI methods, respectively, whereas DDCI2 and DDCI represent suitable approximations to the MR(SD)CI with a smaller CI expansion. The CASCI(2,2)+S and DDCI2 methods (second and third row of Table 5) exhibit some stability with respect to the electronic state chosen to obtain the orbital set and with respect the dimension of the CAS. However, the results thus obtained do not represent any improvement with respect to the CASCI(8,8) results. Clearly, these two methods are not able to include the differential correlation effects.

Results from DDCI are also dependent on whether the orbitals are obtained from the triplet or singlet state. The DDCI calculations from state-specific orbitals lead to the worse results, which is not surprising since, rigorously, the DDCI conditions are only fulfilled when the CI expansions are built from the same orbital set. Interestingly, the DDCI calculations corresponding to the orbitals obtained from the singlet state are stable and do not depend on the size of the CAS used to obtain the orbitals and are very close to experiment. However, the agreement is purely fortuitous since DDCI should be a good approximation to MR(SD)CI which includes all single and double excitations in a variational way and, hence, the 2h−2p missing in the DDCI expansion. However, results in the bottommost row of Table 5 clearly show that the CAS(2,2) description does not provide a good zero-order reference irrespective of whether the orbitals are obtained from CASSCF calculations using a large set or not. One can claim that the failure of MRSDCI calculations is the lack of size consistency which is inherent to any truncated configuration interaction method. Note, however, that while size consistent effects clearly show up when dealing with bond breaking, its effect is almost negligible when dealing with electronic excitations. Therefore, one comes to the conclusion that the minimal CAS reference space is inadequate. This is in agreement with the findings of Suaud et al.[28] showing that that the CAS(2,2) description is

only partly recovered upon use of natural orbitals iteratively obtained from DDCI calculations using the CAS(2,2) as reference space. This procedure is, however, not straightforward, and alternative approaches are desirable. This will be discussed in the next subsection.

3.4. Influence of Geometry in the CASSCF and MRMP Calculations. The discussion above and the results of Suaud et al.[28] about the inadequacy of a CAS(2,2) as reference, unless using iterative natural orbitals, imply that one should rely on a larger active space. The logical choice is the full π valence CAS(8,8) which is too large to be employed as reference in MR(SD)CI and even in DDCI calculations. This leaves one with two choices to include dynamical correlation effects: take into account the effect of single and double excitations out of the CAS by second-order perturbation theory or rely on some selection criterion to build the reference space. Here, we will analyze in detail the first option by using the MRMP method of Hirao[67,67] as implemented in GAMESS[76,77] which is similar to the CASPT2 method employed by Hrovat et al.[23] The last authors reported a quite accurate value, although the limited basis set (6-31G*) and the CASSCF(8,8) were used which seem to leave room for improvement.

The results in subsection 3.2 suggest that using a geometry obtained from a DFT-based method in the MRMP calculations may be a good choice. Table 6 reports the Δ_{vert} and Δ_{adia} values calculated with CASSCF and MRMP using the 6-31G** basis set at the B3LYP, M06, and HSE geometries obtained with the 6-311++G** basis set and also with the CASSCF geometry obtained with the smaller 6-31G*. Except for the case of Δ_{adia} using the CASSCF geometry which can be easily understood from the inability of the CASSCF to describe the geometry of the singlet excited state, the CASSCF and MRMP values appear to be very stable and almost unaffected by the choice of the geometry. This confirms the prediction in subsection 3.2 that the use of the geometry predicted by a reliable DFT-based method is a good alternative. We close this subsection by noting that the MRMP value of roughly 4200 cm^{-1} is in good agreement with the CASPT2 calculations of Hrovat et al.[23] but is still 25% in error with respect to experiment.

3.5. Influence of Basis Set in the CASSCF and MRMP Calculations. It is well recognized that basis set quality is crucial when the property of interest strongly depends on electron correlation effects. To clarify the effect of the basis set in the MRMP calculations two different additional sets of calculations have been carried out. In the first one, the geometry is obtained at the CASSCF/6-31G* and the basis set is increased up to 6-311++G** (Table 7), whereas in the second one the geometry is obtained at the CASSCF level, but at each of the basis sets, explored and correlation consistent basis sets are also included (Table 7).

Analysis of the results in Tables 7 and 8 shows that while the effect of enlarging the basis set is not large, there is a systematic

Table 7. Vertical and Adiabatic Triplet−Singlet (Δ_{vert} and Δ_{adia}) Gap of *m*-Xylylene As Predicted From CASSCF and MRMP with the CAS(8,8) Using Basis Sets of Increasing Size[a]

cm^{-1}	6-31g*		6-31g**		6-311++g**	
	Δ_{vert}	Δ_{adia}	Δ_{vert}	Δ_{adia}	Δ_{vert}	Δ_{adia}
CASSCF	5593	4501	5576	4482	5533	4432
MRMP	4600	4261	4577	4254	4349	4097

[a]In order to separate geometric effects, all values have been computed using the optimized structure as obtained with the CASSCF/6-31G* approach.

improvement of the calculated result. However, even for the largest basis set, the final MRMP value for the adiabatic transition still exhibits a difference of 780 cm^{-1} with respect to experiment with a residual error of 23%, which is not so different from the CASPT2/6-31G* result of Hrovat et al.[23] Thus, the present results seem to indicate that further improvement requires either enlarging the dimension of the CAS or going to higher orders of perturbation theory. Increasing the dimension of the CAS becomes difficult both computationally and conceptually since once all π orbitals have been considered as active, one is left with the full valence CAS which will imply 40 active orbitals and 40 electrons. Going to higher orders of perturbation theory can in principle be achieved by DDCI, but the dimension of the resulting matrix makes this almost impossible. A last possibility consists of selecting some determinants in the CAS as references and carrying out MRSDCI calculations. A series of selected CI calculations have been carried out with the reference determinants chosen on the basis of the extent of their contributions to the CASSCF wave function. This set of calculations employs the 6-31G** basis set and the geometry obtained at the CASSCF/6-311++G** level and includes as reference the determinants in the CAS(8,8)+S wave function with contributions up to 0.03 or 0.09%. The largest reference space thus constructed contains 18 determinants. Unfortunately, the results for the vertical and adiabatic transitions are not stable with respect to the selection threshold which closes this way.

4. GENERAL DISCUSSION

The systematic study presented in the previous sections illustrates how difficult it is to obtain an accurate result for the triplet−singlet gap of MBDQM and also offers some interesting conclusions and computational strategies for similar systems. For instance, the results of DFT-based calculations appear to be quite robust, and the dependence with respect to the basis set quality and to the molecular geometry is quite small. The main problem here is the dependence with respect to the choice of the exchange−correlation functional. In absence of experimental results it is difficult to assess the

accuracy of the different functionals. However, the fact that experimental results are available for MBDQM facilitates this issue. Clearly, the calculated value of 3607 cm^{-1} in Table 2 for the adiabatic transitions predicted by the M06-2X functional within the extended 6-311++G(3df,3pd) basis set are those closest to experiment with an absolute error of 249 cm^{-1}, or 7% error, only. The agreement becomes even more satisfactory if one considers the value obtained using the CASSCF(8,8)/aug-cc-pVTZ geometry for the triplet and singlet state. These calculations can be regarded as a way to estimate the spin contamination in the geometry on the BS solution,[86,87] as indicated above. The M06-2X calculated value using these geometries is of 3531 cm^{-1} (Table 4) which implies an absolute error of 173 cm^{-1} or 5%. Let us now consider the B3LYP functional which most often represents the default choice. Interestingly, the absolute error of B3LYP for the Δ_{adia} transition in Table 2 is of 769 cm^{-1}, predicted from the corresponding optimized triplet and BS solutions, is only slightly smaller than the one predicted by MRMP out of a CASSCF(8,8) wave function and with a rather extended basis set. This is a clear indication that singlet−triplet gaps predicted by DFT-based calculations within the BS approach are reliable, although the choice of the exchange−correlation functional remains a big issue. Note, in passing by, that the Δ_{apadia} values always deviate more from experiment which is not surprising given the approximations involved.

One can claim that more advanced functionals of the Minnesota can provide values numerically closer to the experimental value. To explore this possibility, an additional set of calculations has been carried out with the recently proposed range-separated hybrid nonseparable meta-GGA MN12-SX functional of Peverati and Truhlar.[88] The vertical and adiabatic triplet−singlet gaps predicted with this functional using the 6-311++G** basis set, and the corresponding optimized geometries are 3985 and 3620 cm^{-1} which are close to the equivalently obtained M06-2X values (4142 and 3615 cm^{-1}), indicating that M06-2X and MN12-SX provide a similar description.

In order to further analyze the predictions from M06-2X and B3LYP, we computed the electron affinity of MBDQM which is also available from the NIPES experiments of Wenthold et al.[22] Using the largest 6-311++G(3df,3pd) basis set, the M06-2X and B3LYP calculations have been carried out for the vertical and adiabatic electron affinity using the optimized geometries of the neutral diradical (triplet) and anion (doublet). In a subsequent step, thermal corrections to energy and enthalpy at the temperature at which experiments have been carried out have been accounted for using the thermochemistry features implemented in Gaussian09. The calculated results, summarized in Table 9, reveal that both B3LYP and M06-2X predict values which are in very good agreement with experiment. The adiabatic values with zero-point corrections being considerably accurate (0.922 and 0.927 for B3LYP and M06-2X,

Table 8. Vertical and Adiabatic Triplet−Singlet (Δ_{vert} and Δ_{adia}) Gap of *m*-Xylylene As Predicted From CASSCF and MRMP with the CAS(8,8) Using Basis Sets of Increasing Size and the Corresponding CASSCF Geometry Optimized with Each Basis Set

cm^{-1}	6-31g*		6-311++g**		aug-cc-pVDZ		aug-cc-pVTZ	
	Δ_{vert}	Δ_{adia}	Δ_{vert}	Δ_{adia}	Δ_{vert}	Δ_{adia}	Δ_{vert}	Δ_{adia}
CASSCF	5593	4501	5531	4433	5535	4455	5585	4473
MRMP	4600	4261	4349	4110	4283	4102	4279	4138

Table 9. Calculated Vertical (EA$_{vert}$), Adiabatic (EA$_{adia}$), and Adiabatic Plus Zero-Point Corrections (EA$_{adia+Z}$) Electron Affinity of *m*-Xylylene As Predicted from B3LYP and M06-2X DFT-Based Methods Using the 6-311++G(3df,3pd) Basis Set

eV	EA$_{ver}$	EA$_{adia}$	EA$_{adia+Z}$
B3LYP	0.843	0.784	0.922
M06-2X	0.875	0.800	0.927
experiment[22]		0.919 ± 0.008	

respectively) with a <1% error with respect to the 0.919 ± 0.008 eV experimental value;[22] which is a remarkable achievement for the calculation of such an elusive property. Therefore, one could conclude that the prediction of triplet–singlet gaps in this type of systems is reasonably well described, at least from the numerical point of view, by hybrid functionals.

The results of the present systematic study concerning the use of explicitly correlated wave function methods are somewhat disappointing, evidencing the difficulty to obtain values which reduce the 22% error with respect to experiment corresponding to the CASPT2 published by Hrovat et al.[23] more than 15 years ago. Nevertheless, a number of important conclusions emerged. First, this is an example where the minimal CAS(2,2) description is hardly correct, needing to rely on iterative natural orbitals from a DDCI calculation out of the CASSCF(2,2) function as shown by Suaud et al.[28] In the present work we attempted to recover the minimal physically grounded CAS(2,2) by relying instead on the orbitals from larger active spaces. Unfortunately, the CASSCF(8,8) calculations lead to orbitals for the triplet and singlet which are very different. This has the consequence that DDCI calculations also fail and even MR(SD)CI out of a CAS(2,2) built from the orbitals of CASSCF(8,8) fail to produce reasonable results. Therefore, one has to rely either on costly and tedious iteratively obtained natural orbitals or on second-order perturbation theory with the CASSCF while using CAS(8,8) as reference. The two approaches lead to similar results, although present results hardly improve over the CASPT2 description of Hrovat et al.[23] though the MRMP scheme is perhaps more adequate and larger basis sets are used.

From the positive point of view, MRMP calculations carried out at different geometries, including those obtained with several density functionals, are quite stable indicating that this is indeed a good option. The effect of the basis set is not unexpectedly larger, but even with quite large basis sets including those of correlation consistent type, the calculated triplet–singlet gap of MBDQM is still large, at about 22% (4097 cm^{-1} with 6-311++G** basis set). The difficulty of the wave function-based methods in describing the triplet–singlet gap arises quite unequivocally from dynamical correlation effects which cannot be recovered unless an even larger CAS is used, but this becomes computationally prohibitive. This is confirmed by the results obtained for the electron affinity of MBDQM. The adiabatic value predicted by CASSCF calculations with CAS(8,8) and CAS(9,8) for the triplet state of the neutral molecule and doublet state of the anion at the corresponding CASSSCF geometry optimized with the 6-311++G** basis set is qualitatively incorrect. Including dynamical correlation through MRMP recovers the correct sign but the calculated value of 0.132 only represents a too poor approximation to the experimental value of 0.919 ± 0.008 eV[22] and also far from the B3LYP and M06-2X corresponding

values in Table 9. Clearly, the CAS(8,8)/CAS(9,8) description is insufficient, and the basis set is also too limited to account for the differential electronic dynamical correlation.

5. CONCLUSIONS

The triplet–singlet gap of MBDQM has been computed by a variety of density functional and wave function-based methods in an attempt to provide a guide in the study of similarly large systems for which the wave function methods become unmanageable. The effect of the basis set and geometry has been separately explored, and a number of conclusions have been reached. These are given below.

(1) Beyond a certain reasonable quality, the triplet–singlet gap of MBDQM predicted by different density functionals does not depend too much on the basis set. Moreover, the geometries predicted by the different functionals are fairly consistent, which means that to investigate the effect of the functional one can use the geometry for the triplet and singlet predicted by any of these functionals.

(2) The triplet–singlet energy gap of MBDQM predicted by different density functionals strongly depends on the choice of the functional to the point that results from the range-separated LC-ωPBE method become unacceptable, probably indicating that the standard parameters for range separation are not at all appropriate for this type of highly conjugated systems. The M06-2X meta-GGA functional provides the best comparison to experiment, and the performance of B3LYP is also good. This good numerical behavior is confirmed by the calculation of the electron affinity which, for both functionals, is in very good agreement with experiment. Nevertheless, the dependence on the functional cannot be ignored.

(3) The use of the BS optimized geometry to compute the adiabatic singlet–triplet gap does not represent a serious problem, although improved agreement with experiment can be obtained by using a more accurate geometry.

(4) The physically meaningful CAS(2,2) description of the triplet–singlet gap of MBDQM cannot be recovered by simply expanding the CAS to the full π valence. In addition, DDCI and MRSDCI values obtained using a CAS(2,2) as reference, but the orbitals from larger CASSCF up to CAS(8,8) are found to lie in a too broad range to validate this strategy.

(5) MRPT calculations out of the CASSCF(8,8) provide a semiquantitative prediction of the triplet–singlet gap of MBDQM especially when using the larger basis sets but give only a modest improvement over the previous CASPT2 values. This happens in spite of the fact that the uncontracted nature of the MRMP scheme facilitates a rescaling of the contribution of CAS determinants in the first order perturbed wave function.

(6) MRPT calculations using the geometry that has been optimized by a given hybrid or meta-GGA functional provide similar values of the triplet–singlet gap of MBDQM, thereby suggesting that this would be a considerably useful strategy.

(7) Finally, the fact that MRCI and MRMP systematically overestimate the triplet–singlet gap may indicate that basis set and reference space requirements are not fulfilled or, alternatively, that the experimental value is slightly affected by the experimental conditions. Note

that the NIPES experiment is carried out in a helium environment at 175−185 K[22] and some energy-transfer mechanism is needed to explain the non-Franck−Condon character of the NIPES spectrum of MBDQM .

The problems encountered here for the wave function description of MBDQM are reminiscent of the previous work by Nachtigall and Jordan[14−16] as well as by Cramer and Smith[17] on tetramethyleneethane and trimethylenemethane, respectively, even if the former represents a different case since it involves a disjoint diradical where two allyl radical moieties are connected through their nodal atoms. These authors concluded that an accurate many-body treatment of a diradical becomes tricky, with somewhat erratic behavior noticed from one methodology to another and sometimes with basis size. The theoretical level of methodology can be raised but with a huge concomitant increase in computing efforts. The present work on a nontrivial diradical provides a convenient and useful guide for what is to be expected from a systematic many-body study of magnetic interactions in largely conjugated organic radicals that may have at least one aromatic ring. Finally, one must warn that previous results of Valero et al.[89] on α-4-dehydrotoluene and biverdazyl radicals suggest that the performance of a given functional, hybrid, or meta GGA, with respect to the triplet−singlet gap is also system dependent and comparison to experiment or to similar systems becomes unavoidable before choosing a given method.

■ ASSOCIATED CONTENT

Ⓢ Supporting Information

Tables S1−S9 of optimized coordinatess, energies, computed S2 expectation values, and calculated S−T energy gaps from both UDFT and WF-based methods. More on UDFT: Optimization − Log file 1−4; Single-point calculation − Log file 5−8; Optimization for doublet − Log file 9−12; Calculation of single point triplet and BS of diradical by taking optimized anion doublet − Log file 13−16; Frequency calculations diradical and electron affinity from Log file 17−20. This material is available free of charge via the Internet at http://pubs.acs.org.

■ AUTHOR INFORMATION

Corresponding Author
*E-mail: francesc.illas@ub.edu.

Notes
The authors declare no competing financial interest.

■ ACKNOWLEDGMENTS

■ REFERENCES

(1) Platz, M. S.; *Diradicals*; Borden, W. T., Ed.; Wiley-Interscience: New York, 1982; pp 1−343.
(2) Dougherty, D. A. *Kinetics and Spectroscopy of Carbenes and Biradicals*; Platz, M. S., Ed.; Plenum: New York, 1990; p 117.
(3) Lewis, G. N.; Lipkin, D. *J. Am. Chem. Soc.* **1942**, *64*, 2801.
(4) Porter, G. *Proc. R. Soc. London* **1950**, *A200*, 284.
(5) Biewer, M. C.; Biehn, C. R; Platz, M. S.; Despres, A.; Migirdicyan, E. *J. Am. Chem. Soc.* **1991**, *113*, 616.
(6) Wenthold, P. C.; Lineberger, W. C. *Acc. Chem. Res.* **1999**, *32*, 597.
(7) Rajca, A. *Chem. Rev.* **1994**, *94*, 871.
(8) Iwamura, H.; Koga, N. *Acc. Chem. Res.* **1993**, *26*, 346.
(9) Borden, W. T.; Davidson, E. R. *J. Am. Chem. Soc.* **1977**, *99*, 4587.
(10) Ovchinnikov, A. A. *Theor. Chim. Acta* **1978**, *47*, 297.
(11) Lieb, E. H. *Phys. Rev. Lett.* **1989**, *62*, 201.
(12) Trindle, C.; Datta, S. N. *Int. J. Quantum Chem.* **1996**, *57*, 781.
(13) Trindle, C.; Datta, S. N.; Mallik, B. *J. Am. Chem. Soc.* **1997**, *119*, 12947.
(14) Nachtigall, P.; Jordan, K. D. *J. Am. Chem. Soc.* **1992**, *114*, 4143.
(15) Nachtigall, P.; Dowd, P.; Jordan, K. D. *J. Am. Chem. Soc.* **1992**, *114*, 4741.
(16) Nachtigall, P.; Jordan, K. D. *J. Am. Chem. Soc.* **1993**, *115*, 270.
(17) Cramer, C. J.; Smith, B. A. *J. Phys. Chem.* **1996**, *100*, 9664.
(18) Moreira, I.; de, P. R.; Illas, F. *Phys. Chem. Chem. Phys.* **2006**, *8*, 1645.
(19) Neese, F. *Coord. Chem. Rev.* **2009**, *253*, 526.
(20) Bencini, A.; Totti, F. *J. Chem. Theory Comput.* **2009**, *5*, 144.
(21) Wright, B. B.; Platz, M. S. *J. Am. Chem. Soc.* **1983**, *105*, 628.
(22) Wenthold, P. G.; Kim, J. B.; Lineberger, W. C. *J. Am. Chem. Soc.* **1997**, *119*, 1354.
(23) Hrovat, D. A.; Murcko, M. A.; Lahti, P. M.; Borden, W. T. *J. Chem. Soc., Perkin Trans. 2* **1998**, *5*, 1037.
(24) Lineberger, W. C.; Borden, W. T. *Phys. Chem. Chem. Phys.* **2011**, *13*, 11792.
(25) Fort, R. C., Jr; Getty, S. J.; Hrovat, D. A.; Lahti, P. M.; Borden, W. T. *J. Am. Chem. Soc.* **1992**, *114*, 7549.
(26) Wang, T.; Krylov, A. I. *J. Chem. Phys.* **2005**, *123*, 104304.
(27) de Graaf, C.; Sousa, C.; Moreira, I.; de, P. R.; Illas, F. *J. Phys. Chem. A* **2001**, *105*, 11371.
(28) Suaud, N.; Ruamps, R.; Guihéry, N.; Malrieu, J. P. *J. Chem. Theory Comput.* **2012**, *8*, 4127.
(29) Datta, S. N.; Jha, P. P.; Ali, E. M. *J. Phys. Chem. A* **2004**, *108*, 4087.
(30) Ali, E. M.; Datta, S. N. *J. Phys. Chem. A* **2006**, *110*, 2776.
(31) Ali, E. M.; Datta, S. N. *J. Phys. Chem. A* **2006**, *110*, 13232.
(32) Latif, I. A.; Hansda, S.; Datta, S. N. *J. Phys. Chem. A* **2012**, *116*, 8599.
(33) Pal, A. K.; Hansda, S.; Datta, S. N.; Illas, F. *J. Phys. Chem. A* **2013**, *117*, 1773.
(34) Datta, S. N.; Pal, A. K.; Hansda, S.; Latif, I. A. *J. Phys. Chem. A* **2012**, *116*, 3304.
(35) Mitani, M.; Mori, H.; Takano, Y.; Yamaki, D.; Yoshioka, Y.; Yamaguchi, K. *J. Chem. Phys.* **2000**, *113*, 4035.
(36) Mitani, M.; Yamaki, D.; Takano, Y.; Kitagawa, Y.; Yoshioka, Y.; Yamaguchi, K. *J. Chem. Phys.* **2000**, *113*, 10486.
(37) Mitani, M.; Takano, Y.; Yoshioka, Y.; Yamaguchi, K. *J. Chem. Phys.* **1999**, *111*, 1309.
(38) Ditchfie, R.; Hehre, W. J.; Pople, J. A. *J. Chem. Phys.* **1971**, *54*, 724.
(39) Hehre, W. J.; Ditchfie, R.; Pople, J. A. *J. Chem. Phys.* **1972**, *56*, 2257.
(40) Dunning, T. H., Jr. *J. Chem. Phys.* **1989**, *90*, 1007.
(41) Hariharan, P. C.; Pople, J. A. *Theor. Chim. Acta* **1973**, *28*, 213.
(42) Clark, T.; Chandrasekhar, J.; Spitznagel, G. W.; Schleyer, P. V. R. *J. Comput. Chem.* **1983**, *4*, 294.
(43) Frisch, M. J.; Pople, J. A.; Binkley, J. S. *J. Chem. Phys.* **1984**, *80*, 3265.
(44) Kendall, R. A.; Dunning, T. H., Jr.; Harrison, R. J. *J. Chem. Phys.* **1992**, *96*, 6796.

(45) Becke, A. D. *J. Chem. Phys.* **1993**, *98*, 5648.

(46) Zhao, Y.; Truhlar, D. G. *J. Chem. Phys.* **2006**, *125*, 194101.

(47) Zhao, Y.; Truhlar, D. G. *J. Phys. Chem. A* **2006**, *110*, 13126.

(48) Zhao, Y.; Truhlar, D. G. *Theor. Chem. Acc.* **2008**, *120*, 215.

(49) Heyd, J.; Scuseria, G. E.; Ernzernhof, M. *J. Chem. Phys.* **2003**, *518*, 8207; *ibid* **2006**, *124*, 219906(E).

(50) Vydrov, O. A.; Scuseria, G. E. *J. Chem. Phys.* **2006**, *125*, 234109.

(51) Illas, F.; Moreira, I.; de, P. R.; Bofill, J. M.; Filatov, M. *Phys. Rev. B* **2004**, *70*, 132414.

(52) Illas, F.; Moreira, I.; de, P. R.; Bofill, J. M.; Filatov, M. *Theor. Chem. Acc.* **2006**, *115*, 587.

(53) Filatov, M.; Shaik, S. *Chem. Phys. Lett.* **1998**, *288*, 689.

(54) Filatov, M.; Shaik, S. *Chem. Phys. Lett.* **1999**, *304*, 429.

(55) Slipchenko, L. V.; Krylov, A. I. *J. Chem. Phys.* **2002**, *117*, 4694.

(56) Moreira, I.; de, P. R.; Costa, R.; Filatov, M.; Illas, F. *J. Chem. Theory Comput.* **2007**, *3*, 764.

(57) Valero, R.; Illas, F.; Truhlar, D. G. *J. Chem. Theory Comput.* **2011**, *7*, 3523.

(58) Noodleman, L. *J. Chem. Phys.* **1981**, *74*, 5737.

(59) Noodleman, L.; Davidson, E. R. *J. Chem. Phys.* **1986**, *109*, 131.

(60) Noodleman, L.; Peng, C. Y.; Case, D. A.; Mouesda, J. M. *Coord. Chem. Rev.* **1995**, *144*, 199.

(61) Caballol, R.; Castell, O.; Illas, F.; Malrieu, J. P.; Moreira, I.; de, P. R. *J. Phys. Chem. A* **1997**, *101*, 7860.

(62) Yamaguchi, K.; Takahara, Y.; Fueno, T.; Nasu, K. *Jpn. J. Appl. Phys.* **1987**, *26*, L1362.

(63) Yamaguchi, K.; Jensen, F.; Dorigo, A.; Houk, K. N. *Chem. Phys. Lett.* **1988**, *149*, 537.

(64) Yamaguchi, K.; Takahara, Y.; Fueno, T.; Houk, K. N. *Theor. Chim. Acta* **1988**, *73*, 337.

(65) Hirao, K. *Int. J. Quantum Chem.* **1992**, *S26*, 517.

(66) Hirao, K. *Chem. Phys. Lett.* **1992**, *190*, 374.

(67) Hirao, K. *Chem. Phys. Lett.* **1992**, *196*, 397.

(68) Hirao, K. *Chem. Phys. Lett.* **1993**, *201*, 59.

(69) Miralles, J.; Castell, O.; Caballol, R.; Malrieu, J. P. *Chem. Phys.* **1993**, *172*, 33.

(70) Malrieu, J. P. *J. Chem. Phys.* **1967**, *47* (11), 4555.

(71) Foresman, J. B.; Head-Gordon, M.; Pople, J. A.; Frisch, M. J. *J. Phys. Chem.* **1992**, *96*, 135.

(72) Harrison, J. F. *Chem. Rev.* **2000**, *100*, 679.

(73) Helgaker, T.; Coriani, S.; Jorgensen, P.; Kristensen, K.; Olsen, J.; Ruud, K. *Chem. Rev.* **2012**, *112*, 543.

(74) Malrieu, J. P.; Caballol, R.; Calzado, C. J.; de Graaf, C.; Guihéry, N. *Chem. Rev.* in press, DOI: 10.1021/cr300500z.

(75) Frisch, M. J.; Trucks, G. W.; Schlegel, H. B.; Scuseria, G. E.; Robb, M. A.; Cheeseman, J. R.; Scalmani, G.; Barone, V.; Mennucci, B.; Petersson, G. A.; Nakatsuji, H.; Caricato, M.; Li, X.; Hratchian, H. P.; Izmaylov, A. F.; Bloino, J.; Zheng, G.; Sonnenberg, J. L.; Hada, M.; Ehara, M.; Toyota, K.; Fukuda, R.; Hasegawa, J.; Ishida, M.; Nakajima, T.; Honda, Y.; Kitao, O.; Nakai, H.; Vreven, T.; Montgomery, J. A., Jr.; Peralta, J. E.; Ogliaro, F.; Bearpark, M.; Heyd, J. J.; Brothers, E.; Kudin, K. N.; Staroverov, V. N.; Kobayashi, R.; Normand, J.; Raghavachari, K.; Rendell, A.; Burant, J. C.; Iyengar, S. S.; Tomasi, J.; Cossi, M.; Rega, N.; Millam, N. J.; Klene, M.; Knox, J. E.; Cross, J. B.; Bakken, V.; Adamo, C.; Jaramillo, J.; Gomperts, R.; Stratmann, R. E.; Yazyev, O.; Austin, A. J.; Cammi, R.; Pomelli, C.; Ochterski, J. W.; Martin, R. L.; Morokuma, K.; Zakrzewski, V. G.; Voth, G. A.; Salvador, P.; Dannenberg, J. J.; Dapprich, S.; Daniels, A. D.; Farkas, Ö.; Foresman, J. B.; Ortiz, J. V.; Cioslowski, J.; Fox, D. J. *Gaussian 09*, revision A.1; Gaussian, Inc.: Wallingford, CT, 2009.

(76) Schmidt, M. W.; Baldridge, K. K.; Boatz, J. A.; Elbert, S. T.; Gordon, M. S.; J. Jensen, H. S.; Koseki, N.; Matsunaga, K.; Nguyen, A.; Su, S.; Windus, T. L.; Dupuis, M. J.; Montgomery, A. *J. Comput. Chem.* **1993**, *14*, 1347.

(77) Gordon, M. S.; Schmidt, M. W. 1167−1189, In *Theory and Applications of Computational Chemistry: the first forty years*; Dykstra, C. E., Frenking, G., Kim, K. S., Scuseria, G. E., Eds.; Elsevier: Amsterdam, 2005.

(78) Ben Amor, N.; Maynau, D. *Chem. Phys. Lett.* **1998**, *286*, 211; CASDI program: Package developed at the Laboratoire de Chimie et Physique Quantiques, Université Paul Sabatier, Toulouse (France).

(79) Aquilante, F.; de Vico, L.; Ferré, N.; Ghigo, G.; Malmqvist, P.-A.; Pedersen, T.; Pitonak, M.; Reiher, M.; Roos, B. O.; Serrano-Andrés, L.; Urban, M.; Veryazov, V.; Lindh, R. *J. Comput. Chem.* **2010**, *31*, 2240.

(80) Andersson, K.; Malmqvist, P.-Å.; Roos, B. O.; Sadlej, A. J.; Wolinski, K. *J. Phys. Chem.* **1990**, *94*, 5483.

(81) Andersson, K.; Malmqvist, P.-Å.; Roos, B. O. *J. Chem. Phys.* **1992**, *96*, 1218.

(82) Angeli, C.; Cimiraglia, R.; Evangelisti, S.; Leininger, T.; Malrieu, J. P. *J. Chem. Phys.* **2001**, *114*, 10252.

(83) Rivero, P.; Moreira, I.; de, P. R.; Illas, F.; Scuseria, G. E. *J. Chem. Phys.* **2008**, *129*, 184110.

(84) Rivero, P.; Moreira, I.; de, P. R.; Scuseria, G. E.; Illas, F. *Phys. Rev. B* **2009**, *79*, 245129.

(85) Johnson, B. G.; Gill, P. M. W.; Pople, J. A. *J. Chem. Phys.* **1993**, *98*, 5612.

(86) Malrieu, J. P.; Trinquier, G. *J. Phys. Chem. A* **2012**, *116*, 8226.

(87) Saito, T.; Thiel, W. *J. Phys. Chem. A* **2012**, *116*, 10824.

(88) Peverati, R.; Truhlar, D. G. *Phys. Chem. Chem. Phys.* **2012**, *14*, 16187.

(89) Valero, R.; Costa, R.; Moreira, I.; de, P. R.; Truhlar, D. G.; Illas, F. *J. Chem. Phys.* **2008**, *128*, 114103.

Before closing the discussion devoted to *m*-xylylene diradical, it is worth commenting a result that appeared after the publication of the work.

In the text it is stated that a possible reason for the constant overestimation of the calculated triplet-singlet gap with respect to the measured one, might be matrix effects. This means that part of the energy of the photo-detached electron would be lost by interaction with the medium through which it propagates, till being measured. However, the appearance of a similar experimental work (*J. Am. Chem. Soc.*, **2015**, *137* (28), 9094–9099) on a related molecule, the 1,2,4,5-tetramethylenebenzene (TMB), might provide an alternative explanation. In this work they report an excellent agreement for the triplet-singlet gap between experiment ($\Delta E_{TS} = -3.5$ Kcal/mol) and theory ($\Delta E_{TS} = -3.6$ Kcal/mol). The experimental technique is the same as the one for the *m*-xylylene diradical, i.e., NIPES. Similarly, the level of theory that they use is full π-valence CASPT2, also employed in the *m*-xylylene case but with an error of 22%. In looking for differences between the two molecules that might account for the differential agreement between theory and experiment, one realises that in TMB the two unpaired electron are located inside the six-membered ring, whereas in the *m*-xylylene they are in the pending methyl groups. Thermally activated vibrational modes might result in rotation of the two methyl groups with respect to the π-conjugated phenyl ring, decreasing the triplet-singlet gap in *m*-xylylene, as depicted in Figure 4.3.1.
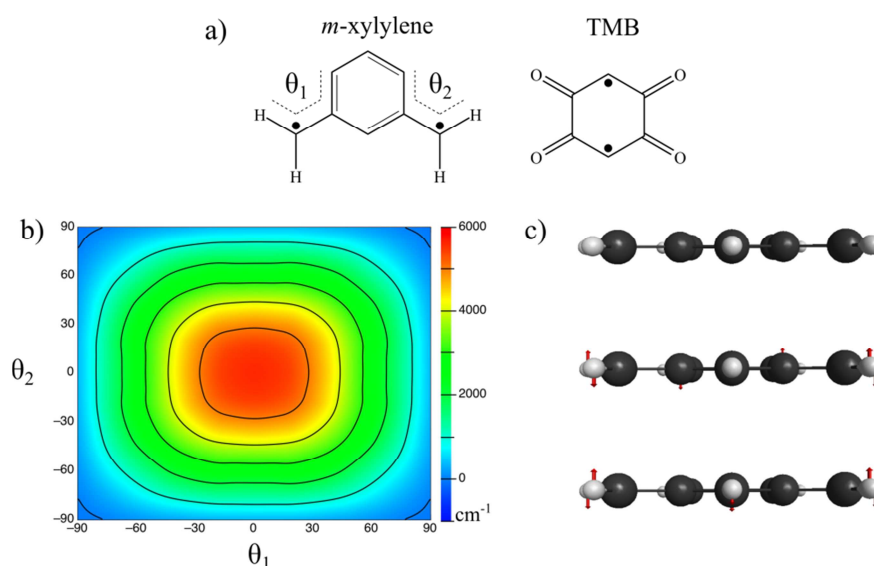

Figure 4.3.1. a) comparison of *m*-xylylene and TMB molecular structures. b) CAS(8,8)SCF triplet-singlet gap values (cm^{-1}) in the restricted optimization map for the m-xylylene. c) Planar view of m-xylylene and depiction of two low frequency (544 and 566 cm^{-1}) normal vibrational modes involved in the torsion of the methyl groups. The frequencies are calculated in the minimum found for the CAS(8,8)SCF triplet.

4.3.2.   Paper #4.2.

Theoretical and Computational Investigation of Meta-Phenylene as Ferromagnetic Coupler in Nitronyl Nitroxide Diradicals

REGULAR ARTICLE

Theoretical and computational investigation of *meta*-phenylene as ferromagnetic coupler in nitronyl nitroxide diradicals

**Arun K. Pal · Daniel Reta Mañeru ·
Iqbal A. Latif · Ibério de P. R. Moreira ·
Francesc Illas · Sambhu N. Datta**

Abstract We predict the magnetic exchange coupling constant (J) for 27 *m*-phenylene-based nitronyl nitroxide (NN) diradicals with nine different substituents in three unique (common *ortho*, *ortho*–*meta* and common *meta*) positions on the coupler unit by using the broken-symmetry density functional methodology. For all investigated diradicals, J values are computed using B3LYP, B3LYP-D3 and M06-2X functionals with 6–311+G(d,p) basis set. The J_{M06-2X} value is larger than J_{B3LYP} and closer to the observed value for the unsubstituted species. Substitutions at common *ortho* position always produce a greater angle of twist between the spin source and the coupler units. When the twist angle is very large, the nature of intramolecular magnetic interaction changes from ferromagnetic to antiferromagnetic. In these cases, the coupler–NN bond order becomes small. Substitution at the common *meta* position of *m*-phenylene in the diradical has little steric and hydrogen-bonding effects. Electron-withdrawing groups reveal a specific trend for single-atom substitution. An *ortho* substitution generally decreases J and a *meta* substitution always increases J with a decreasing $-I$ effect. Variation of J with planarity as well as Hammett constant is investigated. The nucleus-independent chemical shift value is found to decrease from the corresponding mono-substituted phenyl derivatives. The dependence of J on these factors is explored.

Keywords Diradical · Magnetic coupling constant · DFT · Dihedral angle · Inductive effect · NICS(1)

A. K. Pal · I. A. Latif · S. N. Datta (✉)
Department of Chemistry, Indian Institute of Technology
Bombay, Powai, Mumbai 400076, India
e-mail: sndatta@chem.iitb.ac.in

D. R. Mañeru · I. P. R. Moreira · F. Illas
Departament de Química Física and Institut de Química Teòrica I
Computacional (IQTCUB), Universitat de Barcelona,
C/Martí i Franqués 1, 08028 Barcelona, Spain

1 Introduction

Stable diradicals play an important role in research on magnetic materials of organic origin [1–3]. The intramolecular as well as the intermolecular magnetic interactions control the magnetic properties of materials [4]. The intramolecular magnetic interaction depends on the nature of the radical centers and the coupler [5–7], whereas the intermolecular interaction depends on the ground-state spin of individual molecules and the crystal structure of molecular solids [8].

In an oversimplified model, the intramolecular magnetic property of a diradical arises from the spin–spin interaction of the two unpaired electrons in two different orbitals through a (π-conjugated) spacer [6]. In case the two orbitals are near degenerate, the initial zeroth-order degeneracy of singlet–triplet total energy is lifted by electron–electron repulsion, and in case of a significant overlap between the singly occupied orbitals, the singlet lies below the triplet. This is known as the Heitler–London spin exchange between the spins of opposite sign [9]. Contrary to this, interaction between electrons in orthogonal nonbonding orbitals results in a triplet ground state. The nature of the magnetic exchange interaction, antiferromagnetic and ferromagnetic, can be predicted from the symmetry of the π-electron topology [10], starred/and non-starred rule [11], spin polarization scheme [12] and, more specifically, from

spin alternation rule in the unrestricted SCF treatment [13, 14].

Thiele and Schlenk diradicals provide the classical examples of antiferromagnetic and ferromagnetic spacers, respectively [6, 15–17]. In the latter case, *m*-phenylene is the coupler unit. In fact, *m*-phenylene as a general ferromagnetic coupler is observed not only for carbon radical centers or carbenes but also for nitrogen-centered radicals such as nitroxyl and nitronyl nitroxide (NN) radicals. The aza analog of *m*-phenylene ferromagnetically couples spin sources even like transition metal ions such as Cu(II) and V(IV) [18–20].

Sometimes *meta*-phenylene acts as an antiferromagnetic coupler. The conformation of the spin source and the delocalization of spin in the substituents become responsible for this transformation. For example, Rassat et al. [21] and Iwamura et al. [22] found that the unpaired electrons of *m*-phenylene bis-(*tert*-butyl nitroxide) on hetero atoms are antiferromagnetically coupled. These authors considered that *tert*-butyl nitroxide group is twisted out of the conjugation with the *m*-phenylene linker. Iwamura et al. [22] confirmed by X-ray crystallography that the angle of twist of phenylene ring to the plane of *tert*-butyl group is 65° for syn and 75° for anti-conformations. Figure 1 shows a schematic representation of a bis-NN diradical coupled through *m*-phenylene. Borden et al. [23] have theoretically investigated the change of *m*-phenylene from a ferromagnetic coupler at a twist angle of about 0° to an antiferromagnetic one at around 90°. The change occurs due to a selective destabilization of the antisymmetric combination of singly occupied orbitals on each of the radical centers by a σ-orbital of the *m*-phenylene moiety. Mitani et al. [24, 25] have theoretically investigated polyradical systems with *m*-phenylene bridge and found high-spin ground state. Zhang et al. [26] have theoretically investigated the effect of substitution on *m*-phenylene-bridged *m*-xylene diradicals. They found that a simultaneous substitution of electron-donating and electron-withdrawing groups at *m*-phenylene and radical centers and vice versa gives rise to a singlet state or a very small S-T gap. In a recent work on *meta*-xylylene [27], we found that the hybrid B3LYP and

M06-2X functionals provide singlet–triplet gaps comparable to experiment. In the present work too, we will come across a few cases where the *meta*-phenylene coupler produces singlet diradicals.

The main objective of the present work is to investigate the magnetic properties of 27 substituted *m*-phenylene-based bis-NN diradicals using unrestricted density functional theory (UDFT) and the same functionals. We consider nine different substituents on the *m*-phenylene ring, namely –COOH (**1**), –F (**2**), –Cl (**3**), –NO$_2$ (**4**), –Br (**5**), –OH (**6**), –NH$_2$ (**7**), –Ph (**8**) and –CH$_3$ (**9**), in order of decreasing inductive (−I) effect (electron-withdrawing power). Each substituent occupies three unique positions, namely (**a**) common *ortho*, (**b**) *ortho–para* and (**c**) common *meta* sites on the ring (see Fig. 2). We aim to study the effect of electron attracting power of the substituents as well as the effect of the location of substituents. The role of the aromaticity of the coupler unit is also investigated. Kamiyama et al. [28] have examined the singlet–triplet energy gap of the carboxyl derivative **1c** and phenol derivative **6c** (both *common meta* variety) by continuous wave electron spin resonance (ESR) spectroscopy and static paramagnetic susceptibility measurements in the solid state. The experimental *J* values of **1c** and **6c** are ≥ -1.7 cm^{-1} and ≈ 8.7 cm^{-1}, respectively, in glassy solutions of methanol. Hase et al. [29] identified the triplet ground state of **6b** (*ortho–para* variety) from the EPR measurements on the isolated molecules in diluted glassy solutions and found the *J* value of 9.0 cm^{-1} from magnetic susceptibility measurements in the solid state. A problem arises in these cases, as there would be extensive hydrogen bonding of the solvent hydroxyl groups not only with the substituent (COOH and OH groups) but also with the NN moieties. In solid, there would be extensive intermolecular hydrogen-bonding interactions. This is likely to have a differential effect on the relative stability of the singlet and triplet states, thereby influencing in the observed coupling constant. The experimental coupling constants would not correctly represent the coupling constants for the isolated species. The synthesis of **5c** has been accomplished by Catala et al. [7]. The unsubstituted diradical, *meta*-phenylene bis(α-nitronyl nitroxide) or *m*-BNN, has a coupling constant of 34.8 cm^{-1} in MeTHF [30]. To our knowledge, the other molecules have not been synthesized so far.

2 Methodology

We adopt the broken-symmetry density functional (BS-DFT) approach proposed by Noodleman et al. [31–33]. The exchange interaction between the two magnetic centers is expressed by Heisenberg spin Hamiltonian
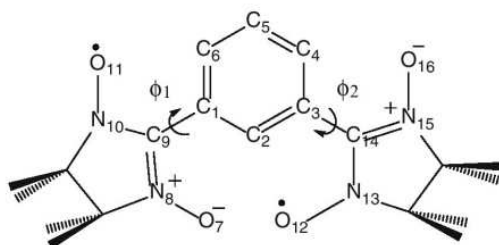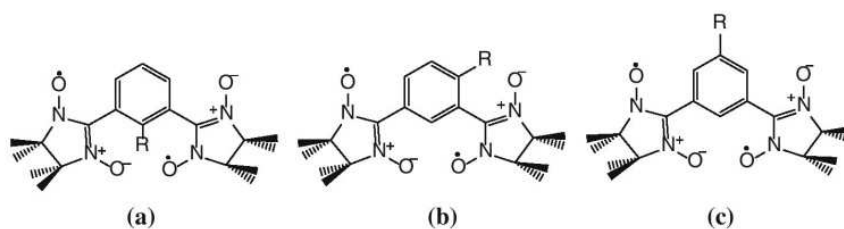

Fig. 1 Schematic representation of *meta*-phenylene bis(α-nitronyl nitroxide) or *m*-BNN

Fig. 2 The series of diradicals under investigation: R is (1) –COOH, (2) –F, (3) –Cl, (4) –NO$_2^-$, (5) –Br, (6) –OH, (7) –NH$_2$, (8) –Ph, (9) –CH$_3$

$$\hat{H} = -2J\hat{S}_1 \cdot \hat{S}_2 \tag{1}$$

where J is the magnetic exchange coupling constant. A negative value of J indicates antiferromagnetic interaction, whereas a positive value indicates the intramolecular interaction to be ferromagnetic. In the spin-projected BS approach due to Ginsberg, Noodleman and Davidson (GND), [34, 35] J can be written as

$$J^{GND} = \frac{E_{BS} - E_T}{S_{max}^2} \tag{2}$$

where E_{BS} is the energy of the broken-symmetry state. For a diradical, $S_{max} = 1$. The spin projection technique is necessary to eliminate the spin contamination in the BS representation of the open-shell singlet. This issue has been discussed elsewhere in detail [36, 37]. In the weak overlap limit, the GND equation produces results that are comparable to the Yamaguchi equation [38, 39]:

$$J^Y = \frac{E_{BS} - E_T}{\langle S_{HS}^2 \rangle - \langle S_{LS}^2 \rangle}. \tag{3}$$

Here, we calculate the magnetic exchange constant using Eq. (3). Since the expectation values of the square spin operator for the high spin and broken symmetry are usually close to 2 and 1, respectively [40], this approach is almost equivalent to that obtained from the general mapping procedure allowing one to deal either with molecular or periodic systems [41].

The molecular geometries of all the 27 species in triplet state are fully optimized at ROHF/6–311G(d,p) level. In general, the ROHF/6–311G(d,p)-optimized geometries turn out to be in good agreement with the crystallographic structures [42]. ROHF with a sufficiently large basis set produces good molecular orbitals, which can be taken as initial guesses for the calculations of BS solutions at the UB3LYP, UB3LYP-D3 and UM06-2X levels using the 6–311+G(d,p) basis set. Also, a large basis set leads to a good triplet geometry. Alternatively, triplet geometry optimization can be done by UDFT methods, though we preferred ROHF for a standard and common starting point for DFT using each functional. For **5** where R = Br, the cc-PVTZ basis set is also used. The Gaussian 03 and Gaussian 09 suites of programs [43, 44] are used in the quantum chemical calculations.

To study the effect of aromaticity of the coupler on the magnetic exchange interaction, the nucleus-independent chemical shift (NICS) is calculated at the B3LYP/6–311+G(d,p) level using the GIAO methodology for all the aromatic rings in each diradical. The NICS values can be calculated at the center of the rings [NICS(0)], but since the σ framework of C–C and C–H affects the π electrons, NICS values are calculated at 1 Å above the ring [NICS(1)] where the π-electron density is generally known to be maximum [45].

Wiberg [46] bond index (order) are calculated by natural bond orbital (NBO) analysis [47, 48] at UB3LYP/6–311+G(d,p) level as implemented in Gaussian 09 [44].

3 Results and discussions

3.1 Coupling constant (J) and $\langle S^2 \rangle$ values

Computed total energy and $\langle S^2 \rangle$ values are given in Tables S1–S3 in the Supporting Information file (page 33–36). The J values calculated with B3LYP, B3LYP-D3 and M06-2X functional for all the species are given in Table 1. The coupling constant is found to follow the order **a** (common *ortho*) < **b** (*ortho–para*) < **c** (common *para*) in every case. An interesting variation of J is found for the species with substitution at the common *ortho* position for both NN fragments (**a** isomers). The calculated J varies from −2.44 to 9.3 cm^{-1}. Negative values are obtained only for **3a** and **8a**. In these cases, the ground state is an open-shell singlet, and the magnetic interaction is antiferromagnetic in nature. The maximum variation of J is found for the *ortho–para* (**b**) species. The calculated J varies from 1.9 to 18.3 cm^{-1}. The *meta* substitution (**c**) always yields a J value in the range of 18.4–24.9 cm^{-1}.

In case of the unsubstituted species, the experimental coupling constant from temperature dependence of EPR signal intensity in MeTHF is ≥34.8 cm^{-1} [30]. Our calculated J with B3LYP and B3LYP-D3 functionals are smaller, about 24 cm^{-1}, whereas M06-2X functional gives a larger value of 32.7 cm^{-1} that is in better agreement with the observed coupling constant. This trend of M06-2X giving a larger coupling constant persists for all substituted diradicals. For any functional, however, the calculated J for

Table 1 Quantum chemically calculated exchange coupling constant (*J*) in cm^{-1} with B3LYP B3LYP-D3 and M06-2X functionals using ROHF/6–311G(d,p)-level triplet-optimized geometry

| Diradicals	6–311+G(d,p) basis set								
	J_{B3LYP}			$J_{\text{B3LYP-D3}}$			J_{M062X}		
Unsubstituted[a]	24.1			24.2			32.7		
Substituted	**a**	**b**	**c**	**a**	**b**	**c**	**a**	**b**	**c**
1	6.90	15.3	23.3[b]	6.71	15.3	23.3[b]	8.37	20.6	32.0[b]
2	9.31	12.9	21.9	9.32	13.0	23.1	12.4	17.8	31.0
3	−2.44	9.33	24.9	−2.44	9.36	25.0	−3.87	12.0	33.3
4	6.13	12.0	22.7	6.14	12.0	22.8	7.59	16.3	31.5
5	2.02	8.34	23.0	2.02	8.37	23.1	2.26	10.6	31.1
6	3.75	18.3[c]	19.9[d]	3.71	18.3[c]	19.9[d]	4.50	27.1[c]	26.3[d]
7	3.92	15.5	19.4	3.95	15.5	19.4	5.35	22.9	25.5
8	−2.74	1.89	18.4	−1.52	1.91	19.6	−2.40	2.04	26.1
9	4.89	11.0	23.6	4.91	11.0	23.6	6.12	14.6	31.7
Using cc-PVTZ									
5	2.19	8.63	23.1	2.24	8.64	23.1	2.52	11.0	31.2

[a] For the unsubstituted *m*-BNN, $J_{\text{obs}} \geq 34.8$ cm^{-1} in MeTHF [30]

[b] For **1c** in glassy solution of methanol, $J_{\text{obs}} \geq -1.7$ cm^{-1} [28]

[c] For **6b** in the solid state, $J_{\text{obs}} = 9.0$ cm^{-1} [29]

[d] For **6c** in glassy solution of methanol, $J_{\text{obs}} \approx 8.7$ cm^{-1} [28]

Fig. 3 **a** *Error bars* for the calculated coupling constant and the extent of spin contamination for the unsubstituted *m*-BNN. **b** Comparison of average dihedral angles, NN–coupler bond length and methyl carbon–nearest ring–carbon distance from X-ray data and ROHF optimization
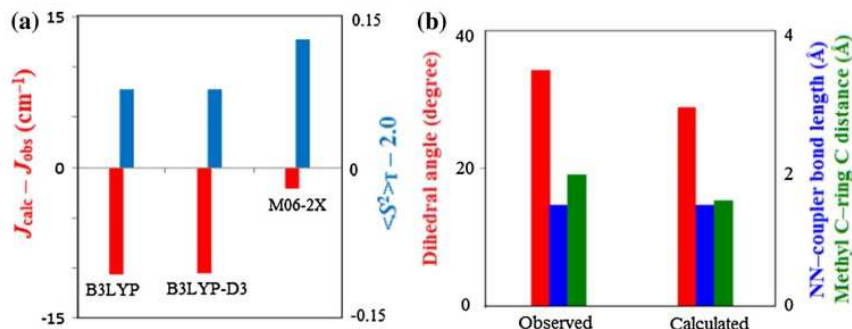
the common *meta* species **c** is comparable to the calculated *J* for the unsubstituted *m*-BNN. As the M06-2X coupling constants for the **c** series are close to the experimental coupling constant of *m*-BNN, we use the M06-2X results for illustration except in common cases.

Figure 3a shows the error bars for the calculated *J* and $<S^2>_{\text{T}}$ of the unsubstituted *m*-BNN compared to the observed values 34.8 cm^{-1} and 2.0 a.u., respectively. Though the spin contamination in triplet is largest for M06-2X, the $\Delta<S^2>$ is approximately equal to 1 and the estimated coupling constant turns out to be nearly correct, in comparison with experiment. In Fig. 3b, we compare the critical features of the observed X-ray crystallographic geometry from Ref. [30] and the ROHF-optimized geometry used here for all functionals. The calculated average dihedral angle is 28.7° compared to the crystallographic 34.1°. The average NN–coupler bond length is 1.470(8) Å (calculated) as against 1.462(4) Å (experimental). In each NN unit, the average methyl carbon–nearest ring–carbon distance is 1.530(4) Å [ROHF/6–311G(d,p)], characteristic of a C–C single bond, whereas the crystallographic distance is

1.905 Å. The reason for the extended bond length in crystal is that the amplitude of motion of each methyl group is really large, as discussed by Shiomi et al. [30]. The error bars for all other geometrical parameters are quite small.

Unfortunately, the coupling constant for **1c** [28], **6b** [29] and **6c** [28] has been determined in glassy solution of methanol and in the solid state. These are found to be quite small, −1.7, 9.0 and 8.7 in cm^{-1}, respectively. The medium provides the scope for extensive hydrogen bonding not only with the NN radical centers but also with the substituents COOH and OH groups in the coupler, and as discussed in Introduction, cannot truly represent the coupling constants for the isolated species. The magnetic measurement on **6b** [29] in the solid state yielded the adiabatic coupling constant that has to be considerably smaller than the vertical one. The estimated M06-2X values for the isolated diradicals are 32.0, 27.1 and 26.3 cm^{-1}, respectively (Table 1).

Kitagawa et al. [49] pointed out that the spin contamination of broken-symmetry solution introduces errors in the optimized geometry and suggested the use of numerical

gradients to correct for the geometry. This aspect has been reinvestigated by Malrieu and Trinquier [50] as well as by Saito and Thiel [51]. Malrieu and Trinquier have suggested an estimation of singlet energy at each configuration and extrapolation of the geometry to obtain the minimum energy of the singlet. Saito and Thiel have derived and implemented analytical gradients for broken-symmetry unrestricted density functional calculations (BS-UDFT) with the removal of spin contamination by Yamaguchi's spin projection method. Geometry optimizations with these analytical gradients (AGAP-opt) yield results consistent with those obtained by Kitagawa et al. These techniques can be adopted to estimate the adiabatic singlet–triplet energy gap, though in this work we calculate only the vertical energy differences.

In all our calculations, the spin contamination in the triplet state is small with $<S^2>_T \sim 2.07$. For the ideal BS state, $<S^2> = 1$, and compared to this value, the spin contamination of the calculated BS states with $<S^2> \sim 1.07$ is also small (~ 0.07). Thus, we retrieve $\Delta <S^2> \approx 1$ that yields, in combination with good relative M06-2X energies, good estimates for the vertical coupling constant (and singlet–triplet energy gap for vertical transition) in **c** species and *m*-BNN.

3.2 Inductive effect

The decreasing trend of $-I$ effect reveals no clear-cut systematic trend for any substituent position. Thus, electron delocalization appears to be the major factor for determining the coupling constant. For the single-atom substituents F, Cl and Br (species **2**, **3** and **5**), however, an approximate pattern emerges for the influence of inductive effect. For the common *ortho* position (**a**), the coupling constant decreases from F to Cl and Br. It becomes very small in the last two cases. However, for Cl, J becomes negative. For the *ortho*–*para* positions (**b**), the coupling constant decreases from F to Cl and from Cl to Br. For *meta* position (**c**), J increases from F to Cl but decreases from Cl to Br. The trends (**b**) and (**c**) can be understood from spin alternation. Any increase in electron density at the common *meta* position, as a result of substitution at *ortho*–*para* position, reinforces the ferromagnetic coupling due to a constructive interference of the spin wave in the coupler with the additional spin that arises from the increase in electron density by $+R$ effect. This effect increases J. An increase in electron density at the *ortho* positions due to a substituent at common *meta* position leads to a destructive interference, and a smaller J value. The trend for (**a**) is similar to that for (**b**), but the excessively small J value can be attributed to the steric effect as discussed in the following. This explanation can fail in the case of a substituent with more than one atom, as the

bond(s) of the substituent might be involved in delocalization, hydrogen bonding, stereo-electronic effect, etc.

3.3 Influence of planarity

The angles of rotation (ϕ_1 and ϕ_2 as in Fig. 1) of NN from the plane of the *m*-phenylene coupler are given in Table 2, which indicates that in general J decreases as ϕ increases. This is because the conjugation between the NN and coupler fragment decreases with the increase in ϕ [22] and is in agreement with our previous work [36, 37]. The larger dihedral angles for **a** and **b** isomers are mainly due to stereo-electronic effects.

The calculated dihedral angles ϕ_1 and ϕ_2 between *m*-phenylene and the two radical centers in the unsubstituted diradical are 26.43° and 26.56° as shown in Table 2. For substituents in the common *meta* position, these vary in a very narrow range, while for substituents in the common *ortho* positions, the dihedral angles become very large and vary widely. The factor of planarity can be defined by $\chi_p = \cos\phi_1\cos\phi_2$. χ_p Will be zero if one of the angles is 90°. But generally, ϕ_1 and ϕ_2 are changed together for maintain the symmetry of the molecule. The species are completely non-planar if $\chi_p = 0$, that is, $\phi_1 = \phi_2 = 90°$. Actually, χ_p becomes zero if one of the angles is 90°, but as it usually happens, both ϕ_1 and ϕ_2 increase simultaneously toward 90°. The molecular frame is planar if $\chi_p = 1$, that is, $\phi_1 = \phi_2 = 0$. This structural feature has limited the width of variation for all calculated coupling constants. In the case of a pronounced deviation from planarity, McConnell's formula [12] indicates an antiferromagnetic coupling, that is, a negative value for the magnetic coupling constant. The strength of the magnetic coupling would be linearly dependent on χ_p that describes the extent of conjugation between the spacer and the two radical centers. Variation of the calculated M06-2X magnetic coupling constant with χ_p is illustrated in Fig. 4a–c. The corresponding B3LYP plots are similar and are shown in the Supporting Information as Figure S1. The figures show linear plots with large positive slopes and small negative intercepts except for the (**c**) series where the slope is extra-large and the intercept is large negative. The (**c**) series differs as the coupling constants are considerably larger. The negative intercept confirms a switch from through-bond spin interaction to McConnell's through-space (spin-dipole–spin-dipole) interaction mechanism [12]. The intercept (that corresponds to $\phi_1 = \phi_2 = 90°$) is relatively large (-27.05 cm^{-1}) for common *meta* substitution that would hardly deflect the two NN rings when the latter are placed perpendicular to the *meta*-phenylene plane. An equal deflection of the two NN moieties leads to a smaller intercept (-3.28 cm^{-1}) for common *ortho* substitution. An unequal deflection spoils McConnell's interaction and

Table 2 Calculated NICS(1), average Wiberg bond index (BO) and the angles of twist (ϕ) for the diradicals in triplet state

Species	NICS(1)		ΔNICS(1)	BO	ϕ_1	ϕ_2
	Diradical[a]	Molecule[b]				
Unsubstituted	−9.43	−10.20	0.77	0.99	26.43	26.56
1a	−9.86		0.29	1.01	44.50	47.09
1b	−9.49	−10.15	0.66	1.03	25.79	43.44
1c	−8.91		1.24	1.04	27.05	29.20
2a	−9.47		0.92	1.02	42.54	52.09
2b	−9.37	−10.39	1.02	1.04	22.44	54.60
2c	−9.44		0.95	1.06	26.04	27.65
3a	−9.58		0.47	1.01	84.05	84.22
3b	−9.23	−10.05	0.82	1.04	25.49	61.04
3c	−9.41		0.64	1.05	25.76	25.76
4a	−9.60		0.70	0.95	50.12	46.72
4b	−9.54	−10.30	0.76	1.06	24.60	48.70
4c	−9.44		0.86	1.05	26.05	28.69
5a	−9.22		0.66	1.01	65.18	57.04
5b	−9.25	−9.88	0.63	1.03	20.81	65.68
5c	−9.02		0.86	1.06	26.68	28.02
6a	−8.78		1.04	1.03	35.20	67.80
6b	−8.80	−9.82	1.02	1.05	27.60	44.07
6c	−9.15		0.67	1.06	30.71	33.11
7a	−7.83		1.10	1.04	43.84	56.60
7b	−8.25	−8.93	0.68	1.06	25.82	51.71
7c	−8.75		0.18	1.05	32.42	32.51
8a	−9.19		0.44	0.99	83.13	83.06
8b	−8.83	−9.63	0.80	1.02	21.81	85.48
8c	−8.84		0.79	1.05	35.08	35.56
9a	−9.32		0.75	1.01	49.92	59.38
9b	−9.44	−10.07	0.63	1.04	22.72	57.50
9c	−9.22		0.85	1.04	27.05	27.18

[a] This work, [b] R-phenyl, Ref. [45]

gives rise to a vanishingly small antiferromagnetic interaction for *ortho–para* substitution (intercept ~ -0.65 cm^{-1}).

Wiberg bond order (BO) for the NN–phenylene connecting bond is greater than 1.0 in all cases except **4a** and **8a**. The larger BO (>1.0) indicates a larger double bond character and hence a greater conjugation, thus a larger J. As all calculated BOs are close to 1, they are not informative here.

3.4 Spin density and SOMO

It is a well-known fact that in the isolated NN radical, almost all the spin densities are equally shared by the NO groups [52, 53]. Mulliken population analysis of spin density in all the triplet diradicals reveals the same trend, that is, almost all the spin density is equally shared by the 4 NO fragments of the 2 NN moieties. A typical example is illustrated in Fig. 5a. In the BS state, again, almost all the spin densities reside on the 2 NO groups of each NN. However, the 2 NO groups have

unequal spin population but of the same sign. A similar spin distribution is found in the other NN fragment, though with an overall opposite sign, as shown in Fig. 5b. The spin density diagrams clearly illustrate the spin alternation in the most stable state.

A diradical has two singly occupied molecular orbitals (SOMOs). According to Borden and Davidson [54, 55], a pair of disjoint SOMOs generally leads to a singlet ground state with negative J, whereas the non-disjoint SOMOs give rise to a triplet ground state. In Fig. 6, we illustrate the nature of SOMOs in the BS solutions of fluoro derivative (**3a**, **3b** and **3c**). The SOMOs for **3a** are manifestly disjoint, whereas **3b** and **3c** have obviously non-disjoint SOMOs. Indeed, we calculate a negative coupling constant for **3a** and positive J values for **3b** and **3c**. Taking the example of **3b**, we also show in this figure that the B3LYP SOMOs only slightly vary from the M06-2X SOMOs. However, the SOMO dictum is known to fail when the frame of conjugation of the diradical strongly deviates from planarity [21, 22].
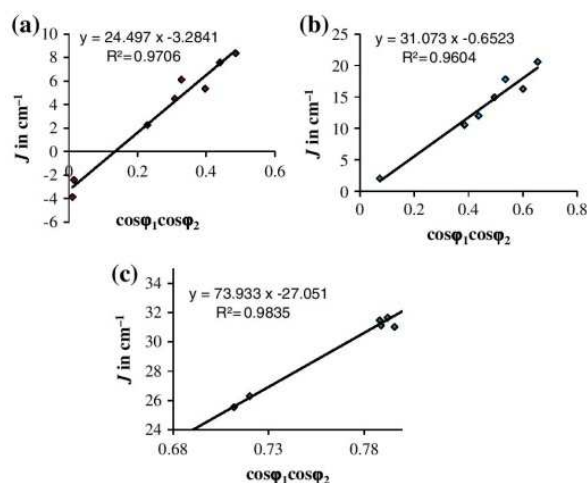
Fig. 4 Calculated J (M06-2X) versus χ_p, the factor of planarity: **a** common *ortho*: J (cm^{-1}) $= -3.28 + 24.50\chi_p$ (RMSD = 0.72); **b** *ortho–para*: J (cm^{-1}) $= -0.65 + 31.07\chi_p$ (RMSD = 1.12); **c** common *meta*: J (cm^{-1}) $= -27.05 + 73.93\chi_p$ (RMSD = 0.64)

3.5 Hammett constant

From the viewpoint of density functional theory (DFT), electronegativity can be defined as the negative of the partial derivative of the energy of an atomic or molecular system with respect to the number of electrons for a constant external potential [56]. Proft et al. [57] have carried out density functional calculations on different alkyl and alkyl alcohol groups and proposed that in gas phase,

electron-withdrawing power increases with increasing electronegativity and hardness of the groups. Proft et al. [57] also verified that as the number of hydrogen atom increases, the electron-withdrawing power of the alkyl or alkyl alcohol group decreases.

Steric effect is too strong for (**a**) and (**b**) type substitutions, and the factor of planarity predominantly determines J in these two cases. Therefore, the variation of J with Hammett constant is checked only for the (**c**) type substitutions. From our previous calculation on Schlenk diradical [58] that is structurally similar to the present organic diradicals, we expect a linear dependence of J on the Hammett constants. This is indeed borne out in Fig. 7 where variation with σ_m is associated with a small slope (1.74) and small standard deviation (0.83). The slope ensures five points to be almost on the straight line. At $\sigma_m = 0$, the intercept 30.69 cm^{-1} may be compared with the input 32.7 cm^{-1} for hydrogen as substituent. Variation of J with Hammett constant shows the correlation of the strength of magnetic interaction with acidity, that is, the electron-withdrawing power of the substituent. This observation has theoretical importance as discussed in Ref. [58]. This effect is visible only for common *meta* position (**c**), but it is masked by steric factor for the other two locations (**a**) and (**b**).

3.6 Nucleus-independent chemical shift (NICS)

NICS is a measure of aromaticity. The significance of negative values of NICS indicates that the systems are

Fig. 5 Mulliken spin density plots (M06-2X) for **1c** and **6c** (a) in triplet (T) and (b) broken-symmetry (BS) solutions

T (**1c**)   **(a)**   T (**6c**)

BS (**1c**)   **(b)**   BS (**6c**)

3a: M06-2X

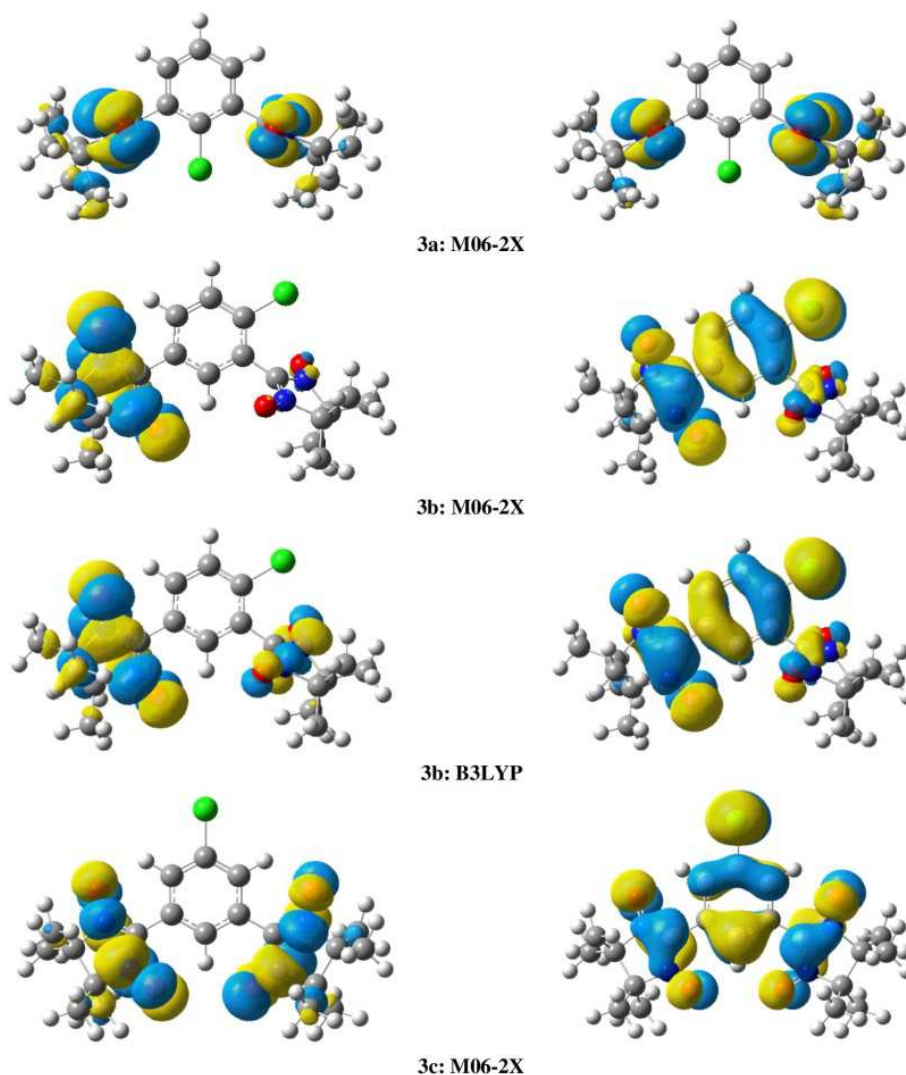3b: M06-2X

3b: B3LYP

3c: M06-2X
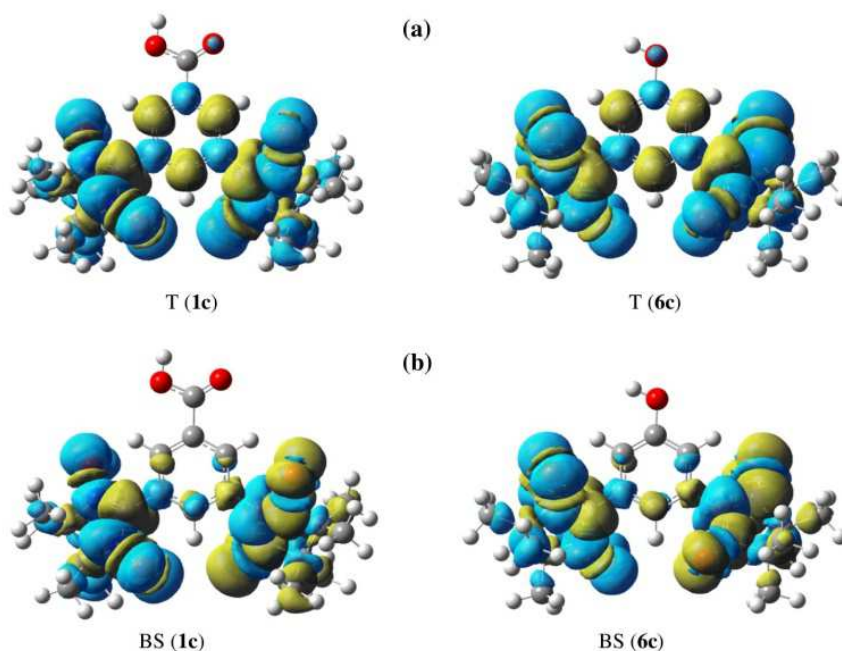
Fig. 6 SOMO plots for the broken-symmetry solutions of the fluorine derivatives of *m*-BNN (**3**). The SOMOs for **3a** are manifestly disjoint, whereas **3b** and **3c** have obviously non-disjoint SOMOs. As shown for **3b**, the B3LYP SOMOs show only a minor variation from the M06-2X diagrams

aromatic and positive values of NICS indicate that the systems are anti-aromatic [59]. The higher the negative value of NICS, the higher will be the aromatic character of any molecular system. Any system with zero NICS value means the system is completely non-aromatic. Schleyer et al. [60] proposed that NICS(1) gives some useful information about aromatic character of different hydrocarbons. The NICS(1) is nucleus-independent chemical shift calculated at a point 1 Å above the center of aromatic ring.

The NICS tensor and its isotropic average (simply, the chemical shift) represent fractional departures from the tensor or average for a reference substance, often tetramethyl silane (TMS). This reference has a C-13 nucleus thoroughly shielded by an almost perfectly spherical charge distribution. A negative value of the chemical shift is taken to imply de-shielding owing to departures from the spherical distribution. For ring systems, it is appealing to consider "ring current" that can define a local magnetic field by circulation of charge around the ring.

The computation of the chemical shift tensor rests on a perturbation-theoretical analysis. The first-order term, a property of the ground state, defines the diamagnetic portion. The second-order term defines the paramagnetic contribution. Its value depends in part on the energy gap between ground and triplet excited states, or more
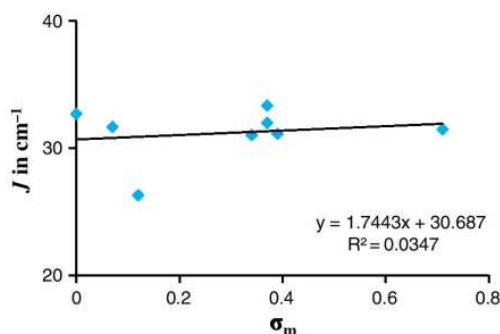
Fig. 7 Plot of calculated J (M06-2X) for type (**c**) species (common *meta* substitution) versus σ_m: J $(cm^{-1}) = 1.74\sigma_m + 30.69$ (RMSD = 0.84)

Fig. 8 Least square fitting of the calculated coupling constant with Eq. (6). The optimized parameters are $A = -442.0$ and $B = -2.931$, with $R^2 = 0.865$ and RMSD 4.31. The series of diradicals are indicated as **a** *red circle*, **b** *blue triangle* and **c** *black square*. The cross in *yellow* represents the unsubstituted *m*-BNN

approximately on the LUMO–HOMO energy gap of a closed-shell molecule. The stabilization characteristic of systems called aromatic is attended by a large LUMO–HOMO energy gap, and any feature of a particular molecule that changes this gap must affect the second-order term in the chemical shift. Thus, we imagine that elevating the HOMO (by a pi-donor) or depressing the LUMO (by a pi-acceptor) would have an adverse effect on the chemical shift. For a diradical, we have to deal with a pair of SOMOs instead of the doubly occupied and virtual couple. The SOMO energy difference (or the LUMO–HOMO energy gap of the coupler) can be viewed as the contributing factor.

3.6.1 Combined dependence

As the original Noodleman formula [31–33]

$$J = \frac{E(BS) - E(T')}{1 + S_{ab}^2} \qquad (4)$$

suggests, the evaluation of J would need a calculation of the overlap of magnetic orbitals Sab. This would provide a transparent intuitive interpretation. However, although identifying the magnetic orbitals is easy for transition metal complexes, it remains a non-trivial task for a moderately large organic diradical. The α-HOMO and β-HOMO in the BS solution may be taken as the magnetic orbitals: This has been attempted before for bis-NN diradicals with linear chain couplers and aromatic couplers, with partial success [37]. Still, the magnetic orbital overlap remains to be related to structural parameters such as BO and dihedral angle so as to generate a clear physical picture.

An alternative way of understanding was put forward by Hoffmann and his group back in 1968. Hoffmann et al. [61] contended that a triplet ground state is favored when the LUMO–HOMO energy gap is small. Later, an
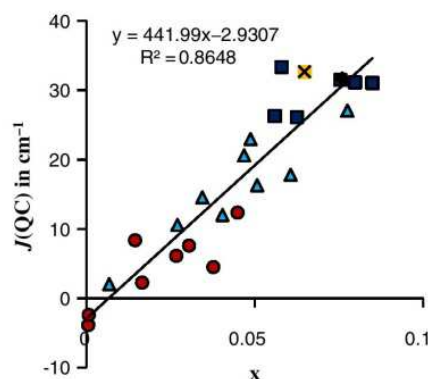
improvement was suggested by Hay et al. [62] that a departure from near degeneracy favors the singlet ground state,

$$E(T) - E(S) = -2K_{ab} + \frac{(\Delta\varepsilon_{ab})^2}{J_{aa} - J_{ab}}, \ (K_{ab} > 0) \qquad (5)$$

where J and K are direct and exchange integrals involving the SOMOs a and b. Again, this formula lacks a direct structural interpretation.

We are interested in a description of J in terms of structural characteristics such as those discussed in Ref. [63]. Coupling of spins would depend on the paramagnetic nature of the coupler. This coupling would be enhanced when there is strong overlap and good energy matching between the SOMOs of radical carriers and the orbitals of coupler. The overlap is strongly affected by geometry. An empirical formula was proposed by Ali et al. [64] for fused-ring couplers:

$$J = A\frac{\Delta NICS(1)\cos\phi_1\cos\phi_2(WBO)}{NICS(1)} + B \quad in \ cm^{-1} \qquad (6)$$

In the original formula of Ref. [64], the term B was not considered; we add it here for the sake of convenience. Equation (6) reflects the interplay of influences for *m*-phenylene-coupled radical sites, regardless of substitution elsewhere on the coupler ring. It includes steric effects through their impact on the torsion angles between the pi system of the coupler and the pi system of the radical carriers. The fractional change in NICS acts as surrogate for the fractional paramagnetic nature of the coupler. Wiberg BO reflects the general strength of interaction between radical centers and *m*-phenylene pi system. The structural characteristics NICS(1), ΔNICS(1), WBO, ϕ_1 and ϕ_2 are listed in Table 2.

Fig. 9 The unique hydrogen bond formation observed for **4a**. No such bond is formed in **4b**. Intramolecular hydrogen bonding is found in **6a** and **6b**. (Similar hydrogen bonds are also observed for **1a**, **7a** and **7b**)
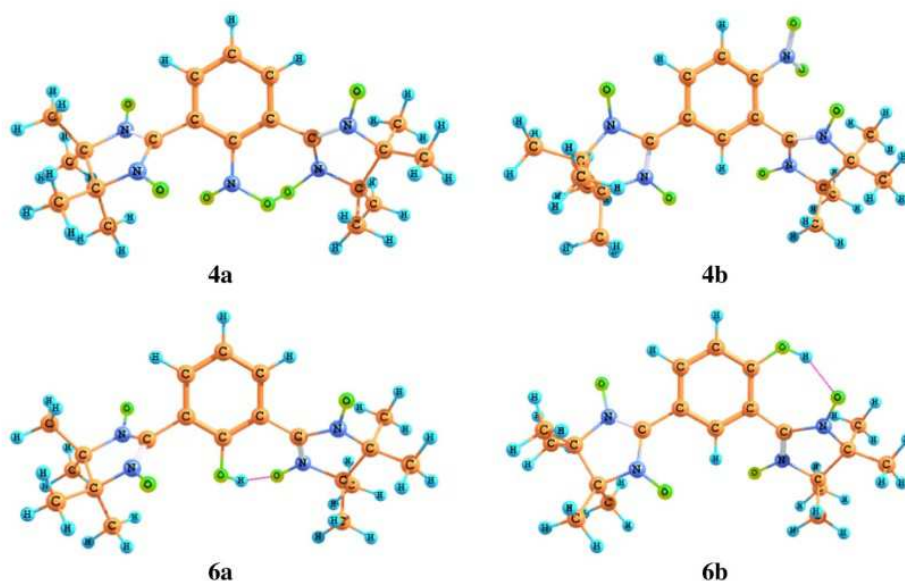
The formula (6) is unique in that it treats (**a**), (**b**) and (**c**) series of diradicals on the same footing, that is, using the same constants A and B. It recognizes the effects of substitution only in terms of the calculated structural characteristics in Table 2. A least square fit is depicted in Fig. 8. A fairly linear dependence is observed between the quantum chemical J and the empirical Eq. (6): $J(QC) = Ax + B$. The optimized values are $A = -442.0$ and $B = -2.931$ with RMSD = 4.31. The slope A can be interpreted as an average proportionality constant for the three series of diradicals including the unsubstituted one, while the B value represents the average intercept that corresponds $\chi_p = 0$. In other words, B is the average coupling constant for the radical center planes being perpendicular to the coupler plane and is necessarily negative as discussed in Sect. 3.3 (spin dipolar interaction—the so-called McConnell mechanism—normally leading to anti-ferromagnetic interactions) and illustrated by Fig. 4.

For the systems studied here, we expect the effects of substitution to be smallest for the c-substituted sites, where the substituent would have electronic but no steric impact. The importance of steric effects would be more serious in b-substituted systems for which there is one *ortho* interaction, and still more severe for the a-substituted systems for which there are two *ortho* substitutions effective conjugation between pi coupler and radical sites.

First, we consider the impact of substitution on NICS(1) of the phenyl system. In the following statements, enhancing NICS makes the value more negative and makes the system more aromatic.

1. Substitutions that enhance NICS(1) on benzene: F > NO_2.

2. Substitutions that decrease NICS(1) on benzene: NH_2 ≫ phenyl > OH > Br.
3. Substitutions with little effect on NICS(1) on benzene: Cl, CH_3, COOH.

Introducing the NN radicals makes NICS(1) for *m*-phenylene more positive and diminishes the aromatic character.

The a-type (*ortho–ortho*) substitution has a major impact on torsion angles especially for phenyl and oddly for chloro groups. The J values are strikingly diminished by a-type substitutions, sometimes changing sign from positive to negative values (amino > phenyl > Cl). The a-type substitutions can either make NICS(1) more positive, reducing aromaticity (amino ≫ hydroxyl > phenyl and bromo), or make NICS(1) more negative, enhancing aromaticity (carboxyl ≫ chloro).

The c-type (common *meta*) substitutions have generally little effect on torsion angles. The c-type substitution generally enhances the Wiberg index slightly. There are small changes for R = phenyl and amino, tending to push them further out of alignment with *m*-phenylene ring, and diminishing J.

The b-type (*ortho–para*) substitution has a more dramatic effect on its *ortho* neighbor's torsion angle, than on the *para* NN. The effect on J is generally intermediate between c-type and a-type substitutions. For hydroxyl and amino, the impact is modest; for phenyl, the impact is large. The b-type substituents have puzzling consequences for NICS(1).

Para hydrogen bonding produces mostly structural effects such as a reduction in the twist angle ϕ as in **6a** and **6b** (Fig. 9), and also a small amount of spin delocalization

effect. The bulky phenyl group leads to an increase in the twist angle in its neighbor, (both ϕ_1 and ϕ_2 in **8a** and only ϕ_2 in **8b**). Thus, **8a** becomes antiferromagnetically coupled, and **8b** is only faintly ferromagnetic (see Tables 1 and 2).

4 Conclusions

The magnetic exchange coupling in 25 diradicals are predicted as ferromagnetic at UB3LYP/6–311+G(d,p), UB3LYP-D3/6–311+G(d,p) and M06-2X/6–311+G(d,p) levels. Species **3a** and **8a** are antiferromagnetically coupled. The substitution at the *meta* position of bis-NN-*m*-phenylene diradicals has little steric and hydrogen-bonding effects. In the case of a large twist of the planes of the spin sources from the plane of the coupler, the nature of interaction changes from ferromagnetic to antiferromagnetic. In these cases, the BO becomes small. The NICS value is found to decrease from the corresponding mono-substituted phenyl derivatives. The coupling constant is more or less linearly dependent on the product of (ΔNICS/NICS) and factor of planarity, with a small but distinctly negative intercept.

5 Supporting information

Log files of all calculations and Ref. [43] and [44]. The materials are available free of charge at http://pubs.acs.org.

References

1. Rajca A, Utamapanya S (1992) J Org Chem 57:1760
2. Wentrup C (2002) Science 295:1846
3. Rajca A, Shiraishi K, Pink M, Rajca S (2007) J Am Chem Soc 129:7232
4. Kahn O (1993) Molecular Magnetism, 2nd edn. Wiley, New York
5. Rajca A (1994) Chem Rev 94:871
6. Matsuda K, Matsuo M, Mizoguti M, Higashiguchi K, Irie M (2002) J Phys Chem B 106:11218
7. Catala L, Turek P, Moigne JL, Cian AD, Kyritsakas N (2000) Tetrahedron Lett 41:1015
8. Benelli C, Gatteschi D (2002) Chem Rev 102:2369
9. McWeeny R (1989) Pure Appl Chem 61:2087
10. Longuet-Higgins HC (1950) J Chem Phys 18:265
11. Ovchinnikov AA (1978) Theor Chim Acta 47:297
12. McConnell HM (1963) J Chem Phys 39:1910
13. Trindle C, Datta SN (1996) Int J Quantum Chem 57:781
14. Trindle C, Datta SN, Mallik B (1997) J Am Chem Soc 119:12947
15. Platz MS, Borden WT (1982) Diradicals, chap 8. Wiley, New York
16. Ioth K (1967) Chem Phys Lett 1:235
17. Dougherty DA (1990) Acc Chem Res 24:88
18. Takano Y, Onishi T, Kitagawa Y, Soda T, Yoshioka Y, Yamaguchi K (2000) Int J Quantum Chem 80:681
19. Ishida T, Kawakami T, Mitsubori S, Nogami T, Yamaguchi K, Iwamura H (2002) J Chem Soc Dalton Trans 60:3177
20. Ishida T, Mitsubori S, Nogami T, Takeda N, Ishikawa M, Iwamura H (2001) Inorg Chem 40:7059
21. Dvolaitzky M, Chiarelli R, Rassat A (1992) Angew Chem Int Ed Engl 31:180
22. Kanno F, Inoue K, Koga N, Iwamura H (1993) J Am Chem Soc 115:847
23. Fang S, Lee M, Hrovat DA, Borden WT (1995) J Am Chem Soc 117:6727
24. Mitani M, Mori H, Takano Y, Yamaki D, Yoshioka Y, Yamaguchi K (2000) J Chem Phys 113:4035
25. Mitani M, Yamaki D, Takano Y, Kitagawa Y, Yoshioka Y, Yamaguchi K (2000) J Chem Phys 113:10486
26. Zhang G, Li S, Jiang Y (2003) J Phys Chem A 107:5573
27. Reta Mañeru D, Pal AK, Moreira IPR, Datta SN, Illas F (2014) J Chem Theory Comput 10:335
28. Kamiyama K, Shiomi D, Hase S, Nishizawa M, Sato K, Kozaki M, Okada K, Takui T (2000) Appl Magn Reson 19:45
29. Hase S, Shiomi D, Sato K, Takui T (2001) J Mater Chem 11:756
30. Shiomi D, Tamura M, Sawa H, Kato R, Kinoshita M (1993) J Phys Soc Jpn 62:289
31. Noodleman L (1981) J Chem Phys 74:5737
32. Noodleman L, Baerends EJ (1984) J Am Chem Soc 106:2316
33. Noodleman L, Peng CY, Case DA, Mouesca JM (1995) Coord Chem Rev 144:199
34. Ginsberg AP (1980) J Am Chem Soc 102:111
35. Noodleman L, Davidson ER (1986) Chem Phys 109:131
36. Ali ME, Vyas S, Datta SN (2005) J Phys Chem A 109:6272
37. Ali ME, Datta SN (2006) J Phys Chem A 110:2776
38. Yamaguchi K, Takahara Y, Fueno T, Nasu K (1987) Jpn J Appl Phys 26:L1362
39. Yamaguchi K, Jensen F, Dorigo A, Houk KN (1988) Chem Phys Lett 149:537
40. Caballol R, Castell O, Illas F, Malrieu JP, Moreira IPR (1997) J Phys Chem A 101:7860
41. Moreira IPR, Illas F (2006) Phys Chem Chem Phys 8:1645
42. Vyas S, Ali ME, Hossain E, Patwardhan S, Datta SN (2005) J Phys Chem A 109:4213
43. Frisch MJ, Trucks GW, Schlegel HB, Scuseria GE, Robb MA, Cheeseman JR, Montgomery JA Jr, Vreven T, Kudin KN, Burant JC et al (2003) Gaussian 03. Gaussian Inc, Pittsburgh
44. Gaussian 09, Revision A.1, Frisch MJ, Trucks GW, Schlegel HB, Scuseria GE, Robb MA, Cheeseman JR, Scalmani G, Barone V, Mennucci B, Petersson GA et al. (2009) Gaussian, Inc., Wallingford
45. Chen Z, Wannere CS, Corminboeuf C, Puchta R, Schleyer PVR (2005) Chem Rev 105:3842
46. Wiberg K (1968) Tetrahedron 24:1083
47. Glendening ED, Reed AE, Carpenter JE, Weinhold F (1990) QCPE Bull 10:58
48. Weinhold F, Landis CR (2001) Chem Educ Res Pract Eur 2:91
49. Kitagawa Y, Saito T, Ito M, Shoji M, Koizumi K, Yamanaka S, Kawakami T, Okumura M, Yamaguchi K (2007) Chem Phys Lett 442:445

50. Malrieu JP, Trinquier GJ (2012) J Phys Chem A 116:8226
51. Saito T, Thiel WJ (2012) J Phys Chem A 116:10824
52. Zheludev A, Barone V, Bonnet M, Delley B, Grand A, Ressouche E, Rey P, Subra R, Schweizer J (1994) J Am Chem Soc 116:2019
53. Novoa JJ, Lafuente P, Deumal M, Mota F (2002) Magnetism: molecules to materials IV, vol 3. Wiley, New York, p 78
54. Borden WT, Davidson ER (1977) J Am Chem Soc 99:4587
55. Constantinides CP, Koutentis PA, Schatz J (2004) J Am Chem Soc 126:16232
56. Parr RG, Donnelly RA, Levy M, Palke WE (1978) J Chem Phys 68:3801
57. Proft FD, Langenaeker W, Geerlings P (1995) Tetrahedron 51:4021
58. Latif IA, Hansda S, Datta SN (2012) J Phys Chem A 116:8599
59. Schleyer PVR, Maerker C, Dransfeld A, Jiao AH, Hommmes NJRVE (1996) J Am Chem Soc 118:6317
60. Schleyer PVR, Jiao H, Hommes NJRVE, Malkin VG, Malkina OL (1997) J Am Chem Soc 119:12669
61. Hoffmann R, Imamura A, Hehre WJ (1968) J Am Chem Soc 90:1499
62. Hay PJ, Thibeault JC, Hoffmann R (1975) J Am Chem Soc 97:4884
63. Datta SN, Trindle CO, Illas F (2013) Theoretical and computational aspects of magnetic organic molecules, vol 6. Imperial College Press, London
64. Ali ME, Datta SN (2006) J Phys Chem A 110:13232

4.3.3.   Paper #4.3.

Triplet–Singlet Gap in Structurally Flexible Organic Diradicals

REGULAR ARTICLE

Triplet–singlet gap in structurally flexible organic diradicals

Daniel Reta Mañeru · Ibério de P. R. Moreira · Francesc Illas

Abstract A key factor in the search of high-spin ground state purely organic molecules concerns the effect of the inherent non-rigid structures on the magnetic and optical properties. This structural feature has not been properly addressed in previous theoretical works. Here, based on the experimentally characterized high-spin ground state of dendritic and star-branched polyradicals, we study four alternant hydrocarbon biradicals that intend to model these effects and, at the same time, provide a first step toward understanding more extended experimental structures. A series of density functional theory (DFT) and of wave function-based methods have been used to explore the richness of structural minima in the corresponding potential energy surfaces and to discuss its effect on the triplet–singlet gap of the proposed model systems. For a given model, the DFT-based B3LYP, M06-2X and MN-12SX methods provide a consistent description. Likewise, a multiconfigurational quasi-degenerate perturbation theory approach with the minimal π space as CASSCF reference is found to provide unbiased results. Despite the conformational richness found for these systems, they all can be described by a reduced set of values referred to only two structural parameters, being those the dihedral angles between the phenyl rings. For a given model, there is no significant change in the triplet–singlet gap depending on the chosen local minima.

D. Reta Mañeru · I. P. R. Moreira · F. Illas (✉)
Departament de Química Física & Institut de Química Teòrica i Computacional (IQTCUB), Universitat de Barcelona,
C/ Martí i Franquès 1, 08028 Barcelona, Spain
e-mail: francesc.illas@ub.edu

1 Introduction

The search of high-spin ground state organic molecules has been inspired and developed by comparison with previous efforts carried out in the field of inorganic chemistry. In this sense, two important landmarks have paved the road to the synthesis of organic magnetic systems. First, the discovery of single-molecule magnets [1] promoted attempts to mimic the behavior displayed by the *nd* ($n = 3, 4, 5$) orbitals in magnetic transition metal complexes to purely organic systems. This implies an open-shell ground state involving $C(2p)$ orbitals only. The second landmark comes from the double-exchange model proposed by Zener [2, 3] to explain the giant magnetoresistive effects observed in manganites since it is strongly related to the more recent work of Shultz and Kumar [4] leading to the first example of enhanced ferromagnetic coupling in a mixed-valence bis(semiquinone) biradical anion that lacks an effective π-type ferromagnetic coupler.

From a single-molecule magnet perspective, the initial roadmap to organic molecules displaying high-spin ground state has been facilitated by theoretical predictions carried out in alternant hydrocarbons. In particular, we mention the seminal work of Longuet-Higgins [5], stating how many non-bonding singly occupied orbitals will be present depending on the number of carbon atoms and double bonds, and the valence bond theory-based study of Ovchinnikov [6], predicting the ground state spin quantum number of a given structure. This theoretical evidence leads to the conclusion that organic molecules with high-spin ground state can be synthesized from non-Kekulé alternant hydrocarbons with

non-disjoint singly occupied molecular orbital (MO) systems [7, 8]. The experimental approach often consists on generating one unpaired electron per center, and it was developed mainly by Rajca et al. [9]. In the strategy followed by Rajca [10] for carbon-centered radicals, the species are obtained from the corresponding polyethers precursors that are treated with lithium metal in tetrahydrofurane (THF), yielding the subsequent carbopolyanions which are further oxidized with iodine at 180 K. This treatment leads to the type of poly-radicals that are generally studied in frozen THF solutions by SQUID magnetometry and often generates a broad set of systems such as di–tri–tetra radicals, star-branched and dendritic polyradicals. Although most of Rajca's research is based on C-centered radicals, recent work has also focused on N-centered radicals, both in diradical [10] and polyradi-cal [11] compounds. An alternative approach for obtaining persistent triplet ground state molecules has recently emerged from research devoted to synthesizing molecules with sin-glet biradical ground state [12]. The referred persistent triplet ground state molecule is a heptazethrene isomer [13] and was synthesized following a strategy similar to the one by Rajca [9], i.e., by oxidation of the corresponding dianion. Clearly, all these strategies result in an appealing approach toward the synthesis of the so-called single-molecule organic magnet.

In this work, following the well-established theoretical framework described in detail in the recent book by Datta et al. [14], we focus on a series of Rajca-type extended systems that are based on the repetition of the *m*-xylylene diradical unit, a system investigated in detail in previous work [15]. Previous works have addressed the possibility to obtain polymeric radicals precisely by considering the *m*-xylylene diradical as a building block. However, impor-tant structural features derived from the particularities of the radical centers have often been overlooked. In fact, the few works dealing with this type of delocalized systems either assume co-planarity of the phenyl rings [16, 17] or neglect the existence of multiple minima [18]. In this sense, it is worth pointing out the many contributions of Barone et al. on providing an accurate way of predicting magnetic interactions in organic radicals (see for instance Ref. [19] and references therein) and the application to the similar problems as those here investigated [20]. However, it is important to note that the focus of these works is on radi-cals which exhibit more markedly localized magnetic cent-ers dominated by σ–π-type orbitals. This is not the case of the present work where the magnetic interactions involve two interconnected π systems. It is also important to men-tion that the work of Barone et al. [21] on nitrogen-based radical centers, also synthesized by Rajca [22], is perhaps better related to the present work although it does not deal with the influence of conformational effects simply because the diradical of interest is structurally rigid. Finally and related to the study of magnetic interactions through space,

it is worth noting the work on verdazyl-based compounds [23]. However, here the focus is on the interaction between magnetic moieties rather than on structurally flexible mag-netic molecules. Here, we go one step further and address the problems derived from the existence of multiple min-ima and their effect on the relative energy of the low-lying electronic states. This constitutes a necessary preliminary step before studying periodic structures that resemble the star-branched and dendritic structures proposed by Rajca [9] where planarity will be the exemption rather than the rule. In this sense, the present work complements a recent study by Pal and Datta [24] on calix[4]arene-based radicals with bis(biphenylene)methyl linkers, which are presented as possible precursors of spin glass and superparamagnets. Following this line of reasoning, the model systems here described would eventually permit one exploring the effect of defect introduction as well as the loss of a radical center in the propagation of spin coupling throughout the system.
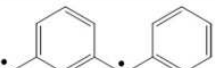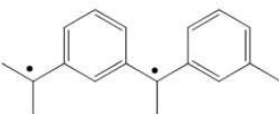
2 Model systems
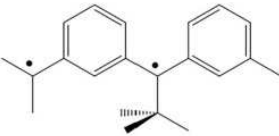
In order to investigate the effect of substituents and of con-formational freedom in polycyclic aromatic hydrocarbons with branched and dendritic structures such as those sug-gested by Rajca [9], a series of model systems have been designed. They all share the skeleton depicted in Scheme 1 where the θ_1 and θ_2 dihedral angles in the molecular frame-work confer a richness of possible structural isomers even including enantiomeric forms. In the simplest system, all substituents are hydrogen atoms so that the resulting com-pound is the 3-methyldiphenylmethyl-diyl diradical, here-after referred to as compound **1**.

To investigate the effect of electron donating groups in the electronic structure of the diradical thus formed and also in the potential energy surface corresponding to the θ_1 and θ_2 dihedral angles, a second model is built where all substitu-ents in Scheme 1 are methyl groups. The resulting system is 1-methyl-3-(2-yl-isopropyl)-3′-methyldiphenylmethyl com-pound **2**. Forcing orthogonality between the two phenyl rings, thus enabling the study of the effect of the extension
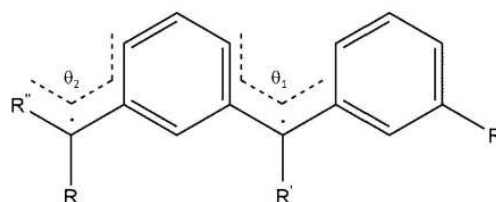
Scheme 1 Schematic representation of studied model systems indi-cating the relevant dihedral angles, the different *R* substituents are listed in Table 1

Table 1 Models for alternant hydrocarbons used in the present work

System	R	R′	R″	Schematic representation	IUPAC name
1	–H	–H	–H		3-Methyldiphenylmethyl-diyl
2	–CH$_3$	–CH$_3$	–CH$_3$		1-Methyl-3-(2-yl-isopropyl)-3′-methyldiphenylmethyl
3	–CH$_3$	*Tert*-butyl	–CH$_3$		1-(Tertbutyl)-3-(2-yl-isopropyl)-3′-methyldiphenylmethyl
4	–H	–H	Phenyl		1,1′-(1,3-Phenylene)bis[1-phenylmethyl]

of the π-system throughout the molecule, may be achieved by introducing a bulky group, such as *tert*-butyl in position R′. The resulting system is 1-(tertbutyl)-3-(2-yl-isopropyl)-3′-methyldiphenylmethyl, referred to as compound **3**. Finally, the introduction of a phenyl group in R″ keeping the rest of substituents as hydrogen depicts the continuation toward the linear polymer introducing also the possibility of a larger delocalization over the molecule. The resulting 1,1′-(1,3-phenylene)bis[1-phenylmethyl]diradical will be referred to as compound **4**.

2.1 Computational approach

We start this section by pointing out that the main focus of the present work is to explore the effect of the conformational richness displayed by the proposed models on the electronic structure properties related to the open-shell character rather than providing an exhaustive discussion of the possible effect of the different available electronic structure methodologies on the reported properties. Hence, fine details of the electronic structure such as zero-field splitting (ZFS) and anisotropy can be safely ignored. Consequently, the different sets of calculations are based on previous experience in several systems [14] and, in particular, on recent systematic work on the *m*-xylylene diradical [15].

The molecular and electronic structure of model systems in Table 1 has been studied using density functional theory (DFT) and wave function-based methods. In a first step, geometry optimization of all systems in the triplet and broken symmetry approach to singlet electronic states has been performed at the DFT level by means of three different exchange–correlation potentials, namely the standard B3LYP hybrid functional [25] which overall provides robust results,

the M06-2X which was found to provide accurate results for the *m*-xylylene diradical [15] and the MN12-SX, one of the latest functionals of the Minnesota family which significantly improves over previous members of the series [26]. These calculations have been carried out using the standard 6-311G** basis set [27, 28] since, for this kind of systems, it has been proven that the results thus obtained do not vary significantly by increasing the basis set size and quality [15]. Nevertheless, this has been further verified using system **2** as a case for study and the more extended 6-311++G** basis set [29].

Since, for each compound, the three DFT geometry-optimized structures are almost identical, vertical and adiabatic triplet–singlet energy differences have always been obtained from the B3LYP-optimized structures, using the broken symmetry approach [30–32] to estimate the open-shell singlet [33] and with the Yamaguchi correction for spin contamination [34–36]. Here, it is important to note that even if alternative approaches exist to describe open-shell singlet states such as those based on spin-flip time-dependent DFT (TD-DFT) methods [37–40], there is strong evidence that, for a given functional and for systems with two unpaired electrons as it is the case here, broken symmetry and spin-flip TD-DFT approaches provide essentially the same description [41]. Nevertheless, in order to have an appropriate unbiased, albeit approximate reference, triplet–singlet gaps have been also obtained from single-point energy calculations at each DFT geometry using a CAS-SCF wave function using minimal—CAS(2,2)—and full π-valence—CAS(14,14)—active spaces. For the minimal CAS, dynamical correlation effects were estimated from second-order multi-reference Møller–Plesset (MRMP) perturbation theory [42–45] calculations, hereafter referred to as MCQDPT that stands for multiconfigurational

Fig. 1 Structural landscape of compound **1** featuring two structural isomers (**1**$_1$ and **1**$_2$), each with an enantiomeric counterpart (**1**$_1$ and **1**$_{1'}$; **1**$_2$ and **1**$_{2'}$) and the corresponding Newman's projections. The transition-state (TS) structures for interconversion of these isomers are also included. θ stands for θ_1 in Scheme 1 since θ_2 remains close to zero in all structures. The *arrows* in the outermost part of the *circle* indicate the local minima that the corresponding transition state connects
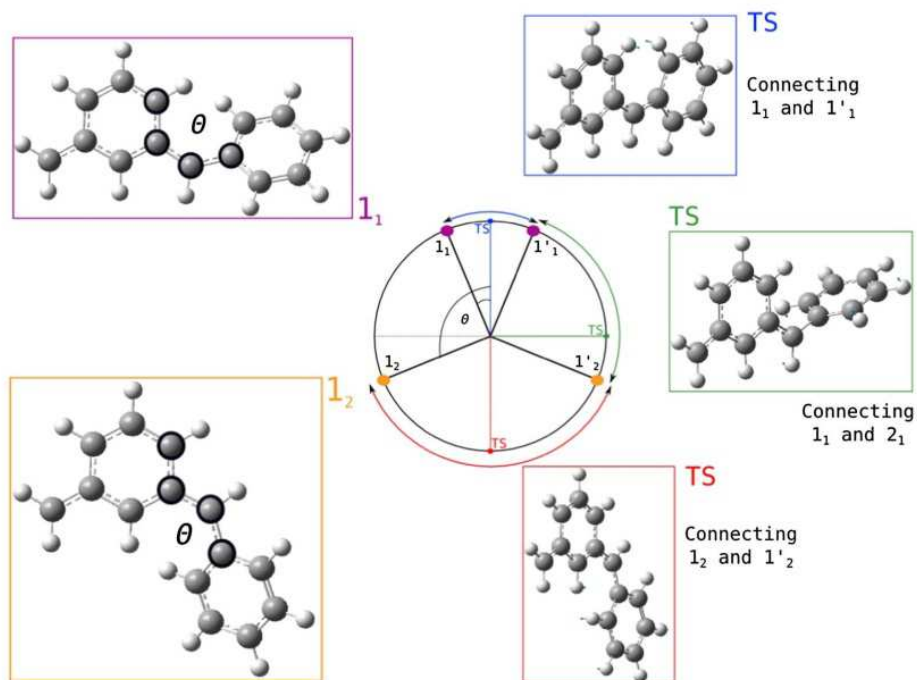
quasi-degenerate perturbation theory. Note, however, that MRMP has some noticeable differences with respect to the broadly used CASPT2 method [46, 47]. These involve essentially the number of states used to span the first-order wave function. In the CASPT2 method, the total energy is obtained from single and double excitations out of the reference wave CASSCF function. However, in MRPT all singly and doubly excited determinants obtained from each of the determinants in the reference wave function are considered. In the language of configuration interaction methods, one would state that CASPT2 uses a contracted reference function, whereas MRPT does not. The use of a contracted/uncontracted reference may be advantageous depending on the particular case although there is not a general rule. The CASSCF and MCQDPT calculations have been carried out using the 6-311G** standard basis set as in most of the DFT calculations except for compound **2** where, because of the rather large size, a 6-31G* basis set was selected.

A brief comment is required when calculating the vertical and adiabatic transitions within the broken symmetry approach. For vertical transitions, one can simply apply the appropriate mapping as illustrated in the review paper by Moreira and Illas [48] or the Yamaguchi formula, which approximately accounts for non-orthogonality of alpha and beta MOs [34–36]. The latter is the choice here because of the larger delocalization of magnetic orbitals in organic radicals [49]. However, for the adiabatic transitions, one should estimate the energy of the decontaminated open-shell singlet at the broken symmetry geometry.

This can simply be done by calculating the energy of the triplet state at that geometry as recently shown in the case of *m*-xylylene [15]

$$\Delta_{TS}^{adia} \equiv \Delta_{adia} = E_{S^i} - E_{T^j} = \frac{2\left(E_{BS^i} - E_{T^i}\right)}{\left\langle S_{T^i}^2\right\rangle - \left\langle S_{BS^i}^2\right\rangle} + E_{T^i} - E_{T^j}$$

(1)

where i and j refer to the molecular geometry of the singlet and triplet, respectively.

3 Results and discussion

3.1 Local minima, isomers and enantiomers

The analysis of the potential energy surface for compounds **1–4** either in the triplet ground state or in the open-shell singlet—represented by a broken symmetry solution—reveals a quite rich landscape with multiple minima corresponding to structural isomers and, depending on the case, enantiomers. The search for stable structures has been carried out for the three different density functionals, and the picture obtained is always qualitatively the same. For simplicity, we will next describe the results corresponding to the B3LYP functional. To illustrate the rich structural landscape above-mentioned, let us take the simplest case of compound **1** where R, R' and R'' substituents in Scheme 1 are all hydrogen atoms. The existence of two (structurally

Fig. 2 Structural landscape of compound **2** featuring four structural isomers (**2**₁, **2**₂, **2**₃ and **2**₄), each with an enantiomeric counterparts (**2**₁′, **2**₂′, **2**₃′ and **2**₄′) and the corresponding Newman's projection through the dihedral angle θ. θ stands for θ_1 in Scheme 1 since θ_2 remains close to zero in all structures
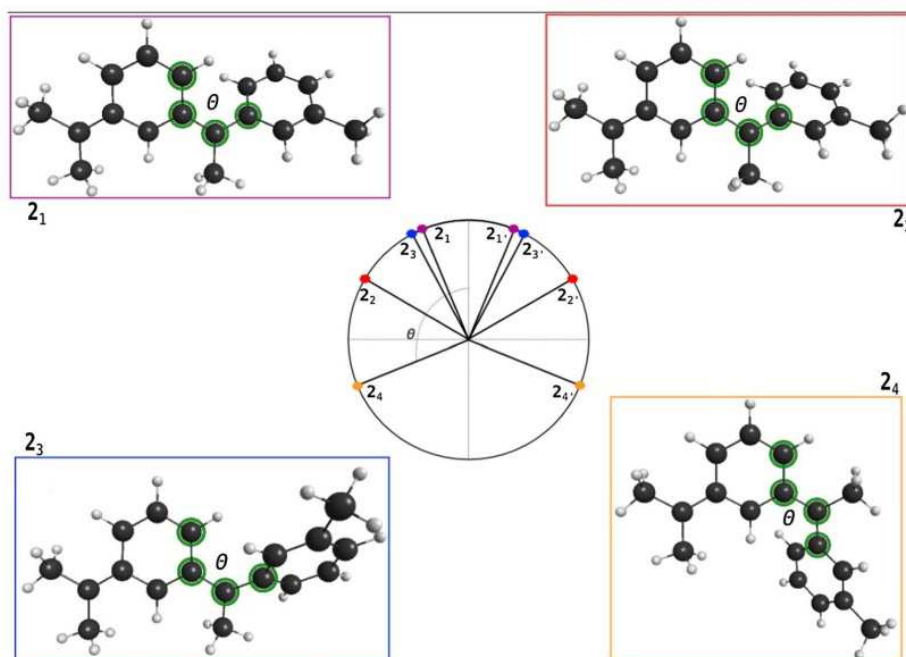
different) phenyl rings separated by a radical center leads to different stable nuclear configurations, which can be easily understood from Fig. 1. A first energy minimum in the triplet potential energy surface is encountered for a situation where the two phenyl rings are separated by an angle of ~17° either through a clockwise or a counter clockwise rotation. The frequency analysis reveals that both structures are minima in the triplet potential energy surface having exactly the same energy and being mirror images, they are enantiomers and will be referred to as 1_1 and $1_{1'}$, respectively. A similar situation is found for the open-shell singlet potential energy surface. The origin of this quite exotic form of enantiomerism—there is no typical asymmetric C—lies in the particular nature of the radical center linking two different rings where the pyramidal sp^3 like hybridization results in three different chemical substituents and one "dangling bond" which effectively acts as the fourth one. The two enantiomers, hereafter referred to as 1_1 and $1_{1'}$, can be interconverted through an appropriate transition-state structure. The search for this stationary saddle point in the potential energy surface led to a structure connecting 1_1 and $1_{1'}$ where the two rings are coplanar and which, in principle [50], corresponds to the appropriate transition state. The energy barrier for interconversion is, however, very small, of a 4.64 kJ mol⁻¹ (387 cm⁻¹). The sp^3 pyramidal character of the radical center linking the two rings has another interesting effect, namely the existence of a second type of minimum energy structure in the triplet potential energy surface where the two rings are now separated by 166° (Fig. 1) and accidentally degenerate with the

previous one with a calculated B3LYP energy difference of 0.02 kJ mol⁻¹ (2 cm⁻¹) only. A slightly larger energy difference of 0.23 kJ mol⁻¹ (20 cm⁻¹) is found between the two broken symmetry solutions, at the same B3LYP level. Again, the rotation from a coplanar situation can be clockwise or a counterclockwise meaning that this new structure does also exhibit two enantiomers that will be denoted as 1_2 and $1_{2'}$ and are connected through a transition state where the two rings are also coplanar opposed by a 180° angle. The energy barrier for interconversion is also of 4.63 kJ mol⁻¹ as in the case of the 1_1 and $1_{1'}$ enantiomers. The different structural isomers 1_1 and 1_2 (or $1_{1'}$ and $1_{2'}$) can also be interconverted through overcoming an energy barrier of 21.79 kJ mol⁻¹ corresponding to a transition-state structure where the two rings are separated by a 90° angle.

The landscape exhaustively described for compound **1** is applicable to the rest of model systems with some variations, which will be now described in some detail. Therefore, the discussion will be limited to the different energy minima without further comments on the energy barriers for interconversion. In compound **2**, the R, R' and R'' substituents in Scheme 1 are all methyl groups. The presence of the methyl groups significantly affects the potential energy surface landscape with the appearance of two new minima which following the notation introduced above are denoted as 2_1, 2_2, 2_3 and 2_4, whereas the corresponding enantiomers are denoted as $2_{1'}$, $2_{2'}$, $2_{3'}$ and $2_{4'}$. The molecular structure of these four energy minima, fully characterized by frequency analysis, involves essentially the relative

Table 2 Vertical and adiabatic triplet–singlet energy differences, Δ_{vert} and Δ_{adia}, respectively, for the minimum energy structures (1_1 and 1_2) of compound **1** as predicted by different density functionals and wave function-based methods using the B3LYP-optimized geometries

Structure	Method	Δ_{vert}	Δ_{adia}
1_1	B3LYP	3,350	2,816
	M06-2X	3,182	2,543
	MN12-SX	2,947	2,455
	CAS(2,2)SCF	1,384	751
	MCQDPT	3,169	2,659
	CAS(14,14)SCF	3,841	2,941
1_2	B3LYP	3,304	2,767
	M06-2X	3,167	2,527
	MN12-SX	2,901	2,398
	CAS(2,2)SCF	1,359	734
	MCQDPT	3,108	2,620
	CAS(14,14)SCF	3,812	2,767

All values are in cm^{-1}. Wave function-based results are obtained using the set of orbitals corresponding to each electronic state

orientation of the phenyl rings as schematically illustrated in Fig. 2. Consequently, the energy differences between these structures are relatively small. For the B3LYP triplet potential energy surface, the most stable structure is 2_3 followed by 2_1, 2_4 and 2_2 lying at 2, 28 and 102 cm^{-1} above 2_3, respectively. In the case of the broken symmetry potential energy surface, the most stable structure is 2_1 followed by 2_4, 2_3 and 2_2 with the corresponding broken symmetry solutions lying at 194, 207 and 218 cm^{-1}, respectively, above that of 2_1. Compound **3** differs from compound **2** only by substitution of the methyl group of the radical center connecting the two rings by a bulkier *tert*-butyl group. Here, only two energy minima have been located in spite of running several optimization geometry calculations starting from the situations corresponding to energy minimum in **2**. The energy difference between 3_1 and 3_2 in the triplet state is of 22 cm^{-1} only, which is similar to the situation described for compound **1**. Finally, compound **4** attempts to mimic the initial step of a polyradical generated from **1**. Hence, it contains three phenyl rings and involves up to five different conformers properly characterized from the corresponding frequency calculations separated by at most 153 cm^{-1} in the triplet state, whereas the broken symmetry solution are separated by at most 130 cm^{-1}.

3.2 Triplet–singlet gaps

The existence of multiple minima, as described above, introduces a certain degree of complexity in the energy difference between the lowest triplet and open-shell singlet states. Therefore, we have chosen to analyze these energy

differences, previously defined as Δ, for each minimum energy structure. Following previous work, vertical and adiabatic (Δ_{vert} and Δ_{adia}) gaps have been calculated where the geometry optimization has been carried out at the B3LYP level. This is justified from the recent systematic work on the *m*-xylylene diradical where it has been shown that the effect of the geometry is much smaller than the one introduced by the method used to estimate the total energy [15].

Let us now discuss in some detail the situation for compound **1** for which results are summarized in Table 2. Several interesting issues emerge from this table. First, the three density functionals predict Δ values that differ at most by 10 %. Moreover, these values are significantly smaller (~30 %) than those predicted for the *m*-xylylene diradical which indeed were in fair agreement with experiment [15], indicating that increasing the extension of the π system can result in energy difference in the range of those expected for magnetic systems which seems to confirm the hypothesis set out in the introduction. The minimal CAS(2,2)SCF wave function badly fails to predict the proper order of magnitude of the triplet–singlet gap although this is remedied by including dynamical correlation effects through the MCQDPT approach. The results thus found are now similar to those predicted by the different density functionals, in particular with the M06-2X, which seemed to provide the best estimate of the triplet–singlet gap in the *m*-xylylene diradical [15]. Part of the correlation effects missing in the CAS(2,2)SCF description are recovered with the full π valence CAS(14,14)SCF although the Δ values are now significantly overestimated because dynamical correlation out of this space is missing. A graphical comparison between the two singly occupied canonic orbitals for compound 1_1, obtained either by a CAS(2,2) SCF or CAS(14,14)SCF description, can be made from inspecting Fig. 3. In line with previous results, the problem of using a minimal CAS(2,2)SCF set of orbitals comes from an inadequate description of the degree of localization of the magnetic orbitals [51, 52]. In these organic diradicals, usually exhibiting a more delocalized π system, the minimal CAS(2,2)SCF description leads to an excessive localization with respect to the full π valence CAS(14,14) SCF description which provides a more accurate reference. This is similar to the case of Cu dinuclear complexes where the minimal CAS(2,2) description also leads to exceedingly localized orbitals [52]. Nevertheless, adding dynamical correlation out of the minimal CAS(2,2)SCF also provides a convenient and less computationally demanding way to recover the appropriate orbitals while including as well the dynamic correlation effects that affect the triplet–singlet energy difference as recently shown for the difficult case of *m*-xylylene [15]. In this sense, MCQDPT calculation on top of the CAS(2,2)SCF seems to be an adequate option

Fig. 3 Graphical representation of the two singly occupied canonic orbitals obtained either by a minimal CAS(2,2)SCF or a full π valence CAS(14,14) SCF calculation for compound **1₁**. The differential localization between the two sets of orbitals also holds for compound **2**
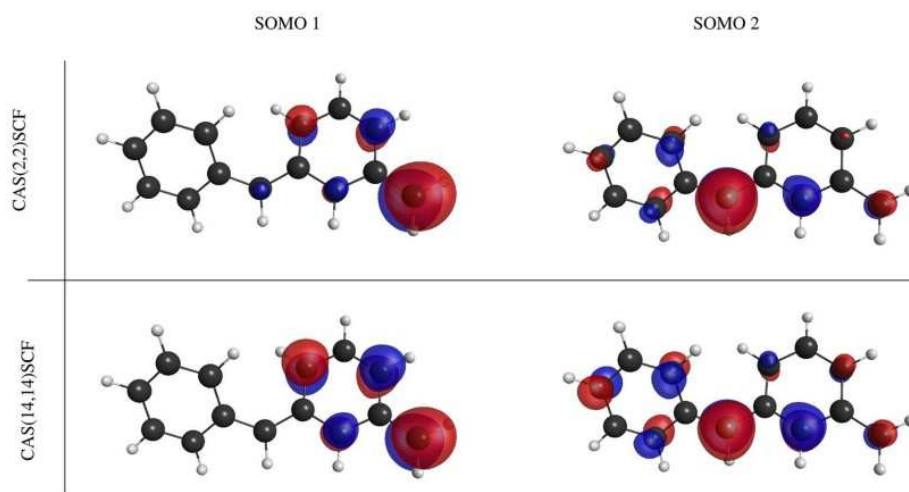

Table 3 Vertical and adiabatic triplet–singlet energy differences, Δ_{vert} and Δ_{adia}, respectively, for the minimum energy structures (2_1–2_4) of compound **2** as predicted by different density functionals and wave function-based methods using the B3LYP-optimized geometries

Structure	Method	Δ_{vert}	Δ_{adia}
2_1	B3LYP	2,737	2,047
	M06-2X	2,610	1,950
	MN12-SX	2,319	1,778
	CAS(2,2)SCF	1,072	655
	MCQDPT	2,512	1,983
	CAS(14,14)SCF	3,499	2,561
2_2	B3LYP	2,168	1,498
	M06-2X	2,017	1,319
	MN12-SX	1,852	1,299
	CAS(2,2)SCF	832	197
	MCQDPT	1,924	1,422
	CAS(14,14)SCF	2,525	1,815
2_3	B3LYP	2,715	2,053
	M06-2X	2,587	1,968
	MN12-SX	2,300	1,752
	CAS(2,2)SCF	1,061	649
	MCQDPT	2,486	1,982
	CAS(14,14)SCF	3,458	2,486
2_4	B3LYP	2,652	1,934
	M06-2X	2,513	1,879
	MN12-SX	2,246	1,689
	CAS(2,2)SCF	1,051	655
	MCQDPT	2,466	1,943
	CAS(14,14)SCF	3,449	2,414

All values are in cm^{-1}. Wave function-based results are obtained using the set of orbitals corresponding to each electronic state

and is the one employed in the larger **2**, **3** and **4** model systems. It is also important to note that the set of molecular orbitals used (MOs) in the MCQDPT calculations is the canonic orbitals of the CAS(2,2)SCF triplet and singlet, respectively. Finally, it is worth pointing out that the above discussion applies equally to the **1₁** and **1₂** minimum energy structures (Table 1).

We now focus the discussion on compound **2**, for which results are summarized in Table 3. As in the previous case, the three different exchange–correlation potentials used yield results that are fairly consistent, and the calculated triplet–singlet gap differs by at most 14 %. Once again, the minimal CASSCF description fails to provide a reliable estimate of the triplet–singlet gap, but the introduction of dynamical correlation out of the minimal space by means of MCQDPT provides values lying in the average value predicted by DFT-based methods. Once more, the extension to the full π valence CAS(14,14)SCF space overestimates the Δ values, confirming that the best strategy for a wave function-based description is provided by a MCQDPT calculation using the CAS(2,2) as reference space. Comparing to compound **1**, the Δ values for the DFT-based methods are in average a 19 % smaller for the case of vertical transitions and a 26 % for the adiabatic ones. This trend is maintained for the case of MCQDPT on top of CAS(2,2)SCF calculations. This observation indicates that another way of decreasing the triplet–singlet gap, and thus approaching the range of magnetic transitions in polycyclic aromatic hydrocarbons with C-centered unpaired electrons, would be the introduction of carefully chosen σ-donating groups directly bonded to the radical center. Finally, **2₁**, **2₃** and **2₄** conformers present the same trend for the Δ values, being **2₂** the

exception with a deviation from the average value for Δ of 20 % in the case of vertical transitions and 25 % for the adiabatic ones.

Table 4 Vertical and adiabatic triplet–singlet energy differences, Δ_{vert} and Δ_{adia}, respectively, for the lowest energy minimum energy structures of compounds **3** and **4** as predicted by different density functionals and wave function-based methods using the B3LYP-optimized geometries

Structure	Method	Δ_{vert}	Δ_{adia}
3₁	B3LYP	3,458	3,084
	M06-2X	3,250	2,720
	MN12-SX	3,000	2,621
	CAS(2,2)SCF	1,221	491
	MCQDPT	3,065	2,755
4₁	B3LYP	2,355	1,994
	M06-2X	2,245	1,841
	MN12-SX	2,065	1,740
	CAS(2,2)SCF	1,090	749
	MCQDPT	2,389	2,067

All values are in cm^{-1}. Wave function-based results are obtained using the set of orbitals corresponding to each electronic state

In view of the trends discussed above for compounds **1** and **2**, we will limit the discussion of the triplet–singlet gap in **3** and **4** to the lowest energy conformer, the differences with respect to the other stable structures being really meaningless. The Δ values for the most stable minima of compounds **3** and **4** are listed in Table 4. They are not reported for the full π valence CAS(14,14)SCF space due to the increasing amount of determinants needed, and because based on the above discussion for compounds **1** and **2**, it is known that these results would overestimate the triplet–singlet gap. Compound **3** presents Δ values similar to the ones of compound **1**, deviating from the decreasing tendency in the triplet–singlet gap in the series of proposed compounds which implies that the substitution of a methyl group in **2** by a of *tert*-butyl group goes in the opposite direction as when introducing the methyl groups in **1** leading to compound **2**. The overall trends are summarized in Fig. 4, displaying the vertical and adiabatic triplet–singlet gaps predicted by the MCQDPT calculations as a function of the dihedral angles θ_1 and θ_2. This figure clearly shows that, in spite of the different nature of the R, R′ and R″ substituents in Scheme 1, the richness of minima showed by the potential energy surfaces can be described by a reduced
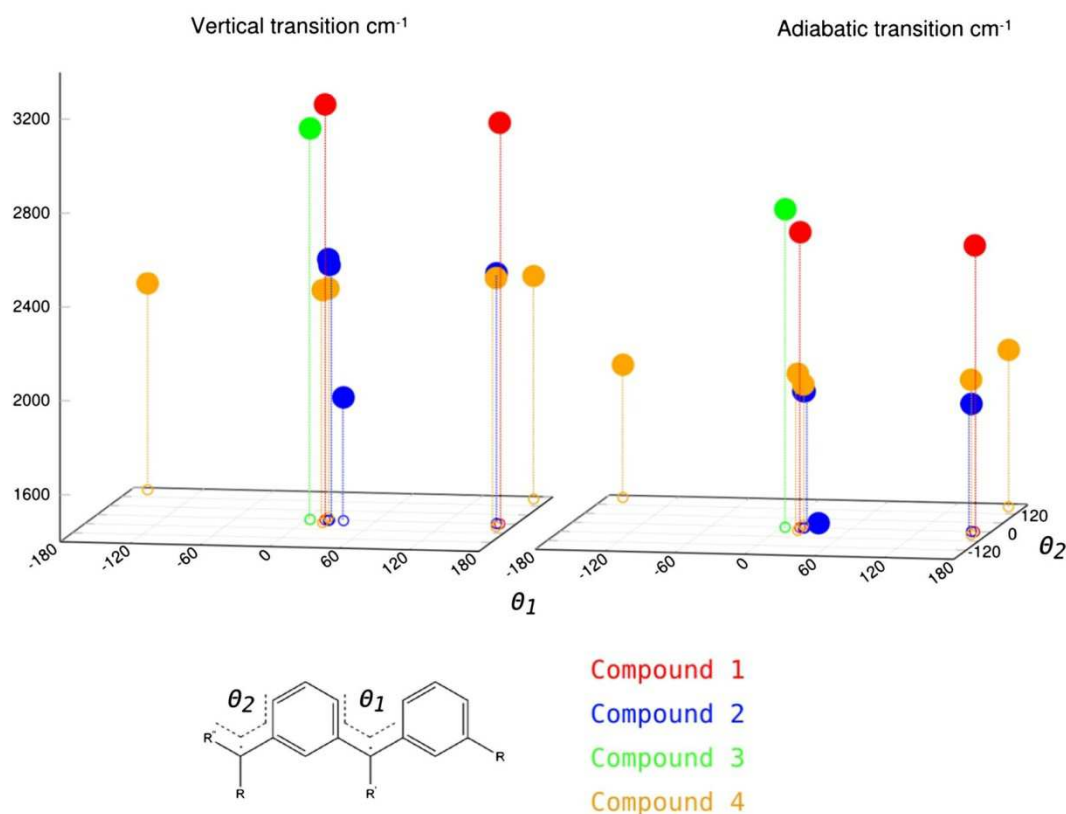

Fig. 4 Schematic representation of the calculated MCQDPT (on top of minimal CAS(2,2)SCF) vertical and adiabatic triplet–singlet gap of compounds **1**–**4** as a function of the dihedral angles θ_1 and θ_2

set of values referred to only two structural parameters, the θ_1 and θ_2 dihedral angles. This represents an important input in a forthcoming study of polymeric radical chains based on these monomers.

Finally it is worth to point out that, as it has already been commented, compound **4** presents the same environment for both of the radical centers, but at the same time introduces a more extended π system. The direct effect is a significant reduction in the triplet–singlet gap, which is evident in Fig. 4. Note also that the trends predicted by DFT and wave function-based methods are similar to those commented for the rest of compounds. Thus, the DFT-based methods yield values that are very similar among each other and to the MCQDPT result on top of the minimal CASSCF calculation. Compound **4** already allows one to imagine the possible conformations that a hypothetic polymer would display, and the importance of the relative position of the phenyl rings in order to predict a linear, helical or any other disposition in the 3D growth of the sought polymer. A study on these issues is currently being carried out in our group.

4 Conclusions

In this work, a series of four compounds chosen to model the star-branched and dendritic structures experimentally characterized by Rajca [9] has been studied by different theoretical methods, the focus being on the richness of structures in their ground state (triplet) potential energy surface and on the triplet–singlet gap. At the DFT level, the B3LYP, M06-2X, MN-12SX functionals were explored, whereas wave function methods include minimal CAS-SCF followed by second-order MCQDPT. In some cases, the full π valence CASSCF has also been explored. In light of the preceding discussion, several conclusions can be extracted, which are listed below.

- There are no stable planar structures of these compounds, which has implications when considering possible polymeric chains.
- The corresponding potential energy surface of these compounds exhibits many low-lying local minima that can be described by only considering the θ_1 and θ_2 dihedral angles. This represents an important input in a forthcoming study of polymeric radical chains based on these monomers, since it reduces drastically the difficulty of choosing the relative position of the phenyl rings in the growth of the polymer.
- The B3LYP, M06-2X and MN12-SX density functionals predict very similar structures for the proposed models, being all of them able to find the several minima of the potential energy surface for each compound.

- Single-point MCQDPT calculations using a minimal CASSCF reference space at the B3LYP-optimized geometries appear to be the best strategy to estimate the triplet–singlet gap in this kind of compounds with wave function-based methods, which is consistent with previous work on *m*-xylylene [15].
- For a given compound, the magnitude of triplet–singlet gap predicted by both DFT and wave function-based methods does not depend significantly on the minimum energy structure chosen to carry out the calculation.
- The triplet–singlet gap predicted by both DFT and wave function-based methods indicates that it is possible to tune this property by appropriate choice of substituents which opens the possibility to keep decreasing the triplet–singlet gap in these high-spin ground state compounds to the limit of entering magnetic transitions.

Therefore, the conclusions from this work, even if based on a limited set of model systems, provide a basis for subsequent studies aimed at predicting polymers exhibiting high-spin ground state, a project that is now under development in our group.

References

1. Kahn O (1993) Molecular magnetism. VCH, New York
2. Zener C (1951) Phys Rev 81:440
3. Zener C (1951) Phys Rev 82:403
4. Shultz DA, Kumar RK (2001) J Am Chem Soc 123:6431
5. Longuet-Higgins HC (1950) J Chem Phys 18:3
6. Ovchinnikov AA (1978) Theor Chim Acta 47:297
7. Borden WT, Davidson ER (1977) J Am Chem Soc 99:4587
8. Lineberger WC, Borden WT (2011) Phys Chem Chem Phys 13:11792
9. Rajca A (1994) Chem Rev 94:871
10. Rajca A, Olankitwanit A, Rajca SJ (2011) Am Chem Soc 133:4750
11. Rajca A, Olankitwanit A, Wang Y, Boratynski PJ, Pink M, Rajca S (2013) J Am Chem Soc 135:18205
12. Sun Z, Zeng Z, Wu J (2014) Acc Chem Res. doi:10.1021/ar5001692
13. Li Y, Huang KW, Sun Z, Webster RD, Zeng Z, Zeng W, Chi C, Furukawa K, Wu J (2014) Chem Sci 5:1908
14. Datta SN, Trindle CO, Illas F (2014) Theoretical and computational aspects of magnetic organic molecules. Imperial College Press, World Scientific Publishing, London. ISBN 978-1-908977-21-2
15. Ma eru DR, Pal KP, Moreira I de PR, Datta SN, Illas F (2014) J Chem Theory Comput 10:335

16. Li S, Ma J, Jiang Y (1997) J Phys Chem A 101:5567
17. Ma H, Liu C, Zhang C, Jiang Y (2007) J Chem Phys A 111:9471
18. Zhang G, Li S, Jiang Y (2003) Tetrahedron 59:3499
19. Barone V, Cacelli I, Ferreti A, Monti S, Prampolini G (2011) J Chem Theory Comput 7:699
20. Barone V, Boilleau C, Cacelli I, Ferreti A, Prampolini G (2013) J Chem Theory Comput 9:1958
21. Barone V, Boilleau C, Cacelli I, Ferreti A, Monti S, Prampolini G (2013) J Chem Theory Comput 9:300
22. Rajca A, Olankitwanit A, Rajca S (2011) J Am Chem Soc 133:4750
23. Rota J-B, Le Guennic B, Robert V (2010) Inorg Chem 49:2010
24. Pal AK, Datta SN (2014) J Phys Chem C 118:27599
25. Becke AD (1993) J Chem Phys 98:5648
26. Peverati R, Truhlar DG (2012) Phys Chem Chem Phys 14:16187
27. Ditchfield R, Hehre WJ, Pople JA (1971) J Chem Phys 54:724
28. Hehre WJ, Ditchfield R, Pople JA (1972) J Chem Phys 56:2257
29. Clark T, Chandrasekhar J, Spitznagel GW, Schleyer PVR (1983) J Comput Chem 4:294
30. Noodleman L (1981) J Chem Phys 74:5737
31. Noodleman L, Davidson ER (1986) J Chem Phys 109:131
32. Noodleman L, Peng CY, Case DA, Mouesca JM (1995) Coord Chem Rev 144:199
33. Caballol R, Castell O, Illas F, Malrieu JP, Moreira I de PR (1997) J Phys Chem A 101:7860
34. Yamaguchi K, Takahara Y, FuenoT, Nasu K (1987) Jpn J Appl Phys 26:L1362
35. Yamaguchi K, Jensen F, Dorigo A, Houk KN (1988) Chem Phys Lett 149:537
36. Yamaguchi K, Takahara Y, Fueno T, Houk KN (1988) Theor Chim Acta 73:337
37. Shao Y, Head-Gordon M, Krylov AI (2003) J Chem Phys 118:4807
38. Wang F, Ziegler T (2004) J Chem Phys 121:12191
39. Krylov AI (2005) J Phys Chem A 109:10638
40. Levine BG, Ko C, Quenneville J, Martinez TJ (2006) Mol Phys 104:1039
41. Valero R, Illas F, Truhlar DG (2011) J Chem Theory Comput 7:3523
42. Hirao K (1992) Int J Quantum Chem S26:517
43. Hirao K (1992) Chem Phys Lett 196:397
44. Hirao K (1992) Chem Phys Lett 190:374
45. Hirao K (1993) Chem Phys Lett 201:59
46. Andersson K, Malmqvist P- , Roos BO, Sadlej AJ, Wolinski K (1990) J Phys Chem 94:5483
47. Andersson K, Malmqvist P- , Roos BO (1992) J Chem Phys 96:1218
48. Moreira I de PR, Illas F (2006) Phys Chem Chem Phys 8:1645
49. Datta SN, Pal AK, Hansda S, Illas F (2013) J Phys Chem A 117:1773
50. Bofill JM, Quapp W (2011) J Chem Phys 134:074101
51. Suaud N, Ruamps R, Guih ry N, Malrieu JP (2012) J Chem Theory Comput 8:4127
52. Angeli C, Calzado CJ (2012) J Chem Phys 137:034104

Before closing the discussion on structurally flexible diradicals, it might be interesting to add the following remarks on a similar triradical molecule.

Consider the molecule depicted in Figure 4.3.3. It can be seen as the next step towards infinite polymers and it guides the discussion presented in paper #4.5. It is an example of three electrons in three centres problem, as the one extensively treated in chapter 3, section 3.4.2. However, here we are not concerned with the mapping approach, and for the purpose of the discussion, we assume as valid the coupling constants extracted by means of density functional calculations.
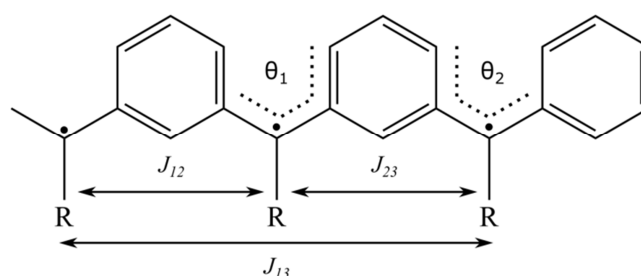
Figure 4.3.3. Schematic representation of the molecule under study (R = H), together with the relevant three exchange coupling constants and two structural parameters.

Following the computational strategy established in paper #4.3, all calculations are performed with the Gaussian-09 suite of programs, using the standard 6-311g(d,p) basis set. Its molecular geometry for the quartet state was optimized using the popular B3LYP hybrid functional. Six different minima were located on the potential energy surface for the quartet state (high-spin). All of them were characterized by calculation the frequencies. At each of the conformations, single point calculations using a variety of density functionals, were performed to extract the magnetic exchange interactions on each local minima. The discussion and the required equations to extract them can be found in section 3.2.1. $S_1 = S_2 = S_3 = 1/2$ trimers of chapter 3, and it will not be repeated again here.

Table 4.3.3.a summarizes the dihedral angles for the six different local minima and the extracted coupling constant values predicted with three different functional. As observed in paper #4.3, the variety of conformers can be described with a reduced set of structural parameters referred to only two dihedral angles. For the purpose of this brief discussion it is worth noting that no matter the adopted conformation, the ground state is the high-spin state ($J > 0$) the coupling constant values remain similarly large. This is in

sharp contrast with what is found in papers #4.1, #4.4 and #4.6, in which structural distortions have a large impact on the magnitude and sign of the coupling constant.

		1	2	3	4	5	6			
	Θ_1	-18.7	-18.0	-18.2	17.4	-164.6	-165.0			
	Θ_2	17.1	-16.4	-16.4	165.5	-166.5	166.7			
		(cm^{-1})							J_{23}/J_{12}	J_{13}/J_{12}
B3LYP	J_{12}	3456	3438	3405	3379	3409	3403			
	J_{23}	2404	2391	2374	2433	2409	2363		0.70	-0.02
	J_{13}	-80.0	-79.2	-86.2	-86.5	-87.6	-86.4			
M062X	J_{12}	3276	3257	3245	3218	3228	3225			
	J_{23}	2270	2264	2248	2313	2295	2256		0.69	-0.02
	J_{13}	-75.0	-74.8	-81.6	-82.6	-84.1	-83.5			
MN12SX	J_{12}	3003	2985	2950	2930	2964	2955			
	J_{23}	2079	2047	2034	2103	2049	2019		0.69	-0.02
	J_{13}	-57.6	-56.7	-62.7	-63.7	-63.0	-64.4			

Table 4.3.3.a Summary of structural parameters (dihedral angles) in the six different local minima characterized (1-6). Magnetic coupling constants (cm^{-1}) at each minimum as predicted with different functional. The rightmost column indicates the relationship between J values in minimum 1, but it is similar in the rest of the geometries.

Additionally, at the quartet minimum predicted by the B3LYP functional, wave function-based calculations were performed to estimate the energetic difference between the three pure spin states, as indicated in Table 4.3.3.b. As discussed in section 3.3. and paper #3.2 of chapter 3, only these values do not provide a way of extracting the three magnetic coupling constants, but one could make use of the constant relationship found for the DFT calculated values (rightmost columns in Table 4.3.3.a), to simplify the spectrum. However, as it was shown in section 3.3 of chapter 3, the agreement between the relationships calculated by means of DFT and effective Hamiltonian theory is not very good, indicating a large delocalization of some BS solutions.

cm^{-1}	ΔE_{Q-D_1}	ΔE_{Q-D_2}
CAS(33)CI	-881	-2751
CAS(33)SCF	-750	-1955
CAS(33)+DDCI	-789	-2432

Table 4.3.3.b. Energy difference values (cm^{-1}) between pure spin states as predicted by the minimal complete active space

4.3.4.   Paper #4.4.

Exchange Coupling Reversal in a High-Spin Organic Triradical Single-Molecule Device

Exchange coupling inversion in a single high-spin organic triradical molecule

R. Gaudenzi,[1] E. Burzurí,[1] D. Reta,[2] I. de P. R. Moreira,[2] S. T. Bromley,[2] C. Rovira,[3] J .Veciana,[3] and H. S. J. van der Zant[1]

[1] *Kavli Institute of Nanoscience, Delft University of Technology, 2628 CJ, Delft, The Netherlands*

[2] *Departament de Química Física and Institut de Química Teórica i Computacional, Universitat de Barcelona (IQTCUB), E-08028 Barcelona, Spain*

[3] *Institut de Ciéncia de Materials de Barcelona (ICMAB-CSIC) and CIBER-BBN, Campus de la UAB, 08193, Bellaterra, Spain*

The magnetic properties of a nanoscale system are inextricably linked to its local environment. Among others, in ad-atoms and inorganic layered structures the exchange interactions result from relative lattice positions, thicknesses and other environmental parameters. Here, we report on a sample-dependent large variation and sign inversion of the magnetic exchange coupling between the three unpaired spins of an organic triradical molecule embedded in a three-terminal solid-state device. The ferro-to-antiferromagnetic transition is due to structural distortions induced by the environment of the solid-state device and results in a high-to-low spin ground state change in a molecule traditionally considered as a robust high-spin quartet. We further show electric tunability of the exchange coupling via the gate electrode. These findings, in accordance with theoretical calculations, help to better understand organic molecule-based materials and may lead to new pathways to control magnetism of individual molecules at the nanoscale.

Magnetism at the nanoscale is often determined by the local environment: the sensitivity of the exchange coupling to the spatial arrangement and its dependence on the interactions between sandwiching layers, spin interfaces, ligands, neighbouring atoms or substrate is well-established. In most cases, these interactions lead to an increase or decrease of the strength of the local magnetism[1–6]. Of special interest is the situation in which the sign of the exchange interaction reverses, leading to a transition from ferromagnetic to antiferromagnetic coupling (or vice versa). Altering the relative positions of the atoms in Fe dimers[7] or varying the thickness of the interlayer in Fe/Cr/Fe structures[8,9] can, for instance, trigger such an inversion.

Owing to their intrinsic flexibility, single molecules form an interesting system to control this exchange reversal. In addition, as building blocks of molecule-based materials, knowledge on variations of the magnetic properties at the individual-molecule scale reveals effects that might go unseen in bulk. A previous work reports variations of the spin excitation energies in single molecules on metallic surfaces[3], but a ferro-to-antiferromagnetic exchange coupling inversion has never been demonstrated.
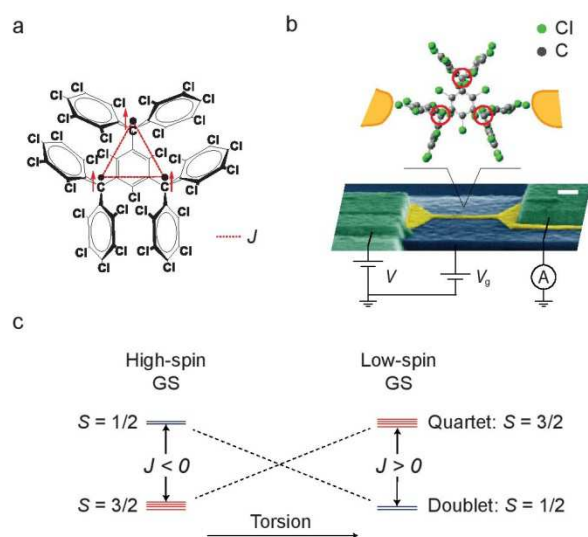

FIG. 1. **The molecule, the device and the exchange coupling inversion mechanism.** (a) Molecular structure of a triradical organic molecule with a C_2 symmetry: the three radical centers, located on the three methyl carbon atoms, are each surrounded by three twisted perchlorinated phenyl rings. The three unpaired electrons are coupled through an exchange interaction, J, schematically represented by red dashed lines. (b) Scanning-electron-microscope micrograph (100-nm scale bar, false color) of the gold nanowire on a AuPd/Al$_2$O$_3$ gate. The molecular junction is created with the molecule bridging the nanogap formed during electromigration. (c) Schematics of the exchange coupling sign flipping mechanism: a torsion applied to the molecule increases the exchange coupling from negative (ferro-) to positive values (anti-ferromagnetic) through zero inducing a change from the $S = 3/2$ high-spin ground state (GS) to a $S = 1/2$ low-spin ground state.

In view of molecular spintronics applications, such a phenomenon is of particular interest in high-spin all-organic molecules - in which magnetism is not connected to the presence of metal ions[10–13] - because of their favorable spin lifetimes[14].

Here, via inelastic electron tunneling spectroscopy (IETS), we map the magnetic states of individual neutral and stable organic triradical molecules. The all-organic molecule of our study exhibits, in solution, a strong fer-
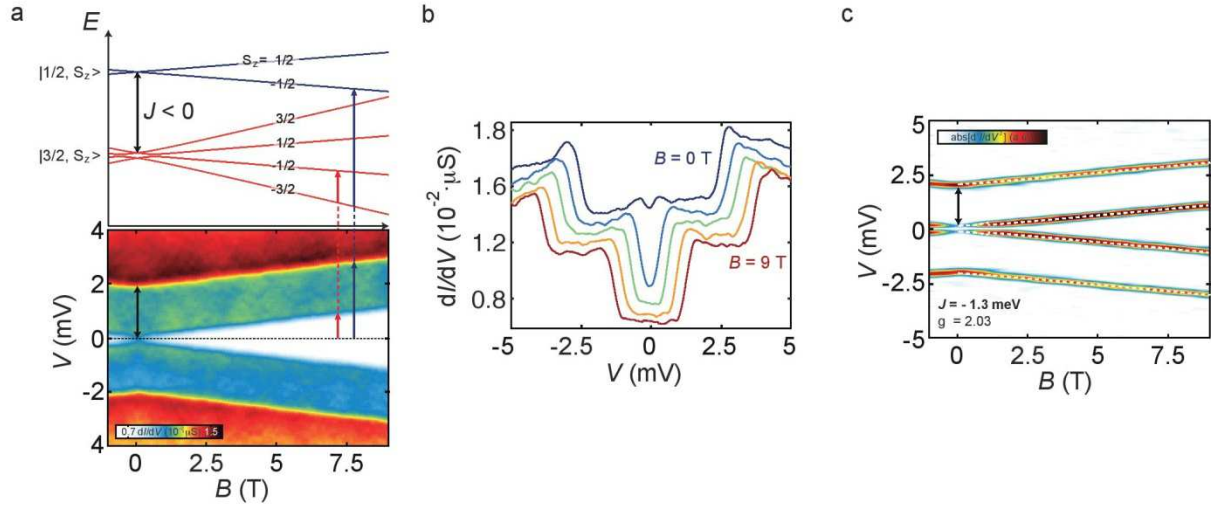
FIG. 2. **Ferromagnetic exchange coupling** J. (color online) (a) dI/dV map (below) measured on sample A as a function of bias voltage and magnetic field. The energy splitting between the low- and the high-energy step is constant in magnetic field and marked by a black double arrow. Above, the energy level scheme of a spin-3/2 system with a ferromagnetic exchange coupling ($J < 0$) and a small anisotropy parameter ($D = 0.06$ meV) as a function of magnetic field. Red and blue arrows indicate the allowed first-order spin-flip processes with $\Delta S_z = \pm 1$ to which the observed steps in dI/dV are ascribed. (b) dI/dV spectra extracted from the map in (a) with a spacing of $\Delta B = 1.8$ T starting from 0 T (offset for clarity). The low-energy excitation exhibits a zero-field splitting of about 0.1 meV. (c) Absolute value $|d^2I/dV^2|$ of the map in (a). The dashed lines superimposed to the experimental data are the fit to the Hamiltonian of equation(1) with $J = -1.3$ meV ($E(|Q\rangle) - E(|D\rangle) = 3/2J$) and $g = 2.03$. The zero-field spitting is clearly visible. All measurements are taken at $T \approx 70$ mK.

romagnetic exchange interaction between its three unpaired electrons. Through the observation of distinct magnetic spectra in different samples, we infer that the exchange coupling significantly decreases in magnitude and can even turn antiferromagnetic when the molecule is embedded in a solid-state device. We attribute the reduction and the sign reversal to small deformations induced by the local environment of the junction and support this hypothesis with theoretical calculations. The analysis demonstrates that the distortions only modify the exchange but not the robust radical character of the three centers, in agreement with previous studies on monoradicals[13].

We use a 2,4,6-hexakis(pentachlorophenyl) mesityltriyl radical molecule[15,16] sandwiched between two gold leads to construct our molecular junction, as schematically depicted in Fig. 1b (see Methods for additional information on the molecule and the junction preparation). The molecule, shown in Fig. 1a, is a neutral triradical with three unpaired electrons on the three methyl carbon atoms. Each one of these atoms, with three chlorinated phenyl rings surrounding it in a propeller-like conformation, forms one of the three elementary radical subunits. The central mesitylene ring is common to the three subunits and is used to magnetically interconnect them. Two of the propellers have the same sense of rotation while the third rotates with an opposite sense, conferring the molecule a C_2 symmetry. Owing to

this architecture and particular orbital topology[17–19], the three radical electrons lie in three distinct non-disjoint, quasi-degenerate, non-bonding singly-occupied molecular orbitals (SOMOs) exhibiting a strong exchange interaction. Previous experiments[15] have demonstrated a robust high-spin quartet ($S_Q = 3/2$) ground state with a low-spin doublet ($S_D = 1/2$) excited state well-separated in energy ($|E(|Q\rangle) - E(|D\rangle)| \gg k_B T$). This characterization is, however, performed in the solid state (crystal) and frozen solution, where the molecules adopt the thermodynamically most stable conformation with a C_2 symmetry.

Electron transport spectroscopy on sample A is presented in Fig. 2 as a function of bias voltage and magnetic field B. Four well-defined conductance steps, symmetrically placed at positive and negative bias, are visible in the dI/dV color map of Fig. 2a and extracted spectra in Fig. 2b. The low- and high-energy steps are located around ± 0.1 meV and ± 2 meV at $B = 0$ T and shift linearly and parallel to each other as the magnetic field is increased. The small low-bias step visible at $B = 0$ T signals the presence of a small zero-field splitting (≈ 0.15 meV). Each finite bias step is associated with the opening of an inelastic electron current channel via an excited state of the molecule. When spin excited states are involved, the steps' position in energy as a function of magnetic field provides a means to read out the molecule's energy spectrum. In the present case, the spectrum is
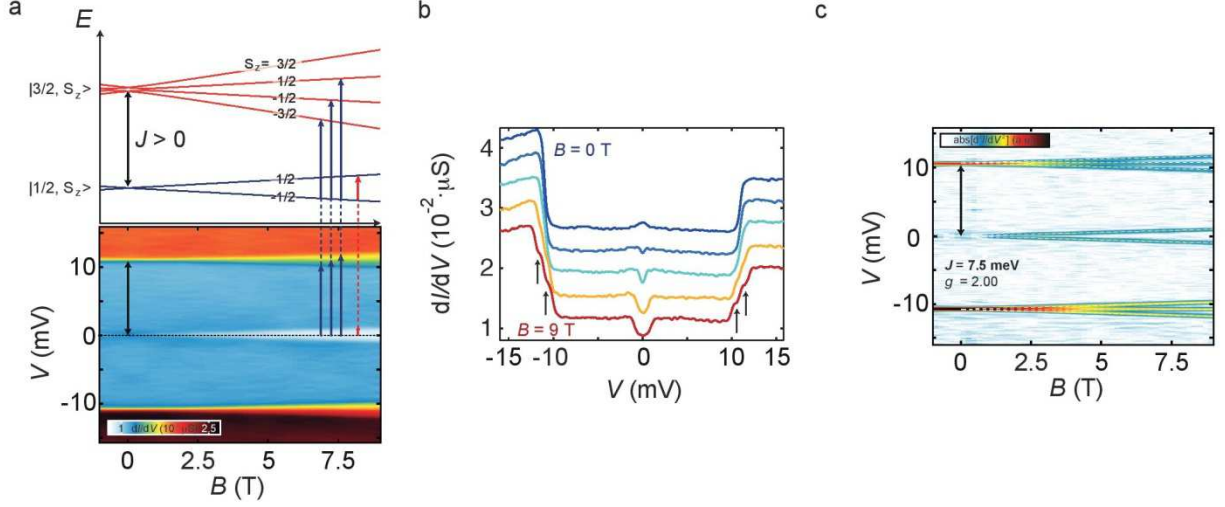
FIG. 3. **Anti-ferromagnetic exchange coupling** J. (color online) (a) dI/dV map measured on sample B as a function of bias voltage and magnetic field. A zero-bias peak and a step are visible at zero magnetic field. At high fields the high energy step is split into three smaller steps, with negative, zero and positive slopes. The upper panel shows the energy level scheme of a spin-3/2 system with an antiferromagnetic exchange coupling ($J > 0$) and a small anisotropy parameter ($D = 0.06$ meV). The colored arrows indicate the allowed processes with $\Delta S_z = 0, \pm 1$ associated with the observed spectrum. (b) dI/dV spectra extracted from the map in (a) with a spacing of $\Delta B = 1.8$ T between 0 T and 9 T (offset for clarity). As the magnetic field increases, the zero-bias peak splits and the two additional steps appear in correspondence of the single step (black arrows). (c) Absolute value $|d^2I/dV^2|$ of the map in (a) with the fit to equation (1) superimposed (dashed lines). The splitting of the zero-bias peak and higher-energy excitation in three smaller staircase-like excitations is clearly visible. The extracted fitting parameters are $J = 7.5$ meV and $g = 2.0$. All measurements are taken at $T \approx 70$ mK.

composed of the eigenstates $|\mathbf{S}, S_z\rangle$ of the spin Hamiltonian:

$$\hat{\mathcal{H}} = \frac{J}{2}\left(\mathbf{S}^2 - \sum_{i=1}^{3}\mathbf{S}_i^2\right) + g\mu_B B_z S_z, \qquad (1)$$

where $\mathbf{S}_i$ denotes the 1/2-spin vectors of the three radical electrons, $\mathbf{S} \equiv \sum_{i=1}^{3}\mathbf{S}_i$ and S_z the total spin and spin projection operators, respectively. The second-order spin excitations induced by the tunneling electrons obey the selection rules $\Delta S_z = 0, \pm 1$. Within this framework, we can respectively assign the low- and high-bias steps seen in Fig. 2a (bottom) to the two spin transitions $|3/2, -3/2\rangle \rightarrow |3/2, -1/2\rangle$ and $|3/2, -3/2\rangle \rightarrow |1/2, -1/2\rangle$ between states of the molecular spectrum in Fig. 2a (top). The former transition takes place within the spin-3/2 ground state multiplet and approaches therefore zero energy at vanishing magnetic fields; the latter transition, on the other hand, involves an excited state belonging to the higher spin-1/2 multiplet and converges to a finite energy at $B = 0$ T.

In Fig. 2c the absolute value $|d^2I/dV^2|$ of the map in Fig. 2a is shown. The dashed line is a fit to the exchange Hamiltonian in equation (1) with an exchange coupling $J = -1.3$ meV and gyromagnetic ratio $g = 2.03$. This negative (ferromagnetic) J favors the high-spin quartet $|3/2, S_z = \pm 3/2, \pm 1/2\rangle$ over the low-spin doublet $|1/2, S_z = \pm 1/2\rangle$. The allowed transitions involve there-

fore $\Delta S_z = \pm 1$, giving rise to the two inelastic steps in the spectrum that increase linearly with magnetic field. A weak non-linearity of the low- and high-bias step evolution for fields $B < 0.5$ T is visible. This can be accounted for by adding a small anisotropy parameter to the spin Hamiltonian of equation (1).

On this sample gate-dependent measurements have also been performed and are shown in figure S1 of the supplementary material. Throughout the entire accessible gate range no sign of resonant transport is seen. This suggests a large SOMO-SUMO (also named SOMO-LUMO-β) gap and supports charge neutrality. While no resonant transport is visible, we observe that an increase in gate voltage results in a sizeable increase of the exchange coupling. This electric field-induced modulation of J amounts to a 9% of its total value. We further note that two other measured samples show a similar set of transitions (see supplementary material). The extracted exchange coupling constants are in those cases $J = -2.2$ meV and $J = -2.3$ meV.

A second group of samples showed a markedly different set of spin transitions and magnetic field evolution. The characteristics are summed up for sample B in Fig. 3. The color map in Fig. 3a displays the dI/dV as a function of bias voltage and magnetic field. A small zero-bias peak and two symmetric conductance steps at about ± 11 meV are visible at $B = 0$ T. The zero-bias peak evolves into
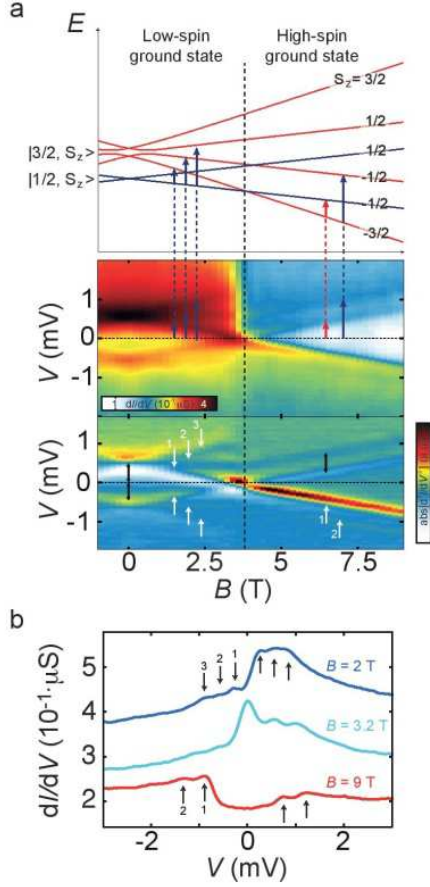
FIG. 4. **Magnetic field control over the ground state.** (color online) (a) dI/dV map (center) measured on sample C as a function of V and B. At low magnetic fields three conductance excitations (indicated by numbers) split in magnetic field. The positive and negative-bias ones numbered 1 cross at $B \approx 3.2$ T (black dashed line). For $B > 3.2$ T, the three lines merge into two steps. The constant energy splitting between the low- and high-energy step is marked by black arrows in the d^2I/dV^2 map (below). Above, the energy diagram of a spin-3/2 system with an antiferromagnetic exchange coupling ($J > 0$) and a small anisotropy parameter as a function of magnetic field. A negative but small J favors the low-spin doublet at low magnetic fields and the high-spin quartet at high magnetic fields. Red and blue arrows indicate the spin-flip processes with $\Delta S_z = 0, \pm 1$. (b) dI/dV spectra extracted from the map in (a) at $B = 2, 3.2$ and 9 T (offset for clarity). The three steps (arrows 1, 2 and 3) present for values $B < 3.2$ T evolve into two steps (arrows 1 and 2) for $B > 3.2$ T.

two steps for increasing magnetic fields and the single high-bias step splits in three smaller steps. The three-fold excitation can be more readily seen in Fig. 3b (black arrows) and Fig. 3c. This last feature is not compatible with the spin-3/2 ground state observed in sample A and indicates a ground state spin $S < 3/2$ together with a

excited multiplet with $S + 1 \leq 3/2$ (either $S = 1/2$ or 0).

The presence of the zero-bias peak and its doublet-like magnetic field evolution indicate a $S = 1/2$ ground state. The energy spectrum corresponding to this case is displayed in Fig. 3a (top). The low-bias step is ascribed to the transition $|1/2, -1/2\rangle \rightarrow |1/2, 1/2\rangle$ within the spin-1/2 ground state multiplet; the high-bias ones are associated with the three allowed transitions to the spin-3/2 multiplet $|1/2, -1/2\rangle \rightarrow |3/2, S_z\rangle$, with $S_z = \{-3/2, -1/2, 1/2\}$, where the selection rule $\Delta S_z = 0$ also applies. Selected spectra extracted from Fig. 3a at different fields are displayed in Fig. 3b. The zero-bias peak is clearly visible in the trace at zero magnetic field. The peak evolves into a dip at $B \approx 1.8$ T and opens up into two inelastic steps at higher fields. The observed weak zero-bias peak is consistent with the presence of Kondo correlations between one of the SOMO unpaired electrons of the spin-1/2 ground state and the electrons in the leads.

Taking the absolute value of the derivative of the map in Fig. 3a, we obtain the $|\mathrm{d}^2I/\mathrm{d}V^2|$ map of Fig. 3c. The splitting with magnetic field in two and three distinct steps of the low- and high-energy excitations respectively is clearly visible. Superimposed we show the result of a fit to equation (1), from which a magnetic exchange coupling $J = 7.5$ meV and $g = 2.0$ are extracted. We have observed a similar magnetic field dependence in two other samples with magnetic exchanges of $J = +3.0$ meV and $J = +0.4$ meV (sample C, shown in Fig. 4). Thus, In these samples, in contrast to sample A, the exchange coupling J is antiferromagnetic (positive) and stabilizes the low-spin doublet over the high-spin quartet.

Measurements in gate performed on sample B are shown in figure S1 of the supplementary material. No sign of charging and resonant transport are present. Analogously to sample A, this indicates a large gap and supports charge neutrality. The electric field-induced modulation of J amounts here to a 2% of its total value.

Figure 4 shows the results of a measurement on sample C displaying an intermediate scenario between the ones observed in sample A and B. The dI/dV and corresponding $|\mathrm{d}^2I/\mathrm{d}V^2|$ color maps of Fig. 4(a) exhibit two conductance steps centered around $\approx \pm 0.55$ meV at $B = 0$ T. For magnetic fields below 3.2 T the steps at positive and negative bias split each into three excitations with positive, zero and negative slopes (numbered 1, 2 and 3 in the $|\mathrm{d}^2I/\mathrm{d}V^2|$ map and the dI/dV linecut of Fig. 4(b)). The two excitations 1 in the positive and negative bias region intersect at $V = 0$ V and $B \approx 3.2$ T (dashed line in Fig. 4(a)). For $B > 3.2$ T only two of the three excitations survive. The zero-bias one emerges as a prosecution of excitation 1 with the same slope, while the finite-bias one continues from 2 with a different slope. The energy difference between the two steps is constant with magnetic field and amounts to ± 0.55 meV. It is important to notice that this value equals the energy of the excitation at zero magnetic field (black arrows in the map of Fig. 4(a)(bottom)). Following the
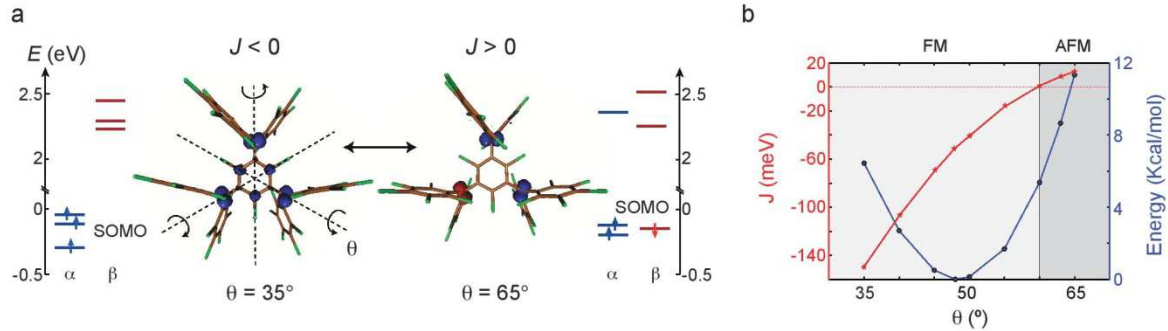
FIG. 5. **Modelling orbitals energies and magnetic exchange coupling.** (color online) (a) Energy level diagram, molecular structure and spin density isosurfaces for two distinct torsion angles θ. A torsion applied to the three peripheral groups with respect to the central ring promotes the flip of one the spins (rightmost diagram) and a further concentration of the spin density onto the orbitals of methyl carbon atoms. (b) Energy and exchange coupling vs. angle θ plot. At the potential energy minimum ($\theta = 47°$) the ferromagnetic exchange energy exceeds room-T. Increasing (decreasing) the torsion angle results into an decrease (increase) of $|J|$ and ultimately to the reversal of its sign.

energy level scheme of Fig. 4(a), the three excitations in the low-field region ($B < 3.2$ T) of the plot are associated with the transitions $|1/2, -1/2\rangle \rightarrow |3/2, S_z\rangle$, with $S_z = \{-3/2, -1/2, 1/2\}$. The low- and high-bias ones in the high-field side ($B > 3.2$ T) are ascribed to the transitions $|3/2, -3/2\rangle \rightarrow |3/2, -1/2\rangle$ and $|3/2, -3/2\rangle \rightarrow |1/2, -1/2\rangle$ respectively. A change from low- to high-spin ground state thus occurs at the crossing point of the two regions ($B = 3.2$ T).

The set of transitions featured in this sample C can be explained with a positive, but small ($J \sim g\mu_B B$) exchange coupling J. This antiferromagnetic coupling favors the low spin state, but only up to a magnetic field equal to $\approx \frac{2}{3}J/g\mu_B$. For higher fields a spin-1/2 to spin-3/2 ground state flip occurs, with a consequent change in the excitation spectrum. Owing to the small J, the magnetic field provides thus a means to effectively control the magnetic ground state. Importantly, the spectra of samples A and B are therefore shown to be connected exclusively via a magnetic field change, with no need for oxidation/reduction of the molecule.

The data show that different samples of the same neutral individual triradical molecule in an electromigrated junction yield values of J spanning from -2.3 meV to $+7.5$ meV, in contrast to the robust value $J \leq -40$ meV obtained from the same molecule in frozen solution[15]. Excluding charging effects on the basis of the gate measurements and large calculated SOMO-SUMO gap, we argue that the local environment of the junction is responsible for the reduction and sign change of J. The mechanism we propose relies on a molecular distortion induced on the molecule by the electrodes. In particular, we argue that the dihedral angle θ (Fig. 5(a) and supplementary material), which defines the relative position of the six peripheral rings with respect to the central one, determines the exchange and depends on the specific arrangement of the molecule between the electrodes, thus giving rise to the observed sample to sample vari-

ation. To test this hypothesis we perform unrestricted DFT-based calculations based on the broken symmetry approach[20-24] for different dihedral angles θ. The J-value at each step is extracted from the energy difference between the high-spin and the broken symmetry solution approaching the spin adapted doublet state (See supplementary materialfor details on the calculations and explicit definition of the dihedral angle).

Spin-unrestricted molecular orbitals and magnetic exchange values resulting from the calculations are shown in Fig. 5. At low angles ($\theta = 35°$) the three spin-up SOMOs present a large energetic separation from the excited LUMO$-\beta$ orbitals. The non-disjoint[19] and near-degenerate character of these SOMOs is at the origin of the preferential high-spin GS. The spin density associated to this configuration is distributed on each of the three radical centers with a remarkable participation on the central phenyl ring. This through-bond delocalization of the unpaired electrons on the central ring determines the large exchange integral contributing to the stabilization of the high spin quartet. The delocalization over the central ring is progressively cut off as a torsion is applied and the dihedral angle increased. At high angles ($\theta = 65°$ is taken here as an example) the spin density on the central ring is completely suppressed and the orthogonality of the SOMOs compromised. The resulting large orbital overlap term favors electron pairing over the unpairing due to the exchange integral, yielding the observed positive (AFM) exchange coupling.

Energy cost and exchange coupling as a function of θ are reported in Fig. 5(b). The most thermodynamically stable conformation, obtained for $\theta = 47°$, is associated with a strong FM interaction. The calculated value ($|J| \approx 40$ meV $> k_bT$, with $T = 300$ K) is consistent with the high-spin ground state observed in room-T measurements on the molecule in frozen solution[15]. J monotonically increases for higher angles and the crossover to an AFM coupling is observed at $\theta = 60°$ at an energetic

cost of only ~ 5 Kcal/mol. The observed tunability of J with gate voltage can also be explained through this model. Provided unequal distances between the three radical electronic orbitals and the gate electrode, the electrostatic force can generate a net torque on the molecule. The torque can consequently result into a change in θ.

This model likely presents a simplified picture of the high complexity inherent to the molecule-electrodes coupled system where other kinds of distortions away from the thermodynamically most stable conformation may occur. Despite its simplicity, the model clearly demonstrates that non-destructive torsions applied to such polyradicals can lead to an inversion of the sign of the exchange coupling. Furthermore, the knowledge of this mechanism opens a pathway to the chemical, mechanical and electrical control of the reversal of magnetic states in individual as well as ensembles of these molecules. For instance, the steric hindrance of the substituents can be engineered to stabilize the antiferromagnetic frustrated configuration in a single molecule.

In summary, we demonstrate that an individual high-spin all-organic triradical molecule in a junction exhibits changes in its exchange coupling between FM and AFM, while maintaining chemical integrity and charge neutrality. The change and sign inversion show, as supported by theory, that at the nanoscale the preference for the high-spin vs. low-spin ground state is not only dictated by the peculiar orbital topology arguments but also by molecular distortions imposed by the surrounding environment. Furthermore, external electric and magnetic fields may effectively control the J-value and its magnetic ground state. These results contribute to the understanding of the influence of the environment on the magnetic properties of molecule-based organic materials and open the way to the control of the magnetic ground states of flexible polyradicals for future molecular spintronics applications.

Methods

Molecule. The studied molecule is the diasteromeric form with a C_2 symmetry of 2,4,6-trichloro-$\alpha,\alpha,\alpha',\alpha',\alpha'',\alpha''$-hexakis(pentachlorophenyl)mesityltriyl radical, prepared as previously reported[15].

Junction preparation. The molecular junction is created starting from a thin gold nanowire which is subsequently electromigrated and let self-break at room temperature in the molecular solution (0.1 mM), as described elsewhere[5]. The nanowire is evaporated on top of an Al/Al_2O_3 acting as a capacitively-coupled gate electrode and insulator. In the present study, six so-formed molecular junctions are investigated.

Experiment. Measurements are performed in high vacuum ($p < 5 \cdot 10^{-4}$ mbar) in a dilution refrigerator (≈ 70 mK) equipped with a superconducting magnet allowing magnetic fields up to 9 T. Current spectra are extracted applying a DC bias voltage V to the gold electrodes while recording current I. The differential conductance dI/dV is then obtained by taking the numerical derivative.

Author contributions J. V. proposed the study of the triradical. E.B., R. G. and H. v.d.Z designed the project. R. G. performed the measurements, C.R. and J. V. synthesized the molecules, D.R., I. de P. R. Moreira and S. T. Bromley performed the calculations. R.G, E.B. and H.v.d.Zant wrote the manuscript. All authors contributed to the interpretation of the data and commented on the manuscript.

Additional Information Supplementary information is available in the online version of the paper. Reprints and permissions information is available online at www.nature.com/reprints.

Competing financial interests The authors declare no competing financial interests.

[1] B. W. Heinrich, G. Ahmadi, V. L. Müller, L. Braun, J. I. Pascual, and K. J. Franke, Nano Lett. **13**, 4840 (2013).

[2] J. J. Parks, A. R. Champagne, T. A. Costi, W. W. Shum, A. N. Pasupathy, E. Neuscamman, S. Flores-Torres, P. S. Cornaglia, A. A. Aligia, C. A. Balseiro, G. K.-L. Chan, H. D. Abruña, and D. C. Ralph, Science **328**, 1370 (2010).

[3] J. A. J. Burgess, L. Malavolti, V. Lanzilotto, M. Mannini, S. Yan, S. Ninova, F. Totti, S. Rolf-Pissarczyk, A. Cornia, R. Sessoli, and S. Loth, Nat. Commun. **6**, 8216 (2015).

[4] E. Burzurí, A. S. Zyazin, A. Cornia, and H. S. J. van der Zant, Phys. Rev. Lett. **109**, 147203 (2012).

[5] E. Burzurí, R. Gaudenzi, and H. S. J. van der Zant, J. Phys. Condens. Matter **27**, 113202 (2015).

[6] O. Kahn and B. Briat, J. Chem. Soc. Faraday Trans. 2 **72**, 268 (1976).

[7] B. Bryant, A. Spinelli, J. J. T. Wagenaar, M. Gerrits, and A. F. Otte, Phys. Rev. Lett. **111**, 127203 (2013).

[8] P. Grünberg, R. Schreiber, Y. Pang, M. B. Brodsky, and H. Sowers, Phys. Rev. Lett. **57**, 2442 (1986).

[9] A. Fert, P. Grünberg, A. Barthélémy, F. Petroff, and W. Zinn, J. Magn. Magn. Mater. **140-144**, 1 (1995).

[10] J. Liu, H. Isshiki, K. Katoh, T. Morita, B. K. Breedlove, M. Yamashita, and T. Komeda, J. Am. Chem. Soc. **135**, 651 (2013).

[11] Y.-h. Zhang, S. Kahle, T. Herden, C. Stroh, M. Mayor, U. Schlickum, M. Ternes, P. Wahl, and K. Kern, Nat. Commun. **4**, 2110 (2013).

[12] S. Müllegger, M. Rashidi, M. Fattinger, and R. Koch, J. Phys. Chem. C. Nanomater. Interfaces **117**, 5718 (2013).

[13] R. Frisenda, R. Gaudenzi, C. Franco, M. Mas-Torrent, C. Rovira,

7

J. Veciana, I. Alcon, S. T. Bromley, E. Burzurí, and H. S. J. van der Zant, Nano Lett. **15**, 3109 (2015).

[14] A. R. Rocha, V. M. García-Suárez, S. W. Bailey, C. J. Lambert, J. Ferrer, and S. Sanvito, Nat. Mater. **4**, 335 (2005).

[15] J. Veciana, C. Rovira, N. Ventosa, M. I. Crespo, and F. Palacio, J. Am. Chem. Soc. **115**, 57 (1993).

[16] J. Sedó, N. Ventosa, D. Ruiz-Molina, M. Mas, E. Molins, C. Rovira, and J. Veciana, Angew. Chemie Int. Ed. **37**, 330 (1998).

[17] H. C. Longuet-Higgins, J. Chem. Phys. **18**, 265 (1950).

[18] A. A. Ovchinnikov, Theor. Chim. Acta **47**, 297 (1978).

[19] W. T. Borden and E. R. Davidson, J. Am. Chem. Soc. **99**, 4587 (1977).

[20] D. Reta Mañeru, R. Costa, M. Guix Márquez, I. d. P. R. Moreira, and F. Illas, J. Chem. Theory Comput. **11**, 3650 (2015).

[21] L. Noodleman, J. Chem. Phys. **74**, 5737 (1981).

[22] L. Noodleman and E. R. Davidson, Chem. Phys. **109**, 131 (1986).

[23] L. Noodleman, C. Peng, D. Case, and J.-M. Mouesca, Coord. Chem. Rev. **144**, 199 (1995).

[24] I. d. P. R. Moreira and F. Illas, Phys. Chem. Chem. Phys. **8**, 1645 (2006).

4.3.5. Paper #4.5.

Folding-Induced Stabilization of Ferromagnetic Helical Polyradicals Based on Triarylmethyl Radical Derivatives
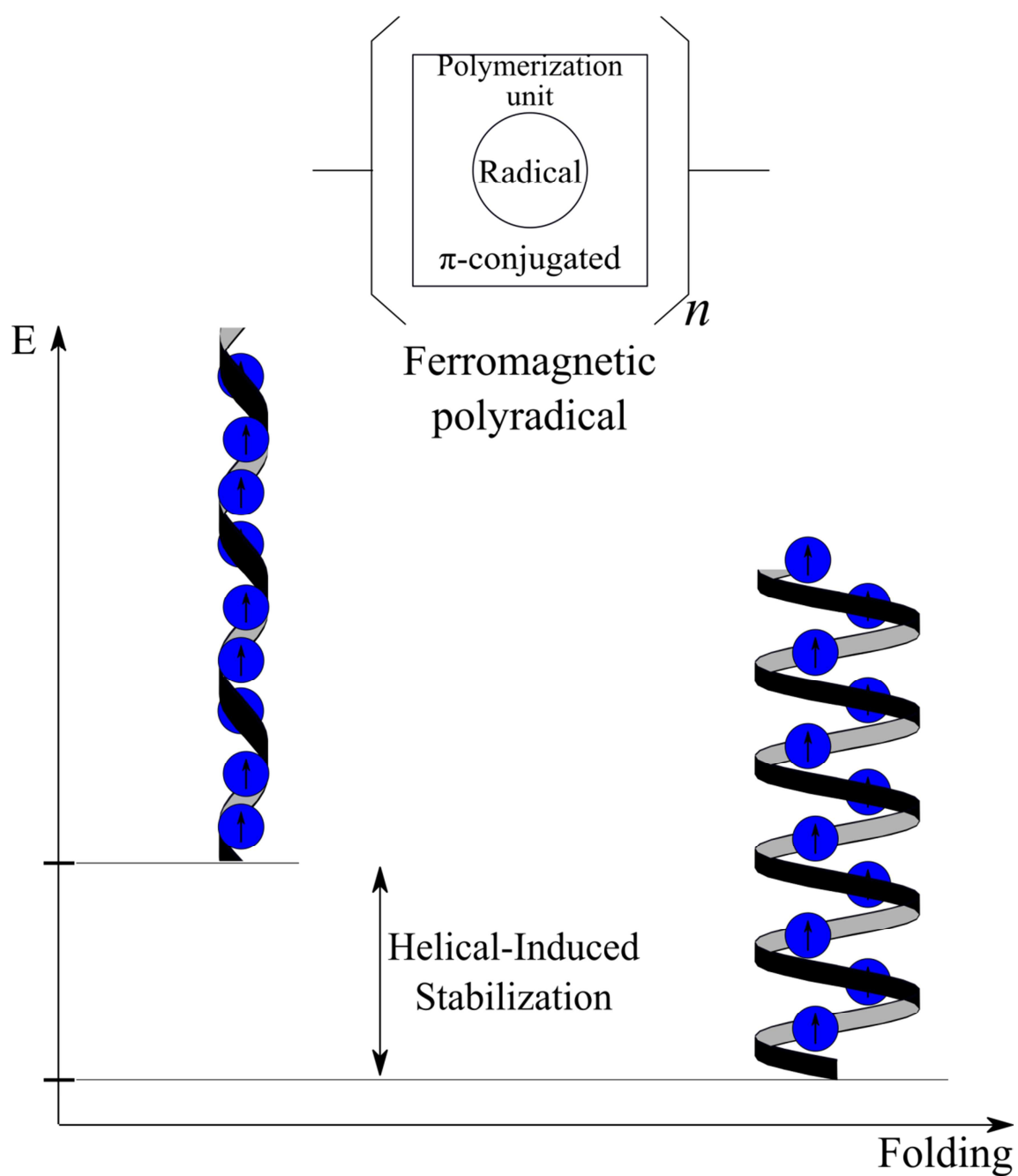
Helical Folding-Induced Stabilization of Ferromagnetic polyradicals based on triarylmethyl radical derivatives

Daniel Reta Mañeru, Ibério de P. R. Moreira, Francesc Illas*

Departament de Química Física & Institut de Química Teòrica i Computacional

(IQTCUB), Universitat de Barcelona, C/Martí i Franquès 1, 08028 Barcelona, Spain

Abstract.-

Magnetic ordering in purely organic π-conjugated materials is a challenging, rare and desirable event. The interest lies on the unique magnetic properties derived from high-spin carbon-based polymers/macromolecules tailored through appropriate synthetic routes. Ground breaking achievements have been reported regarding magnetic ordering in an organic polymer using spin-clusters as building-blocks. This strategy leads to two-dimensional (2D) extended polyradicals with a concomitant loss of appealing macroscopic properties such as expected magnetic anisotropy in elongated shaped macromolecules containing carbon-bearing radicals. Here we provide compelling evidence of a secondary structure-induced stabilization of ferromagnetic polyradicals with robust magnetic properties and strongly suggest revisiting a discarded attempt to obtain polymeric linear-like radicals. An alternative synthetic approach is also proposed, based on polyradicals obtained from discrete molecular precursors long enough to ensure a secondary structure, rather than from polymerization processes.

1. Introduction.

Purely organic magnetic materials constitute a promising approach for the miniaturization of devices with interesting optical, electronic and magnetic properties, all using low cost chemical elements.[1-4] Despite significant advances in the field, critical issues remain when aiming at achieving a strong enough ferromagnetic ordering over a wide range of temperatures and a structural control on the final products.[5]

Up to date, the most successful strategies relied on synthesizing high-spin macromolecules and/or polymers with very large number of carbon bearing unpaired electrons interacting through-bond.[5-14] Particularly, odd alternant polycyclic hydrocarbons with a 1,3-connection are widely used, as envisioned by Mataga.[15] In

these systems, topological arguments ensure non-disjoint, degenerate singly occupied orbitals,[16,17] and ground states with the highest multiplicity.[18] However, within the commonly adopted synthetic route, disruption and even suppression of magnetic interactions is commonly observed, associated to an incomplete generation of the radical centres from the precursor, or to an out-of-plane torsion breaking the π−conjugation.[10,13] That is specially the case for linear, star-branched and dendritic connectivities as recognized long time ago by Rajca *et al.*[5] Precisely, to circumvent this problem an alternative approach based on the use of organic spin clusters was proposed.[5] These building blocks constituted one of the mainstreams in the field of organic magnetism.[12] As a result, most of the subsequent related research led to two dimensional (2D) extended polyradicals[5,14] at the expense of other architectures with lower dimensionalities, as for instance linear or rod 1D chains. Nonetheless, interesting properties associated to an elongated 1D-like polyradical are not present in 2D materials, magnetic anisotropy among them. The contribution of classical dipole-dipole interactions to magnetic anisotropy is known to be a relevant one.[11] Thus, energy barriers for coherent rotation of magnetization are expected to relate to the molecular shape of the polyradicals as well as to its spin density; the latter being especially large in elongated shapes.

In the present work, we investigate the structural and magnetic properties of two 1D-like polyradicals based on odd alternant hydrocarbons and, based on consistent arguments in favour of the structural and chemical stability, provide compelling evidence of helical-induced stabilization of ferromagnetic polyradicals with robust magnetic properties. Interestingly, one of the systems under study was already synthesized by Rajca[8] although its use as magnetic building block was, at that time, discarded because of the uncontrollable impact of chemical defects on the magnetic properties. Considering the novel and interesting predicted properties of these 1D-like elongated magnetic organic systems further research seems mandatory. To this end, a plausible scheme, based on Rajca results,[7] is proposed for an effective synthetic strategy to reach medium size oligomers.

2. Computational details

Calculations for the polymer and oligomer compounds described in the next section have been carried out using the B3LYP[19] hybrid density functional theory based method

including dispersion corrections as proposed by Grimme;[20] the resulting method being referred to hereafter as B3LYP-D. For the polymers, periodic calculations have been carried out using Crystal09 code,[21,22] with the standard 6-21G* basis set for all atoms (H, C) whereas for the decaradical the Gaussian-09 suite of programs[23] was used employing a 6-31G* basis set.[24,25] ITOL values have been fixed to 7,7,7,7,14 to force stringent numerical convergence of energy and gradients and 3 k-points in the 1D irreducible Brillouin zone. Denser k-point meshes do not significantly affect the energy differences defining structure stability or values of magnetic coupling constants.

The description of the magnetic properties is based on the Ising model Hamiltonian

$$\hat{H}^{Ising} = -\sum_{\langle i,j \rangle} J_{ij} \hat{S}_i^z \hat{S}_j^z \tag{23}$$

where J_{ij} is the exchange coupling constant between the $\hat{S}_i^z$ and $\hat{S}_j^z$ localized spin moments and the $\langle i,j \rangle$ symbol indicates that the sum refers to nearest neighbour interactions only. According to Eq. (1), a positive value of the exchange coupling constant J_{ij} corresponds to ferromagnetic (FM) interactions, while negative values describe an antiferromagnetic (AFM) interaction (parallel and antiparallel spins respectively). The number, sign and magnitude of the most relevant J_{ij} determine the low-energy spectrum of the problem and consequently the magnetic ordering of the system. The extraction of the different J_{ij} is based on the mapping approach described elsewhere.[26] A more detailed explanation is provided in the supplementary section 2.

3. Structural features, chemical stability and magnetic properties.

The structures investigated in the present work can be regarded as derivatives of *m*-xylylene diradical extended in 1D (referring to the σ skeleton), with an increasing steric protection of the radical centres, as indicated in Figure 1.

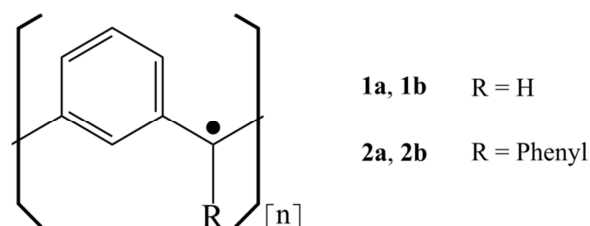|	
1a, 1b	R = H
2a, 2b	R = Phenyl

Figure 1. Schematic representation of investigated polymers. The different notation for each polymer indicates the conformation adopted (a stands for linear and b for helical).

Polymer **1** is a good model to investigate magnetic interactions and the different adopted conformations. Polymer **2** is a Gomberg-based[27] polyradical. To the best of our knowledge, polyradical **1** has never been synthesized. On the contrary, polyradical **2** was synthesized by Rajca,[8] following the carbopolyanion method. The obtained precursor polymer was reported to have an average number of 30 potential radical sites. However, polyradical **2** presented a saturation of the magnetization curve fitting with an average spin value of $S = 2$, corresponding to only 4 $S = 1/2$ sites per molecule. The failure on spreading the magnetic interaction along all potential radical sites was assigned to chemical defects, such as incomplete oxidation of the carbopolyanion precursor. However, no further experimental attempts aiming at improving the generation of radical centres in these linear polyradicals have been pursued. This was largely motivated by the success of spin clusters as building blocks for synthesizing 2D extended polyradicals, as proposed by Rajca.

Theoretically, the electronic structure of polyradicals **1** and **2** has been extensively studied.[28–32] In contrast, despite early indications by Yoshizawa *el al.*,[32] structural effects and their impact on the σ-π separation have been generally overlooked. Conformational freedom in these flexible structures introduces a degree of complexity that cannot be ignored.[33] In fact, the appearance of a preferential helical conformation as a secondary structure brings interesting macroscopic properties at variance with purely linear 1D polyradicals where no ferromagnetism is expected.[34] Additionally, the secondary structure introduces an effective manner for sterically protecting the radical centres.

In the present work, the molecular structure of all polymers has been fully optimized for the electronic ground state (ferromagnetic solution) and for linear and helical conformations. In all cases a local minimum was located and analysis of the corresponding structures evidences that inclusion of dispersion is crucial in defining the preference for the helical conformation. Coordinates of the primitive cells for the optimized structures including dispersion corrections, are in the supplementary section 1. A preference for a helical conformation has been found for all the studied polymers, especially once dispersion terms are taken into account. The helical conformation of polymers **1** and **2** is 2.8 and 2.5 kcal/mol per magnetic centre, respectively, more stable than the linear one. These values are very similar to the parallel displaced pi-stacking

interaction of the benzene dimer calculated by means of very accurate CCSD(T) ab-initio wave function-based methods with large basis sets.[35]

Figure 2 compares the linear and helical conformation of polymer **1** and **2**. It also presents the cell parameters per magnetic centre and distances relating the carbon-bearing radicals as obtained when considering dispersion corrections. Note that the number of magnetic carbon atoms per cell is six in the linear conformations and three for the helical ones. The introduction of phenyl rings in polymer **2** promotes a large $\pi-\pi$ interaction along the direction of the polymer, resulting in an effective stabilization with respect to the linear conformation. Figure 2 also includes the band gap values for the different polymers in the ferro and most stable antiferromagnetic phases. For a given conformation, the almost constant band-gap values around 2 eV, either for the ferro or antiferromagnetic order, indicates that the magnetic centres are stable and that magnetic properties do not alter the electronic structure of the polymer. Additionally, the similar values for the different conformations ensure a comparable behaviour no matter the geometry adopted. Density of states and band diagram for ferro and antiferromagnetic solutions of polymer **2a** are in supplementary section 3.
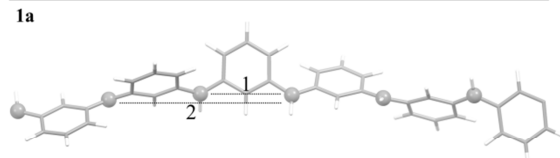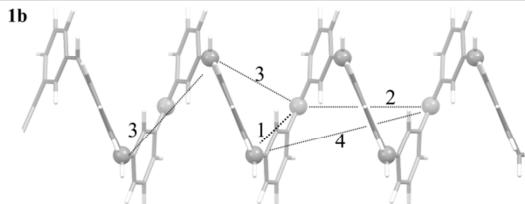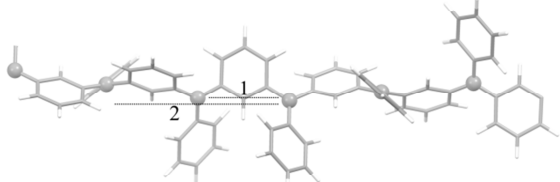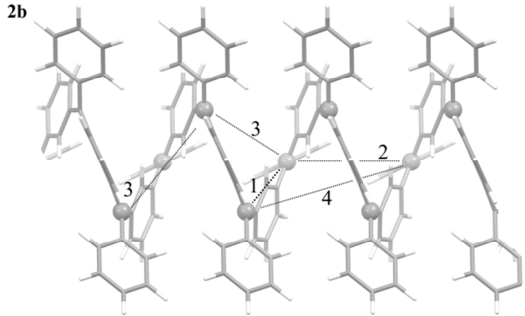
	Distance (Å)				Band gap (eV)
	cell	1	2	3	4	
1a	29.63	4.9	9.9			2.4 / 2.1
2a	29.66	5.0	10.0			2.0 / 1.8
1b	6.16	5.0	6.2	6.1	9.4	2.4 / 2.2
2b	5.69	5.0	5.7	6.0	8.9	2.0 / 1.8

Figure 2. a) Schematic representation of the optimized geometries of polymers **1** and **2** adopted for a linear and helical conformation. Ball atoms indicate the radical centres. b) Structural and band gap

(ferro/antiferro solution) information of polymers **1-2** extracted from the optimized geometries taking into account dispersion corrections.

Finally, concerning the discussion on structural features, it could be argued that increasing chemical stability of the radical centres might be an effective way of promoting more robust properties of the resulting 1D-like polyradical. For this purpose, steric hindrance might be considered as an approach as noted in the increase of stability when passing from the Gomberg radical[27] to perchlorinated substituted PTM radical.[36]. Thus, a polymer based on PTM units represents a limiting case to further verify this hypothesis although the large steric hindrance may difficult obtaining stable structures, in line with the reported work on related 2D polyradical dendrimers.[9,37–39] However, currently there is a large library of available PTM-derivatives with only certain Chlorine-substituted positions.[4] Such catalogue could be used for a revisited synthesis of related polymer **2**, in order to achieve a compromise between gained stabilization of the radical centres through steric protection and a conformational freedom to adopt a relaxed secondary structure.

	Type of structure					
Polymer	Linear		Helix			
	$\Delta E_{FM\text{-}AFM}$ (cm^{-1})					
1	-1920		-2312			
2	-1134		-1447			
	Spin densities					
1	0.717		0.678			
2	0.642		0.631			
	Magnetic exchange interactions (cm^{-1})					
	J_1	J_2	J_1	J_2	J_3	J_4
1	328	-8	388	0.2	-10	-0.3
2	202	-6	292	0.1	-5.0	-4.0

Table 1. Energetic difference between the ferromagnetic and the most stable antiferromagnetic phases as predicted from the B3LYP-D calculations. Negative value implies a more stable ferromagnetic state. Spin densities and magnetic exchange interactions per magnetic centre are also reported.

In order to obtain information regarding the magnetic properties, single point calculations for different broken symmetry solutions were carried out at each of the obtained optimized geometries in the ferromagnetic ground state solution. Table 1 summarizes the most important results, evidences that for all conformations the ferromagnetic order is the ground state and the calculated value of the FM-AFM energy difference is large enough to ensure ferromagnetism even at room temperature ($J \gg kT$). This is of paramount importance when aiming at designing a material with robust

magnetic properties. Table 1 also presents the exchange interaction values per magnetic centre for polymers **1** and **2** for the structure optimized including dispersion. Details on the definition of the magnetic cells, associated computed energies and equations for the extraction of the magnetic coupling constants are in the supplementary section 2. It is worth noticing that a different conformation introduces changes in the magnetic topology as indicated in Figure 2, and consequently on the magnitude and number of the relevant exchange interactions. Thus, in the linear conformation there are two relevant magnetic interactions only that occur in an almost straight line, resulting in a quasi-1D magnetic chain. Contrarily, a helical conformation implies a distribution of the radical centres along the interior of the helix, resulting in larger number of nearest magnetic neighbours, leading to a quasi-3D magnetic system. Moreover, the helical conformation introduces a privileged direction for magnetic interactions to transmit.

To check whether the appearance of a secondary structure is an effect of an infinite polymeric structure, decaradicals (10 magnetic sites) molecular units have been optimized. Cartesian coordinates of the optimized structures are in supplementary section 4. For derivatives from both polymers **1** and **2**, the helix shape remained intact, indicating that it is a stable local minimum, and the ground state keeps being the high-spin state (supplementary section 4.3). On the contrary, local minima for the linear derivatives were not located, although a clear tendency to compact the secondary structure is observed. This indicates that if the polyradical is large enough, the interruption of the magnetic path at the extremes does not destroy either the adopted secondary structure or the local magnetic interactions occurring in the interior. Very importantly, this conclusion shows that materials based on 1D-like polyradicals do not necessarily require precursors obtained through polymerization processes, but rather discrete units long enough for a secondary structure to form and stabilize the radical centres.

4. Conclusions.

This work presents a theoretical study of the structural, electronic structure features and magnetic properties of two 1D-like polyradicals based on odd alternant hydrocarbons and presenting the radical centres in the backbone of the π-conjugated polymer, connected through a 1,3-phenylene unit.

The present results show that, as predicted by Yoshizawa *et al.*,[32] structural flexibility plays a crucial role allowing two linear (**1a**, **2a**) and helical (**1b**, **2b**) conformations. As a result of the π-π interactions, the helical conformation is preferred in all cases and dispersion terms appear to be crucial. Additionally, the existence of a helix as a secondary structure promotes stabilization of the radical centres by steric hindrance and one can safely argue that additional steric protection of the radical centres could be achieved using PTM derivatives although this may require controlling the interplay between steric congestion and structural freedom.

For the polymers under scrutiny, the particular topology of the π-system in the repeating unit ensures a high-spin ground state,[15–18] as fully confirmed by the present state of the art calculations. In fact, the energy of the ferromagnetic ground state is well below the one of the most stable antiferromagnetic phase implying that the ferromagnetic behaviour will be maintained even at room temperature. Therefore, the predicted magnetic properties are robust and the values of the magnetic coupling constants per radical centre are remarkably large compared to the typical exchange interaction found in coordination complexes,[40] rarely exceeding 100 cm^{-1}. Moreover, the preferred helical conformation introduces a more complex magnetic topology, which resembles to a 2D cylindrical network. This certainly has an impact in the expected macroscopic properties of the material, especially when compared to the linear conformation.

Finally, relying on the successful synthesis of a robust $S = 3/2$ ground state triradical[7] from a discrete precursor with three potential radical sites, one could extrapolate the argument to precursors with a larger but constant number of potential radical sites for obtaining well defined polyradicals. Attempts in this directions have been pursued, but imposing a conformational restriction for making the system totally planar (section 4.3 in[5]). This strategy led to unsuccessful results, which could be explained by the impossibility for adopting a secondary structure. As indicated by the investigated decaradical, the key point would be to work with precursors long enough to ensure the appearance of a secondary structure, stabilizing the radical centres. In this way one would avoid the implicit drawbacks of a polymerization process in which it is only possible to obtain a distribution of molecules around an average molecular mass, and topological defects are difficult to prevent. From a synthetic point of view, working with a defined precursor provides a simple starting point to improve the optimization of

starting point to improve the optimization of the chemical process to generate the polyradicals quantitatively. Given that the synthesis of the molecular precursor is affordable, it would be possible to obtain polyradicals with a constant number of radical sites, very stable ferromagnetic ground state, large magnetic interactions and secondary structure-induced anisotropy. To finalize, note that by applying an external magnetic field one could think of aligning and separating the discrete units which may open the way to purely organic magnetic devices.

Acknowledgements

REFERENCES

(1)   Veciana, J. *Π-Electron Magnetism From Molecules to Magnetic Materials*; Veciana, J., Ed.; Springer-Verlag: Berlin, 2001.

(2)   Blundell, S. J.; Pratt, F. L. Organic and Molecular Magnets. *J. Phys. Condens. Matter* **2004**, *16* (24), R771–R828.

(3)   Sanvito, S. Molecular Spintronics. *Chem. Soc. Rev.* **2011**, *40* (6), 3336.

(4)   Ratera, I.; Veciana, J. Playing with Organic Radicals as Building Blocks for Functional Molecular Materials. *Chem. Soc. Rev.* **2012**, *41* (6), 303–349.

(5)   Rajca, A. The Physical Organic Chemistry of Very High-Spin Polyradicals. *Adv. Phys. Org. Chem.* **2005**, *40*, 153–199.

(6)   Iwamura, H. *High-Spin Organic Molecules and Spin Alignment in Organic Molecular Assemblies in Advances in Physical Organic Chemistry, Volume 26*; Academic Press: London, 1990.

(7)   Rajca, A.; Utamapanya, S. Poly(arylmethyl) Quartet Triradicals and Quintet Tetraradicals. *J. Am. Chem. Soc.* **1993**, *115* (6), 2396–2401.

(8)   Utamapanya, S.; Kakegawa, H.; Bryant, L.; Rajca, A. High-Spin Polymers. Synthesis of 1,3-Connected Polyarylmethane and Its Carbopolyanion and Polyradical. *Chem. Mater.* **1993**, *5* (8), 1053–1055.

(9)   Veciana, J.; Rovira, C.; Ventosa, N.; Crespo, M. I.; Palacio, F. Stable Polyradicals with High-Spin Ground States. 2. Synthesis and Characterization of a Complete Series of Polyradicals Derived from 2,4,6-Trichloro-

.α.,.α.,.α.',.α.',.α.'',.α.''-Hexakis(pentachlorophenyl)mesitylene with S = 1/2,. *J. Am. Chem. Soc.* **1993**, *115*, 57–64.

(10)   Rajca, a; Utamapanya, S. Toward Organic-Synthesis of a Magnetic Particle - Dendritic Polyradicals with 15 and 31 Centers for Unpaired Electrons. *J. Am. Chem. Soc.* **1993**, *115* (9), 10688–10694.

(11)   Rajca, A. Organic Diradicals and Polyradicals: From Spin Coupling to Magnetism? *Chem. Rev.* **1994**, *94*, 871–893.

(12)   Rajca, A.; Wongsriratanakul, J.; Rajca, S. Magnetic Ordering in an Organic Polymer. *Science* **2001**, *294*, 1503–1505.

(13)   Rajca, A. From High-Spin Organic Molecules to Organic Polymers with Magnetic Ordering. *Chemistry* **2002**, *8* (21), 4834–4841.

(14)   Shishlov, N. M. From the Gomberg Radical to Organic Magnets. *Russ. Chem. Rev.* **2007**, *75*, 863–884.

(15)   Mataga, N. Possible Ferromagnetic States of Some Hypothetical Hydrocarbons. *Theor. Chim. Acta* **1968**, *10* (4), 372–376.

(16)   Longuet-Higgins, H. C. Some Studies in Molecular Orbital Theory I. Resonance Structures and Molecular Orbitals in Unsaturated Hydrocarbons. *J. Chem. Phys.* **1950**, *18* (3), 265.

(17)   Borden, W. T.; Davidson, E. R. Effects of Electron Repulsion in Conjugated Hydrocarbon Diradicals. *J. Am. Chem. Soc.* **1977**, *99* (14), 4587–4594.

(18)   Ovchinnikov, A. A. Multiplicity of the Ground State of Large Alternant Organic Molecules with Conjugated Bonds. *Theor. Chim. Acta* **1978**, *47*, 297–304.

(19)   Becke, A. D. Density Functional Thermochemistry. III. The Role of Exact Exchange. *J Chem Phys* **1993**, *98*, 5648–5652.

(20)   Grimme, S. Semiempirical GGA-Type Density Functional Constructed with a Long-Range Dispersion Correction. *J. Comput. Chem.* **2006**, *27* (15), 1787–1799.

(21)   Dovesi, R.; Orlando, R.; Civalleri, B. CRYSTAL: A Computational Tool for the Ab Initio Study of the Electronic Properties of Crystals. *Z. Krist.* **2005**, *220*, 571–573.

(22)   Dovesi, R.; Saunders, V. R.; Roetti, C.; Orlando, R.; Zicovich-Wilson, C. M.; Pascale, F.; Civalleri, B.; Doll, K.; Harrison, N. M.; Bush, I. J.; D'Arco, P.; Llunell, M. CRYSTAL09 User's Manual. *University of Torino*. Torino 2009.

(23)   Frisch, M. J.; Trucks, G. W.; Schlegel, H. B.; Scuseria, G. E.; Robb, M. A.; Cheeseman, J. R.; Scalmani, G.; Barone, V.; Mennucci, B.; Petersson, G. A.; Nakatsuji, H.; Caricato, M.; Li, X.; Hratchian, H. P.; Izmaylov, A. F.; Bloino, J.; Zheng, G.; Sonnenberg, J. L.; Hada, M.; Ehara, M.; Toyota, K.; Fukuda, R.;

Hasegawa, J.; Ishida, M.; Nakajima, T.; Honda, Y.; Kitao, O.; Nakai, H.; Vreven, T.; Montgomery, J. A., J.; Peralta, J. E.; Ogliaro, F.; Bearpark, M.; Heyd, J. J.; Brothers, E.; Kudin, K. N.; Staroverov, V. N.; Kobayashi, R.; Normand, J.; Raghavachari, K.; Rendell, A.; Burant, J. C.; Iyengar, S. S.; Tomasi, J.; Cossi, M.; Rega, N.; Millam, J. M.; Klene, M.; Knox, J. E.; Cross, J. B.; Bakken, V.; Adamo, C.; Jaramillo, J.; Gomperts, R.; Stratmann, R. E.; Yazyev, O.; Austin, A. J.; Cammi, R.; Pomelli, C.; Ochterski, J. W.; Martin, R. L.; Morokuma, K.; Zakrzewski, V. G.; Voth, G. A.; Salvador, P.; Dannenberg, J. J.; Dapprich, S.; Daniels, A. D.; Farkas, Ö.; Foresman, J. B.; Ortiz, J. V.; Cioslowski, J.; Fox, D. J. Gaussian, Inc. Wallingford CT 2009.

(24)   Hariharan, P. C.; Pople, J. A. The Influence of Polarization Functions on Molecular Orbital Hydrogenation Energies. *Theor. Chim. Acta* **1973**, *28* (3), 213–222.

(25)   Francl, M. M.; Pietro, W. J.; Hehre, W. J.; Stephen Binkley, J.; Gordon, M. S.; DeFrees, Douglas, J.; Pople, J. A. Self-Consistent Molecular Orbital Methods. XXIII. A Polarization-Type Basis Set for Second-Row Elements. *J. Chem. Phys.* **1982**, *77* (7), 3654.

(26)   Moreira, I. de P. R.; Illas, F. A Unified View of the Theoretical Description of Magnetic Coupling in Molecular Chemistry and Solid State Physics. *Phys. Chem. Chem. Phys.* **2006**, *8* (14), 1645–1659.

(27)   Gomberg, M. An Instance of Trivalent Carbon: Triphenylmethyl. *J. Am. Chem. Soc.* **1900**, *22* (11), 757–771.

(28)   Tyutyulkov, N.; Schuster, P.; Polansky, O. Band Structure of Nonclassical Polymers. *Theor. Chim. Acta* **1983**, *63* (4), 291–304.

(29)   Tyutyulkov, N.; Polansky, O. E.; Schuster, P.; karabunarliev, S.; Ivanov, C. I. Structure and Properties of Non-Classical Polymers II. Band Structure and Spin Densities. *Theor. Chim. Acta* **1985**, *67* (3), 211–228.

(30)   Tyutyulkov, N. N.; Karabunarliev, S. C. Structure and Properties of Nonclassical Polymers. III. Magnetic Characteristics at Finite Temperatures. *Int. J. Quantum Chem.* **1986**, *29* (5), 1325–1337.

(31)   Yoshizawa, K.; Tanaka, K.; Yamabe, T. Ferromagnetic Coupling through M-Phenylene. Molecular and Crystal Orbital Study. *J. Phys. Chem.* **1994**, *98* (7), 1851–1855.

(32)   Yoshizawa, K.; Hoffmann, R. Potential Linear-Chain Organic Ferromagnets. *Chem. - A Eur. J.* **1995**, *7*, 403–413.

(33)   Reta Mañeru, D.; Moreira, I. D. P. R.; Illas, F. Triplet–singlet Gap in Structurally Flexible Organic Diradicals. *Theor. Chem. Acc.* **2015**, *134*, 18.

(34)   Lieb, E.; Mattis, D. Theory of Ferromagnetism and the Ordering of Electronic Energy Levels. *Phys. Rev.* **1962**, *125* (1), 164–172.

(35)   Sinnokrot, M. O.; Valeev, E. F.; Sherrill, C. D. Estimates of the Ab Initio Limit for π−π Interactions: The Benzene Dimer. *J. Am. Chem. Soc.* **2002**, *124* (36), 10887–10893.

(36)   Ballester, M.; Riera-Figueras, J.; Castaner, J.; Badfa, C.; Monso, J. M. Inert Carbon Free Radicals. I. Perchlorodiphenylmethyl and Perchlorotriphenylmethyl Radical Series. *J. Am. Chem. Soc.* **1971**, *93* (9), 2215–2225.

(37)   Rovira, C.; Veciana, J.; Armet, O.; Castañer, J.; Riera, J.; Vincent, E.; Radhakrishna, P. A Study of Triarylmethyl Diradicals as Magnetic Models for Organic Ferromagnets. *Mol. Cryst. Liq. Cryst. Inc. Nonlinear Opt.* **1988**, *156* (1), 301–310.

(38)   Veciana, J.; Rovira, C.; Crespo, M. I.; Armet, O.; Domingo, V. M.; Palacio, F. Stable Polyradicals with High-Spin Ground States. 1. Synthesis, Separation, and Magnetic Characterization of the Stereoisomers of 2,4,5,6-Tetrachloro-.α.,.α.,.α.',.α.'-Tetrakis(pentachlorophenyl)-M-Xylylene Biradical. *J. Am. Chem. Soc.* **1991**, *113* (7), 2552–2561.

(39)   Ruiz-Molina, D.; Veciana, J.; Palacio, F.; Rovira, C. Drawbacks Arising from the High Steric Congestion in the Synthesis of New Dendritic Polyalkylaromatic Polyradicals. *J. Org. Chem.* **1997**, *62* (26), 9009–9017.

(40)   Wannarit, N.; Pakawatchai, C.; Mutikainen, I.; Costa, R.; Moreira, I. de P. R.; Youngme, S.; Illas, F. Hetero Triply-Bridged Dinuclear copper(II) Compounds with Ferromagnetic Coupling: A Challenge for Current Density Functionals. *Phys. Chem. Chem. Phys.* **2013**, *15* (6), 1966–1975.

Helical Folding-Induced Stabilization of Ferromagnetic polyradicals based on triarylmethyl radical derivatives

Daniel Reta Mañeru, Ibério de P. R. Moreira, Francesc Illas*

Departament de Química Física & Institut de Química Teòrica i Computacional

(IQTCUB), Universitat de Barcelona, C/Martí i Franquès 1, 08028 Barcelona, Spain

<u>Index of Supplementary Information.</u>

1. Primitive cell coordinates of optimized polymers structures for the ferromagnetic solution.

    1.1. Linear conformation. Polymers **1a** and **2a**.

    1.2. Helical conformation. Polymers **1b** and **2b**.

2. Energy expressions, computed absolute energies and definition of magnetic solutions required for the extraction of magnetic exchange interactions.

    2.1. Linear conformation. Polymers **1a** and **2a**

    2.2. Helical conformation. Polymers **1b** and **2b**.

3. Density of States and Band Structure diagrams for FM and AFM solutions of polymer **2b**.

4. Optimized geometries (high-spin solution) of the different decaradicals derived from polymers **1b** and **2b** and calculated energetic differences for the decaradical derived from polymer **2b**.

    4.1. Optimized geometry of discrete helical decaradical derived from **1b**.

    4.2. Optimized geometry of discrete helical decaradical derived from **2b**.

    4.3. Calculated energetic differences in the helical decaradical derived from **2b**

1. Primitive cell coordinates of optimized polymers structures for the ferromagnetic solution.

1.1. Linear polymers. Six magnetic centres per cell. Magnetic atoms 1-6.

For reasons of space, this information is not displayed here, but it can be requested from the authors

1.2. Helical polymers. Three magnetic centres per cell.

For reasons of space, this information is not displayed here, but it can be requested from the authors

2. Energy expressions, computed absolute energies and definition of magnetic solutions required for the extraction of magnetic exchange interactions.

We adopt an Ising spin Hamiltonian for the extraction of magnetic interactions. The Ising Hamiltonian is expressed as

$$\hat{H}^{Ising} = - \sum_{<i,j>} J_{ij} \cdot \hat{S}_i^z \cdot \hat{S}_j^z$$

2.1. Linear conformation.

The magnetic cell used for the extraction of the magnetic interactions is the same cell used for the optimization of the polymer, and therefore contains six magnetic centres. The computed absolute energies for the different magnetic solutions are given in Table S. I.1. The associated energy expressions according to the Ising Hamiltonian and the computed energetic differences for the solutions FM-AFM2 are indicated in Table S. I.2. Figure S. I.1 specifies how the different FM-AFM2 magnetic solutions are defined.

Solution	Energy (hartree)	
	1a	**2a**
FM	-1616.4013668690	-3001.1249851480
AFM1	-1616.3926198107	-3001.1196340643
AFM2	-1616.3928287815	-3001.1198010527

Table S. I.1 Absolute computed energies for the different magnetic solutions required for the extraction of the magnetic exchange constants.

Solution	energy	ΔE_{FM-AFM}	Calculated ΔE_{FM-AFM} (cm-1)	
			1a	**2a**
FM	$-6/4\,(J_1+J_2)$			
AFM1	$-1/2\,(J_1+J_2)$	$-J_1-J_2$	-1919.75734	-1174.427088
AFM2	$1/2\,(-J_1+J_2)$	$-J_1-2J_2$	-1873.893552	-1137.777372

Table S. I.2. Energy expressions associated to each of the magnetic solutions in the linear conformation. Computed absolute energies and associated energy differences referred to the ferromagnetic phase for all magnetic cells used in the helical conformation.
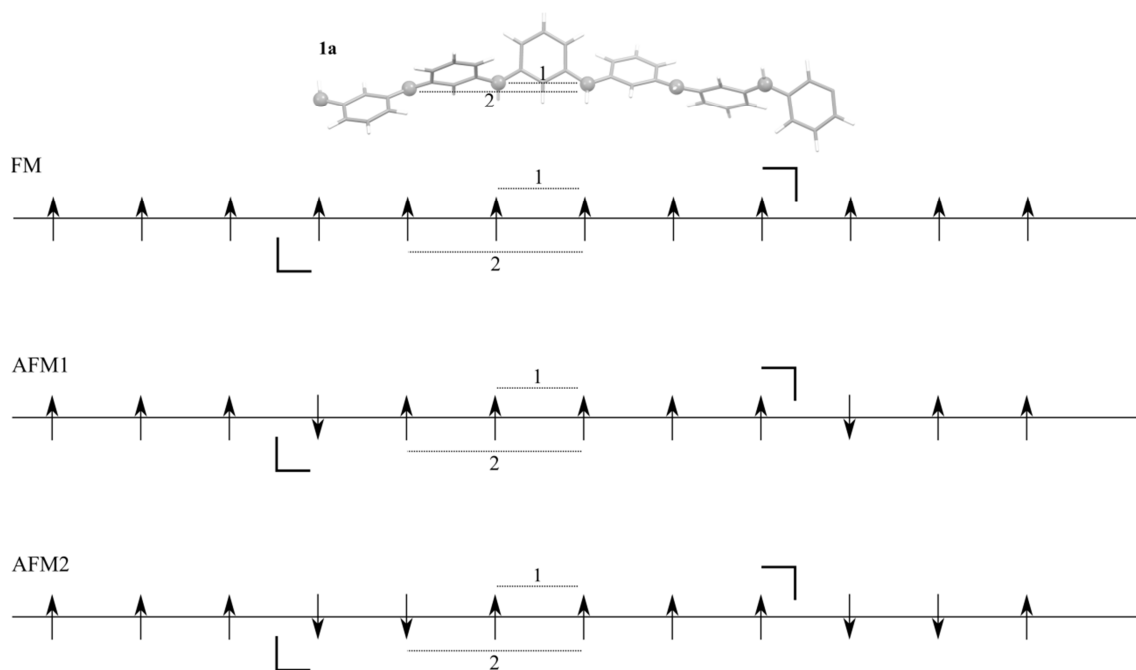

Figure S. I.1. Schematic representation of the magnetic solutions (indicated in brackets) used to extract all relevant magnetic interactions.

2.1. Helical conformation.

The magnetic cell used for the extraction of the magnetic interactions is double the cell used for the optimization of the polymer, and therefore contains six magnetic centres. The computed absolute energies for the different magnetic solutions are given in Table S. I.3. The associated energy expressions according to the Ising Hamiltonian and the computed energetic differences for the solutions FM-AFM4 are indicated in Table S. I.4. Figure S. I.2 specifies how the different FM-AFM4 magnetic solutions are defined.

	Energy (hartree)	
Solutions	**2a**	**2b**
FM	-1616.427910044	-3001.151038859
AFM1	-1616.417569494	-3001.143326321
AFM2	-1616.407237511	-3001.135616547
AFM3	-1616.407225306	-3001.135559183
AFM4	-1616.417829211	-3001.143528848

Table S. I.3. Absolute computed energies for the different magnetic solutions required for the extraction of the magnetic exchange constants.

Cell	energy	$\Delta E_{\text{FM-AFM}}$	Calculated $\Delta E_{\text{FM-AFM}}$ (cm-1)	
			1b	**2b**
FM	$\frac{1}{2}(-3J_1 - 3J_2 - 3J_3 - 2J_4)$			
AFM1	$\frac{1}{2}(-J_1 - J_2 - J_3)$	$-J_1 - J_2 - J_3 - J_4$	-2269.5	-1692.7
AFM2	$\frac{1}{2}(J_1 - 3J_2 + J_3 + J_4)$	$-2J_1 - 2J_3 - 2J_4$	-4537.1	-3384.8
AFM3	$\frac{1}{2}(J_1 + J_2 + J_3 + J_4)$	$-2J_1 - 2J_2 - 2J_3 - \frac{3}{2}J_4$	-4539.8	-3397.4
AFM4	$\frac{1}{2}(-J_1 + J_2 + J_3 + J_4)$	$-J_1 - 2J_2 - 2J_3 - \frac{3}{2}J_4$	-2212.5	-1648.3

Table S. I.4. Energy expressions and the resulting energy difference referred to the ferromagnetic phase for all magnetic cells used in the helical conformation.
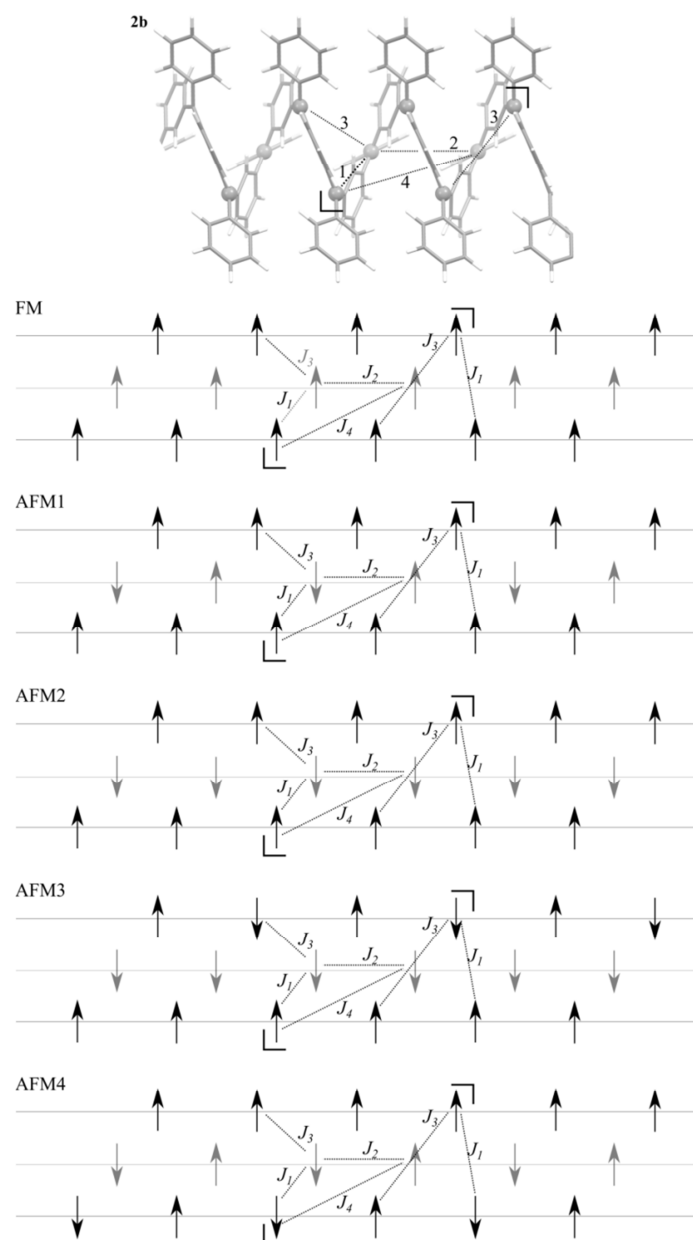
Figure S. I.2. Schematic representation of the magnetic cells (indicated in brackets) used to extract all relevant magnetic interactions.

3. Density of States and Band Structure plots for FM and AFM solutions of polymer 2b.

Figure S. I. 3. represents the density of states for both ferro and antiferromagnetic solutions. Note that the AFM solution is defined as the solution where each single spin is surrounded by two spins of opposite sign. This solution was not used to compute the exchange coupling constants in the previous section, but is normally the reference for reporting band gap values, since it represents the most unfavourable case for ferromagnetic ordering. In line with what was discussed in the main text, the value of

the band gap is 2 and 1.7 eV for FM and AFM solutions respectively. This is an indication of the stability of the radical centres and of the robustness of the magnetic properties.
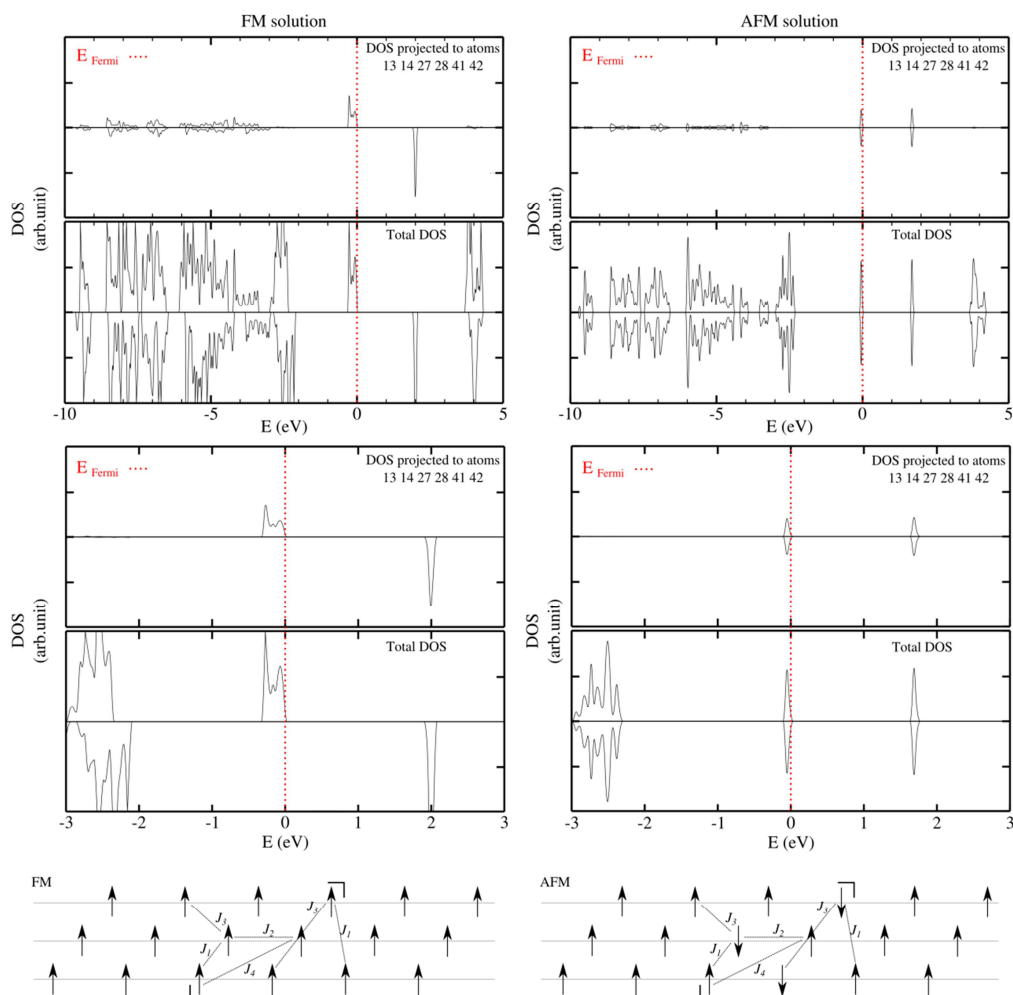

Figure S. I. 3. Density of states of ferromagnetic (FM) and antiferromagnetic (AFM) solutions of polymer **2b**. The definition of the magnetic cell used is also indicated.

Figure S. I. 4 introduces the band diagram for both ferro and antiferromagnetic solutions as defined for the density of states representations. As it can be seen, the bands are quite flat and show little dispersion.
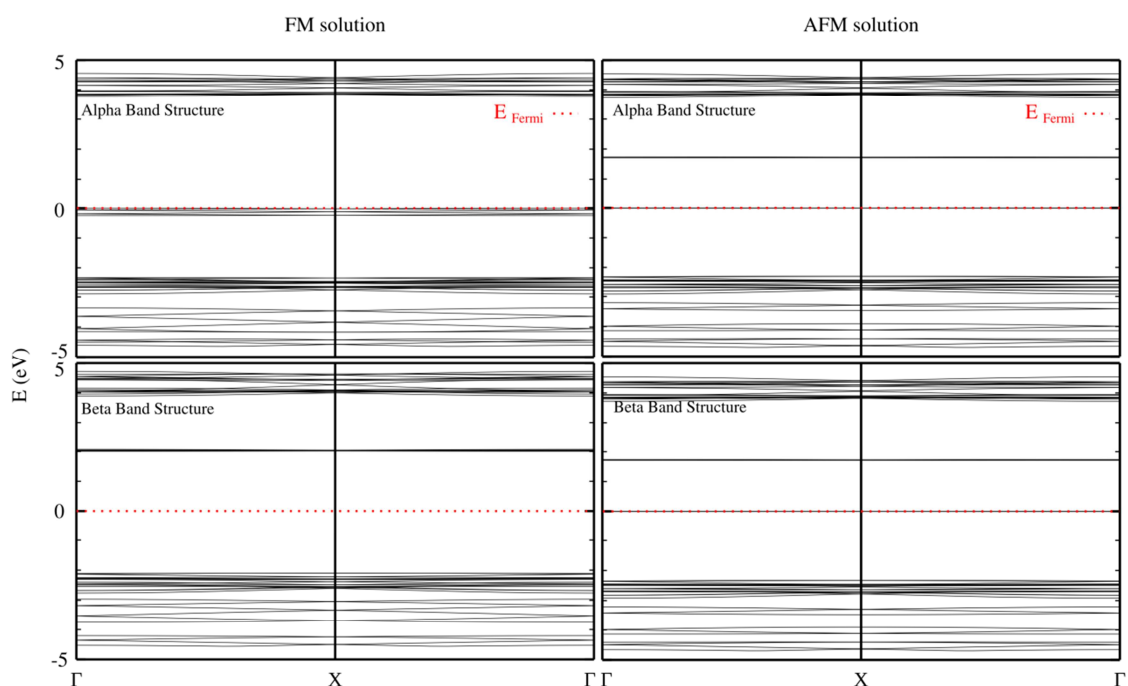
Figure S. I. 4. Band diagram of ferro and antiferro solutions of polymer **2b**

4. Optimized geometries (high-spin solution) of the different decaradicals derived from polymers 1b and 2b and calculated energetic differences for the decaradical derived from polymer 2b.

For reasons of space, the Cartesian coordinates of decaradicals derived from polymer **1b** and **2b** are not displayed here, but it can be requested from the authors

4.3 Calculated energetic differences in the helical decaradical derived from **2b**.

Molecular units presenting ten magnetic centres have at least six solutions with different multiplicity, ranging from $S = 5$ (undecet) to $S = 0$ (singlet). Within the mapping approach, one can approximate the pure spin states through broken symmetry solutions to extract magnetic exchange interactions, provided a correct spin projector is defined. Here, however, we use the broken symmetry solutions to approximate the energetic difference between the several states with different multiplicity. The high-spin state is well described with a single determinant of the type $|\alpha\alpha\alpha\alpha\alpha\alpha\alpha\alpha\alpha\alpha\rangle$, which, by convenience will be represented as $|10\alpha\rangle$. Similarly, the other five low-spin states can be approximated by single determinants of the type $|9\alpha1\beta\rangle$, $|8\alpha2\beta\rangle$, $|7\alpha3\beta\rangle$, $|6\alpha4\beta\rangle$ and $|5\alpha5\beta\rangle$, respectively. For each multiplicity in the low-spin cases, there are several

broken symmetry solutions with similar energy, depending on where the beta spin density is located. In a non-systematic manner we investigated some of the different solutions, and no relevant change was observed. Table S. I.5 reports the energetic differences among the high-spin solution and the most stable low-spin solution found in each case. It clearly illustrates that also in the molecular case, the high spin is the ground state and it is well above the most stable antiferromagnetic solution.

2b derived			
Solution	Absolute energy (a.u.)		ΔE (cm^{-1})
$\lvert 10\alpha \rangle$	−5240.53686416		
$\lvert 9\alpha 1\beta \rangle$	−5240.53539632	$\lvert 10\alpha \rangle - \lvert 9\alpha 1\beta \rangle$	-322
$\lvert 8\alpha 2\beta \rangle$	−5240.53411933	$\lvert 10\alpha \rangle - \lvert 8\alpha 2\beta \rangle$	-602
$\lvert 7\alpha 3\beta \rangle$	−5240.53179894	$\lvert 10\alpha \rangle - \lvert 7\alpha 3\beta \rangle$	-1112
$\lvert 6\alpha 4\beta \rangle$	−5240.53195893	$\lvert 10\alpha \rangle - \lvert 6\alpha 4\beta \rangle$	-1077
$\lvert 5\alpha 5\beta \rangle$	−5240.53183543	$\lvert 10\alpha \rangle - \lvert 5\alpha 5\beta \rangle$	-1104

Table S. I.5. Absolute energies (a.u.) and the corresponding energy difference (cm^{-1}) referred to the most stable state (high-spin) as calculated in the optimized geometry of the polymer **2b** derived decaradical. Negative values for ΔE imply a high-spin ground state.

4.3.6.   Paper #4.6.

Design of Triarylmethyl-Based 2D Polyradical Materials Showing Controllable Magnetic and Optical Properties through Elastic Distortions

Design of Triarylmethyl-Based 2D Polyradical Materials showing Controllable Magnetic and Optical Properties through Elastic Distortions.

Daniel Reta Mañeru, Isaac Alcón, Stefan Bromley, Ibério de P. R. Moreira

Departament de Química Física & Institut de Química Teòrica i Computacional (IQTCUB), Universitat de Barcelona, C/Martí i Franquès 1, 08028 Barcelona, Spain

Abstract

Control over the electronic structure of extended systems by means of externally induced structural distortions is a promising route towards multifunctional materials. In this work we computationally design a planar network using as building blocks stable triarylmethyls organic radicals and simple mesitylene units to link the radical molecules. The resulting stable, two-dimensional π-conjugated ferromagnetic organic polyradical shows a linear correlation between electronic properties and the externally induced distortions. Bringing together stable triarylmethyls and the concept of surface covalent organic framework appears as a promising strategy to obtain such systems.

Introduction

π-conjugated polyradicals represent nowadays one of the main strategies for achieving purely organic multifunctional materials.[1–3]

Among the basic constituents employed for such purpose, triarylmethyls (TAMs) radicals are the most important building blocks.[4] TAMs belong to the odd-alternant polycyclic aromatic hydrocarbon class and are composed of three aryl rings bonded to a central methyl carbon atom, where their unpaired electron mainly resides, as depicted in Scheme 1. In these compounds, the stability of the radical centre is tightly related to the steric protection of the radical centrs. Thus, the simplest TAM, the triphenylmethyl (TPM) originally reported by Gomberg in 1900[5] and derivatives are known to last only for few minutes in solution at room conditions before reacting with atmospheric oxygen,[5] and to undergo dimerization reactions.[6] However, a larger protection by substituting all hydrogen atoms in TPM by chlorine atoms results in the perchlorotriphenylmethyl (PTM), a remarkably stable radical synthesized by Ballester et

al.[7] The versatility offered by the inclusion of different substituents in the aryl positions, has allowed the syntheses of many different TAMs derivatives.[7–14]

One of the most outstanding uses of TPM as a radical building block was developed by Rajca *et al.*[4] in the field of organic magnetism, coining the concept of spin cluster. Within this strategy, the first example of an organic polymer magnet was reported,[15] showing an approximate *S* value of 5000 and magnetic order below 10 K. Owing to the improved chemical stability of the PTM, these building blocks have been widely exploited,[2] as for instance for the preparation of electro-active self-assembled monolayers,[16,17] mixed-valence compounds,[18] donor-acceptor systems,[19] robust magnetic triradicals,[20] porous-organic radical frameworks (POFs)[21] or metal-organic frameworks (MOFs).[22] Such diversity has led to very interesting properties for material science such as enhanced electrical conductivities,[23] optical absorption bands[24] or magnetoresistance phenomena.[25]

The intrinsic molecular-structure/spin-localization relationship in TAMs has been recently revealed computationally.[26] This work manifests a linear dependence between spin-localization and the average cosine squared of the dihedral angle ($<\cos^2\varphi>$) of each aryl ring with the central carbon atom plane, which is consistent with π–overlap arguments.[27–29] Additionally, this relationship does not depend on the chemical functionalization or temperature.[26] It is then reasonable to think that manipulating the spin localization by structural means represents a powerful tool for controlling the associated properties that arise from spin-spin interactions. However, to the best of our knowledge, no explicit TAM device or material has been made or designed towards this direction.

The work reported in this letter aims at bridging this gap, bringing together the concepts of two-dimensional covalent organic frameworks (2D-COFs)[30,31] and TAMs radicals.[4] Thus, we propose a TAM-based 2D π-conjugated polyradical for which the twist of the aryl rings can be controlled by external mechanical strain. By means of density functional calculations we study the structure, chemical stability and magnetic coupling under the effect of the external strain and its impact on the material properties. We find that a gradual distortion is followed by smooth changes on the magnetic and optical properties without largely affecting the chemical stability of the radical centres within the network, which is crucial for potential applications of the material.

Computational details.

The structure is modelled by a single slab in vacuum, as shown in Figure 1. All the different structures reported herein were fully optimized with the hybrid PBE0[32] functional within the FHI-AIMS code,[33,34] using "light" numerical basis sets. Aiming to mimic the strain that a planar system might experience on top of a certain substrate, we performed a series of restricted optimizations, increasing systematically one of the cell parameters (from zero to five Å) and optimizing the other, while keeping constant the vacuum level.

For the calculation of electronic structure and magnetic properties, we use the Crystal09 code,[35,36] the B3LYP[37] hybrid density functional based method with the standard 6-21G* basis set for all atoms.[38,39] ITOL values have been fixed to 7,7,7,7,14 to force stringent numerical convergence of energy and gradients and a shrinking factor of 6 in the 2D irreducible Brillouin zone, using the Monkhorst-Pack scheme to define the reciprocal space.

The description of the magnetic properties is based on the Ising spin Hamiltonian[40]

$$\hat{H}^{Ising} = -\sum_{\langle i,j \rangle} J_{ij}\hat{S}_i^z\hat{S}_j^z \tag{1}$$

where J_{ij} is the exchange coupling constant between the $\hat{S}_i^z$ and $\hat{S}_j^z$ localized spin moments and the $\langle i,j \rangle$ symbol indicates that the sum refers to nearest neighbour interactions only. According to Eq. (1), a positive value of the exchange coupling constant J_{ij} corresponds to ferromagnetic (FM) interactions, while negative values describe an antiferromagnetic (AFM) interaction (parallel and antiparallel spins respectively). The number, sign and magnitude of the most relevant J_{ij} determine the low-energy spectrum of the system and, consequently, the magnetic structure of the system. The extraction of the different J_{ij} is based on the mapping approach described elsewhere.[41]

Results and discussion

As suggested by Mataga[42] in 1968, hypothetical linear and 2D arrangements of *m*-xylylene diradical[43] and TAM radicals, might present high-spin ground states. More recently, Rajca *et al.*[15] provided the first experimental proof that these networks can be

achieved. However, the magnetic properties of the resulting system persist only at low temperature, presumably due to the instability of the polyradical. Therefore, it would be desirable to count with strategies that allow preparing stable organic polymer magnets with larger critical temperature and chemical stability at ambient conditions. A step in this direction can be done working with building blocks that are already very stable themselves, such as PTMs.

In fact, following early achievements on the preparation of porous organic frameworks (POFs)[22] and molecular organic frameworks (MOFs),[21] one could take advantage of PTMs stability over surfaces[17,44] in order to obtain 2D-SCOFs. Important advantages are derived from this strategy, since it offers 2D ordered covalently bonded networks where the different molecular constituents occupy ordered positions in the mono-layer. Monolayer 2D-COFs are normally achieved when prepared on specific surfaces (surface covalent organic frameworks, SCOFs)[45] but they can also be prepared in solution,[46] obtaining a multi-layered or porous material. As proved experimentally in graphene monolayers and bilayers,[47,48], structural distortions can be introduced by carefully bending the supporting substrate, due to the 2D-fashion order. Thus, since a clear molecular-structure/spin-localization relationship exists in TAMs,[26] stretching might represent an effective way to change the electronic properties of TAM-based 2D-SCOFs π-conjugated polyradicals.

Based on these strategies, here we report the computational design and study of two hypothetical 2D-COFs. Figure 1 schematically compares the building blocks used by Rajca et al.,[15] and the ones used in this work, together with the resulting extended system. 2D-TPM stands for the system obtained from TPMs (R = H), while 2D-PTM stands for the system obtained from PTMs (R = Cl) (Figure 1). The design of our TAM-based 2D-COFs deliberatively aims to obtain a planar material with stable radical centres. Planarity is required so the external strain affects efficiently the twist of the phenyl rings only. 1,3-phenylene is known to be a good coupling unit to promote strong ferromagnetic interactions,[49] and consequently, TAM units should be connected through the meta-position of their aryl rings to avoid formation of quinoidal structures. However, due to the propeller-like structure of most TAMs, a 1,3-connectivity would probably lead to non-planar structures preventing the formation of the 2D-network in solution or on surface. Thus, as depicted in Figure 1, we consider the use of benzene units to connect three TAM units through their para-positions, hence ensuring the

planarity of the 2D-network. Comparatively, the network of the system proposed by Rajca *et al.* is much more rigid to external distortions due to the calix[4]arene-based radicals.

For both the proposed 2D-TPM and 2D-PTM structures, all atoms coordinates and cell parameters are optimized. In the minimum energy structures, the radical centres lay on a plane defining the central element of the slab. These radical centres are connected with all TAM aryl rings twisted by 34° and 40° respectively, with respect to the network plane. These twist angle values coincide with the calculated for the TPM and PTM single molecules.[26] Calculations are performed on the fully optimized structure (relaxed) and two restricted optimized points with different degree of distortion, denoted semi-distorted and distorted. Table 1 summarizes all relevant values concerning energetic differences between the low-lying magnetic states, band gaps and spin densities. As for the case of discrete molecules,[26] these properties correlate very well with the corresponding $<\cos^2\varphi>$ values (see supplementary information). Both 2D-TPM and 2D-PTM relaxed structures show a high-spin ground state. The spin density in these cases spreads between the radical centres and the phenyl rings surrounding them, which are also shared by other TPM units. According to Borden and Davidson,[50] the non-disjoint character of the singly occupied orbitals (SOMOs) in odd alternant hydrocarbons, favours the high-spin state. The applied strain produces a partial twisting of certain aryl rings, leading to a localization of the spin density in the radical centre with a concomitant suppression of spin density on the shared phenyl rings. Thus, the radical centres become magnetically independent and in the most distorted structure, the high-spin and low-spin solutions become almost degenerate. When comparing both systems, the bulky chlorine atoms in the 2D-PTM force much larger dihedral angles than in the 2D-TPM case, which translates into smaller energy separation between the low-lying magnetic states. Consequently, the 2D-PTM network presents much more reduced $<\cos^2\varphi>$ variation for the same applied strain, when compared to the 2D-TPM network (see section 1 of supplementary information). The values of calculated band gaps in Table 1 indicate several things. First, its value depend to a given extent on the used functional, but for a given functional the trends are the same. Second, these values correspond to energies in the range of visible radiation, meaning that if synthesized, they might display a given colour which might change by structural stress. Third, the relatively small and linear variation that the applied distortions induce in this property

indicates that the distortions do not destroy the electronic structure of the material suggesting a comparable chemical stability. Finally, the fact that they remain constant for the high- and low spin-solutions (for the 2D-TPM case) suggests that the spin density is well-localized in the radical centres and that magnetic properties do not alter the electronic structure of the network. These considerations are further justified by the observation of the same trends for the spin densities on the radical centres.

Concerning the magnetic properties, calculations have been carried out only on the 2D-TPM system. The restricted optimizations performed introduce gradual twisting moves of the aryl rings, which distorts the equilateral triangle relating the three radical centres in the unit cell. This is schematically depicted in Figure 2. Thus, for the relaxed geometry there is only one J_1 inside the triangle, and almost twice further, J_2 relates two radical centres through the pore; in the distorted geometries the equilateral triangle is lost, and J_1 converts into J_{1a} and J_{1b}. The unit cell consist of all three geometries contains three radical centres, which, for the extraction of two different magnetic exchange interactions does not provide enough magnetic solutions. Therefore, the magnetic cells used for the extraction of magnetic interactions are twice the unit cell in one of the directions. Table 2 presents the calculated magnetic coupling constant values for the three relaxed, semi-distorted and distorted geometries. Details on the extraction of these values can be found in the supplementary information. For the semi-distorted and distorted geometries, J_2 has been ignored in view of the negligible value in the relaxed case. The calculated values for the three geometries indicate a ferromagnetic interaction, although in the distorted geometry, the ferromagnetic solution is practically degenerate with the antiferromagnetic one.

Conclusions.

This work presents a theoretical study of the structural, electronic structure features and magnetic properties of two monolayer TAM-based polyradicals, showing the radical centres lying on a plane that defines the central element of the slab, and how those are affected by external mechanical strain.

Two systems have been designed: 2D-TPM and 2D-PTM. Both share a phenyl ring as building block, but one is based on TPM radical and the other on PTM. PTM is known to be stable over surfaces[17] indicating that it could be deposited to generate the 2D-SCOF. However, for the TPM case, due to the less sterically protected radical

centre, it might be desirable to deposit it in its precursor form (ether), and if the monolayer is successfully formed, proceed with the carbanion method to generate the radical centres.[51,52] In fact, this strategy might bring an additional advantage in terms of generating the radical centres, because an ordered layer would present radical precursors more easily accessible than in the case of structurally disordered polymers[53] or star-branched dendrimers.[4] This would decrease the impact that chemical defects (absence of radicals at some TAM sites) have in suppressing the magnetic interactions defining the 2D magnetic topology in the material.[4]

Both systems, when fully optimized, present a high-spin ground state. The energetic separation with the rest of low-spin solutions is calculated to be larger for the 2D-TPM case, because the bulky chlorine atoms of PTM introduce dihedral angles that force a considerable spin-localization.

There exists a clear correlation between the aryl ring twists and all the properties derived from a different extent of spin-localization over the radical centres, such as spin density, band gap, ΔE_{FM-AFM} and J coupling values. This offers a powerful mechanism to control electronic properties of TAM-based 2D-SCOFs by external means.

The calculated J coupling constant values are small. This indicates that this type of networks might not be appropriate for magnetic materials, but rather for other interesting optical properties.
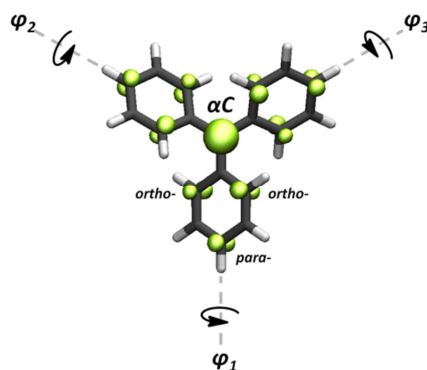
Scheme 1. Triarylmehtyl general molecular structure. The unpaired electron mainly resides on the central carbon atom (αC) but also partially delocalizes to the ortho- and para- positions of each aryl ring.
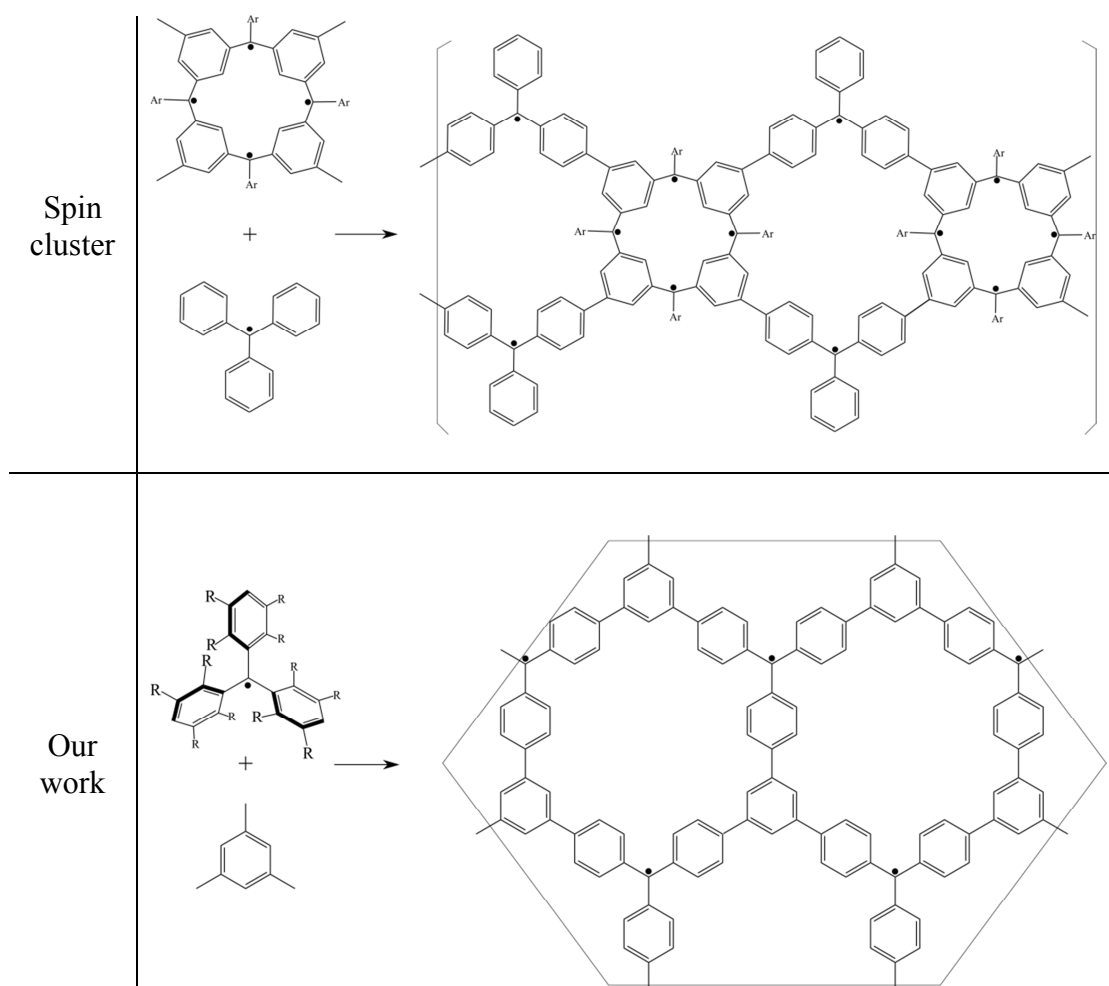

Figure 1. Schematic comparison of the building blocks used and the resulting extended 2D polyradicals introduced by Rajca et al. and the ones used in this work. The possibility of introducing an external strain that affects the triaryl twist angles without distorting too much the planarity of the system, is more effficiently achieved within our proposal. Within our proposal, two prototype TAM-based 2D-COFs are designed and studied. When the TAM presents all R = H, the structure is designated as 2D-TPM; when it presents all R = Cl, the obtained structure is named 2D-PTM. The substituents are not shown in the extended structure for clarity.
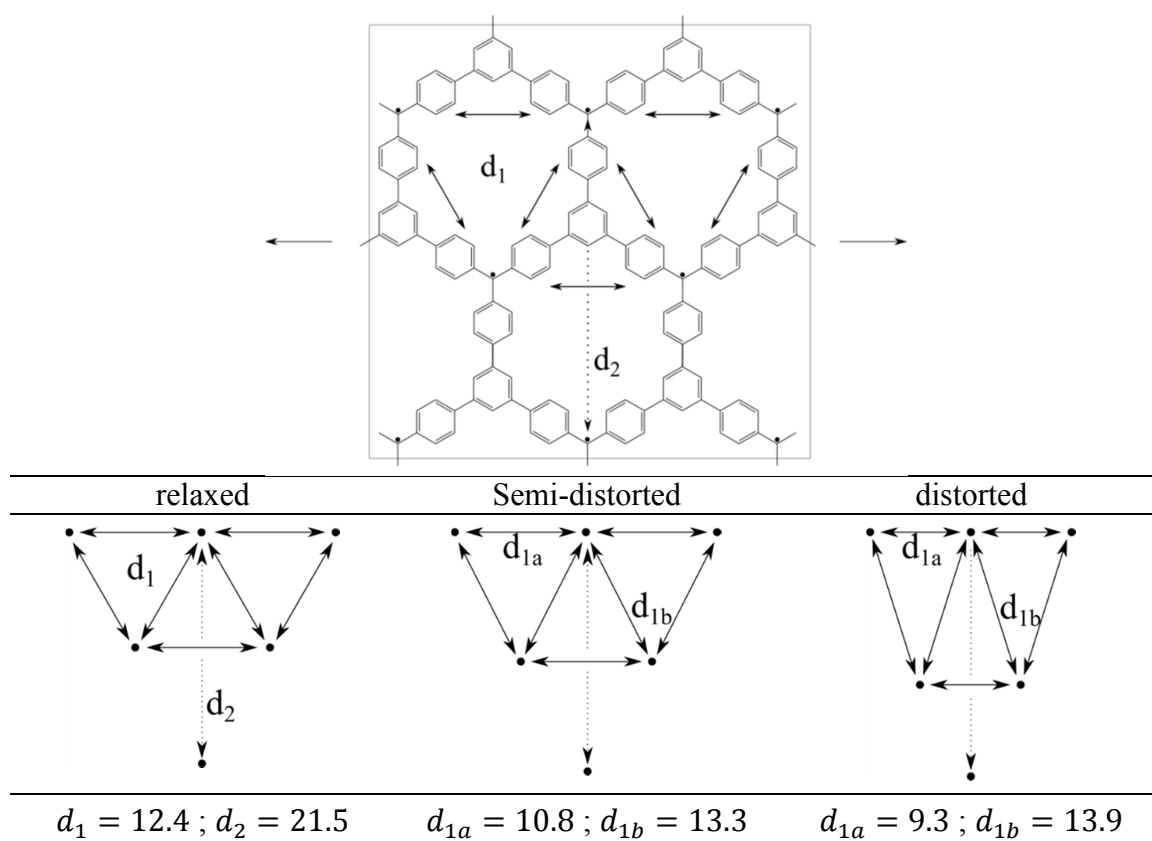
relaxed	Semi-distorted	distorted
$d_1 = 12.4 \, ; \, d_2 = 21.5$	$d_{1a} = 10.8 \, ; \, d_{1b} = 13.3$	$d_{1a} = 9.3 \, ; \, d_{1b} = 13.9$

Figure 2. Schematic representation of the most relevant distances between the radical centres, and how they are affected by external strain. Down most row indicates the actual values (Å) for these distances in 2D-TPM. Note that for the semi-distorted and distorted cases, d_2 has been ignored.

	2D-TPM			2D-PTM		
	Relaxed	Semi-distorted	Distorted	Relaxed	Semi-distorted	Distorted
	Calculated energy differences per magnetic centre (cm^{-1})					
ΔE_{FM-AFM_1}	-16.0	-4.8	-0.1	-3.0	-1.8	-0.6
ΔE_{FM-AFM_2}	-32.1	-14.0	-0.3			
	Band gap (eV)					
FM	1.8 (2.2)	1.9 (2.4)	2.4 (2.8)	(2.9)	(2.9)	(3.0)
AFM_1	1.8	2.0	2.4			
	Averaged spin density at the radical centres					
FM	0.604	0.693	0.807	0.816	0.842	0.848
AFM_1	0.604	0.693	0.807	0.816	0.842	0.848
AFM_2	0.604	0.693	0.807			

Table 1. Summary of electronic properties on both structures investigated, at each of the geometries. For the band gap values, the results are obtained from B3LYP (PBE0) calculations.

2D-TPM			
	relaxed	Semi-distorted	distorted
J_{1a}	5.5	0.18	0.001
J_{1b}	5.5	2.33	0.06
J_2	-0.006	-	-

Table 2. Magnetic coupling constants per magnetic centre (cm^{-1}) for the 2D-TPM, at each of the geometries investigated. The corresponding J2a J2b values in semi- and distorted geometries have not been calculated but are expected to be of the same order as in the relaxed geometry (see distances in Table 1).

REFERENCES

(1)   Veciana, J. *Π-Electron Magnetism From Molecules to Magnetic Materials*, Ed.; Sprin.; Berlin, 2001.

(2)   Ratera, I.; Veciana, J. Playing with Organic Radicals as Building Blocks for Functional Molecular Materials. *Chem. Soc. Rev.* **2012**, *41* (6), 303–349.

(3)   Train, C.; Norel, L.; Baumgarten, M. Organic Radicals, a Promising Route towards Original Molecule-Based Magnetic Materials. *Coord. Chem. Rev.* **2009**, *253* (19-20), 2342–2351.

(4)   Rajca, A. The Physical Organic Chemistry of Very High-Spin Polyradicals. *Adv. Phys. Org. Chem.* **2005**, *40*, 153–199.

(5)   Gomberg, M. An Instance of Trivalent Carbon: Triphenylmethyl. *J. Am. Chem. Soc.* **1900**, *22* (11), 757–771.

(6)   Neumann, W. P.; Penenory, A.; Stewen, U.; Lehnig, M. Sterically Hindered Free Radicals. 18. Stabilization of Free Radicals by Substituents as Studied by Using Triphenylmethyls. *J. Am. Chem. Soc.* **1989**, *111* (15), 5845–5851.

(7)   Ballester, M.; Riera-Figueras, J.; Castaner, J.; Badfa, C.; Monso, J. M. Inert Carbon Free Radicals. I. Perchlorodiphenylmethyl and Perchlorotriphenylmethyl Radical Series. *J. Am. Chem. Soc.* **1971**, *93* (9), 2215–2225.

(8)   Ballester, M.; Castañer, J.; Riera, J.; Ibáñez, A.; Pujadas, J. Inert Carbon Free Radicals 2. Monofunctionalized Tetradecachlorotriphenylmethyl Radicals and Related Compounds. *J. Org. Chem.* **1982**, *47*, 259–264.

(9)   Ballester, M.; Riera, J.; Castañer, J.; Rovira, C.; Veciana, J.; Onrubia, C. Inert Carbon Free Radicals. 4. Spin Labeling of Amino Acids and Peptides. *J. Org. Chem.* **1983**, *48* (21), 3716–3720.

(10)   Juliá, L.; Ballester, M.; Riera, J.; Castañer, J.; Ortin, J. L.; Onrubia, C. Inert Carbon Free Radicals. 9. The First Perchlorinated Triarylmethyl and Fluorenyl

Radicals with a Heteroaromatic Ring, and Related Compounds. *J. Org. Chem.* **1988**, *53*, 1267–1273.

(11) Staab, H. A.; Kuo-chen, C.; Ruland, A. Synthese Und Reaktionen von a-Hydroxy- Und a-Halogen-a-Aryl[1 .n]paracyclophanen. *Chem. Ber.* **1982**, *115*, 1765–1774.

(12) Sabacky, M. J.; Johnson, C. S.; Smith, R. G.; Gutowsky, H. S.; Martin, J. C. Triarylmethyl Radicals. Synthesis and Electron Spin Resonance Studies. *J. Am. Chem. Soc.* **1967**, *89*, 2054–2058.

(13) Neunhoeffer, O.; Haase, H. Dioxa-Dihydrocoranthryl, Ein Eingeebnetes Triphenylmethylradikal. *Chem. Ber.* **1958**, *91* (9), 1801–1805.

(14) Gabellieri, C.; Mugnaini, V.; Paniagua, J. C.; Roques, N.; Oliveros, M.; Feliz, M.; Veciana, J.; Pons, M. Dynamic Nuclear Polarization with Polychlorotriphenylmethyl Radicals: Supramolecular Polarization-Transfer Effects. *Angew. Chem. Int. Ed. Engl.* **2010**, *49* (19), 3360–3362.

(15) Rajca, A.; Wongsriratanakul, J.; Rajca, S. Magnetic Ordering in an Organic Polymer. *Science* **2001**, *294*, 1503–1505.

(16) Crivillers, N.; Mas-Torrent, M.; Vidal-Gancedo, J.; Veciana, J.; Rovira, C. Self-Assembled Monolayers of Electroactive Polychlorotriphenylmethyl Radicals on Au(111). *J. Am. Chem. Soc.* **2008**, *130* (16), 5499–5506.

(17) Mas-Torrent, M.; Crivillers, N.; Rovira, C.; Veciana, J. Attaching Persistent Organic Free Radicals to Surfaces: How and Why. *Chem. Rev.* **2012**, *112*, 2506–2527.

(18) Lloveras, V.; Vidal-Gancedo, J.; Figueira-Duarte, T. M.; Nierengarten, J. F.; Novoa, J. J.; Mota, F.; Ventosa, N.; Rovira, C.; Veciana, J. Tunneling versus Hopping in Mixed-Valence Oligo-P-Phenylenevinylene Polychlorinated Bis(triphenylmethyl) Radical Anions. *J. Am. Chem. Soc.* **2011**, *133* (15), 5818–5833.

(19) Guasch, J.; Grisanti, L.; Jung, S.; Morales, D.; D'Avino, G.; Souto, M.; Fontrodona, X.; Painelli, A.; Renz, F.; Ratera, I.; et al. Bistability of Fc-PTM-Based Dyads: The Role of the Donor Strength. *Chem. Mater.* **2013**, *25* (5), 808–814.

(20) Veciana, J.; Rovira, C.; Ventosa, N.; Crespo, M. I.; Palacio, F. Stable Polyradicals with High-Spin Ground States. 2. Synthesis and Characterization of a Complete Series of Polyradicals Derived from 2,4,6-Trichloro-.α.,.α.,.α.',.α.',.α.'',.α.''-Hexakis(pentachlorophenyl)mesitylene with S = 1/2,. *J. Am. Chem. Soc.* **1993**, *115* (d), 57–64.

(21) Roques, N.; Maspoch, D.; Luis, F.; Camón, A.; Wurst, K.; Datcu, A.; Rovira, C.; Ruiz-Molina, D.; Veciana, J. A Hexacarboxylic Open-Shell Building Block:

Synthesis, Structure and Magnetism of a Three-Dimensional Metal–radical Framework. *J. Mater. Chem.* **2008**, *18* (1), 98–108.

(22)   Maspoch, D.; Ruiz-Molina, D.; Wurst, K.; Domingo, N.; Cavallini, M.; Biscarini, F.; Tejada, J.; Rovira, C.; Veciana, J. A Nanoporous Molecular Magnet with Reversible Solvent-Induced Mechanical and Magnetic Properties. *Nat. Mater.* **2003**, *2* (3), 190–195.

(23)   Crivillers, N.; Munuera, C.; Mas-Torrent, M.; Simão, C.; Bromley, S. T.; Ocal, C.; Rovira, C.; Veciana, J. Dramatic Influence of the Electronic Structure on the Conductivity through Open- and Closed-Shell Molecules. *Adv. Mater.* **2009**, *21* (10-11), 1177–1181.

(24)   Simão, C.; Mas-Torrent, M.; Crivillers, N.; Lloveras, V.; Artés, J. M.; Gorostiza, P.; Veciana, J.; Rovira, C. A Robust Molecular Platform for Non-Volatile Memory Devices with Optical and Magnetic Responses. *Nat. Chem.* **2011**, *3* (5), 359–364.

(25)   Frisenda, R.; Gaudenzi, R.; Franco, C.; Mas-Torrent, M.; Rovira, C.; Veciana, J.; Alcon, I.; Bromley, S. T.; Burzurí, E.; van der Zant, H. S. J. Kondo Effect in a Neutral and Stable All Organic Radical Single Molecule Break Junction. *Nano Lett.* **2015**, *15* (5), 3109–3114.

(26)   Alcón, I.; Bromley, S. T. Structural Control over Spin Localization in Triarylmethyls. *RSC Adv.* **2015**, *5* (119), 98593–98599.

(27)   Adam, F. C.; Weissman, S. I. Electron Spin Resonance and Electronic Structure of Triphenylmethyl. *J. Am. Chem. Soc.* **1958**, *80* (11), 2057–2059.

(28)   Karplus, M.; Fraenkel, G. K. Theoretical Interpretation of Carbon-13 Hyperfine Interactions in Electron Spin Resonance Spectra. *J. Chem. Phys.* **1961**, *35* (4), 1312–1323.

(29)   Maki, A. H.; Allendoerfer, R. D.; Danner, J. C.; Keys, R. T. Electron Nuclear Double Resonance in Solutions. Spin Densities in Triarylmethyl Radicals. *J. Am. Chem. Soc.* **1968**, *90* (16), 4225–4231.

(30)   Ding, S.-Y.; Wang, W. Covalent Organic Frameworks (COFs): From Design to Applications. *Chem. Soc. Rev.* **2013**, *42* (2), 548–568.

(31)   Côté, A. P.; Benin, A. I.; Ockwig, N. W.; O'Keeffe, M.; Matzger, A. J.; Yaghi, O. M. Porous, Crystalline, Covalent Organic Frameworks. *Science* **2005**, *310* (5751), 1166–1170.

(32)   Adamo, C.; Barone, V. Toward Reliable Density Functional Methods without Adjustable Parameters: The PBE0 Model. *J. Chem. Phys.* **1999**, *110* (13), 6158.

(33)   Havu, V.; Blum, V.; Havu, P.; Scheffler, M. Efficient Integration for All-Electron Electronic Structure Calculation Using Numeric Basis Functions. *J. Comput. Phys.* **2009**, *228* (22), 8367–8379.

(34) Blum, V.; Gehrke, R.; Hanke, F.; Havu, P.; Havu, V.; Ren, X.; Reuter, K.; Scheffler, M. Ab Initio Molecular Simulations with Numeric Atom-Centered Orbitals. *Comput. Phys. Commun.* **2009**, *180* (11), 2175–2196.

(35) Dovesi, R.; Orlando, R.; Civalleri, B. CRYSTAL: A Computational Tool for the Ab Initio Study of the Electronic Properties of Crystals. *Z. Krist.* **2005**, *220*, 571–573.

(36) Dovesi, R.; Saunders, V. R.; Roetti, C.; Orlando, R.; Zicovich-Wilson, C. M.; Pascale, F.; Civalleri, B.; Doll, K.; Harrison, N. M.; Bush, I. J.; et al. CRYSTAL09 User's Manual. *University of Torino*. Torino 2009.

(37) Becke, a D. Density Functional Thermochemistry. III. The Role of Exact Exchange 98:5648-52. *J Chem Phys* **1993**, *103* (3-4), 361–363.

(38) Hariharan, P. C.; Pople, J. A. The Influence of Polarization Functions on Molecular Orbital Hydrogenation Energies. *Theor. Chim. Acta* **1973**, *28* (3), 213–222.

(39) Francl, M. M.; Pietro, W. J.; Hehre, W. J.; Stephen Binkley, J.; Gordon, M. S.; DeFrees, Douglas, J.; Pople, J. A. Self-Consistent Molecular Orbital Methods. XXIII. A Polarization-Type Basis Set for Second-Row Elements. *J. Chem. Phys.* **1982**, *77* (7), 3654.

(40) Ising, E. Beitrag Zur Theorie Des Ferromagnetismus. *Zeitschrift für Phys.* **1925**, *31* (1), 253–258.

(41) Moreira, I. de P. R.; Illas, F. A Unified View of the Theoretical Description of Magnetic Coupling in Molecular Chemistry and Solid State Physics. *Phys. Chem. Chem. Phys.* **2006**, *8* (14), 1645–1659.

(42) Mataga, N. Possible Ferromagnetic States of Some Hypothetical Hydrocarbons. *Theor. Chim. Acta* **1968**, *10* (4), 372–376.

(43) Wenthold, P. G.; Kim, J. B.; Lineberger, W. C. Photoelectron Spectroscopy of M -Xylylene Anion. **1997**, *7863* (16), 1354–1359.

(44) Mugnaini, V.; Calzolari, A.; Ovsyannikov, R.; Vollmer, A.; Gonidec, M.; Alcon, I.; Veciana, J.; Pedio, M. Looking Inside the Perchlorinated Trityl Radical/Metal Spinterface through Spectroscopy. *J. Phys. Chem. Lett.* **2015**, No. 111, 2101–2106.

(45) Liu, X.-H.; Guan, C.-Z.; Ding, S.-Y.; Wang, W.; Yan, H.-J.; Wang, D.; Wan, L.-J. On-Surface Synthesis of Single-Layered Two-Dimensional Covalent Organic Frameworks via Solid-Vapor Interface Reactions. *J. Am. Chem. Soc.* **2013**, *135* (28), 10470–10474.

(46) Ding, H.; Li, Y.; Hu, H.; Sun, Y.; Wang, J.; Wang, C.; Wang, C.; Zhang, G.; Wang, B.; Xu, W.; et al. A Tetrathiafulvalene-Based Electroactive Covalent Organic Framework. *Chemistry* **2014**, *20* (45), 14614–14618.

(47)   Zhao, J.; Wang, G.; Yang, R.; Lu, X.; Cheng, M.; He, C.; Xie, G.; Meng, J.; Shi, D.; Zhang, G. Tunable Piezoresistivity of Nanographene Films for Strain Sensing. *ACS Nano* **2015**, *9* (2), 1622–1629.

(48)   Ni, Z. H.; Yu, T.; Lu, Y. H.; Wang, Y. Y.; Feng, Y. P.; Shen, Z. X. Uniaxial Strain on Graphene: Raman Spectroscopy Study and Band-Gap Opening. *ACS Nano* **2008**, *2* (11), 2301–2305.

(49)   Gallagher, N. M.; Olankitwanit, A.; Rajca, A. High-Spin Organic Molecules. *J. Org. Chem.* **2015**, *80* (1), 1291–1298.

(50)   Borden, W. T.; Davidson, E. R. Effects of Electron Repulsion in Conjugated Hydrocarbon Diradicals. *J. Am. Chem. Soc.* **1977**, *99* (14), 4587–4594.

(51)   Rajca, A. A Polyarylmethyl Carbotetraanion. *J. Am. Chem. Soc.* **1990**, *112*, 5889–5890.

(52)   Rajca, A. A Polyarylmethyl Quintet Tetraradical. *J. Am. Chem. Soc.* **1990**, *112* (7), 5890–5892.

(53)   Utamapanya, S.; Kakegawa, H.; Bryant, L.; Rajca, A. High-Spin Polymers. Synthesis of 1,3-Connected Polyarylmethane and Its Carbopolyanion and Polyradical. *Chem. Mater.* **1993**, *5* (8), 1053–1055.

Supplementary Information

Design of Triarylmethyl-Based 2D Polyradical Materials showing Controllable Magnetic and Optical Properties through Elastic Distortions.

Daniel Reta Mañeru, Isaac Alcón, Stefan Bromley, Ibério de P. R. Moreira

Departament de Química Física & Institut de Química Teòrica i Computacional (IQTCUB), Universitat de Barcelona, C/Martí i Franquès 1, 08028 Barcelona, Spain

Index of Supplementary Information.

1. Correlation between ΔE_{FM-AFM}, band gaps, spin densities and magnetic coupling constant values with $<\cos^2\varphi>$ for both 2D-TPM and 2D-PTM structures at each of the relaxed, semi-distorted and distorted geometries.

2. Band structure for the 2D-TPM systems at the relaxed and distorted geometries.

3. Details on the definition of different magnetic solutions for the extraction of all relevant magnetic exchange interactions.

1. Correlation between ΔE_{FM-AFM}, band gaps, spin densities and magnetic coupling constant values with $\langle\cos^2\varphi\rangle$ for both 2D-TPM and 2D-PTM structures at each of the relaxed, semi-distorted and distorted geometries.

This section shows graphically the linear correlation between calculated one-electron properties and the $\langle\cos^2\varphi\rangle$ value.
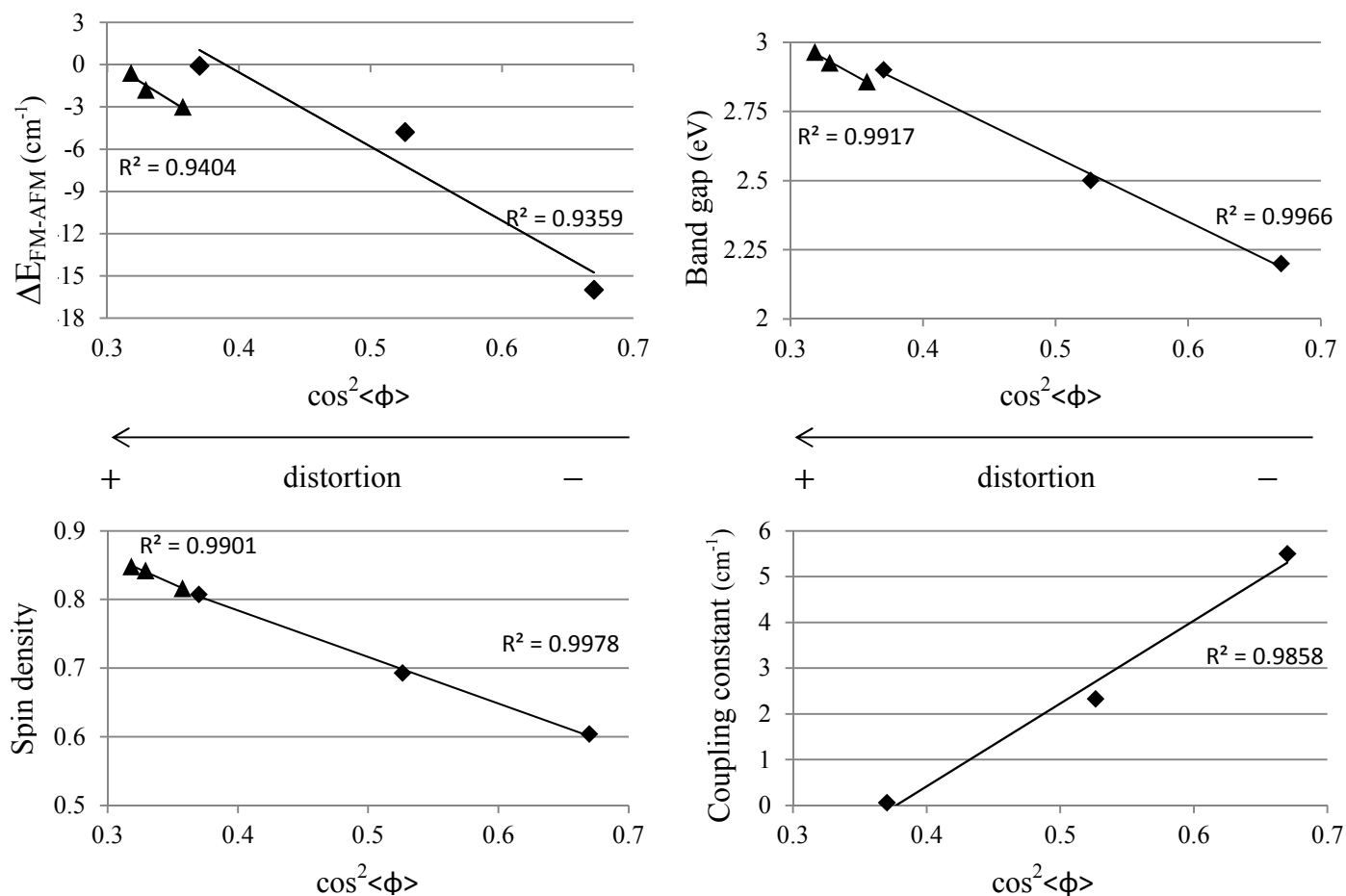

Figure SI.1.Linear correlation between ΔE_{FM-AFM} (cm^{-1}), bandgap (eV), spin density at the radical centres and coupling constant values (cm^{-1}) against average $\langle\cos^2\varphi\rangle$ for the different geometries (relaxed, semi-distorted and distorted) for 2D-TPM (rhombohedral) and 2D-PTM (triangle). All values are calculated with B3LYP[1] functional in Crystal09 program,[2,3] except for the band gaps which are calculated with PBE0[4] in AIMS.[5]

As observed in Figure SI.1, there exists a clear linear correlation between the one-electron properties on the material and aryl ring twist. Indirectly, it manifests the linkage between molecular structure and spin-localization. Note that for all properties, the region of allowed distortions for the 2D-PTM (triangles) is much more reduced as compared to 2D-TPM (rhombohedral).

2. Band structure for 2D-TPM systems at the relaxed and distorted geometries.

In this section is presented the band structures of the 2D-TPM systems at the relaxed and distorted geometries, as calculated with the B3LYP functional and Crystal09 program.
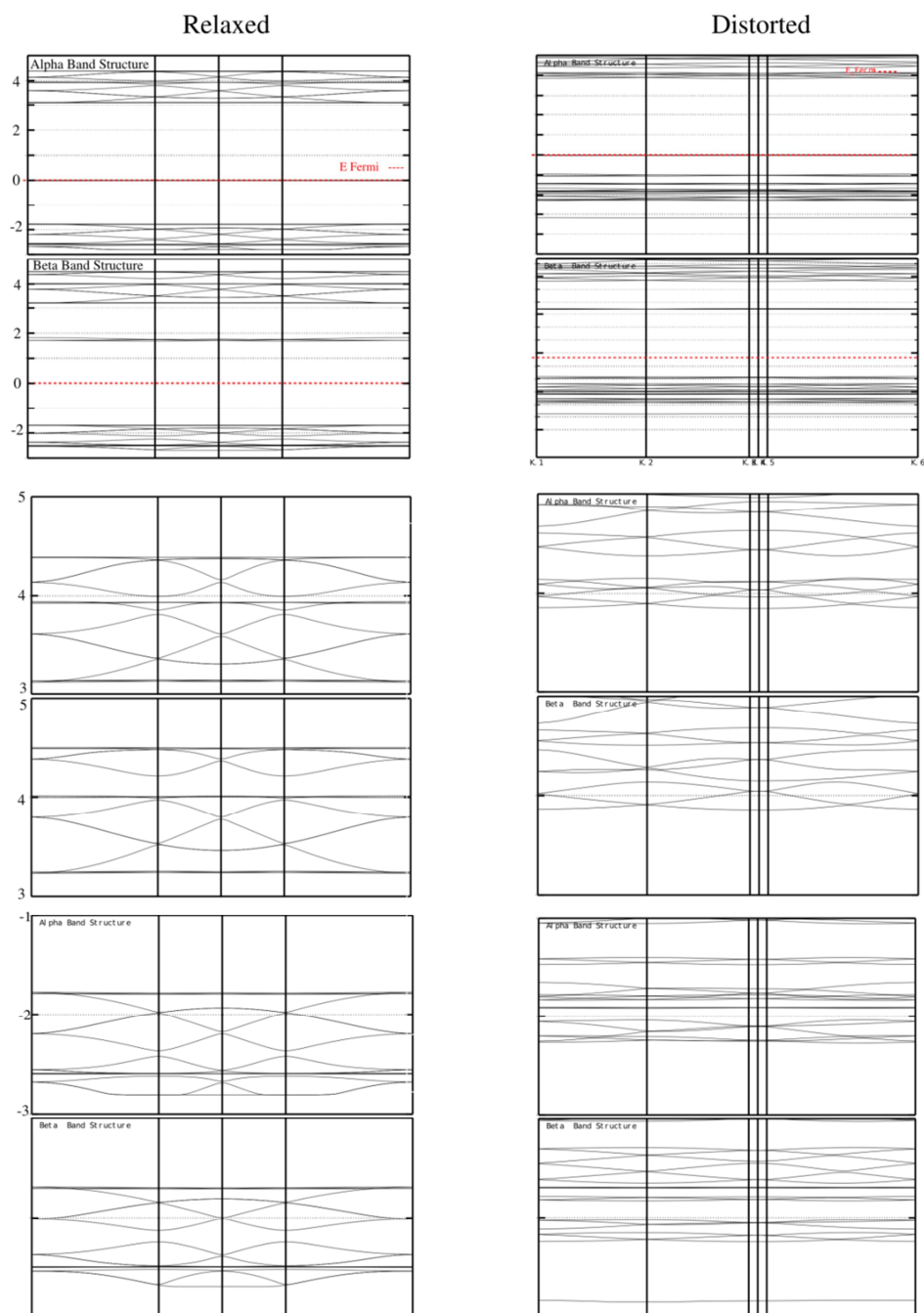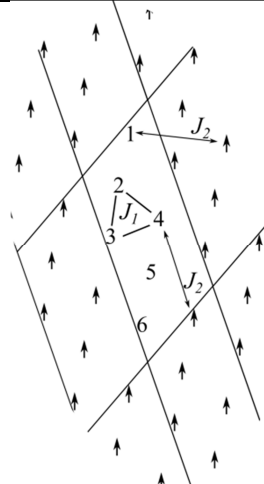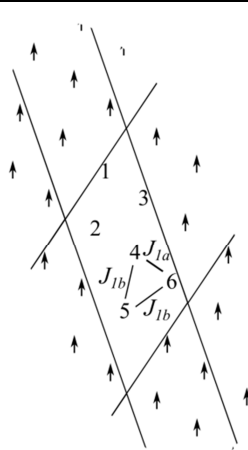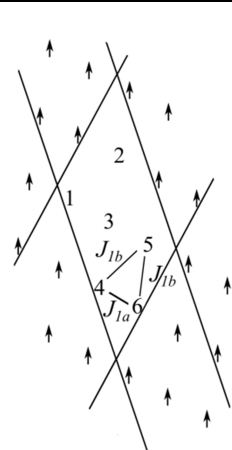

Figure SI.2. Calculated band structure for the 2D-TPM system. Leftmost and rightmost columns stand for the relaxed and distorted geometries, respectively. Highest row shows the band structure in a range of energies from -3 to 5 eV. For clarity, unoccupied and valence bands are zoomed in the middle and down most rows, respectively.

From Figure SI.2, one can see that the band gaps in these systems is ruled by the dispersion of the bands. A closer inspection of the shape of the occupied bands indicates that the dispersion of the bands also changes with the distortion, as an expression of the localization of the unpaired electrons.

3. Details on the definition of different magnetic solutions for the extraction of all relevant magnetic exchange interactions.

The description of the magnetic properties is based on the Ising spin Hamiltonian[6]

$$\hat{H}^{Ising} = -\sum_{\langle i,j \rangle} J_{ij}\hat{S}_i^z\hat{S}_j^z \qquad (1)$$

2D-TPM		
relaxed	Semi-distorted	distorted

solution	$FM = 123456$ $AFM_1 = 1\bar{2}3456$ $AFM_2 = 1\bar{2}34\bar{5}6$		$FM = 123456$ $AFM_1 = 12345\bar{6}$ $AFM_2 = 1\bar{2}3\bar{4}5\bar{6}$		$FM = 123456$ $AFM_1 = 12345\bar{6}$ $AFM_1 = 1\bar{2}3\bar{4}5\bar{6}$

Energy expressions					
	E	ΔE_{FM-AFM}	E	ΔE_{FM-AFM}	E	ΔE_{FM-AFM}
FM	$-\dfrac{9}{2}(J_1+J_2)$		$-\dfrac{1}{2}(3J_1+6J_2)$		$-\dfrac{1}{2}(3J_1+6J_2)$	
AFM_1	$-\dfrac{1}{2}(3J_1+5J_2)$	$-3J_1-2J_2$	$-\dfrac{1}{2}(J_1+2J_2)$	$-J_1-2J_2$	$-\dfrac{1}{2}(J_1+2J_2)$	$-J_1-2J_2$
AFM_2	$\dfrac{1}{2}(3J_1-9J_2)$	$-6J_1$	$\dfrac{1}{2}(-3J_1+6J_2)$	$-6J_2$	$\dfrac{1}{4}(2J_1+5J_2)$	$-\dfrac{1}{4}(8J_1+17J_2)$

Calculated energy differences per magnetic centre (cm^{-1})		
ΔE_{FM-AFM_1}	-16.0	-4.8	-0.1
ΔE_{FM-AFM_2}	-32.1	-14.0	-0.3

Coupling constant values per magnetic centre (cm^{-1})		
J_{1a}	5.5	0.18	0.001
J_{1b}	5.5	2.33	0.06
J_2	-0.006	-	-

Table SI.1. Schematic representation of the magnetic solutions used to extract the relevant coupling constants in each geometry of the 2D-TPM system, corresponding energy expressions as predicted by Ising spin Hamiltonian, calculated energy differences and associated coupling constants values.

In order to extract all relevant magnetic interactions, it was necessary to define a magnetic cell which is double in one direction the unit cell. Thus, the magnetic cell shows six different radical centres which provide enough linearly independent equations to extract the coupling constants. The different magnetic solutions used are denoted FM, AFM1 and AFM2, as depicted in Table SI.1. With the energy expressions for each of the magnetic states obtained with Ising spin Hamiltonian, and the calculated energy differences associated with this states, based on the mapping approach[7] one can extract all relevant magnetic interactions.

REFERENCES

(1)   Becke, a D. *J Chem Phys* **1993**, *103* (3-4), 361–363.

(2)   Dovesi, R.; Orlando, R.; Civalleri, B. *Z. Krist.* **2005**, *220*, 571–573.

(3)   Dovesi, R.; Saunders, V. R.; Roetti, C.; Orlando, R.; Zicovich-Wilson, C. M.; Pascale, F.; Civalleri, B.; Doll, K.; Harrison, N. M.; Bush, I. J.; D'Arco, P.; Llunell, M. *University of Torino*. Torino 2009.

(4)   Adamo, C.; Barone, V. *J. Chem. Phys.* **1999**, *110* (13), 6158.

(5)   Havu, V.; Blum, V.; Havu, P.; Scheffler, M. *J. Comput. Phys.* **2009**, *228* (22), 8367–8379.

(6)   Ising, E. *Zeitschrift für Phys.* **1925**, *31* (1), 253–258.

(7)   Moreira, I. de P. R.; Illas, F. *Phys. Chem. Chem. Phys.* **2006**, *8* (14), 1645–1659.

4.4. Summary and Discussion of Results.

The ultimate goal of this chapter is to provide sound arguments that allow obtaining a purely π–conjugated organic polyradical interacting through-bond, with large *S* value, high-spin ground state, robust ferromagnetic properties, strong magnetic anisotropy and chemical stability.

The structure of section 2 is aimed at introducing each of the necessary arguments that present and explain the sought goal. Thus, it has dealt with the following reasoning:

- To justify why odd alternant hydrocarbons present high-spin ground state despite being neutral molecules with an even number of electrons.
- To select specific odd alternant hydrocarbons as building blocks, on the basis of a promotion of high-spin ground state and the introduction of chemical stability when used to form polyradicals.
- To choose the most convenient coupling scheme in order to promote both interesting macroscopic properties and the appearance of stabilizing secondary structure by means of intramolecular dispersion interactions.

Figure 11 summarizes the previous discussion, explicitly pointing at the requirements for obtaining the desired properties.
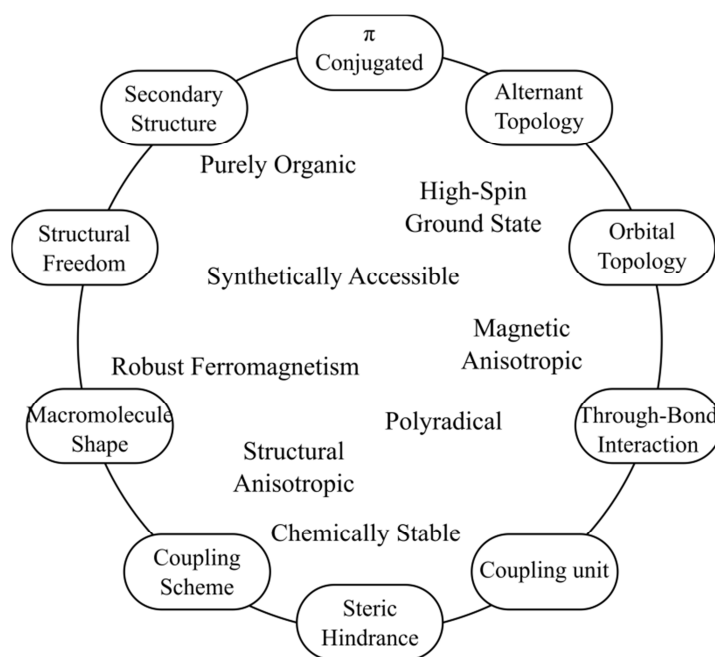

Figure 11. Schematic summary of the requirements (circumference) to obtain the targeted goal (inside the circle).

Keeping this in mind, the series of publications (#4.1-6) have explored different aspects of the electronic structure of odd alternant hydrocarbons, which constituted the necessary steps towards formulating effective and valuable proposals for obtaining the desired materials.

Paper #4.1 performs an extensive computational study on the most basic constituent of all molecules discussed in this chapter, the *m*-xylylene (molecule **9**) diradical. The availability of experimental data on the large triplet-singlet gap[17], made it a perfect reference systems to benchmark the correct methodology for treating related extended compounds. It also served as an exercise for the author to enter the field of computational chemistry methods, and more particularly, to introduce the problematic of correlated electronic states, since before his PhD studied his research was purely experimental. The experimental setup used to access the triplet-singlet gap, is based on measuring the kinetic energy of a photo detached electron from the anion radical, which is associated to the fine vibrational structure of the neutral molecule. The resolution of the fine vibrational structure indicates that it is an adiabatic process, and therefore to correctly describe it theoretically, one has to account for the different geometries on both the triplet and singlet states. Paper #4.1 discusses this particular subject when optimizing the geometries with wave function and density functional-based methods, as suggested by Malrieu *et al.*[66] Despite the apparent simplicity of the molecule (C_8H_8), the majority of computational strategies used to describe its triplet-singlet gap resulted in an overestimation with respect to the experimental value. Despite that, results of DFT-based calculations appear to be quite robust, and the dependence with respect to the basis set quality and to the molecular geometry is quite small. The main problem is the dependence with respect to the choice of the exchange−correlation functional. The difficulty of the wave function-based methods in describing the triplet−singlet gap arises quite unequivocally from dynamical correlation effects which cannot be recovered unless an even larger CAS is used, but this becomes computationally prohibitive. Overall, the M06-2X meta-GGA functional provides the best comparison to experiment.

Paper #4.2 investigates the role of *m*-phenylene as a strong ferromagnetic coupling unit between two nitronyl nitroxides radicals. It addresses the impact that substituents in the phenyl ring have on the magnitude of exchange coupling constant, and the effect of the density functional used to describe it. Particularly, this work investigates the role of

planarity, providing a first word of caution on the importance of structural freedom to properly define the triplet-singlet gap, and consequently the magnetic interactions among unpaired electrons. Despite sharing the same coupling unit, the calculated values for these compounds are much smaller than the ones reported in paper #4.1. This is due to the different nature of the spin-carrier units.

Paper #4.3 studies extended *m*-xylylene derivatives (simplified versions of molecule **11**) with different substituents. It focuses on the non-planarity of the compounds, at variance with similar theoretical studies which assume planarity of the systems, and it finds a large structural flexibility at a very low energetic cost. The richness of minima showed by the potential energy surfaces can be described by a reduced set of values referred to only the two dihedral angles This study constitutes a necessary preliminary step before studying periodic structures and enlightened how hypothetical polyradicals might be extended, as explicitly investigated in paper #4.5. Surprisingly the very different molecular geometries (conformational minima) are connected through transition states that lay very close in energy, resulting in very flat potential energy surfaces. In none of them, the σ−π separation is ensured, but still, they show a high-spin ground state well below in energy from the open-shell singlet. This is in sharp contrast with the *m*-xylylene diradical (paper #4.1) for which a slight distortion penalizes energetically the triplet state (Figure 4.3.1.).

Paper #4.4 is a joint experimental and theoretical work on a robust triradical molecule (based on molecule **13**) sandwiched between two gold electrodes. The molecule presents a different magnetic topology than the one in papers #4.3, since three radical centres are connected through *meta-* of the same phenyl ring. The experimental technique used to inspect the low-lying magnetic states of the molecule is inelastic electron tunnelling spectroscopy and agree with DFT-based calculations. Here small structural distortions, which are assumed to be induced by the electrodes, totally determine the ground state of the molecule, provoking even a crossing of magnetic states. This work, in comparison to paper #4.3 clearly shows that the adopted coupling scheme (section 2.6.3) induces different response of the ground state to structural distortions, which needs to be addressed when looking for robust magnetic properties on a material.

Paper #4.5 could be seen as a natural continuation of paper #4.3 where *m*-xylylene unit is infinitely extended. It reports the appearance of a secondary structure in 1D-like polyradicals, which induces a stabilization of the radical centres while keeping very strong ferromagnetic interactions among them, and orientates the direction of magnetic anisotropy. In line with paper #4.3, largely different conformations do not alter the high-spin nature of the ground state, neither modify dramatically the calculated coupling constant values. Additionally, it also proposes to revisit a discarded synthetic route based on long enough, but still discrete molecular precursors, to ensure the appearance of a helical structure that induces stabilization. This would avoid the uncontrollable impact of the defects imposed by the synthetic route in polymeric precursors

Paper #4.6 investigates an alternative manner to the one proposed by Rajca *et al.*[57] for extending a π-conjugated polyradical system in 2D, by means of triarylmethyl (TAMs) units connected through phenyl rings. This work exploits the stability of different chlorine-substituted derivatives of the Gomberg radical[42] (molecule **12**) when deposited over surfaces[44] and proposes making use of surface covalent organic frameworks (SCOFs) to design 2D-based TAMs polyradicals showing controllable electronic properties by means of external distortions. The work focuses on two model systems, depending whether the TAM building block is simply the Gomber[42] or the PTM[43] radical. By gradually applying a strain in one of the directions of the plane, it is found that the electronic properties, such as spin densities, band gaps, ΔE_{FM-AFM} and magnetic coupling constants, follow a linear correlation with the dihedral angles that is directly linked to the spin localization on the radical centres. The calculated magnetic coupling constants are relatively low, and as commented, are also largely affected by the distortion till the point of vanishing.

Considering all discussed articles, one can safely conclude that the magnetic topology introduced by the coupling scheme, entirely determines the response of the ground state to distortions, and points at the fact that the best strategy for obtaining robust ferromagnetic properties in organic compounds relies on linear π-conjugated molecular polyradicals.

CHAPTER FIVE

Conclusions

The conclusions of this thesis can be divided in two, depending on the systems under study. However, there are some that are common.

From a methodological point of view, DFT-based calculations introduce a large dependence of the choice of the functional on the calculated magnetic coupling constant values, but in general provide reliable and consistent trends. On the other hand, wave function-based methods offer a more rigorous treatment of the electronic structure of the problem, and consequently a better description of the magnetic exchange interactions. However, it is very limited by the size of the system.

On the accurate description of magnetic exchange interactions in the studied coordination compounds.

By a detailed analysis of the mapping approach, we have identified the spin systems for which the formulation given by Noodleman is not appropriate. Particularly, the Ni-V and Ni-Cu heterobinuclear complexes investigated in paper #3.1, demonstrate that if the pure spin states are expressed as a linear combination of determinants that do not correspond to the broken symmetry determinants, a univocal spin projector cannot be defined.

An alternative formulation of the mapping approach, following previous work on the group, is proposed and generalized to the case of three-electron three-centre problems.

The proposed alternative makes direct use of the energy of the broken symmetry solutions and maps them into the energy expectation values of the corresponding broken symmetry solutions of the HDVV Hamiltonian. Therefore, it does not require using a spin projector.

The validity of this proposal is checked by comparison to experiment and by means of effective Hamiltonian theory, and it is found to provide consistent magnetic coupling values.

Effective Hamiltonian theory allows a direct comparison between the HDVV and the effective Hamiltonian matrix elements. This, applied to three-centre three-electron problem, permits an ab initio extraction of all relevant two-body magnetic coupling constants between nearest neighbours, without making any assumptions on the

symmetry of the problem. Additionally, the comparison between the effective Hamiltonian and the spin model Hamiltonian provides information on the Heisenberg character of the system.

Finally, for the trinuclear Cu(II) case studied in paper #3.2, the calculated coupling constant value present a large dependence on the functional used. However, the relationship between the coupling constants is found to be almost constant for the different functionals used. Additionally, the consistent values obtained in model dinuclear systems indicate that the magnetic interaction is local, and it offers a simple manner of extracting the magnetic exchange interactions in complex polynuclear systems.

On the theoretical description and computational design of purely π−conjugated organic polyradical interacting through-bond, high-spin ground state with large *S* value, robust ferromagnetic properties, strong magnetic anisotropy and chemical stability.

A purely organic compound showing robust ferromagnetic interaction in a wide range of temperature has yet not been achieved, despite the numerous attempts. It is a task that involves very complex synthetic routes and characterization techniques, together with a critical and very difficult to control interplay between the generation of unpaired electrons, structural distortions and chemical stability of the radical centres.

Density functional theory using hybrid functionals, particularly B3LYP, provides a reliable computational strategy to describe the multiple local minima in these structurally flexible organic radicals.

Structural features play a crucial role in the definition of magnetic properties in π−conjugated polyradicals interacting through-bond. Particularly, they introduce effective manners to increase the stability of the compounds while enhancing robust ferromagnetic properties

For extended polyradical systems, especially those presenting large π−π interactions, the inclusion of long-range dispersion corrections is of paramount importance to properly describe the minima in the potential energy surface, and consequently, the magnetic interactions.
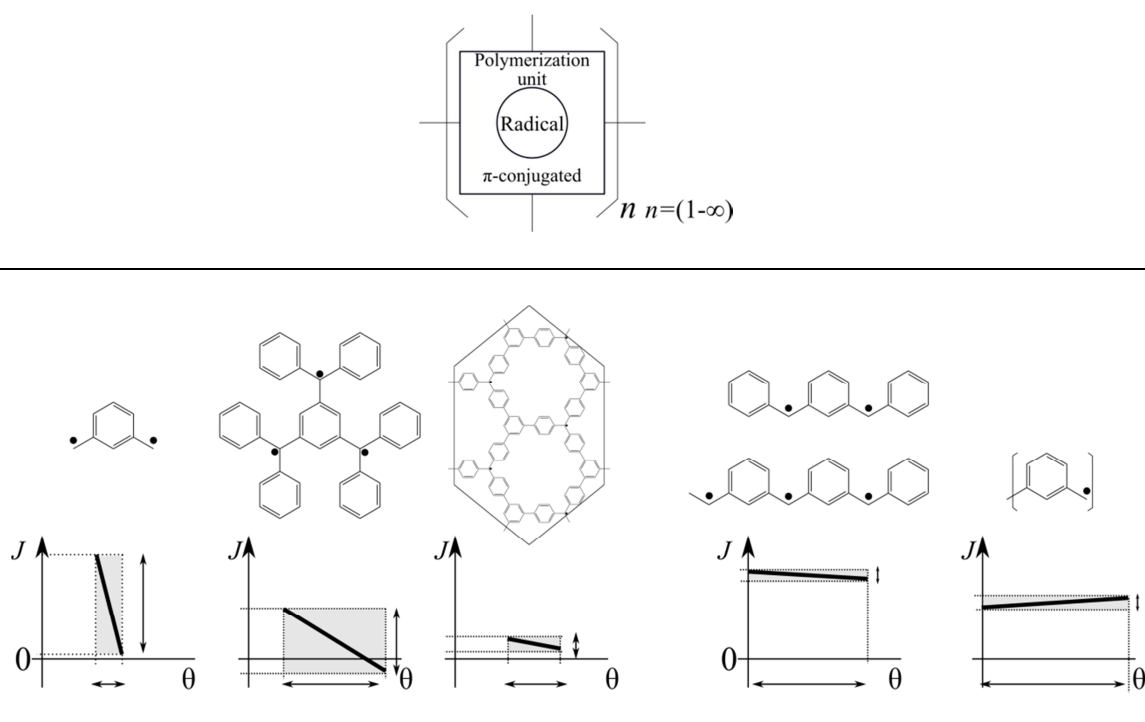
Figure 1. Schematic representation of the overall trends observed throughout this thesis. *J* represents the dominant magnetic coupling constant (positive values indicate ferromagnetism). θ is a representation of a given collective coordinate capturing the torsion in the system in the different systems studied in this thesis. Grey areas highlight how the allowed distortion in the system affects the dominant magnetic coupling constant.

Apart from the already mentioned ones, Figure 1 schematically summarizes the main conclusions of this thesis with respect to magnetic interaction in π−conjugated odd alternant organic polyradicals. Those are:

All organic systems investigated in this thesis can be divided in two, according to the effect of structural distortions on the dominant magnetic coupling constant, as indicated in the left-most and right-most columns in Figure 1. For the *m*-xylylene diradical, small distortions (θ) imply large variations of the coupling value (*J*), as a consequence of a missing auxiliary π−conjugated system to delocalize the unpaired electron if a distortion happens. For the triradical molecule, the range of allowed distortions is larger, and its impact gets to reverse the sign of the exchange coupling constant. On the 2D polymeric systems, the distortions experienced by the network are limited because of the planarity of the system, and the coupling constant value remains positive but very small. In contrast, the systems extended in one dimension present a very large structural flexibility, but no matter the conformation adopted, they show very strong ferromagnetic coupling. Additionally, as a consequence of the structural

flexibility, there are secondary structures that induce a net stabilization of the high-spin ground state.

Altogether, this thesis proposes using linear π-conjugated polyradicals, based on molecular units derived from Gomberg radical, to achieve robust ferromagnetic properties in stable purely organic systems.

Contribution to Publications

The results of this thesis are presented as a compendium of publications which are co-authored by more than just the author of this thesis. This chapter describes the contribution of the author to each of the publications.

<u>Paper #3.1.</u>

Spin adapted versus broken symmetry approaches in the description of magnetic coupling in heterodinuclear complexes. Costa, R.; Valero, R.; **Reta Mañeru, D**.; Moreira, I. de P. R.; Illas, F. *J. Chem. Theory Comput.,* **2015***, 11,* 1006−1019.

Contribution: Carrying out all the wave function-based calculations, analysing the data and helping with the writing of the manuscript.

<u>Paper #3.2.</u>

Handling Magnetic Coupling in Trinuclear Cu(II) Complexes. **Reta Mañeru, D.**; Costa, R.; Mañé, M. G.; Moreira, I. de P. R.; Illas, F. *J. Chem. Theory Comput.* **2015**, *11* (8), 3650–3660.

Contribution: Carrying out all the wave function-based calculations, interpreting and analysing the data, writing the Newton-Raphson code and helping with the writing of the manuscript.

<u>Paper #4.1.</u>

The Triplet-Singlet Gap in the *m*-xylylene Radical: A Not So Simple One. **Reta Mañeru, D.**; Pal, K. P.; Moreira, I. de P. R.; Datta, S. N.; Illas, F. *J. Chem. Theory Comput.,* **2014**, *10*, 335.

Contribution: Carrying out all the calculations, interpreting and analysing the data and helping with the structuration and writing of the manuscript.

<u>Paper #4.2.</u>

Theoretical and computational investigation of meta-phenylene as ferromagnetic coupler in nitronyl nitroxide diradicals. Pal, K. P.; **Reta Mañeru, D.**; Latif, I. A.; Moreira, I. de P. R.; Illas, F.; Datta, S. N. *Theor. Chem. Acc.* **2014**, *133*, 4, 1472.

Contribution: Helping with the writing of the manuscript.

<u>Paper #4.3.</u>

Triplet-singlet gap in Structurally Flexible Organic Diradicals. **Reta Mañeru, D.**; Moreira, I de P.R.; Illas, F. *Theor. Chem. Acc.* **2015,** *18*, 134.

Contribution: Proposing the study, carrying out all the calculations, interpreting and analysing the data and helping with the structuration and writing of the manuscript.

<u>Paper #4.4.</u>

Exchange Coupling Inversion in a Single High-Spin Organic Triradical Molecule. Gaudenzi, R.; Burzuri, E.; **Reta Mañeru, D.**; Moreira, I. de P. R.; Bromley, S. T.; Rovira, C.; Veciana, J.; van der Zant, H. S. J. Submitted

Contribution: Carrying out all the calculations, proposing the model that rationalizes the experimental results and helping with the structuration and writing of the manuscript.

<u>Paper #4.5.</u>

Helical Folding-Induced Stabilization of Ferromagnetic polyradicals based on triarylmethyl radical derivatives. **Reta Mañeru, D.**; Moreira, I. de P. R.; Illas, F. Submitted

Contribution: Proposing the study, carrying out all the calculations, interpreting and analysing the data and writing the manuscript.

<u>Paper #4.6.</u>

Design of Triarylmethyl-Based 2D Polyradical Materials Showing Controllable Magnetic and Optical Properties through Elastic Distortions. **Reta Mañeru, D.**; Alcón, I.; Bromley, S. T.; Moreira, I. de P. R. Under preparation.

Contribution: At the moment of submission of this thesis, carrying out all the calculations concerning magnetic properties, interpreting and analysing the data and writing the manuscript.

In addition to the publications that constitute the present thesis, the following articles are also co-authored by the Ph.D. candidate

Discovery of the K_4 Structure Formed by a Triangular π Radical Anion. Mizuno, A.; Shuku, Y.; Suizu, R.; Matsushita, M.; Tsuchiizu, M.; **Reta Mañeru, D.**; Illas, F.; Robert, V.; Awaga, K. *J. Am. Chem. Soc.* **2015***, 137 (24),* 7612–7615 (Communication)

Identifying atomic sites in N-doped pristine and defective graphene from ab initio core level binding energies. Bellafont, N. P.; **Reta Mañeru, D.**; Illas, F. *Carbon.* **2014**, *76,* 155-164.

Characterization of a robust Co(II) fluorescent nanomagnet deposited intact on HOPG. Heras Ojea, M. J.; **Reta Mañeru, D.**; Rosado, L.; Zuazo, J. A.; Castro, G. R.; Tewary, S.; Rajamaran, G.; Aromí, G.; Jiménez, E.; Sañudo, E. C. *Chem. Eur. J.* **2014**, *20,* 10439-10445.

Nanoparticles of Ni(II) and Co(II) Metallo-Organic Molecular Materials. Heras Ojea, M. J.; Pons-Balagué, A.; **Reta Mañeru, D.**; Sañudo, E. C. *J. Nanopart. Res.,* **2014**, 16:2209.

New Nanostructured Materials: Nanostructuration of a Fluorescent Magnet Based on Acridine Yellow. **Reta Mañeru, D.**; Heras Ojea, M. J.; Rosado, L.; Aromí, G.; Zuazo, J.; Castro, G.; Sañudo, E. C. *Polyhedron*, **2013**, *66,* 136. ICMM 2012.

Microwave Assisted Synthesis in Coordination Chemistry. Pons-Balagué, A.; Heras Ojea, M. J.; Gairaud, M. L.; **Reta Mañeru, D.**; Teat, S. J.; Costa, J. S.; Aromí, G.; Sañudo, E. C. *Polyhedron*, **2013**, *52*, 781.

CAPITULO SIETE

Resumen en Castellano

En la siguiente memoria se presenta un resumen de la tesis doctoral que lleva por título "Comprensión y predicción del acoplamiento magnético en sistemas complejos: de complejos inorgánicos a poliradicales orgánicos".

7.1. Introducción.

El desafío para comprender el origen del magnetismo en la materia y los fenómenos asociados que se desprenden de él, han requerido un notable esfuerzo por parte de algunas de las mentes científicas más brillantes. En el proceso, han ofrecido formas fundamentalmente nuevas de describir la materia e impulsado profundas transformaciones tecnológicas en las sociedades. El estudio del origen del magnetismo en la materia está íntimamente relacionado con el nacimiento de la mecánica cuántica, ya que para explicar los fenómenos magnéticos observados en la materia, es necesario contar con una teoría que explique la estructura atómica.

El desarrollo de la mecánica cuántica permitió racionalizar el conjunto de fenómenos magnéticos que ocurren en la materia. Los primeros intentos de aplicar la teoría cuántica al campo del magnetismo fueron llevados a cabo por Heisenberg en 1928. Se dedicó a la racionalización del ferromagnetismo observado en los metales, donde se cumple el supuesto de spines localizadas debido a la naturaleza d y f de las capas de los iones metálicos. En última instancia, la interacción isotrópica entre los momentos de spin localizados se puede describir mediante el Hamiltoniano fenomenológico introducido por Heisenberg[1]

$$\widehat{H} = -\sum_{\langle i,j \rangle} J_{ij} \widehat{\boldsymbol{S}}_i \cdot \widehat{\boldsymbol{S}}_j \tag{1}$$

donde J_{ij} es la constante de acoplamiento magnético entre los centros $\widehat{\boldsymbol{S}}_i$ y $\widehat{\boldsymbol{S}}_j$ localizados de spin y $\langle i,j \rangle$ indica que la suma se refiere a las interacciones entre vecinos más cercanos únicamente. En este modelo, un valor positivo o negativo del parámetro J_{ij} implica interacción ferromagnética o antiferromagnética entre los momentos de spin del centro i con el j, respectivamente. Una simplificación del anterior Hamiltoniano fue introducida por Ising,[2] quien consideró únicamente las componentes z de los operadores de spin

$$\hat{H}^{Ising} = -\sum_{\langle i,j \rangle} J_{ij} \hat{S}_i^z \cdot \hat{S}_j^z \qquad (2)$$

Estos modelos son esenciales para la interpretación de muchos fenómenos magnéticos que se derivan de la existencia de momentos de spin localizados. Por lo tanto, estos dos Hamiltonianos son fundamentales para el trabajo presentado en esta tesis, y se encontrarán a lo largo de la discusión

Históricamente, el magnetismo se ha dedicado a los compuestos inorgánicos, en su mayoría sólidos iónicos con centros paramagnéticos metálicos (Fe, Co, Ni, Cu, Mn), responsables de sus propiedades magnéticas macroscópicas. Sin embargo, en las últimas décadas, el estudio de las propiedades magnéticas se ha extendido hacia enfoques basados en sistemas moleculares, cubriendo áreas muy diversas que incluyen compuestos organometálicos[3–5] y moléculas puramente orgánicas.[6–8]

El principal interés de esta tesis se encuentra en el estudio de las propiedades magnéticas de moléculas orgánicas sin centros metálicos. La existencia de electrones desapareados en estos sistemas, que son los responsables de las propiedades magnéticas más relevantes, proviene de argumentos topológicos que se explicarán en detalle más adelante. El estudio del magnetismo en los compuestos puramente orgánicos requiere un enfoque totalmente diferente con respecto al de los compuestos con centros metálicos. Para los sistemas puramente orgánicos, todos los fenómenos se deben a electrones en orbitales *s* y *p*, y la ausencia de átomos pesados permite descartar los efectos asociados al acoplamiento de spin-órbita. Por otra parte, en este tipo de sistemas, la densidad de espín está deslocalizada, en general, sobre un conjunto de átomos que participan en un sistema π−conjugado, en comparación con los centros metálicos donde las capas abiertas son electrones en orbitales *d* o *f*.

En una primera aproximación, los sistemas radicalarios orgánicos se pueden clasificar dependiendo de si la interacción entre los centros magnéticos es a través del espacio[9,8] (por ejemplo nitronyl nitroxidos o compuestos de tranferencia de carga) o a través de enlace[10,11] (sistemas π−conjugados). Existe una importante diferencia derivada de estos mecanismos diferentes: en aquellos radicales que interactúan a través del espacio, los electrones desapareados se encuentran en cada una de las entidades moleculares que forman un cristal, el cual se mantiene unido por medio de interacciones de largo alcance, como por ejemplo, interacción π−π. En estos sistemas, el parámetro

crítico que afecta a las propiedades magnéticas es la distancia entre esas unidades, la cual a su vez depende en gran medida de factores externos como la temperatura o la presión. Alternativamente, aquellos sistemas radicales en los que la interacción se da a través del enlace, implican que la interacción magnética se produce dentro de una unidad molecular unida covalentemente. Otro aspecto comparativamente diferente es que mientras en los sistemas que interaccionan por el espacio, cada unidad que interactúa presenta un único electrón desapareado, los sistemas en los que la interacción se da a través del enlace pueden presentar un número variable de centros de radicalarios dentro de cada unidad molecular. Además, estas unidades moleculares pueden ser estructuralmente flexibles. Esta última característica introduce algunos problemas implícitos que no pueden pasarse por alto, como por ejemplo, deformaciones moleculares de bajo coste energético asociadas a la isomería conformacional, que afectan el camino de la interacción magnética de una manera mucho más compleja que en los cristales moleculares. En última instancia, como consecuencia de la flexibilidad estructural, es esperable que en estos sistemas aparezcan grados de ordenamiento supramoleculares, como estructuras secundarias. Por lo tanto, es una característica que debe ser considerada en las estrategias que pretendan describir correctamente las propiedades magnéticas de este tipo de sistemas.

Sin embargo, un aspecto fundamental, previo al estudio de la interacción magnética, es asegurar que la existencia de los electrones desapareados. Para ello, los argumentos de estabilidad son cruciales. Hay dos estrategias principales para estabilizar electrones desapareados en moléculas orgánicas. El primero se basa en una protección estérica del centro radicalario, conocida como estabilización cinética. Su ejemplo representativo es el aumento de la estabilidad cuando se pasa del radical de Gomberg[12] a su derivado clorado, el PTM.[13] La segunda estrategia se basa en la introducción de un sistema π–conjugado que permita una deslocalización del electrón desapareado, lo que facilita que participe en varias formas resonantes, resultando en una estabilización energética neta.[14,15] Un ejemplo representativo de este tipo son moléculas con un fuerte carácter aceptor-donador, que permitan procesos redox, que resultan en radicales cargados, como por ejemplo la molécula tetracyanoethylene (TCNE)[16] y tetracianoquinodimetano (TCNQ)[17] Aquí, el electrón desapareado aparece como una consecuencia de un proceso de transferencia de carga. Sin embargo, el enfoque de esta

tesis se centra sobre los radicales orgánicos neutros que presentan un número par de electrones.

A continuación se presentan una serie de radicales orgánicos que han sido sintetizados experimentalmente (ver Ilustración 1). La Ilustración 1 sigue el mismo razonamiento que la discusión previa sobre radicales, presentando en la primera columna ejemplos de radicales interaccionando a través del espacio, y en la última radicales interaccionando a través de enlace. La columna del medio presenta un tipo de sistemas, los polímeros radicalarios, que se pueden considerar una mezcla de los dos previamente introducidos. Estos consisten en una unidad polimérica de la que cuelga un radical persistente. En función de la conformación adoptada por la estructura polimérica, los centros radicalarios tienen varias maneras de interaccionar. Finalmente, las diferentes filas de la Ilustración 1 se corresponden con el tipo de átomo sobre el que se encuentra el electrón desapareado. Filas *a), b), c)* y *d)* se corresponden con carbono, nitrógeno, oxígeno y heterociclos con azufre, respectivamente. La presentación de todos estos sistemas pretende hacer notar la cantidad de posibilidades a la hora de elegir los componentes básicos para obtener sistemas extendidos poliradicalarios.

En esta tesis, en base a criterios de las dimensionalidades que se pueden obtener (lo que determina la topología magnética) y estabilidad de los centros radicalarios, la mayor parte de la investigación se centra en sistemas π-conjugados, poliradicalarios que interaccionan a través de enlace, con los electrones desapareados sobre átomo de carbono (columna de la derecha, fila *a)* de la Ilustración 1. Además, criterios adicionales son el de conseguir un sistema puramente orgánico, con un estado fundamental de muy alto spin, interacción ferromagnética entre los electrones desapareados muy grande y una estabilidad química de los centros radicalarios que asegure que se pueda sintetizar.

Estos sistemas representan el enfoque conceptual más importante para esta tesis. De hecho, el capítulo 4 está completamente dedicado a esta clase de moléculas. Es razonable pensar que si la interacción magnética se da a través del enlace, la naturaleza de la unidad de acoplamiento juega un papel crucial en la definición de la interacción magnética. De hecho, está bien establecido experimentalmente que las unidades de meta-fenil promueven las interacciones ferromagnéticas; la conjugación π facilita la deslocalización de los electrones no apareados lo que aumenta su interacción y la conexión 1,3 a través de un anillo de seis miembros no permite formas resonantes
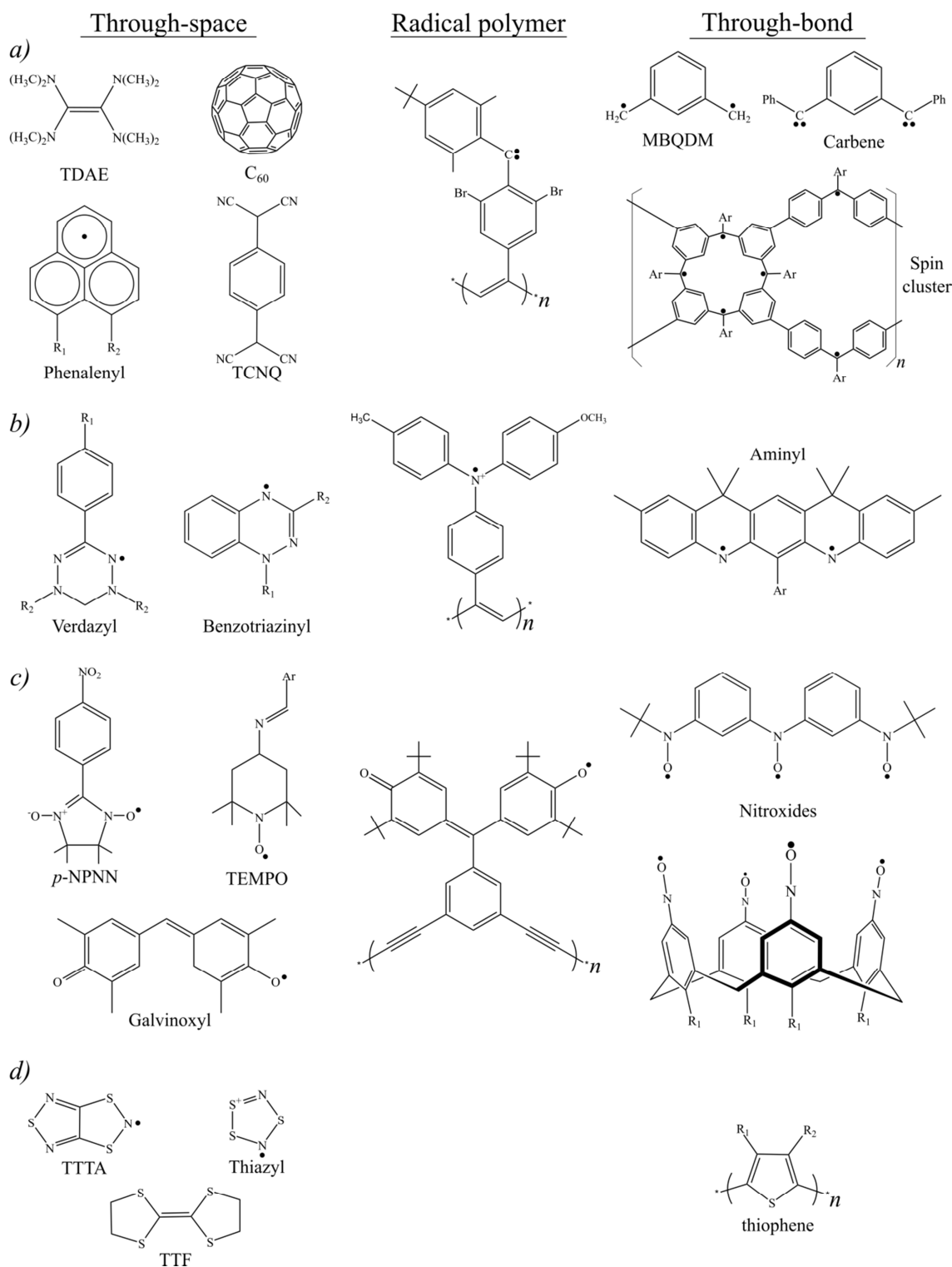
Ilustración 1. Estructura molecular de algunos compuestos orgánicos radicalarios experimentalmente reportados. Cada fila corresponde al diferente átomo en el que reside el electrón desapareado. a), b) y c) representan carbono, nitrógeno, y oxígeno, respectivamente. d) son compuestos que contienen azufre. Cada columna representa el tipo de interacción entre los electrones desapareados: a través de espacio, polímeros radicales y a través de enlace.

que involucren capas cerradas, lo que resultaría en un emparejamiento de los electrones desapareados con la consiguiente desaparición de las propiedades magnéticas de interés. Por esta razón, la mayoría de los compuestos que se discuten aquí presentan esta topología, basada en unidades 1,3-phenylene. Este campo de investigación ha experimentado dos contribuciones importantes. La primera está basada en unidades de C_{60} buckminsterfullereno, pero no será tratada en este resumen. La otra contribución, muy relevante para el propósito de esta tesis, fue presentado por Rajca,[10] quien, tras una extensa investigación sobre cómo enfocar la síntesis de compuestos orgánicos poliradicalarios para promover propiedades magnéticas robustas,[10] introdujo el concepto de clústeres de espines. Este enfoque es una manera eficaz para evitar la supresión de la interacción magnética entre los electrones desapareados. Tal interrupción aparece a menudo debido a la ruta experimental requerida para generar los centros radicalarios (el método carbanión, que implica la oxidación de los precursores de poliéter) y la inherente flexibilidad estructural de los compuestos, lo que puede dar lugar a una torsión tan grande de la molécula, que la conjugación del sistema π se rompe, y con ella la interacción entre electrones desapareados.

7.2. Metodología.

El objetivo de esta sección es introducir los conceptos básicos que permiten el uso de la teoría cuántica para calcular la estructura electrónica de un conjunto dado de partículas, es decir, una molécula, como una manera exacta para describir sus propiedades. Entre la gran cantidad de propiedades que se puede calcular dentro de los métodos actuales, el de interés a lo largo de esta tesis es el magnetismo, que orienta la discusión hacia algunas formulaciones específicas capaces de describirlo.

Para un sistema dado de N electrones y M núcleos interaccionando, decrito por los vectores posición $\mathbf{r}_i$ and $\mathbf{R}_A$ respectivamente, los estados quánticos estacionarios que definen el sistema se obtienen resolviendo la ecuación de Schrödinger en su forma no relativista e independiente del tiempo:

$$\widehat{H}\Psi_i = E_i\Psi_i \tag{3}$$

donde $\hat{H}$ es el operador hamiltoniano asociado al sistema, E_i es la energía de un estado estacionario dado y Ψ_i es la función de onda que lo describe. En unidades atómicas, el Hamiltoniano se escribe como

$$H = -\sum_{i=1}^{N}\frac{1}{2}\nabla_i^2 - \sum_{A=1}^{M}\frac{1}{2M_A}\nabla_A^2 + \sum_{A=1}^{M}\sum_{B>A}^{M}\frac{Z_A Z_B}{R_{AB}} + \sum_{i=1}^{N}\sum_{j>i}^{N}\frac{1}{r_{ij}} - \sum_{i=1}^{N}\sum_{A=1}^{M}\frac{Z_A}{r_{iA}} \tag{4}$$

O, de forma más compacta,

$$\hat{H} = \hat{T}_N + \hat{T}_e + V_N + V_e + V_{Ne} \tag{5}$$

En esta ecuación, M_A es la relación de la masa del núcleo de la A y la masa de un electrón, Z_A es el número atómico del núcleo A, ∇_A^2 y ∇_i^2 son los operadores Laplacianos que implican la diferenciación con respecto a las coordenadas del núcleo y de electrones A y electrón i, respectivamente, $r_{iA} = |\bar{r}_i - \bar{r}_A|$ es la distancia entre el electrón i y el núcleo A y $r_{ij} = |\bar{r}_i - \bar{r}_j|$ es la distancia entre el electron i y j y $R_{AB} = |\bar{R}_A - \bar{R}_B|$ es la distancia entre los núcleos A y B.

El primer y segundo términos son los operadores de energía cinética nucleares y electrónicos, respectivamente. Términos tercero y cuarto representan el núcleo-núcleo y electrón-electrón repulsión, respectivamente. El último término representa la atracción de Coulomb entre los electrones y núcleos.

Utilizando la aproximación de Born-Oppenheimer, se pueden desacoplar los movimientos de los ectrones y de los núcleos. Esto resulta en trayectorias de los núcleos que se mueven en superficies potenciales que vienen de resolver la parte electrónica. Con esta aproximación, eqn (3) se puede reescribir como

$$\hat{H}_{elec}\Psi_i = E_{elec}\Psi_i \tag{6}$$

Este es el problema electrónico. La aproximación más común para resolver este problema se basa en la aproximación de Hartree-Fock. Es una formulación que utiliza un único determinante de Slater para describir el estado fundamental de un sistema de N electrones. La función de onda se expresa

$$|\Psi_0\rangle = |\chi_i\chi_j\cdots\chi_N\rangle \tag{7}$$

Dentro de las aproximaciones discutidas, el principio variacional permite obtener el conjunto óptimo de los orbitales de spin $\{\chi_i\}$ que minimizan la energía electrónica y es la mejor aproximación al estado fundamental del sistema N-electrones

$$E_0 = \langle\Psi_0|\widehat{H}_{elec}|\Psi_0\rangle = \sum_i \langle i|h|i\rangle + \frac{1}{2}\sum_{ij} \langle ij\|ij\rangle \tag{8}$$

Una restricción adicional a los orbitales de spin es que permanezcan ortonormales $\langle\chi_i|\chi_j\rangle = \delta_{ij}$. La ecuación para los spin orbitales óptimos es la ecuación integro-diferencial de Hartree-Fock

$$h(1)\chi_i(1) + \sum_{i\neq j}\left[\int d\mathbf{x}_2|\chi_j(2)|^2 r_{ij}^{-1}\right]\chi_i(1) - \sum_{i\neq j}\left[\int d\mathbf{x}_2\chi_j^*(2)\chi_i(2)r_{ij}^{-1}\right]\chi_j(1)$$
$$= \varepsilon_i\chi_i(1) \tag{9}$$

donde

$$h(1) = -\frac{1}{2}\nabla_i^2 - \sum_A \frac{Z_A}{r_{iA}} \tag{10}$$

es un operador de monoelectrónico que describe la energía cinética y la energía potencial de atracción a los núcleos de un solo electrón. Los otros dos términos en el lado izquierdo representan dos operadores bielectrónicos, llamados los operadores Coulomb J_j y de intercambio K_j, respectivamente. La energía orbitálica del orbital de spín χ_i es ε_i Las integrales asociadas a estos operadores son

$$h_{ii} = \langle\chi_i(1)|h|\chi_i(1)\rangle \tag{11}$$
$$J_{ij} = \langle\chi_i(1)\chi_j(2)|r_{ij}^{-1}|\chi_i(1)\chi_j(2)\rangle \tag{12}$$
$$K_{ij} = \langle\chi_i(1)\chi_j(2)|r_{ij}^{-1}|\chi_j(1)\chi_i(2)\rangle \tag{13}$$

La integral de Coulomb J_{ij} representa la repulsión que el electrón i causa al j, mientras que la integral de intercambio K_{ij} no tiene un equivalente físico clásico, ya que su origen se encuentra en el principio de antisimetría. Este tipo de interacción es responsable de la correlación de electrones con el mismo spin.

Basado en la aproximación mono configuracional que se acaba de discutir, se pueden expresar las funciones que describen los estados magnéticos, en base a los operadores de Fock. Por ejemplo, considérese el caso de dos electrones en dos orbitales en interacción, lo que resulta en un estado triplete (los dos electrones tienen el mismo espín) y en otro singlete (los dos electrones tienen espines opuestos). Las configuraciones que describen estos estados son, para el singlete

$$
\begin{aligned}
\left| \,{}^1\Psi_1^2 \right> &= 2^{-1/2}\left(\left|\Psi_{\overline{1}}^{\overline{2}}\right> + \left|\Psi_1^2\right> \right) \\
&= \frac{1}{2}[\psi_1(1)\psi_2(2) + \psi_1(2)\psi_2(1)](\alpha(1)\beta(2) - \beta(1)\alpha(2))
\end{aligned} \tag{14}
$$

y para el triplete

$$
\begin{aligned}
\left| \,{}^3\Psi_1^2 \right> &= 2^{-1/2}\left(\left|\Psi_{\overline{1}}^{\overline{2}}\right> - \left|\Psi_1^2\right> \right) \\
&= \frac{1}{2}[\psi_1(1)\psi_2(2) - \psi_1(2)\psi_2(1)](\alpha(1)\beta(2) + \beta(1)\alpha(2))
\end{aligned} \tag{15}
$$

Utilizando estas funciones para expresar la energía de los dos estados, en la aproximación Hartree-Fock, conduce a

$$
\left< \,{}^1\Psi_1^2 \middle| H \middle| {}^1\Psi_1^2 \right> = h_{11} + h_{22} + J_{12} + K_{12} \tag{16}
$$

$$
\left< \,{}^3\Psi_1^2 \middle| H \middle| {}^3\Psi_1^2 \right> = h_{11} + h_{22} + J_{12} - K_{12} \tag{17}
$$

Lo que resulta en la siguiente expresión para la diferencia de energía entre el triplete y el singlete

$$
\left< \,{}^3\Psi_1^2 \middle| H \middle| {}^3\Psi_1^2 \right> - \left< \,{}^1\Psi_1^2 \middle| H \middle| {}^1\Psi_1^2 \right> = -2K_{12} \tag{18}
$$

Es decir que, en esta aproximación, la diferencia de energía entre los estados magnéticos es dos veces la integral de intercambio. K_{ij} (ecuación (13)) siempre positiva, por lo que si los orbitales usados para expresar el triplete y el singlete son similares, el triplete es dos veces K_{12} más estable. K_{ij} es una integral sobre el espacio, por lo que cuanto mayor sea la región espacial compartida por los orbitales del triplete y del singlete, mayor su valor, y en principio, mayor la diferencia de energía entre el estado de alto espín y el de bajo espín, que es precisamente uno de los requisitos que se buscan para que un sistema presente propiedades magnéticas robustas. Sin embargo, el

promover grandes regiones del espacio compartidas por los orbitales del triplete y singlete también introduce un efecto contraproducente, ya que el valor del solapamiento entre orbitales aumenta. Este se expresa como una integral en el espacio,

$$S_{12} = \int \psi_1^* \psi_2 dV \tag{19}$$

Al contrario que K_{ij}, la integral de solapamiento favorece que los electrones desapareados ocupen un único orbital molecular, lo que elimina las propiedades magnéticas de interés.

Por lo tanto, en una primera aproximación, la estabilidad relativa de los estados de alto espín con respecto a estados de bajo espín, se consigue mediante un balance de las integrales de intercambio y solapamiento. En este punto, los argumentos topológicos[18] son cruciales, ya que proveen maneras de aumentar K_{ij} y reducir S_{ij}. La idea clave es tener orbitales de tipo π, por lo tanto extendidos por toda la molécula, pero degenerados y ortogonales, lo que penaliza S_{ij} mientras que aumenta K_{ij}.

Estos argumentos topológicos indican las características estructurales que deben tener las moléculas, los cuales se traducen en estructuras conjugadas alternantes, con formas no-Kekulé y orbitales moleculares mono ocupados que no puedan ser localizados sobre diferentes regiones de la molécula.

7.3. Extracción precisa del acoplamiento magnético en complejos de coordinación.

Una descripción teórica precisa de la estructura electrónica en compuestos de coordinación magnéticos es previa a la extracción de las constantes de acoplamiento magnético más relevantes. El conocimiento de estos acoplamientos permite establecer relaciones magneto estructurales, lo que ayuda en el diseño de sistemas con propiedades mejoradas. Debido a la naturaleza de los estados de baja energía de este tipo de sistemas, normalmente se requiere una precisa de la correlación electrónica estática y dinámica. Idealmente, uno desearía poder tratar la estructura electrónica con la elevada de por los métodos basados en la función de onda multi referencial, tales como CASSCF, CASPT2 o MRCI, al coste computacional de enfoques mono

determinantales, como los métodos basados en la teoría del funcional de la densidad. Ese es precisamente el objetivo del *mapping*.

El enfoque del *mapping* aparece como una manera precisa y computacionalmente eficiente de extraer las interacciones magnéticas en complejos de metales de transición, radicales orgánicos y sistemas periódicos.[19] Para un sistema magnético dado, est enfoque consiste en la descripción de la energía y la distribución electrónica de los estados de espín puros por medio de soluciones de simetría rota, utilizando un proyector de espín.

En un sentido general, el método se basa en una asociación uno-a-uno entre tres espectros de energías, siendo uno el espectro exacto y los otros dos son los correspondientes a los Hamiltonianos modelo de espín, tal como se representa esquemáticamente en Ilustración 2. En primer lugar, aprovecha el hecho de que el Hamiltoniano exacto no relevista e independiente del tiempo y el de HDVV conmutan con el operador de espín total. Esto significa que existe un conjunto de funciones que son funciones propias de ambos Hamiltonianos, lo que establece una relación uno a uno entre sus valores y funciones propias. Y en segundo lugar, explota la correspondencia entre los espectros HDVV y de las funciones propias del Hamiltoniano de Ising, que se pueden asignar a soluciones de simetría rota (BS), como fue originalmente desarrollado por Noodleman[20–22]. Entonces, el principal objetivo es hacer coincidir de manera unívoca los tres espectros, lo que permitirá una extracción teórica precisa de la interacción magnética basada en métodos *ab initio*.
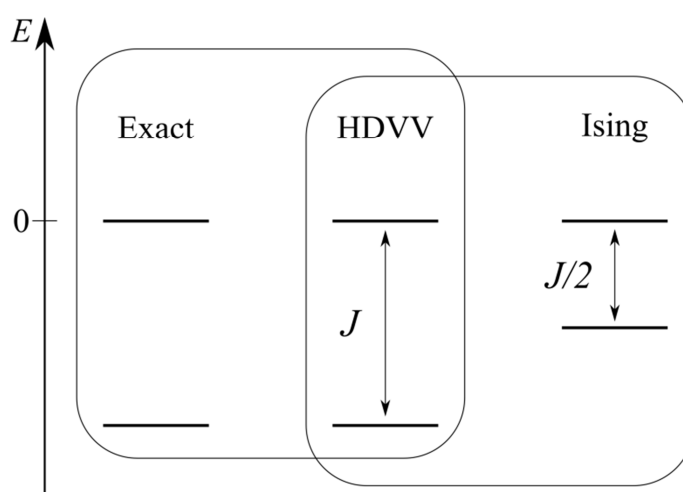

Ilustración 2. Representación de la idea que subyace en el método del *mapping*.

Sin embargo, el *mapping* presenta al menos dos puntos débiles. El primero hace referencia al projector de spin; el segundo a situaciones en las que no se cuente con suficientes diferencias de energía entre estados puros de espín para extraer los acoplamientos magnéticos relevantes.

En lo que concierne al primer problema, los complejos heterobinucleares representan un ejemplo paradigmático. Considérese un sistema en el que uno de los centros magnéticos presenta dos electrones desapareados acoplados en un triplete local, el cual interacciona con otro centro que tiene un único electrón desapareado. Esta situación se representa esquemáticamente en Tabla 1.

	Funciones adaptadas al spin	BS
$S_a=1$ $S_b=1/2$	$\lvert Q, \tfrac{1}{2}\rangle = \tfrac{1}{\sqrt{3}}\left(\lvert a_1 a_2 \bar{b}_1\rangle + \lvert a_1 \bar{a}_2 b_1\rangle + \lvert \bar{a}_1 a_2 b_1\rangle\right)$	$\lvert a_1 a_2 b_1\rangle$
a_2 ↑ ↓ ↑ b_1 a_1 ↑	$\lvert D, \tfrac{1}{2}\rangle = \tfrac{2}{\sqrt{3}}\lvert a_1 a_2 \bar{b}_1\rangle - \tfrac{1}{\sqrt{6}}\left(\lvert a_1 \bar{a}_2 b_1\rangle + \lvert \bar{a}_1 a_2 b_1\rangle\right)$	$\lvert a_1 a_2 \bar{b}_1\rangle$; $\lvert \bar{a}_1 \bar{a}_2 b_1\rangle$

Tabla 1. Representación esquemática de un complejo heterobinuclear con un triplete local sobre el centro *a* y un doblete sobre el centro *b*. Las soluciones adaptadas al espín y las de simietría rota también se muestran.

Como se puede comprobar, las funciones puras de espín $\lvert Q, 1/2\rangle$ y $\lvert D, 1/2\rangle$, las cuales representan el estado cuartete y doblete respectivamente, son combinaciones lineales de determinantes que imponen la ruptura del triplete local sobre el centro *a*. Sin embargo, todas las soluciones de simetría rota deben mantener el triplete local, ya que la energía asociada con romperlo es muy elevada, lo que hace que no sea un estado magnético. A pesar de ello, mediante un mapping del valor esperado del operador de espín, se puede establecer qué solución de simetría rota es la apropiada para la extracción de la interacción magnética.

En lo que concierne al segundo problema, un complejo trinuclear de Cu(II) ejemplifica la problemática. En un sistema de tres electrones en tres centros, el espectro HDVV se compone de un quartete y dos dobletes. Las expresiones de sus funciones de onda y energías son

$$\lvert Q\rangle = \lvert 3/2, 3/2\rangle = 3^{-1/2}(\lvert \alpha\alpha\beta\rangle + \lvert \alpha\beta\alpha\rangle + \lvert \beta\alpha\alpha\rangle) \tag{20}$$

$$\lvert D_1\rangle = \lvert 1/2, 1/2\rangle = 2^{-1/2}(\lvert \alpha\alpha\beta\rangle - \lvert \alpha\beta\alpha\rangle) \tag{21}$$

$$\lvert D_2\rangle = \lvert 1/2, 1/2\rangle = 6^{-1/2}(\lvert \alpha\alpha\beta\rangle + \lvert \alpha\beta\alpha\rangle - 2 \cdot \lvert \beta\alpha\alpha\rangle) \tag{22}$$

$$E_Q = -1/4 \cdot (J_{12} + J_{13} + J_{23}) \tag{23}$$

$$E_{D_1} = 1/4 \cdot (J_{12} + J_{13} + J_{23}) - {}^1\!/_2 \cdot X \tag{24}$$

$$E_{D_2} = 1/4 \cdot (J_{12} + J_{13} + J_{23}) + {}^1\!/_2 \cdot X \tag{25}$$

$$X = (J_{12}^2 + J_{13}^2 + J_{23}^2 - J_{12} \cdot J_{13} - J_{12} \cdot J_{23} - J_{13} \cdot J_{23})^{1/2} \tag{26}$$

Por lo tanto, si no se assume ninguna simplificación en términos de simetría, hay tres constantes de acoplamiento magnético pero sólo dos diferencias de energía, por lo que el sistema de ecuaciones no se puede resolver. Un modo de solucionarlo es asumir alguna relación de simetría que permita reducir el espectro, como se indica en Tabla 2.
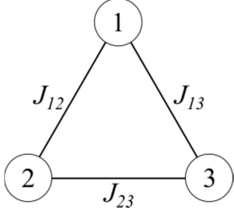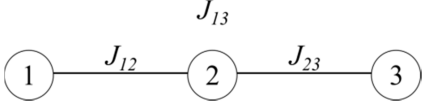
equilateral	linear
$J_{12} = J_{23} = J_{13} = J$	$J_{12} = J_{23} = J ; J_{13} = 0$
$X = 0$	$X = J$
$E_Q = -\dfrac{3}{4} \cdot J$	$E_Q = -\dfrac{1}{2} \cdot J$
$E_{D_1} = E_{D_2} = E_D = \dfrac{3}{4} \cdot J$	$E_{D_1} = 0 \; ; E_{D_2} = J$
$E_Q - E_D = -\dfrac{3}{2} \cdot J$	$E_Q - E_{D_1} = -\dfrac{1}{2} \cdot J \; ; E_Q - E_{D_2} = -\dfrac{3}{2} \cdot J$

Tabla 2

Para solucionar estos problemas, y basados en estudios previos en el grupo, se propone una formulación alternativa del mapping, que utiliza directamente los valores de energía de las soluciones de simetría rota y los mapeo con los valores esperados de las funciones de simetría rota en el Hamiltoniano HDVV.

Esta propuesta se ha validado por comparación con el experimento y mediante teoría del Hamiltoniano efectivo.

7.4. Estudio teórico de sistemas puramente orgánicos de alto espín.

Esta sección pretende alcanzar varios objetivos. En primer lugar, presentar y justificar los argumentos que conducen al uso de un conjunto muy particular de moléculas orgánicas para obtener sistemas de alto espín. Estas moléculas son hidrocarburos policíclicos alternantes con estructuras no Kekulé y con orbitales moleculares mono ocupados (SOMOs en inglés) que no pueden ser confinados a regiones diferentes del sistema conjugado. En segundo lugar, introducir y discutir diferentes formas de unir estas unidades moleculares para conseguir sistemas poli radicalarios extendidos, con el fin de promover la estabilidad química de los centros radicalarios y unas propiedades ferromagnéticas robustas, definidas en un amplio intervalo de temperaturas. Por último, en este capítulo también sirve para presentar y contextualizar parte del trabajo desarrollado en esta tesis como un intento de avanzar en este campo del magnetismo orgánico.

Desde un punto de vista cualitativo, la introducción de la conjugación da lugar a una deslocalización de los orbitales que albergan los electrones desapareados. Esto implica los electrones desapareados interactúan entre sí en regiones más extensas. Si no se aplican otras restricciones, el solapamiento entre orbitales (eqn(19)) dará lugar a una interacción que superará la integral de intercambio directo (eqn. 13) resultando en un emparejamiento de los electrones desapareados y la consecuente formación de una capa cerrada, lo que suprimiría cualquier propiedad magnética interesante.

Afortunadamente, los argumentos topológicos en sistemas conjugados alternantes, permiten definir orbitales de tipo π que, si bien definidos sobre las mismas regiones de espacio, son degenerados y ortogonales, lo que penaliza el solapamiento entre orbitales al mismo tiempo que intensifica la integral de intercambio directo. Estos argumentos topológicos indican las características estructurales que deben tener las moléculas, los cuales se traducen en estructuras conjugadas alternantes, con formas no-Kekulé y orbitales moleculares mono ocupados que no puedan ser localizados sobre diferentes regiones de la molécula. Un sistema conjugado de electrones π se denomina alternante si sus átomos se pueden dividir en dos conjuntos, de modo que ningún átomo de un conjunto está directamente vinculado a cualquier otro átomo del mismo conjunto. Por construcción, la degeneración se fija (a través de la topología), y el problema sobre la preferencia del estado de espín se reduce a términos relacionados con la integral de

intercambio. Manteniendo en mente que el objetico es conseguir sistemas orgánicos, π-conjugados, con un estado fundamental de alto espín y propiedades ferromagnéticas robustas, el propósito de la siguiente sección consiste en discutir las mejores maneras de acoplamiento de unidades radicalarias.

Uno de los aspectos más importantes a tener en cuenta para conseguir sistemas poliradicalarios de alto espín está relacionado con cómo se acoplan las diferentes unidades magnéticas. Para ello, el 1,3-fenil es una unidad que promueve interacciones ferromagnéticas fuertes, siempre y cuando no haya distorsiones estructurales importantes que rompan la conjugación por la que sucede la interacción. Por ello, todas las estructuras estudiadas en este apartado de la tesis están basadas en extensiones en una o dos dimensiones de esta unidad básica. La Ilustración 3 resume diferentes maneras de acoplar las unidades magnéticas. El primer esquema de acoplamiento es el denominado esquema ferromagnético. Esta estrategia se basa en la existencia de una unidad de acoplamiento ferromagnético (fCU) que conecta los electrones no apareados en una red alternante. La multiplicidad del estado fundamental del polyradical resultante se espera que sea $S = n/2$ donde n es el número de centros radicalarios. Esto es consecuencia de los argumentos topológicos aplicados a la unidad de acoplamiento (generalmente un 1,3-fenil). Sin embargo, hay dos clases distintas de poliradicales que resultan de este esquema de acoplamiento, dependiendo de la disposición de los centros radicalarios. Los poliradicales que pertenecen a la Clase **I** presentan los centros de espín dentro del sistema π que media la interacción entre espines. Esto da como resultado polímeros con los centros radicalarios dentro de la unidad de repetición. La repetición de estas unidades básicas se puede llevar a cabo a través de un crecimiento lineal, ramificado en estrella, dendrítico o mediante una conectividad macrocíclica. Los poli radicales que pertenecen a la Clase **II** tienen los centros de espín colgantes unidos al sistema π. Este es el esquema de acoplamiento que cuenta con la mayor cantidad de ejemplos descritos en la literatura, especialmente polyradicals Clase **I**
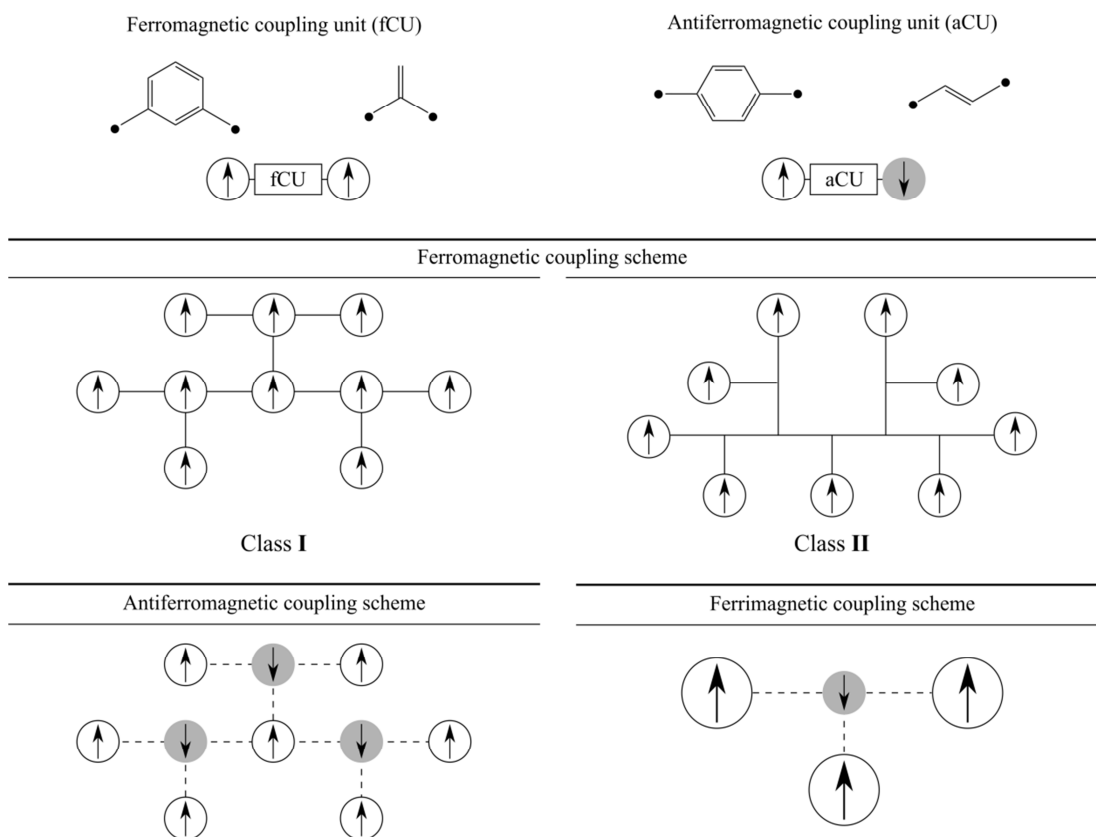
Ilustración 3. Representación de unidades que promueven una interacción ferro- y antiferromagnetica y de los resultants schemas de acoplamiento que surgen de su combinación. Las rayas sólidas indicant interacción ferromagnética y las punteadas interacción antiferromagnética.

7.5. Resumen y discusión de resultados.

Esta tesis establece un enfoque teórico y computacional para la descripción y la predicción de las interacciones de intercambio magnéticos en una variedad de sistemas complejos. Estos incluyen dos principales familias de compuestos. El primer conjunto está formado por complejos de coordinación inorgánicos, presentando centros magnéticos localizados y estructuras cristalinas bien definidas. La segunda familia se compone hidrocarburos policíclicos alternantes impares para los que los argumentos topológicos garantizan la existencia de electrones no apareados. Considerando diferentes esquemas de acoplamiento (dimensionalidades) y el papel de la flexibilidad estructural, el objetivo principal del estudio que se presenta es mejorar la estabilidad de los centros de radicales y promover una interacción ferromagnética robusta entre ellos. Por lo tanto, la tesis ha sido estructura de tal manera que los diferentes capítulos tratan varios aspectos que son necesarios tener en cuenta para la presentación de una discusión rigurosa sobre los objetivos de la tesis.

El capítulo 1 compara explícitamente ejemplos de radicales orgánicos en los que la interacción entre electrones desapareado se da a través del espacio y a través del enlace. Esta discusión proporciona argumentos experimentales para la elección de la familia de radicales orgánicos que interaccionan a través de enlace. El capítulo 2 presenta los fundamentos teóricos en los que se basan todas las metodologías de cálculo de estructura electrónica utilizadas en este trabajo. El capítulo 3 proporciona una manera precisa de extracción de constantes de acoplamiento magnético en sistemas localizados con parámetros estructurales bien definidos. En el capítulo 4 se presentan y discuten argumentos sólidos para diseñar un poliradical puramente orgánico con conjugación π interactuando a través de enlace, con un valor de S grande, estado fundamental de alto espín, propiedades ferromagnéticas robustas, fuerte anisotropía magnética y estabilidad química.

La parte más metodológica de la tesis intenta definir maneras precisas de extraer las interacciones magnéticas en sistemas complejos basadas en la estrategia del mapping. Al señalar dos deficiencias principales que hacen que el enfoque de mapeo estándar propuesto por Noodleman no sea directamente aplicable a ciertos sistemas de espín, y siguiendo el trabajo desarrollado en el grupo, se propone un enfoque alternativo y se aplica al problema de tres centros tres electrones. Este enfoque se verifica adicionalmente mediante la comparación con datos experimentales y por medio de la teoría de Hamiltoniano efectivo, para construir un Hamiltoniano efectivo de espín ab initio.

Con respecto a la parte que trata sistemas orgánicos de alto espín, se puede afirmar que esta sección de la tesis es el que ha recibido la mayor atención y esfuerzo, sobre todo debido a la enorme cantidad de trabajos publicados, tanto teóricos como experimentales, que tuvo que ser asimilada. Al mismo tiempo, también ha sido la más satisfactoria, por el desafío que constituía, la cantidad y la calidad de las publicaciones producidas y porque me ofreció la posibilidad de trabajar en estrecha colaboración con investigadores experimentales. El objetivo final de este capítulo es proporcionar argumentos sólidos que permitan obtener un polyradical puramente orgánico con conjugación π interactuando a través de enlace, con valor grande de S, estado fundamental de alta multiplicidad, propiedades ferromagnéticas robustas, fuerte anisotropía magnética y estabilidad química. La Ilustración 4 resume la discusión

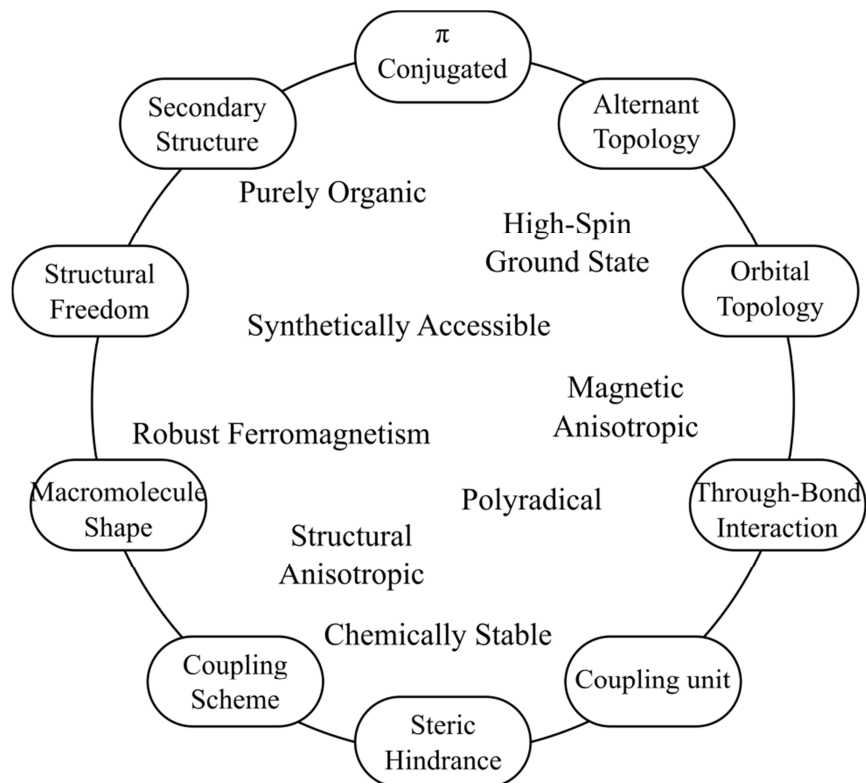anterior, señalando explícitamente a los requisitos para obtener las propiedades deseadas.

Ilustración 4. Resumen de los requrimientos (indicados en la circunferencia) y de las propiedades buscadas (dentro del círculo), para un material magnético puramente orgánico.

7.6. Conclusiones.

Las conclusiones de esta tesis se pueden dividir en dos, dependiendo de los sistemas estudiados. Sin embargo, hay algunos que son comunes.

Desde un punto de vista metodológico, los cálculos basados en DFT introducen una gran dependencia de la elección de la funcional en los valores constantes de acoplamiento magnético calculados, pero en general proporcionan tendencias fiables y consistentes. Por otro lado, los métodos basados en la función de onda ofrecen un tratamiento más riguroso de la estructura electrónica del problema, y por consiguiente una mejor descripción de las interacciones de intercambio magnéticos. Sin embargo, están muy limitado por el tamaño del sistema.

Sobre la descripción exacta de las interacciones de intercambio magnéticos en compuestos de coordinación estudiados.

Por un análisis detallado del *mapping*, hemos identificado los sistemas de espín para los que la formulación propuesta por Noodleman no es apropiada. En particular, los complejos heterobinuclear Ni-V y Ni-Cu investigados en papel # 3.1, demuestran que si los estados puros de espín se expresan como una combinación lineal de los determinantes que no corresponden a los determinantes simetría rota, un proyector de espín unívoco no se puede definir.

Una formulación alternativa del *mapping*, en base trabajos anteriores llevados a cabo en el grupo, se ha propuesto y generalizado para el caso de los tres electrones tres centros.

La alternativa propuesta hace uso directo de la energía de las soluciones de simetría rotos y los asigna a los valores esperados de la energía de las correspondientes soluciones de simetría rota del HDVV hamiltoniano. Por lo tanto, no requiere el uso de un proyector de espín.

La validez de esta propuesta se comprueba mediante la comparación a los datos experimentales y por medio de la teoría de Hamilton efectiva. Los valores obtenidos para el acoplamiento magnético son consistentes.

La teoría de Hamilton efictivo permite una comparación directa entre el los elementos matriciales de la representación del Hamiltoniano HDVV y el efectivo. Esto,

aplicado al problema de los tres centros tres electrones, permite una extracción ab initio de todas las interacciones magnéticas de dos cuerpos, a primeros vecinos, sin hacer ninguna suposición sobre la simetría del problema. Además, la comparación entre el hamiltoniano efectivo y el Hamiltoniano modelo de espín ofrece información sobre el carácter de Heisenberg del sistema.

Por último, para el Cu (II) trinuclear caso estudiado en el papel # 3.2, el valor del acoplamiento magnético calculado presentan una gran dependencia con el funcional utilizado. Sin embargo, la relación entre las constantes de acoplamiento se encuentra que es casi constante para los diferentes funcionales utilizados. Además, los valores consistentes obtenidos en sistemas modelo de dinucleares indican que la interacción magnética es local, y ofrece una manera sencilla de extraer las interacciones de intercambio magnéticos en sistemas polinucleares complejos.

Sobre la descripción teórica y diseño computacional de poliradicales puramente orgánicos π-conjugados, interaccionando a través de enlace, con estado fundamental de alto espín con valores grande *S*, propiedades ferromagnéticas robustas, fuerte anisotropía magnética y estabilidad química.

Un compuesto puramente orgánico que muestre interacción ferromagnética robusta en un amplio rango de temperatura todavía no se ha alcanzado, a pesar de los numerosos intentos. Es una tarea que implica rutas sintéticas y técnicas de caracterización muy complejas, junto con un balance crítico y muy difícil de controlar entre la generación de electrones desapareados, distorsiones estructurales y estabilidad química de los centros radicalarios.

La teoría del funcional de la densidad, utilizando funcionales híbridos, particularmente B3LYP, ofrece una estrategia computacional fiable para describir los múltiples mínimos locales en estos radicales orgánicos estructuralmente flexibles.

Las características estructurales juegan un papel crucial en la definición de las propiedades magnéticas en poliradicales π-conjugados que interactúan a través de enlcae. En particular, estas características estructurales introducen maneras eficaces para aumentar la estabilidad de los compuestos al tiempo que mejoran las propiedades ferromagnéticas.

Para los sistemas poliradicales extendidos, especialmente los que presentan interacciones π–π, la inclusión de correcciones de dispersión de largo alcance es de suma importancia para describir adecuadamente los mínimos en la superficie de energía potencial, y, en consecuencia, las interacciones magnéticas.

Aparte de los ya mencionados, Figura 1 resume esquemáticamente las principales conclusiones de esta tesis con respecto a la interacción magnética en poliradicales orgánicos impares alternantes π-conjugados. Esos son:
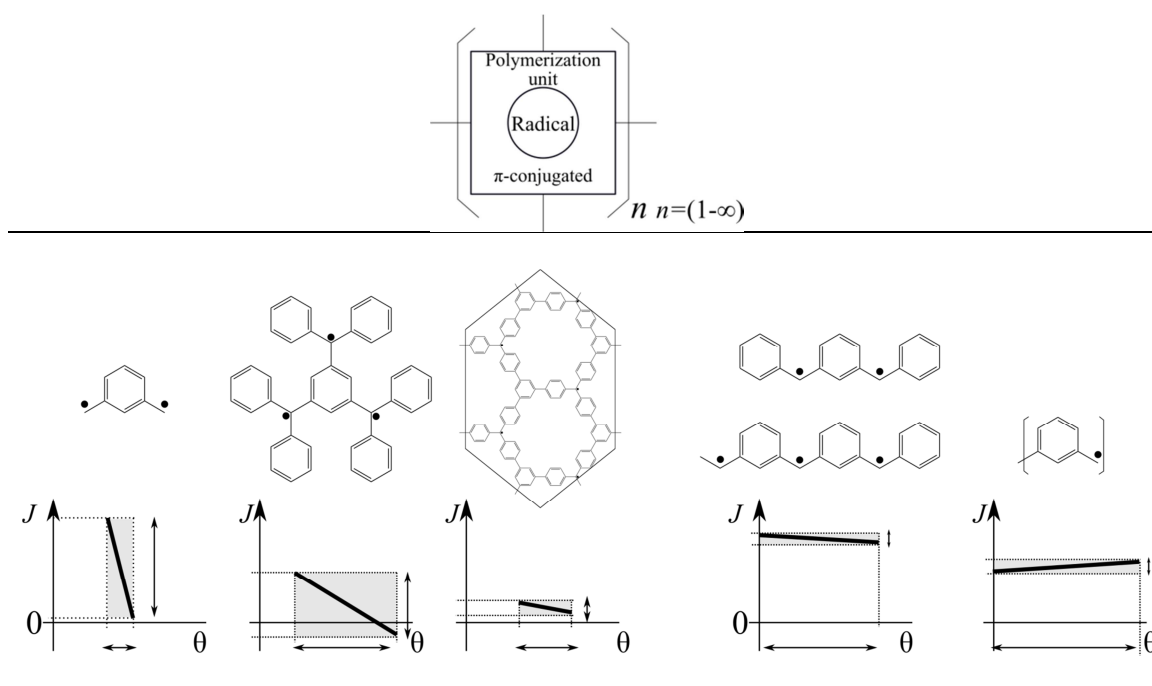

Ilustración 5. Representación esquemática de las tendencias generales observadas a lo largo de esta tesis. J representa la constante de acoplamiento magnético (valores positivos indican ferromagnetismo). θ es una representación de un colectivo dado a coordinar la captura de la torsión en el sistema. Áreas grises destacan cómo la distorsión permitida en el sistema afecta a su constante de acoplamiento magnético

Todos los sistemas orgánicos investigados en esta tesis se pueden dividir en dos, según el efecto de las distorsiones estructurales en la constante de acoplamiento magnético dominante, como se indica en las columnas izquierda y derecha en la Ilustración 5. Para el dirradical *m*-xylyleno, pequeñas distorsiones (θ) implican grandes variaciones del valor de acoplamiento (J), como consecuencia de la falta de un sistema π–conjugado auxiliar para deslocalizar el electrón desapareado si una distorsión ocurre. Para la molécula triradical, la gama de distorsiones permitidas es más grande, y su impacto consigue invertir el signo de la constante de acoplamiento de intercambio. En los sistemas poliméricos en 2D, las distorsiones experimentadas por la red son limitadas

debido a la planaridad del sistema, y el valor de acoplamiento magnéticos se mantiene positivo, pero muy pequeño. En contraste, los sistemas extendidos en una dimensión presentan una gran flexibilidad estructural, pero no importa la conformación adoptada, muestran muy fuerte acoplamiento ferromagnético. Adicionalmente, como consecuencia de la flexibilidad estructural, hay estructuras secundarias que inducen una estabilización neta del estado fundamental de alto spin.

Para concluir, esta tesis propone utilizar poliradicales lineales π-conjugados, basados en unidades moleculares derivados de radicales tipo Gomberg, para lograr propiedades ferromagnéticas robustas en sistemas puramente orgánicos estables.

(1)   Heisenberg, W. *Zeitschrift für Phys.* **1928**, *49* (9-10), 619–636.

(2)   Ising, E. *Zeitschrift für Phys.* **1925**, *31* (1), 253–258.

(3)   Kahn, O. *Molecular magnetism*; VCH: New York, 1993.

(4)   Carlin, R. L. *Magnetochemistry*; Springer-Verlag, 1986.

(5)   Gatteschi, D.; Sessoli, R.; Villain, J. *Molecular Nanomagnets*; Oxford University Press: Oxford, 2006.

(6)   Lahti, P. M. *Magnetic Properties of Organic Materials*; Lahti, P. M., Ed.; Marcel Dekker, Inc: New York, 1999.

(7)   Rajca, A. *Chem. Rev.* **1994**, *94*, 871–893.

(8)   Miller, J. S.; Drillon, M. *Magnetism: Molecules to Materials IV*; Miller, J. S., Drillon, M., Eds.; Wiley-VCH Verlag GmbH & Co. KGaA, 2002.

(9)   Miller, J. S.; Drillon, M. *Magnetism: Molecules to Materials II*; Miller, J. S., Drillon, M., Eds.; Wiley-VCH Verlag GmbH & Co. KGaA, 2002.

(10)   Rajca, A. *Adv. Phys. Org. Chem.* **2005**, *40*, 153–199.

(11)   Shishlov, N. M. *Russ. Chem. Rev.* **2007**, *75*, 863–884.

(12)   Gomberg, M. *J. Am. Chem. Soc.* **1900**, *22* (11), 757–771.

(13)   Ballester, M.; Riera-Figueras, J.; Castaner, J.; Badfa, C.; Monso, J. M. *J. Am. Chem. Soc.* **1971**, *93* (9), 2215–2225.

(14)   Feixas, F.; Matito, E.; Poater, J.; Solà, M. *Chem. Soc. Rev.* **2015**, *44* (18), 6434–6451.

(15)   Trinquier, G.; Malrieu, J.-P. *Chem. - A Eur. J.* **2015**, *21*, 814–828.

(16)   Zheludev, A.; Grand, A.; Ressouche, E.; Schweizer, J.; Morin, B. G.; Epstein, A. J.; Dixon, D. A.; Miller, J. S. *J. Am. Chem. Soc.* **1994**, *116* (16), 7243–7249.

(17)   Acker, D. S.; Harder, R. J.; Hertler, W. R.; Mahler, W.; Melby, L. R.; Benson, R. E.; Mochel, W. E. *J. Am. Chem. Soc.* **1960**, *82* (24), 6408–6409.

(18)   Gutman, I.; Polansky, O. E. *Mathematical concepts in organic chemistry*; Springer-Verlag: New York, 1986.

(19)   Moreira, I. de P. R.; Illas, F. *Phys. Chem. Chem. Phys.* **2006**, *8* (14), 1645–1659.

(20)   Noodleman, L. *J. Chem. Phys.* **1981**, *74*, 5737–5743.

(21)   Noodleman, L.; Davidson, E. R. *Chem. Phys.* **1986**, *109* (1), 131–143.

(22)   Noodleman, L.; Peng, C. Y.; Case, D. A.; Mouesca, J.-M. *Coord. Chem. Rev.* **1995**, *144*, 199–244.